TESIS DE LA UNIVERSIDAD DE ZARAGOZA

2012

39

Ahmed Mohammed Hussain El Kenawy El

Spatio-temporal variability of surface air temperature in northeastern Spain

Departamento

Geografía y Ordenación del Territorio

Director/es

Vicente Serrano, Sergio Martín
López Moreno, Juan Ignacio

ISSN 2254-7606

Prensas de la Universidad Universidad Zaragoza

Universidad Zaragoza
1542

Tesis Doctoral

SPATIO-TEMPORAL VARIABILITY OF SURFACE AIR TEMPERATURE IN NORTHEASTERN SPAIN

Autor

Ahmed Mohammed Hussain El Kenawy El Sayed

Director/es

Vicente Serrano, Sergio Martín
López Moreno, Juan Ignacio

UNIVERSIDAD DE ZARAGOZA

Geografía y Ordenación del Territorio

2012

SPATIO-TEMPORAL VARIABILITY OF SURFACE AIR TEMPERATURE IN NORTHEASTERN SPAIN

A Dissertation submitted for the Degree of Doctor in Philosophy in the Department of Geography and Land Management

University of Zaragoza

Presented by

Ahmed Mohammed Hussain El Kenawy El Sayed

MSc in Environmental Informatics, University of Leicester, UK (2007)

Supervisor

Dr. Sergio Martin Vicente-Serrano

Instituto Pirenaico de Ecologia, Consejo Superior de Investigaciones Cientificas (CSIC), Zaragoza

Co-Supervisor

Dr. Juan Ignacio López Moreno

Instituto Pirenaico de Ecologia, Consejo Superior de Investigaciones Científicas (CSIC), Zaragoza

Summer 2012

To

My little kid Kareem

“If you cannot do great things, do small things in a great way.”

Napoleon Hill (1883-1970)
American writer

Sergio Martín Vicente Serrano y Juan Ignacio López Moreno, científicos titulares del Departamento de Procesos Geoambientales y Cambio Global del Instituto Pirenaico de Ecologia (Consejo Superior de Investigaciones Científicas)

CERTIFICAN:

Que Don Ahmed Mohammed Hussain El Kenawy El Sayed ha realizado bajo nuestra dirección el trabajo que, para optar al grado de Doctor en Geografía, presenta con el título:

"Spatio-temporal variability of surface air temperature in northeastern Spain", y

Que el trabajo se ajusta a los objetivos establecidos en el proyecto de Tesis Doctoral aprobado el 16 noviembre de 2009, por el Departamento de geografía y Ordenación del Territorio y ratificado por la Comisión de Doctorado.

Y para que así conste, firmamos la presente Certificación en Zaragoza a 25 de Mayo de 2012 para los efectos que sean oportunos.

Fdo. Sergio M. Vicente Serrano Fdo. Juan I. López-Moreno

ACKNOWLEDGMENTS

My thanks go to all the people who have supported, accompanied and guided me throughout my PhD. First of all I would like to acknowledge Dr. Sergio Martin Vicente-Serrano for giving me the opportunity to continue my postgraduate studies in his research group. I also acknowledge my second supervisor, Dr. Juan Ignacio Lopez-Moreno, for his inspiring discussions. Both have been great motivators, given me their endless support, extensive insights and fruitful guidance throughout my work. They gave me the opportunity to live in Zaragoza for more than four years, a city which I admire very much. I would also like to thank Dr. Nathaniel Brunsell from the Atmospheric Research Group at the University of Kansas for his support during my academic visit to the USA. Also, I am greatly indebted to Dr. Petr Stepanek from the Czech Hydrometeorological Institute for his very useful advice in general and his ProClim software in particular.

I am also very grateful to all my colleagues in *Instituto Pirenaico de Ecologia* for the very pleasant working atmosphere for the duration of this study. I specially thank to Arben, Yacine, Javier, Marta, Hugo, Jorge and Edmond for their invaluable help in all the aspects of this study. Many thanks also due to all the administrative and technical people including: Cecilia, Trinidad, and Jose Manuel. I extend sincere gratitude to Consejo Superior de Investigaciones Cientificas (CSIC) for the financial support of this work through the JAE scholarship program.

My wife, thank you for believing in me. Many thanks for your support, motivation and inspiration. You provided me the balance during hard times.

This work has been supported by the research projects CGL2011-27574-CO2-02, and CGL2011-27536 financed by the Spanish Commission of Science and Technology and FEDER, ACQWA (FP7-ENV-2007-1- 212250) financed by the VII Framework Programme of the European Commission, “Efecto de los escenarios de cambio climático sobre la hidrología superficial y la gestión de embalses del Pirineo Aragonés” financed by “Obra Social La Caixa” and the Aragón Government and Influencia del cambio climático en el turismo de nieve, CTTP01/10, Financed by the Comisión de Trabajo de los Pirineos.

ABSTRACT

From the climatological point of view, northeast Spain is an area of large interest due its varied geographical, topographical and climatic characteristics. In this work, a spatially and temporarily high-resolution daily dataset of temperature was developed for northeastern Spain. Data derived from a high number of observatories (1583) spanning some period between 1900 and 2006 was tested for internal and external consistency to check data quality. To improve data completeness, a linear regression model was then utilized to infill gaps in the daily temperature series using the best correlated data from nearby sites. Discontinuities in the reconstructed series were then determined by combining the results of three homogeneity relative tests: the Standard Normal Homogeneity Test (SNHT), the Easterling and Peterson two-phased regression method, and the Vincent test. The newly complied dataset seems to be more robust and reveals more coherent spatial and temporal patterns of temperature compared with the original dataset. This finding was confirmed by means of a suite of statistics (e.g., semivariance models and L-moment statistics). From the temporal and spatial perspectives, the new dataset comprises the most complete register of temperature in northeast Spain (1900-2006), with a reasonably spatial coverage. Therefore, this database provides a more reliable base for studying temperature changes and variability in the region.

This thesis analyzed the surface air temperature variability and trends over the study domain for the 20th century based on the new compiled dataset. An assessment of long-term change and variability of temperature was provided using a dataset of 19 observatories from 1920 to 2006. In addition, a more detailed analysis of the spatial and temporal variability of maximum, minimum, and mean temperatures, and the

diurnal temperature range (DTR) was also carried out employing 128 observatories spanning the period from 1960 to 2006. In general, maximum, minimum, and mean temperatures increased significantly, mostly from contributions in the late decades of the 20st century. At the seasonal scale, the analysis revealed that the weakest trends (mostly insignificant at the 95% level [$p<0.05$]) were observed during autumn, while the strongest warming rates were found during summer and spring. Spatially, the observed warming was more robust in the coastal portions compared with mainland observatories.

Spatial and temporal characteristics of extreme temperature events were also investigated. A total of 21 indices were used to assess changes in the cold and warm tails of the daily temperature distribution, calculated at the annual timescale. The presence of trends in temperature extremes was assessed by means of the Mann-Kendall statistic. However, prior to assessing trends, the autocorrelation function (ACF) and bootstrap methodologies were used to account for the influence of serial correlation and cross-correlation on the trend assessment. In general, the observed changes were more prevalent in warm extremes than in cold extremes. The results indicated a significant increase in the frequency and intensity of most of warm extremes. An increase in warm nights (TN90p: 3.3 days decade^{-1}), warm days (TX90p: 2.7 days decade^{-1}), tropical nights (TR20: 0.6 days decade^{-1}) and the annual high maximum temperature (TXx: 0.27ºC decade^{-1}) was detected in the 47-year period (1960-2006). In contrast, majority of the indices related to cold extremes (e.g., cold days [TX10p], cold nights [TN10p], very cold days [TN1p], and frost days [FD0]) demonstrated a decreasing but statistically insignificant trend. Spatially, similar to temperature means, the coastal areas along the Mediterranean Sea and the Cantabrian Sea experienced stronger warming compared with mainland areas.

In this thesis, a procedure for classifying daily temperature extremes into homogenous regions was also presented and evaluated. This procedure employed characteristics of temperature extremes calculated for summer (JJA), including temperature frequency (e.g., warm days), intensity (e.g., warmest day), and duration (e.g., maximum length of warm spell). Following the results of the principal components analysis (PCA) and the Ward´s method of clustering, the study area was divided into four homogenous sub-regions: the Mediterranean region, the mainland and the Cantabrian region, the moderately elevated areas westward and southward, and the mountainous region. The quality of this clustering was evaluated and ensured by means of an internal cluster validation measure (Silhouette width). Overall, the delineated sub-regions were proved as homogenous in terms of both the geographic and climatic meanings. The temporal evolution of the long-term (1960-2006) temperature extremes was assessed for each of these sub-regions. The Mediterranean and the highly elevated regions revealed the strongest signals in both day-time and night-time extremes.

This study also explored the forcing mechanisms that can explain temperature variability at seasonal timescales. The results indicated that this variability can markedly be connected to variations in the large-scale atmospheric patterns. Notably, the Eastern Atlantic (EA), the Scandinavian (SCA), and the Western Mediterranean Oscillation (WeMO) patterns exerted significant influences on temperature variations in the study domain. Temperature tended to increase during the positive (negative) modes of the EA (WeMO and SCA) patterns. Also, the possible physical processes and mechanisms favoring for the occurrence of the anomalous extreme heat events (very warm days [VWD: daily Tmax>99th percentile] and very cold nights [VCN: daily Tmin<1st percentile]) were examined. This included

configurations of Seal level pressure (SLP) and 200hPa and 500hPa geopotential height fields. The occurrence of VCN was mainly associated with predominance of the meridional circulation over much area of the Western Europe, with strong advection of cool air from northern continental Europe and the North Atlantic. On the other hand, the most likely factors contributing to VWD were the north-eastward displacement of the Atlantic subtropical high and the increase in the European blockings. In spite of the small spatial extent of the study domain (approximately 160,000 km^2), the results interestingly confirmed that circulation patterns had spatially variable influences on both temperature means and extremes.

This work also assessed how well a set of regional climate models (RCMs) can reproduce observed changes in seasonal temperatures over northeastern Spain. The projected changes in seasonal temperatures were assessed under the A1B emission scenario of climate change for the 21st century based on comparison of the control period (1971-2000) and two future time slices: 2021-2050 and 2071-2100. The results indicated that the current substantial warming will continue during the 21st century. The largest temperature changes were projected for the second half of the 21st century, with the strongest trends being on the order of 0.7 and 0.5°C $decade^{-1}$ in summer and winter, respectively. The results demonstrated a rapid increase in wintertime minimum temperature and summertime maximum temperature. Spatially, almost the whole domain will be dominated by a positive temperature anomaly during the 21st century, relative to the present climate (1971-2000), with the largest warming in the central Ebro valley and the least over the Pyrenees and near the Cantabrian coast. In order to assess how the lower and upper tails of temperature distributions will change over the 21st century and whether these changes will be consistent with changes in the mean in both the sign and the magnitude, an analysis of the trends in various time-varying percentiles

(e.g., the 10th, 25th, 75th and 90th) was performed on a seasonal basis. Linear trends of temperature percentiles showed clear warming trend over the late decades of the 21st century (2071-2100), compared with both the mid century (2021-2050) and the observed (1971-2000) changes. The largest warming was projected for the lower (upper) percentiles of the minimum (maximum) temperature distributions during summer (winter). A warming rate of 0.9ºC and 0.8ºC decade^{-1} was observed for the 10th and 25th percentiles of summer minimum temperature, whereas the 75th and 90th percentiles of wintertime maximum temperature distribution increased by 0.5ºC and 0.6ºC decade^{-1}, respectively. In addition, the results indicated that, among all seasons, summer will exhibit the largest interannual variability of temperature in the future. This increase could drastically increase the probability of exhibiting more extremely warm events in the region. This study also emphasized that changes in the upper and lower tails of temperature distribution may not follow the warming rate of the mean. This suggests that much of changes in the temperature percentiles will be driven by a shift in the entire distribution of temperature rather than only changes in the central tendency.

In such a complex climatic and geographic region, an assessment and attribution of regional temperature variability based on high-quality, long-term and dense network of observatories can be advantageous for extracting finer scale information, which may prove useful for the vulnerability assessments and the development of local adaptation strategies for various disciplines such as hydrology, agriculture, water resources management, ecology and human health.

RESUMEN

El noreste de España es un área de gran interés por su variedad geográfica, topográfica y climática. En el marco de este trabajo se ha desarrollado una base de datos de temperatura diaria para el noreste de España de una elevada densidad espacial. Se ha utilizado un gran número de observatorios (1583) con datos desde 1900 hasta 2006. La calidad de los datos fue examinada atendiendo a su consistencia interna y externa. Los datos ausentes fueron rellenados mediante modelos lineales de regresión utilizando las series cercanas de temperatura diaria que mostraban mejor correlación. Una vez reconstruidas las series, se aplicaron tres test de homogeneidad para detectar posibles discontinuidades: El *Standard Normal Homogeneity Test* (SNHT), el método de regresión de dos fases *Easterling and Peterson,* y el test de *Vincent.* Diversos análisis estadísticos (e.g., semivariance modelos and L-moment statistics) han confirmado que la base de datos resultante muestra una mayor coherencia espacial y temporal que la base de datos original. La base de datos obtenida representa el conjunto de datos de temperatura más completo del noreste de España para el periodo 1900-2006, siendo una base de datos idónea para estudiar la variabilidad y el cambio de la temperatura en la región.

Esta tesis analiza la variabilidad y tendencia de las temperaturas en la zona de estudio durante el siglo XX. 19 series de temperatura han sido utilizadas para analizar el periodo 1920-2006, mientras que para análisis más detallados de la variabilidad espacial y temporal de las temperaturas máximas, mínimas, medias y rango diario (DTR) se utilizaron 128 observatorios que cubren el periodo 1960-2006. Se ha detectado un incremento generalizado de las temperaturas, determinado en gran medida por la evolución que han mostrado en las últimas décadas del periodo de estudio. Estacionalmente, los análisis indican que las tendencias más moderadas

han sucedido durante otoño, mientras el mayor calentamiento se ha detectado en verano y primavera. Espacialmente, el calentamiento detectado resulta mucho más consistente en las zonas de costa frente al detectado en los observatorios en zonas de interior.

También se ha estudiado el comportamiento espacial y temporal en la ocurrencia de eventos extremos. Un total de 21 índices fueron seleccionados para caracterizar los extremos fríos y cálidos de la distribución de frecuencias de las series de temperatura diaria. La existencia de tendencias temporales se detectaron mediante el test de Mann-Kendall. Además funciones de autocorrelación (AF) y la técnica de *bootstrap* sirvió para eliminar el efecto de la correlación serial y la croscorrelación en la detección de tendencias. En general, los cambios observados son más marcados en la ocurrencia de eventos fríos que cálidos. Un incremento en la ocurrencia de noches cálidas (TN90p: 3.3 días/década), días cálidos (TX90p: 2.7 días/década), noches tropicales (TR20: 0.6 días/década) and la temperatura máxima más alta anual (TXx: 0.27ºC/década) se encontró para el periodo1960-2006. La mayoría de los índices relacionados con extremos fríos (p.e., días fríos [TX10p], noches frías [TN10p], días muy fríos [TN1p], y días de helada [FD0]) mostraron un descenso que generalmente no fue estadísticamente significativo. Parecido a lo observado con las temperaturas medias, las zonas costeras Mediterráneas y Cantábricas mostraron un mayor calentamiento respecto a las zonas de interior.

Se ha clasificado la zona de estudio en cuatro regiones homogéneas según la ocurrencia, intensidad y duración de eventos de temperaturas extremas aplicando Análisis de Componentes Principales (PCA) y análisis clúster (método *Ward*). Las regiones identificadas han sido: la Mediterránea, la Cantábrica, el sector Ibérico y

las estaciones más elevadas del Pirineo y el Sistema Ibérico. La robustez de la clasificación se validó utilizando el estadístico de *Silhouette.* La evolución temporal de los eventos extremos en las series más largas (1960-2006) muestra un comportamiento distinto entre las diferentes regiones. La región mediterránea y los observatorios en zonas de montaña mostraron la señal más clara de calentamiento tanto en las temperaturas máximas y mínimas.

Este trabajo también ha analizado los mecanismos atmosféricos que pueden explicar la variabilidad térmica. Los resultados indican que los cambios observados en las temperaturas y sus diferencias espaciales y estacionales están relacionados con patrones atmosféricos de gran escala. En particular el patrón del Atlántico Este (EA), el patrón Escandinavo (SCA) y la Oscilación del Mediterráneo Occidental (WeMO) ejercen un papel muy importante en la variabilidad térmica de la zona de estudio. La temperatura tiende a incrementarse durante las fases positivas (negativas) del patrón EA (SCA y WeMO). Los posibles mecanismos físicos que favorecen la ocurrencia de los días más cálidos (TX99) y noches frías (TN1) han sido también examinados utilizando series diarias de presión a nivel de superficie (SLP) y las alturas geopotenciales de 200hPa y 500hPa. La ocurrencia de noches muy frías (VCN) está asociada a un incremento de la circulación meridional sobre grandes áreas de Europa occidental, con una clara advección de aire frío del norte de Europa y el Atlántico norte. La situación más favorable para la ocurrencia de días muy cálidos (VWD) es un desplazamiento norte-este del anticiclón Atlántico subtropical y situaciones de bloqueo sobre Europa. Sin embargo, los resultados confirman que los patrones de circulación afectan de forma espacialmente diferenciada a las temperaturas medias y extremas.

Este trabajo también ha analizado la capacidad de los modelos climáticos regionales (RCMs) de reproducir los cambios observados en las temperaturas a escala estacional en la zona de estudio. Las series de temperatura simuladas, asumiendo un escenario de emisión de gases de efecto invernadero A1B, para dos periodos del siglo XXI (2021-2050) y (2071-2100), se han comparado a los simulados para un periodo control (1971-2000). Los resultados indican que los procesos de calentamiento van a continuar durante el siglo XXI, acelerándose en sus últimas décadas. El mayor incremento corresponde a verano e invierno, con unos ratios de calentamiento de 0.7 y 0.5 ºC por década respectivamente. Espacialmente, se espera un mayor incremento térmico en las zonas del interior del valle del Ebro, y un calentamiento más suave en el área pirenaica y la costa del Cantábrico. Se ha valorado la magnitud de los cambios proyectados en distintas partes de la distribución de frecuencia de las temperaturas, y sus efectos sobre los cambios en el signo y magnitud de los valores medios. Para ello se han aplicado análisis de tendencia a las series de evolución temporal de distintos percentiles (p.e., los percentiles 10, 25, 75 y 90) tanto en el periodo control como en los dos periodos futuros (2021-2050 y 2071-2100). El mayor calentamiento ha afectado a los percentiles más bajos (altos) de la temperatura máxima (mínima) de las distribuciones de verano (invierno). Se ha estimado un ritmo de calentamiento de 0.9 y 0.8ºC por década para los centiles 10 y 25 de la temperatura mínima de verano, mientras los percentiles 75 y 90 de la temperatura máxima de invierno pueden aumentar 0.5 y 0.6ºC por década respectivamente. Los resultados indican que verano mostrará la mayor variabilidad interanual en las próximas décadas. Este incremento puede aumentar notablemente la probabilidad de ocurrencia de eventos extremos cálidos en la región. Los cambios en los extremos de la distribución de frecuencia de las series de temperatura no siguen necesariamente el ritmo de

calentamiento de la temperatura media, sugiriendo que los cambios proyectados para los distintos percentiles se deben a una alteración completa de la distribución de frecuencia y no sólo de sus valores centrales.

La detección y caracterización de la variabilidad y cambio de las temperaturas mediante el uso de una red de observatorios de gran longitud y elevada densidad espacial han resultado de gran utilidad en una región tan compleja desde un punto de vista climático y geográfico. La información generada puede resultar de gran interés para valorar la vulnerabilidad de la región ante los efectos del cambio climático proyectado, permitiendo el desarrollo de estrategias de adaptación en sectores como la gestión de los recursos hídricos, agricultura, ecología y salud.

Contents

LIST OF TABLES

LIST OF FIGURES

LIST OF ABBREVIATIONS

A	Anticyclones
ACF	Autocorrelation Function
AEM	Agencia Estatal de Meteorologia
AnClim	Analysis of Climate datasets (software)
ANOVA	One-way Analysis of Variance
AR	Autoregressive Process
AR4	The 4th Assessment Report
C	Cyclones
CA	Cluster Analysis
CDF	Cumulative Distribution Function
CFCs	Chloroflurocarbons
CH4	Methane
CHE	Confederación Hidrográfica del Ebro
CO2	Carbon dioxide
CRU	Climate Research Unit
CV	Coefficient of Variation
DJF	December-January-February (winter season)
DTR	Diurnal Temperature Range
EA	East Atlantic Oscillation
EAWR	East Atlantic/ Western Russian Oscillation
ECA	European Climate Assessment
ELPIS	A Dataset of Local-Scale Daily Climate Scenarios for Europe
EMULATE	European and North Atlantic daily to MULtidecadal climATE variability
E-OBS	Observational Gridded Daily Dataset for Europe
EV	Explained Variance
FD0	Frost Days
GCMs	Global/General Climate Models
GHCN	Global Historical Climatology Network
GHG	Green House Gases
GPM	Geopotential meters
GSL	Growing Season Length
ID0	Ice Days
IDW	Inverse Distance Weighting interpolation algorithm
IPCC	Intergovernmental Panel on Climate Change
IVE	Inter-annual Variability Error
JJA	June-July-August (summer season)
KMO	Kaiser-Meyer-Olkin Test
MA	Moving Average
MAM	March-April-May (spring season)
MBE	Mean Bias Error
MO	Mediterranean Oscillation
MSL	Mean Sea Level
N2O	Nitrous Oxide
NAO	North Atlantic Oscillation

NCDC	National Climate Data Center
NCEP/NCAR	National Centers for Environmental Prediction-National Center for Atmospheric Research
NDJFM	November-December-January-February-March (Cold half of the year)
NESAT	North-Eastern Spain Adjusted Temperature dataset
NH	Northern Hemisphere
NOAA	National Oceanic and Atmospheric Administration
O3	Ozone
OLS	Ordinary Least Squares
PCA	Principal Component Analysis
PDF	Probability Density Function
PPM	Part Per Million
PPB	Part Per Billion
PROCLIM	PROcessing CLImatological datasets (software)
PRUDENCE	Prediction of Regional scenarios and Uncertainties for Defining European Climate change and Effects
R	Pearson Correlation Coefficient
RCMs	Regional Climate Models
Rho	Non-parametric Spearman Test
RHTs	Relative Homogeneity Tests
SCA	Scandinavian Oscillation
SDATS	Spanish Daily Adjusted Temperature Series
SLP	Surface Level Pressure
SNHT	Standard Normal Homogeneity Test
SON	September-October-November (autumn season)
SPEI	Standardized Precipitation Evapotranspiration Index
SPI	Standardized Precipitation Index
SRES	Special Report on Emissions Scenarios
SST	Surface Sea Temperature
STARDEX	Statistical and Regional dynamical Downscaling of Extremes for European regions
Stdev	Standard deviation
SU	Summer Days
TFPW	Trend Free Pre-Whitening
Tmax	Daily maximum temperature
Tmean	Daily mean temperature
Tmin	Daily minimum Temperature
VCN	Very Cold Nights
VWD	Very Warm Days
WD	Warm Days
WeMO	Western Mediterranean Oscillation
WHO	World Health Organization
WMO	World Meteorological Organization
YK	Yule–Kendall Skewness measure

CHAPTER ONE INTRODUCTION

1. INTRODUCTION

The following introductory paragraphs provide an overview of the research context, the fundamental questions of this thesis, and the framework applied for this work. Finally, a summary of each main chapter is given in the thesis outline.

1.1. Climate Change

Climate change is one of the most pressing global problems, which is likely projected to become a progressively more significant threat in the next decades. Natural scientists have described it as perhaps the preeminent environmental risk confronting the world in the 21st century. Indeed, there is increasing evidence that climate is changing worldwide and most of the pronounced change is mainly observed during the past few decades (IPCC, 2007). Some potentially climate driven changes include observed changes in sea level, snow cover, ice extent, species extinctions and distributions, and extreme weather events. Changes in climate can be attributable to internal and external variability. The influence of external factors on climate system can be broadly seen in the context of radiative forcing. In its 4th Assessment Report (AR4) in 2007 the IPCC indicated that there is a very high confidence (99% probability) that recent climate change is mainly driven by anthropogenic influences rather than natural variations. Recently, Jansen et al. (2007) emphasized this notion indicating that the global climate change cannot be explained without considering the role of the human activities. This finding has also been confirmed by Hegerl et al. (2007) who indicated that the observed change in the global climate during the 20th century cannot fully be attributed to the internal variability of climate. In other words, the significant anthropogenic warming, mainly caused by burning fossil fuels, industry,

deforestation, land-use changes that modify surface albedo and other man-made activities, has induced considerable alterations of the global energy balance leading to both positive and negative radiative forcings (Ruddiman, 2003). Overall, the key role of increasing the GHG concentrations in the atmosphere is the imbalance between incoming and outgoing radiation. A clear positive radiative forcings is the rise of greenhouse gas (GHG) concentrations such as carbon dioxide (CO2), methane (CH4), nitrous oxide (N2O), ozone (O3) and chloroflurocarbons (CFCs) (Figure 1.1). From 1970 to 2004, the atmospheric CO2 concentration has raised from 180 parts per million (ppm) to 385ppm, while the Methan has elevated from 715 parts per billion (ppb) to 1790ppb (IPCC, 2007).

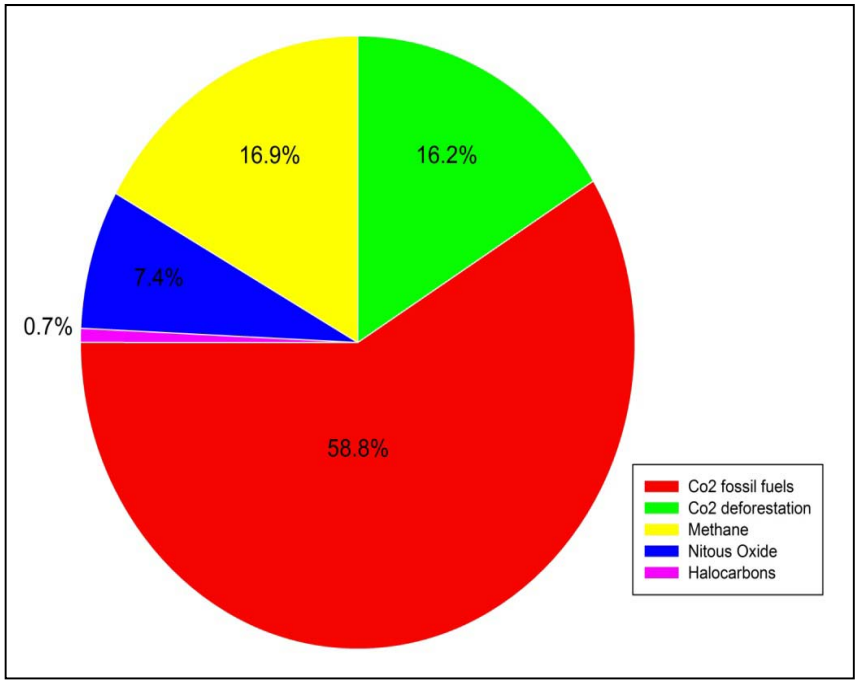

Figure 1.1: The key GHG with positive feedback on the global energy (IPCC, 2007)

Contrarily, other atmospheric components such as aerosols (e.g., sulphur) have a negative forcing, inducing below-normal temperatures. The GHG absorb the long wavelength (infrared) radiation, causing a reduction of the outgoing radiation in the atmosphere and in turn increase in temperature. In order to keep a radiative equilibrium between the Earth surface and the atmosphere, the GHG provides a driving force for heating the Earth.

Climate change, as induced by modifications in the energy balance of the earth system, can not only be linked to the anthropogenic forcing. Natural forcings can, to some extent, be another driver of climate change and variability. Internal variability in the climate system can be due to, among others, changes in solar radiation, orbital characteristics, volcanic eruptions or natural greenhouse gases (e.g., water vapor). For instance, Beer et al. (1998) attributed the coldest temperature during the late half of the 17th century to a reduction in solar activity. During this period Luterbacher et al. (2004) also found the coldest winter on record across Europe, with a negative anomaly of −3.6ºC. In their study to assess the strength of the Asian monsoon over the last 9000 years, Wang et al. (2005) found cycles in the monsoon activity, that are compatible with variations in solar activity. In the same context, numerous studies attributed much of warming during the first half of the 20th century to increasing solar irradiance. Similarly, large and short lived volcanic eruptions can be seen as a significant natural radiative forcing, which likely induce a cooling of the global temperature (Hansen and Lacis, 1990). Following Barry and Chorley (1992), the volcanic eruptions emitted from El Chichon (March 1982) significantly accounted for a reduction of the global temperature in the following decade, as these volcanic particles scattered the short-wave radiation and in turn increased the surface albedo causing

cooling. Contrarily, the increase in sunspots, which occurs on an 11-year cycle, often results in a rise of solar radiation emission, particularly when they are mainly centered close to the equator of the sun (Albregtsen and Maltby, 1981).

Taken together, it is important to gain knowledge about changes in external forcing affecting the global climate as well as the internal dynamics of the climate system. This approach addresses the principal question whether the observed warming is an ongoing trend driven by “unusual” external forcings or simply due to natural internal variability. This approach could therefore improve the understanding of the way in which the present climate behaves. Furthermore, it contributes to better projections of future climate changes.

According to the IPCC (2007), natural systems are more vulnerable to climate change as a consequence of their limited adaptive capacity. Nonetheless, the vulnerability of these systems may considerably vary according to the geographic location and time, besides the effect of other social, economic, and environmental conditions. The literature on the response of natural systems and human ecosystems to climate change is large and growing. For example, numerous recent works have linked changes in ecosystem structure and function, including changes in species physiology, phenology, distributions, community composition, to changes in climate (e.g., Hellman 2002; Oberhauser and Peterson 2003; Parmesan and Yohe 2003; Root et al. 2003; Thomas et al., 2004; Visser and Both, 2005; Parmesan, 2006). One example is Thomas et al. (2004) who projected an extinction of roughly 15-37% of species in the next 50 years, due to climate change. Several studies have also addressed the direct or indirect effects of climate change. A representative example is the drastic

consequences of the 2003 European summer, the warmest summer over the last 1500 years as revealed by Luterbacher et al. (2004). According to the WHO (2003), this unprecedented heat event caused more than 30,000 fatalities (at least 15,000 in France), besides economic losses of US$ 14 billion resulting principally from the devastating consequences of forest fires and crop losses.

Under climate change conditions, more attention has recently been paid to understand climate variability and change, particularly with the rapid improvement of the instrumental measurements. Correspondingly, substantial progress has also been made to assess the wide-ranging impacts of increasing atmospheric carbon dioxide concentration and globally rising temperatures. In this regard, an increasing number of studies endeavored to further understanding of changes in climate mean and extremes. Particular concern has been pertained to investigate long-term changes in temperature and precipitation patterns, being the most common variables describing climate change.

Nonetheless, while climate change is a global phenomenon, its effects are not homogenous in all regions of the world. The magnitude and impacts of climate change on ecosystems, health, energy demand and human activities vary from region to another. Therefore, assessing impacts of climate change at a more local and regional scale is critical and more important for ecosystem dynamics and human societies. Understanding changes in climatic patterns and the dynamics behind them at finer spatial scale is a key to assessing their possible changes in the future, which could provide high quality advice to local policymakers for adaption and mitigation.

1.2. Global Warming

While the term “climate change” is generally used to denote long-term and significant changes in the Earth’s pattern of weather, including different variables (e.g., temperature, precipitation, wind, cloudiness, dew point, evapotranspiration, snow…etc), whether due to natural variability or anthropogenic influences, the phrase “global warming”, on the other hand, is commonly used to refer to human-induced temperature rise, which has already and will continue to occur. Historically, the warming effect induced by the enhanced greenhouse effect was first recognized by Jean-Baptiste Fourier in 1827 (Wallington et al., 2004). Few years later, the Swedish chemist Svante Arrhenius estimated the effect of a doubling of the atmospheric carbon dioxide concentrations on the global temperature by 5-6ºC. Recently, ongoing scientific evidence supports this claim based on results derived from various proxies such as tree rings, ice cores and ocean sediments, suggesting higher increase in the global mean surface temperature during the last few decades relative to periods since at least the last millennium. This warming is mainly driven by the enhanced greenhouse effect resulting from anthropogenic, or human-caused, emissions of greenhouse gases (carbon dioxide, methane, nitrous oxide, halocarbons, and ozone) to the atmosphere.

During the course of the 20th century, the global warming occurred at a linear rate of 0.7°C decade^{-1} (IPCC, 2007). As indicated in Figure 1.2, this warming has been more pronounced over the past 25 years (1.8°C decade^{-1}). Globally the 1990s and 2000s were the warmest decades on record, and the 1990, 1994, 1998, 2003 and 2010 were the warmest years. Based on reconstructed temperature time series since 1500, Luterbacher et al. (2004) concluded that the global trends in temperature during the

latter half of the 20th century are very likely higher than during the past five decades. This feature has also been found for the global land (Figure 1.2, left panel), the northern hemisphere (Figure 1.2, right panel) and Europe (Figure 1.3). The increase in temperature during the last two decades of the 20th century was the largest compared with the past 130 years. In general, the observed warming has not been uniform over space and time (Jones and Moberg 2003). The observed anomalous temperatures during recent decades can be seen as one of the most arising effects of the global warming. According to the IPCC (2007), this unusual warming mostly corresponds to a rapid increase in the carbon dioxide concentration, which was markedly larger in the last two decades (1.9 ppm per year) compared to previous decades (1.4 ppm per year from 1960 to 2005).

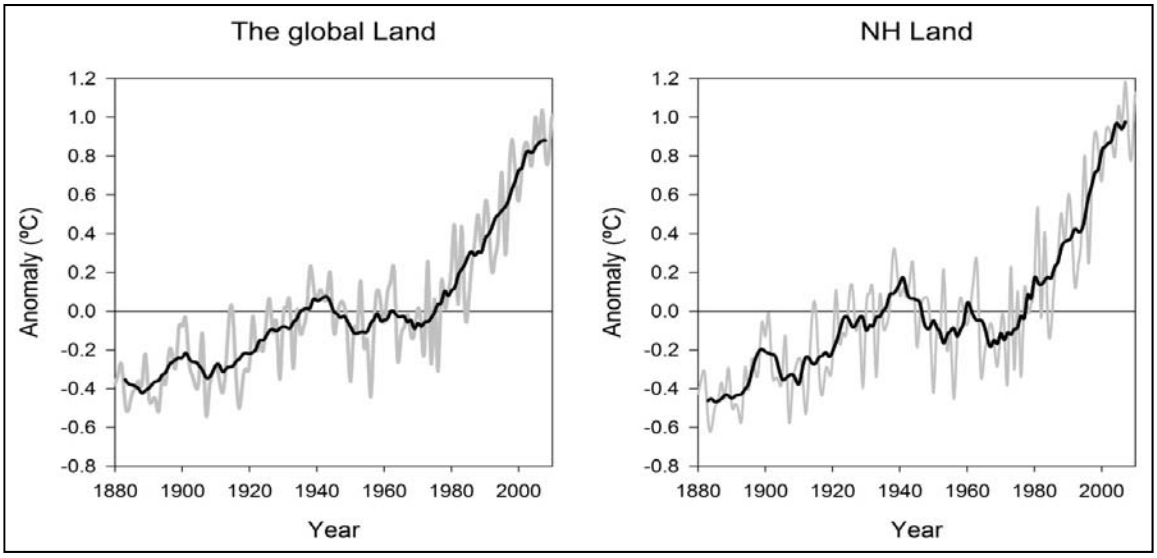

Figure 1.2: (Left) Annual anomalies of (left) the global average land-surface and (right) northern hemisphere (NH) land-surface air temperature (ºC) from 1880 to 2010. The anomalies were calculated relative to normal mean over the base period 1961-1990. Solid line indicates the smoothed curve using a 7-yrs low pass filtering. The original data were derived from CRU (Jones et al., 2001).

Numerous studies confirmed global warming at regional, continental and global scales (e.g., Jones et al., 1999; Jones and Moberg, 2003). Nevertheless, this observed warming has not been uniform over space and time (Jones and Moberg, 2003). It has been noted that a great part of this warming was in the mid and high latitudes, particularly during the cold season, suggesting more increase in minimum temperature than in maximum temperature. This feature corresponds to a tendency towards a narrower yearly temperature range.

Numerous recent works on the Earth's climate make clear that the recent global warming will continue in the future in response to elevated atmospheric greenhouse gases, indicating a tendency of temperature to increase over large areas of the world. Based on predictions from numerous global climate models (GCMs), the IPCC (2007) reported that the global average temperature will further increase by a range from 1.4 to 5.8ºC by the end of the 21st century, in response to an increase in CO2 concentrations by as much as 350%. Temperature increase in Europe is consistent with this global trend. Some authors have consistently projected a significant increase in surface air temperatures over Europe within the 21st century (e.g., Kjellström, 2004; Moberg and Jones, 2004; Deque et al., 2005). For example, Parry (2000) studied the future climatic trend in Europe and found that the mean temperature might increase by 2–6.3°C at the end of this century. A more recent work by Schar et al. (2004) also projected an increase in the annual mean temperature over Europe, concluding that the unusual 2003 summer will become increasingly more common by the end of the current century, as the climate progressively warms.

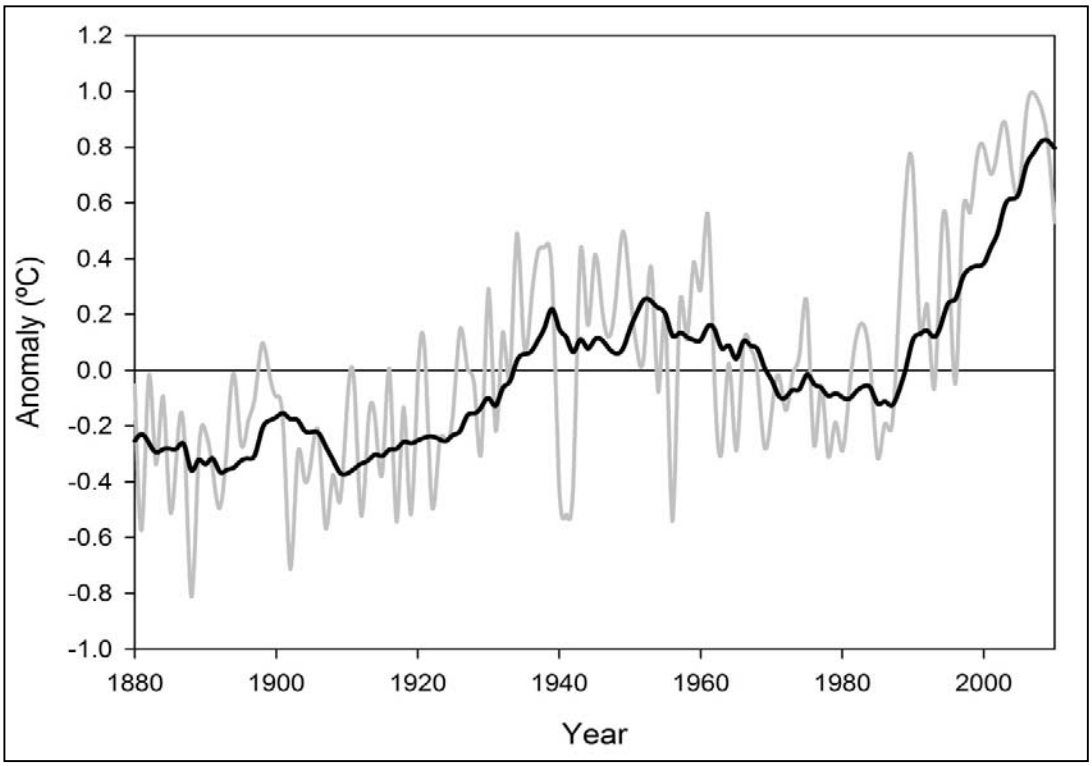

Figure 1.3: Annual anomalies of the European land & ocean air temperature (ºC) from 1880 to 2010. The anomalies were calculated relative to the normal mean over the base period 1961-1990. Solid line indicates the smoothed curve using a 10-yrs low pass filtering. The original data were derived from CRU (Jones et al., 2001).

Similarly, In response to the global warming, much more attention has recently been paid to assess the potential impacts of future climate change on both natural environments (e.g., Thomas et al., 2004; Ryan et al., 2008) and human activities (e.g., Patz et al., 2005; Ruiz-Ramos and Minguez, 2010). These efforts are largely motivated by the fast improvement in the capability of numerical climate models, which allow not only for improving their spatial resolution but also including more physical processes (e.g., cloud formation, aerosol influences, radiation balance and atmospheric fronts). In this context, numerous European projects have designed experiments to dynamically downscale regional climate projections from GCMs to regional scale by means of

either dynamical or statistical approaches. Numerous modeling studies have been accomplished with a selection of the high-quality simulation data provided by some of these projects, such as PRUDENCE (Christensen et al., 2007), STARDEX (Haylock et al., 2006), ENSEMBLE (Hewitt and Griggs, 2004) and MISTRA-SWECIA (Kjellstrom, 2007). With these high-resolution climate simulations, it has been possible to quantitatively assess possible future impact of global warming, to perform model inter-comparison studies and to assess the possible impacts of anthropogenic climate change on natural environments and socio-economic activities.

1.3. Temperature Changes

Temperature is a climate variable of high importance from the view of various areas including, among others, hydrology, agriculture, ecology, ecosystem, health and energy. The estimation of temperature changes is critical to understanding land surface–atmosphere interactions. This is principally because it is a key variable in both the water and energy cycles in the globe. As indicated in Figure 1.4, among different feedbacks, surface air temperature determines the magnitude of fluxes of outgoing longwave, sensible, latent and ground (surface) heat. In addition, it controls, to some extent, the proportion of rainfall partitioned into runoff through evaporation process. Also, surface temperature can largely affect crop yields through changes in the length of the growing season. Similarly, the number of days that lie outside physiological tolerable limits may negatively affect the regional biodiversity (Root et al. 2003). Thus, assessing changes in surface air temperature can be of particular importance for different hydrological, environmental and societal applications.

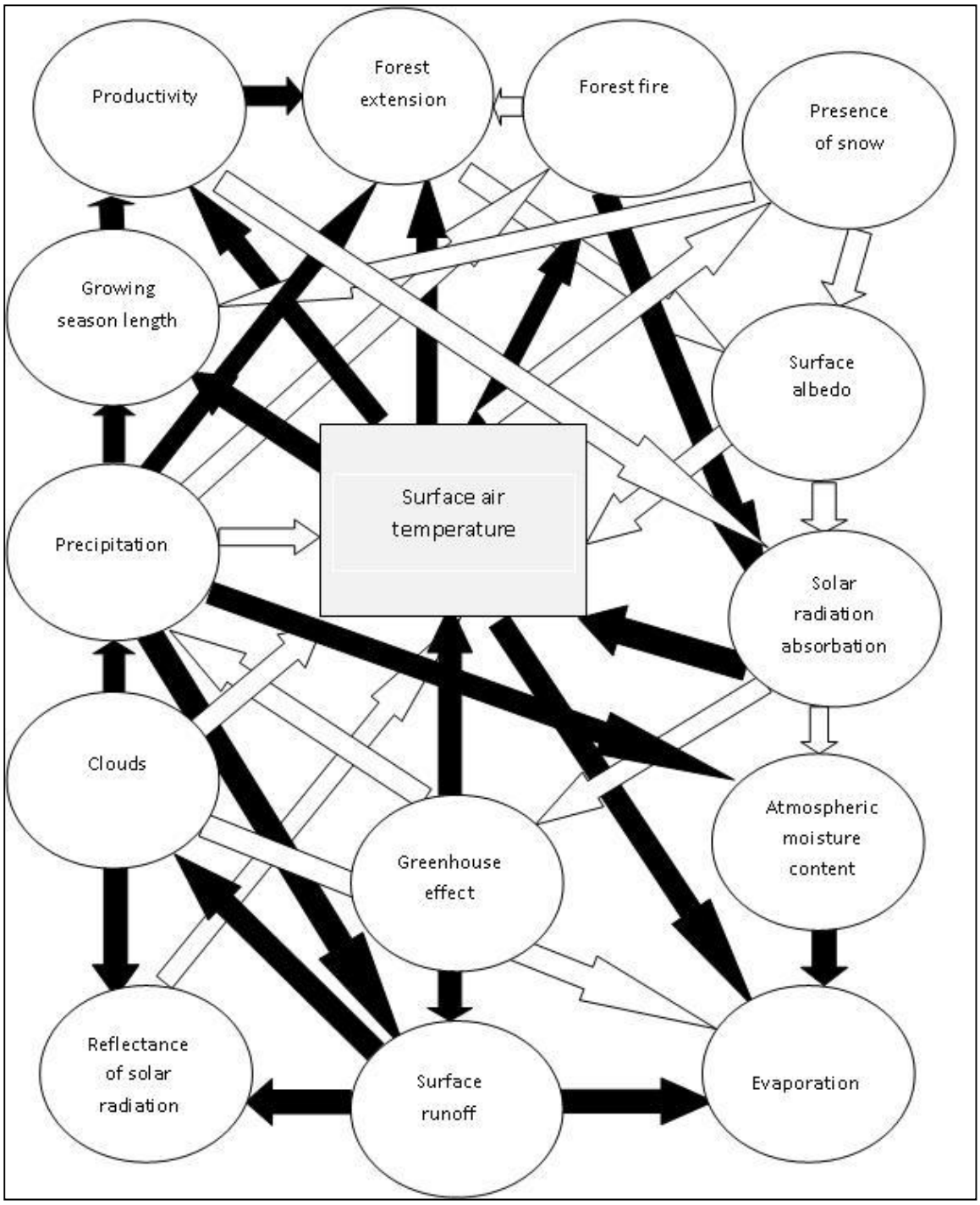

Figure 1.4: Surface air temperature as a key component in many hydrological, climatic, energy transfer and environmental interactions. Black (white) arrows indicate positive (negative) feedbacks.

Due to the adverse societal, economic and environmental potential impacts, there has been increasing interest in the analysis of temperature variability and trends over the last few decades (Diaz and Murnane, 2008; Solomon et al., 2007). The spatial and temporal variability of surface air temperature have increasingly been the focus of climatic research worldwide (e.g., Jones et al., 1999a; Folland et al., 2001). Global changes in the character of temperature have been observed in the past decades (Jones et al., 1999a; Jones and Moberg, 2003). For instance, Jones and Moberg (2003) reported that the global average earth surface temperature had increased by about 0.7°C in the 20th century. The most prominently observed changes were an increase in the mean during summer and winter periods, suggesting less seasonal variations.

At a more localized scale, there is a good deal of evidence on significant increases in average temperature over Europe in recent decades (Klein Tank et al., 2005). The average increase in the observed annual mean temperature across the continent was 0.8ºC. The strongest changes were observed in northwestern Russia and southern Europe, particularly the Iberian Peninsula (Beniston et al., 2007; Della-Marta et al. 2007a,b). In their study on Switzerland, Scherrer et al. (2004), for example, found the most significant changes in mean temperature during summer. Also, roughly half of the north Atlantic warming since the last ice age was noted in the last decade (NRC, 2002).

While the early detection of anthropogenic change in mean temperature is of growing concern, the impacts of climate change on society are more likely to be connected to extreme events. Typically, climate change detection is more often associated with the

analysis of changes in extreme events than with changes in the mean (Katz and Brown, 1992; Meehl and Tebaldi, 2004). Recently, there have been a number of extreme cold and heat events that have caused loss of lives and serious economic damages to private property and infrastructure. For this reason, much attention has recently been paid to learn more about the frequency and intensity of extreme temperature events, as being induced by climate change (e.g., Easterling et al., 2000; Jones et al., 2001; Frich et al., 2002; Klein Tank and Konnen, 2003; Kostopoulou and Jones, 2005; Moberg and Jones, 2005; Vincent et al., 2005; Alexander et al., 2006; Moberg et al., 2006; Brown et al., 2008). Some of impact studies gave much more concern to assess influences of extreme temperature events on different aspects of human life including: mortality, comfort, ecology, agriculture, and hydrology (Schindler, 1997; Ciais et al., 2005; Garcia-Herrera et al., 2005; Patz et al., 2005). Among them, the immediate impacts of extreme events on mortality (Karl and Knight, 1997, Garcia-Herrera et al., 2005), hospital admissions (Diaz et al., 2002), forestry (Miller and Urban 1999), ecology (Chust et al., 2011), agriculture (Adams et al., 1998), water resources (Vicente-Serrano et al., 2011a), tourism (Breiling and Charamza, 1999), energy demand (Smoyer-Tomic et al., 2003) and other socio-economic sectors (Hanemann et al., 2011) have been discussed. Overall, majority of studies have analyzed temperature extremes at different spatial scales ranging from the regional to the global. In general, most of the findings revealed significant upward (downward) trend in duration and frequency of warm (cold) extremes. Examples of these extreme events are found regularly in instances around the world (e.g., Haylock and Nicholls, 2000; Klein Tank and Konnen, 2003; Barriopedro, et al., 2011). The study by Alexander et al. (2006) gave the most current assessment of changes in observed daily temperature extremes from 1951 to 2003 at the global scale. They concluded that changes in

temperature extremes were mainly linked to daily minimum temperatures. More than 70% of the global land areas showed a significant rise (decrease) in the annual amount of warm nights (cold nights). At a narrower scale, Frich et al. (2002) similarly found positive trends in warm extremes in Europe, the USA, China, Canada and Australia.

With a more focus on the European continent, one can designate the August 2003 heat wave and the January 2012 cold wave as examples for extreme temperature events causing drastic impact and damage. According to Christopher and Gerd (2003), the unusual summer heat wave of 2003 had a significant influence on numerous European communities. For the Mediterranean region, a series of studies has also put a great deal of effort into exploring the behavior of temperature extremes (e.g., Maheras et al., 1999; Meehl and Tebaldi, 2004; Della-Marta et al., 2007a,b; Kuglitsch et al., 2010). According to Meehl and Tebaldi (2004), among the European regions, the Mediterranean is more vulnerable to intense, frequent and severe extreme heat events during the late of the 20th and the early 21st century.

1.4. Temperature Changes in the Iberian Peninsula: a general context

While assessment of temperature trends at a global scale is markedly important, it is also of great interest to explore temperature variability at local and regional scales, which could have wide-ranging impacts on human society and the natural environment (e.g., agriculture, hydrology, human health.... etc). Recently, numerous studies have investigated temperature behavior in the Iberian Peninsula. The spatial coverage of these works varies considerably from the whole peninsula or Spain (e.g., Oñate and Pou, 1996; Hulme and Sheard, 1999; Rodriguez-Puebla et al., 2001b; Brunet et al.,

2001, 2005, 2006, 2007a), sub-regions (e.g., Esteban Parra et al., 1995, 2003; Morales et al., 2005; Miro et al., 2006; Martinez et al., 2010) to a specific observatory (e.g., Serra et al., 2001). According to these works, the temperature increase in the Iberian Peninsula was even higher than the global average. Hulme and Sheard (1999) noted that the annual mean temperature increased by 1.6ºC during the last century. The strongest warming was detected since the mid of the 1970s. Nonetheless, this warming did not occur everywhere and in all seasons, but since 1972 it clearly dominated during winter and summer and over land areas. Notably, the warmest years during the 20th century occurred after 1990. Similarly, Brunet et al. (2007a) analyzed long-term variability of temperature in Spain employing a new daily adjusted dataset of the longest and quality records 22 Spanish daily time series covering the period 1850-2005. According to this study, the mean temperature increased at a rate of 0.10ºC decade^{-1} over the mainland Spain. Most of this increase attributed to the warming in maximum temperature, which raised at a rate twice the minimum temperature. Among the regional studies, Quereda et al. (2000) reported a strong trend in the annual mean temperature in the Spanish Mediterranean region during the period between 1870 and 1996 (0.71ºC decade^{-1}). This warming has also been noted by Pausas (2004) who examined temperature variability in the eastern Mediterranean Peninsula using a daily dense network of 350 observatories and Miro et al. (2006) who analyzed daily summer temperature in a Mediterranean area (Valencia) for the period 1958-2003.

Over the last few decades, many studies have also put a great deal of effort into exploring the behavior of temperature extremes in Iberia (e.g., Prieto et al., 2004; Brunet et al. 2007b; Bermejo and Ancell, 2009; Rodriguez-Puebla et al., 2010). Among these studies, Brunet et al. (2007b) assessed variability of temperature extremes in

Spain over the course of the 20th century. They reported evidence of larger changes in high temperature extremes than low temperature extremes. Based on daily data from 26 observatories coupled with a gridded dataset, Rodriguez-Puebla et al. (2010) recently investigated spatial and temporal changes in warm days and cold nights across the Iberian Peninsula during 1950-2006. At a more localized scale, Miro et al. (2006), for example, reported a significant increase in the frequency of warm and extreme temperature days in Valencia from 1958 to 2003. Lana and Burgueño (1996) examined spatial distribution of extreme minimum temperature in Catalonia (NE Spain) during the cold season (December-March). Also, Burgueño et al. (2002) analyzed daily temperature extremes at the Fabra station (Barcelona).

1.5. Knowledge gaps

Anthropogenic greenhouse gas emissions are a key driver of recent changes in temperature means and extremes. However, these effects will not be homogeneous across the globe. In other words, the regional temperature change may vary markedly from the global average temperature change, and therefore assessment of temperature change and variability should be undertaken at a regional scale to explore the extent to which regional temperature variability interacts with the global warming. This kind of detailed regional analysis of temperature variations is still demanded in the Iberian Peninsula given that it is bounded by the Atlantic Ocean and the Mediterranean Sea, which makes its climate largely influenced by the complex interactions of the Mediterranean and the Atlantic configurations. As a part of the western Mediterranean, the Iberian Peninsula has been proposed by many authors as “warm spot” region in terms of the global warming (e.g., Giorgi, 2006, Coppola and Giorgi, 2010). Indeed, a considerable portion of the peninsula is mountainous with clear topographical gradient,

which makes it more sensitive to climate change.. The complex land–sea interactions along with latitude, altitude and orography variations make the local and regional climate very variable. Topography and continentality may also produce more or less complicated patterns of temperature and therefore the impact of changes in temperature can largely depend on these local and regional conditions. For example, differences in topography can cause local variations in the angle at which the solar radiation gets to the ground surface. Also, the aspect and the slope may considerably affect the magnitude of surface heating and cooling. For instance, as a portion of the northern hemisphere, south-facing slopes of the peninsula often receive more nearly direct solar radiation relative to north-facing slopes. The impacts of these local patterns may vary from season to season. In addition, the natural environment in the peninsula is characterized by its unique flora, fauna and ecosystems which make it more vulnerable to even slight variations in temperature (Pasho et al., 2011a, b). In this context, mesoscale and regional-scale climate processes can play a key role in this diversity. Taken together, the magnitude and rate of observed, and even simulated, changes in temperature can depend on these local conditions.

In Iberia, the regional studies which have investigated temperature behavior almost exclusively give much more concern to the Mediterranean region as a consequence of availability of dense station network (e.g., Quereda et al., 2000; Pausas, 2004; Miro et al., 2006, Martinez et al., 2010), but generally there is less focus on mainland and the Cantabrian regions. Also, some of these studies were restricted to very smaller number of observatories, where reliable data were available (e.g., Lana and Burgueño, 1996; Burgueño et al., 2002) for the Fabra station (Barcelona).

From the temporal perspective, so far, there is no comprehensive view of the long-term variability of temperature at the regional and sub-regional scales in a way that can significantly contribute to more accurate and robust assessment of climate variability and change. Indeed, changes of temperature variability over the earlier decades of the 20th century have poorly been addressed. The only few exceptions (e.g., Brunet et al., 2007a) were generally based on a very limited number of observatories. In a similar way, while numerous studies were conducted to trace spatial and temporal patterns of precipitation in Iberia, as traditionally being the most important climate variable over the peninsula (e.g., Martin-Vide, 2004; Begueria-Portugues and Vicente Serrano, 2006; Costa and Soares; 2009a; López-Moreno et al., 2010), there are only very few assessments of trends in temperature means and extremes (e.g., Lana and Burgueño, 1996; Burgueño et al., 2002; Prieto et al., 2004; Brunet et al. 2007a,b; Bermejo and Ancell, 2009; Rodriguez-Puebla et al., 2010). In these regional studies, some regions (e.g., NE Spain) have received less concern.

In the same context, an increasing range of studies have projected changes in precipitation in the peninsula, allowing for assessing model-to-model differences (e.g., Sumner et al., 2003; Rodriguez-Puebla and Nieto, 2010; Sanchez et al., 2011; Vicente-Serrano et al., 2011b). On the other hand, a comprehensive assessment of temperature projections at the regional and sub-regional scales is still lacking and worth investigating. Some studies have already been made to assess future temperature rise over the Peninsular Spain (e.g., Taplador et al., 2009; Errasti et al., 2011; Brands et al., 2011a). Among them, Brands et al. (2011a), for example, employed 12 different GCMs to assess their ability to simulate the Probability Density Function (PDF) of daily temperature at various pressure levels over southwestern

Europe, including Iberia. Other studies also undertook assessment, but only for a particular region including: the Spanish Mediterranean (Vargas et al., 2008), the Pyrenees (López-Moreno et al., 2008b), NW the peninsula (Brands et al., 2011b; Gimeno et al., 2011) and the Basque Country (Gonzalez-Aparicio and Hidalgo, 2011). Nonetheless, the main challenges to these works are: (i) the lack of complete, reliable and spatially dense observational temperature datasets, which can be used for validation purposes and in turn ensuring the robustness of the future projections. For example, under the A1B emission scenario, Gonzalez-Aparicio and Hidalgo (2011) employed a very limited number of observatories to assess future changes in a suite of temperature-derived extreme indices over the Basque Country (northern Spain). (ii) Due to lack of dense network of observatories, most of the simulations employed GCMs to project changes in the future. GCMs are always inappropriate to describe climate at the regional scale compared with RCMs. This is particularly because regional climate is largely influenced by complex topographical variations, land-sea contrasts, and marked gradients of vegetation and land cover, which are difficult to capture by the coarse resolution of GCMs (on average 50 km). (iii) Previous work examining simulated changes in temperature has not explicitly indicated how they are related to the climatological probability distribution. The question still remains, at either national or regional scales, how far changes in the upper and lower tails of temperature distribution are driven by changes in the central tendency or whether they are actually related to shift in the entire distribution of temperature. In this regard, further assessment is needed motivating by the notion that the impacts of future changes on natural environments and human activities are more likely associated with changes in climate variability and extreme events than with changes in the mean conditions (Ciais et al., 2005; Barriopedro et al., 2011). At the local and regional

scales, changes in the upper and lowermost temperature records are particularly important for different reasons. First, extreme events are exceptional from the statistical point of view given that they are located at the upper and lower tails of temperature distributions, which could give a good indication on the possible impact of global warming on temperature change and variability in terms of both changes in the mean and standard deviation. Second, the sensitivity of both natural systems and human welfare to changes in temperature are maximized when changes in the mean corresponds to changes of similar sign and magnitude in extreme events. Expectedly, the impacts of future temperature changes on mortality, human health and even biological adaptation mechanisms, among others, will largely be more severe under frequent and intense extreme temperature records. Therefore, an assessment and attribution of the dependency between changes in the mean and extreme events can be valuable for different climate impact and assessment studies. For this reason, there is an essential need to explore not only future changes of the mean climate state but also changes of the warm/cold tail of temperature distribution at the regional scale.

To conclude, it can be seen that despite the well-studied precipitation changes and distributions in many areas across the Iberian Peninsula, there are gaps in current knowledge with respect to temperature response to climate change, particularly at the regional scale. Unfortunately, owing to low density of observatories or data quality limitations, spatial and temporal variability of temperature are still poorly understood at the regional and sub-regional scales. Numerous datasets still include gaps that are distributed randomly in space and time as a consequence of various institutional and financial constraints. Other datasets suffer from lack of data quality assurance, as a

consequence of relocation of the meteorological observatories, which degrades the utility of daily climate datasets in much of the peninsula.

Due to lack of spatially dense and temporarily complete, homogenous and reliable time series, most studies focusing on temperature response to climate change in Iberia have focused on the whole peninsula or employed low density of observatories (e.g., Morales et al., 2005; Brunet et al., 2006, 2007a). Details and sources about different available climate datasets in the peninsular Spain are listed in Table 1.1. One representative example is Brunet et al. (2006) who developed a new daily adjusted dataset of 22 time series of maximum and minimum temperatures in the whole Spain. Although this dataset covers a long period (1850-2003), the coverage is still inadequate for several spatial studies. For this reason, there is still a necessity for the improvement of daily datasets for monitoring, detecting and attributing changes in temperature. Recently, developing complete and homogenous climatic datasets has been of considerable interest in Iberia. Nonetheless, most of the recent works have mainly been devoted to precipitation (e.g., Romero et al., 1998; Eischeid et al., 2000; Brunetti et al., 2006; Vicente-Serrano et al., 2010) and to a less extent to temperature (Eischeid et al., 2000; Brunet et al., 2006).

Developing a new compiled dataset with high spatial and temporal resolution can improve the understanding of temperature variability and changes at the regional scale. Daily complete, long and homogenous datasets can provide a more detailed analysis of temperature changes and variability at the regional scale. Moreover, the complex orography of the Iberian Peninsula requires high density of observatories to capture temperature variability. In their study on the Mediterranean region, Gao et al.

(2006) found that the spatial variability of temperature in Iberia has a clear fine scale structure, mainly induced by the complex topography. This dataset can therefore help determining how regional temperature responds to the global change. More specifically, assessment of possible changes of temperature at a regional scale encompasses a large spatial and temporal variation, which may indicate how local and regional climate systems will react to the global changing climate.

Also, acknowledging the possible consequences of climate change processes on different natural and socioeconomic systems (e.g., hydrology, forestry, crop production, energy demand…etc), it is still important to assess the magnitude and spatial extent of temperature changes at a more detailed spatial scale. While climate change is a global phenomenon, issues in addressing this problem will vary markedly from one region to another worldwide.

In this motivate, developing reliable and homogenous compiled temperature dataset can also be very useful for a wide variety of applications, including, for example, characterization of extreme events (e.g., warm and cold spells), climate risk assessment (e.g., frost), hydrological and environmental modeling, and verification of numerical model simulations to assessing possible future impacts of climate change. Understanding climatic changes at this high spatial and temporal resolution can contribute to consistent prediction of future behavior of temperature. Therefore, the potential impacts of climate change largely depend on regional context. This strongly implies that any development plans must have a regional character and requires an assessment at a more regional scale. The regional assessment of observed and projected temperature variations can therefore provide considerable responses to vital

questions which may arise by local policy makers attempting to adopt and mitigate the global change. Such kind of assessment can also be valuable to improve adaptation and mitigation polices at more local scale.

Table 1.1: List of sources and description of selected datasets covering northeastern Spain

Reference	Variables	Temporal resolution	Region	Type	Time period
The Global Historical Climatology Network version2 (GHCN)(Vose et al., 1992)	Precipitation, temperature, sea-level pressure and air pressure	monthly	Globe	-land based	morf 1950 ot raen tneserp
The Global daily Climatology Network version 1, US National Climate Data Centre, NCDC, (Gleason, 2002)	Precipitation and temperature	daily	Globe	-land based	-2001 1840
Herrera et al., 2012	Precipitation	daily	Spain (0.2º resolution)	Gridded dataset	1950-2003
Haylock et al., 2008	Precipitation and temperature	daily	Europe (different resolutions)	Gridded dataset	1950-2006
ECA&D (Klein Tank et al. 2002 and Klok and Tank, 2009)	Precipitation and temperature	daily	Europe	Land-based	1900-2006
ELPIS (Semenov et al. 2010)	Precipitation. Temperature and solar radiation	daily	Europe (25km)	Gridded dataset	1982-2008
E-OBS (Hofstra et al., 2009)	Precipitation and temperature	daily	Europe (0.25º resolution)	Gridded dataset	1950-2006
EMULATE (Moberg et al., 2006)	Precipitation and temperature	daily	Europe	Land-based	morf 1850 ot raen tneserp
SDATS (Brunet et al., 2006)	temperature	daily	Spain	Land-based	1850-2003
NESATv2 (north-eastern Spain Adjusted Temperature) (http://wwwa.urv.cat/centres/Departaments/geografia/clima/archive.htm)	temperature	monthly	Catalonia	Gridded dataset	1869-1998

1.6. Study area: geographical perspectives and climate characteristics

In this section, an overall image of the main geographical characteristics of the northeast Spain and its climates is provided in the following paragraphs.

1.6.1. Location and geographical setting

The study area occupies the northeastern region of the Iberian Peninsula. It extends over 18 administrative provinces, namely Alava, Barcelona, Burgos, Cantabria, Castellón, Girona, Guadalajara, Guipuzcoa, Huesca, La Rioja, Lleida, Navarra, Palencia, Soria, Tarragona, Teruel, Vizcaya and Zaragoza (Figure 1.5). It covers an area of about 159,424 km^2, which covers approximately 1/4 of the whole area of the Iberian Peninsula. As illustrated in Figure 1.5, the domain roughly lies in a spatial window between the latitudes of 39° 43' N and 43° 29' N, and the longitudes of 05° 01' W and 03° 17' E. This geographical position makes the region unique from the climatic perspective as; first, it includes the most southern arid and semiarid region in the European continent. Second, with the latitudinal location, the dynamics of the mid latitude circulation and the subtropics are thoroughly linked and compete against each other. This region also encompasses a variety of geological and geographical settings that are expressed in a diversity of fluvial regimes and biological diversity.

1.6.2. Topography

As depicted in Figure 1.6 (upper panel), the study area is heterogeneous in terms of terrain complexity, with elevation up to 3000 m a.s.l. (the Pyrenees). In particular, the elevation across the domain varies from 0 to 3404 m, with a mean elevation of 775.4 m above mean sea level (m.s.l). However, the elevation varies greatly over short distances, suggesting high spatial gradient of elevation. The Ebro depression is the

main physiographic unit as it represents approximately 53.7% of the whole domain. It extends inland along a northwest-southeast axis. This depression is a semi-enclosed basin, surrounded by mountain belts including the Pyrenees (north), the Cantabrian belt (northwest), the Catalan chain (east) and the Iberian system (south and southwest) (Figure 1.6, lower panel).

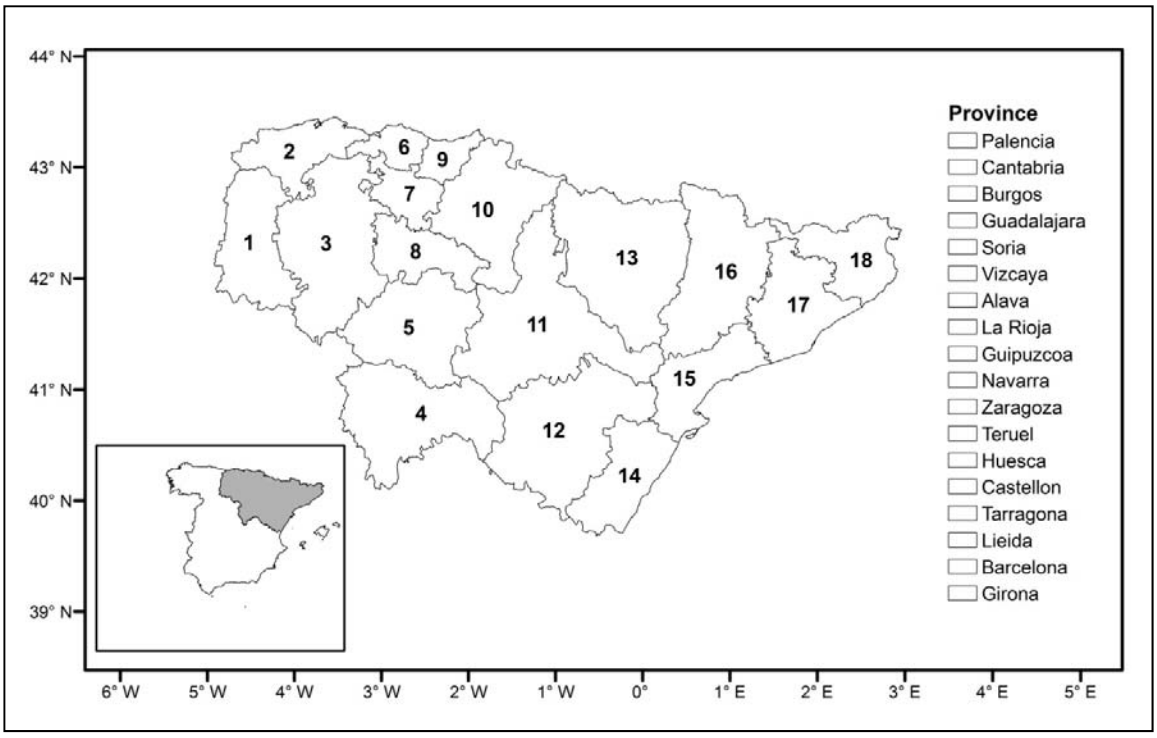

Figure 1.5: Location of the study domain and its administrative provinces.

1.6.3. Hydrology

Hydrologically, the largest Mediterranean river of the Iberian Peninsula and the study area is the Ebro, with a basin of nearly 85,000 km^2 and a channel length of 930 km (Figure 1.7). The Ebro River originates from the southern facing slopes of the Cantabrian Range and the western Pyrenees before connecting to the Mediterranean Sea through a smaller opening in the Ebro Delta at Tortosa (180 km south of

Barcelona) (Bejarano et al., 2010). The Pyrenees contributes nearly 70% of the total water runoff (López-Moreno et al., 2006). Major tributaries include Gallego, Aragon, Cinca, Segre, Jalon, Huerva, Zadorra and Ginel. In its middle reach, the river has a floodplain of an extent of 739 km^2, representing the most extensive one in the peninsula (Ollero, 2010).

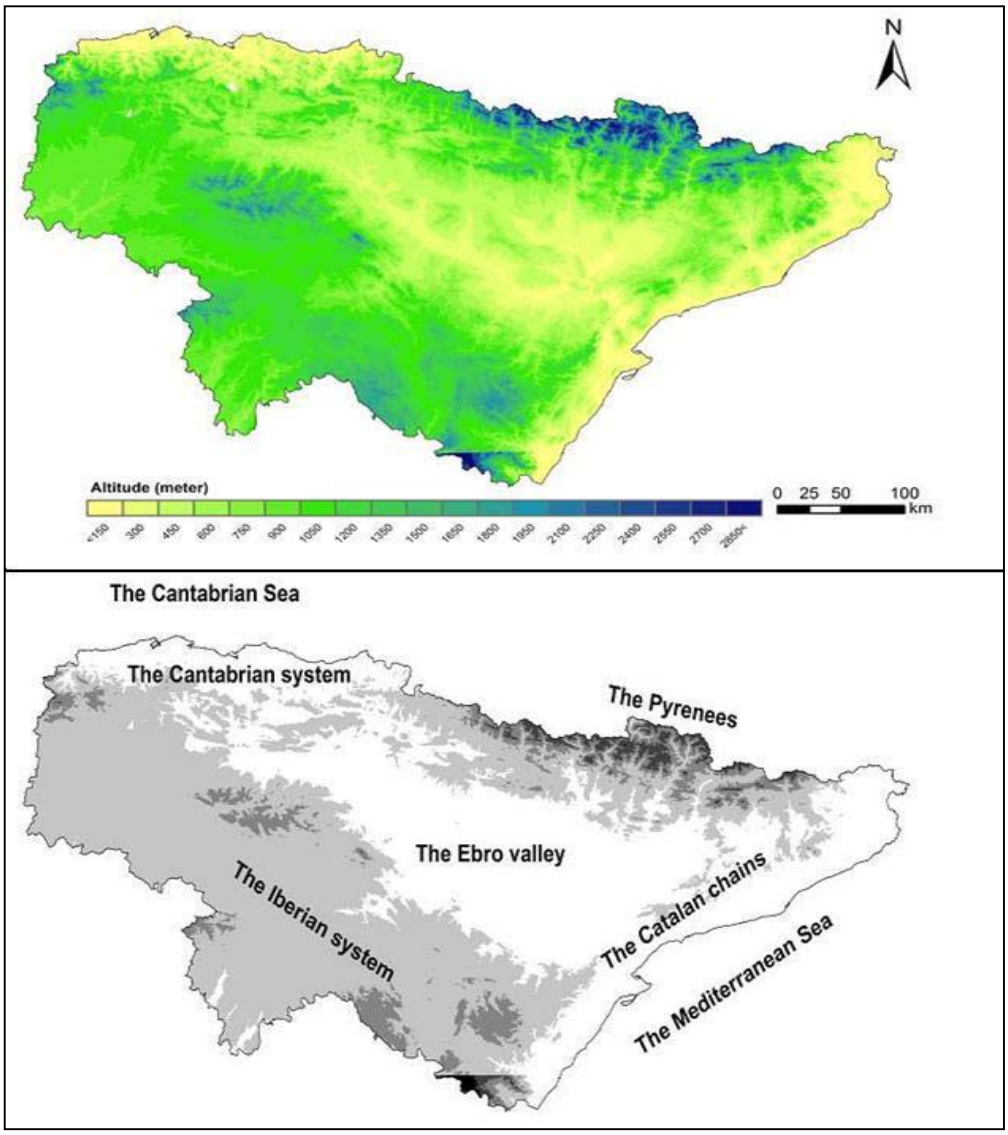

Figure 1.6: (Upper) Topography of the study domain and, (lower) its main physiographical units.

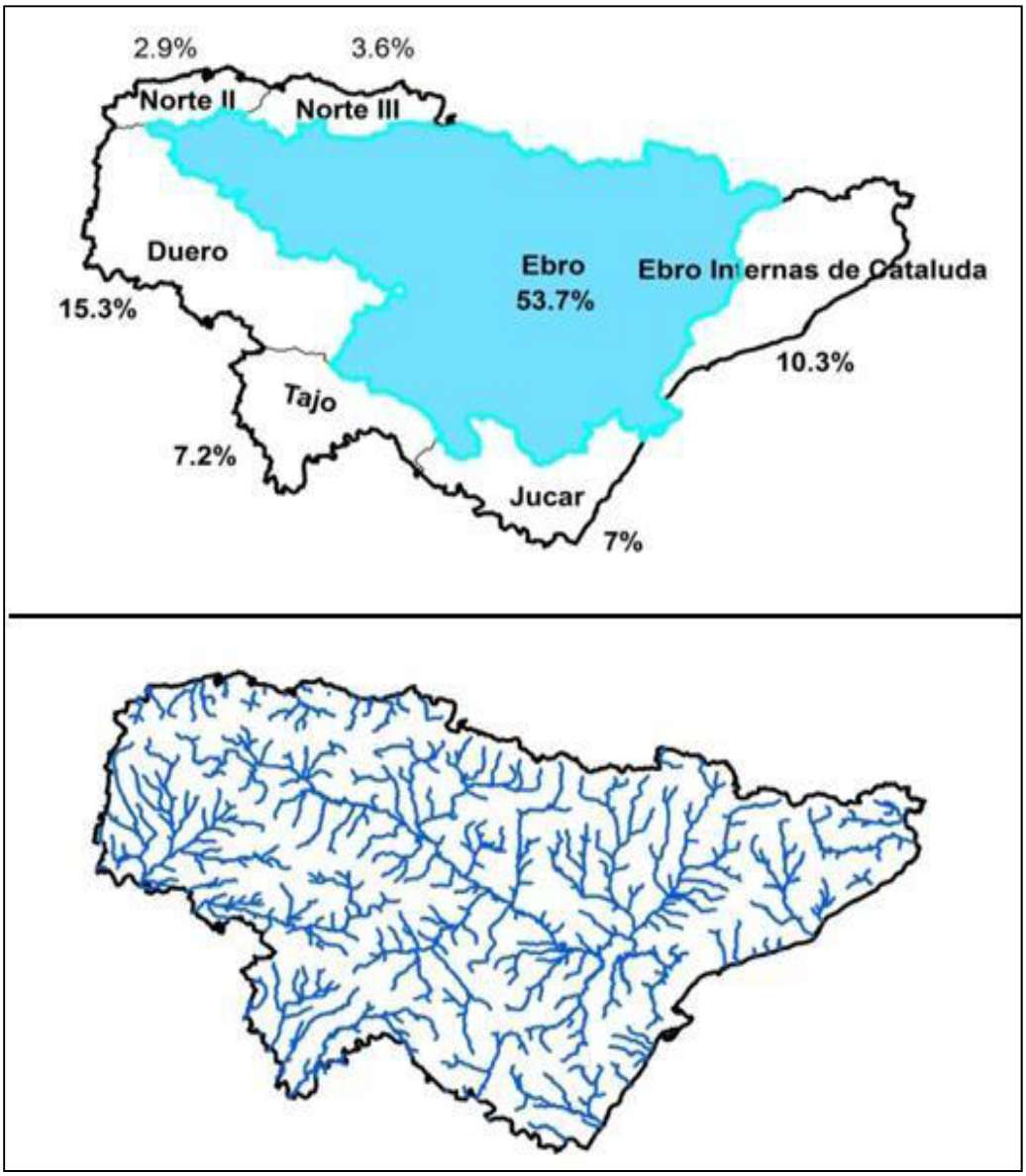

Figure 1.7: (Upper) the main hydrological divisions and, (lower) drainage network in the study domain. The percentages indicate the area represented by each basin.

From the hydrological perspective, the flow peak of the Ebro occurs during February, while low water levels occur during summer (particularly in June). This is mainly because the rainfall originating over the Atlantic affects the headwaters of the Ebro during winter and early spring. Historically, the Ebro has constituted a major component of the Spanish water policy. The Confederación Hidrográfica del Ebro

(CHE) (http:// www.chebro.es), found in 1926, is the oldest basin agencies in the world. Recently, there has been intense exploitation of water resources for sectors of agriculture irrigation, electricity production, cattle breeding, domestic consumption and industrial activities. According to Bouza-Deaño et al. (2008), the water of the Ebro is usually used for agriculture and cattle breeding (89.3%), domestic supply (7.2%) and industrial activities (3.5%).

1.6.4. Climate

While the study domain has a relatively small geographical space, it encompasses large variations of climates, including oceanic, Mediterranean, continental and mountainous. According to the Koeppen classification (1936), much of the study domain is defined as a semiarid Mediterranean climate (BWh); a classification that has also been confirmed by Thornthwaite (1948) (see Peel et al., 2007). In the study domain, there are clear climate contrasts between the continental portions and the closing coasts. Also, there is a strong gradient from central flatland areas to adjacent mountainous belts. More specifically, the climate is highly varied, from semi-arid conditions in central portions (i.e., the Ebro valley), moderate conditions along the Mediterranean and the Cantabrian regions to mountainous climate. This diversity in climate comes mostly from weather systems interactions with a complex terrain that includes from sea-land interfaces to mountainous ranges. The interaction of the atmospheric circulation, the latitude, the altitude, the terrain topography, vegetation cover, the land-sea interactions and the atmospheric circulation are the main factors contributing to climate variations in the region (Rodriguez-Puebla et al., 1998; López-Bustins et al., 2008; Vicente-Serrano et al., 2009). From a global perspective, this region encompasses a climatic gradient between mid-latitude and subtropical regimes.

Also, it is situated in a transitional zone where the Mediterranean configurations and the Atlantic influences at the mid-latitudes are the main driving forces of the regional climate. These closing seas are the most important source of moisture for surrounding land areas. The climate is therefore influenced by the large-scale configurations, originating from the north Atlantic and the Mediterranean. The various modes of the large-scale atmospheric circulation include, among others, the north Atlantic subtropical High and Sea Surface Temperature (SST). Generally, winters are characterized by cyclonic disturbances and negative pressure anomaly whereas subtropical high pressure system is prevalent during summers.

Figure 1.8 indicates the annual cycle of mean temperature in the region. As indicated, January is the coldest month with an average surface air temperature of 5.2ºC, meanwhile July is the warmest month with an average of 21.4ºC. The mean annual temperature fluctuations are about 16.2ºC in the whole region. The annual temperatures range from about 17.9ºC in the lowest sites in the Ebro valley to 5ºC in the mountain areas. However, due to the complex topography of the region, the annual diurnal range, defined as the difference between the highest maximum temperature and the lowest minimum temperature in the year, is apparently high suggesting more continental influences in the region. For example, the mean maximum temperature during summer may reach 45ºC in the Ebro valley; meanwhile winter mean minimum temperatures may fall below -15ºC in very elevated sites in the Iberian system and the Pyrenees. This also suggests great interannual contrasts. This contrast is also evident over space, as revealed in Figure 1.9, in which interannual variations of mean temperature at three different observatories with varied elevation are plotted. It can be noted that temperature variations are elevation dependent. The highest temperatures

often occur in the flattened areas in the Ebro valley (e.g., Zaragoza airport, Zaragoza) and in areas close to the Mediterranean Sea (e.g., Sort Piraguisme, Lleida). On the other hand, mountainous areas (e.g., Pantano de Compuerto, Palencia) and areas close to the Cantabrian Sea are relatively cooler. However, it is noteworthy indicating that this temperature-elevation dependency may vary from one season to another as a consequence of influences of other local variables such as the slope, aspect, land cover, vegetation canopy, and maritime influences.

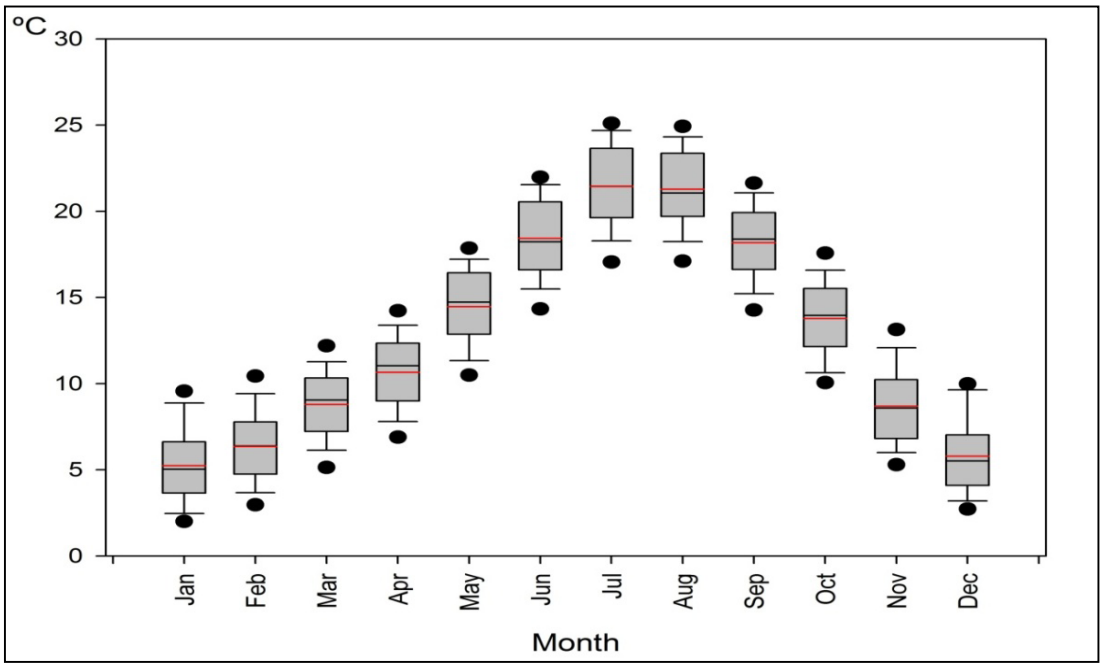

Figure 1.8: The annual cycle of mean temperature climatology in the study domain, calculated as the long-term average for the period 1960-2006. The median, 10th, 25th, 75th and 90th percentiles are shown as vertical boxes. The red line represents the mean while the dots indicate the 5th and 95th percentiles.

The study region also includes diverse pluviometric regions, varying from arid, semi-arid to humid. According to Martin-Vide and Olcina (2001), the precipitation isoline between 600 and 800 mm/year distinguishes between the humid and arid areas,

meanwhile isoline between 300 and 350 mm/year differentiates the arid from the semi-arid regions. The humid area (above 1000 mm/year) is mainly located to the north close to the Cantabrian Sea and over the mountain ranges (e.g., the Iberian, Cantabrian and Catalan systems and the Pyrenees). Dry conditions occur in central portions, particularly over the Ebro valley and along the Mediterranean littoral area to the east.

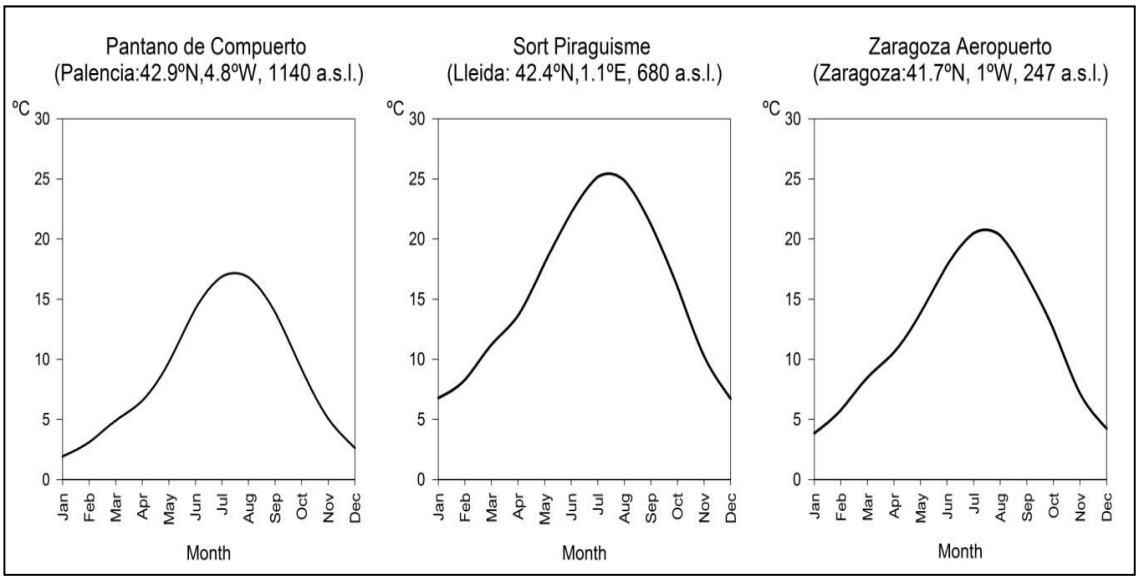

Figure 1.9: Interannual variability of mean temperature climatology at three different observatories in the study domain, calculated as the long-term average for the base period 1960-2006. The altitude is given in meters.

As illustrated in Figure 1.10, precipitation is mainly concentrated in spring and autumn. The dry conditions typically prevail in the period from June to September, The average of total precipitation varies from 25.6mm (July) to 64.1mm (October). There are also large spatial variations, with a remarkable gradient from south to north and from east to west (De-Castro et al., 2005; Gonzalez-Hidalgo et al., 2010). These spatial contrasts are presented in Figure 1.11, which compares the interannual variations of

total precipitation at three different localities in the region. As illustrated, the precipitation peak is located in October, with values ranging from 22.4 mm at Artieda (Navarra) to 71.2 mm at Segorbe (Castellon). On the other hand, total precipitation in the drier month varied from 7.9 mm in August at Artieda (Navarra) to 24.2 mm in July at Huesca Monflorite (Huesca). Most annual precipitation falls as snow in mountainous regions (e.g., the Pyrenees). A more detailed summary of the climate of the study area can be found in Capel-Molina (1981) and Font-Tullot (1983).

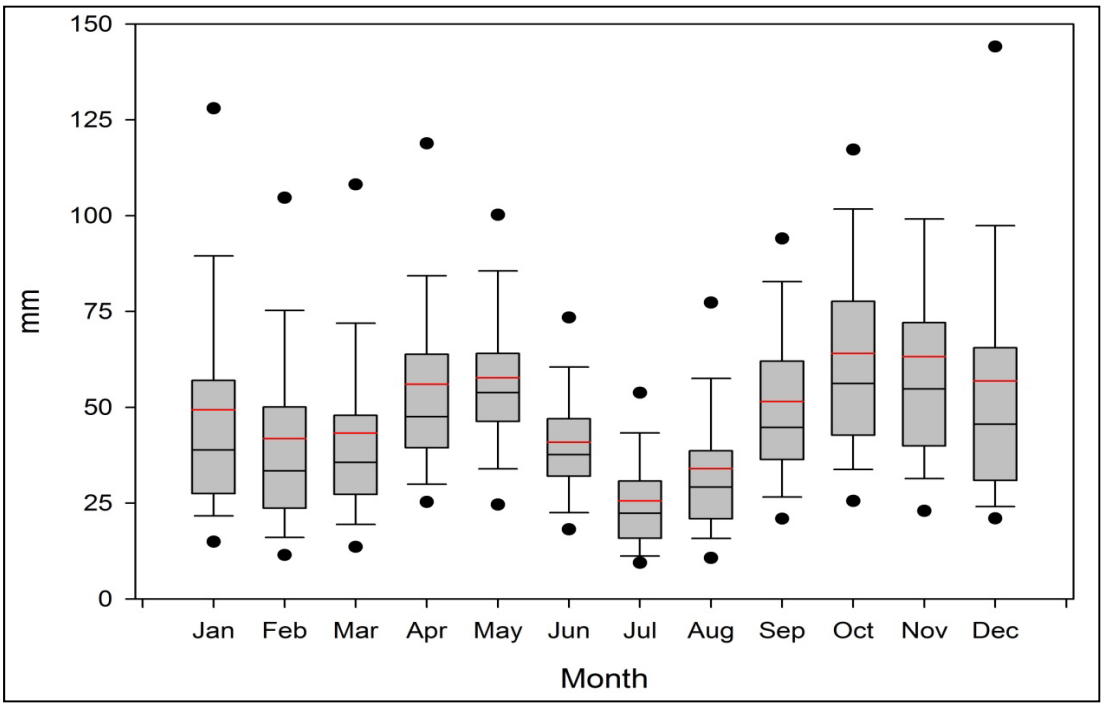

Figure 1.10: The annual cycle of total precipitation climatology in the study domain, calculated as long-term average for the period 1960-2006. The median, 10th, 25th, 75th and 90th percentiles are shown as vertical boxes. The red line represents the mean while the dots indicate the 5th and 95th percentiles.

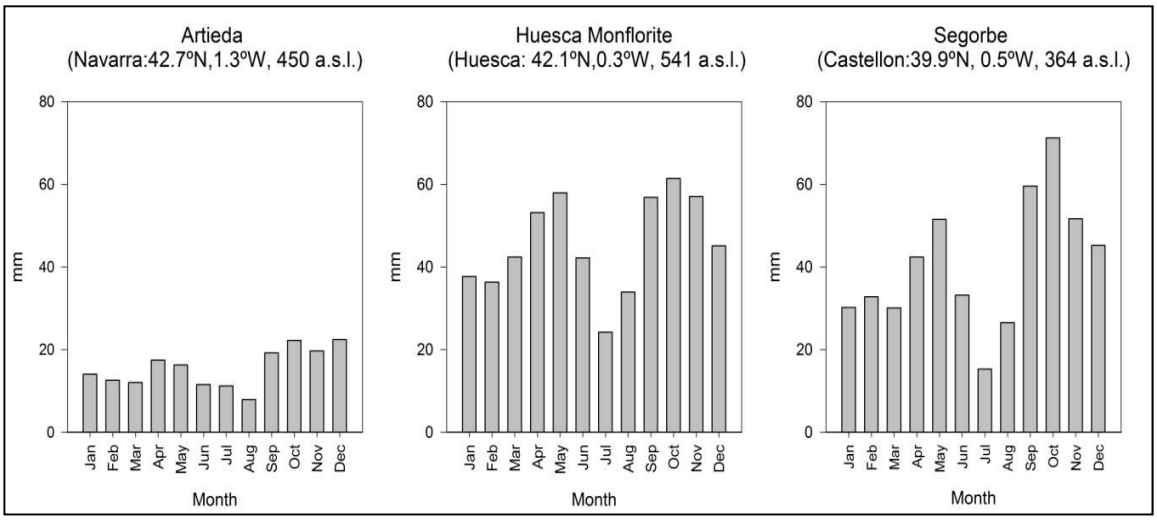

Figure 1.11: Interannual variability of precipitation climatology in three different there observatories in the study domain, calculated for the base period 1960-2006. The altitude is given in meters.

1.7. Aims of the thesis

The main focus of this thesis is to improve the understanding of the regional variability of temperature in northeast Spain using daily temperature dataset. The research line examines the observed space-time variability of temperature means and extremes from 1960 to 2006.

The primary objectives of this study were:

- To develop a complete, reliable and homogenous daily temperature dataset for northeastern Spain, with the aim of improving the spatial and temporal coverage of temperature time series in the study domain. This new compiled dataset was developed using a very dense network of 1583 daily raw time series distributing across the region. Herein, this research also aspires to assess the methodology used to quality control, reconstruct and adjust breaks

(inhomogeneities) in the series on trends, spatial and temporal coherence, and statistical properties of the final series. In order to draw a comparison between the series before and after adjustments, a suite of different statistical methods (e.g., semivariance models, L-moment statistics, and Pearson order moment correlation) was used to accomplish this task. There are emphasizing needs to develop temperature dataset with high spatial and temporal resolution for the study area.

- To examine spatial and temporal variability of surface air maximum, minimum and mean temperatures and daily temperature range (DTR) at both seasonal and annual timescales during the period from 1960 to 2006. This aim extends further to analyze the possible physical causes behind the observed regional variability. The purpose was to quantify possible large-scale atmospheric configurations that control the observed local trends.

- To analyze extreme heat events based on (i) defining extreme events by means of both arbitrary and percentile-based thresholds, (ii) calculating their linear trends, and (iii) tracing spatial variability of the observed trends. To meet this goal, trends in daily maximum and minimum temperatures were assessed using 21 extreme temperature indices.

- To divide the study domain into regions as homogenous as possible based on the information derived from a set of extreme temperature indices using the Principal Component Analysis (PCA) and Cluster Analysis (CA), and to assess the connections between spatial and temporal variability of temperature

extremes in the defined sub-regions on the one hand and the main modes of atmospheric circulation over Western Europe and the Mediterranean region on the other hand.

- To examine the spatial and temporal variability of the anomalous severe heat events over the study domain. This incorporates very warm days (VWD) and very cold nights (VCN). The anomalous extreme days were first defined using the uppermost (99th: VWD) and lowermost (1st: VCN) percentiles of daily maximum and minimum temperature distributions, respectively. Then, the main spatial modes corresponding to these very extreme events were identified. Further aim involves the analysis of large-scale atmospheric circulation patterns at different geopotential levels (200hPa and 500hPa) as well as at the Mean Sea Level (MSL) to identify synoptic conditions favoring for the occurrence of these extreme days and explain their spatial structure.

- To evaluate the capability of different RCMs to represent regional temperature variability as simulated from the Special Report on Emissions Scenarios (SRES) A1B moderate greenhouse gasses emission scenario for the 21st century. This study investigated 9 regional climate simulations from the EU-ENSEMBLES project and examined projected climate change signals for the near future (2021-2050) and far future (2071-2100), with respect to present-day climatic conditions (1971-2000). Through this aim, this thesis endeavored to (i) assess potential uncertainties of future projections through a detailed comparison of the individual model-projections, (ii) to quantify the projected climate change signal of mean maximum and minimum temperature on a seasonal basis, (iii) to simulate the regional

climatology of the anomalous severe extreme events in the region, (iii) to evaluate projected changes in a set of time-varying percentiles (e.g., the 10th, 25th, 75th and 90th) representing the cold and warm tails of temperature distributions under the future warming conditions, (iv) to determine whether changes in extreme events may already be consistent with simulated changes in the central tendency and in turn how the distribution of daily maximum and minimum temperature will change seasonally in the future,

1.8. Outline of the thesis

This thesis is structured as follows: chapter 1 is intended to give a brief overview on the scientific background of the research topic and its arising questions. In addition to a literature review that summarizes the current state of knowledge, a short geographical and climatological description of the study domain supplements this introduction. Chapter 2 outlines the full protocol applied to develop a spatially and temporarily high-resolution dataset of temperature for northeast Spain. The daily dataset development is complemented with statistical analyses focusing on the robustness of the final dataset. A comparison between the dataset before and after homogeneity adjustment is also provided. Chapter 3 provides a detailed description of the methodological framework employed to trace the observed and projected changes in surface air temperature during the 20th and 21st century. The chapter on methods also includes theoretical explanations on some of the techniques and statistical tests used in this work. This will include basic equations, numerical methods, and physical parameterizations used. Chapter 4, “Results”, is devoted to present the primary research results, organized around the research questions. In chapter 5, “Discussion”, an insight of the results is given, providing a comparison with similar studies and

findings. In chapter 6 a summary and the main concluding remarks are presented. Chapter 7 gives an outlook on possible future developments of the present work. Finally, the appendix section includes the supplementary material to this thesis. This Ph.D. study has resulted in six manuscripts, whose full citations are included in appendix B.

1.8. Significance of the study

The novelty of this work is that, as opposed to most previous studies, it depends on a new developed dataset which represents the most complete register and the densest network of temperature observatories in the study area. Therefore, this work is critical to understanding the variability of temperatures changes in the region and can therefore contribute to better understanding of the impact of climate change in this climatically complex region. This study also gives much more concern to changes in the both the moderate and most severe extreme events in the region. While this study, similar to previous works, has been confined to use a threshold value of 10 (90) percentiles of daily minimum (maximum) temperature distribution to define an extreme event, the uppermost (99th) and lowermost (1st) intervals of daily data distributions were also considered in temperature extreme events analyses. Understanding the spatial and temporal variability of these unusual events and the driving forces behind their variability has received less concern in climate research and thus remain poorly understood. In the framework of this thesis not only the present changes in temperature are of importance, but there is also a focus on the future behavior. In this regard, the inclusion of simulations from different RCMs to assess future climate projections of seasonal temperature and their spatial variations raises the potential of

certainty about the final conclusions that are to be drawn in this work. The findings could thus improve our understanding and prediction of the long-term trends of temperature simulations, which could be of particular importance for different disciplines in the region such as hydrology, water resources management and ecology. Overall, understanding changes in temperature patterns and the dynamics behind them is a key to assessing the possible changes in the future and thus can provide high quality advice to societies for mitigation. The gained results can be placed in a larger climate context, providing insights into the long-term behavior of temperature and its driving forces in the Iberian Peninsula, the Mediterranean region and southwestern Europe.

CHAPTER

TWO

DATASET DEVELOPMENT AND DESCRIPTION

2. DATASET DEVELOPMENT AND DESCRIPTION

2.1. Introduction

In recent years, there is ongoing global increase about climate change and its natural and socioeconomic consequences (e.g., water resources, hydrology, forestry, agriculture, energy...etc). Assessing these impacts requires climate datasets of high spatial and temporal resolution. Beside data availability, the quality and homogeneity of climate series are prerequisites for detailed and trustworthy climate studies. Complete, reliable and spatially dense climatic datasets are mandatory for different types of climatic analyses (Eischeid et al., 2000). For example, an appropriate analysis of climate variability and trends necessitates climatic datasets of fine spatial and temporal resolution. If the inhomogeneities are not accounted for properly, the results of climate analyses based on the non-adjusted data can be erroneous and misleading (Peterson et al., 1998).

The study domain is characterized by its complex topography, moderately high latitude, and transitional location between the Atlantic and the Mediterranean configurations. In addition, this domain encompasses diverse climate regimes, varying from semi-arid to humid, continental to maritime and lowlands to mountainous. Therefore, assessing temperature changes in a region of these high geographical and climatic contrasts necessitates a dataset of high spatial and temporal resolution. Unfortunately, the insufficient number of temperature observatories and its uneven spatial distribution has been the main features of recent studies focusing on air temperature change and variability in the region. In addition, most long-term time series covering the region are generally affected by some inhomogeneities caused by changes in instruments, observers, site displacements, observing practices, and the

surrounding environment (e.g., urbanization, land use and vegetation canopy). These inhomogeneities in temperature data do not make possible to consider temporal variations as induced only by climate processes.

In this chapter, a detailed description of the different techniques conducted to reconstruct, quality control and test homogeneity of the available time series is provided. In general, the rationale behind this multistep procedure was to improve quality, temporal extension and spatial coverage of temperature time series in the study region. This chapter is structured in four main parts. A description of the original dataset is given in section 2.2. The methodology employed to check data quality, infill gaps, and test homogeneity of daily temperature time series are outlined in sections from 2.3 to 2.7. An assessment of the possible impact of data adjustment (correction) on spatial and temporal characteristics of the final temperature time series is included in section 2.8. Finally, a description of the final adjusted dataset is presented in section 2.9.

2.2. Raw dataset description

This study employed a database of 1583 daily maximum and minimum temperature time series spanning some period between 1900 and 2006. This dataset was provided by the Spanish Meteorological Agency (*Agencia Estatal de Meteorologia, AMET*). The spatial distribution of temperature observatories is illustrated in Figure 2.1. A quick inspection of the network of stations clearly reveals that the spatial density of stations is inhomogeneous across the administrative 18 provinces. As depicted in Figure 2.2, the most data-rich provinces are Barcelona, Guipuzcoa and Cantabria with a density of 1 station for each 481.9, 493.6 and 515.5 km^2, respectively. In contrast, the coarser

coverage is found in Soria, Guadalajara and Burgos, with a density of 1 station for an extent of 3430.4, 2711.8 and 2458.9 km^2, respectively. The average of inter-station distance in the whole dataset is nearly 23.7 km.

In terms of topography, majority of observatories are located in lowlands and moderately elevated areas. Figure 2.3 informs that 34, 52.7, 73.6 and 86 % of observatories are situated in sites below than 300, 500, 800 and 1000 m, respectively. Areas above 1500 m are only represented by 2.6% of the network observatories.

Temporarily, the stations density markedly differs with a sharp increase from 1970 onwards (Figure 2.4). About 21.3 % of stations extend back to 1950 or earlier, while 98.7 % of the observatories have their most recent records until 2002.

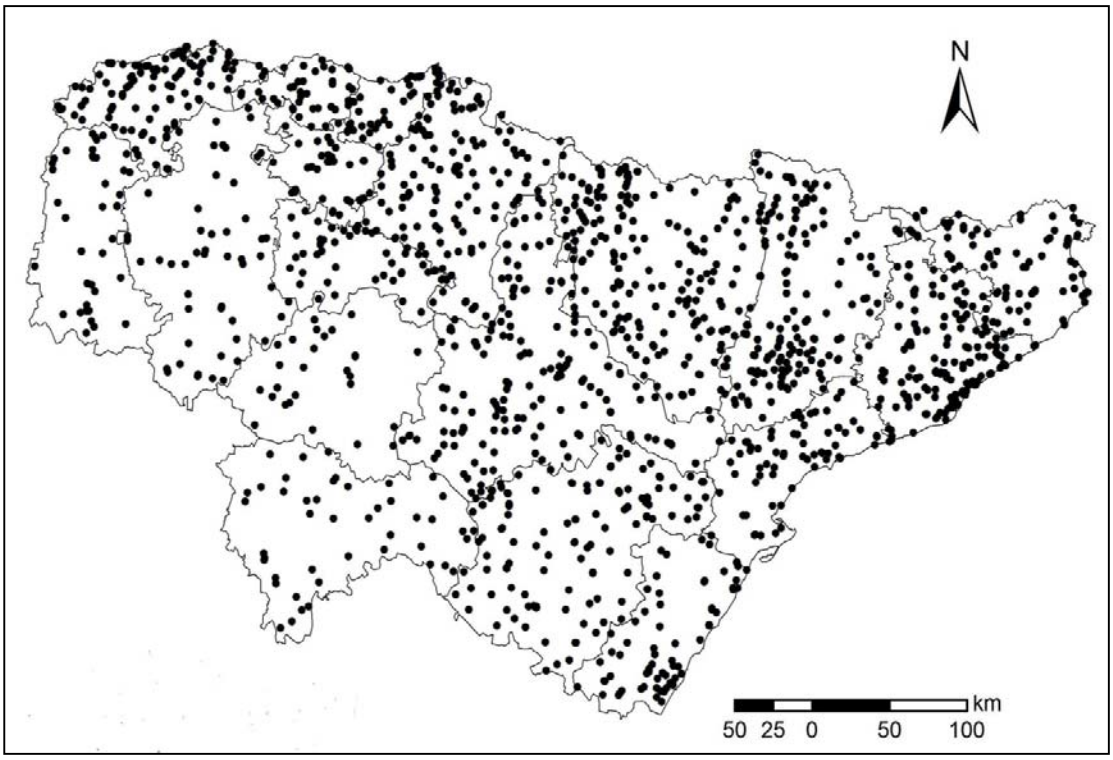

Figure 2.1: Location of the study area and spatial distribution of temperature observatories in the original dataset (*N*=1583).

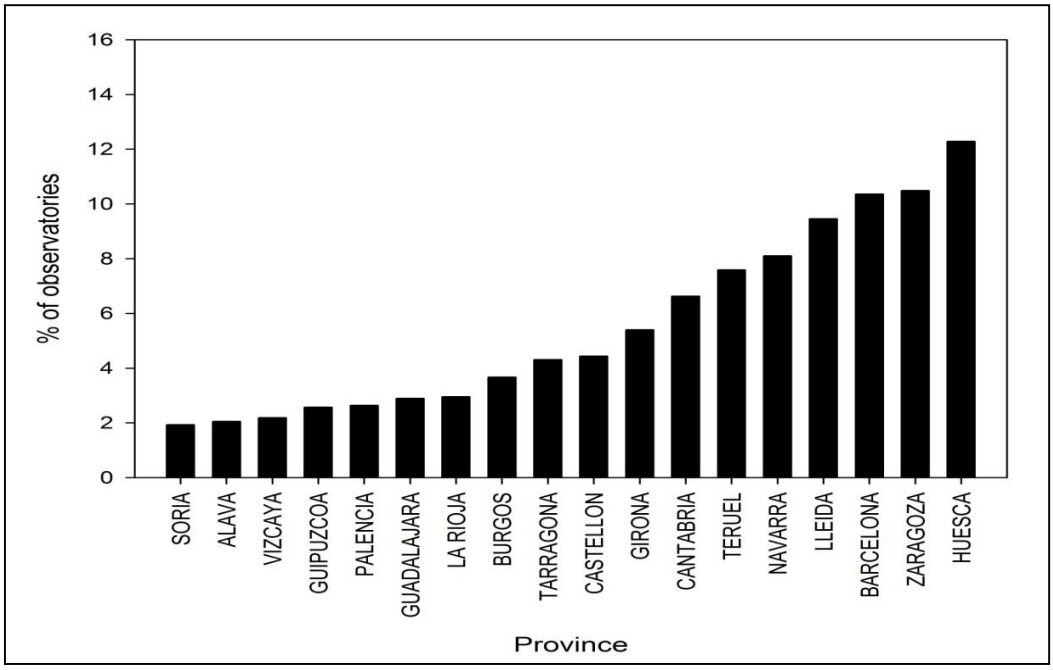

Figure 2.2: Distribution of temperature observatories according to the province.

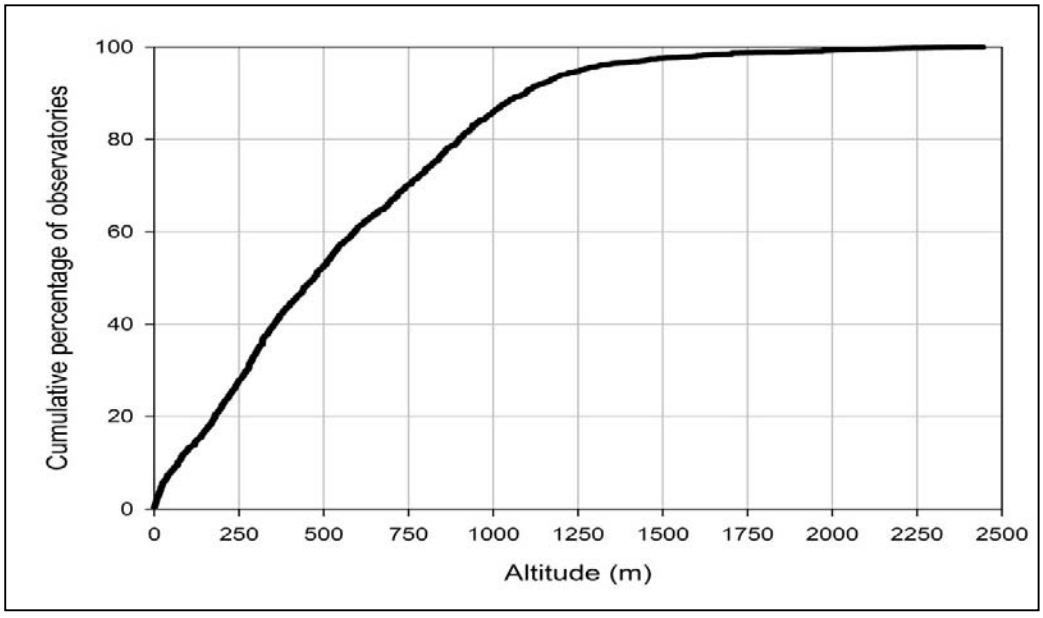

Figure 2.3: The cumulative distribution of the number of observatories as a function of altitude. Altitude is given in meters.

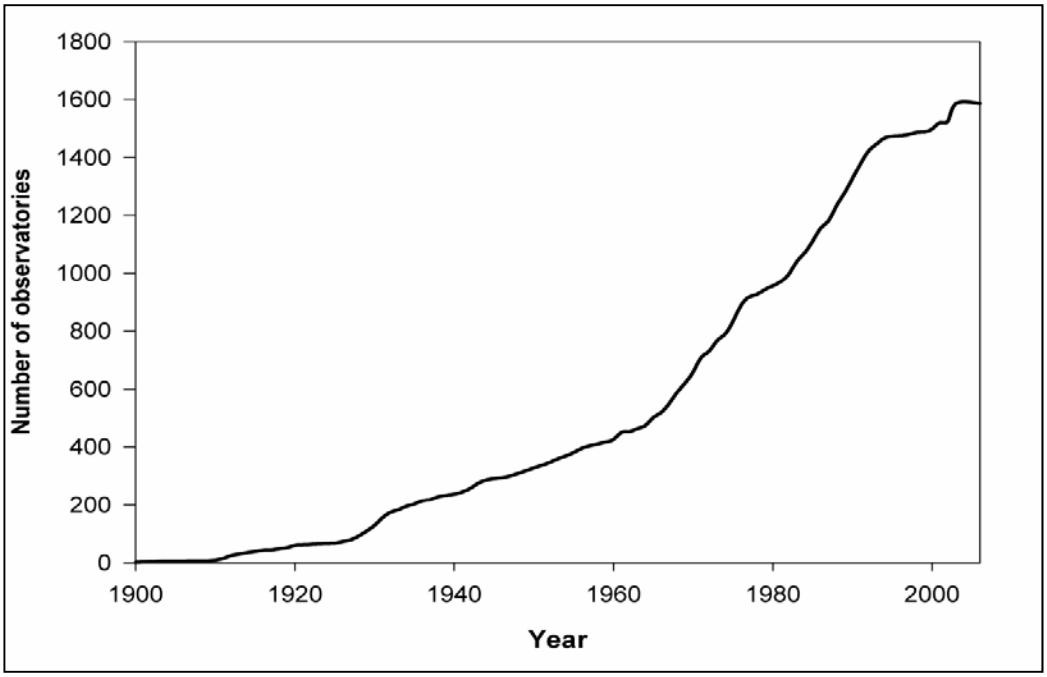

Figure 2.4: The number of available daily maximum-minimum temperature observatories in the original dataset from 1900 to 2006.

As illustrated in Figure 2.5, the raw dataset, particularly those series with long-term temperature records (e.g.,> 50 yrs), suffers from presence of missing values and temporal gaps. Changes in stations opening, closing and locations are being the reason. More importantly, Figure 2.5 indicates that parts of the available observatories have archives of instrumental climate records which, in some cases, date back to the first decades of the 20th century. Also, the region provides promising amount of data, as revealed by the dense network of observatories, which can allow for potential reconstruction of very useful long-term temperature time series making a good use of data from short interval time series (e.g., < 30yrs).

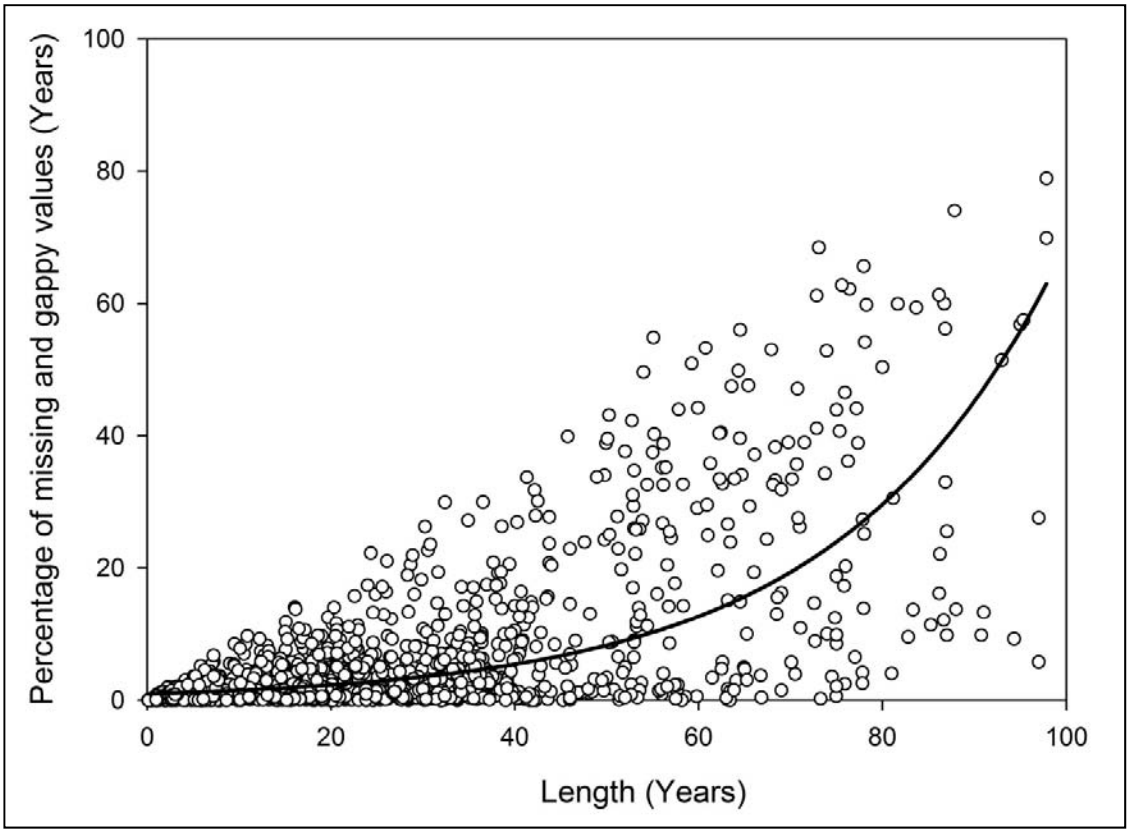

Figure 2.5: Scatter plot representing the relationship between the length (in years) and the percentage of missing values in the time series of the original dataset. The solid line indicates the best fitted model curve. The length is defined as the difference between the opening date of the observatory and its more recent record.

In the following section, a full description of the multistep approach used for quality control, reconstruction and homogenization of the daily temperature series is detailed. A scheme that represents the different steps of this procedure is summarized in Figure 2.6.

2.3. Quality control of daily time series

Quality control is a fundamental task to remove incorrect data and to check for data consistency and reliability (Feng et al., 2004). In this work, the original series were subjected to several quality checks. First, typical tests were performed to identify systematic errors, which resulted from different sources (e.g., archiving, transcription, and digitization). This can include non-existent dates, Tmin ≥ Tmax, Tmax > 50ºC, Tmin < - 50ºC and runs of at least 7 consecutive days with identical records. Next, the data were screened for internal consistency by comparing the value in question against other values in the same time series following Reek et al. (1992).

Finally, the data were checked for external consistency by comparing each time series with nearby sites. The rationale behind this procedure was to trim outliers that markedly differ from the majority of neighbors while keeping the valuable extreme information. To accomplish this task, daily data of each testable observatory were compared with a minimum of 3 nearby observatories located within a maximum distance of 30 km. More specifically, the rank of each value in a testable time series was obtained as a quantile of all values in this series. Then, these quantiles were compared with the quantiles of nearby stations for each particular day. Values which exceed a user-defined difference threshold in this between-station comparison was flagged and set to missing values. In order to screen for appropriate interquantiles range threshold, this research tested different thresholds (e.g., 0.1, 0.2, 0.3, etc) using a random subset representing 1 % of all time series.

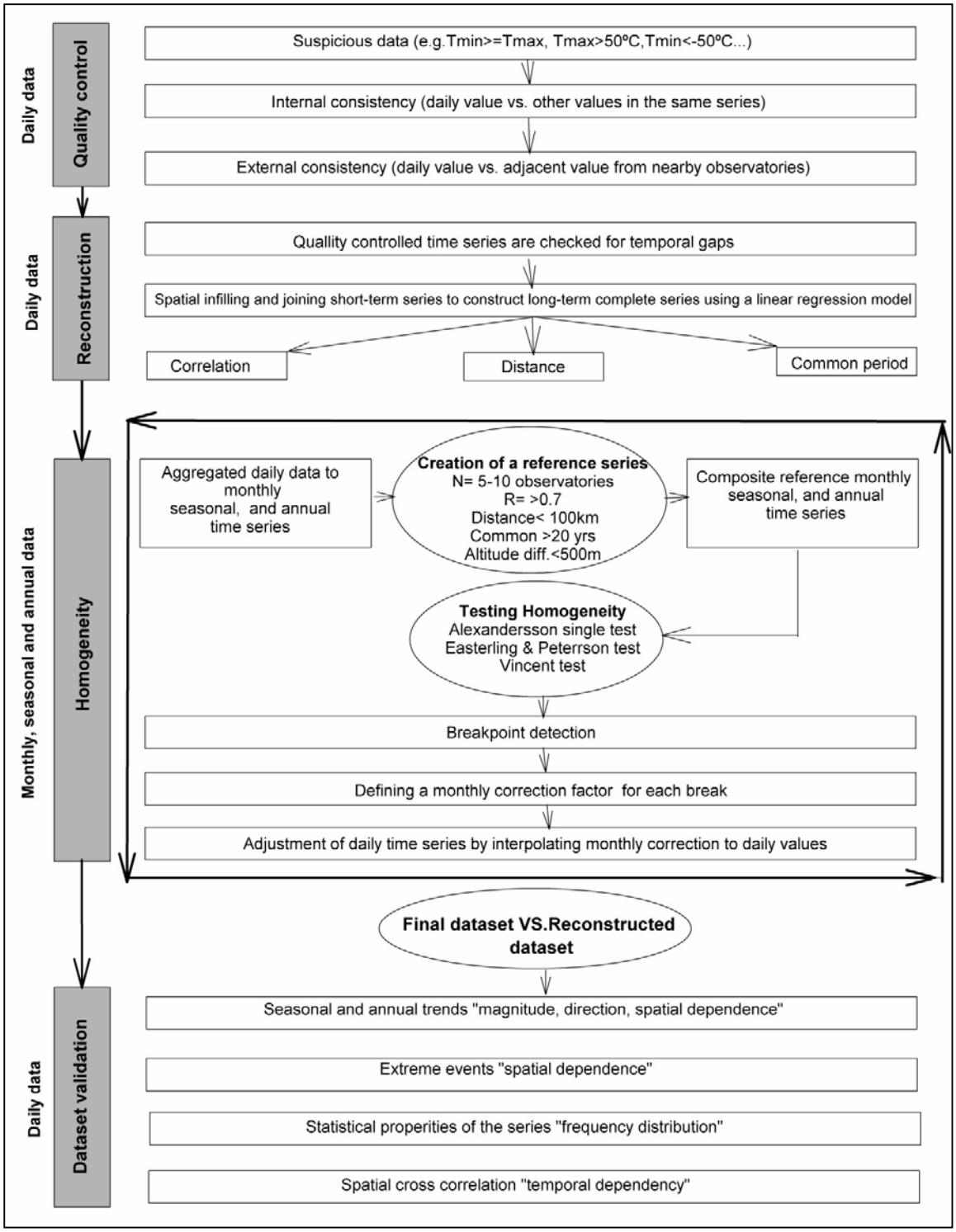

Figure 2.6: Schematic representation of the integrated approach applied to quality control, reconstruction, and homogenization of daily temperature time series in the study area. Shaded areas indicate the main steps.

The results suggested a threshold of 0.5 as a more suitable compromise for all seasons apart from winter, whereby a more restricted threshold (0.3) was set. This was principally done to account for the thermal and dynamical conditions originating from topography influences in winter. As the study domain is topographically complicated, the topography can significantly influence different atmospheric and climate processes through modification or blocking atmospheric flows and air masses. In areas of strong topography gradient, meso-scale weather systems can be found as a result of thermodynamic processes associated with the vertical (ascending and descending) movement of air (Barry and Chorley, 1987; Whiteman, 2000). Accordingly, the spatial dependency among observatories can markedly degrade over short distances. A similar approach was recently adopted by Stepanek et al. (2009) and Vicente-Serrano et al. (2010) to detect erroronous records in climate data.

2.4. Reconstruction of daily time series

Short-term and fragmented time series may introduce noise to estimates of long-term climate changes. This is the typical case in many climatic datasets worldwide, where many gaps are introduced in the series. Peterson and Vose (1997) indicated that short or fragmented series may significantly alter the magnitude and sign of climate variability trends, particularly at regional-scale resolution. For this reason, many techniques have recently been applied for serial reconstruction in climatology including, for example, the neural artificial network (Rigol et al., 2001), interpolation algorithms (Vicente-Serrano et al., 2010), and the singular spectrum analysis (Ghil et al., 2002). The basic idea behind these methods is to obtain long-term complete dataset using all available data within a region. In general, the reconstruction can be

carried out as a function of the weighted distance (Shen et al., 2001) and/or correlation (Young, 1992). Nevertheless, these approaches differ in their applicability according to terrain complexity and spatial density of stations (Allen and DeGaetano, 2001; Hofstra et al., 2010). For instance, many interpolation techniques (e.g., optimal interpolation, Kriging, and splines-surface fitting) can give good results in regions with no gradients (Jarvis and Stuart, 2001a, b). Contrarily, their performance in terms of both bias and amount of variance is predominantly poor in areas of complex terrain or uneven density of observatories (Romero et al., 1998; Eischeid et al., 2000; Hubbard and You, 2005). In such environments, the regression-based methods can be a superior solution. These methods take into account data from adjoining stations with the best temporal correlation and the highest spatial dependence. The primary advantage of these methods is that they show less sensitivity to outliers (Romero et al., 1998), and can therefore better represent systematic temperature differences associated with topographic influences in heterogeneous regions (Hubbard and You, 2005). Compared to other meteorological variables, such as precipitation, temperature often has a statistically normal distribution. Accordingly, the regression-based approaches seem to be an adequate choice for this research. In literature, numerous previous studies proved the advantages of the regression methods to reconstructing temperature time series relative to other methods (e.g., Eischeid et al. 1995; Allen and DeGaetano, 2001; Hubbard and You, 2005; You et al., 2008).

In this work, the standard linear regression model was simply applied to estimate missing value at the target observatory on a given day (*i*), as follows:

$$Y_i = a + bx_i \tag{2.1}$$

where a refers to the intercept, b is the slope between the y (target) and x (neighboring) time series and y_i and x_i are the values of the target and neighboring stations at the day *i*.

This research took advantage of the large number of available observatories in the original dataset to rebuild long-term time series based on comprising nearby series of short time span. It is assumed that information introduced from nearby stations identically reflects uniform climatic conditions of the target station. To accomplish this task, the daily temperature series of the original dataset were firstly divided in two broad groups. The first category included all the series that are still in operation (2004 or more recently), hereafter labeled as target series. This step resulted in 668 target observatories. The remaining data (915 observatories) were served as a pool for the reconstruction process. Since the final output of the reconstruction procedure is largely influenced by the selected neighboring stations, a set of similarity measures (distance and correlation) is used to rebuild the target series. The procedure for the pre-selection of the adequate neighbors only comprised those stations which fulfilled a set of restricted multi-criterion, including: a) a minimum common observing period of 4 years shared by the target station, b) a positive correlation coefficient exceeding 0.90, and c) location within a radius of 15 km around the target station. This procedure helped avoiding suspicious information and only sacrificing quality-assured data that experienced similar climate conditions to the target observatory. In order to maximize the series length, priority of infilling a target station was firstly given to the longest nearby series that best correlated with the target station. For this reason, the stations were firstly ranked on the basis of the available record length and data completeness. When data from an adjacent series were used to reconstruct a target station, they

were automatically discarded from the bulk series to avoid introduction of redundancy information. The redundant information can actually decrease the reconstruction skill since they can dismiss important information from other nearby sites. However, it is worthwhile to indicate that the regression model was applied iteratively to maximize the value of information used from all nearby observatories. Nevertheless, the number of surrounding stations for each target (candidate) station was not fixed in time as it depended on data availability on each particular day.

2.5. Homogeneity testing

Most long-term climatological time series are often affected by a number of non-climatic factors that make these data unrepresentative of the actual climate variations. These factors include, for example, changes in observatory locations, observers, surrounding environments, measurement practices or instruments (Peterson et al., 1998, Costa and Soares, 2009b). Historically, numerous attempts have already been made to develop appropriate methods to detect and correct inhomogenities at low temporal resolution (i.e., monthly and annual) (e.g., Alexandersson, 1986; Jones et al., 1986; Petrovic, 2004). However, less attention has been devoted toward testing homogeneity of climatic data at daily and sub-daily resolution (e.g., Vincent et al., 2002; Wijngaard et al., 2003). This task is more challengeable due to noise and high variability introduced in daily data compared with monthly and annual data. A comprehensive review of different homogenization approaches is given in Peterson et al. (1998) and Costa and Soares (2009b). In absence of accurate, complete and well-documented metadata (i.e., station history), the relative homogeneity tests (RHTs), which rely on comparing the station´s own data with its neighborings, are favored to identify supporting evidence of significant changes on observational routines. The NE

Spain dataset shows a typical example. The relative homogeneity test procedure included two main steps: the creation of reliable reference series and the application of proper homogeneity tests.

Building reference time series is mandatory for undertaking the relative homogeneity tests. The reference time series is assumed to reveal the same variability of weather and climate exhibited in the candidate station. In this regard, this research used composite reference series to test homogeneity of each candidate series. This was mainly because temperature shows less spatial variations compared to other climatic variables, such as precipitation, which can vary greatly over space. Similar to previous works (e.g., Peterson and Easterling, 1994; Klein Tank et al., 2002; Vicente-Serrano et al., 2010), this work brought together factors of distance, correlation, elevation dependence, and stations density to select the most useful sites to create reliable composite reference series. Herein, nearby observatories with high temporal correlation were assumed to exhibit the same variability of weather and climate. More specifically, the reference series were composited from nearby localities lying within a maximum distance of 100 km, with correlation greater than 0.7. In practice, a distance threshold of 100 km was considered as high enough so as to secure reasonable number of nearby stations in sparse network areas (e.g., southwestern portions). In the same sense, although higher correlation coefficient is desirable to build a reliable reference series, a threshold of 0.8 between the candidate and the reference series still suits the purpose of this work given that the correlation was computed between the first difference series (X_{t+1}-X_t) to avoid additional inhomogeneities from the reference series. This correlation threshold was in the range being considered in numerous previous studies (e.g., Peterson et al., 1998; Vicente-Serrano and López-Moreno,

2006; Costa and Soares, 2006; Stepanek et al., 2008; Savic et al., 2010). In addition to distance and correlation thresholds, a minimum overlap period of 20 years of records between the candidate and nearby observatories was also set. This common period is long enough to construct reliable composite reference series. Furthermore, it helped overcoming the problem of discontinuities in the nearby series. Lastly, a maximum altitude difference of 500 m between the candidate and the nearby sites was adopted to limit the influence of topographical gradients.

Based on the aforementioned criteria, a well-defined monthly reference series was created for each testable series using a weighted average of data from the highly correlated neighboring stations following the standard procedure of Peterson and Easterling (1994), as follows:

$$T_{R,i} = \frac{T_{R1,i} \times R_1^2 + T_{R2,i} \times R_2^2 + T_{R3,i} \times R_3^2 + T_{R4,i} \times R_4^2 + T_{R_n,i} \times R_i^2}{R_1^2 + R_2^2 + R_3^2 + R_4^2 + R_n^2} \quad (2.2)$$

where $T_{R,i}$ is the reference series for the *i* month, $T_{R_n,i}$ is the value of temperature in the neighboring observatory *n* during the month *i*, R_I is the correlation coefficient between the first difference time series of the target (candidate) series and the neighboring observatory *n* during the month *i*.

Herein, it is noteworthy indicating that the values of the selected nearby stations were firstly standardized by their mean and standard deviation for each month independently. This procedure reduces possible biases from the reference series. In general, the procedure to create the reference series was run automatically using the PROCLIM-DB software (Stepanek, 2008). However, it is worthwhile to indicate that

although the main target was to obtain a homogenous dataset at daily resolution, the reference series were created at monthly, seasonal and annual timescales. This helped avoiding problems released from the high variability of daily data at small spatial scales (Feng et al., 2004). Indeed, daily data exhibit a complex and non-linear behavior. Therefore, they may comprise nonlinear events resulting from very local processes, such as orography and surface albedo. The combination of the high day to day differences and the generally high spatial heterogeneity of the climate add another difficulty to capture daily variations in the reference series.

Detecting breakpoints in the time series is one of the most relevant problems among those addressed by the RHTs. In practice, there is no one single test to be recommended as optimal to detect breaks in all situations (Costa and Soares, 2009b). This is mainly because RHTs vary in their theoretical background, algorithms and sensitivities to detecting breaks in the series. Thus, application of different statistical methods could largely improve the degree of certainty related to the detectable breaks in the series, especially when metadata is unavailable (Wijngaard et al., 2003). This approach has been favored by many researchers to verify the possible discontinuities in climatic time series (e.g., Wijngaard et al., 2003; Costa and Soares, 2009b). In this research, three well-established RHTs were chosen to test homogeneity of the series, including: the Standard Normal Homogeneity Test (SNHT) for a single break (Alexandersson, 1986), the Easterling and Peterson test (Easterling and Peterson, 1995) and the Vincent method (Vincent, 1998). The SNHT single break test determines the most significant break in the time series and has the advantage of detecting breaks close to the beginning and the end of the series (Wijngaard et al., 2003). For this reason, it has increasingly been recommended to define the breaks in

climatic series (e.g., Slonosky et al., 1999; Wijngaard et al., 2003). On the other hand, the Easterling and Peterson two-phase regression-based technique has the advantage of detecting multiple breaks in the series, specifically when they are very close in time (Easterling and Peterson, 1995). More recently, Vincent (1998) proposed a multiple linear regression approach to identify multiple breaks in temperature series, particularly undocumented change points. Vincent et al. (2002) used this test to identify multiple breaks in the daily Canadian temperature series.

In this study, all the RHTs were carried out at monthly, seasonal and annual timescales. These temporal resolutions fulfilled normality, which is a prerequisite for the SNHT. Moreover, seasonal resolution allowed a better detection of inhomogeneities given that some sources of inhomogeneity show different impacts from season to season (e.g., summer vs. winter). The AnClim software developed by Stepanek (2004) was used for testing homogeneity. Only detectable breaks at a confidence level of 95% ($p<0.05$) were considered statistically significant. Following this approach, all possible inhomogeneities in the series were defined and grouped together. This procedure enabled to detect all possible inhomogenities in the series because it did not only identify the same break in one series, but it also allowed tracking down inhomogenities not identified by any of the other two tests. Recalling that the underlying hypothesis of the RHTs is based on comparing the mean from two sides of the data, inhomogeneities found within the first and the last 5 years of the series were not considered. As a consequence of the reduced sample size close to the boundaries of the series, there is an increasing probability to have high T values (Hawkins, 1977). Previous studies rejected inhomogenities 5 years or more at the start

and/or the end of the series, particularly if they are not fully explained by metadata (e.g., Gonzalez-Rouca et al., 2000, Gokturk, et al., 2008).

The homogeneity adjustments make it possible to consider temporal variations of temperature time series as caused only by climate variations. Therefore, an adjustment (correction) model was applied to account for statistically significant abrupt changes. The correction factor was computed for each month individually based on a comparison of percentiles of the differences between the candidate and the reference series before and after any detectable break. To obtain daily corrections, the pre-defined monthly corrections were interpolated into the daily time series following the approach described by Sheng and Zwiers (1998) and recommended by Vincent et al., (2002). This procedure is advantageous in various ways. First, it reduces discontinuities on the first and last days of each month (Vincent et al., 2002). Second, it maintains characteristics of daily extreme events, such as frequency and intensity. Lastly, it preserves temperature trends and variability presented in monthly temperatures. Altogether, it can be expected that the homogenized daily temperature series will be compatible with those of monthly resolution.

Finally, it is worthwhile to indicate that testing homogeneity was applied iteratively as all time series in the dataset were considered repeatedly as candidate and reference series. However, more restricted criteria were considered in this iterative procedure. First, multiple reference series were used as alternative to the composite reference series to test homogeneity. Accordingly, each candidate time series was tested independently and iteratively against each of the best correlated 5 neighboring stations. Although this procedure involved intensive use of the data, it reduced the possible effects of temperature spatial variation originating from terrain complexity in

the study domain. In the following iterations homogeneity was tested again using the composite reference series, but applying more restricted criteria (e.g., r= > 0.9, number of observatories<= 10). This procedure mainly aimed to verify the regional consistency among nearby sites. At this stage, combining both multiple and composite reference series and testing all the time series several times was important to ensure that the final dataset is relatively free from any significant breaks.

2.6. Impacts of the adjustment protocol on trends and statistical properties of the series

Evaluation of the impact of series adjustment is of great importance to determining the reliability of the final time series for different climate analyses such as trends and climate extremes. Given that homogenization procedures are more subjective and therefore can have adverse and complex influences on time series, many authors (e.g., Peterson et al., 1998; Vincent et al., 2002) highlighted the importance of identifying the possible impacts of inhomogeneity adjustment on climatic data. In this research, a set of techniques was used to account for such possible impacts. Herein, the main hypothesis was that the degree to which a station's data reveals spatial and temporal coherence with their immediate surroundings can be a good indication of the reliability of the applied methodology. Therefore, the validity of the final dataset can be evaluated by examining spatial and temporal characteristics of the new dataset, as compared to the original dataset. All the assessment tests were applied to a set of 98 observatories covering the period from 1950 to 2006. The spatial distribution of these observatories is given in Figure 2.7.

Firstly, linear trends of maximum and minimum temperatures were calculated at seasonal and annual timescales before and after eliminating inhomogeneities. The main purpose was to assess the relative influence that the homogeneity procedure exerted on the trend assessment in terms of both the magnitude and sign (direction) of the trend. The significance of the trends was assessed using the nonparametric Spearman (*Rho*) test at a confidence level of 95% (p value < 0.05). The Spearman Rho statistic was computed, as follows:

$$Rho = 1 - \frac{6\sum_{i=1}^{n}(R_i - i)^2}{n(n^2 - 1)} \qquad (2.3)$$

where R_i is the rank of *i*th observation in the time series and *n* is the length of the time series.

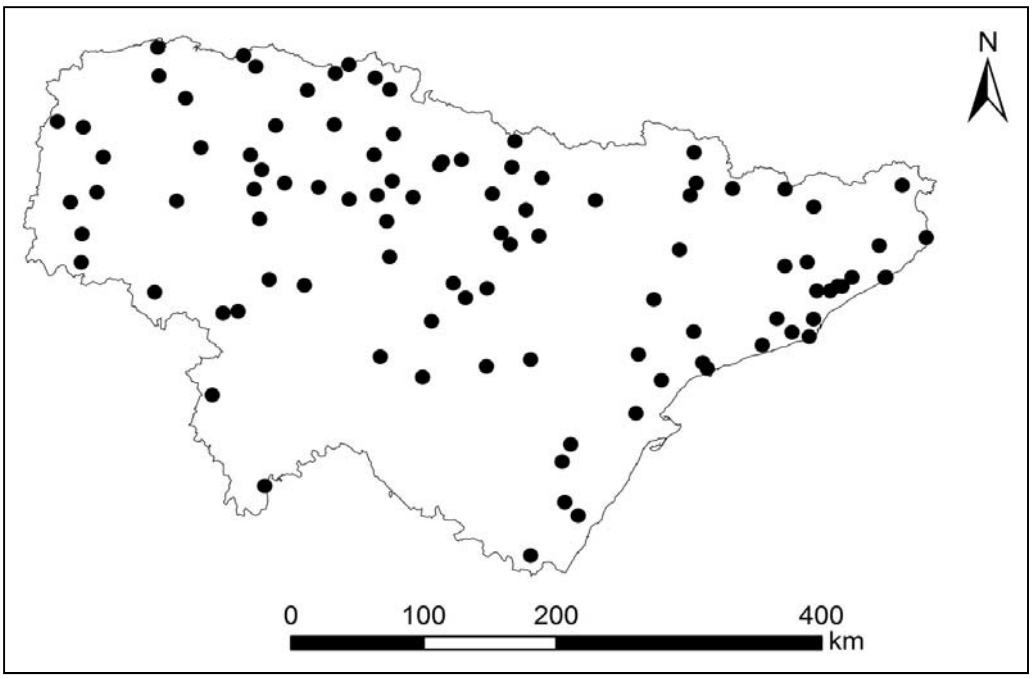

Figure 2.7: Spatial distribution of temperature observatories from 1950 to 2006 (*N*=98).

This test is robust to outliers and does not assume prior probability distribution of the residuals. The slope was estimated using the ordinary least squares (OLS) fitting and expressed in ºC per decade. Seasonal averages were obtained from monthly data for each year and defined as winter (December-February; DJF), spring (March-May; MAM), summer (June-August; JJA), and autumn (September-November; SON). A comparison between the trends sign (direction) before and after corrections was conducted by means of the cross-tabulation analysis, which illustrated pairwise relationships between the categories of the trend signs (i.e., significant positive [+], significant negative [-], and statistically insignificant [N]). In this context, the pivot tables were constructed to represent the cross-categorized frequency data in a matrix format following the results of the trend assessment.

To assess the degree of spatial dependence between the seasonal and annual trends before and after homogeneity correction, the semivariance models were computed for the magnitude of change. A detailed explanation of semivariance theory can be found in Webster and Oliver (2001). Semivariance analysis has widely been applied in ecology (e.g., Urban et al., 2000) and climatology (e.g., Vicente-Serrano et al., 2010) to detect scales of variability in spatial data. The semivariance describes the spatial variance as a function of distance between the observatories. The value of the semivariance decreases as the pair of data points is separated by a short distance, meanwhile it increases when the distance increases. In this study this geostatistic was employed to analyze variations in spatial structure of the trends before and after homogeneity correction. It can be expected that the semivariance will be lower after correcting inhomogeneities as a consequence of introducing a relatively free-of-error and homogenous series. Spatial semivariance was obtained, as:

$$\gamma(h) = \frac{1}{2N(h)} \sum_{i=1}^{N(h)} [Z(s_i) - Z(s_i - h)]^2 \quad (2.4)$$

where y(h) is semivariance at lag distance *h*, *N (h)* is the number of station pairs that are separated by *h* distance, *Z (si)* and *Z (si+h)* are the values of *Z* variable in stations *si* and *si* + *h*.

Secondly, adjustment of the series may alter the probability distribution of extreme temperature (e.g., frequency and intensity). Therefore, this study used two extreme temperature indices to assess possible impacts of adjustment on occurrence of extreme values. In practice, the annual count of warm and cold days before and after breaks adjustment was computed for each daily time series from 1950 to 2006. The warm (cold) day was simply defined as the day higher (lower) than the 90th (10th) percentile of the average maximum (minimum) temperature. The definition of extreme values based on the percentiles is objective, site-independent and facilitates direct comparisons between regions of diverse climates (Jones et al., 1999). However, it is worthwhile to indicate that the key question behind this analysis was to assess the way in which the adjustment procedure affected spatial continuity of the trends rather than the trends themselves. Therefore, the spatial continuity of the extreme temperature trends before and after homogenization was compared using semivariance of the magnitude of change.

Thirdly, to determine how the adjustment procedure affected the statistical distribution of daily temperature values in the series, a suite of statistical indicators were computed for the time series before and after correction. In this regard, L-moment statistics were computed for each independent daily maximum and minimum time series before and

after homogeneity correction. These statistics provide information on the scale (L-coefficient of variance [t_2]), shape (L-coefficient of skewness [t_3]), and peakedness of the series (L-coefficient of kurtosis [t_4]). L-moment statistics are independent of the sampling size and also resistant to outliers. Moreover, they show less bias in comparison with other conventional product moments, such as standard deviation, skewness and kurtosis. These statistics have therefore been used in climatological and hydrological studies (e.g., Guttman, 1993; Guttman et al. 1993; Vicente Serrano et al., 2010). More details on the L-moment theory are given in Asquith (2003). In short, the L-moment coefficients are defined according to Hosking and Wallis (1997), as follows:

$$\tau_2 = \frac{\lambda_2}{\lambda_1} \tag{2.5}$$

$$\tau_3 = \frac{\lambda_3}{\lambda_2} \tag{2.6}$$

$$\tau_4 = \frac{\lambda_4}{\lambda_2} \tag{2.7}$$

where ($\lambda_1, \lambda_2, \lambda_3, \lambda_4$) are the probability-weighted moments (PWMs) defined by Greenwood et al. (1979), as:

$$\lambda_1 = \beta_0 \tag{2.8}$$

$$\lambda_2 = 2\beta_1 - \beta_0 \tag{2.9}$$

$$\lambda_3 = 6\beta_2 - 6\beta_1 + \beta_0 \quad (2.10)$$

$$\lambda_4 = 20\beta_3 - 30\beta_2 + 12\beta_1 - \beta_0 \quad (2.11)$$

The PWMs of order *r* is given by:

$$\beta_r = \frac{1}{N}\sum_{i=1}^{N}\left(1 - F_i\right)^r x_i \quad (2.12)$$

where F_i is the cumulative distribution of a given ordered sample ($x_1 < x_2 < x_3 < x_i$) calculated, as:

$$F_i = \frac{i - 0.35}{N} \quad (2.13)$$

Also, to get a closer picture of the spatial structure of L-moment coefficients, values of these statistics were also plotted against distance by means of the semivariance models before and after inhomogeneities correction.

Lastly, while the statistical methodologies described above can provide a guidance to assessing the reliability of the final dataset, perhaps the most outstanding feature to assess the effect of the homogeneity procedure is to account for the correlation between the time series before and after correcting breaks. In this research an assessment of this effect was achieved by deriving the Pearson correlation matrix between temperature series at different distance orders. The correlation matrix was computed for both the original series (i.e. raw and corrected) and the series of first differences (X_{t+1}-X_t) for the raw and corrected data. Considering the correlation between the first difference series is of special interest to give insights into the strength of the temporal dependency among the series after isolating the influence of

inhomogeneities which may be introduced in the independent series. Overall, introducing inhomogeneities in the series is assumed to degrade correlation among nearby sites and, in this study, the inter-station correlation could act as a kind of filtering for non-adjusted series.

2.7. Homogeneity testing results

Table 2.1 summarizes the percentage of flagged data following the quality control procedure. On average, the percentage of erroneous data was higher for minimum (0.11%) than for maximum temperature (0.09%). The highest errors for maximum and minimum temperatures occurred during spring and summer, respectively. Spatially, the fraction of flagged data was greater in station-dense areas (e.g., Catalonia and Cantabria), compared with relatively sparse areas (e.g., Burgos and La Rioja). One representative example for the erroronous data was the daily minimum temperature at the observatory of San Mateo (Castellon) which recorded -88.8ºC on the second day of January in 1960. Figure 2.8 also illustrates an example of one outlier detected in daily maximum temperature at the observatory of Pamplona on 23rd June 1983, in which the percentile of this daily value was 0.37, which differed largely from other neighboring observatories (0.75±0.82). This value was flagged and set as missing value.

After quality control checks, a linear regression model was used to comprise nearby and best correlated series of short-term span in order to rebuild long-term time series. Figure 2.9 illustrates an example of the reconstruction procedure. As presented in Figure 2.9.A, the reconstructed wintertime daily minimum temperature time series at

the observatory of Calatorao Cooperative (9428E, Zaragoza) has records from 1940 to 2006 as a consequence of joining data from two nearby sites (9425I and 9432).

Table 2.1: Summary statistics of the flagged data following the quality control procedure. The numbers refer to the fraction of the flagged data in daily maximum (Tmax) and minimum (Tmin) temperature series. The mean indicates the average of the flagged data for the whole dataset, while the lowest (highest) shows the maximum (minimum) percentage of flagged data at the station-based level.

		Winter	Spring	Summer	Autumn	Annual
Tmax	**Lowest**	0	0	0	0	0
	Highest	0.47	0.97	0.55	0.6	1.99
	Mean	0.01	0.04	0.02	0.02	0.09
Tmin	**Lowest**	0	0	0	0	0
	Highest	0.52	1.41	1.35	0.99	3.85
	Mean	0.02	0.02	0.04	0.03	0.11

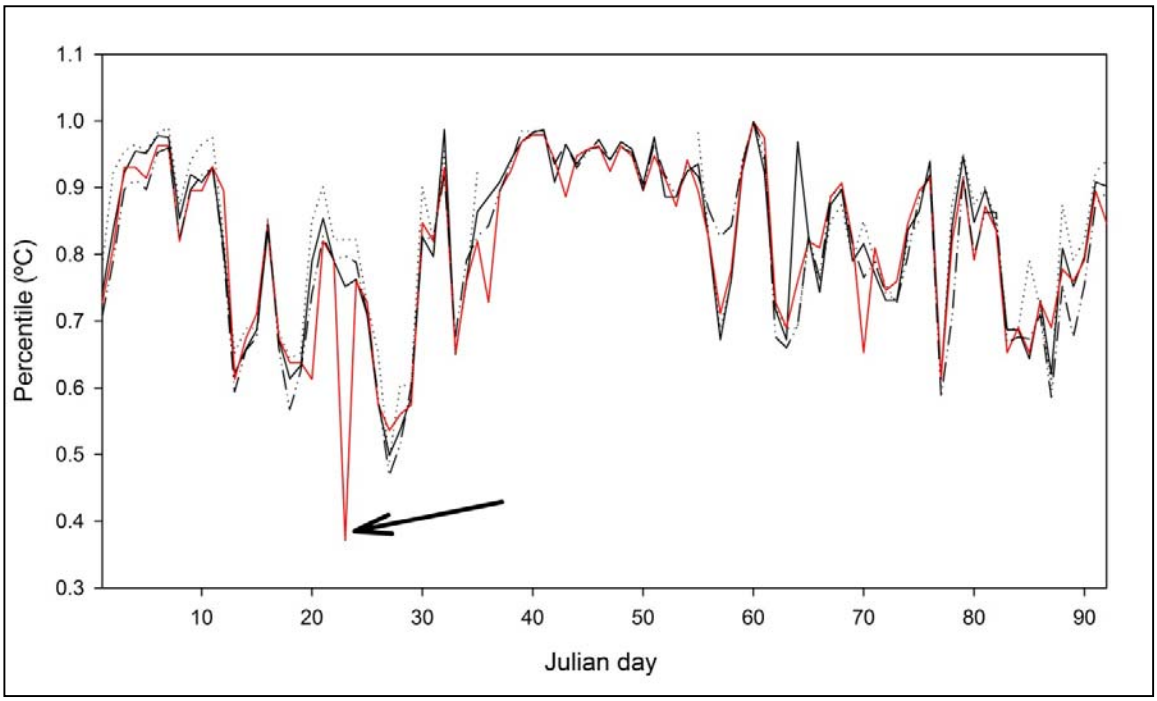

Figure 2.8: The percentiles of the daily summer temperature at the observatory of Pamplona (red line) and its nearby observatories. The percentiles were calculated for each day in the period from 1st June to 31st August in 1983 (total of 92 Julian days), relative to the entire daily records of each observatory.

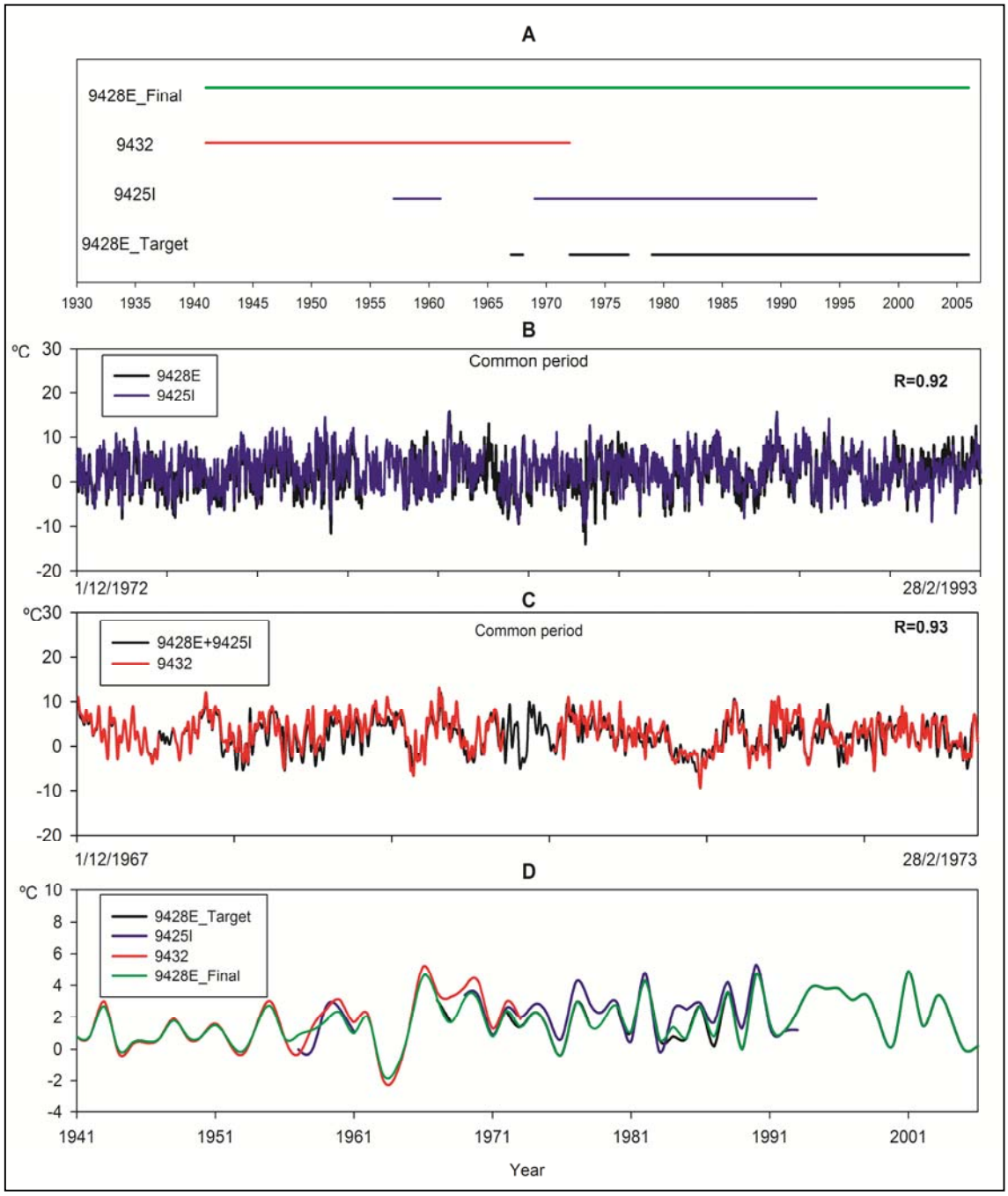

Figure 2.9: The reconstructed wintertime minimum temperature series at the observatory of Calatorao Cooperative (9428E, Zaragoza) based on joining data from two nearby sites (9425I and 9432). Pearson correlation coefficient (*r*) indicates the correlation between the reconstructed time series and each of the nearby observatories. The green line denotes the final time series.

The temporal evolution of the final reconstructed series fits well that of the nearby localities (9425I: *r*= 0.92, 9432: *r*= 0.93). This clearly implies that this procedure can provide a robust basis for the series reconstruction. The quality-controlled reconstructed daily dataset of 668 maximum-minimum temperature series covering some periods between 1900 and 2006 was then subjected to homogeneity testing and adjustment.

One of the most common problems in handling long-term climate data is the presence of inhomogenities. Box plots summarizing the criteria used to building the composite reference series are illustrated in Figure 2.10. On average, values of the 10 best correlated neighboring observatories with average distance lower than 50 km were considered to create the reference series for both maximum and minimum temperature series. More importantly, the Pearson correlation coefficient was generally higher than 0.9 for a vast majority of observatories, with only very few exceptions. Taken together, these criteria comply with the common standards required to build reliable reference series in previous homogeneity studies. Figure 2.11 illustrated two example reference time series created for two target (candidate) time series. The first corresponds to May maximum temperature at the observatory of Sabadell Aerodromo [Barcelona], while the latter informs about August minimum temperature at the observatory of Reus Aeroport [Tarragona].

Table 2.3 summarizes the homogeneity testing results for maximum and minimum temperature time series. As presented, only 12 (17) time series out of the whole maximum (minimum) temperature datasets were not testable due to lack of closing observatories, poor correlation or shortness of the series (< 20yrs). Table 2.3 also demonstrates that 307 (46%) and 302 (45.2%) of the minimum and maximum

temperature time series, respectively, did not show statistically significant inhomogeneities. However, 82 (79%) of the minimum (maximum) temperature series classified as homogenous were relatively short (generally < 30 yrs). Majority of the series longer than 30 years experienced some homogeneity problems. The results indicate, for instance, that maximum and minimum temperature time series of more than 40 (50) years of records had an average of 2.7(3) and 2.3 (2.6) breakpoints, respectively.

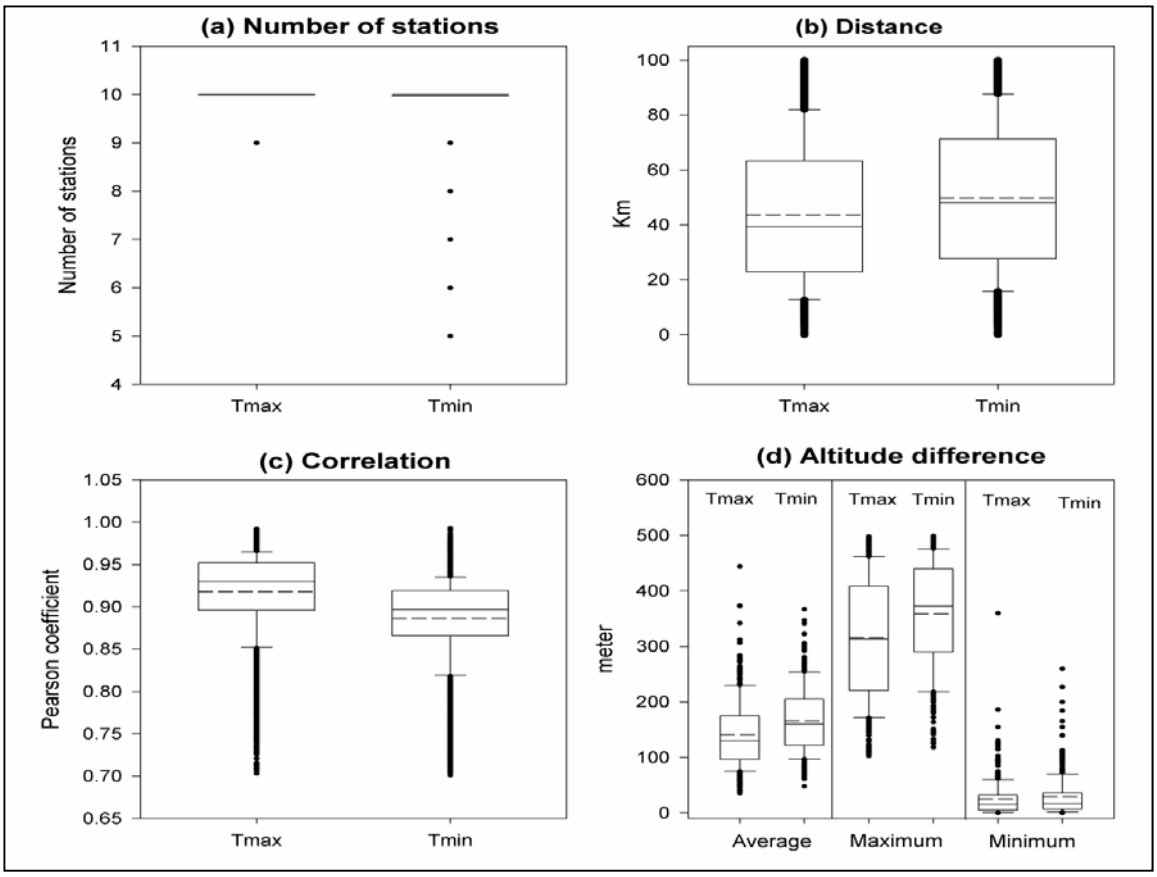

Figure 2.10: Box plots summarizing (a) the number of nearby observatories (b) distance threshold, (c) Pearson correlation threshold and, (d) altitude difference of the series used to create the composite reference series for break detection. Dotted line indicates the mean. The median, 10th, 25th, 75th and the 90th percentiles are plotted as vertical boxes with errors bar.

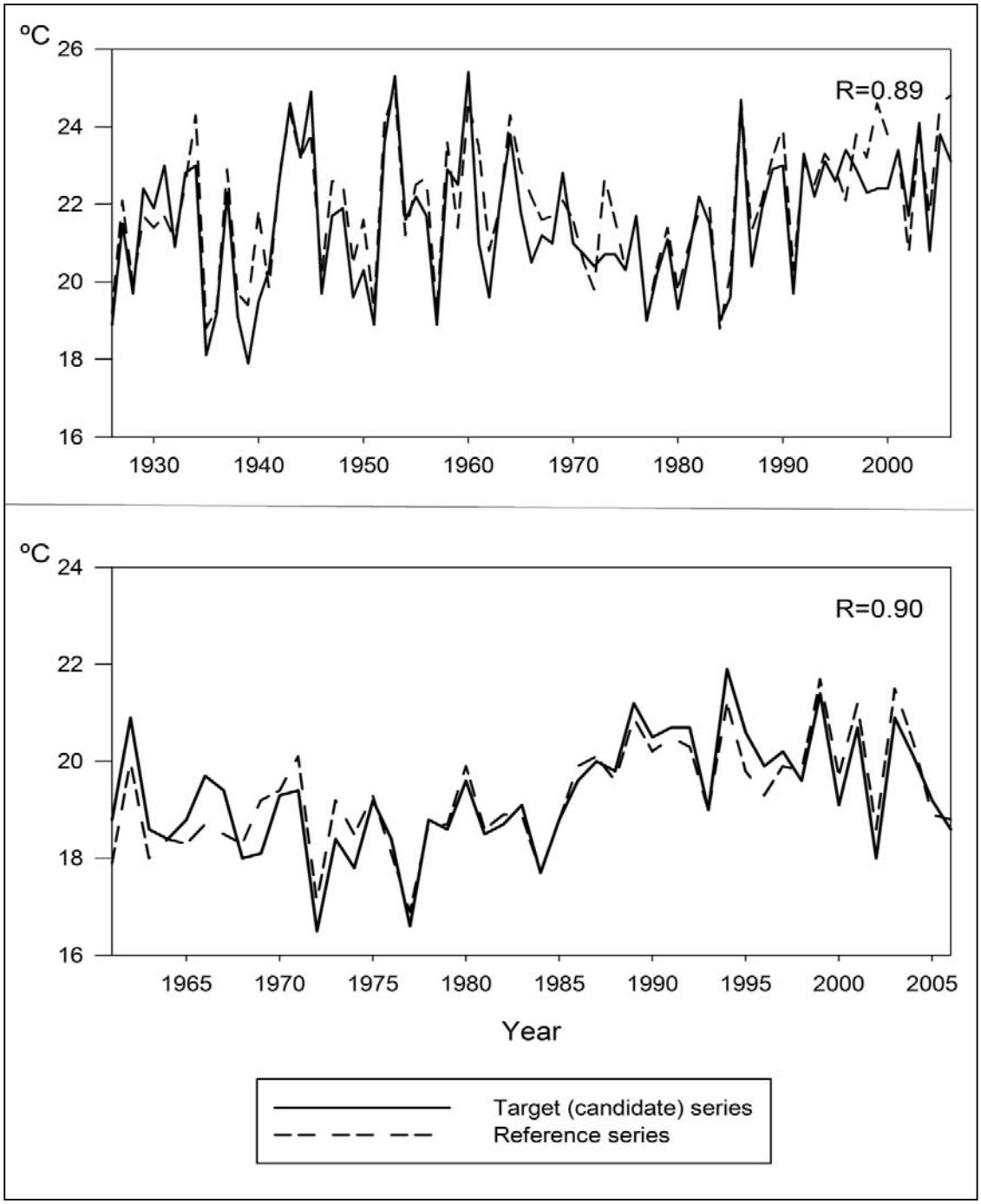

Figure 2.11: The composite reference time series for (a) May maximum temperature at the observatory of Sabadell Aerodromo [Barcelona] and (b) August minimum temperature at the observatory of Reus Aeroport [Tarragona]. Pearson correlation coefficients between the target (candidate) and the reference time series are provided.

Table 2.3: Summary of the homogeneity testing results (significance level =95%)

	Tmin	Tmax
Number of testable series	651	656
Number of non-testable series	17	12
Total number of the series	668	668
Number of homogenous series	307	302
Number of series with significant breaks	344	354
Total number of significant breaks	865	969

Table 2.3 also suggests that the number of inhomogeneities was larger for maximum temperature (n = 969) than for minimum temperature (n = 865). This can largely be attributed to the high spatial correlation among maximum temperature time series, which makes it easier to detect even small shifts in the series. Another possible reason is that the impact of station relocations, as a common cause of inhomogeneities, is expected to be minimal during nighttime due to low vegetation activity (Stepanek and Mikulová, 2008).

As presented, the reconstruction procedure only accounted for 10.3 and 10.4 % of the detectable inhomogeneities in maximum and minimum temperature, respectively. These breaks often occurred when joining very short-term fragments from different time series. Temporarily, majority of the breaks dated back to the 1970s and 1980s for both maximum and minimum temperature, which agrees well with other earlier studies (e.g., Tuomenvirta, 2001; Wijngaard et al., 2003; Auer et al., 2005). Spatially, inhomogeneities were randomly distributed for both maximum and minimum temperature suggesting that these breaks can be attributed to changes in instruments or observing practices. Nonetheless, it is noteworthy mentioning that most of strong inhomogeneities in terms of the amount of change were mainly localized in complex

terrain regions (e.g., the Pyrenees and the Iberian system). This is reasonable given that stations in high elevated regions are more vulnerable to changes in locations and/or surrounding environment as climate conditions are less stable relative to lowlands (Tuomenvirta, 2001). This finding also comes in agreement with previous works (e.g., Tuomenvirta, 2001; Syrakova and Stefanova, 2008).

A comparison between the performances of the three RHTs revealed that the SNHT was markedly efficient in detecting the most significant break in the series. Although the gradual breaks were not determined using the single shift SNHT, the regression-based methods (i.e., the Easterling & Peterson method and the Vincent method) were proven to have more power in defining such multiple breaks. Overall, the statistically significant breaks ($p<0.05$) defined by one or more of the three tests were combined altogether for each particular observatory. Then, a monthly correction model was applied to account for each detectable break. Figure 2.12 shows the frequency distribution of the correction factors applied to adjust seasonal maximum and minimum temperature datasets. The correction factor did not vary greatly from one season to another. However, there was a bias to decrease temperature means after correction. On average, the magnitudes of the correction factor were generally higher for minimum temperature than for maximum temperature. The decrease in the means of maximum temperature largely occurred during summer (-0.04ºC) and spring (-0.05ºC). In all seasons, a correction factor higher than 1ºC was needed only in very few series.

Figures 2.13 and 2.14 illustrate the results of the SNHT applied to two different time series. The results corresponding to summer maximum temperature at the observatory of Fuenterrabia aeropuerto (Guipuzoca) are given in Figure 2.13.

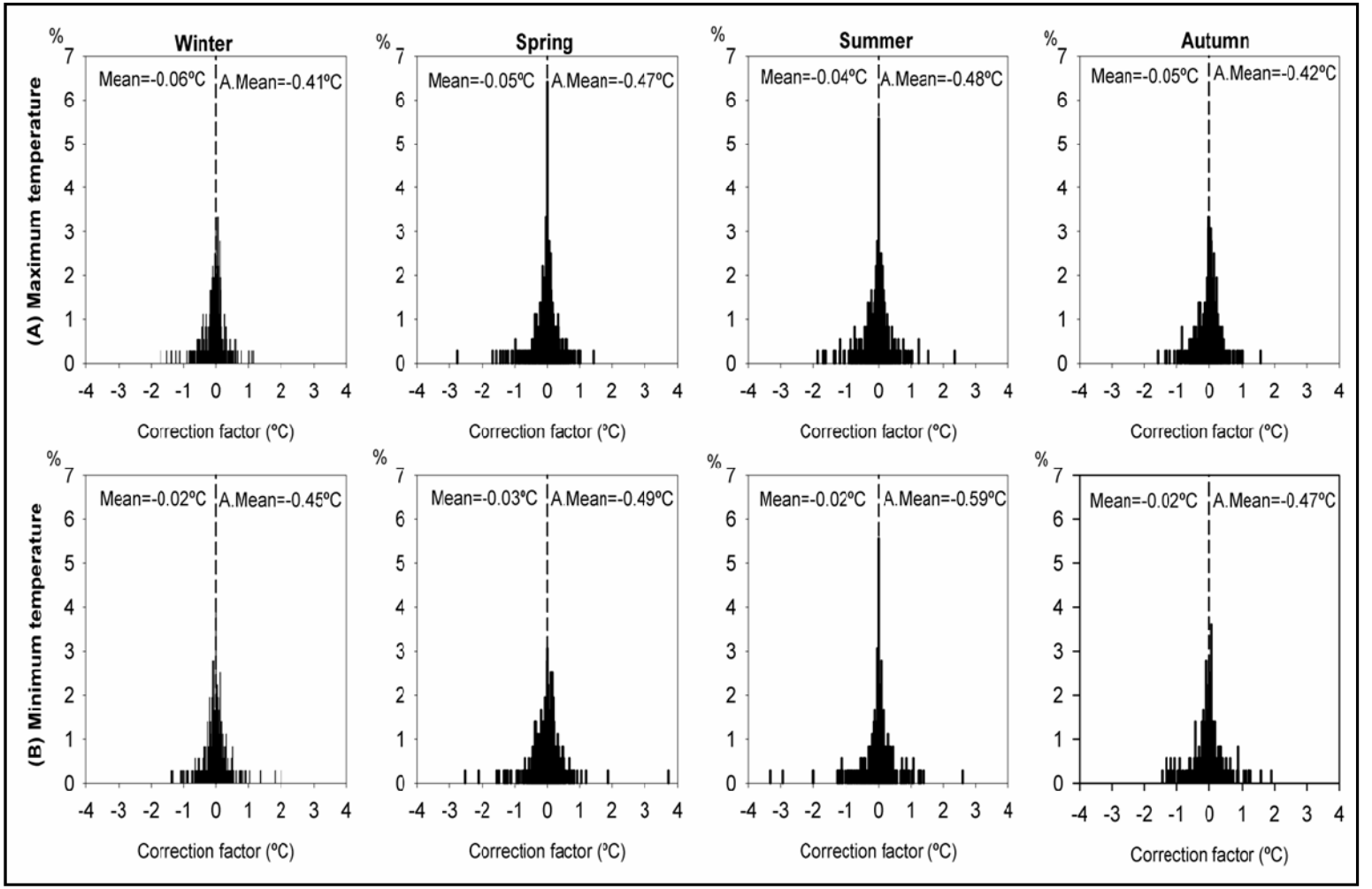

Figure 2.12: Frequency distribution of the correction factors (ºC) applied to a) maximum and b) minimum temperature time series averaged for each season. The values of the mean (absolute mean) of the correction factors averaged for all time series are also provided. Vertical ine denotes the average.

As shown, T statistic reached its critical value (95% significance level) around the year 1968. Nonetheless, the displacement from the mean disappeared after eliminating the detected inhomogeneity. Another example is presented in Figure 2.14, which corresponds to spring minimum temperature at Els Hostalets de Balenya (Barcelona). As illustrated, a statistically significant break was presented close to the year 1956. The differences between the candidate and the reference series and their t-test results indicate that T-value for the adjusted data was below the 95% confidence limit.

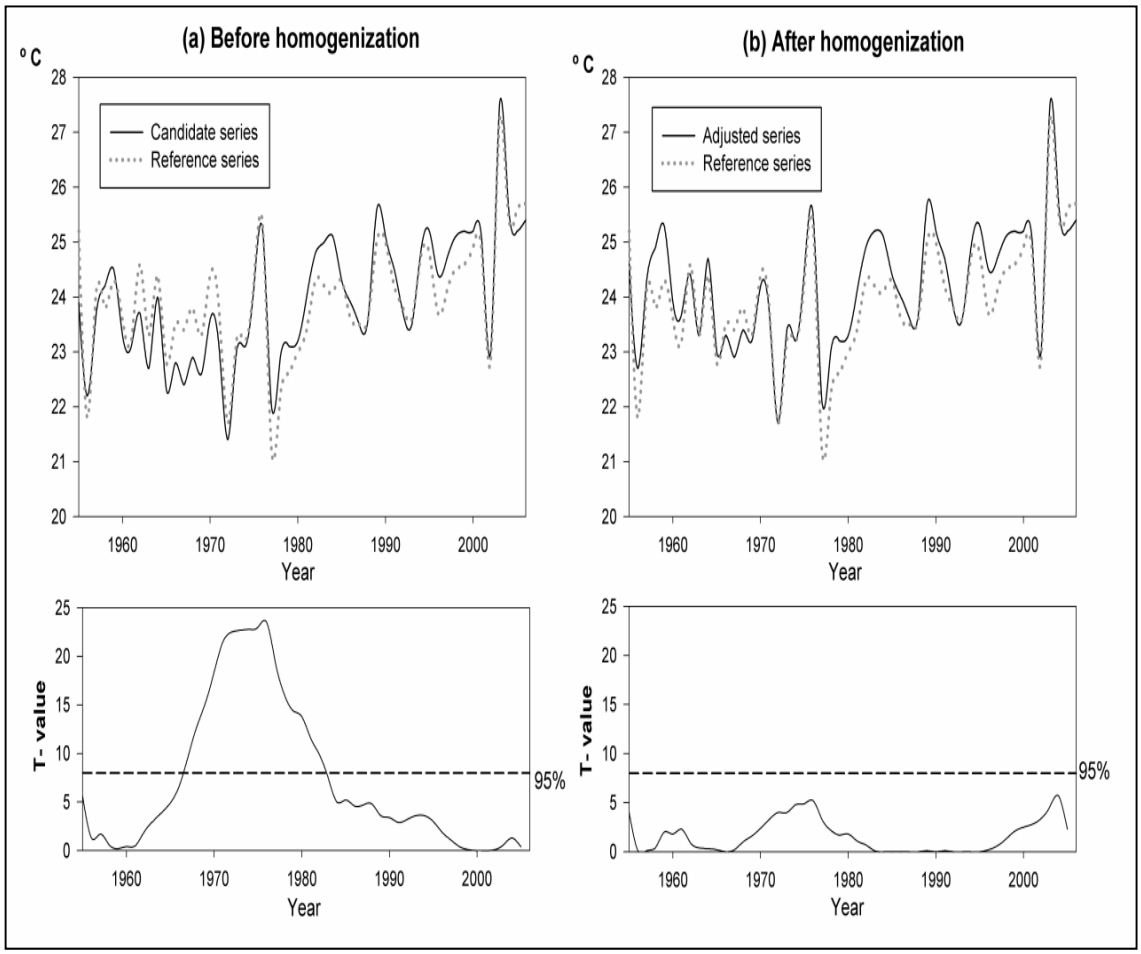

Figure 2.13: Test results of the SNHT applied to summer maximum temperature series at Fuenterrabia aeropuerto, [Guipuzoca] (a) before and (b) after homogeneity corrections. Dashed lines indicate the 95% significance level. The test statistic (T) is plotted against the critical value.

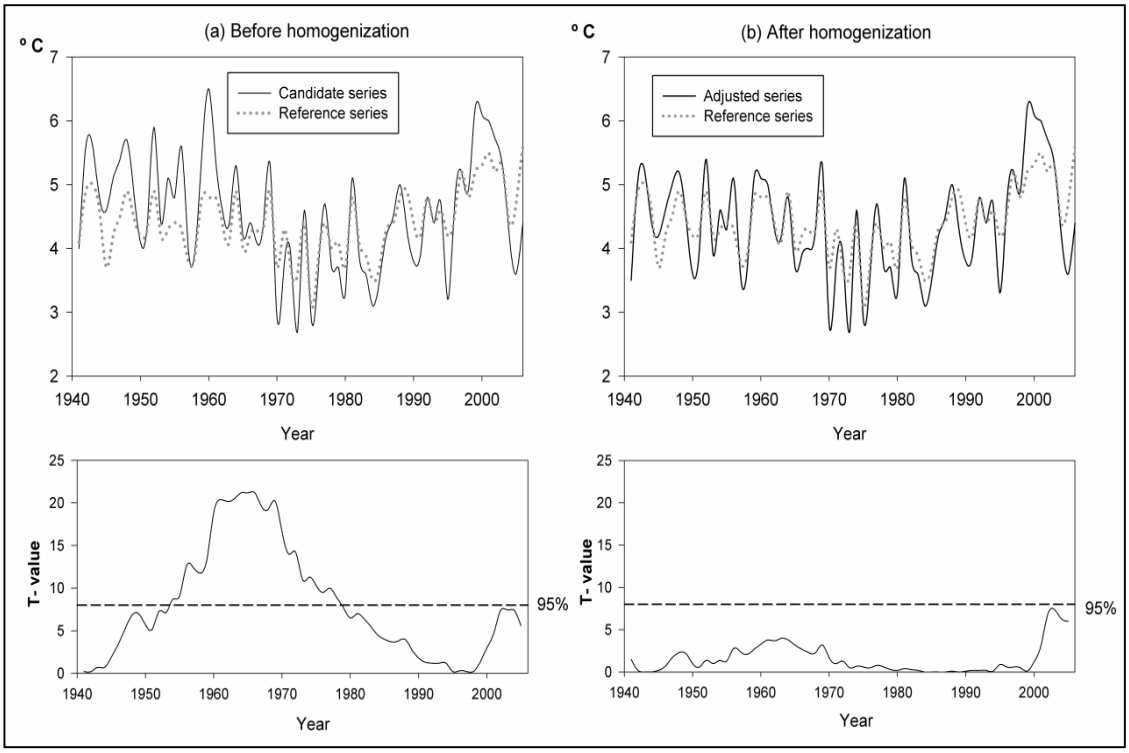

Figure 2.14: Same as Figure 2.13, but for spring minimum temperature series at Els Hostalets de Balenya [Barcelona].

2.8. Indicators on the reliability of the adjusted dataset

In the following section, an evaluation of the reliability of the newly developed daily adjusted dataset is outlined. The aim was to assess the sensitivity of temperature series to the adjustment procedure in terms of any significant change in their statistical properities (e.g., the mean, variance, extremes and statistical distribution).

2.8.1. Impact of the homogeneity protocol on trends

Table 2.4 presents the results of the cross-tabulation analysis applied to trends in the annual maximum and minimum temperature for each pair of stations (i.e. before and after homogeneity correction). In this section, construction of the pivot tables was only

restricted to the annual trends to give an indicative example of the cross-categorized frequency of the trends. In general, the results did not largely reflect considerable differences in the sign (direction) of the trends. As shown in Table 2.4, the cells lie off the diagonal of the pivot table (grey shading) implies that the corrections did not affect trends direction The oppositely directed trends were only evident in 25 (25.5 %) and 44 (44.9 %) of maximum and minimum temperature series, respectively. This clearly implies that in most cases the adjustment had no discernible effect on the direction of the gained trends. Perhaps this arises from the small correction factors applied to the majority of observatories at the monthly scale, which in turn disappear when aggregated to the annual timescale (refer to Figure 2.12). Another possible explanation can be linked to the fact that most of the detectable inhomogeneities were found in the 1970s and 1980s, a period which exhibited a remarkable warming trend worldwide (Jones and Moberg, 2003). Under this warming, the low magnitudes of correction factors failed to alter the direction of the observed variability in the series.

Spatial differences between the trends in the raw and corrected annual temperature series are illustrated in Figure 2.15. It seems that the adjustments had a very local impact on trends, whereby observatories located along the Mediterranean coast experienced more warming after homogeneity correction. This is more apparent for minimum temperature. The picture is almost uniform since the trends of the series before and after adjustment showed coherent spatial structure of the signs. A quick inspection of the trend assessment results indicates that the most convincing impact of adjustments on trends was mainly related to changes in the magnitude rather than the sign (direction) of the trend.

Table 2.4: Results of the cross-tabulation analysis applied to trends in annual maximum and minimum temperature series from 1950 to 2006 before and after homogenization. Significance is assessed at the 95% level. Numbers between brackets indicate the fraction of observatories.

After homogenization	Before homogenization					
	Maximum temperature			Minimum temperature		
	Positive	Negative	Insignificant	Positive	Negative	Insignificant
Positive	63 (64.3 %)	2 (2 %)	18 (18.4 %)	49 (50 %)	5 (5.1 %)	36 (36.8 %)
Negative	0 (0 %)	0 (0 %)	0 (0 %)	0 (0 %)	0 (0 %)	0 (0 %)
Insignificant	5 (5.1 %)	0 (0 %)	10 (10.2%)	1 (1 %)	2 (2 %)	5 (5.1 %)
Total	98			98		

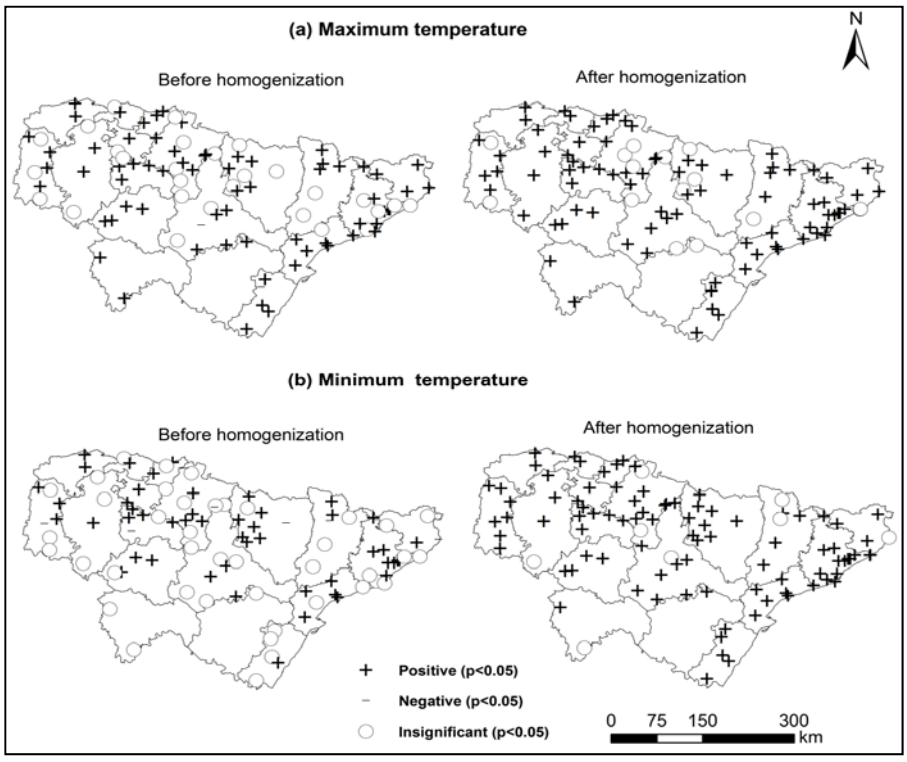

Figure 2.15: Spatial distribution of the trends in the annual (a) maximum and (b) minimum temperature time series before and after homogeneity corrections. Trend calculation is based on the period 1950-2006 and statistical significance is assessed at the 95% level.

Figure 2.16 depicts scatter plots showing the differences in the magnitude of the linear trends (ºC decade^{-1}) between the original and adjusted time series. For most seasons, the trends after correction were not linearly consistent with those before correction. The correction was generally in the range of -0.23 (summer minima) to 0.17 (autumn maxima). This suggests a considerable impact of the adjustment procedure on the slope of both seasonal and annual time series.

One typical example corresponding to the observatory of Yebra de Basa (Huesca) is shown in Figure 2.17. The linear fit of the raw and homogenized series indicates that both series showed uptrend over the period from 1950 to 2006. Nevertheless, the tendency toward warmer conditions was weaker after adjusting the series (0.1ºC decade^{-1}), compared with the series prior to correction (0.3ºC decade^{-1}). Another example corresponding to the annual minimum temperature at the observatory of San Sebastian “Igueldo” [Guipuzcoa] confirmed the same finding as minimum temperature showed slightly more warming (0.22ºC decade^{-1}) after adjusting the series (Figure 2.18).

In the same sense, Figure 2.19 strongly suggests that the temporal behavior of the adjusted series as predicted by the semivariance models was spatially more dependent compared with the raw series. This higher spatial continuity was markedly apparent in all seasons for both maximum and minimum temperatures. Given that eliminating inhomogenities likely reduces signal-to-noise ratio in the time series, it can thus be expected that the homogeneity adjustment accounted for the improvement in the spatial continuity of the trends after correction.

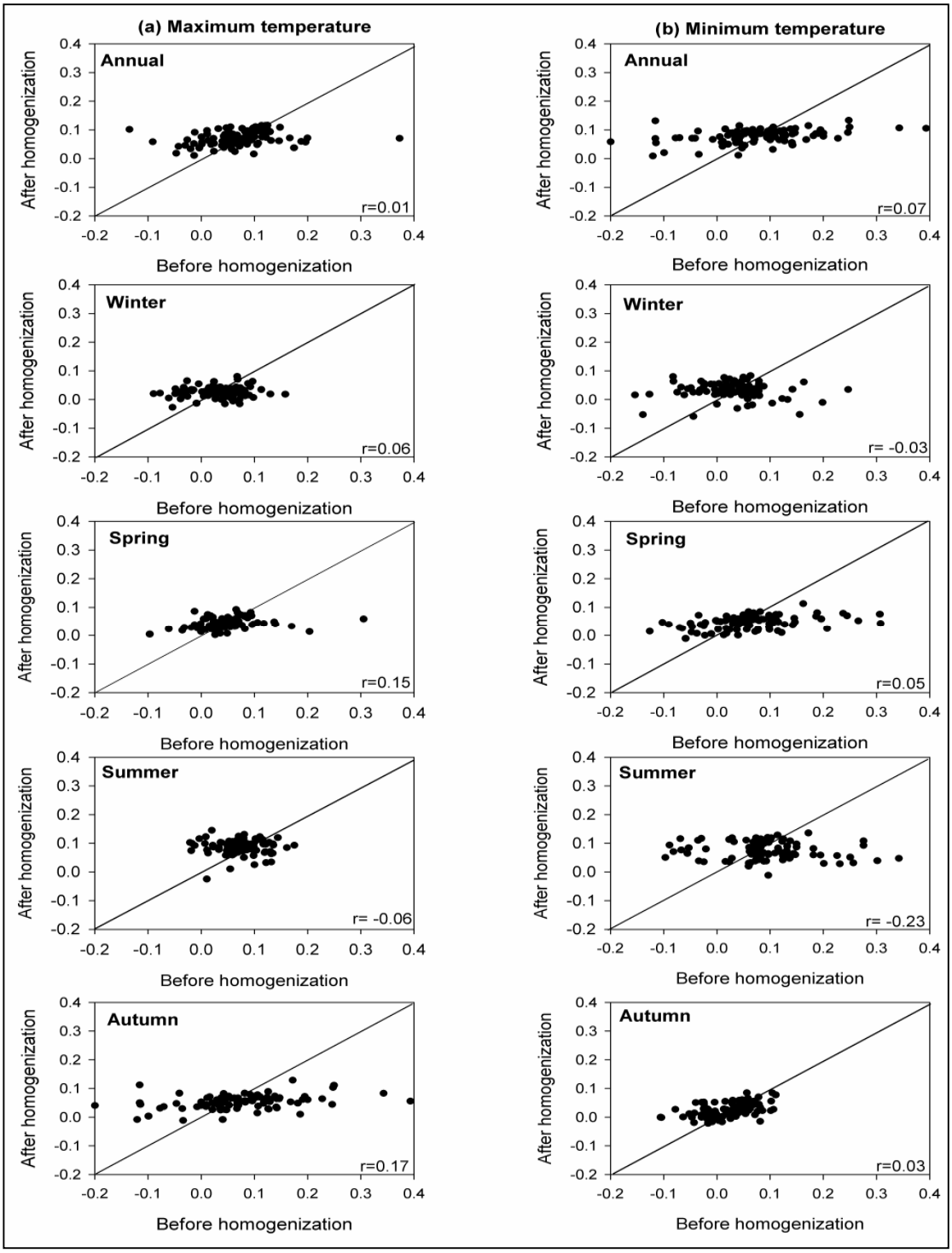

Figure 2.16: Scatter plots of the magnitude of the trends (ºC decade^{-1}), as derived from the seasonal and annual trend analysis for (a) maximum and (b) minimum temperature before and after homogeneity corrections. The trends were assessed for the period from 1950 to 2006.

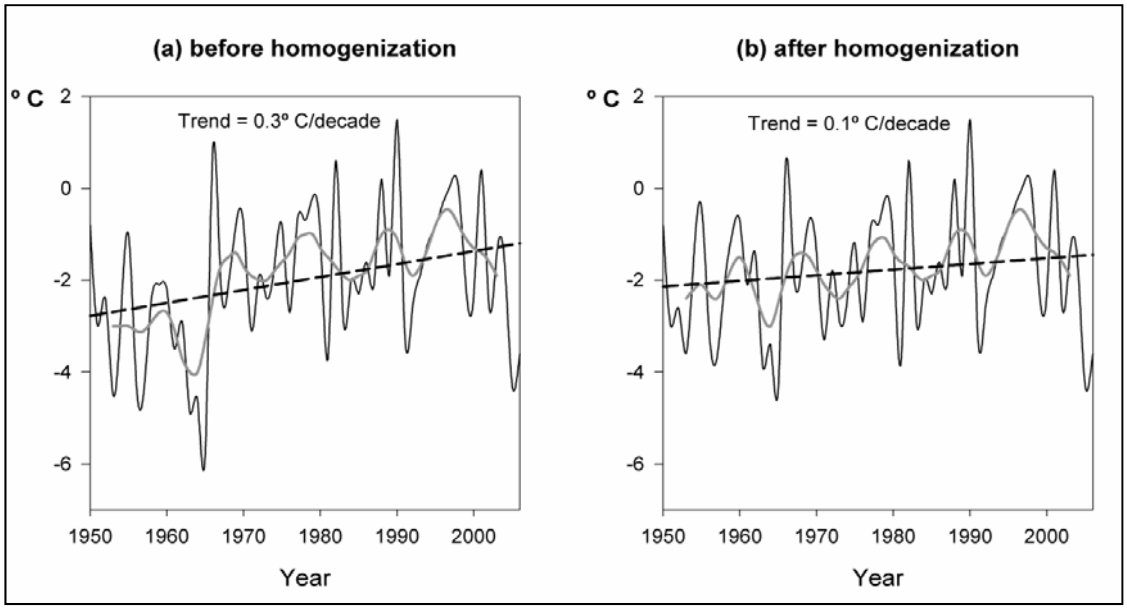

Figure 2.17: Trends in wintertime minimum temperature at the observatory of Yebra de Basa (Huesca) (1950-2006) (a) before and (b) after homogeneity corrections. Gray line corresponds to a low-pass filter of 9-years.

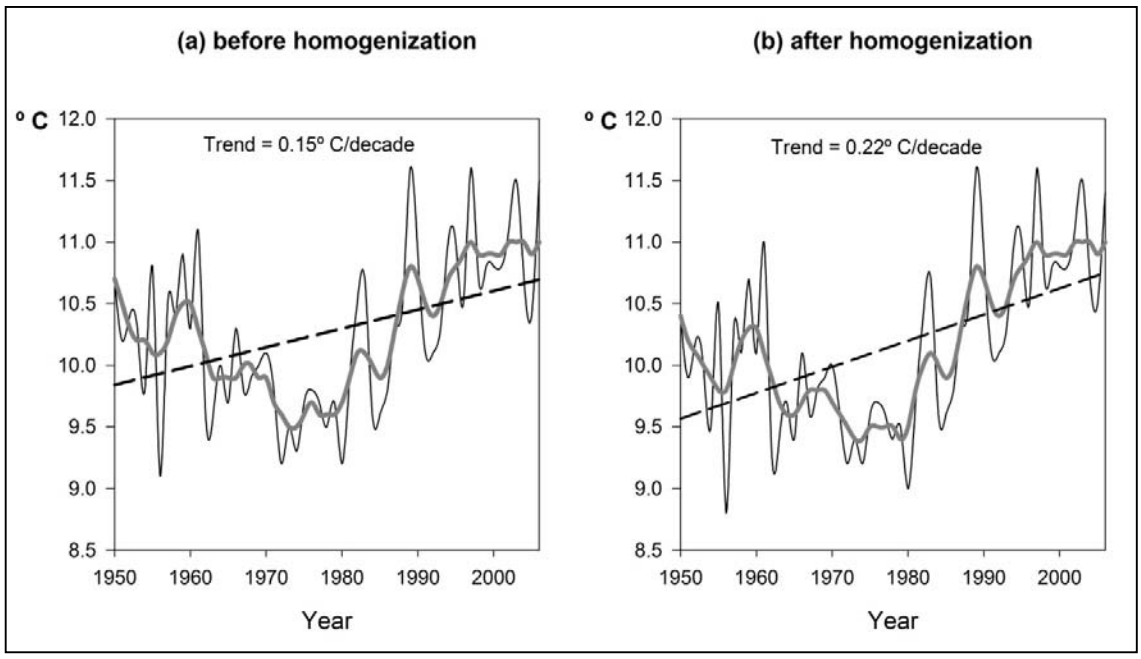

Figure 2.18: Same as Figure 2.17, but for annual-average minimum temperature at the observatory of San Sebastian “Igueldo” [Guipuzcoa].

2.8.2. Impact of the homogeneity protocol on extreme events

The homogeneity procedure applied in this work may affect extreme temperatures in different ways including: frequency, intensity and persistence. Figure 2.20 compares the semivariance models of the trends in warm and cold days indices before and after homogeneity correction. A quick visual inspection of the semivariance models indicates that the spatial heterogeneity of the series markedly decreased after applying the homogeneity correction.

Trends in extreme events did show high level of spatial consistency for the adjusted series, as neighboring observatories tended to have more identical patterns. In contrast, the raw series exhibited certain abrupt jumps over small distances. This implies that the variance of the raw data was higher, suggesting a weaker spatial component. By contrast, the high spatial continuity of the corrected data simply indicates that the spatial coherence among observatories was predominantly attributed to similar temporal evolution at short distances. It is worthwhile to indicate that the influence of adjustments on spatial dependency of cold days climatology was slightly less apparent compared with warm days (Figure 2.19). This can primarily be linked to the fact that minimum temperature during wintertime shows higher spatial variability compared with other seasons, as a consequence of the joint effect of strong circulation influences and high topographic-induced thermal contrasts. Overall, the high degree of spatial coherence in temperature extremes after correcting inhomogeneities provides a strong guidance on the reliability of the adjusted dataset.

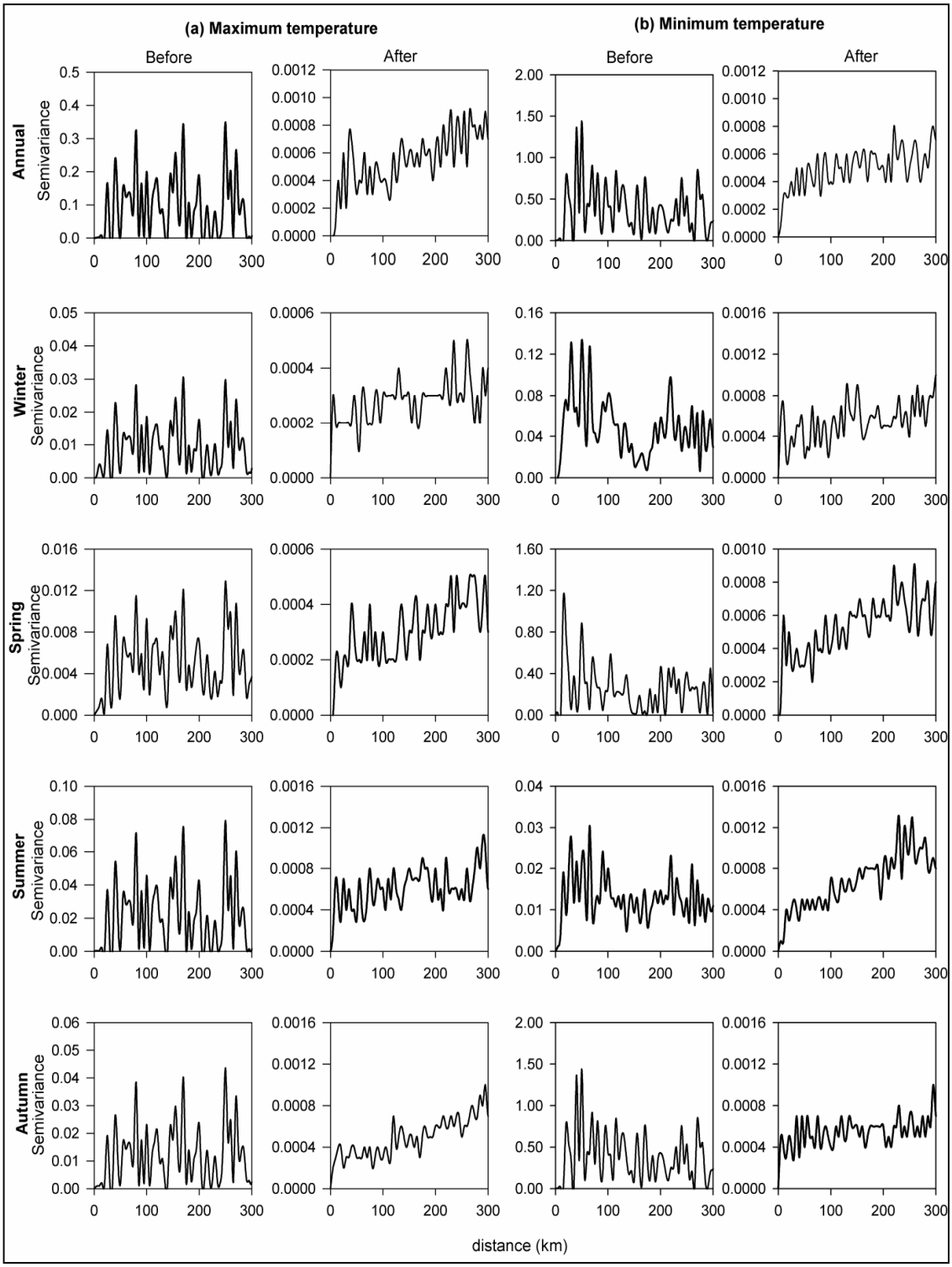

Figure 2.19: Semivariance of the magnitude of the annual and seasonal trends for (a) maximum and (b) minimum temperature before and after homogeneity corrections.

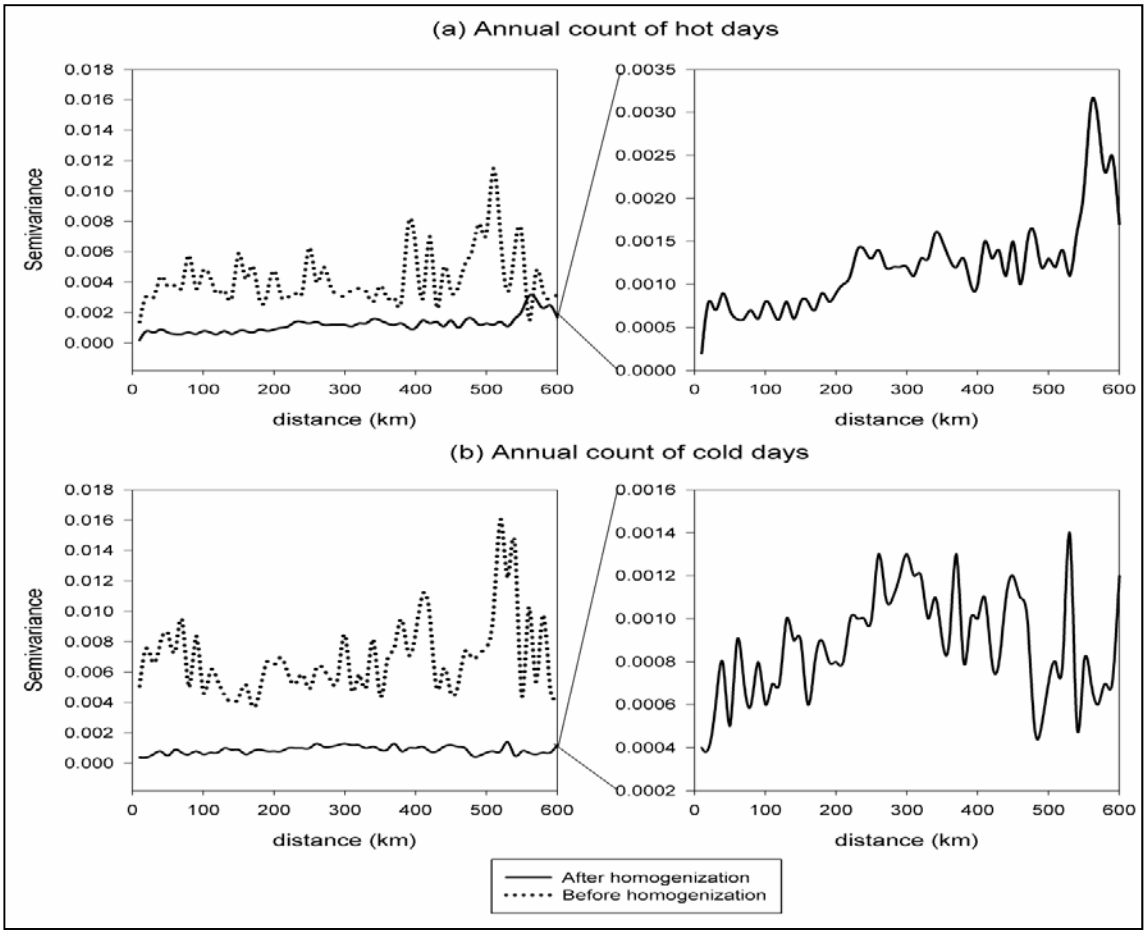

Figure 2.20: Semivariance of the magnitude of trends in the annual count of (a) warm and (b) cold days calculated for the 57-year time series (1950-2006) before and after homogeneity corrections.

2.8.3. Impact of the homogeneity protocol on statistical properties of the series

Figure 2.21 shows the relationships between L-moment statistics (i.e. variance, skewness and kurtosis) before and after homogenization. A comparison of the parent distribution of L-moments permits the assumption that the frequency distribution of temperature series before and after adjustment was generally coincided with a clear linear well-fit. This was evident for both maximum and minimum temperature time

series, whereby strong and statistically significant positive correlations were remarkably apparent between the series before and after adjustment (generally r > 0.8). This clearly implies that the statistical attributes of the adjusted series in terms of variance, skewness and kurtosis were almost attained to similar values as inferred from the series prior to the homogeneity adjustment. The observed bias in the frequency distribution of a few time series was generally negligible.

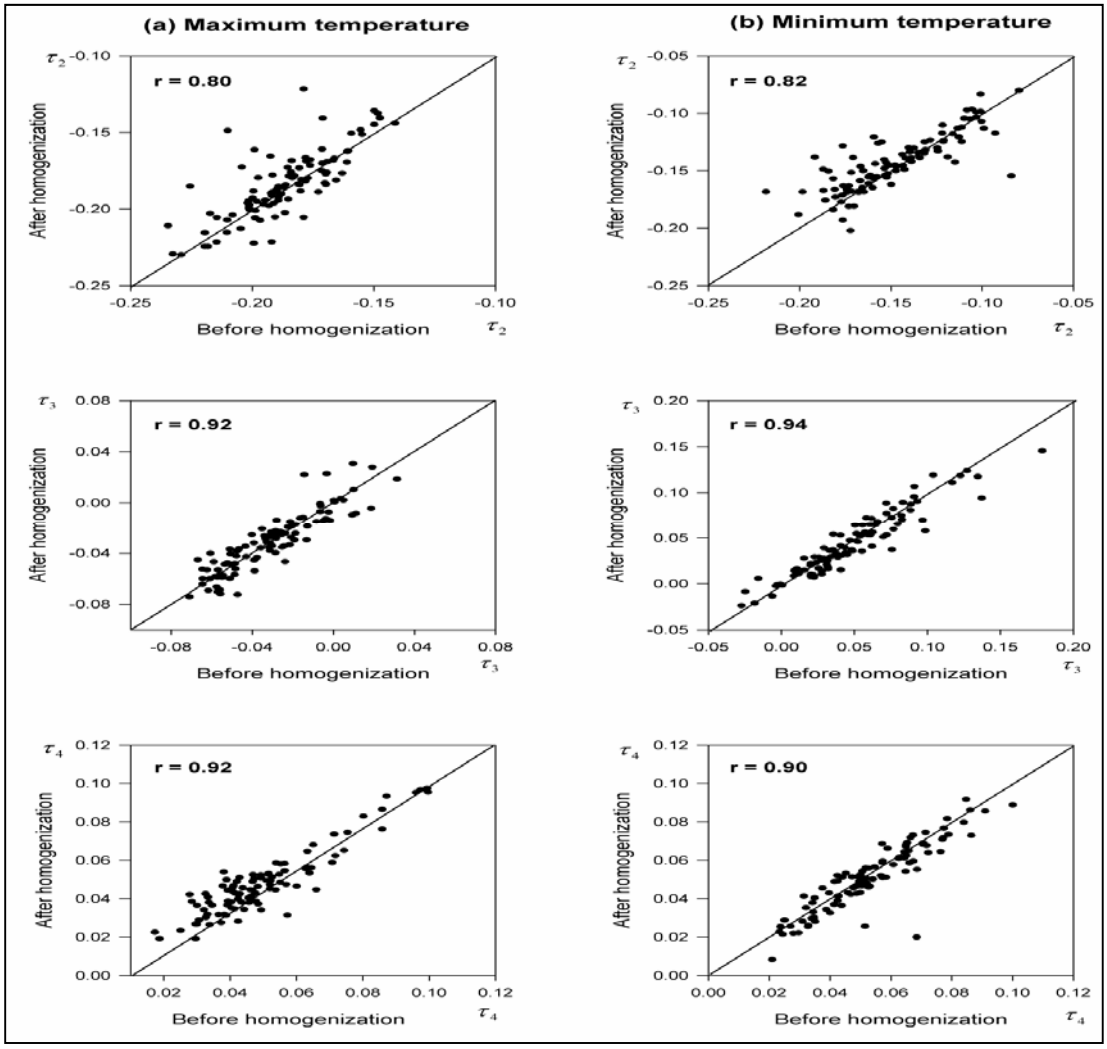

Figure 2.21: L-moment coefficients calculated for (a) maximum and (b) minimum temperature time series before and after homogeneity corrections.

Taking these results together, it can be noted that the homogenous dataset preserved the same statistical distribution of the original dataset. The same finding was also confirmed by means of the semivariance models as illustrated in Figure 2.22.

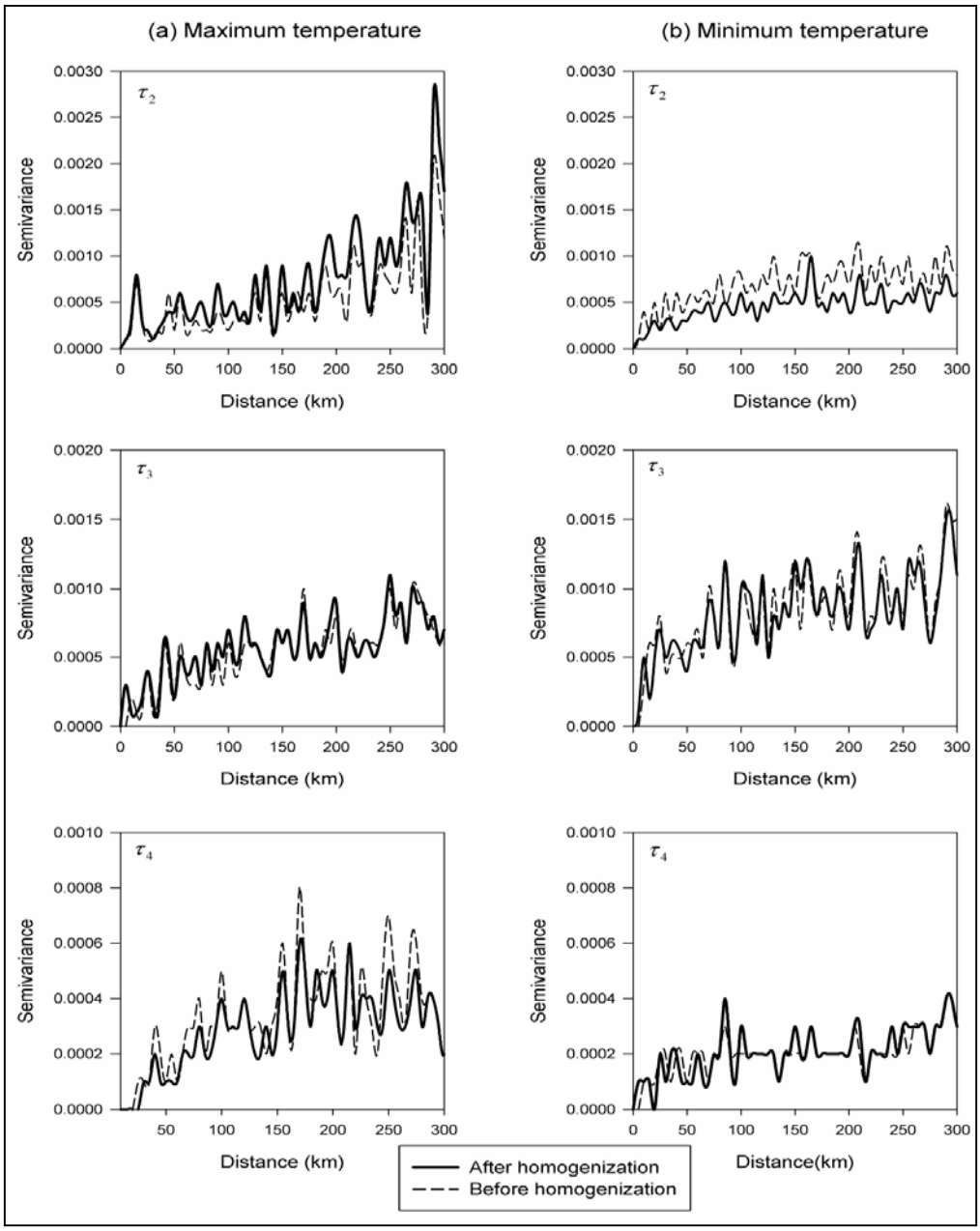

Figure 2.22: Semivariance of L-moment coefficients of (a) maximum and (b) minimum temperature time series before and after homogeneity corrections.

The semivariance models of L-moment statistics reveal that the statistical properties of the adjusted series were rather similar to those of the raw series. In addition, the spatial association of L-moment coefficients still suggests a decrease in the spatial association between the series as distance increases. Distant observatories likely had larger variance which in turn pointed toward heterogeneous spatial patterns. This also gave good indication on the spatial dependence of the statistical attributes of the series after homogeneity correction.

2.8.4. Impact of the homogeneity protocol on inter-station correlation

Inter-station correlation is one of the most important features that can describe the improvement in the temporal dependency of the dataset after eliminating inhomogenities. Figure 2.23 depicts the inter-station correlation before and after correcting inhomogeneities. It clearly reveals higher inter-station correlations for the adjusted series with relevance to the raw data for both maximum and minimum temperatures. This was particularly the case for correlation matrices calculated for the original as well as the first difference series. As Peterson and Easterling (1994) demonstrated that correlation coefficients among the series are very sensitive to the presence of inhomogeneities, the inter-station correlation improved as a consequence of the removal of the noise from the series after adjusting the detectable breaks. Figure 2.23 also indicates that the inter-station correlation was higher among nearby locations, while it gradually decreased beyond large distances. This demonstrates that the homogenized dataset is spatially dependent, with more similar temporal variability among nearby sites. This finding implies that the new compiled dataset is more robust to capture the regional variability of temperature across the study region.

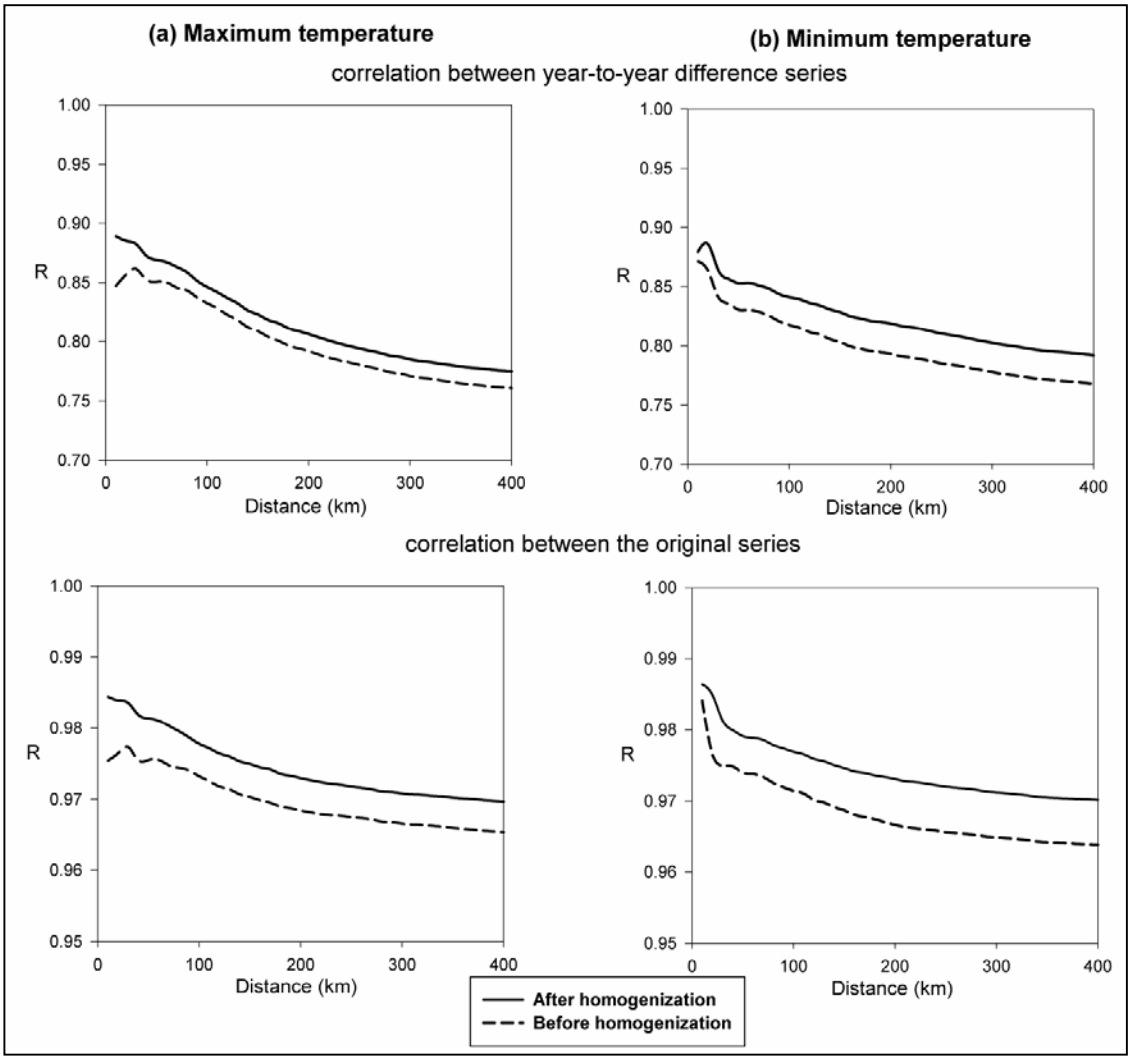

Figure 2.23: Average Pearson correlation coefficient of (a) maximum and (b) minimum temperature time series computed for all observatory pairs as a function of distance before and after homogeneity corrections. The upper (lower) panel belongs to the first-difference (original) temperature dataset.

2.9. The final dataset: a description and evaluation

In this work a dense daily temperature database spanning the period between 1900 and 2006 was developed for northeastern Spain. The main focus of this study was to employ all available information in the original dataset (1583 raw series) provided by

the Spanish Meteorological Agency to build a spatially and temporarily high-resolution temperature dataset. Figure 2.24 illustrates the temporal evolution of the number of available series in the newly compiled dataset. The temporal coverage of the new dataset clearly improved in terms of series completeness. The number of complete and homogenous time series that dates back to 1920, 1950, 1960 and 1970 is 19, 98, 128 and 189, respectively. A list of all available observatories in this adjusted dataset and their main spatial and temporal characteristics is provided in Appendix A.

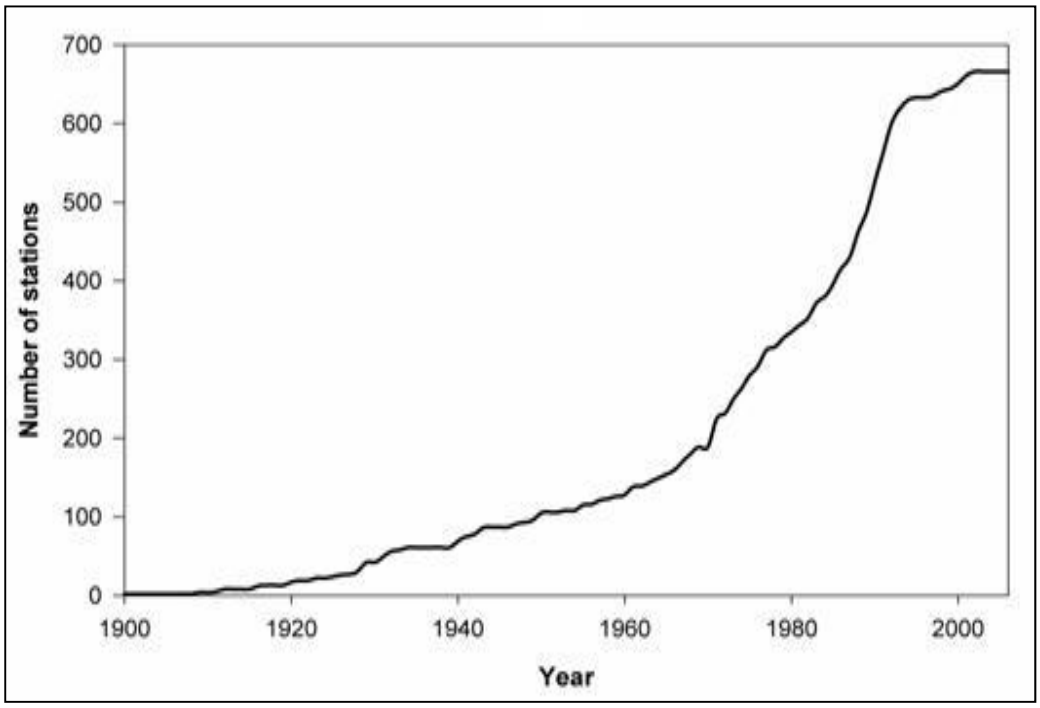

Figure 2.24: The number of the final complete and homogenous temperature series for the period from 1900 to 2006.

The spatial distribution of the final dataset is given in Figure 2.25, while their distribution according to the administrative province is shown in Figure 2.26. Both figures inform that the spatial density of the series is satisfactory across much of the

study domain (e.g., Catalonia and Lerida in the east, and Cantabria and Vizcaya in the northwest), with the exception of some areas in the southern and south-central portions (e.g., Soria and Guadalajara). This is expectable due to lack of station density in such regions in the original network.

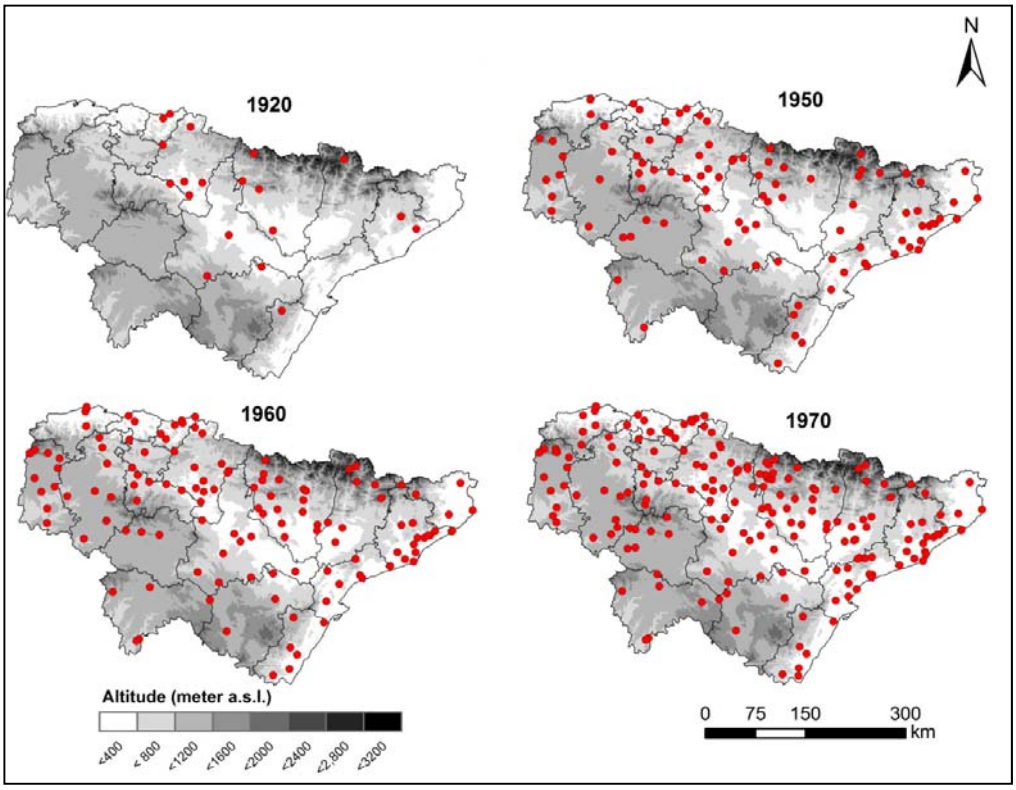

Figure 2.25: Spatial distribution of the final network of complete and homogenous temperature series from 1900 to 2006.

As illustrated in Figure 2.25, the densest network is found from 1970 onwards. During this period, the observatories distribution across portions of the mountainous areas (e.g., the Pyrenees and the Iberian system) is irregular since only 14.4 % of observatories are located above 1000 m. As depicted in Figure 2.27, the observatories are mainly located in the elevation range of 6 up to 1920 m a.s.l., with the majority of them (70.1 %) being placed at elevations below 800 m a.s.l. This uneven vertical

distribution is expected given that higher elevations were not adequately represented by the data in the original dataset.

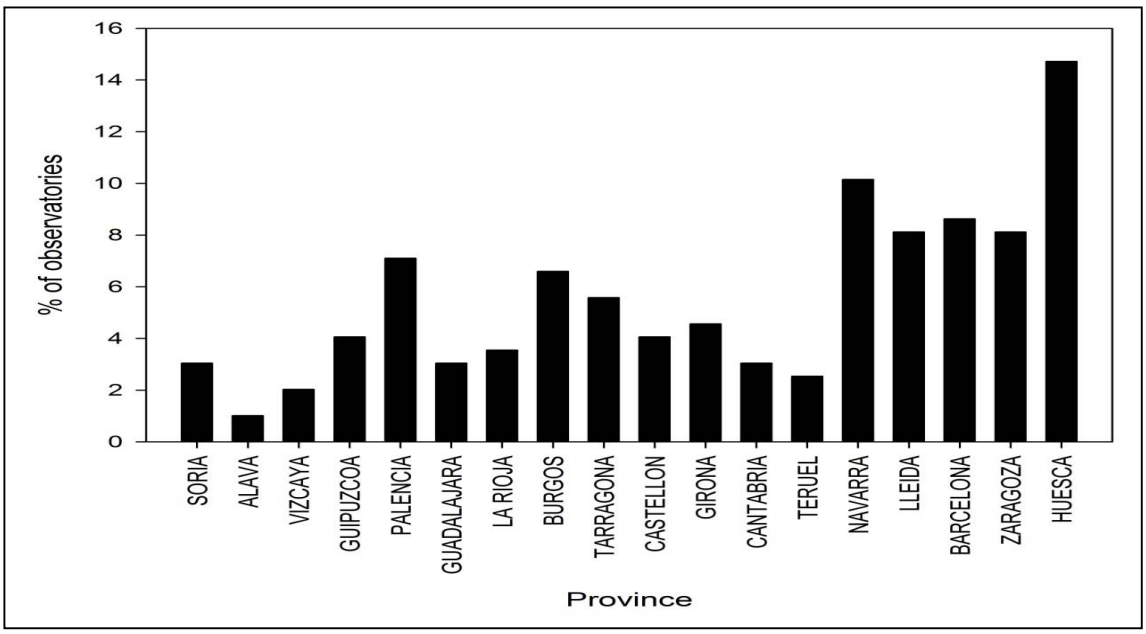

Figure 2.26: Distribution of the final dataset according to the province from 1970 to 2006.

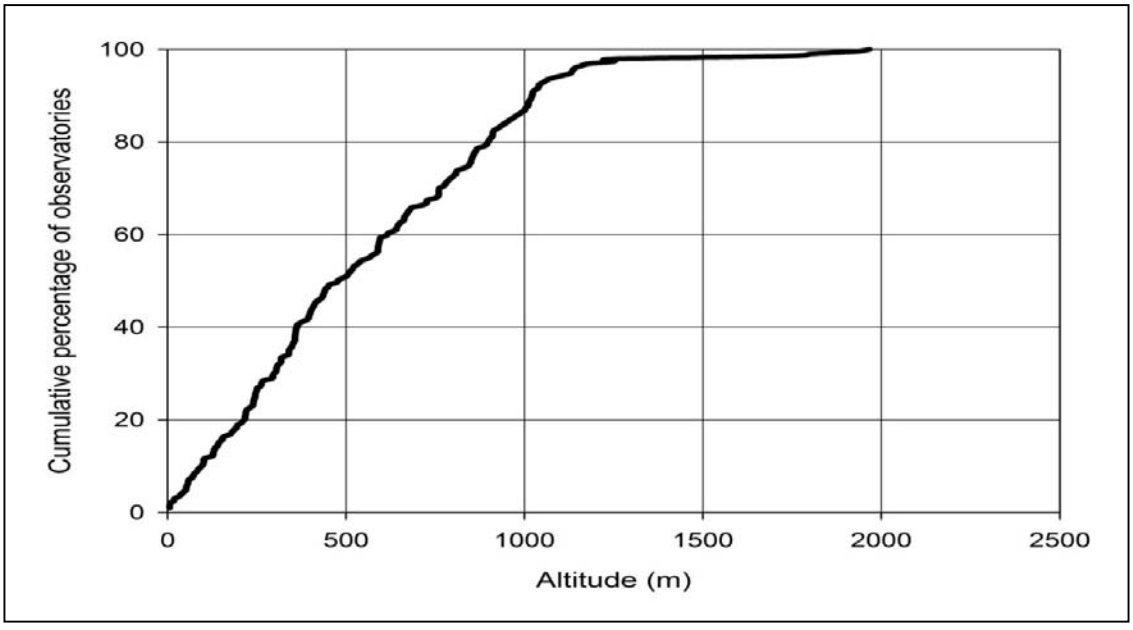

Figure 2.27: The cumulative distribution of the number of observatories in the final dataset as a function of altitude from 1970 to 2006.

2.10. Summary

In this work the procedure used to create the daily adjusted dataset for northeast Spain can be seen with confidence. This dataset passed through multiple steps to assure its quality, completeness and homogeneity. The original dataset was first quality controlled to remove anomalous and suspious data. This procedure was proved to be sensitive to trim outliers and keep only valuable extremes. A linear regression model was then undertaken to infill gaps in daily temperature series using information captured from the surrounding observatories. This regression model is simple, straightforward, applicable and robust when dealing with extreme values. Furthermore, it accounted for the dependency between temperature and topography gradients, particularly in areas of complex terrain. To account for possible breakpoints in the reconstructed time series, three well-established RHTs were used to test homogeneity of the series at monthly, seasonal and annual timescales. Afterwards, a monthly correction factor was calculated and interpolated to daily values to eliminate inhomogeneities from the daily series. A combination of the results of three homogeneity tests was advantageous because these tests had different sensitivities to defining discontinuities in the time series. Moreover, this approach helped determining not only strong breakpoints in temperature time series, but also small shifts.

In this thesis, a great deal of effort being put into developing techniques to assess how the homogeneity methodology affected spatial and temporal characteristics of the final time series. For this reason, this work provided a suite of statistical tests for screening of different aspects in which the break correction can affect temperature series. By means of the spatial semivariance statistic and L-moment statistics, it was possible to look at a broad array of time series characteristics (e.g., means, extreme values and

frequency distribution). These methodologies were applied comparatively to the series before and after adjustment to realistically evaluate impacts of the break correction on the final dataset. In practice, the semivariance models were proven as efficient in describing and analyzing spatial structure of temperature means and extremes. L-moment statistics also provided a consistent tool to assess changes in the statistical properities of the series (i.e., variance, kurtosis, and skewness). Following these techniques, it was clearly evident that the homogeneity adjustment significantly improved the spatial and temporal structure of both temperature means and extremes. Given that evaluation of the impact of homogeneity routines on final climatological products has not obtained much attention in the literature, these methodologies can offer a useful approach for the assessment of homogeneity impacts on climate time series. In general, these methodologies are objective, flexible, reproducible, and can therefore be applied in similar environments.

To conclude, this newly compiled database comprises the most complete and homogenous time series of maximum and minimum temperature for northeastern Spain. From the spatial and temporal perspectives, this dataset is unique and represents an advance compared with previous datasets available for surface air temperature in the Iberian Peninsula. Considering the high spatial and temporal resolution of the final dataset, it can contribute to better understanding of space-time variability of temperature and its driving causes at both local and regional scales. Moreover, this dataset can be useful to understanding the causes and impacts of local and regional climate changes on hydrological systems, ecosystems, natural resources and human activities. In the study domain, this feature is of high importance due to its complex topography and diverse climates. Moreover, this dataset considerably

overlaps with some available precipitation datasets over the region (e.g., Vicente-Serrano et al., 2009). For instance, from 1960 to 2006, 82.8% of temperature observatories have adjacent precipitation data. This sounds important as it permits a detailed regional analysis of the combined effect of temperature and precipitation on different disciplines in the region. Finally, this developed climatology can enhance the grid resolution of any climatic study in future with more potential to validate climate simulations from Regional Climate Models (RCMs).

CHAPTER THREE

METHODOLOGICAL FRAMEWORK

3. METHODOLOGICAL FRAMEWORK

3.1. Introduction

The primary objective of this thesis was to determine quantitatively the observed and projected changes of surface air temperature in northeastern Spain and to assess the main drivers behind this variability. The following paragraphs will elaborate the methods used to achieve this goal in more detail. Unless mentioned, the analyses were based on daily maximum and minimum temperatures of a dataset of 128 observatories spanning the period from 1960 to 2006. The prerequisites for selecting these observatories for subsequent analyses include length, data completeness (i.e., no missing values), and quality (i.e., consistence and homogenous data). Also, as previously detailed, this dataset is free from the effects of non-climatic factors (e.g., urbanization, industrialization and changes in surrounding environments). This is critical to ensure that the observed changes in temperature across the study domain reflect natural variability and/or global warming rather than non-climatic processes.

The (1960-2006) time interval was selected as a base period in this thesis due to the observed rise in the global temperature since the 1960s, as reported in many previous studies (e.g., Jones et al., 1999). Additionally, the dataset offered a reasonable spatial density of temperature observatories from 1960 onwards, which can adequately give insights into the main climate regimes across much of the study domain. Locations of the weather observatories belonging to the 1960-2006 period are illustrated in Figure 3.1. The analyses were conducted at both seasonal and annual timescales. Seasons were defined as: winter (December-February; DJF), spring (March-May; MAM), summer (June-August; JJA) and autumn (September-November; SON).

3.2. Observed changes in seasonal and annual mean temperatures

Seasonal and annual changes in maximum, minimum, and mean temperatures and DTR were assessed using the ordinary least squares (OLS) method, while the significance of the observed trends was tested at a confidence interval of 95% using the non-parametric Spearman *Rho* statistic. In case of normally distributed and serially independent climate variables (e.g., temperature), the OLS method often yields the maximum likelihood estimator of the regression coefficients. In the same context, the Spearman *Rho* is advantageous because it is robust to outliers and does not assume prior probability distribution of the residuals (Sneyers, 1990). The slope of the least squares regression was used to assess the magnitude of change and was expressed in units of ºC per decade. In this analysis, the trend was firstly calculated for a subset of 19 observatories that has data from 1920 to 2006. The availability of a reasonable number of temperature time series, which dates back to the earlier decades of the 20th century, motivates a detailed assessment of such long-term changes in temperature across the study domain. This kind of assessment has poorly been addressed in previous studies in the region in particular and over Iberia in general. The spatial distribution of temperature observatories covering the period from 1920 to 2006 is presented in Figure 3.2 and their main characteristics are provided in Table 3.1. The analysis was then extended to the denser network from 1960 to 2006 in order to obtain a more detailed regional assessment of temperature variability. In this work, 3000 Monte Carlo simulations were used following the procedure described by Kundzewick and Robson (2000). This procedure was applied to each season and annually. Numerous previous studies applied this technique to resampling climate data at random. This procedure aimed to ensure that the observed variability in climate data is

real and not a statistical artifact originating from suspious variability (e.g., Lettenmaier at al., 1994; Adamowski and Bougadis, 2003).

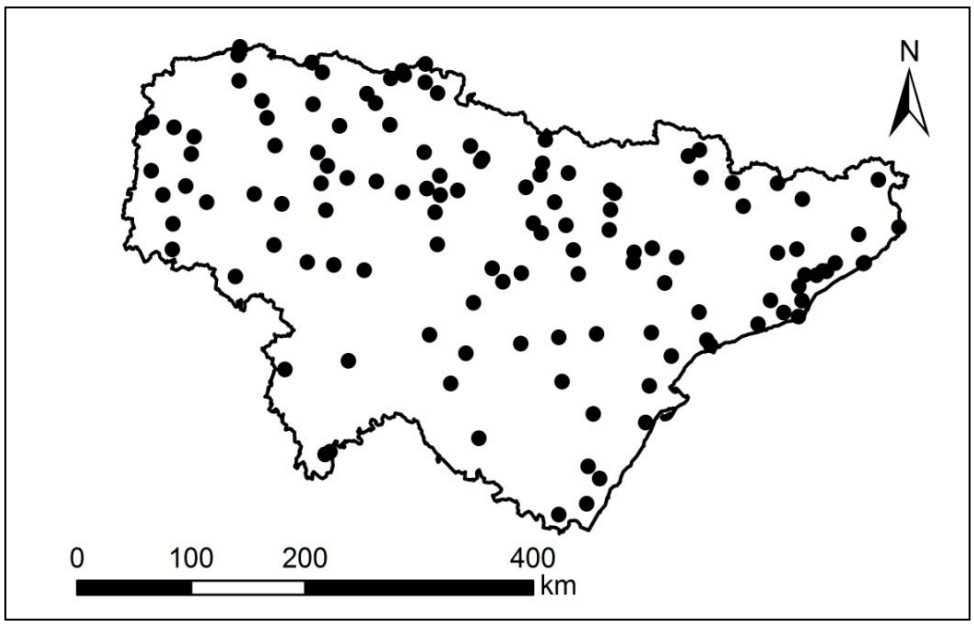

Figure 3.1: Spatial distribution of temperature observatories from 1960 to 2006.

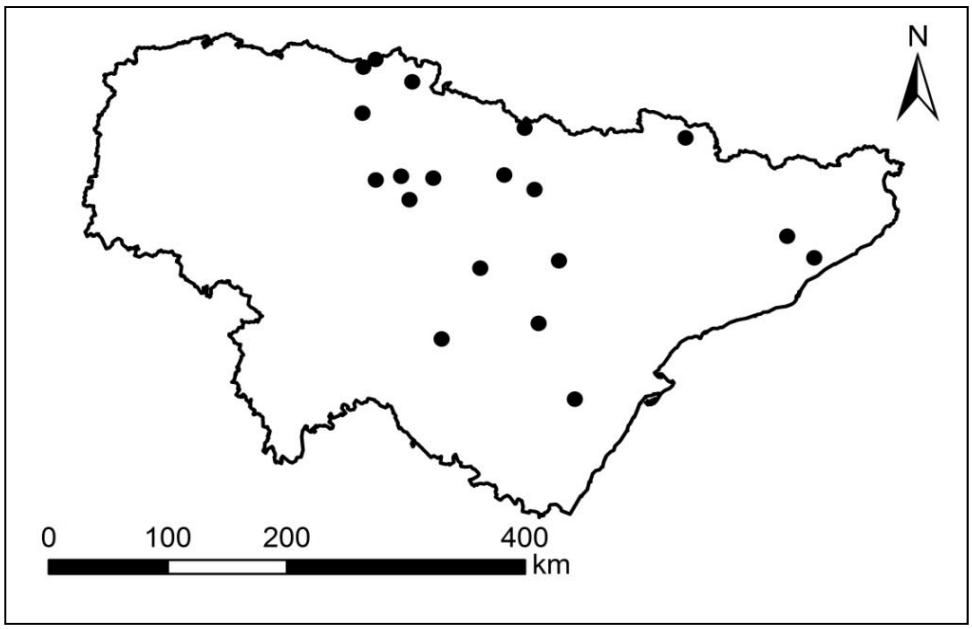

Figure 3.2: Spatial distribution of temperature observatories from 1920 to 2006.

A low-path Gaussian filter was then applied to the original time series to smooth out the interannual variability and provide more robust trends by removing high-frequency fluctuations from the data (Sneyers, 1992).

Table 3.1: List of the observatories used for trend analysis from 1920 to 2006.

WMO CODE	OBSERVATORY	PROVINCE
0120	MOIA	BARCELONA
0213	CARDEDEU	BARCELONA
1006	SANTESTEBAN	NAVARRA
1024E	SAN SEBASTIAN 'IGUELDO'	GUIPUZCOA
1035U	AYA-LAURGAIN	GUIPUZCOA
9174	SARTAGUDA	NAVARRA
9198	CANFRANC LOS ARA/ONES	HUESCA
9246	CARCASTILLO LA OLIVA	NAVARRA
9269	ALSASUA	NAVARRA
9281	FALCES	NAVARRA
9283	CADREITA	NAVARRA
9390	DAROCA OBSERVATORIO	ZARAGOZA
9434	ZARAGOZA AEROPUERTO	ZARAGOZA
9474	LA PEðA 'EMBALSE'	HUESCA
9547	LA PUEBLA DE HIJAR	TERUEL
9562	MORELLA	CASTELLON
9657	ESTERRI D'ANEU	LLEIDA
9900	NUENO	HUESCA
9910	PALLARUELO DE MONEGROS	HUESCA

To reveal the overall picture of temperature variations in the study area as a whole, regional series of maximum, minimum, and mean temperatures and DTR were constructed on an annual basis and for all seasons. The regional series were built using two different manners. Over the period 1920-2006, a regional series based on the arithmetic average of the daily records from the 19 observatories belonging to this time interval was composed. This approach is simple, straightforward, and standard when dealing with a limited and a sparse station network. Recalling that the regional

series for the period 1960-2006 were built from a dense network of 128 observatories, a weighted average from all the observatories on the basis of the scale of the area on which the series is aggregated was computed by means of the Thiessen polygon method (Jones and Hulme, 1996). This approach is advantageous given that the spatial coverage of the data is relatively uneven in particular areas (e.g., southern portions), which may distort the large-scale area average. In other words, this method controls the bias that can be yielded from averaging regions with a higher spatial density of observing stations.

3.3. Observed changes in temperature extreme events

3.3.1. Definition of temperature extreme events.

Extreme weather refers to infrequent, but significant, departures from the normal weather conditions. Climate change may affect extreme temperatures in different ways (e.g., frequency, intensity, persistence). However, assessment of changes in weather extremes remains a challenge because of the rare occurrence of these events. In particular, the likelihood of this assessment also decreases significantly with increasing rarity of the event (Frei and Schär, 2001; Klein Tank and Können, 2003; Schär et al., 2004). In literature, there is no unique definition of extreme event as several definitions have already been proposed and applied in recent climate studies (e.g., Alexander et al., 2006; IPCC, 2007). In these studies, climate indices are commonly used to provide a convenient summary of the changing state of the climate. In climate change studies, indices of extreme events can describe different aspects of these events (e.g., frequency, intensity and persistence).

In this work, a set of 21 indices were used to examine spatial and temporal variability of temperature extremes. In this work, all the indices were calculated on an annual basis for each independent time series during the 47-year period (1960-2006). Table 3.2 provides a detailed description of these indices grouped into three main categories. In this work, it is beneficial to apply various climate indices to obtain a broad and more reliable picture of temperature behavior in the study area. It is believed that inclusion of different definitions of temperature extremes can make the assessment more representative and objective, particularly for capturing micro-climatic characteristics. Also, comparing the results on trends from different climate indices is important to explore whether the observed trends are internally consistent over the region. Furthermore, the information derived from different indices could be valuable for climate change impact studies. Indeed, the influence of anthropogenic climate variability on changes in a single extreme index (e.g., warm nights) cannot be clearly distinguished in space. This is simply because any given characteristic of an extreme event still has a probability to be influenced by natural variability. Moreover, inclusion of only one feature could be spatially biased or might have a limited effect on both natural and human environments. For example, summer days (SU25) may not be viewed as extremes over lowlands with gentle topography. For these reasons, using various characteristics of extreme events (e.g., frequency, intensity and persistence) could improve the understanding of their changing likelihood under global warming. The different aspects and properties of extreme temperature on the one hand, and the various applications of these characteristics for climate impact and assessment studies on the other hand, can be brought together best if the various aspects of extremes are considered.

Table 3.2: List of all temperature indices and their definitions.

	Index	Definition	Unit
Cold extremes	Cold days ($TX10_p$)	Percentages of days with maximum temperatures lower than the 10th percentile.	days
	Cold nights ($TN10_p$)	Percentages of days with minimum temperatures lower than the 10th percentile.	days
	Frost days (FD0)	Number of days with minimum temperature < 0 ^oC per year.	days
	Ice days (ID0)	Number of days with maximum temperature < 0 ^oC per year.	days
	Coldest night (CN)	Lowest daily minimum temperature.	^{o} C
	Very cold nights ($TN1_p$)	Number of days with minimum temperature <1st percentile per year.	days
	Annual high minimum (TN_x)	Maximum value of monthly minimum temperature.	^{o} C
	Annual low minimum (TN_n)	Minimum value of monthly minimum temperature.	^{o} C
Warm extremes	Warm days ($TX90_p$)	Percentages of days with maximum temperatures higher than the 90th percentile.	days
	Warm nights ($TN90_p$)	Percentages of days with minimum temperatures higher than the 90th percentile.	days
	Summer days (SU25)	Number of days with maximum temperature >25 ^oC per year.	days
	Warmest day (WD)	Highest daily maximum temperature.	^{o} C
	Very warm days ($TX99_p$)	Number of days with maximum temperature >99th percentile per year.	days
	Tropical nights (TR20)	Number of days with minimum temperature >20 ^oC per year.	days
	Annual high maximum (TX_x)	Maximum value of monthly maximum temperature.	^{o} C
	Annual low maximum (TX_n)	Minimum value of monthly maximum temperature.	^{o} C
Variability extremes	Temperature sums (T_{sums})	Sum of Tmax days >17^o C – days Tmax < 17 ^oC	^{o} C
	Intra-annual extreme temperature range (Intr)	Difference between the highest Tmax and the lowest Tmin in the year.	^{o} C
	Diurnal temperature range (DTR)	Monthly mean difference between Tmax and Tmin.	^{o} C
	Standard deviation of Tmean (Stdev)	Standard deviation of daily mean temperature from the Tmean normal.	^{o} C
	Growing Season Length (GSL)	Annual count of days between the first span of at least 6 days with Tmean >5 ^oC. and first span after 1st july of 6 days with Tmean < 5 ^oC.	days

As indicated in Table 3.2, the indices were defined in different ways, varying from a certain fixed threshold (e.g., summer days [SU25] and tropical nights [TR20]) to a percentile-based threshold (e.g., very cold nights [TN1p], warm days [TX90p], and cold days [TX10p]). In general, the percentile-based indicators are defined as days passing the warmest/coldest deciles at one tail of the observed probability distribution of maximum and minimum temperatures. In this work, the percentiles were computed at each site for the entire period from 1st January 1960 to 31st December 2006 to account for both cold and warm temperatures. This is a commonly used method to determine extreme values in climatology (Salinger and Griffiths, 2001; Alexander et al., 2006; Trenberth et al., 2007; IPCC, 2007). Recently, a growing number of studies have dealt with changes in temperature extremes using indices representing count of days crossing climatolological percentile thresholds (e.g., Prieto et al., 2004, Brunet et al., 2007b, Rodriguez-Puebla et al., 2010). For example, Prieto et al. (2004) assessed changes in cold days over peninsular Spain in the period from 1955 to 1998 using a threshold of the 5th percentile of Tmin distribution during the cold half of the year (NDJFM). Similarly, Brunet et al. (2007b) studied changes in cold nights (Tmin<10th percentile) and warm days (Tmax>90th percentile) across the Spanish territory from 1850 to 2005. These definitions are objective, site-independent, and facilitate direct comparisons between regions of different climates (Choi et al., 2009). The study area is a typical case, whereby complex terrain and diverse climates are evident. As illustrated in Figure 3.3, an exploratory screening of the 90th percentile of maximum temperature calculated from 1st January 1960 to 31st December 2006 revealed considerable differences. Overall, the values varied from 20ºC at Port del Compte [Lleida, 1800 m a.s.l] to 34.8ºC at Salto de Zorita [Guadalajara, 642 m a.s.l].

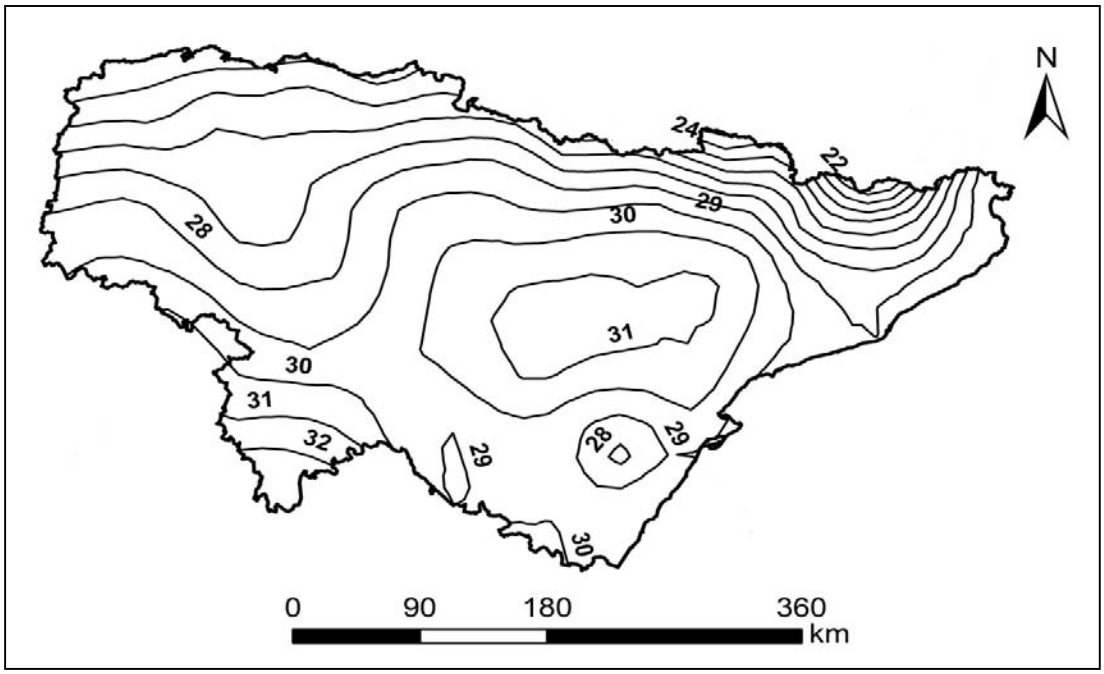

Figure 3.3: Spatial distribution of the 90th percentile magnitude calculated for the annual maximum temperature from 189 observatories covering the period 1970-2006.

On the other hand, the arbitrary-based definitions of temperature extremes identified data outlying pre-fixed thresholds. For instance, frost days (FD0) were defined as days with daily minimum temperature below 0ºC. Previous works also adopted these arbitrary thresholds (e.g., Klein Tank and Konnen, 2003). Calculation of temperature indices in that way is straightforward and more appropriate for climate impact assessments, particularly at fine spatial scales. Also, these definitions can be more valuable when the defined thresholds have physical, hydrological or biological meaning (Politano, 2008). Lastly, some other indices were employed to analyze the relationship between maximum and minimum temperature. This group of indices includes intra-annual extreme temperature range (Intr), diurnal temperature range (DTR), and standard deviation of the daily mean (Stdev). For example, Stdev index is

used as a measure of the departure from the mean condition. Under the global warming, Stdev values are expected to be higher during warm years. Therefore, it can be a good indicator of temperature interannual variability.

In practice, all the selected indices are relevant to the Spanish context. They encompass the most important aspects of temperature extremes, including: intensity, frequency, and variability. In addition, they summarize characteristics of both moderate weather events (e.g., SU25, TX90p, and TN10p) and extremely severe events (e.g., TX99p and TN1p). These indicators have been previously validated by the World Meteorological Organization (WMO, 2009), the European Climate Assessment (ECA) (http://eca.knmi.nl/), and the European project of Statistical and Regional dynamical Downscaling of Extremes (STARDEX EU) for extreme temperature research (http://www.cru.uea.ac.uk/projects/stardex/).

3.3.2. Trends calculation: methodological considerations.

Previous studies dealing with changes in climate extremes have investigated the possible sources of uncertainty in trend assessment (Caussinus and Mestre, 2004; Moberg and Jones, 2005; Zhang et al., 2005). According to these studies, trend assessment of extreme events can have a level of uncertainty arising from many sources such as serial correlation, cross-correlation, data inhomogenities, and the period of investigation. For instance, Zhang et al. (2005) assessed the influence of inhomogenities in the time series on calculation of the percentile-based indices. Also, Moberg and Jones (2005) underlined the way in which overestimated exceedance rates at the boundaries of the selected base period can affect trend assessment. A closely related problem that has also been extensively discussed in many climatological (e.g., Aguilar et al., 2005; Zhang et al. 2005; Vincent et al. 2005; Aguilar

et al. 2009; Vincent et al., 2011) and hydrological (e.g., Yue et al., 2002; Burn and Cunderlik, 2004; Yue and Wang, 2004) studies is the presence of serial correlation and spatial correlation in the time series. Following these studies, it is essential to look at such confounding effects to assure the reliability of the trend results obtained in this work. In this section, the possible influence of serial correlation and spatial autocorrelation on trend assessment is addressed.

3.3.2.1. Serial correlation

Typical time series data are usually statistically dependent due to existence of non-random components, such as persistence, cycles or trends (WMO, 1966). Among them, serial correlation often occurs in climatic time series, whereby warm (cold) years are more likely to be followed by warm (cold) years. The Mann-Kendall statistic is not robust against serial correlation in that a positive serial correlation in a time series can incorrectly increase the probability of rejecting the null hypothesis (H_0) of no trend (Yue et al., 2002; Yue and Wang, 2002). According to Cox and Stuart (1955), positive serial correlation between the observations would increase the chance of significant answer (i.e., presence of trend), even in the absence of a trend. Thus, it is necessary to ensure the randomness of the extreme temperature series before testing for the significance of trends. In literature, this effect can be eliminated from the time series before applying trend tests, or by modifying the original trend test to account for this effect (Hamed, 2008). Previous researchers have used the autocorrelation function (ACF) to eliminate the effects of serial correlation prior to trend assessment. Box and Jenkins (p.33, 1970) suggested use of the ACF when the number of values (n) is close to 50 and the number of lags is at most $n/4$. In this work, all serial correlation coefficients of the time series were calculated for lags from 0 to 14. This was

principally done to increase the ability of the test to define serial correlation at different lag times. When the lag-1 correlation coefficient was significant at the 95% level ($p<0.05$), the presence of serial correlation was verified and removed from the detrended series prior to perform the trend analysis following a Trend Free Pre-Whitening (TFPW) procedure. This method has been suggested by Yue et al. (2002), as a modification of the standard pre-whitening method developed by Von Storch and Navarra (1995). The TFPW procedure is outlined below:

1. The first step assessed the statistical significance of the trend using the Mann-Kendall non-parametric test and estimated the trend component (β) by a linear least squares method, as:

$$\chi = a + \beta t \tag{3.1}$$

where *a* is a constant, *β* is the slope and *t* is time.

2. The second step eliminated the monotonic trend (β) from the observed data series, yielding a de-trended series, as:

$$Y_i = S_i - \beta i \tag{3.2}$$

where Y_i is the value of the de-trended series at time *i* and S_i is the observed value at time *i* .

3. The third step calculated the lag-1 serial correlation coefficient (μ1) for the de-trended series and assessed its statistical confidence ($\rho<0.05$). If μ1 was statistically insignificant, the Mann-Kendall results derived from (Eq. 3.1) was applied directly to the original time series. Otherwise, the pre-whitening procedure was accomplished by removing the lag-1 autoregressive process (AR [1]) from the de-trended time series, as follows:

$$Y_i'' = Y_i - \mu_1 Y_{i-1} \tag{3.3}$$

where $Y_i^{''}$ is the pre-whitened series at time *i*. Herein, the AR (1) process was favored over the moving average (MA) process because the linear trend component is the commonly assumed model for temperature time series.

4. The fourth step added back the component of the trend (β) to the pre-whitened series $Y_i^{''}$ to obtain a serially independent time series.
5. Finally, the statistical significance of the trend was assessed for the serially independent series by means of the Mann-Kendall statistic at the 95% significance level.

The aforementioned approach has been frequently used to remove serial correlation from time series in hydrology (e.g., Yue et al., 2002; Burn and Cunderlik, 2004) and climatology (e.g., Zhang et al., 2000).

3.3.2.2. Cross-correlation

It is generally recognized that cross-correlation in climatological dataset can likely influence the accuracy of trends assessment (Lettenmaier at al., 1994). The cross-correlation can increase the probability of detecting a trend in the time series while there is no trend. Basically, closer observatories are more likely to show similar trends. This likely reduces the number of independent time series and, in turn, the effective number of freedom degrees for trend tests (Douglas et al., 2000). Further discussion of possible impacts of cross-correlation on trend assessment can be found in Lettenmaier at al. (1994), Douglas et al. (2000), Adamowski and Bougadis (2003) and Kurbis et al. (2008).

In literature, numerous bootstrap resampling schemes have been developed to account for spatial correlation in climatological datasets (e.g., Lettenmaier at al., 1994; Douglas et al., 2000; Adamowski and Bougadis, 2003; Kurbis et al., 2008). The rationale behind this procedure was to determine whether local changes or trends observed at individual observatories are related to the global (field) trend obtained for the whole region. In this context, it is well-known that temperature shows high spatial dependency in comparison with other climate variables (e.g., precipitation). Therefore, in order to assess the impact of cross-correlation, it is important to remove the temporal structure from the original dataset so that all the series become non-stationary. One possible way is to resample the original data at random. This procedure will preserve the correlation and dependence structure of the original data because the same year will be sampled from the original time series in each run. In this work, a bootstrap resampling procedure was applied to evaluate the significance of trends at both the global and local level. Simply, the estimated global significance derived from *n* samples for a particular index was compared with the observed local significance computed for the individual observatories (*n*=128). The bootstrap resampling procedure is summarized in the following steps:

1. A set of 1000 Monte Carlo simulations with a length of 47-year was generated for each time series at random from the observed data (1960-2006). Following Kundzewick and Robson (2000), the simulated time series were extracted from the original dataset by replacement with equal probability. According to this step, each particular index had two sets (original with 128 time series, and simulated with 128*1000 time series).

2. The statistical significance of each time series in the original and the simulated datasets was assessed using the Mann-Kendall statistic. The percentage of the trends that are significant at each α % level was defined. Then, the global (field) significance level was computed as the arithmetic mean of the local significance levels at the individual observatories for each index.

3. The probability of obtaining a trend in the resampled series was compared with the original data for each index. Given that the bootstrap samples had no restricted assumptions in terms of statistical distribution, the Cumulative Distribution Function (CDF) was selected to compare between the observed and the simulated datasets at specific levels of statistical significance. In this sense, the non-exceedance probability (P) was calculated using the Weibull distribution, as:

$$P = \frac{r}{B + 1} \tag{3.4}$$

where r is the rank of the data and B is number of the simulated series (1000 in this work).

Douglas et al. (2000) applied a similar approach to define the global significance for low flow rates of streams in the USA.

3.3.2.3. Trend calculation

To account for amount and sign of changes in the derived temperature indices, linear trend was computed using the ordinary least squares (OLS) method. The significance of the trend was assessed using the Mann-Kendall's tau test at the 95% significance

level (p value<0.05). The Mann-Kendall statistic is a rank-based nonparametric test, which is advantageous compared to parametric tests such as the Pearson's correlation coefficient. This is mainly because it is robust to outliers and does not assume an underlying probability distribution of the data series (Moberg et al., 2006). For this reason, this statistic has widely been used in climatological and hydrological applications (e.g., Zhang et al., 2005; Choi et al., 2009).

Let $x_1, x_2, x_3, x_4, \ldots . x_n$ represent *n* data points where x_j represents the data point x at time j. The Mann-Kendall statistic (*S*) can be computed according to Kendall (1975), as follows:

$$S = \sum_{i=1}^{n-1} \sum_{j=i+1}^{n} sign \quad (x_j - x_i) \tag{3.5}$$

where x_j and x_i are the sequential data values and *n* is the length of the data series, and

$$sign \quad (x_j - x_i) \begin{cases} =1 \text{ if } x_j - x_i > 0 & (3.6) \\ =0 \text{ if } x_j - x_i = 0 & (3.7) \\ =-1 \text{if } x_j - x_i < 0 & (3.8) \end{cases}$$

A positive value of *S* is an indicator of an increasing trend, and a negative value indicates a decreasing trend.

Herein, it is worthwhile to indicate that, for each particular extreme index, the trend assessment was conducted for each individual observatory in the period 1960-2006. In addition, the trend was also calculated for the regional series which were obtained for the whole region for each particular index. The rationale behind this procedure was to

test whether detected trend in temperature extremes at each station occurred due to local conditions or revealed a large-scale spatial coherence. In this regard, the regional series were created on the basis of a weighted average of all values in the temperature observatories across the study area. The weight was a function of the surface (area) represented by each observatory following the Thiessen polygon method (Jones and Hulme, 1996).

3.4. Spatial regionalization of extreme events.

Due to the complex topography, latitude and land–sea interactions, climate of the study domain may experience more or less complicated mesoscale patterns of temperature. The possible impacts of climate change in the region can therefore largely depend on the local and regional conditions. In this context, capturing spatial variability of temperature over the study domain sounds important. Nonetheless, this has often been a challengeable task due to the low density of observatories, which fails to represent the complex orography of the domain. Recently, the availability of high spatial and temporal resolution of temperature data in the newly compiled daily dataset in the region can strongly enhance a detailed assessment of spatial modes of temperature in the domain.

In this work, the preference was given to spatially regionalize extreme events rather than mean conditions. Indeed, climate change detection is more often associated with the analysis of changes in extreme events than with changes in the mean (Katz and Brown, 1992). Indeed, while the warming of the mean may be gradual, the effects of extreme weather events, as induced by climate change, are severe and immediate (Richardson et al., 2009). Moreover, the sensitivity of both natural systems and human

welfare to temperature is maximized during extreme heat events. Also, the impacts of extreme events on mortality, human health and even biological adaptation mechanisms will largely be more severe under the extreme temperature values. For instance, Diaz et al. (2006) found that rates of mortality can dramatically increase when daily maximum temperature exceeds the 95th percentile of the local distribution of maximum temperature.

In northeastern Spain, understanding the spatial variability of temperature extreme events is critical for many reasons. First, spatial regionalization of temperature extremes can be an effective tool not only to obtain a detailed knowledge on spatial variability of extremes at local and regional scales, but also to identify driving forces and mechanisms that may influence these spatial variations. Second, this spatial regionalization can be of particular interest for numerous fields, such as agriculture, human health, urban development and planning, and water resources management. Third, obtaining meaningful spatial patterns of extreme events in the region could facilitate the development of appropriate adaptation strategies to cope with issues arising from climate change. The outcome of any adaption policy is inherently maximized when considered at local and regional scales.

Interestingly, while a growing number of studies have dealt with changes in temperature extremes over Iberia using indices representing count of days crossing climatolological percentile thresholds (e.g., Prieto et al., 2004; Brunet et al., 2007b; Rodriguez-Puebla et al., 2010), majority of these studies have been confined to use a moderate threshold value of 90 or 95 percentiles of daily temperature distribution to define an extreme warm event and, on the other hand, the 5 or 10 percentiles of daily minimum temperature to define cold events (e.g., Prieto et al., 2004; Brunet et al.,

2007b). During the last two decades, a lot of record-breaking temperatures have been observed in the study domain (e.g., summers of 1998, 2003 and 2010 and winters of 2010 and 2012). In winter 1956, the study domain also recorded an exceptional cold spell, in which minimum temperature reached -32ºC at some mountainous sites in the Pyrenees (Estany Gento, Lerida). Although these record-breaking temperatures can be seen as one of the most arising effects of the global warming, they have received little consideration in literature with the exception of only very few works (e.g., Garcia-Herrera et al., 2005; Medina-Ramon et al., 2006; Brown et al., 2008), compared with other measures of moderate extremes which are not as far into the tails of the daily temperature distributions. Among these few studies, Brown et al. (2008) defined the anomalous warm (cold) days using the 98.5 (1.5) percentiles as thresholds. Also, Medina-Ramon et al. (2006) studied the risk of death for days with temperature above the 99th percentile.

Taken together, it is believed that assessing spatial structure of anomalous extreme events in such a complex region is as much important as exploring spatial structure of moderate extreme events. This can mainly be due to specific reasons. First, these anomalous events are very exceptional from the statistical point of view as they are located at the utmost tails of temperature distributions, which could give a good indication of the impact of global warming on temperature change and variability in the region in terms of both changes in the mean and standard deviation. Second, as reported by many previous studies (e.g., Przybylak, 2000; Barriopedro et al., 2011), attribution of changes in extreme events can vary considerably according to the time scale in question. In other words, important information regarding the characteristics of extreme events can be dismissed when anomalies are calculated at longer timescales

(e.g., monthly or seasonal). For example, there is some doubt whether or not characteristics of the warmest/coldest day of a month will be captured when computing monthly or seasonal anomalies. In this regard, the most extreme days reveal more analogous events regardless of the scale under consideration. Third, although these events are considered "short-term" extremes since they represent events that only occur very few times per year; they are characterized by outstanding magnitudes with large spatial extent (e.g., the 2003 summer over the Western Europe, 2010 summer over the Eastern Europe and the 2012 winter over Central and Eastern Europe). Lastly, attribution of changes in these extremely severe events is largely viewed as driven by larger, longer lasting and more dynamically complex physical processes. While, many regional studies suggest that changes in temperature extremes can largely be explained by large-scale processes (e.g., Hurrell, 1995; Slonosky et al., 2001; Sáenz et al., 2001; Brunet et al., 2007b; Rodriguez-Puebla et al. 2010), unfortunately, this dependency has poorly been investigated and still under debate for the anomalous extreme events. Majority of studied linked moderate extreme events to atmospheric circulation. For example, Rodriguez-Puebla et al. (2010) examined the association between warm days (TX90p) and cold nights (TN10p) and large scale fields, including SLP and 500hPa. One possible reason for this deficit is that assessing significance of changes in such anomalous events can be statistically hampered by insufficient sample size for the intended analyses given that very low (high) daily temperatures do not necessarily occur every year at each location. In general, assessing spatial variability of these anomalous events is a key to understanding the physical processes favoring for their occurrence.

3.4.1. Spatial regionalization of moderate extreme events

In this research, the spatial regionalization of moderate extreme events was restricted to summer (JJA) season. Summer was chosen because this is the season which exhibited the strongest signal of temperature variations in the study domain (El Kenawy et al., 2012). Moreover, the environmental, economical and societal impacts of these events on physical (e.g., agriculture, ecology, forest fire, and hydrology) and human environments (e.g., mortality, and energy demand) are more pronounced during the summer periods. A representative example over the study area is the unrelenting 2003 summer heat wave, in which some sites at the Pyrenees reached their maximum value on record exceeding the 35°C threshold.

In this work, multivariate statistical techniques (i.e., principal component analysis [PCA] and cluster analysis [CA]) were used to divide the study region into subregions as homogenous as possible. Herein, the aim beyond this classification was to identify synoptic conditions associated with extreme events in the defined sub-regions. This involves the connection with large-scale atmospheric circulation patterns at the mean sea level (MSL). These multivariate techniques have increasingly gained acceptance to identify homogenous regions in many fields, such as hydrology (e.g., Love et al., 2004), geology (e.g., Reimann et al., 2002), forestry (e.g., Schulte and Mrosek, 2006), soil sciences (e.g., Young and Hammer, 2000), and ecology (e.g., Camiz and Pillar, 2007). In atmospheric research, these techniques have also been carried out at different spatial and temporal scales ranging from regionalization of a specific climate variable such as precipitation (e.g., Wolting et al., 2000), temperature (e.g., Coronato and Bisigato, 1998), and evapotranspiration (e.g., Mohan and Arumugam, 1996) to synoptic classification, including air masses (e.g., Bejaran and Camilloni, 2003) and

large-scale atmospheric circulation and weather types (e.g., Romero et al., 1999; Esteban et al., 2006). In Iberia, these techniques have also been a common tool to obtain homogenous climate regions, with the aim of understanding spatial variability of climate and its physical causes (e.g., Martin-Vide and Gomez, 1999; Muñoz-Diaz and Rodrigo, 2004; Vicente-Serrano, 2006; Serra et al., 2010). For instance, Martin-Vide and Gomez (1999) classified Spain into distinct regions based on the length of dry spells over the period 1951-1990. Similarly, Muñoz-Diaz and Rodrigo (2004) divided Spain into relatively homogenous pluviometric regions using seasonal time series covering the period from 1912 to 2000. More recently, Vicente-Serrano (2006) obtained a regionalization of drought in the Iberian Peninsula employing a monthly precipitation dataset.

To obtain a reasonable classification (regionalization) of summer temperature extremes, a set of selected 14 indices which likely represent most of the variability of these extremes was considered. In particular, these indices potentially included many aspects of changing climate conditions including frequency, intensity and persistence. Those indices were retrieved from the daily dataset corresponding to summers over the period from 1960 to 2006. A list of the indices and their description is given in Table 3.3. Summer season is defined as June to August. Much of the warm extremes typically occur during these June–August peak season months, for which the amount and distribution of temperature generally determine the overall severity during this season. An exploratory analysis of the local distribution of daily maximum and minimum temperatures suggested that little number of warm extremes (e.g., warm days) may remain for the late spring (May) or early autumn (September). Thus, evaluating the behavior of warm extremes only for June–August was employed to

assess extreme temperature variations. For instance, the number of summer days (SU25) was defined as the total number of days per summer with maximum temperature over 25°C. Warm days (TX90p) index was defined based on days in which maximum temperature exceeding the climatological 90th percentile of the local daily temperature distribution during summers from 1960 to 2006. In order to measure the severity of heat stress during summer season, the maximum duration of consecutive warm days was considered using a centered moving window of consecutive (*n*) days exceeding the 90th percentile of daily maximum distribution. These criteria were applied in various studies (e.g., Jones et al., 1999; IPCC, 2007; Fang et al., 2008). Assessing the behavior of consecutive and long lasting warm days can provide invaluable information in impact assessment studies, particularly those related to hydrological and environmental modeling.

3.4.1.1. Statistical analysis:

In this section, a detailed description of a two-step statistical procedure to obtain homogenous regions of summer extreme temperature is provided. First, for each observatory, the magnitude of the trend was obtained from the slope of the linear regression of the 47-yrs (1960-2006) time series by means of the OLS method. This was applied for each particular index. Then, the climatic information as summarized by the trends of the different temperature indices was reduced using factor analysis. The second step examined the spatial regionalization by application of the cluster analysis to the scores of the retained factors gained in the first step. This two-step procedure has previously been recommended by several climate regionalization studies (e.g., Baeryswil and Rebetez, 1997; Romero et al., 1999; Papadimas et al., 2011). As has been proposed by these studies, it was necessary to apply factor analysis prior to cluster analysis to minimize autocovariance in the dataset.

Table 3.3: List of the indices of summer temperature extremes and their definitions.

Index	Description	Symbol	Unit
Max_monthly_min	Maximum value of monthly minimum temperature in summer.	TNx	º C
Max_monthly_max	Maximum value of monthly maximum temperature in summer.	TXx	º C
Min_monthly_min	Minimum value of monthly minimum temperature in summer.	TNn	º C
Min_monthly_max	Minimum value of monthly maximum temperature in summer.	TXn	º C
Diurnal temperature range	Monthly mean difference between Tmax and Tmin.	DTR	º C
Intra-annual extreme range	Difference between maximum Tmax and minimum Tmin in summer.	INTR	º C
Temperature sums	Sum of Tmax days >17º c – days Tmax < 17 ^{o}C in summer.	Tsums	º C
Warmest day	Highest daily maximum temperature.	WD	º C
Spell	Maximum length of consecutive days with daily maximum temperature higher than the 90th percentile	Spell	days
Summer days	Number of days with maximum temperature >25 ^{o}C during summer.	SU25	days
Warm days	Percentages of days with maximum temperatures higher than the 90th percentile.	TX90p	days
Warm nights	Percentages of days with minimum temperatures higher than the 90th percentile.	TN90p	days
Max_ summer	Highest daily maximum temperature in summer months	Max_Summer	º C
Min_summer	Lowest daily maximum temperature in summer months	Min_Summer	º C

3.4.1.1.1. Principal Component Analysis (PCA)

The PCA is a statistical method commonly used in climate research to analyze large multivariate datasets and derive the main spatial patterns of climate variables. It is necessarily to remove redundancy in the original data matrix. This redundancy was assessed by the Kaiser-Meyer-Olkin (KMO) test of sampling adequacy. This statistic is often used to test whether there is statistical dependence among a set of variables. In order to reduce the multidimensionality associated with the large number of input variables (i.e., 14 variables by 128 cases), a PCA (S-mode) was applied for the magnitude of trends (ºC decade^{-1}) calculated for the defined extreme indices. Following this mode, the input data had a structure of *n* variables (columns) by *n* observatories (rows). Herein, the raw data were standardized by their mean and standard deviation in order to facilitate comparison between input variables of different scale units (e.g., days and ºC). Also, recalling that temperature parameters are standardized and normally distributed, as being tested in this dataset; a data matrix based on the inter-station correlation was obtained to characterize the levels of the relationships among the input variables. The correlation matrix was favored compared with the covariance matrix because it gives equal weights to all years involved in the analysis. This seems important in this research because the covariance matrix was expected to give more weighting to the warmer years (events) during recent decades.

Selection of appropriate number of PCs that can adequately represent most information of the original dataset is an important decision in PCA. According to the Kaiser criterion, only PCs with eigenvalues greater or equal to 1.0 were extracted. In addition, the results of the Velicer´ minimum average partial test (MAP) and the Scree plot were considered. The Scree plot represents the difference between the natural

logarithms of successive eigenvalues versus component number. The Velicer test is an exploratory factor analysis test, which is based on the matrix of partial correlations. This test has proven superior to different techniques to define the best number of factors (Zwick and Velicer, 1986; Wood et al. 1996). The retained PCs were then rotated by means of the varimax orthogonal technique. This procedure facilitates spatial reasoning of the PCs that later became important to objectively cluster the variables. Then, the observatories were assigned to factors based on their maximum factor loadings.

Herein, it was important to indicate that the PCA results were validated to ensure the stability of the obtained factors and their scores. More specifically, it was necessary to ensure that the obtained results were not variable dependent given that this work is based on employing a set of indices (variables) for regionalization. For this reason, a sensitivity analysis of the input dataset was performed to see whether the obtained factors and their explained variance will change when one or more indices (variables) are removed.

3.4.1.1.2. Cluster analysis

Cluster analysis is a multivariate technique commonly used to classify observations into groups according to similarity in their quantitative characteristics (DeGaetano, 2001). The outcome of clustering analysis is heavily dependent on the pre-processing procedures, such as selection of a “best” clustering algorithm, similarity function, number of clusters, and weights of input variables. A comprehensive review of the cluster analysis algorithms is given in Gong and Richman (1995).

In this work, in order to detect the best spatial classification of summer temperature extremes, the standardized PC scores were used as a basis for the cluster analysis procedure. There have been numerous studies comparing the performance of hierarchical and non-hierarchical algorithms of clustering (e.g., Kalkstein et al., 1987). Since the accuracy of non-hierarchal methods (e.g., k-means) is very sensitive to the selection of the centroids points and also the order in which data are processed; the preference was given to the hierarchical techniques. These methods are particularly preferred when a priori knowledge of data structure is inadequate. In this sense, the hierarchical Ward´s method was chosen. In terms of the statistical accuracy, the Ward algorithm has been found superior to other methods in various climatic applications (e.g., Romero et al., 1999; DeGaetano, 2001). This algorithm is an ANOVA-type approach which explicitly minimizes the within-group similarity and maximizes the between-group similarity (Bonell and Summer, 1992).

Another important decision in the clustering procedure was to define the “accurate” number of clusters to be retained. Overall, a greater number of clusters are not desirable for practical uses and may introduce noisy patterns that could not be justified in terms of the climatological reasoning. In the same sense, an inadequate number of clusters may cause missing of valuable information. For this reason, a consideration of only spatially prolonged patterns that could have the most significant environmental, economic and social impacts is more preferred. Other factors than these spatially large-scale patterns are likely to reveal very local modes of extreme events. In literature, there seems no uniform criterion to decide on the number of clusters. Milligan and Cooper (1985), for example, introduced 30 different statistics to define a relatively appropriate number of clusters. To ensure the reliability of the defined

number of clusters, multiple statistics are desirable to check for agreement between results. In this work, two different statistics were used: the agglomeration coefficient of squared Euclidean distance and the Wilk´ Lambda test. The agglomeration coefficient reveals change in squared Euclidean distance between the two most dissimilar observatories in combined clusters at each stage. A large increase in agglomeration coefficient shows the optimal number of clusters as it indicates that inhomogeneous clusters are being merged. On the other hand, the Wilk´ Lambda is a multivariate statistic of variance, defined as the ratio of the within group variance to the total variance (Everitt and Dunn, 1991). Lower values of this statistic assume that the source of total variation in the dataset is due to the between-groups variance. It can therefore be employed as an indicative statistic to test the best cluster solution.

3.4.1.1.3. Clustering validation

It is known that most clustering algorithms do not provide estimates of clusters significance. This is typically the case for the hierarchical methods, in which clustering algorithms may incorrectly aggregate some observations into misclassified clusters. For example, the Ward algorithm allows crisp clustering in which each observation is assigned to a unique partition (cluster) and cannot be reassigned to alternative cluster whenever more appropriate (Gong and Richman, 1995). Given that the selected clustering procedure was unsupervised as the number of clusters was defined objectively, it was important to verify its goodness of fit. The “optimum” cluster is generally defined by two principal characteristics: isolation and compactness. Isolation indicates the degree to which the clusters are significantly different from each other. Compactness, on the other hand, shows the degree to which observations in a particular cluster are coherent. In this thesis, the Silhouette width index, mainly based

on proximity matrix, was chosen to evaluate the homogeneity of the final clusters. This index (Rousseeuw, 1987) is defined as:

$$S_i = \frac{b_i - a_i}{\max\{a_i, b_i\}} \quad (3.9)$$

where a_i is the intracluster distance (average distance of the observatory (i) to all observatories in the same cluster), while b_i refers to the intercluster distance (the average distance of the same observatory to observatories in another cluster). The Silhouette average width was simply calculated by averaging the coefficients of observatories belonging to each independent clustering. This index is favorable compared with other clustering validity measures (e.g., Dunn index and Davies-Bouldin index) for two reasons. First, it does not only indicate validity of the entire clustering, but it also provides a measure of the extent to which each individual observatory closely matches its cluster. Second, this statistic is robust to outliers, noisy observatories and number of clusters (Rousseeuw, 1987). According to this measure, it is possible to re-assign an observatory to an alternative cluster to satisfy the homogeneity conditions. Overall, values of the Silhouette width are limited to the interval [-1, 1]. Values close to 1 correspond to clusters that are compact and well separated from other clusters. When the intercluster distance of an observatory is equal or less than the intracluster distance, a decision was objectively made to reassign this observatory to another cluster with the lowest intercluster distance. the silhouette coefficient was then re-calculated iteratively until all observatories had a positive silhouette coefficient (i.e., $b_i > a_i$).

In addition to the silhouette coefficient, the quality of the obtained clusters was also assessed by means of the one-way analysis of variance (ANOVA) described by von

Storch and Zwiers (1999). This analysis compares the statistical difference between the obtained clusters before and after validation. Since the main target of the clustering algorithm is to obtain the most significant ANOVA by dividing the dataset into discrete groups (Trigo et al., 1999), a comparison between the F ratios of the ANOVA for the dataset before and after validation can be used as a measure of validation. Higher value of the F ratios is desirable as it indicates an increase (decrease) in the between-groups (within-groups) variations.

3.4.1.2. Trend calculation

For the established final clusters, a regional series was calculated for each cluster based on averaging values of the observatories belonging to this cluster for each particular index. This procedure is twofold. First, it helped comparing trends in temperature extremes from both spatial and temporal perspectives. Second, it allowed spatial patterns to be linked with underlying mechanisms, such as atmospheric circulation. To provide a more proper definition of the regional series, a weighted average of all observatories belonging to each cluster was computed. Herein, the weight was based on the Silhouette coefficient of each observatory, giving larger weights to observatories that were close in their similarity. Simply, high value of the Silhouette coefficient for a particular observatory indicates that it can better reflect the overall characteristics of its cluster (sub-region) than those observatories located at cluster boundaries, with coefficients rather close to 0. Linear trends in the defined indices time series were analyzed for each particular cluster (sub-region) by means of the ordinary least squares method (OLS) and the statistical significance was assessed using the Mann-Kendall statistic at the 95% level of significance.

3.4.2. Spatial regionalization of anomalously severe extreme events

In this section, the methodology to capture the dominant spatial modes of very extreme temperatures events across the region is detailed. This research used a statistical criterion focusing only on changes in very rare and exceptional events defined by days exceeding a given percentile of the historical records. First, very cold nights (VCN) and very warm days (VWD) were defined. In this research, the 1 and 99% intervals were used as threshold values to determine the VCN and VWD, respectively. For each observatory, these percentiles were calculated based on the local distribution of daily temperature time series in the period from 1960 to 2006. The VCN were selected from the days fell below the 1st percentile of the distribution of daily minimum temperature calculated for the winter season, whereas the VWD were defined as days exceeding the 99th percentile of daily maximum temperature distribution during the warm season. This means that, on average, about 1.23 (1.2) days per year would be considered as anomalously warm (cold). The definition of these extreme conditions using the percentiles is more advantageous relative to arbitrary-based definitions. This definition facilitates direct comparison between these extremes in regions with different climates. Due to the complex topography and geography of the study area, temperature varies irregularly over short distances suggesting sharp spatial gradients. Accordingly, there is no absolute single temperature value that can be considered as very extreme over the full domain. Figure 3.3 shows the frequency distribution of maximum (minimum) temperatures during summer (winter) at three different observatories across the region. The 99th percentile calculated for the warm season was over 39ºC in Zaragoza airport (the Ebro valley), which dropped sharply to 26.1ºC at Port del Compte (Lleida, 1800 m a.s.l). Correspondingly, the definition of VCN ranged between -6.6ºC at Port del Compte

(Lleida) and 1ºC at Bilbao airport close to the Cantarbrian Sea. These examples give strong evidence on high spatial contrasts across the region.

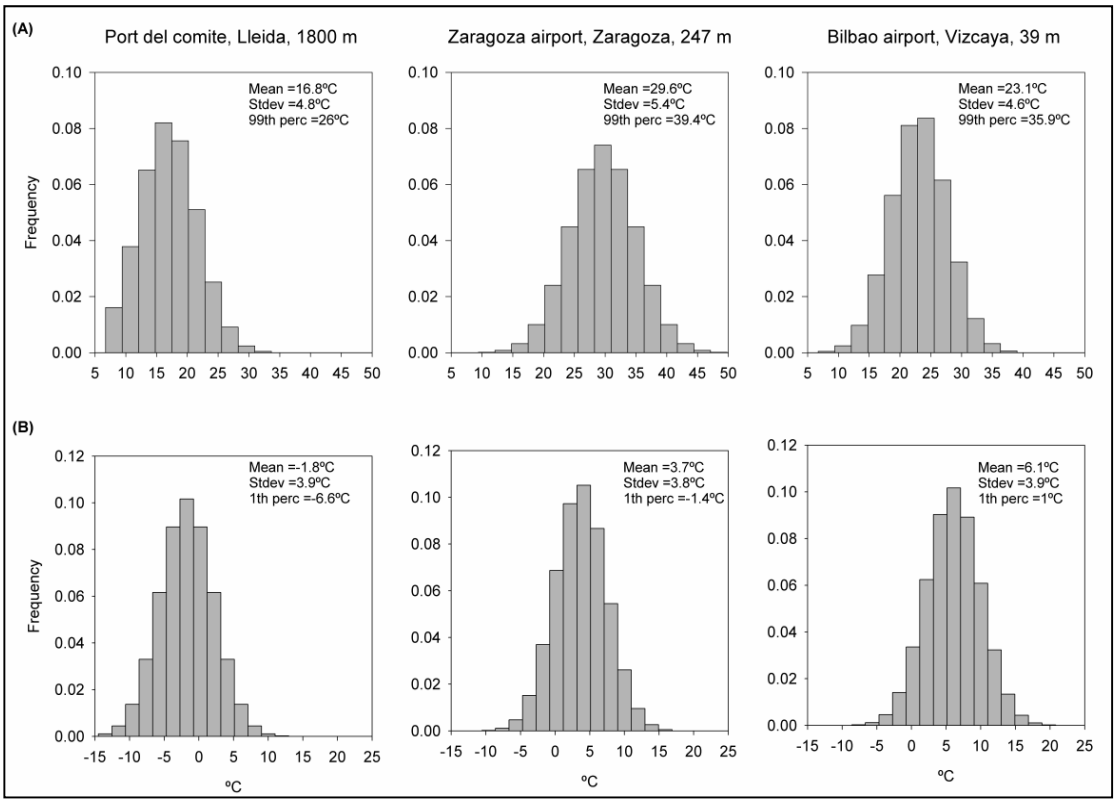

Figure 3.4: Frequency distributions of (a) summertime (MJJA) maximum temperature and (b) wintertime (NDJF) minimum temperature (lower panels) for various daily temperature series. All calculations were made for the period from 1960 to 2006.

After defining these anomalous days, daily anomalies were defined as departures of daily values at each observatory from long-term monthly means (1960-2006). The anomalies were calculated on a monthly basis so that these anomalies were the result of removing the mean seasonal cycle. Only those days that were recorded as very extreme in at least 10 observatories were considered in the PC analysis. This procedure simply aimed to account for those spatially prolonged events that could likely have broad and significant impacts on both natural and human environments.

Other small-scale spatial patterns often reveal very local extreme events, which are physically difficult to interpret, particularly in such a topographically complicated region. Finally, the S-mode of PCA was applied to temperature anomalies corresponding to VWD during the summer season (MJJA) and VCN during the winter season (NDJF). The spatial structure of the leading modes was provided by the scores of the leading PC factors.

3.5. Attribution of driving forces and mechanisms

After detecting the spatial and temporal changes in temperature means and extremes over the study area, this thesis paid particular attention to attribute these changes by explaining the possible forces and mechanisms beyond them. It is assumed that the regional variability of temperature in such a region of complex topography and climate can be linked to both large-scale forces (e.g., atmospheric circulation, land-sea interaction) and local and regional forces (e.g., soil moisture, precipitation variability). Numerous works concluded that the distinctive spatial and temporal variability of climate in the peninsula has often been described as being driven by the atmospheric circulation (Sáenz et al., 2001a, b; Brunet et al., 2007b; Rodriguez-Puebla et al. 2010). For example, Sáenz et al. (2001b) explored relationships between winter temperature variability in the northern Iberian Peninsula and the general atmospheric circulation. In this research, the observed changes in temperature were evidently linked to their possible influencing factors. This helped to understand the importance of different factors influencing observed changes and also project the extent of temperature changes to be expected in the region should any of these factors vary in the future. Attribution of changes in temperature is important for studies of climate change, hydrological modeling and simulation, and agriculture.

3.5.1. Driving forces of variability of seasonal temperature means

The atmospheric processes governing climate changes can be distinguished in two main groups: thermodynamical and dynamical processes (Emori and Brown, 2005). The dynamic processes indicate changes in the atmospheric circulation patterns, which refer to a large and persistent pattern of pressure anomalies that determine the main flow of air masses affecting the climate of broad geographical regions (Hurrell, 1995). On the other hand, the thermodynamic processes are mainly related to changes in the land-atmosphere coupling, such as soil moisture, cloudiness and moisture content of the air.

3.5.1.1. Teleconnections

It is assumed that large-scale circulation pattern likely govern changes in the mean temperature. This is simply because these circulation patterns are favoring for atmospheric flows from one direction for consecutive days, which can be responsible for changes in the mean temperature. To account for the possible causes of seasonal temperature variability, the influence of a range of teleconnection indices was examined in this thesis. These patterns included the North Atlantic Oscillation (NAO), the East Atlantic (EA), the East Atlantic/ Western Russian (EAWR), and the Scandinavian (SCA) patterns. In addition, other oscillations dominating over the Mediterranean basin were also are represented, including the Western Mediterranean Oscillation (WeMO) and the Mediterranean Oscillation (MO). Previous works suggested these indices as main drivers of the climate variability in the Iberian Peninsula (e.g., Hurrell, 1996; Sáenz et al., 2001a, b; Slonosky et al., 2001; Martin-Vide and López-Bustins, 2006; Philipp et al., 2007; Vicente-Serrano et al., 2009) and the Mediterranean (e.g., Maheras and Kutiel, 1999). Overall, the selected

teleconnections summarize a wide variety of flows that affect climate variability in the Iberian Peninsula.

The NAO is a north hemispheric mode calculated as the difference between the high surface pressure in the Azores and the sub-polar low pressure near Iceland. It has a north-south dipole, with one center over Iceland and the other with opposite sign over the mid-latitudinal Atlantic (Hurrell, 1995). Similarly, the EAWR pattern has two main action centers: the first is located in the Caspian Sea and the latter is found over the Western Europe. The EA teleconnection index resembles the NAO in terms of its geographical domain. Nonetheless, it has a more southward shift toward low latitudes (Canary Islands: 25ºN, 25ºW). It has also a well-defined north monopole, south of Iceland and west of the United Kingdom near 52.5ºN, 22.5ºW (Barnston and Livezey, 1987; Murphy and Washington, 2001). The SCA is a dipole with a main center over Scandinavia and minor centers across Western Europe. The data related to the NAO, EAWR, EA, and SCA atmospheric circulation indices were supplied by Climate Prediction Center, NOAA/NCEP, USA (http://www.cpc.noaa.gov/data/teledoc/telecontents/shtml) from 1960 to 2006.

The MO index has been provided by Palutikof (2003) as the difference in the SLP anomalies between Gibraltar (Spain) and Lod (Israel), while the WeMO has been recently developed by Martin-Vide and López -Bustins (2006) as a dipole between San Fernando, Spain (36º 17'N, 06º 07'W) and Padua, Italy (45º 24'N, 11º 47'E). The monthly MO index was obtained from the Climate Research Unit, East Angelia University, UK (http://www.cru.uea.ac.uk/_andrewh/moi.html), whereas the WeMO

data were compiled by the Climatology Group, University of Barcelona (http://www.ub.es/gc/English/wemo.htm).

The Pearson correlation coefficient was used to quantify the relationships between the large-scale atmospheric circulation and seasonal and annual temperature time series. Nonetheless, prior to running the correlation analysis, the monthly series were detrended (by removing the linear trend) and standardized (by their mean and standard deviation). Detrending the series was important to remove the possible influence of the trends and interannual variability of the series on the strength of the correlation. In the same context, the anomalous temperature series were also standardized to assure consistency given that the time series of the anomalous circulation modes are already standardized.

A more detailed analysis was then undertaken to explore the association between the dominant circulation modes responsible for temperature variations, as reveled by the correlation results, and their corresponding anomalous sea level pressure. The rationale was to support the interpretation of mechanisms that govern the linkage between temperature variations and atmospheric circulation. For this purpose, daily dataset of surface level pressure (SLP) provided by the NCEP/NCAR reanalysis datasets was considered for the period from 1960 to 2006 on a regular grid of 2.5º x 2.5º resolution (http://www.esrl.noaa.gov/psd/) (Kalnay et al., 1996). The data were retrieved for the spatial domain between the ranges of 20ºW-35ºE and 20-60ºN. This window coupled different oceanic-land influences (e.g., the Atlantic, Mediterranean, European and the Sahara configurations) that may possess a joint effect on temperature variations in the study area. In addition, this large window relatively limits

the possible impact of local factors (e.g., topography and land use), which may interrupt the SLP configurations when small spatial window is used.

3.5.1.2. Land-atmosphere coupling forces

Numerical studies provide more evidence that the earth's climate is the result of a dynamic equilibrium in which the atmosphere, the ocean and land surfaces interact interchangeably together (Douville, 2003). In this context, while the large-scale atmospheric modes can exert a strong control on temperature variations, temperature variations can also be driven by other processes. While configurations of atmospheric flow can adequately explain temperature variability in the region in all seasons, they cannot adequately describe temperature variations, particularly during summer season. For instance, the thermally forced circulation plays a key role during summer periods, coupled with other heat sources such as heat radiation, maximum insolation, clear skies and light wind.

The enhanced land-atmosphere coupling processes can be related to changes in surface net radiation (Wild et al., 2005), stability and blockings (Beniston et al., 1994), cloudiness (Vautard et al., 2009) and soil moisture (Fischer et al., 2007). Nonetheless, the impacts of these processes are difficult to isolate since they are coupled with each other. For example, incoming solar radiation is often affected by changes in cloudiness. Also, the increased clouds could cause positive soil moisture feedbacks as a consequence of the more solar radiation reaching the surface (Ek and Holtslag, 2003).

In order to assess the impact of land-atmosphere coupling, the dependency between temperature variability in the region in the one hand and cloud cover and soil moisture characteristics on the other hand was assessed.

Among land-atmosphere coupling forces, cloudiness is a key factor that influences the Earth's radiation budget. The strong role of the seasonal cycle of insolation suggests that climate system is very sensitive to changes in cloudiness, particularly during summer. Cloudiness directly affects the global climate system by transferring energy in the atmosphere. The decrease in cloudiness often affects energy and heat transfer throughout insolation, suggesting above-normal temperature during the daytime. Conversely, cloudy days are mostly linked to decrease in sunshine and in turn less evaporation and more cooling. Dai et al. (1997) explained the association between surface air temperature and cloudiness in the context of radiation fluxes.

The climate of the study area is also more likely to be influenced by changes in soil moisture. This is mainly because the domain is located in the mid-latitudes between dry and wet conditions. Simply, low soil moisture at the surface level can often cause a decrease in latent cooling and thus above-normal temperature. Previous studies linked changes in soil moisture with climate variations (e.g., Koster et al., 2004; Seneviratne et al., 2006; Fischer et al., 2007). A recent study by Seneviratne et al. (2006) confirmed that much of variation in summer temperature in the transitional zones over Europe is attributed to land-atmosphere, including depletion in soil moisture.

The daily data of cloud cover fraction (%) and volumetric soil moisture between 0-10 cm below ground level (%) were derived from the daily NCEP/NCAR reanalysis data

provided by the NOAA/OAR/ESRL PSD (http://www.nws.noaa.gov) for the period from 1960 to 2006. The data were only extracted for the grids that cover the study domain. For both cloud cover and soil moisture fields, daily data from six grids, covering the domain at a resolution of 2º latitude by 1.87º longitude, were used to obtain a regionally averaged time series for the whole domain. The standardized anomalies of cloud cover and soil moisture were calculated with respect to the base period 1960-2006. It is noteworthy indicating that the anomalies were calculated for each month independently. This was principally made to remove the effect of the annual cycle. Then the monthly anomalies were aggregated for each season. Pearson correlation coefficient was computed between the standardized anomalies of maximum, minimum and mean temperatures in the one hand and the standardized anomalies of soil moisture and cloud cover on the other hand. The correlation was calculated for each season independently and the significance of the correlation was assessed at the 95% level ($p<0.05$).

3.5.2. Driving forces of extreme events variability

3.5.2.1. Driving forces of moderate extreme events variability

To explore the extent to which atmospheric circulation determines spatial patterns of summer temperature extremes, the EA, SCA, and EAWR circulation patterns were considered. Those patterns were significantly linked to the homogenous regions of temperature extremes, as previously defined (refer to section 3.4). For each established sub-region, the Pearson correlation coefficient (r) was simply computed between the regional series obtained for each index of summer extremes and the time series of the atmospheric circulation at the 95% confidence level (p value < 0.05).

However, it is noteworthy indicating that the time series of extreme events were detrended prior to computing correlation in order to remove the possible influence of the time series interannual variability and limit the effect of monotonic trend on the strength and significance of correlation. Also, the time series were standardized for the base period 1960-12006 to have zero mean and unit variance. This was principally performed before calculating the correlation to confirm that all the time series were equally weighted.

For those leading circulation modes which showed significant influence on variations of summer temperature extremes, the canonical correlation was performed to assess the relationship between SLP anomalies (independent variable) covering much of Europe, the Atlantic and North Africa and summertime temperature (dependent variable) in the study domain. This spatial domain is large enough to encompass all regions that include forcings and circulations which directly affect temperature climate over the study domain.

Canonical correlation is a multivariate statistical technique commonly used to calculate linear combinations between two datasets (i.e., predictors and predictands). This technique is advantageous compared with other multivariate statistics (e.g., multivariate regression) in that it can provide station scale information on the correlation between the dependent and independent variables. Recently, this analysis has increasingly been employed to explore interrelations between climate datasets (e.g., Bartzokas et al., 1994; Xoplaki et al., 2003b; Lolis et al., 2004). For instance, Xoplaki et al. (2003a) used this technique to explore links between the Mediterranean summer temperature and associated physical process (e.g., SST, 300hPa and 700-

1000hPa thickness). A more comprehensive review of the canonical correlation and its theory can be found in Dillon and Goldstein (1984) and Lolis et al. (2004).

Prior to application of the canonical correlation, factor analysis was first applied on both fields (i.e. summer temperature and SLP data) corresponding to the positive/negative phase of the significant modes (e.g., NAO+, SCA-). This procedure aimed to reduce the dimensionality of the original datasets. Then, only those PCs that explain more than 5% of the total variance were retained and the time series scores corresponding to these retained components were used as input variables in the canonical correlation.

Simply, the canonical correlation aims to calculate linear combinations between two datasets: predictors (x) and predictands (y). These combinations are calculated iteratively to maximize the relationship between the x and y datasets. Each dataset has a group of variables (i.e., X_1, X_2, X_3, X_n for X dataset and y_1, y_2, y_3, y_n for y). The linear combination between x and y is then defined, as:

$$W_1 = a_1x_1 + a_2x_2 + a_3x_3 + ... + a_nx_n \quad (3.10)$$

$$V_1 = b_1y_1 + b_2y_2 + b_3y_3 + ... + b_my_m \quad (3.11)$$

where a_1, a_2, a_3,…a_n are the canonical coefficients for the first variate (W_1) corresponding to the predictor (x) dataset. On the other hand, b_1, b_2, b_3,…b_m are the canonical coefficients for the first variate (V_1) corresponding to the predictand dataset (y). Then, the canonical correlation is computed between the two canonical variates W_1 and V_1, as;

$$C_1 = correl(V_1, W_1) \quad (3.12)$$

Then a new set of variates are computed and the canonical correlation is calculated in the same way as:

$$C_2 = correl(V_2, W_2), C_3 = correl(V_3, W_3), \ldots\ldots, C_q = correl(V_q, W_q) \quad (3.13)$$

where $q = \min(n, m)$ (3.14)

The loadings corresponding to each canonical variate are also provided by the canonical correlation output. In this analysis, the predictors and the predictands are usually arbitrary, particularly when there is no priori information about the direction of the dependency between the two input datasets. In this study, temperature anomalies were used as predictands, while large-scale circulation (e.g., SLP anomaly) was used as predictors. More specifically, the canonical correlation required two datasets: (i) local predictand (i.e., scores of retained factors for summer mean temperature during summers of specific circulation mode [e.g., positive/negative EA]), and (ii) large-scale predictors (i.e., scores of the retained factors for SLP corresponding to the circulation mode). Following the results of the Chi-square and Wilk´ Lambda statistics of variance, only significant canonical pairs (variates) at the *p*-value<0.05 were retained and explained. For each particular circulation mode, the statistically significant canonical function that explained the largest proportion of summertime temperature variance was retrieved and mapped.

3.5.2.2. Driving forces of anomalously severe extreme events variability

The influence of SLP on temperature extremes may be interrupted by local conditions (e.g., vegetation canopy, land use changes and topography), it is therefore important

to consider not only the patterns of level pressure at surface, but also the influence of atmospheric circulation patterns at various pressure heights (e.g., 200hPa and 500hPa). In mid latitudes, changes in climate at the regional scale can largely be understood by studying configurations in large-scale atmospheric circulation at different heights (Hurrell, 1995). In order to identify the most favorable synoptic conditions to the occurrence of very extreme events (i.e., VWD and VCN), changes in three synoptic fields corresponding to these days were chosen. These circulation patterns represent the mean sea level (MSL) pressure at surface, besides the low (500hPa) and mid (200hPa) troposphere fields. These height levels were proven to be among the best predictors of climate variability in the Iberian Peninsula (Rodriguez-Puebla et al., 2001a; Brunet et al., 2007b; Vicente-Serrano et al., 2011b), the Mediterranean (Xoplaki et al., 2003a) and Europe (Pozo-Vazquez et al. 2001; Slonosky and Yiou 2002). These physical processes emphasize not only the land-sea interactions at the ground level (i.e., MSL), but they also summarize the overlying air connections (i.e., height field). While the influence of MSL might be minimized in areas of complex topography as has been reported in previous works (e.g., Simmonds and Murray, 1999), pressure at high levels of the troposphere does not exhibit diurnal variation and accordingly shows more robustness to local effects (Beniston et al., 1994). Thereby, configurations of pressure at the troposphere levels can be viewed as a good indicator of air advection. Moreover, using geopotential data at different heights (approximately 1500-5000 m) can largely identify whether anomalous temperature variations at the ground are forced by different modes of pressure at mid and shallow troposphere.

The data utilized to explore co-variability between temperature anomalies during the extreme heat days and their corresponding SLP and height fields were the daily anomalies for the winter/summer months of (i) SLP, 200hPa and 500hPa obtained from the large-scale National Centers for Environmental Prediction-National Center for Atmospheric Research (NCEP/NCAR) reanalysis on a regular grid of 2.5º x 2.5º resolutions (http://www.esrl.noaa.gov/psd/) (Kalnay et al., 1996) and (ii) anomalies of temperature during VWD/VCN corresponding to 128 observatories covering the study domain from 1960 to 2006. The daily anomalies were obtained using the long-term monthly means calculated over the period from 1960 to 2006. The data for the geopotential fields were obtained for a large window (25ºW-35ºE and 30ºN-65ºN), encompassing vast areas of Central and Western Europe along with part of northern and eastern portions of the Atlantic Ocean. This spatial extent is large enough to capture the co-variability between local temperature and their large-scale driving forces.

In this work, climate composites for the different atmospheric levels were first plotted, allowing detecting circulation patterns that represent these high-order extreme events. Second, the daily anomalies of SLP and the upper air 200hPa and 500hPa geopotential heights corresponding to VWD and VCN were separately subjected to PCA. The rationale behind this procedure was to determine the most important spatial modes of these circulations so that they can be linked to the prominent modes of extreme events by means of the canonical correlation analysis. To meet this goal, the PCA of S-mode was applied separately for daily anomalies of (i) summer anomalous warm temperature, (ii) winter anomalous cold temperature. Also, to reduce dimensions of the data of geopotential fields, the daily anomalies of (i) SLP, (ii) 200hPa, and (iii)

500hPa fields corresponding to these extreme days were considered in a PCA analysis. For each independent dataset, only those PCs that explained more than 5% of the total variance were retained and the time series scores corresponding to these retained components were used as input variables in the canonical correlation. Following the results of the Chi-square and Wilk´ Lambda statistics, only significant canonical variates were maintained to explain the dependency between anomalous temperature in the region (dependent variable) and geopotential height fields (independent variable). At this stage, the co-variability was calculated between each pair of datasets (i.e., VWD-SLP, VWD-200hPa, VWD-500hPa, VCN-SLP, VCN-200hPa and VCN-500hPa).

3.5. Future changes of temperature during the 21st century

Understanding the impacts of future climate change on northeast Spain, a region characterized by complex climatological and topographical features, is important for different environmental, hydrological, agricultural and socioeconomic applications. Recently, RCMs have been important tools in assessing the effect of climate change, as induced by the increase of GHG (Wetterhall et al., 2007). These models are a simplified representation of complex and non-linear climate system and its physical processes. These models have progressively been developed in the recent decades enforced by the rapid increase in computational capacity. RCMs are favored compared with GCMs to adequately capture the characteristics of regional climate variability as their computational grid are relatively fine (≈ 25 km), which makes them an adequate choice to reasonably capture the sub-regional scale climate features that may affect temperature variations, such as topography, leeside effects and land use/cover changes. This sounds advantageous over the study domain due to its topographic

complexity, which exerts a strong control on temperature variations. The complex topography of the study domain enhances the importance of small-scale processes in model simulations, suggesting that RCMs are always more appropriate to describe climate at the regional scale. Regional climate is largely influenced by complex topographical variations, land-sea contrasts, and marked gradients of vegetation and land cover, which are difficult to capture by the coarse resolution of GCMs (on average 50 km). According to the IPCC (2007), reliable RCMs projections are now available for many regions worldwide, with a remarkable advance in model resolution and the simulation of important physical processes for regional climate. A number of researches have used predictable climate scenarios to assess future changes in temperature (e.g., Kjellström, 2004; Moberg and Jones, 2004; Deque et al., 2005; Errasti et al., 2011; Brands et al., 2011a).

3.6.1. Description of observational and modeled datasets

In order to assess the potential effects of future climatic conditions, this work used projected daily maximum and minimum temperature data derived from regional downscaled climate model simulations available as part of the ENSEMBLE European project. Further information on the ENSEMBLE models and their simulations can be found in (http://ensemblesrt3.dmi.dk/, Hewitt and Griggs, 2004). The ENSEMBLE simulations are among the most updated ensembles of climate change projections over Europe. For this reason, they have been investigated quite thoroughly in numerous climate simulation studies across different regions of the European continent (e.g., Hewitt and Griggs, 2004; Brands et al., 2011a). Under the ENSEMBLE, the gridding space of the daily dataset has, on average, a 0.25º × 0.25° latitude/longitude resolution (approximately 25 km spatial interval).

In this work, maximum and minimum temperature data for an ensemble of 9 comprehensive RCMs driven by 5 different GCMs were used to assess future climate change projections under the IPCC SRES (Special Report on Emissions Scenarios) A1B emission scenario, which corresponds to a medium level of CO2 emissions to the atmosphere. Under this scenario, the concentration of CO2 is expected to reach 720 ppm by the end of this century (Nakicenovic et al., 2000). These models were chosen based on the availability of simulations under the A1B scenario until the end of the 21th century. They have extensively been employed for climate simulation studies (e.g., Beniston, and Goyette, 2007; Boé and Terray, 2008; Kostopoulou et al., 2009). Table 3.4 gives a summary of the models used in this work and their experiments. As presented, the computational domain varies from 256 (ICTP simulation) to 274 grid points (KNMI, MPI, METO, SMHIR simulations), with different horizontal resolution ranges. Comparing the results from different models can represent not only a range of possible different outcomes, but it can also offer an estimate of the degree of uncertainty associated with future climatic predictions (Giorgi and Mearns, 1999). Indeed, inclusion of different climate models to assess future changes can give an idea on inter-model differences, which can be due to different sources of uncertainty such as parameterization schemes and model components (e.g., atmosphere, ocean, and land-surface interactions) (Meehl and Tebaldi., 2004; Haylock et al., 2006).

In this work, three 30-years set of simulations: control period (1971-2000) and two common future scenario periods (2021–2050 and 2071-2100) were undertaken for the study area.

Table 3.4: Summary of RCMs simulations used in the study with their corresponding resolutions.

Acronym	Institute	Driving data	RCM	Resolution (Lat. by Lon.)	Number of grid boxes
CNRM	Météo France (France)	ARPEGE	ARPEGE	0.15º by 0.35º	270
DMI-APREGE	Danish Meteorological Institute (Denmark)	ARPEGE	HIRHAM	0.17º by 0.32º	273
DMI-ECHAMS	Danish Meteorological Institute (Denmark)	ECHAM5	HIRHAM	0.17º by 0.32º	273
DMI-BCM	Danish Meteorological Institute (Denmark)	BCM	HIRHAM	0.17º by 0.32º	273
ICTP	The Abdus Salam Intl. Centre for Theoretical Physics (Italy)	ECHAM5	RegCM	0.18º by 0.30º	253
KNMI	Koninklijk Nederlands Meteorologisch Instituut, (Netherlands)	ECHAM5	RACMO	0.17º by 0.32º	270
METO	Norwegian Meteorological Institute (Norway)	HadCM3Q16	HIRHAM	0.17º by 0.32º	270
MPI	Max-Planck-Institut für Meteorologie (Germany)	ECHAM5	REMO	0.17º by 0.32º	270
SMHI	Swedish Meteorological and Hydrological Institute (Sweden)	BCM	RCAO	0.17º by 0.32º	270

The selection of the (1971-2000) control period is mainly motivated by the fact that this sub-period (1971-2000) was characterized by a warming episode. Numerous studies (e.g., Labajo et al., 1998; Morales et al., 2005) noted a rapid warming in regional temperature over the Iberian Peninsula temperature, mainly from 1972 onwards. At the global scale, numerous studies also confirmed this positive temperature anomaly during the last decades of the 20th century (e.g., Easterling et al., 1997; Jones et al., 1999; IPCC, 2007). Therefore, it is of interest to assess the shifts in the current climate warmer conditions under a future climate change scenario.

In order to improve model skill for prediction it is essential to have a reliable set of observations. In this work, daily maximum and minimum temperature data from 189 long-term, complete and homogenous time series spanning the period from 1971 to 2000 were used to validate the simulations for the control period. Figure 3.2 depicts the spatial distribution of temperature observatories. As illustrated, the weather stations are relatively evenly distributed across the domain; providing an adequate sampling of the large spatial heterogeneity of geography and climate. This is important to guarantee a more accurate projection of temperature future signals at this fine spatial scale.

3.6.2. Model Validation

Prior to assessing the climate change simulations under the A1B emission scenario, it was important to provide an evaluation of the models performance. For this reason, the model simulations were evaluated against the observational temperature data for the control period (1971-2000). To accomplish this task, the observational data were first gridded using the Inverse Distance Weighting (IDW) interpolation algorithm.

Herein, this method worked by taking the nearest 25 stations to the centre of the grid of interest. In order to facilitate direct comparison between the modeled and interpolated datasets, the gridded observational data were delivered on different spatial resolutions so that they exactly overlap the modeled grids for each particular simulation. The rationale behind this procedure was to match the spatial resolution of the modeled data, as presented in Table 3.4, and accordingly maintain consistency between simulated datasets and their corresponding observed grids. Over the study domain, the real-world boundary conditions, e.g., elevation and land cover, vary markedly over short distances. Accordingly, it seems important to maintain both the model and observational grid-points physically-consistent.

In order to evaluate the performance of the models, the uncertainty in the regional climate models projections was assessed by means of the cross-validation statistics. A large number of climate modeling simulations have been assessed in this manner (e.g., López-Moreno et al., 2008b; Vicente-Serrano et al., 2011b). To determine how well the models simulated the main characteristics of the observed temperature (e.g., the mean, standard deviation, skewness, symmetry), the performance of the models was tested by comparing their simulated (predicted) values against observed data. Recalling that future climate projections are manifested as changes in either the mean of the climate and/or changes in its shape (i.e., variance), the possible shifts in the probability of temperature on the tails of the distribution must be considered when validating the models. The validation statistics used in this work included: the Mean Bias Error (MBE), the Yule–Kendall (YK) skewness measure (Ferro et al., 2005), the Inter-annual variability error (IVE) and the Willmott's D index of agreement (Willmott,

1982). The evaluation was carried out independently for each model and for each particular season. The validation estimators are given, as follows:

$$MBE = N^{-1}\sum_{i=1}^{N}(P_i - O_i) \tag{3.15}$$

$$YK = \left[\frac{(pc95 - pc50) - (pc50 - pc5)}{pc95 - pc5}\right]_P - \left[\frac{(pc95 - pc50) - (pc50 - pc5)}{pc95 - pc5}\right]_O \tag{3.16}$$

$$IVE = \left[\frac{Variance - MBE}{\overline{P}}\right]_P - \left[\frac{Variance - MBE}{\overline{O}}\right]_O \tag{3.17}$$

$$D = 1 - \frac{\sum_{i=1}^{N}(P_i - O_i)}{\sum_{i=1}^{N}(|P_i'| + |O_i'|)^2} \tag{3.18}$$

where *N* is the sample size, *O* is the observed value, *P* is the predicted value, i is the counter for individual observed and predicted values, $|P_i'|$ = $P' = P_i - \overline{O}$ and *pci* represents the *i*th percentile.

Combining the results of those statistical measures is recommended because it provides reliable assessment of the models uncertainty. The YK is a measure of asymmetry between the present-day and simulated data, suggesting a "*perfect*" symmetry of data statistical distribution when values are close to 0. On the other hand, the MBE is commonly used to measure the ability of the model to capture the bias against the observational data, through calculating the difference between the observed and predicted value of temperature. The IVE is a measure of the difference between the variance and the bias, reflecting not only changes in the mean between

the observed and simulated values, but also changes in the standard deviation of the series. The Willmott's D coefficient varies from 0 for no skill to 1 for a "*perfect*" forecast of the observed temperature. Conventionally, the modeled and historic data may coincide in terms of changes in the mean (as revealed by the MBE and Willmott's D), whereas they show large differences in terms of deviations from the mean (as suggested by the IVE and YK). Therefore, combining the skill of different statistical estimators is more beneficial in this research.

While the previous accuracy statistics focused on the statistical properties of the time series (e.g., the mean, variance and skewness), it was also important to verify that the models are skillful in reproducing the spatial patterns of the observed temperature. This sounds important given that the models can probably show good agreement between the magnitudes of change in the mean of temperature series while they introduce different regional features. As reported by many previous works (e.g., Kirono and Kent, 2011), it is important to assess the performance of the models by assessing their ability to capture not only the temporal evolution of temperature but also its spatial pattern. For this purpose, the S-mode of the Principal Component Analysis (PCA) was applied to both the observed and simulated seasonal time series for each ensemble member and for each season independently. A similar approach was recently used by Hertig et al. (2010). In short, those ensembles with high loadings, which showed consistent sign with those of the observed loadings in terms of the sign onto the leading vector, were retained. This approach provides a rigorous assessment of whether the model represents the spatial pattern of interannual variations.

To address the uncertainty of the use of different models under the A1B emission scenario, this work preferred to calibrate climate model outputs using an inter-model

average of the ensembles with the “best” performance, as suggested by the validation outputs. Considering the central estimate of various models, which may differ in their fundamental assumptions, can provide valuable information for climate impact assessments and adaption strategies. In addition, the use of multiple climate realizations for simulating temperature change and variability makes the prediction more robust as it gives more accurate quantification of various sources of uncertainty in model performance. Numerous works gave reasonable seasonal forecasts of climate through the use of multiple RCMs (see e.g., Landman et al., 2001). In this work, the decision was made to select the models with the “*best*” performance defined on the basis of their overall skill with respect to all the statistics used for the validation purpose.

3.6.3. Statistical analysis

3.6.3.1. Future changes in the mean and standard deviation

In order to look at changes in the mean state of climate and their corresponding inter-annual variations, changes in the mean and standard deviation were calculated over the periods of consideration: 1971-2000, 2021-2050 and 2071-2100. For each particular season, the anomalies were calculated relative to the base period (1971-2000).

3.6.3.2. Future changes in the time-varying percentiles

While the early detection of anthropogenic change in mean temperature is of great interest, the impacts of future change on society are more likely to be connected to extreme climatic events. It is therefore important to identify the changes in climatic extremes that are expected under climate change conditions, and to determine whether such changes may already be consistent with simulated changes in the mean

conditions. In this work, projected changes in the time-varying percentiles of maximum and minimum temperatures were assessed for each season. This allowed for exploring the manner in which the distributions of daily maximum and minimum temperature may change over time. Detecting of such changes can also provide valuable information for various climate impact studies (Meehl et al., 2000). Similar to other global (e.g., Caesar and Alexander, 2006) and regional (e.g., Beniston and Stephenson, 2004; Robeson, 2004) studies, the *i*th percentile magnitude was calculated on a seasonal basis for each ensemble member, where *i* stands for the 10th, 25th, 75th and 90th percentiles. Lower percentiles (i.e., 10th and 25th) were used as indicators of changes in the cold tail of temperature distributions, whereas the upper percentiles (i.e., 75th and 90th) gave an indication on changes in the warm tail.

For both the mean and time-varying percentiles time series, trends were examined in order to define the magnitude (expressed in °C decade^{-1}) and direction of ongoing temperature change. Linear trends were computed using the ordinary least square (OLS) method and the significance of the trend was assessed using the Kendall's tau test. The statistical significance was assessed at the 95% confidence level (p-value<0.05).

In order to explore to what extent the variation and trends in the time-varying percentiles are linked to changes in the mean temperature, the mean and the percentiles seasonal time series were uncentered for each grid following the approach detailed by Beniston and Stephenson (2004) and Ferro et al. (2005). Simply, the aim was to decrease the scale (spread) of the data and subsequently their interannual variations by subtracting out their median (i.e., the 50th percentile). Given that the magnitudes of the median and the mean are very close when the data have a

symmetric (Gaussian) distribution, which is the common case for temperature data, it can be expected that the interannual variation of the percentiles can be linked to changes in the mean when the time series are uncentered. Finally, to account for the strength of relationship between changes in the mean temperature and its corresponding time-varying percentiles, the Pearson correlation coefficient (*r*) was simply computed between the uncentered time-varying percentiles time series and the uncentered mean time series for each independent season. The statistical significance of this relationship was assessed at the 95% level of confidence ($p<0.05$).

3.6.3.3. Future changes in extreme events

Recently, a lot of record-breaking temperatures have been observed in Iberia during the most recent years (e.g., 1995, 1998, 2003, 2005, 2010 and 2012). One clear example over northeast Iberia is the unrelenting summer 2003 heat wave (+2.7 standard deviation relative to the 1960-2006). The observed strong warming in both summer and winter mean temperatures in the study domain from 1960 to 2006 (El Kenawy et al., 2012) and the sensitivity of the region to more severe heat stress, as a consequence of varied climatology and geography, provide motivation for exploring the manner in which extreme temperature will respond to elevated greenhouse gas emissions in future. Manny studies found that warmer summers and winters are expected to be common in the next decades (e.g., Schär et al., 2004; Beniston et al. 2007). To address this question, transient experiments from the 9 high-resolution RCMs were evaluated under the intermediate-emission A1B scenario (IPCC, 2007). The horizontal resolution of this ensemble of models enables to resolve mesoscale processes (forces) related to complex terrain and land use/cover features affecting variability of very extreme events over the study domain. Herein, the models with the

"best" performance in term of their ability to reproduce the observed temperature characteristics (i.e., bias and variation) were chosen. Then, the VCN and VWD were analyzed on a grid-point basis. The 1st (99th) percentile of daily minimum (maximum) temperatures were calculated at each grid point for each of the best models for two future time slices: 2021-2050 and 2071-2100. The frequency of VWD (VCN) was defined as the total number of these extreme events per each summer (winter).

CHAPTER FOUR

RESULTS

4. RESULTS

This chapter presents the key results of the detectable spatial and temporal patterns of temperature changes during the 20th century. It also provides results related to the driving atmospheric mechanisms behind these changes. Finally, it outlines the main findings related to future changes of temperature means and extremes under the A1B emission scenario during the 21st century.

4.1. Observed changes in the seasonal and annual means

4.1.1. Temperature long-term changes (1920-2006)

Figure 4.1 shows the temporal evolution of temperature anomalies of the regional series over the period from 1920 to 2006. This assessment employed a subset of 19 observatories covering the complete period. As depicted, maximum temperature showed a positive anomaly during the 1940s, 1980s, 1990s and 2000s. This warming was much more pronounced during the 1940s followed by the 1990s and the 2000s. This behavior was broadly consistent at both the annual and seasonal timescales. However, a visual inspection of temperature anomalies suggests a sudden and strong increase in the maximum, minimum and mean temperatures during the last three decades. The warmest years from 1920 to 2006 were obviously restricted to the past two decades. Over this period, the 1990, 1994, 1998, 2003, and 2006 were identified as anomalously warm years. For instance, the anomaly of summer maximum temperature during 1990, 2003, and 2006 was 1.2, 3.7 and 1.4ºC, respectively. In the same way, the coldest maximum temperature on record were found during the period from 1950 to the mid of the 1970s. For example, the anomaly of the annual maximum temperature in 1972 was -1.6ºC.

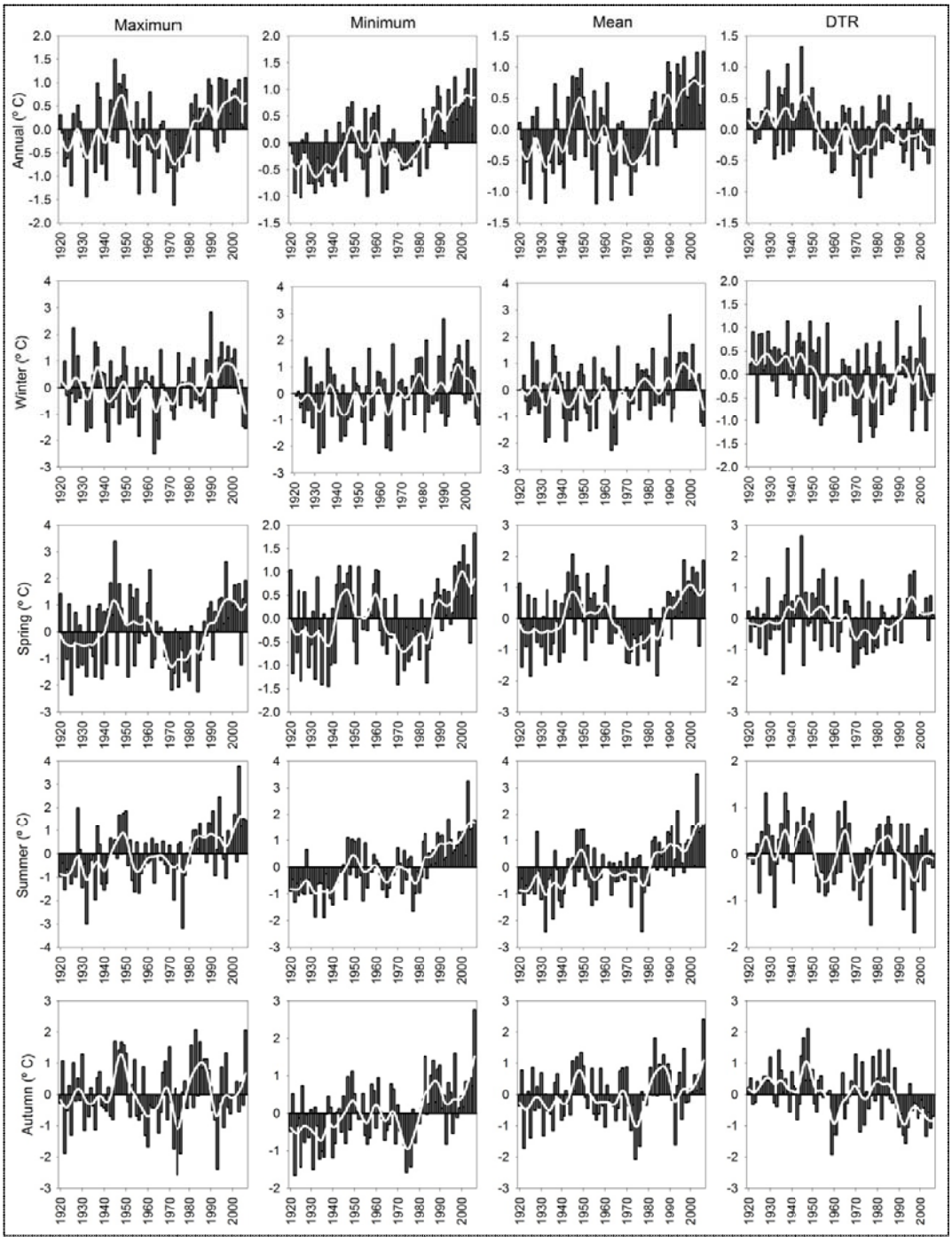

Figure 4.1: Temporal evolution of the seasonal and annual temperature anomalies (ºC) of the regional time series for the period 1920-2006, shown as bars. The anomalies were calculated based on departures from the long-term means over the period 1920 to 2006. White lines show a low Gaussian filter of 11 years.

Figure 4.1 also informs that the annual minimum temperature exhibited a cooling period that prevailed until the late of the 1940s, inversed then by a slight increase during the early years of the 1950s. The 1980s showed a remarkable return to the warming which dominated over the most recent decades. Correspondingly, a clear warming period took place fot most seasons during the mid of the 1940s and the 1950s, followed by a long lasting decrease until the mid of the 1970s. Two clear examples are the years 1956 and 1972 in which the annual minimum temperature showed a negative anomaly, reaching -1 and -0.50ºC during 1956 and 1972, respectively.

While the coldest minimum temperature on record were mainly experienced during the earlier decades (e.g., 1920s, 1930s and 1960s), the last decades of the 20th century exhibited an exceptionally positive anomaly. This probably implies that the uptrend observed in minimum temperature over the long-term period (1920-2006) is largely attributable to the rapid warming during the last few decades. In contrast to winter and autumn, the annual behavior of minimum temperature anomalies was broadly consistent with the behavior of anomalies during summer and spring.

Contrarily, the temporal evolution of the annual DTR anomalies was more consistent with anomalies during winter and autumn rather than in summer and spring. In earlier decades (prior to 1950), DTR demonstrated a positive anomaly due to the higher increase in maximum temperature than in minimum temperature. This feature was reversed in the last five decades of the century.

Table 4.1 summarizes the linear trends of the temperature regional series at seasonal and annual timescales. The significance was assessed at the 95% significance level ($p<0.05$). Overall, the results demonstrate that there was a statistically significant uptrend in the maximum, minimum, and mean temperatures at both the annual and seasonal scales. However, this observed warming was not uniform over time. In particular, maximum temperature showed stronger warming during summer and spring than in winter and autumn. Also, the warming in minimum temperature during the cold half of the year (i.e., winter and spring) was slightly higher with respect to the warm half of the year. The only exception was found during summer as maximum temperature experienced more rapid warming (0.2ºC decade^{-1}), relative to all other seasons (0.02 ± 0.08ºC decade^{-1}). This upward trend can be translated into an increase in summer temperature varying from roughly 1.7ºC (maximum temperature) to 2.1ºC (minimum temperature) over the 87-yrs. By contrast, the trend for autumn and winter was generally lower than summer and spring though being statistically significant at the 95% level.

The maximum and minimum temperature signals were apparently revealed in the temporal evolution of the diurnal temperature range (DTR), which reached the significance threshold only in autumn and winter, suggesting a decreasing trend. During spring, DTR showed no trend as minimum and maximum temperatures increased at a similar rate of change (0.08ºC decade^{-1}).

Table 4.1: Seasonal and annual trends in temperature regional series for the period 1920-2006 (ºC decade $^{-1}$).

	Annual	Winter	Spring	Summer	Autumn
Maximum	**0.08**	0.04	**0.08**	**0.20**	0.02
Minimum	**0.14**	**0.11**	**0.08**	**0.24**	**0.14**
Mean	**0.11**	**0.07**	**0.08**	**0.22**	**0.08**
DTR	**-0.06**	**-0.07**	0.00	**-0.04**	**-0.12**

4.1.2. Temperature seasonal and annual trends (1960-2006)

In order to assess how temperature changes vary across the study domain, a detailed regional assessment of temperature variability was conducted from 1960 to 2006, based on a dense network of observatories from 128 observatories.

4.1.2.1. Maximum temperature

Table 4.2 summarizes the seasonal and annual trends of maximum temperature over the period 1960-2006. In general, there was a general warming trend across the study domain in most seasons. As indicated in Table 4.2, majority of observatories (87.5, 83.6, 86, and 92.2%) showed warming trend in annual, summer, winter, and spring temperatures, respectively. The only exception can be seen in autumn since only 29.7% of observatories showed a positive trend, while almost 43% of the observatories exhibited a negative tendency at the 95% level.

Spatially, there were considerable variations in terms of the magnitudes of the trends suggesting that this warming had a spatial component. As depicted in Figure 4.2, the warming was higher in the regions close to the Mediterranean

Sea and the Cantabrian Sea, and to less extent in mainland observatories, particularly during summer, winter, and spring. However, this general picture suggested some seasonal differences. For instance, the Mediterranean coast showed less warming during winter and spring with respect to the Cantabrian observatories, whereas it exhibited more robust warming during summer, particularly in Catalonia. Another interesting aspect was the dominance of a statistically insignificant pattern of trends in the Ebro basin during autumn. Also, a tendency toward faster warming at high elevation was evident relative to low elevation. This gradient was more pronounced during summer periods as the Pyrenees and the Iberian system experienced more warming compared with closing lowlands. It was also noted that the strong warming in southern portions of the study domain was markedly confined to summer and spring. Another important feature was that the spatial distribution of the trends at the annual scale seemed to be spatially more consistent with the distribution of trends in summer and spring than in winter and autumn.

Table 4.2: Number of observatories with statistically significant trend ($p<0.05$) for temperature variables, classified as: + statistically significant positive; - statistically significant negative; N statistically insignificant. The trends were calculated for the period 1960-2006. Total number of observatories is 128.

Variable	Winter			Spring			Summer			Autumn			Annual		
	N	+	-	N	+	-	N	+	-	N	+	-	N	+	-
Maximum	16	110	2	10	118	0	21	107	0	70	38	20	3	124	1
Minimum	41	79	8	23	104	1	11	116	1	41	81	6	18	108	2
Mean	20	107	1	9	119	0	9	119	0	59	61	8	11	117	0
DTR	43	64	21	49	66	13	53	38	37	37	16	75	48	48	32

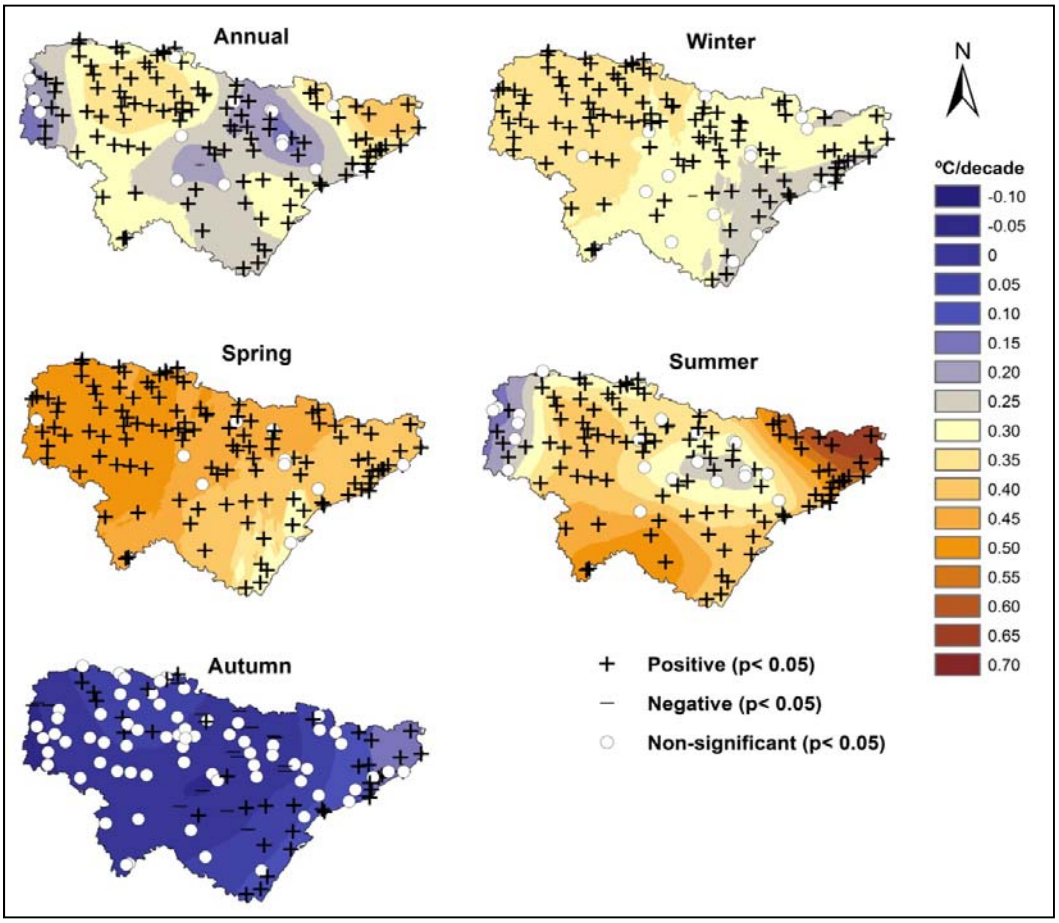

Figure 4.2: Seasonal and annual trends in maximum temperature over the period 1960-2006. The degree of change is expressed in ºC decade^{-1}.

4.1.2.2. Minimum temperature

Figure 4.3 shows the spatial distribution of seasonal and annual trends in minimum temperature over the 1960-2006 interval. Similar to maximum temperature, the trend was globally positive throughout the study area. Also, the strongest warming occurred during summer and spring, whereas autumn exhibited weak warming. The degree of warming varied considerably throughout the study domain though being very similar to those of maximum temperature. In particular, the strongest increase in minimum temperature was noted at coastal stations, with more observatories with statistically significant trend close to the

Cantabrian Sea, particularly during wintertime. The continental observatories exhibited the lowest temperature rise, suggesting strong spatial gradient from the coast to mainland. Also, of interest, the annual, winter, and summer temperatures indicated a south-north gradient with less warming in southern sites.

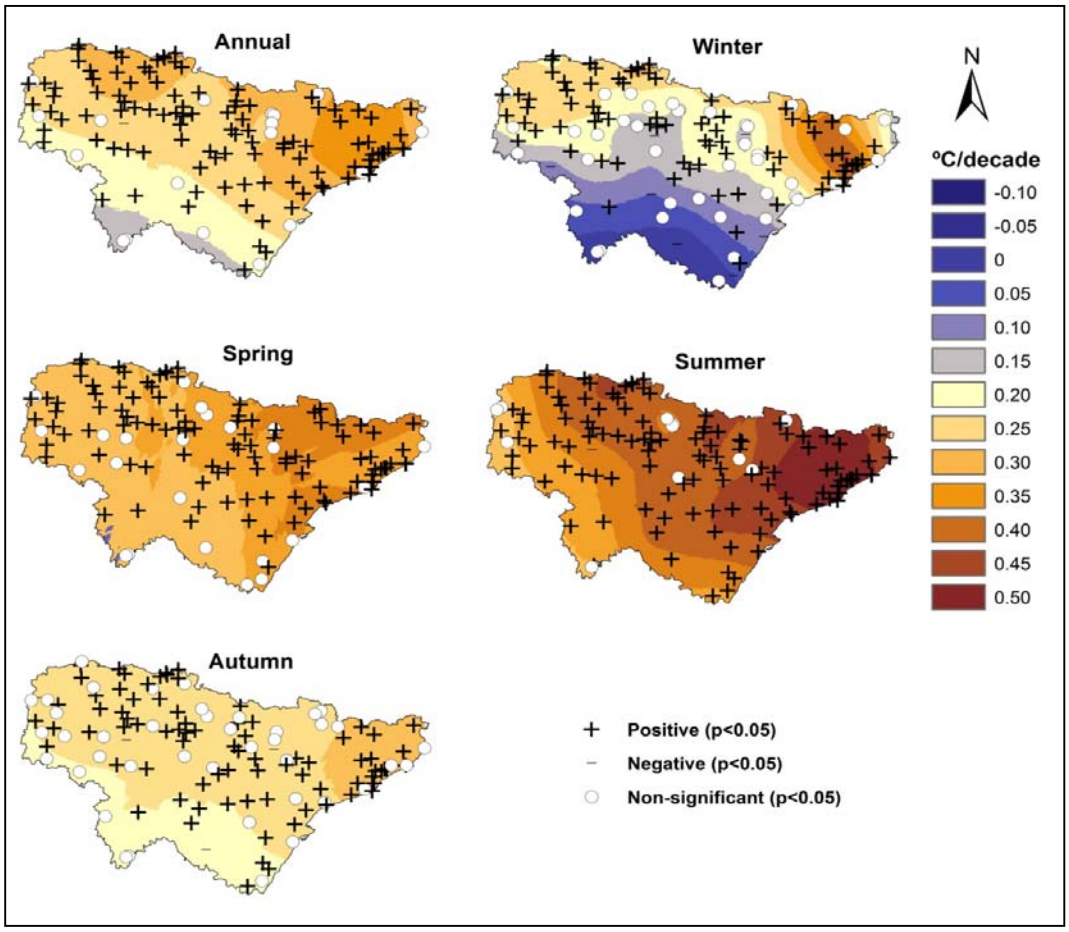

Figure 4.3: Same as Figure 4.2, but for minimum temperature**.**

4.1.2.3. Mean temperature

Table 4.2 summarizes the mean temperature trends according to their statistical significance. The strongest change occurred during summer and spring, whereas the lowest change took place in autumn. In particular, more observatories did show insignificant trend during autumn (46.1%), whereas most observatories

exhibited statistically significant trends during summer, spring (93%) and winter (84.5%).

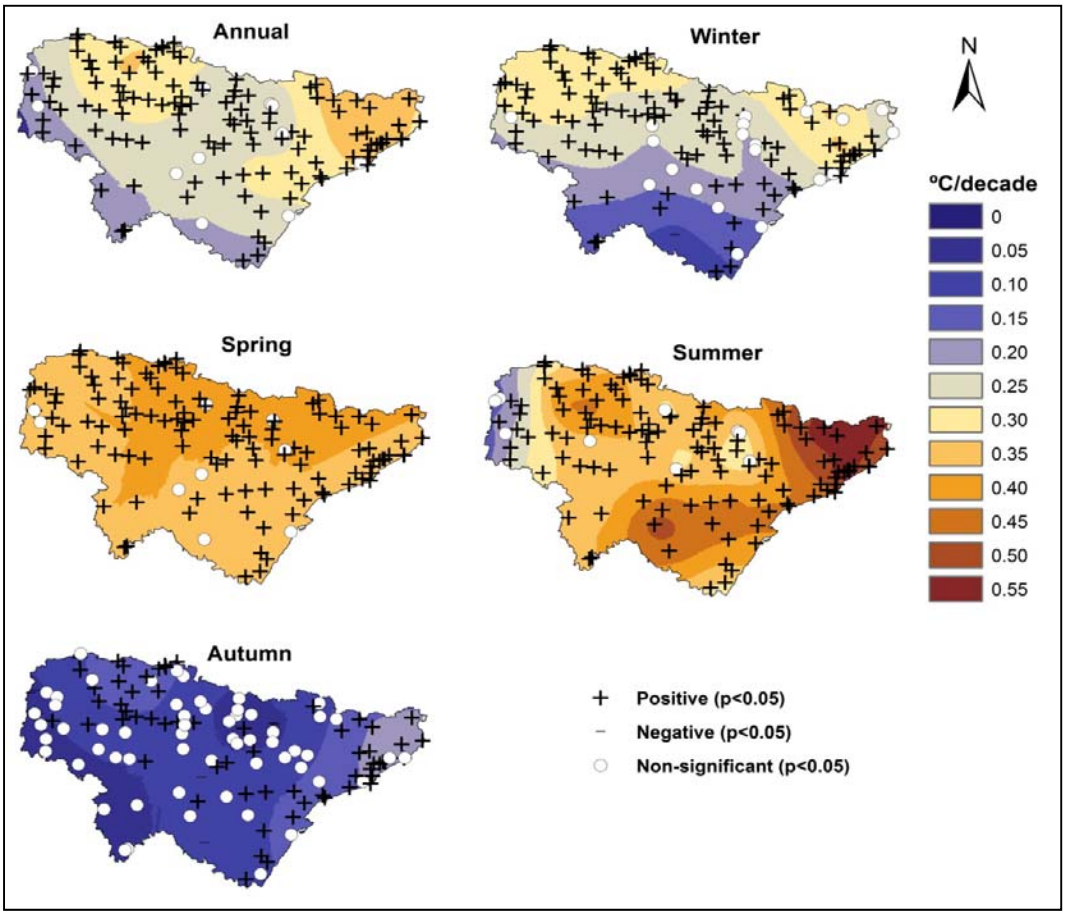

Figure 4.4: Same as Figure 4.2, but for mean temperature**.**

Figure 4.4 depicts the spatial distribution of trends in mean temperature from 1960 to 2006. The spatial patterns of mean temperature seemed to be consistent with those observed for maximum and minimum temperatures, with strong signal in coastal areas than in continental observatories. However, this warming was less pronounced along the Mediterranean (Cantabrian) coast during winter and spring (summer). In contrast to other seasons, more insignificant trends tended to be located in mainland observatories during autumn.

4.1.2.4. Diurnal temperature range (DTR)

Figure 4.5 illustrates the spatial distribution of trends of seasonal and annual DTR, while Table 4.2 summarizes these trends. Table 4.2 suggests three seasons with positive trend (summer, winter, and spring); meanwhile autumn was the only season with a decreasing trend in much of the study area. Conversely, during winter and spring, more observatories showed a statistically significant positive trend. This can probably imply that DTR had a seasonal cycle, with higher range during cold seasons (i.e., winter and spring) and lower values in warm seasons (i.e., summer and autumn). Spatially, it seems that DTR did not exhibit a particular structure. Nonetheless, it showed more uptrend over continental observatories during winter and spring. By contrast, majority of inland observatories experienced negative tendencies in autumn and summer, although many of them were statistically insignificant during summer ($p<0.05$). Overall, there was some evidence on a divergent behavior of DTR (i.e., positive and negative), when compared with the evolution of maximum, minimum and mean temperatures.

Temporarily, a comparison of the 1960–2006 trends, as summarized in Table 4.3, with the changes over the longer period 1920–2006 (Table 4.1) illustrates that the observed warming in the 1960-2006 interval may indeed belong to a longer trend (1920-2006). However, a quick comparison between trends in the seasonal and annual temperatures during the periods 1920-1959 and 1960-2006, as revealed in Tables 5.3 and 5.4 clearly shows that the warming during recent decades was mainly responsible for much of the upward trend found through the

entire period 1920-2006. Most seasonal and annual trends during the period from 1920 to 1959 were found statistically insignificant ($p<0.05$). The only exception corresponded to summer season in which temperature experienced upward trend though being weaker than trends recorded in recent decades. For example, the warming rate of the annual mean temperature from 1960 to 2006 was approximately twice as high in the period from 1920 to 1959. Interestingly, spring mean temperature showed an outstanding warming rate in recent decades (0.66ºC decade^{-1}). Similarly, summer experienced a trend during the period 1960-2006 approximately twice as high in the period 1920-2006.

Table 4.3: Seasonal and annual trends in temperature regional series for the period 1960-2006 (ºC decade^{-1}). The regional series were aggregated based on data from 128 observatories

	Annual	Winter	Spring	Summer	Autumn
Maximum	**0.25**	**0.18**	**0.32**	**0.43**	0.07
Minimum	**0.21**	**0.10**	**0.19**	**0.39**	**0.19**
Mean	**0.33**	**0.14**	**0.66**	**0.41**	**0.13**
DTR	**0.13**	**0.08**	**0.51**	0.04	**-0.12**

Bold numbers are significant at the 0.05 level following the Rho Spearman test.

Table 4.4: Seasonal and annual trends in temperature regional series for the period 1920-1959 (ºC decade^{-1}). The regional series was calculated based on data from 19 observatories

	Annual	Winter	Spring	Summer	Autumn
Maximum	0.12	-0.11	0.28	0.22	0.11
Minimum	**0.17**	0.02	0.18	**0.30**	0.19
Mean	0.15	-0.05	0.24	**0.26**	0.15
DTR	-0.05	-0.13	0.12	-0.08	-0.07

Bold numbers are significant at the 0.05 level following the Rho Spearman test.

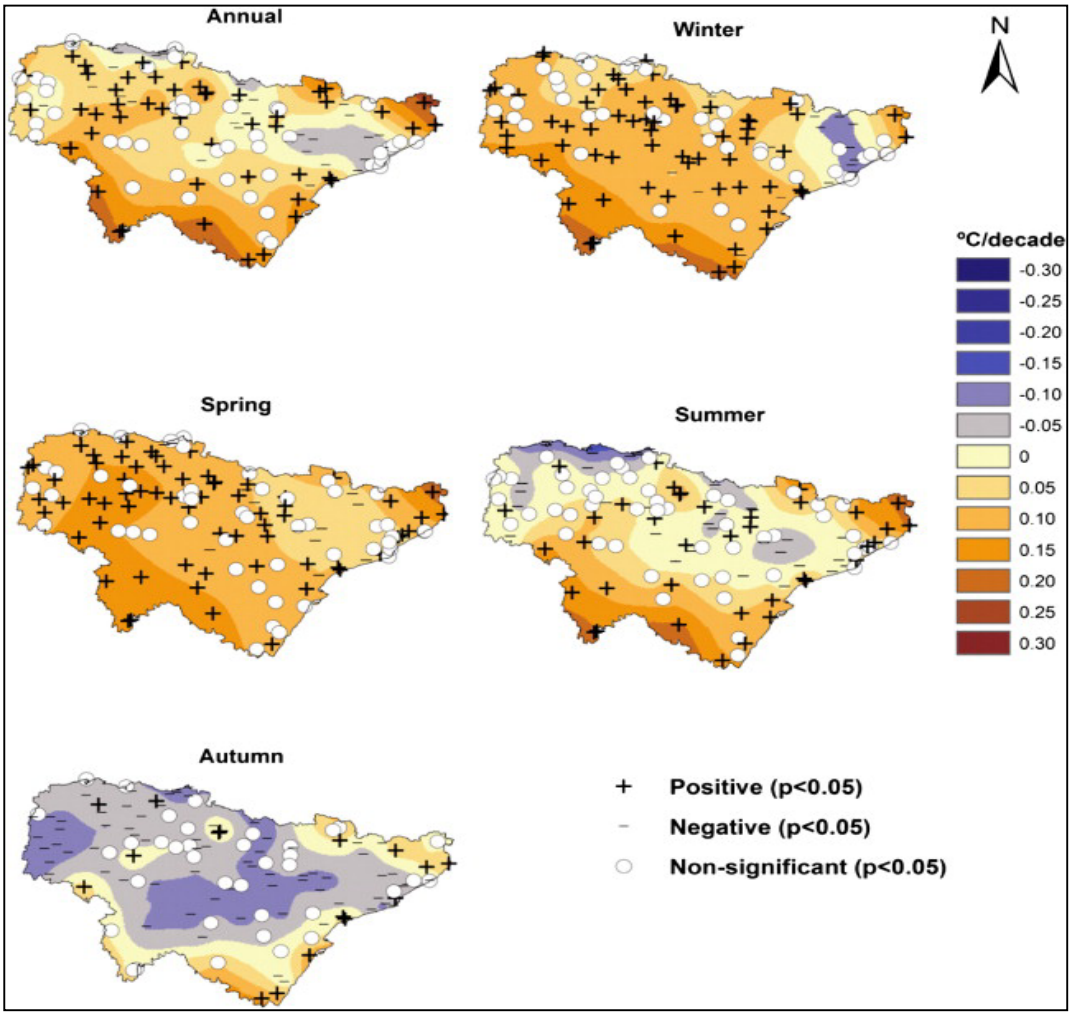

Figure 4.5: Same as Figure 4.2, but for DTR**.**

Spatially, a quick comparison between Figures 4.2, 4.3 and 4.4 clearly shows that warming in maximum, minimum, and mean temperatures was dominated across much of northeastern Spain. Accordingly, it can be inferred that the cooling periods of the year got shorter relative to the warmer periods. Recalling that the observatories used in this study are located within both urban and non-urban localities and also given that the series have been previously homogenized to limit effects of non-climate factors (e.g., urbanization), the observed upward

trends in most of observatories reveal that this increase had a climatological meaning. It can therefore be due to natural climate variability and/or global warming induced mainly by GHG. Nonetheless, the strength of this warming was inconsistent across the study domain and among seasons. The strongest signals were found during spring and summer, whereas this increase was less marked in autumn.

4.2. Observed changes in temperature extreme events

In this section, the results on the analysis of trends in daily maximum and minimum temperature, as derived from a suite of extreme temperature indices described in Table 3.2, are presented. The spatial and temporal variability of these indices are also outlined.

4.2.1. Randomness testing

Presence of serial correlation in time series can affect the ability of the Mann-Kendall's test to correctly assess the significance of trends. In this study, the serial correlation coefficients were computed for lags up to 14. In general, the ACF results confirm that a majority of the time series of extreme events did not show significant serial correlation at the lag-1. A large proportion of the time series was serially independent and did not exhibit short-term persistence. This suggests considerable year-to-year variability in the time series of the investigated indices. Figure 4.6 illustrates an example of the cold days (TX10p) time series at the observatory of Barcelona Airport. As presented, the lag-1 serial correlation coefficient was insignificant at $p<0.05$. This suggests that the series was free from serial correlation. In a few cases, however, the time series showed significant serial correlation. In such cases, the prewhitening procedure was used

to limit the effect of serial correlation before applying the trend test. One obvious example corresponding to the warmest days (WD) time series at Amurrio observatory (Alava) is given in Figure 4.7. As depicted, the time series presented a significant lag-1 serial correlation coefficient (Figure 4.7.A), as more than 5% of the sample autocorrelations exceeded the upper confidence limit. To eliminate the serial correlation, the pre-whitening procedure was applied and the Mann-Kendall test was then undertaken for the pre-whitened series. Figure 4.7.B shows the lag-1 correlation after removing the effect of the serial correlation.

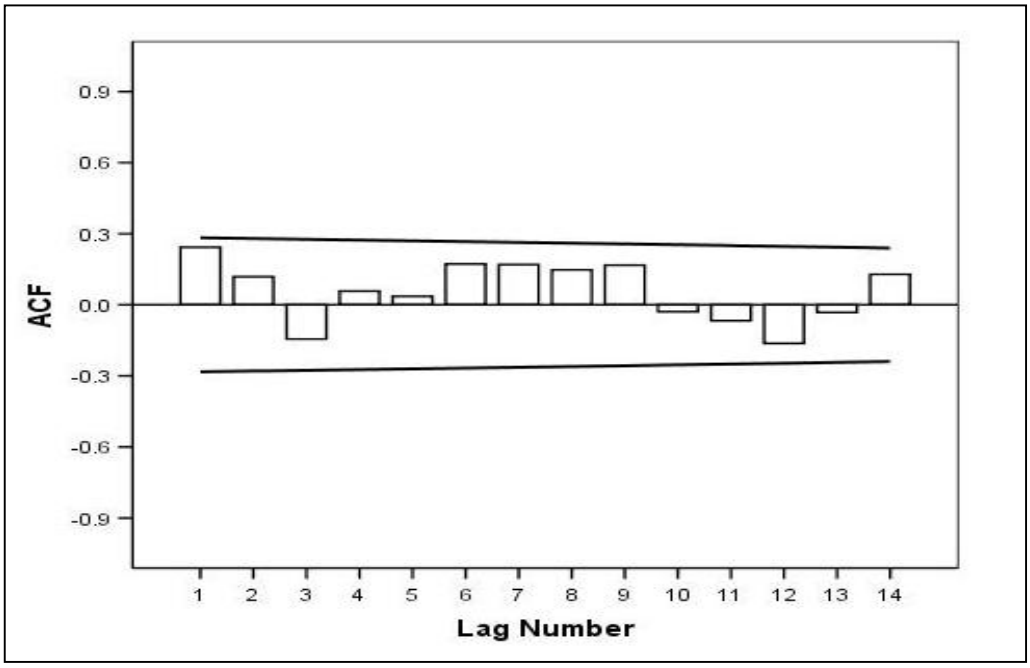

Figure 4.6: Autocorrelation function for the cold days (TX10p) time series at the observatory of "airport of Barcelona" obtained by taking 14-year differences (solid line refers to the upper and lower limit of the 95 % significance level given by ± 1.96 ($1/\sqrt{n}$) where *n* = 47 for the period 1960-2006.

In the same context, to account for the possible impact of cross-correlation on trend assessment, the cumulative probability distribution functions (cdf) of both the Monte Carlo simulations and the observed series are plotted in Figure 4.8.

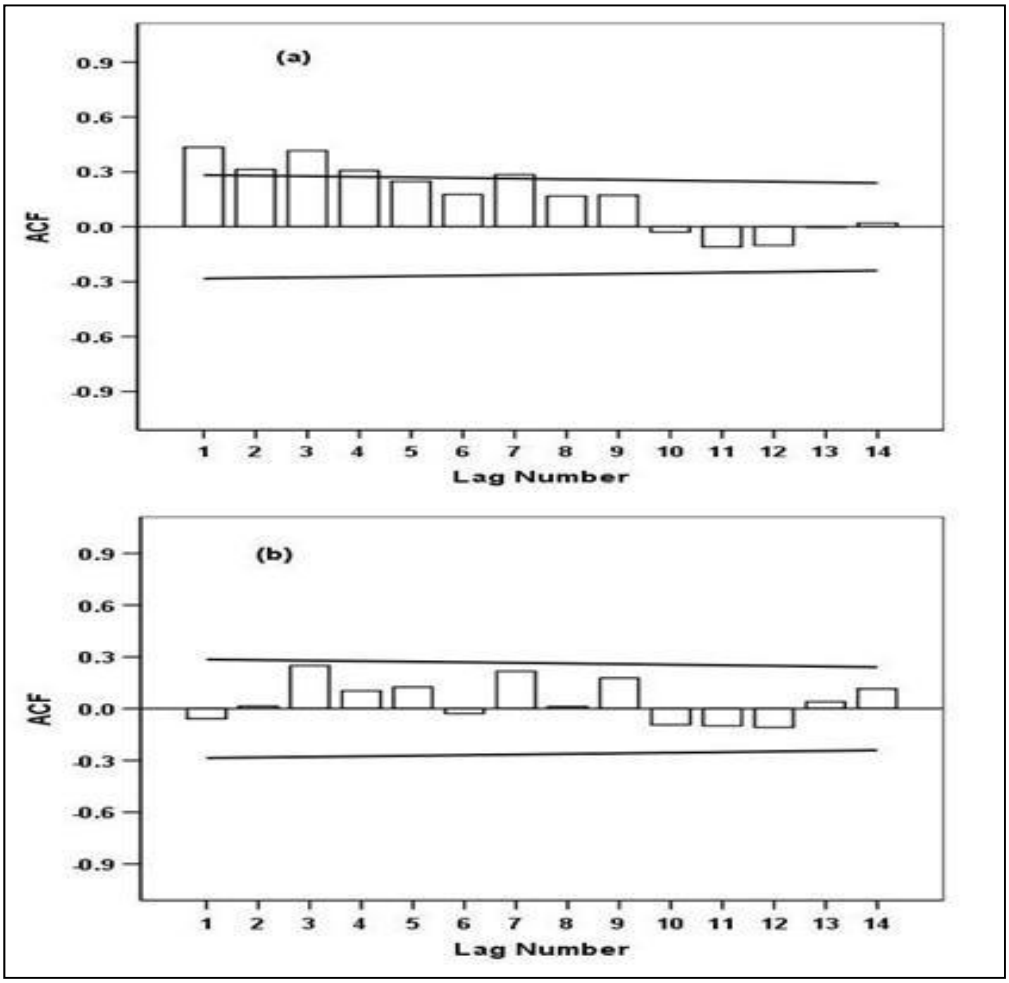

Figure 4.7: Same as Figure 4.6, but for the warmest day (WD) time series at the observatory of Amurrio [Alava province].

In this figure the simulated series were compared with the observed series at different statistical significance levels. Overall, the results indicate that the influence of regional cross-correlation on trend assessment had negligible impact. A comparison of the field significance of the observed and resampled data confirms that the empirical probability distribution of the observed data was

smaller than that of the simulated data at a p-value of 0.025, and larger at a p-value of 0.975.

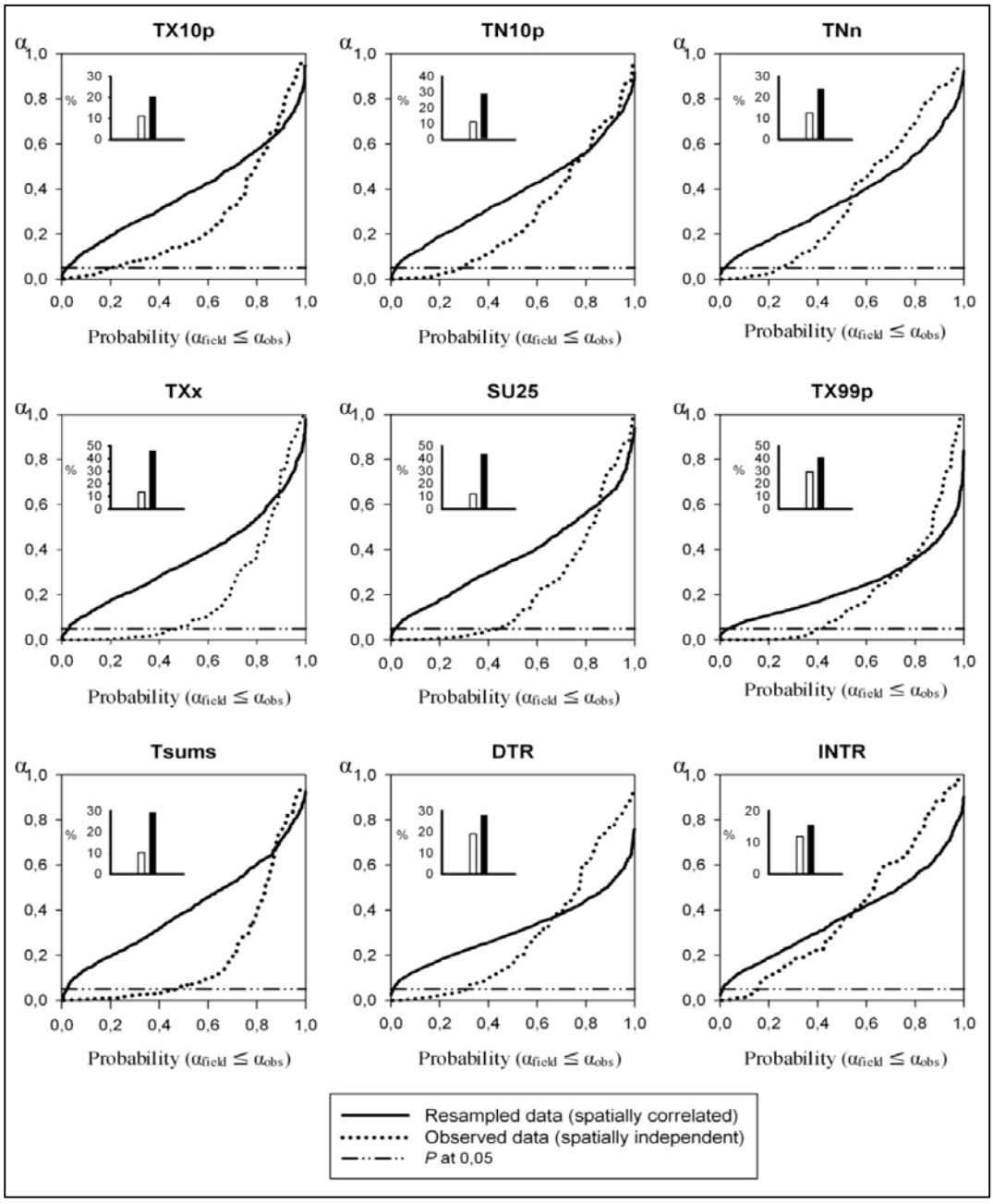

Figure 4.8: The empirical cumulative distribution function (cdf) of the significance levels of the trends for the resampled and observed data for a selected number of indices. Bar lines in the upper panel show percentage of the observed series (■) and the resampled series (□) with statistically significant trend at p<0.05.

This simply implies that the observed data were statistically significant at p-value <0.05. In addition, the total number of series with significant trends at the 95% confidence level was generally larger than those obtained from the 1000 Monte Carlo runs. This suggests that the observed trends in the extreme temperature time series were greater than the number of the trends that were expected to occur by chance. The pattern of the obtained trends at the individual observatories was thus independent from climate noise and did reflect a global trend. Accordingly, it can be concluded that the local trends obtained from the original dataset were field significant.

Taking the cross-correlation and the serial correlation results together, it can be implied that the trend results are robust and could not be substantially biased by either the serial correlation or the cross-correlation.

4.2.2. Spatial and temporal variability of temperature extremes

This section gives an overview of the trend results for each investigated extreme index. Table 4.5 summarizes the results from the application of the Mann-Kendall test. Figures 5.9, 5.10, and 5.11 show the spatial patterns of the trend for each index in terms of the direction (sign) of change and its statistical significance.

4.2.2.1. Changes in warm extremes

Table 4.5 summarizes the results of the Mann-Kendall test for warm temperature indices. As indicated, there was a general upward tendency in majority of warm extremes for both frequency and intensity indices. On average, this increasing was more evident for indices of warm nights (TN90p) [96.1% of observatories],

warm days (TX90p) [93.8%], and the annual high of maximum temperature [91.4%]. However, warm extremes related to night-time showed more significant trends compared with day-time indices. For example, tropical nights (TR20) and warm nights (TN90p) showed upward trend in 47.7 and 73.4% of observatories respectively. In contrast, warmest day (WD), very warm days (TX99p), and summer days (SU25) reached the significance level only in 28.9, 39.8, and 43.8% of observatories, respectively. Given that the warm events mainly occur during summer (JJA), this finding demonstrates that the cold tail of temperature distribution increased more rapidly than the warm tail during summer periods. Table 4.5 also indicates that more observatories (46.1%) showed statistically significant trends in the annual high maximum temperature (TXx), relative to the annual low maximum temperature (TXn) (32%). This implies more increase in maximum temperature in summer than in winter over the period from 1960 to 2006.

Table 4.6 shows the associations in the trend directions for each pair of warm temperature extremes. As presented, most of frequency indices showed a relatively high agreement between the signs of the trends. For instance, warm days (TX90p) exhibited the same direction of trends of summer days (SU25), very warm days (TX99p) and tropical nights (TR20) in 76.6, 74.2 and 61.7% of observatories, respectively. The same behavior was confirmed between temperature intensity indices (e.g., TXx and WD). These strong associations favor for the occurrence of similar spatial patterns.

Table 4.5: Results of trend analysis for cold, warm and variability extremes (significance was assessed at the 95% level). Abbreviations of the indices correspond to those listed in Table 3.2).

Category	Index	Positive			Negative		
		Sig.	Non-Sig.	Total (%)	Sig.	Non-Sig.	Total (%)
Cold extremes	**TX10p**	0.8	13.3	**14.1**	19.5	66.4	**85.9**
	TN10p	3.1	22.7	**25.8**	25.8	48.4	**74.2**
	FD0	1.6	24.2	**25.8**	27.3	46.9	**74.2**
	ID0	0.0	14.8	**14.8**	16.4	68.8	**85.2**
	CN	18.8	42.2	**61.0**	2.3	36.7	**39.0**
	TN1p	0.8	34.3	**35.1**	17.2	47.7	**64.9**
	TNx	69.5	24.2	**93.7**	0.8	5.5	**6.3**
	TNn	19.5	44.5	**64.0**	4.7	31.3	**36.0**
Warm extremes	**TX90p**	56.3	37.5	**93.8**	0.0	6.2	**6.2**
	TN90p	73.4	22.7	**96.1**	1.6	2.3	**3.9**
	SU25	43.8	42.2	**86.0**	0.0	14.0	**14.0**
	WD	28.9	50	**78.9**	1.6	19.5	**21.1**
	TX99p	39.8	42.2	**82.0**	1.6	16.4	**18.0**
	TR20	47.7	38.3	**86.0**	1.6	12.5	**14.1**
	TXx	46.1	45.3	**91.4**	0.0	8.6	**8.6**
	TXn	32.0	56.3	**88.3**	0.8	10.9	**11.7**
Variability extremes	**Tsums**	46.9	46.9	**93.8**	0.0	6.2	**6.2**
	Intr	12.5	43	**55.5**	3.1	41.4	**44.5**
	DTR	12.5	36.7	**49.2**	15.6	35.2	**50.8**
	Stdev	15.6	57.1	**72.7**	0.0	27.3	**27.3**
	GSL	14.8	52.3	**67.1**	1.6	31.3	**32.9**

Figure 4.9 shows the spatial patterns of trends of warm extremes. As illustrated, while the majority of observatories in the study domain showed upward tendency, considerable regional differences were revealed. The coastal areas along the Cantabrian Sea and the Mediterranean Sea mainly exhibited the largest warming, whereas much of the continental areas showed insignificant trends. This spatial structure of the trends was evident for indices related not only to day-time warm extremes (e.g., TX90p, WD, SU25, and TX99p), but also to night-time warm extremes (e.g., TN90p and TR20). Nevertheless, a pattern of positive

trends in night-time extremes was also found over the Ebro valley, which was not shown for day-time extremes.

Table 4.6: Cross-tabulation of the sign of the trends (statistically positive, statistically negative, and statistically insignificant) for each pair of warm and variability extreme indices

Index	TX90p	TN90p	SU25	WD	TX99p	TR20	TXx	TXn	Tsums	Intra	Stdev	GSL	DTR
TX90p		65.6	76.6	63.3	74.2	61.7	77.3	54.7	71.9	50	46.9	49.2	40.6
TN90p			53.1	41.4	52.3	66.4	53.9	37.5	59.4	29.7	29.7	32.0	26.6
SU25				66.4	69.5	52.3	74.2	59.4	71.9	54.7	59.4	60.2	47.7
WD					85.9	55.5	73.4	57.0	59.4	75.8	68.0	65.6	53.1
TX99p						51.6	78.1	55.5	65.6	66.4	61.7	59.4	49.2
TR20							62.5	49.2	53.9	47.7	47.7	51.6	46.9
TXx								57.0	68.0	57.0	60.2	57.8	46.1
TXn									53.1	56.3	53.9	71.1	57.0
Tsums										53.9	56.3	53.9	44.5
Intra											75	72.7	62.5
Stdev												71.9	61.7
GSL													60.2
DTR													

Figure 4.10 reveals the temporal evolution of warm nights (TN90p) at three different observatories. As illustrated, there was a very strong upward trend at Bilbao Airport along the Cantabrian Sea (7.3 days decade^{-1}) and Blanes observatory on the Mediterranean Sea (6.57 days decade^{-1}). In contrast, the mainland observatory of Zaragoza Airport experienced less warming (3.29 days decade^{-1}). This gives indications on considerable spatial differences in the behavior of warm extremes, with strong continental-coastal gradient.

Figure 4.11 illustrates the regional series of each warm extreme index. In agreement with the upward tendency exhibited for most of the indices at the station-based level, an increasing trend in the regional series of warm days (TX90p), warm nights (TN90p), very warm days (TX99p), and tropical nights (TR20) were also expected.

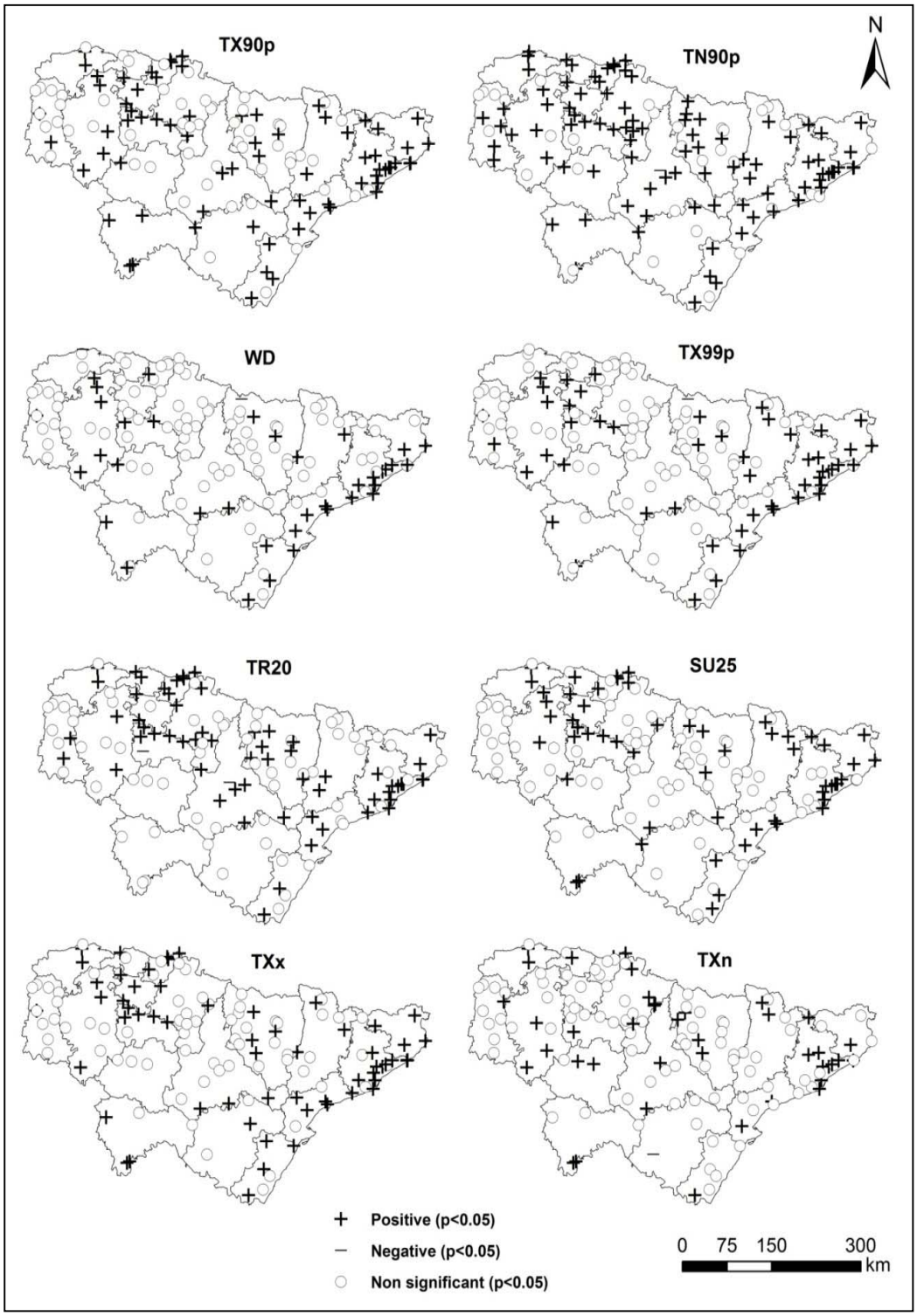

Figure 4.9: Spatial distribution of the trends in warm extreme indices over the period 1960-2006.

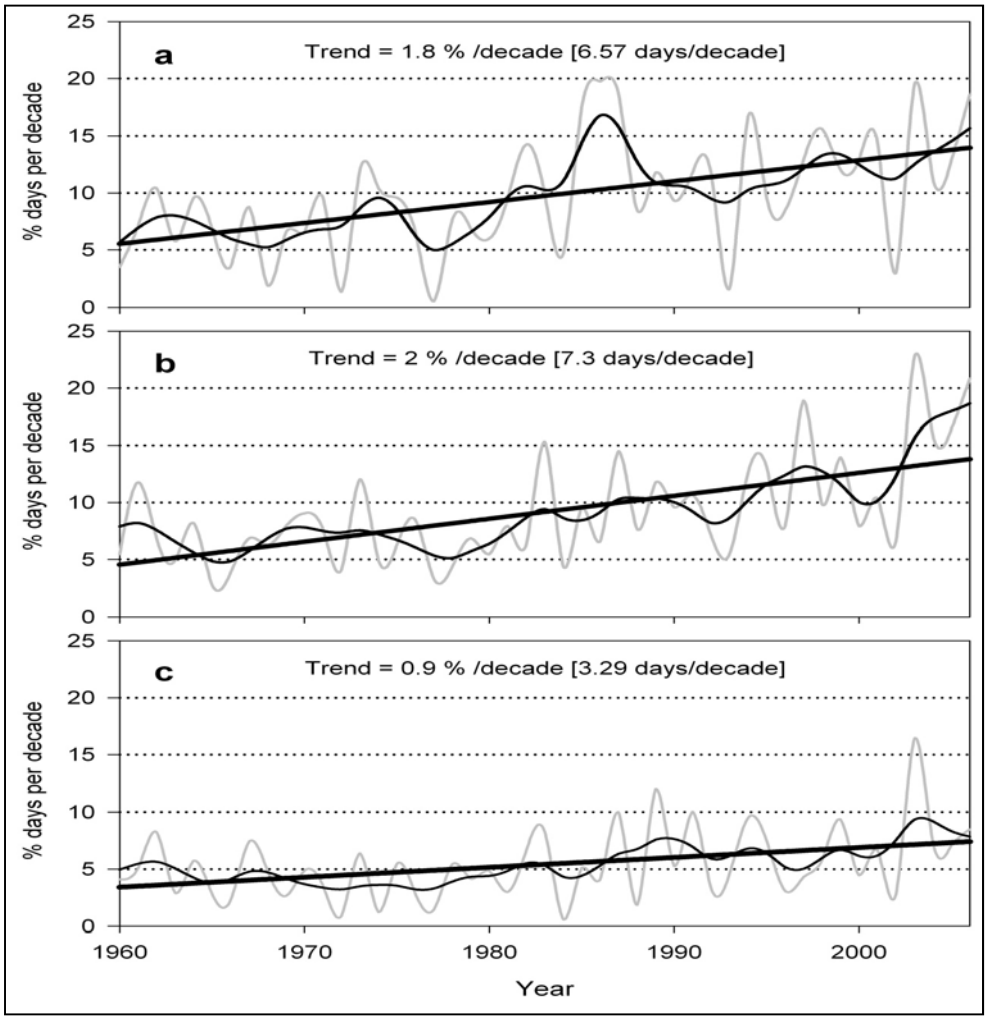

Figure 4.10: Temporal evolution and trends in warm nights (TN90p) time series at three different observatories: (a) Blanes (Mediterranean station), (b) airport of Bilbao (Cantabrian station), and (c) airport of Zaragoza (mainland station). The solid line represents the linear regression. The thin black line represents a 7-year running mean.

As illustrated, the regional trends suggested positive trend in all indices for 1960-2006. The strongest trends were mainly accompanied to warm nights (TN90p) and warm days (TX90p). The regional trends indicate that warm days (TX90p) and warm nights (TN90p) significantly increased by 0.74 (2.7 days decade^{-1}) and 0.91% (3.3 days decade^{-1}), respectively. In contrast, tropical nights (TR20) and

summer days (SU25) showed less warming, with a rate of 0.61 and 2.2 days decade^{-1}, respectively. As illustrated in Figure 4.11, most of the warming trends in TX90p, TN90p, TX99p, and TR20 occurred during the last two decades; with unusual peak in 2003. A gradual increasing trend was also observed for other indices from 1960 to 2006 (e.g., TXx and TXn).

4.2.2.2. Changes in cold extremes

Table 4.5 also shows the trend results of the cold temperature indices. In general, it is evident that majority of indices corresponding to frequency of cold extremes showed negative trends, though being statistically insignificant in most observatories. For instance, 85.9, 85.2 and 74.2 % of observatories exhibited a declining tendency in cold days (TX10p), ice days (ID0), cold nights (TN10P), and frost days (FD0), respectively. By contrast, the indices corresponding to the intensity of cold extremes, including coldest night (CN) and the annual low minimum temperature (TNn), showed statistically significant trends in fewer number of observatories (61 and 64 % of observatories, respectively).

Among all indices, the annual high minimum temperature (TNx) was the only index that indicated a significant trend ($p<0.05$) across much of the study domain (69.5% of observatories). This implies that the trends in the probability distribution of the cold tail of temperature were more linked to the trends in the intensity of temperature than to the frequency of cold events. As indicated in Table 4.5, the number of observatories that experienced downward tendency in the day-time cold indices (e.g., TX10p and ID0) was generally larger than those of night-time indices (e.g., TN10p, FD0, and CN). Nonetheless, the night-time

indices reached the statistical significance level ($p<0.05$) in more observatories compared with day-time indices.

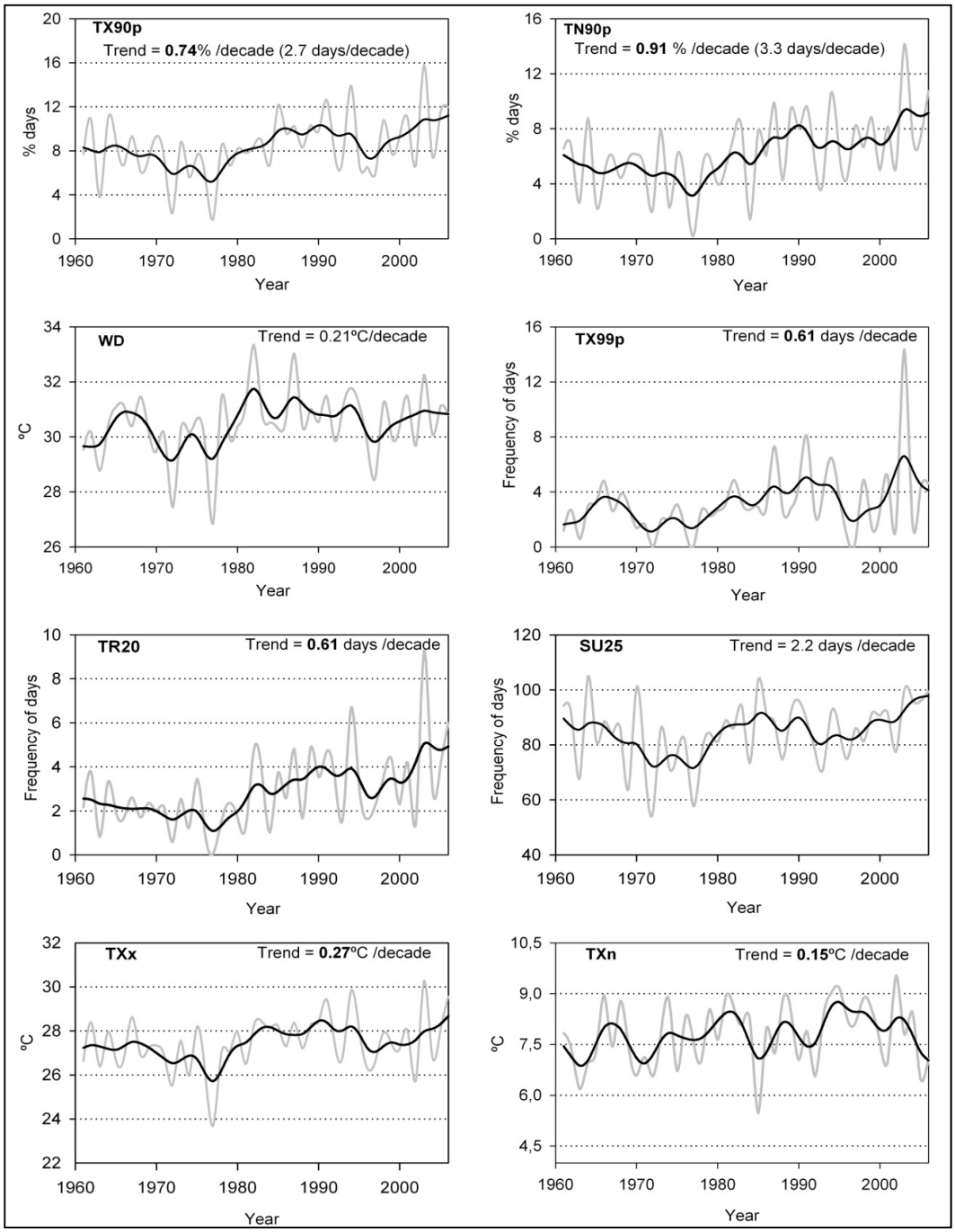

Figure 4.11: Temporal evolution and trends in the regional series of warm extreme indices over the period 1960-2006. Bold numbers refer to significant trends ($p<0.05$). Black line represents a 7-year running mean.

For instance, cold nights (TN10p) and frost days (FD0) were statistically significant in 25.8 and 27.3% of observatories respectively, meanwhile cold days (TX10p) and ice days (ID0) reached the confidence level only in 19.5 and 16.4% of observatories, respectively. This finding indicates more warming in the cold tail of winter temperature than the warm tail over the period from 1960 to 2006.

Table 4.7 presents the association in the sign (direction) of the trend for each pair of cold temperature indices. As shown, there was a high level of consistency in the temporal evolution of the frequency indices, as revealed by coincidences in the sign of the trends. For instance, 84.4% of observatories showed the same sign (direction) of changes in cold nights (TN10p) and frost days (FD0). Similarly, there was a high level of agreement (82.8% of observatories) between the direction of trends in very cold nights (TN1p), and both cold nights (TN10p) and cold days (TX10p). This suggests strong consistency between indicators of the frequency of cold temperature. This high consistency also implies that variability in the frequency of cold extremes had a “global” character over the region, with few spatial differences. This can probably suggest that variations in the frequency of cold extremes are more attributable to large-scale physical processes more than local conditions (e.g., topography). As indicated in Table 4.7, the annual low minimum temperature (TNn) showed higher agreement with frequency indices, compared with the annual high minimum temperature (TNx). This confirms the previous finding on the rapid increase (warming) in the cold tail of temperature distribution during the cold season.

Table 4.7: Cross-tabulation of the sign of the trends (statistically positive, statistically negative, and statistically insignificant) for each pair of cold and variability extreme indices

Index	TX10P	TN10P	FD0	ID0	CN	TN1P	TNX	TNn	Tsums	Intra	Stdev	GSL	DTR
TX10P		63.3	64.8	74.2	63.3	71.1	24.2	60.2	43.0	65.6	65.5	68.0	57.0
TN10P			84.4	64.8	64.1	82.8	25.0	64.1	35.9	62.5	59.4	64.8	66.4
FD0				67.2	63.3	82.8	23.4	63.3	35.9	58.6	60.2	62.5	64.8
ID0					66.4	73.4	26.6	64.8	43.8	71.1	68.8	71.9	60.2
CN						73.4	41.4	82.8	55.5	66.4	68.8	78.1	60.2
TN1P							25.0	69.5	43.0	68.0	69.5	73.4	70.3
TNX								37.5	53.1	31.3	35.9	33.6	31.3
TNn									49.2	62.5	64.8	78.1	54.7
Tsums										53.9	56.3	53.9	44.5
Intra											75.0	72.7	62.5
Stdev												71.9	61.7
GSL													60.2
DTR													

Figure 4.12 depicts the spatial distribution of the trends in cold extreme indices. In general, there were no marked spatial patterns across the study domain as trends were not evident in specific regions. However, there was a slight tendency to locate more negative trends in inland observatories for cold days (TX10p), frost days (FD0) and very cold nights (TN1p). By contrast, coldest night (CN) and the annual low minimum (TNn) revealed a spatial structure, whereby coastal observatories eastward showed rapid warming. In the same sense, the annual high minimum (TNx) showed a broad and spatially consistent pattern of positive trends, although this warming was markedly less evident in the southern and south-central portions of the study area.

Figure 4.13 illustrates the temporal evolution and trends in the regional series of cold temperature indices. Over the period from 1960 to 2006, the regionally weighted occurrence of cold days (TX10p), cold nights (TN10p), very cold nights

(TN1p), frost days (FD0) and ice days (ID0) decreased by 1.2, 0.8, 0.11, 1.35 and 0.19 days decade^{-1}, respectively. Among cold extremes, the annual high minimum temperature (TNx) exceptionally showed a statistically significant uptrend (0.3ºC decade^{-1}). Overall, the low temporal variability of most of the cold indices at the regional scale agreed well with those observed at the individual sites.

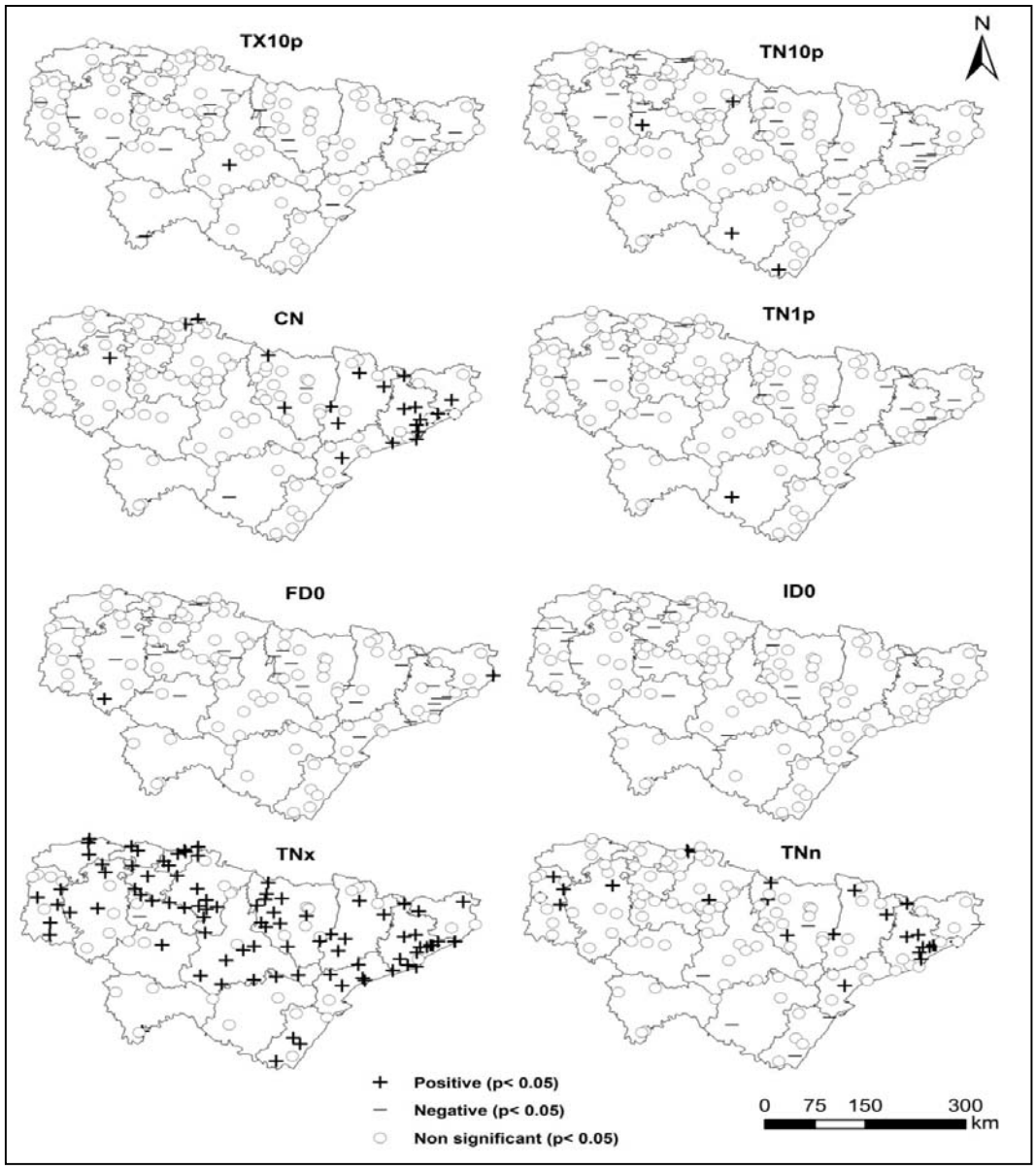

Figure 4.12: Same as Figure 4.9, but for cold extreme indices.

A visual inspection of the temporal evolution of cold temperature indices clearly reveals a multidecadal character (Figure 4.13).

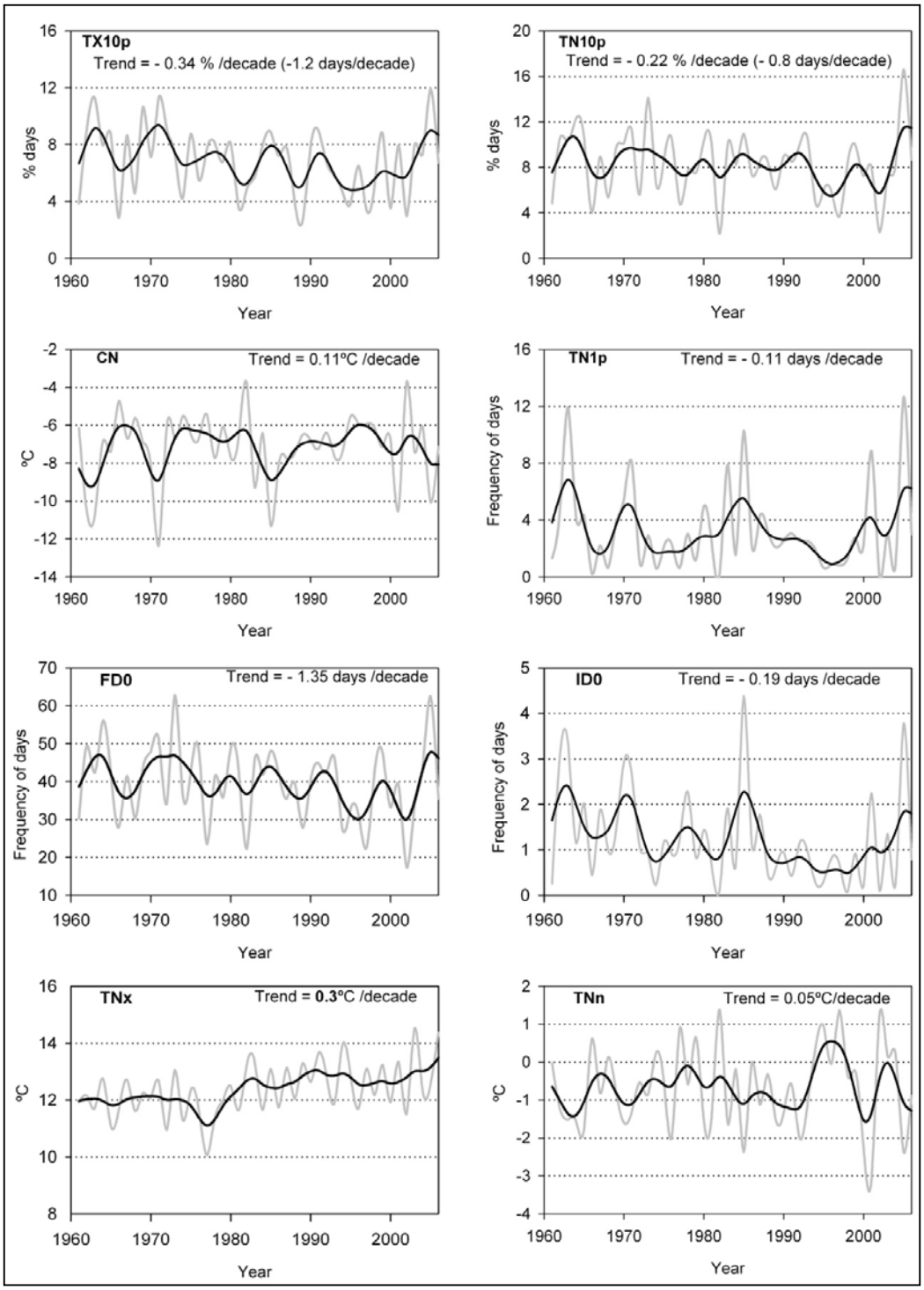

Figure 4.13: Same as Figure 4.11, but for cold extreme indices.

Temporarily, the inter-decadal variability of the cold indices is more apparent compared with the long-term changes. This can be expected given that cold extremes are mostly retained to winter (DJF), a season in which climate is largely driven by large-scale atmospheric flows. These flows vary considerably from year to year. As shown in Figure 4.14, a decadal comparison of the frequency of cold extremes over the period from 1960 to 2006 indicates that there were more colder events during the 1960s and 1970s (e.g., TX10p and ID0). However, they had markedly been less frequent during the last two decades. This high decadal variability could decrease the ability of the trend test to detect a long-term statistically significant linear trend over the whole period.

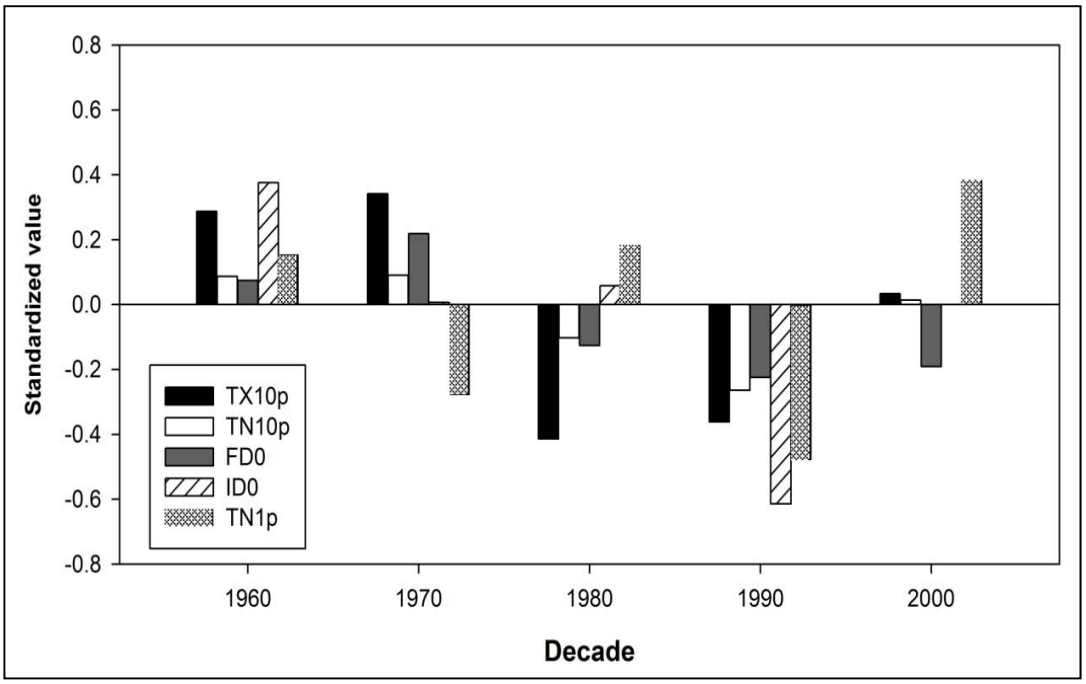

Figure 4.14: Decadal variation of a set of selected cold temperature frequency indices, averaged for the whole study domain. The annual number of events was standardized by their mean and standard deviation to account for the varying scale units of the indices (i.e., ºC and days).

4.2.2.3. Changes in variability extremes

A summary of the Mann-Kendall results regarding trends in variability indices is also given in Table 4.5. In general, no trends were evident in most of temperature variability indices ($p<0.05$). Nevertheless, most of the observatories exhibited a clear upward tendency in indices of temperature sums (Tsums) (93.8%), the standard deviation of mean temperature (Stdev) (72.7%), and the growing season length (GSL) (67.1%). On the other hand, the tendency in the diurnal temperature range (DTR) was mixed between positive (49.2%) and negative (50.8%). Among all indices, temperature sums (Tsums) was the only indicator which showed a statistically significant trend ($p<0.05$) in almost half of the observatories (46.9%). Tables 5.6 and 5.7 summarize the association in trend significance between variability indices on the one hand and warm and cold extremes on the other. A comparison between Tables 5.6 and 5.7 suggests that variability indices showed higher degree of agreement with cold extremes than with warm extremes. For instance, the signs of the trends in the interannual extreme temperature range (INTR) matched those of ice days (ID0), very cold nights (TN1p), coldest night (CN), cold days (TX10p) and cold nights (TN10p) in 71.1, 68, 66.4, 65.5 and 62.5% of observatories, respectively. Contrarily, it coincided with the trends of warm nights (TN90p), tropical nights (TR20) and warm days (TX90p) only in 29.7, 47.7 and 50% of observatories, respectively. These results suggest that the behavior of variability indices in the study area is associated more with changes in the low tail of temperature distribution than in the warm tail. As expected, temperature sums (Tsums) exhibited similar temporal patterns to warm extremes including: warm days (TX90p) and summer days

(SU25) (71.9%), the annual high maximum temperature (TXx) (68%), and very warm days (TX99p) (65.6%).

Figure 4.15 illustrates the spatial distribution of variability indices. Overall, the indices were spatially independent, suggesting a very low spatial consistency across the study area. However, some local differences can also be highlighted. For instance, most of the significant upward trends in the growing season length (GSL) tended to be located in the northeastern portions (Catalonia) and at the highly elevated areas (e.g., the Pyrenees). Also, mainland observatories showed more significant trends in the diurnal temperature range (DTR) compared with coastal regions.

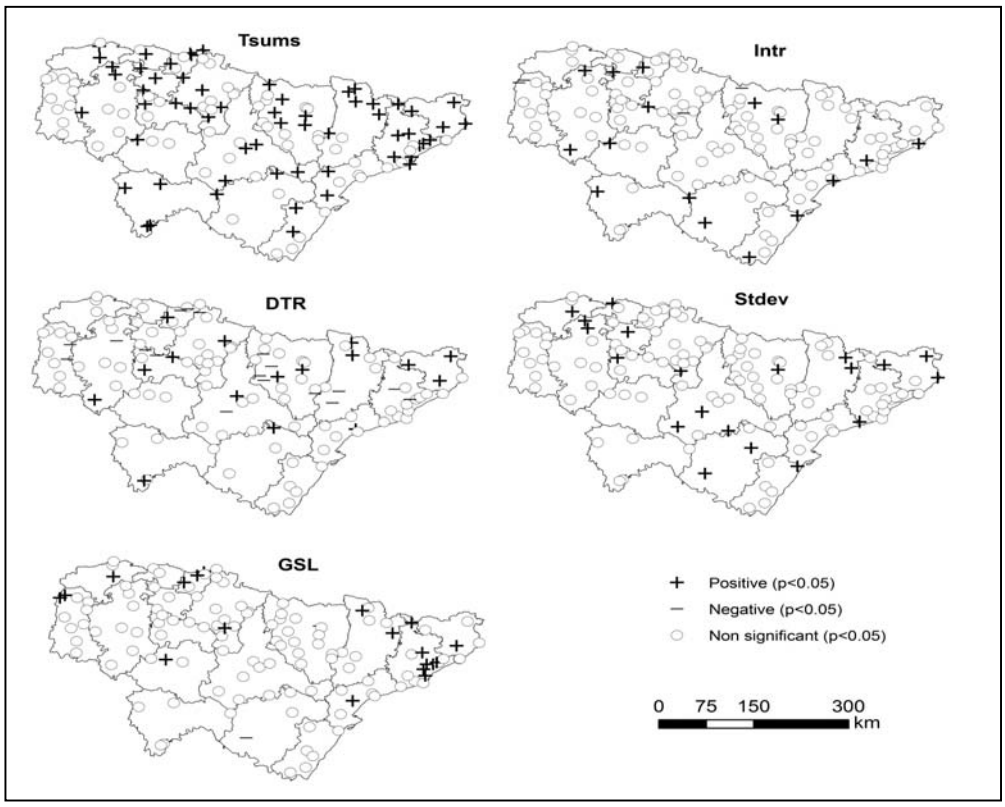

Figure 4.15: Same as Figure 4.9, but for variability indices.

Figure 4.16 shows the temporal evolution and trends in the regional series of variability indices. All indices had no trends at the regional scale ($p<0.05$). For instance, the regional series of the diurnal temperature range (DTR) experienced a very weak warming (0.02ºC decade^{-1}). Also, the length of the growing season (GSL) showed insignificant increase by 0.33 days decade^{-1} from 1960 to 2006. The only exception corresponded to temperature sums (Tsums), which indicated a clear statistically significant upward trend (118.8ºC decade^{-1}). In general, the overall insignificant trend observed for most of the regional series came in agreement with the results obtained for the individual observatories.

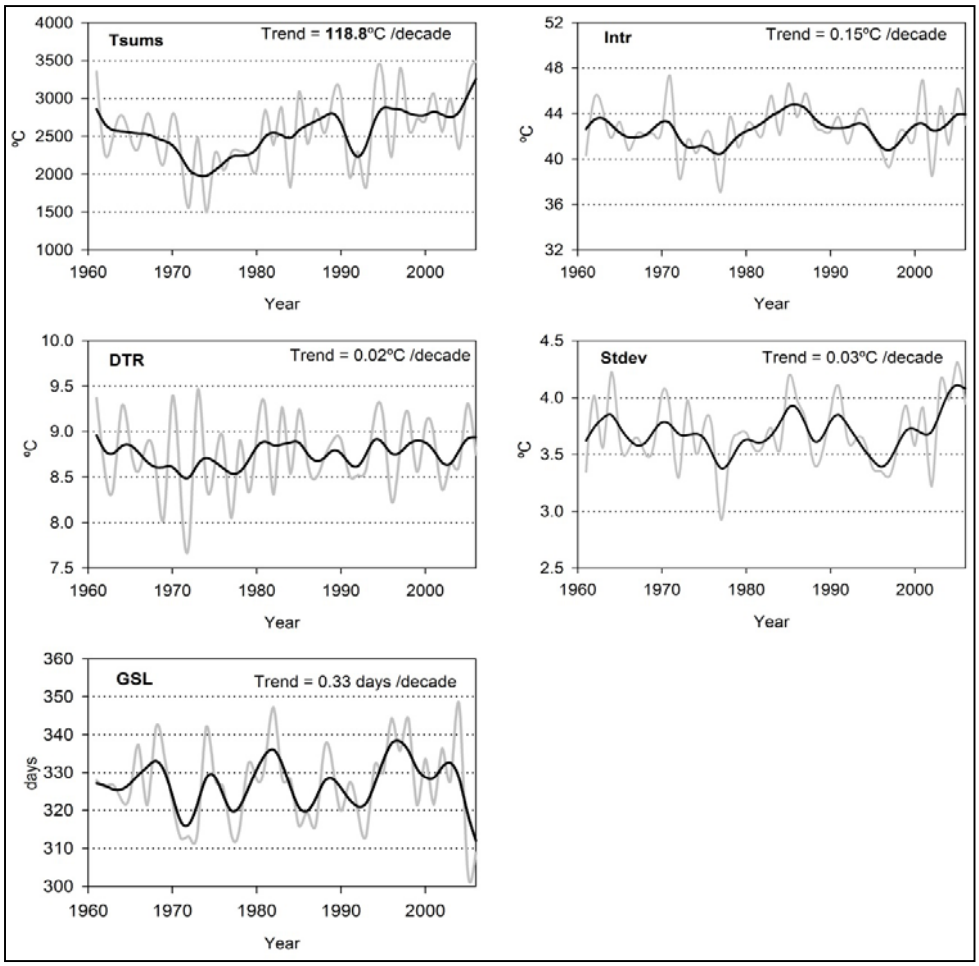

Figure 4.16: Same as Figure 4.11, but for variability indices.

4.3. Spatial regionalization of extreme events.

4.3.1. Regionalization of moderate extreme events.

In this section, the results on the statistical procedure used for classifying daily summer temperature extremes in the study domain into homogenous regions are presented. The evaluation of this scheme is also outlined.

4.3.1.1. PCA results

Kaiser statistic supports the use of PCA to reduce data dimensionality when the KMO value is greater than 0.5 (Norusis, 1988). In this work, the overall KMO statistic among the input variables reached 0.81, with a very high significance level (99 %). This strongly suggested a high level of dependence among the input variables (indices). For this reason, it was necessary to use the PCA to reduce dimensions of the input data. Following the PCA results, the Scree plot showed that the magnitude of the eigenvalues dropped sharply after the third principal component (Figure 4.17). In the same sense, the statistical results of the Velicer test indicate a possible cutoff point at 3 factors that represents the lowest squared and 4th power partial correlations. Accordingly, three significant principal components were retained. Those three PCs explained together 84.32 % of the total explained variance (EV) in the original data. Due to the small-explained variance (15.68 %) of the high-order modes and their small differences, they were not considered in this study. This amount of variance can be originated to local factors that are not physically meaningful and thereby they are difficult to interpret.

The loadings of the PC1 (29.46 % of the EV) revealed aspects on the spatial variability of the night-time summer temperature (e.g., Min_summer, TNn,

TN90p, and TNx). On the other hand, the PC2 (27.43 % of the EV) incorporated those variables that were mostly correlated with the day-time summer temperature (e.g., Max_summer, TXx, TX90p, SU25 and WD). The first component was therefore seen as a measure of “minimum” summer temperature extremes; meanwhile the second component was interpreted as a measure of “maximum” summer temperature extremes. The PC3 (27.34 % of the EV) did not distinctly explain specific pattern since it combined effects of both maximum and minimum temperature (e.g., DTR and Tsums).

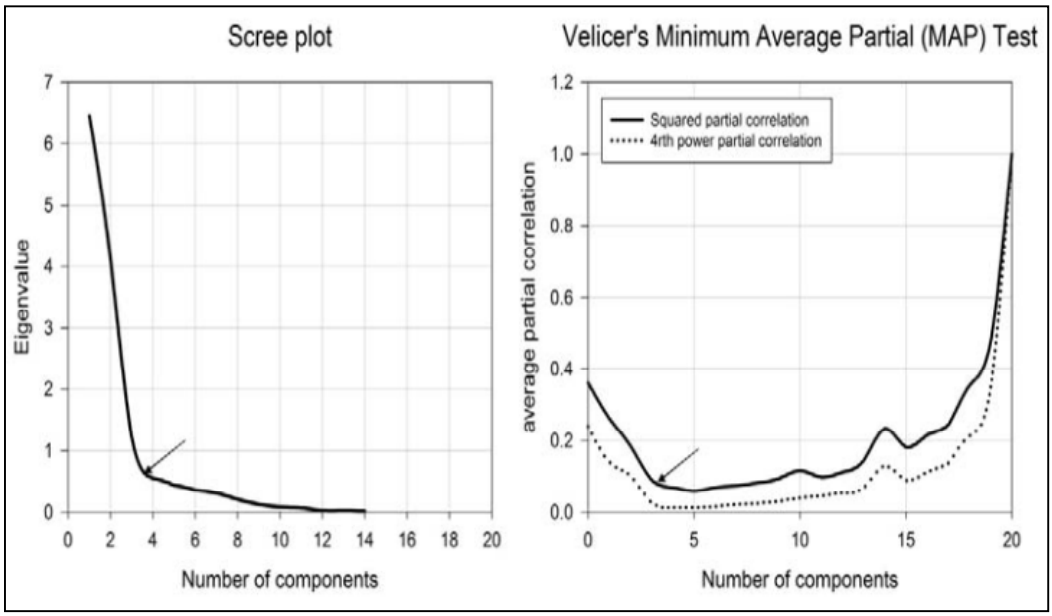

Figure 4.17: Results of diagnostic statistics for determination of the optimum number of PCs. including Scree plot (left), and Velicer minimum average partial test (right).

4.3.1.2. Clustering results:

In order to group objectively those observatories presenting a similar temporal evolution of summertime extremes, the dominant distribution patterns were

identified by applying the cluster analysis to the retained factor scores. As illustrated in Figure 4.18, the results of both the agglomeration coefficient and the Wilks´ Lambda statistic were grouped together, suggesting 4 solutions as the optimum number of clusters. Thus, the final decision was made to partition the clusters at 4 groups. Using more than 4 clusters may not be useful because no meaningful spatial patterns can be explored. In other words, clusters beyond these leading four sub-regions were expected to reflect small-scale patterns, which are often attributable to local factors that are difficult to interpret. In topographically complicated areas, differences in land surface characteristics such as vegetation canopy and surface albedo can induce local changes in surface heat exchanges with the atmosphere and in turn cause local disturbances in the dominant patterns of extreme events. Overall, the resulting number of clusters represented the range of climatological conditions, which can conventionally be accepted over the region. In other words, the spatial modes suggested by the cluster analysis are thought of as representing the main modes of the regional climate regimes according to the previous knowledge (i.e., continental, Mediterranean, oceanic and mountainous). Therefore, the four sub-regions that exhibited similar characteristics of summer temperature extremes were identified. Hereafter, those sub-regions are referred to as: CL1, CL2, CL3 and CL4.

In order to evaluate homogeneity of the established clusters, the Silhouette coefficient was applied. The results showed that the clustering partitions were not completely homogenous. According to this coefficient, almost 16 (12.5%)

observatories were assigned to “inappropriate” clusters. Figure 4.19 compares the Silhouette width for the defined clusters before and after validation.

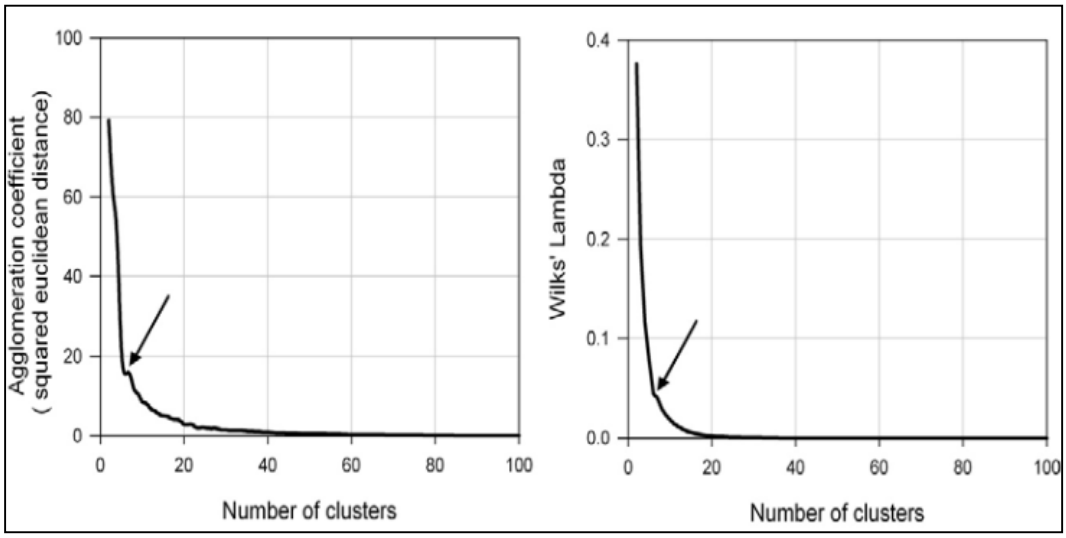

Figure 4.18: Plots of the agglomeration coefficient of squared Euclidean distance (left), and the Wilk´s Lambda statistic (right) as diagnostic tests to define the number of clusters.

As illustrated, some observatories belonging to CL2, CL3 and CL4 had negative Silhouette values, which indicate that the intracluster distance was higher than intercluster distance. Figure 4.19 also indicates how the Silhouette width coefficient improved after validating the clustering, specifically for CL1 and CL4. All coefficient values became positive and higher than those before validation. In particular, the average of the coefficient increased from 0.54 (0.23) to 0.62 (0.39) for CL1 (CL4). This can be seen as an indicator of higher between-group variation and lower within-group variation. In other words, the observatories belonging to each cluster were well-separated from other clusters and correspondingly compacted better within their clusters. This finding was also confirmed by ANOVA results for the four clusters (groups). The results indicated

that F values increased after validation. For instance, for CL2, the F ratio increased from 45.16 to 49.46 as variations between groups increased from 66.31 to 69.18, while the within-group variations decreased from 60.69 to 57.82.

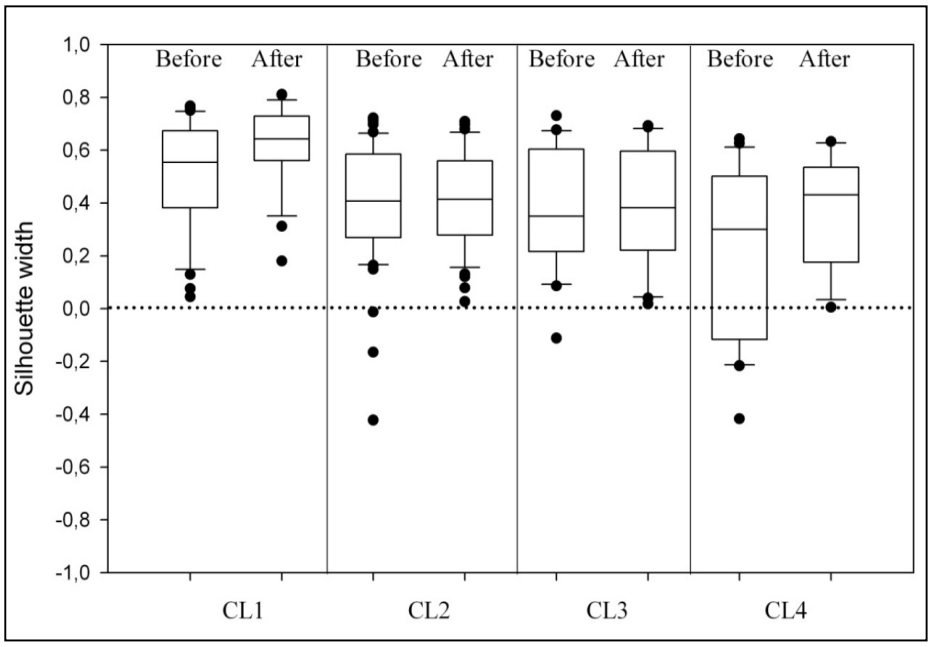

Figure 4.19: Silhouette width for the defined clusters before and after clustering validation.

Figure 4.20 shows the spatial distribution of the observatories corresponding to the delineated clusters. As noted, the number of stations varied considerably among clusters. CL2 represented the densest cluster (45.3% of observatories) with broad spatial distribution, followed by CL1 (25%), CL3 (21.1%), and CL4 (8.6%). This suggests remarkable geographic and climatic contrasts between the defined sub-regions. The delineated sub-regions had a geographical feature, with relatively clear physiographic boundaries. Presumably, the defined clusters showed marked distinction between inland and coastland regions as well as lowlands and highly elevated areas. In few cases, there is a low consistency

among nearby observatories. This can probably be due to the joint effect of local topography and synoptic conditions.

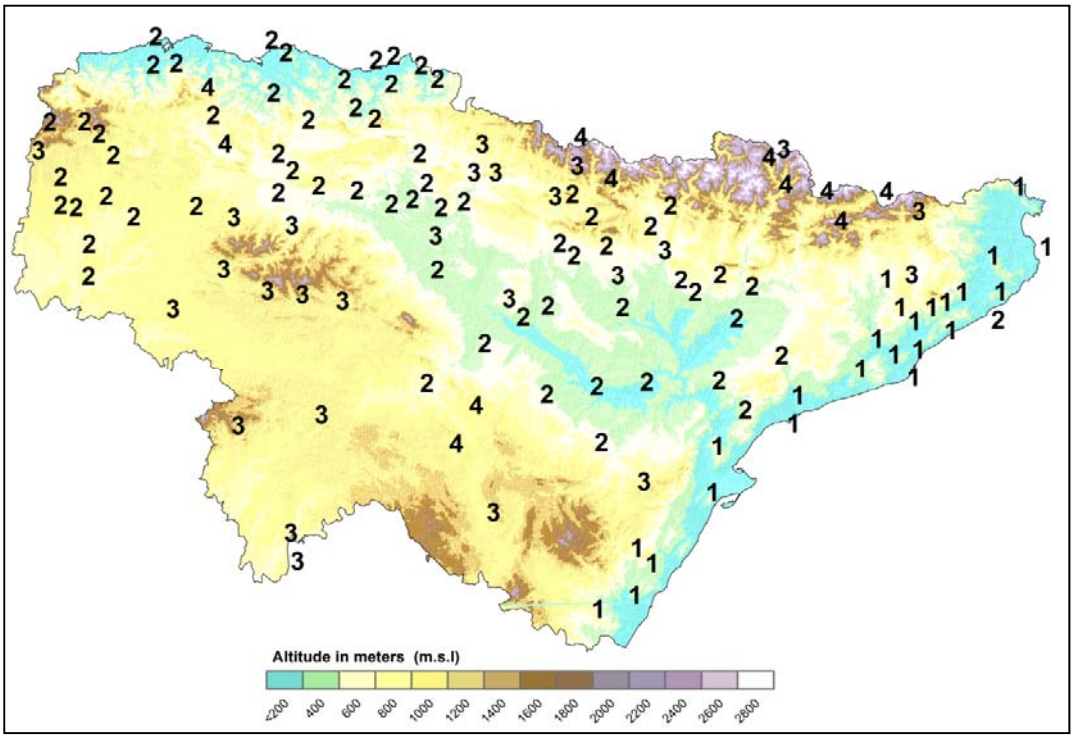

Figure 4.20: Spatial distribution of the observatories delineated to the four homogenous sub-regions following the cluster validation results.

As illustrated in Figure 4.21, it can be clearly seen that elevation and distance to the sea significantly contributed to the spatial variability of summer temperature extremes in the study domain. Spatial variations of summertime extremes matched well with changes in elevation. This was particularly the case for observatories belonging to CL3 and CL4 whose mean elevation was 773.1 and 1101.4 m, respectively. On the other hand, CL1 suggested a joint effect of topography and land-water interaction. In addition to their proximity to the sea

with average distance of approximately 14.8 km, the CL1 observatories generally located at lowlands with mean elevation of 174.9 m.

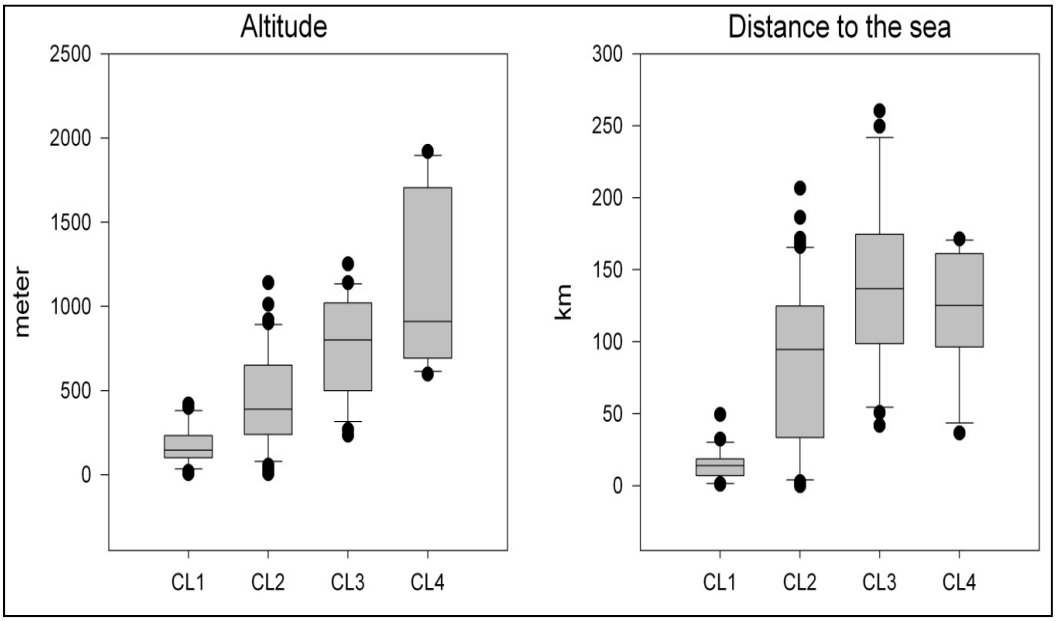

Figure 4.21: Boxplots showing intracluster differences as a function of altitude (left panel) and distance to surrounding water bodies (right panel). The median, 10th, 25th, 75th and the 90th percentiles as vertical boxes are plotted with errors bar.

With respect to continentality effects, both CL3 and CL4 exhibited clear continental influences (average distance to the sea equals 143.3 and 122.6 km, respectively), compared with the less continental CL1. This finding can be clearly seen in Figure 4.21, where the orientation of the clusters was likely controlled by continentality and orography. For instance, CL1 was generally meridian along the Mediterranean coast, whereas CL4 had an east-west orientation along the Pyrenees Mountains.

Spatially, CL1 was mainly situated along the coastline of the Mediterranean Sea capturing possible maritime influences of the Mediterranean, whereas CL2 was located close to the Atlantic Ocean and penetrated eastward through the Ebro valley in central portions. This sub-region mostly included leeward sites of the main mountain regimes (i.e., the Pyrenees system in the north and the Cantabrian system in the west). On the other hand, CL3 corresponded to stations located mainly in the moderately elevated areas southward and westward, corresponding to the foothills of the Iberian mountains. This partition (group) of observatories was characterized by a relatively low maximum and minimum temperature, as a consequence of the local orographic effects. A cluster encompassing the Pyrenees Mountains, together with some scattered high elevation sites in the Iberian system, was also distinctly identified in CL4.

4.3.1.3. Temporal evolution of summertime extreme indices

Table 4.8 summarizes the linear trends in the regionally weighted time series of summertime temperature extremes for the established four sub-regions over the period from 1960 to 2006. In general, the overall tendency in temperature extremes was clearly toward warming for all sub-regions. However, this warming had a spatial component. Figure 4.22 illustrates the temporal evolution of a set of the regionally weighted time series of temperature extremes, selected as indicative examples. As presented, the strongest signals were found in the most elevated areas (CL4) and in the Mediterranean (CL1) for both day-time and night-time temperature indices. From 1960 to 2006, warmest day (WD), for instance, significantly increased at a rate of 0.71ºC and 0.44ºC decade^{-1} for CL1 and CL4, respectively. The percentage of warm nights (TN90p) per summer also showed

uptrend, with an increase of 3.88 and 2.86% per decade for CL1 and CL4, respectively. This suggests that orography and the Mediterranean maritime influences play a key role in the temporal evolution of summer extremes in NE Spain.

Table 4.8: Trends of extreme temperature indices for the defined four sub-regions, suggested by the cluster analysis results. Only bold numbers are statistically significant at the 95% level following the Mann-Kendall results).

Index	CL1	CL2	CL3	CL4	Unit per decade
Max_summer	**0.56**	**0.24**	**0.47**	**0.71**	ºC
TXn	**0.55**	0.34	**0.66**	**0.85**	ºC
TXx	**0.62**	0.18	**0.34**	**0.59**	ºC
SU25	**2.77**	1.06	**2.42**	**3.63**	days
TX90P	**4.11**	0.89	**1.75**	**2.61**	days
WD	**0.71**	0.09	**0.34**	**0.44**	ºC
Min_summer	**0.44**	**0.46**	0.11	**0.60**	ºC
TN90P	**3.88**	**2.83**	0.40	**2.86**	days
TNn	**0.44**	**0.48**	0.16	**0.64**	ºC
TNx	**0.52**	**0.48**	0.09	**0.60**	ºC
Spell	**1.29**	0.24	**0.41**	**0.54**	days
Tsums	**51.65**	24.76	**53.11**	**125.02**	ºC
DTR	**0.12**	**-0.22**	**0.36**	0.11	ºC
INTR	**0.45**	-0.29	0.35	-0.11	ºC

On the other hand, CL2 (mainly located in the Ebro valley and along the Cantabrian sea) showed statistically significant warming trend only for night-time extremes (e.g., TNn, TN10p and TNx), whilst trends in day-time extremes were generally weaker and insignificant at the 95% level. Contrarily, day-time extremes exhibited a remarkable significant trend in CL3 (denoted to moderately elevated areas), whereas night-time extremes had no trend in this sub-region.

More importantly, the results confirm that high mountain areas (CL4) responded more rapidly to the global warming relative to mainland (CL2) and moderately

elevated areas (CL3). This can be clearly seen in the trends of the indices of Max_summer (0.71ºC decade^{-1}), TXn (0.85ºC decade^{-1}), TXx (0.59ºC decade^{-1}), SU25 (3.63 decade^{-1}), Min_summer (0.60ºC decade^{-1}), TNn (0.64ºC decade^{-1}) and TNx (0.60ºC decade^{-1}). and Tsums (125.02ºC decade^{-1}). These results can be of particular importance in the context of the possible impacts of the global climatic change on behavior of temperature extremes in areas of complex topography.

A comparison between the scores of the observatories belonging to each cluster, as previously been derived from PCA, is provided in Figure. 5.23. The loading factors corresponding to the three defined PC3 after varimax rotation coincided with the final clustering membership after validation. Both distributions had a spatial structure. As illustrated, CL1 (the Mediterranean) was bidirectional along PC1 confirming large temporal variability of day-time extremes. Contrarily, it had only positive loadings along the PC2 axis, suggesting less variability of night-time extremes. This probably suggests rapid increase in mean maximum temperature and the corresponding daytime extreme events near to the Mediterranean coast. This feature came in direct contrast with CL2 observatories (mainland low areas), which mostly showed opposite (negative) scores on the daytime extremes factor (PC2). This simply suggests rapid (weak) warming in daytime (nighttime) extremes in the Mediterranean (mainland) observatories and vice versa. This result coincided well with the results obtained for the mean thermal conditions in the region, which suggested a continental-coastal gradient. In the same manner, the scores in highly elevated areas (CL4; mean altitude=1101.4 m) were not consistent with those of lowlands (CL2; mean altitude=174.9 m). As illustrated,

CL4 (CL2) observatories had positive (negative) scores along the PC3 (PC1) and vice versa.

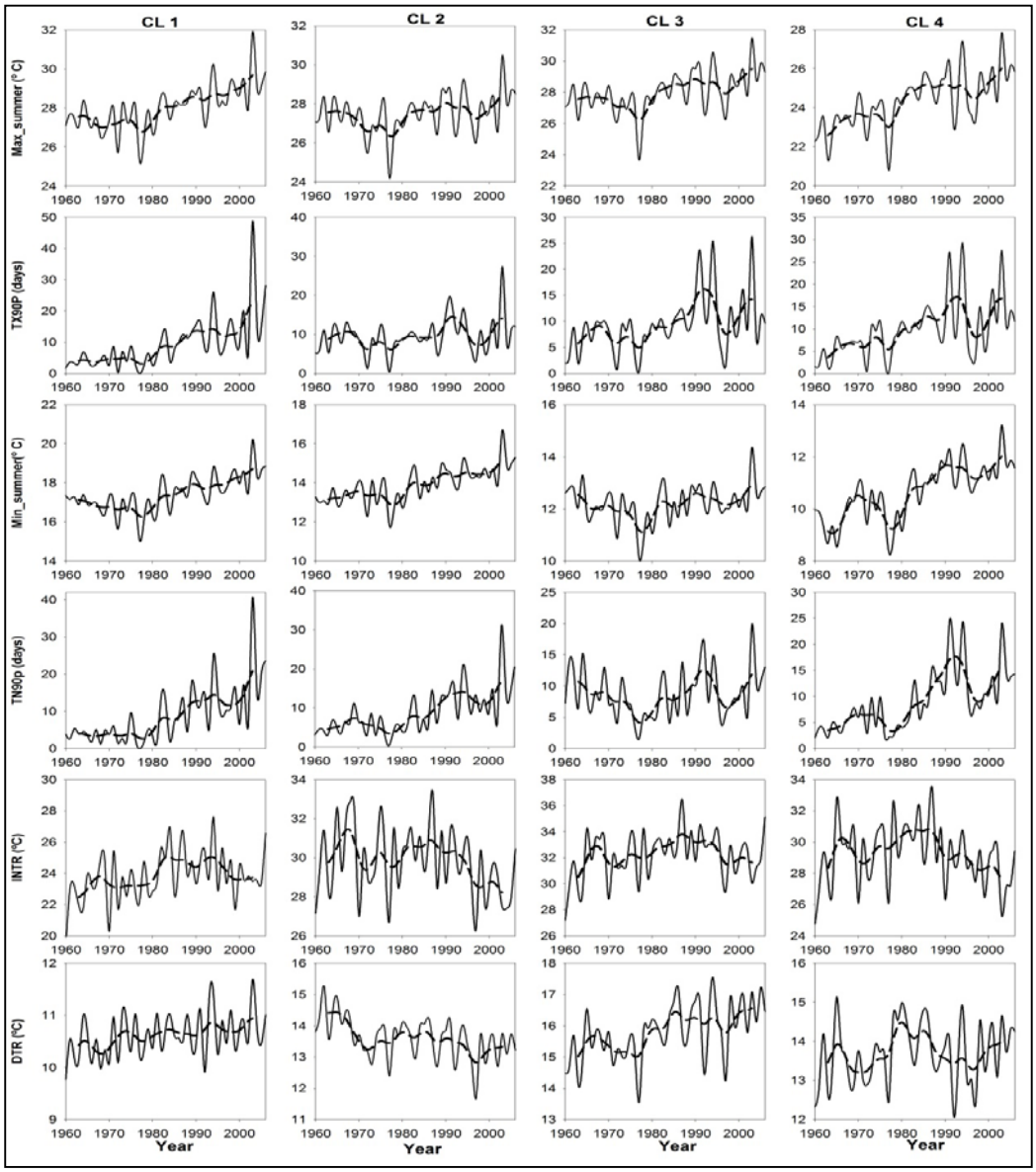

Figure 4.22: Temporal evolution of a set of temperature indices time series from 1960 to 2006. Max_summer (TX90p) represents an example of intensity (frequency) index of day-time temperature, while Min_summer (TN90p) represents an example of intensity (frequency) index of night-time temperature. INTR and DTR represent indices of temperature variability. Dashed line refers to a 9-year low Gaussian filter.

This also suggests a relatively contrasted behavior of extreme events between high and low elevated areas. Given that the linear trends along the CL2 and CL4 were generally positive, this contrast can mainly be seen in the amount (magnitude) change rather than the direction (sign). Taken together, it can be clearly implied that the defined sub-regions have climatic and topographic meanings.

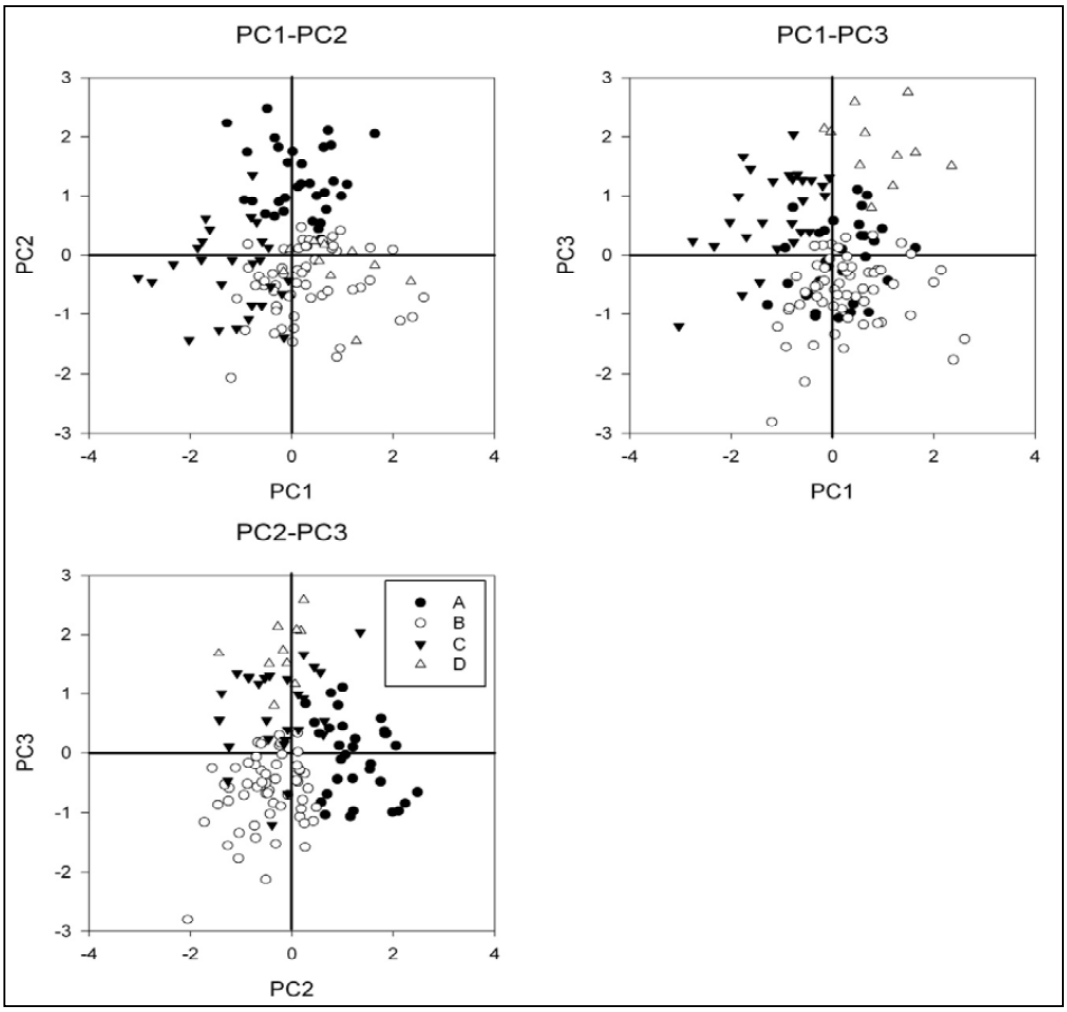

Figure 4.23: Scatter plots of the scores of the observatories delineated to the four sub-regions distributed along PC1, PC2 and PC3 axes. A, B, C, D corresponds to CL1, CL2, CL3 and CL4, respectively.

4.3.2. Regionalization of anomalously severe extreme events.

A PCA was carried out to the anomalies of very warm days (VWD: total days 292) and very cold nights (VCN: total nights 192) recorded in the period 1960-2006 in order to explore the main spatial modes of their variability across the study domain. For each observatory, the VWD (VCN) was defined as days above (below) the 99th (1st) percentiles of daily maximum (minimum) temperature distribution calculated for summer (winter) season. Figure 4.24 (upper panel) shows the leading four modes of wintertime VCN variability. These modes explained together 68.6% of the VCN variance. The first and second modes explained majority of variance with 30.2 and 24.7%, respectively. Only those factors that explained more than 5% of the total variance were mapped.

The spatial modes corresponding to these factors were physically meaningful and thereby they can be interpreted. Figure 4.24 (lower panel) presents the spatial distribution of the retained factors for VWD. The results also suggest four leading rotated PCs that explain together 79.9% of the total variance, with 39.4 and 26.7% for the first and second modes, respectively.

A quick comparison between the spatial modes of VCN and VWD reveals some interesting findings. First, the effects of small-scale features on the occurrence of the anomalous heat days were more highlighted during winter season (unexplained variance equaled 31.4%) than in summer (unexplained variance equaled 20.1%). This can be seen in the context that minimum temperature is more likely to be influenced by very local conditions (e.g., local topography and land use), relative to maximum temperature. These local features can further

influence the advection or/and vertical motions of atmospheric flows that explain the occurrence of VCN. These conditions can significantly affect low temperature distribution through sensible and latent heat fluxes near to the surface.

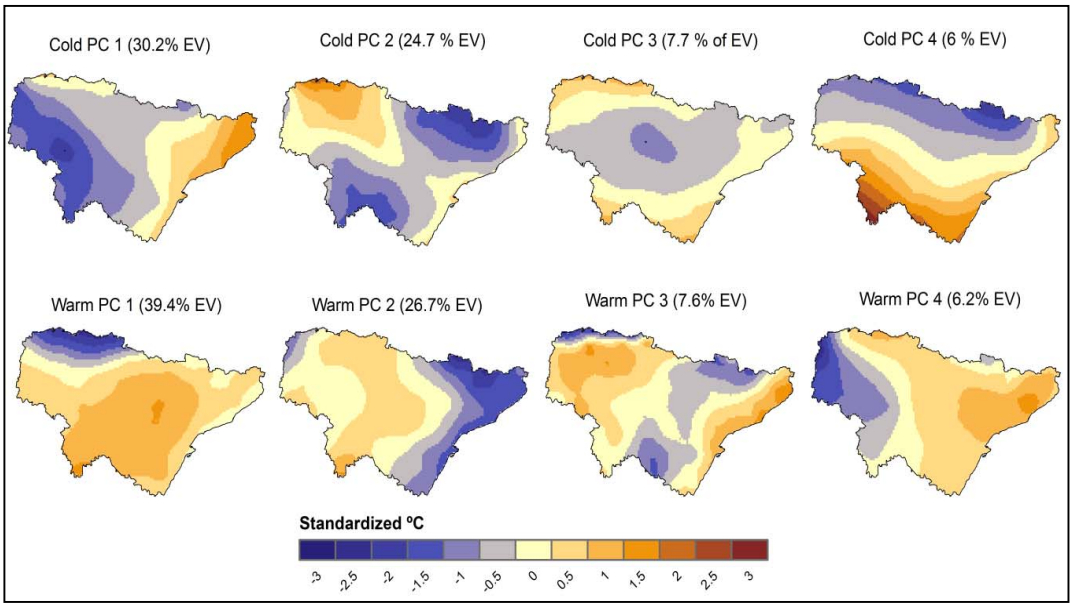

Figure 4.24: Spatial patterns of the scores of the leading principal components for VCN (upper) and VWD (lower). The legend indicates the regression coefficients of the temperatures onto the different PCs.

Another important finding is that the sub-regional spatial patterns of VCN were largely controlled by topography. Contrarily, land-sea interactions exerted strong influence on the spatial structure of VWD, with more severe extreme events in continental areas (Figure 4.24). One clear example is the first mode of VCN which revealed more cold extreme events over elevated areas northwest, whereas lower standardized temperature in the second mode is mainly assigned to elevated areas in the north (Pyrenees) and the south (the Iberian system), compared with lowlands. On the other hand, the first and second modes of VWD suggest stronger influence of continentality against the Atlantic (PC1) and the

Mediterranean (PC2) configurations. For PC3 and PC4, the combined effect of elevation and land-sea interactions can be seen.

4.4. Attribution of driving forces and mechanisms

Spatial and temporal variability of temperature are often described as driven by the joint effect of both the large-scale atmospheric circulation and small-scale physical processes (e.g., convective processes, soil moisture, topography, land use).

4.4.1. Driving forces of variability of seasonal temperature means

4.4.1.1. Teleconnections

To assess the possible influence of large-scale dynamics on temperature variations in the study domain, correlation between standardized anomalies of temperature and a set of teleconnection indices was computed. These indices summarize atmospheric circulation modes in the northern hemisphere. The association was assessed at seasonal and annual timescales for the 1960-2006 interval. Figure 4.25 summarizes correlation between the general atmospheric circulation patterns and seasonal and annual temperature time series. In general, the results suggested a predominant influence of the EA, SCA, and WeMO patterns on interannual variability of temperature. Other atmospheric circulation patterns (i.e., the NAO, EAWR, and MO) did not show significant correlation with temperature variations. Exclusively, the NAO correlated positively and significantly with maximum temperature during wintertime. In contrast to other thermal variables, the correlation between the atmospheric circulation modes and DTR appeared to be weak at both seasonal and annual timescales. DTR only

showed statistically significant correlation with the SCA pattern during winter, spring, and autumn.

A visual inspection in Figure 4.25 clearly indicates a statistically significant positive correlation between the EA and temperature in all seasons. This relationship was found much stronger during winter, suggesting that the EA pattern was the dominant mode responsible for interannual variability of temperature during this season. The average Pearson correlation coefficient (*r*) between the EA high mode and winter maximum (minimum) temperatures was 0.51(0.57). The only exception corresponded to maximum temperature during summer, which showed insignificant correlation with the positive EA mode in majority of observatories. As illustrated in Figure 4.25, apart from winter, most correlations with the SCA and the WeMO patterns were found negative and statistically significant ($p<0.05$). Exceptionally, the association of minimum temperature with the WeMO and SCA patterns did not reach the statistical significance level during winter and autumn. It seems that the influence of these modes on temperature variations was only significant during spring and summer.

Figure 4.25 also informs that the circulation modes interacted differently with temperature in the study domain as the correlations for majority of modes were mixed between positive and negative. This probably informs that there were spatial differences in the response of seasonal temperature to these modes of atmospheric circulation. For this reason, the spatial structure of the relationship between seasonal temperature and atmospheric patterns was assessed.

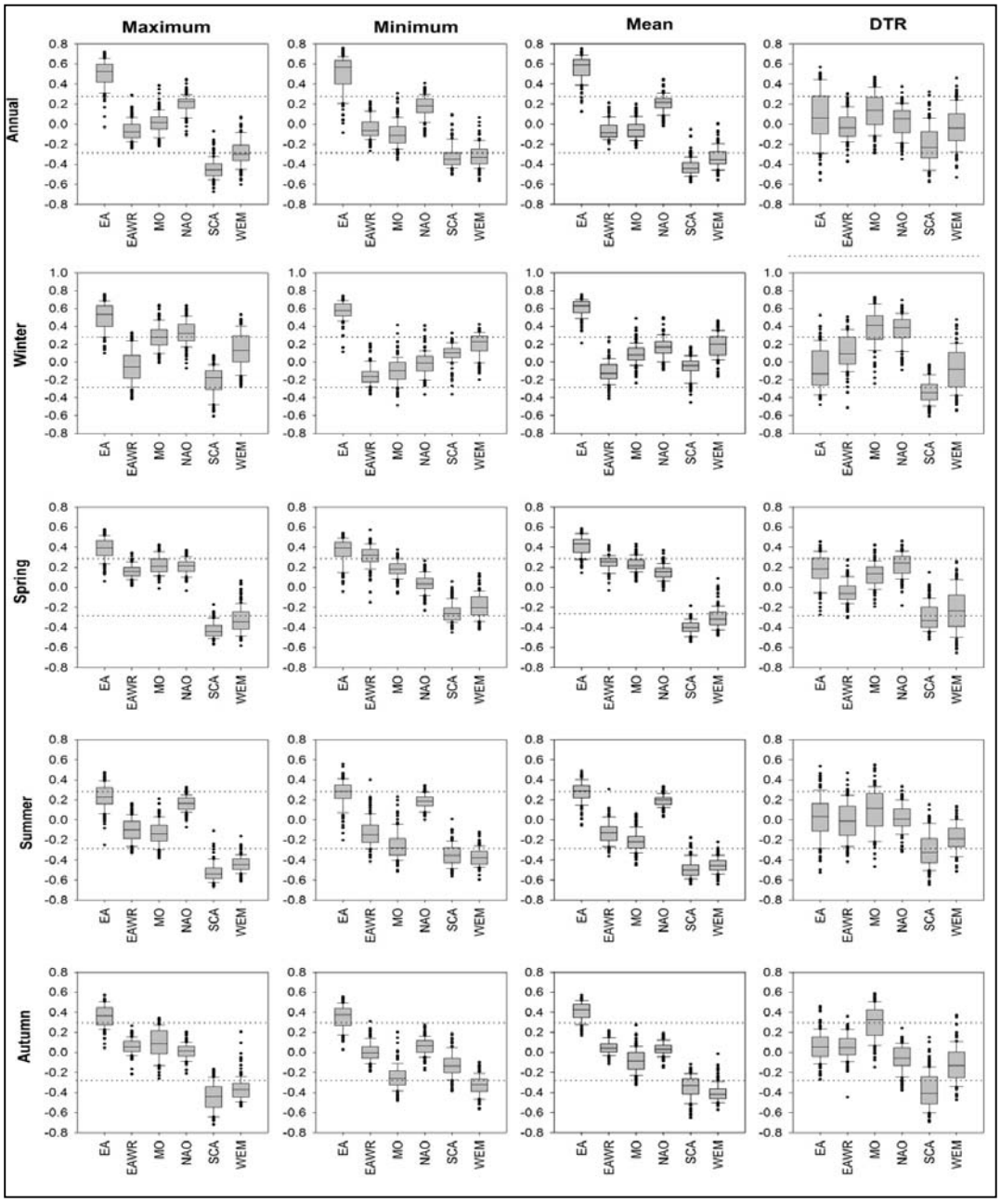

Figure 4.25: Scatter plots of the Pearson correlation coefficients (*r*) calculated between the detrended anomalies of seasonal and annual maximum, minimum, and mean temperatures and DTR and the main large-scale atmospheric circulation. Dotted lines show the upper and lower limits of the 95% significance level. The median, 10th, 25th, 75th and the 90th percentiles as vertical boxes are plotted with errors bar.

However, given that most thermal variables (i.e., maximum, minimum and mean) showed more or less similar connections with atmospheric modes in terms of the correlation sign (direction), as revealed in Figure 4.25, the intention was only confined to explore the dependency between the leading atmospheric circulation modes in the region and mean temperature. The spatial structure of the relationship between seasonal mean temperature and atmospheric patterns is presented in Figures from 5.26 to 5.29.

Figure 4.26 depicts the spatial patterns summarizing the response of winter mean temperature to atmospheric circulation. As illustrated, the connection between the EA pattern and mean temperature showed a broad and consistent spatial pattern, suggesting a large-scale signature of this pattern over the study domain. Nonetheless, this relationship was apparently stronger close to the Cantabrian Sea and in the northeastern portions of the study domain. By contrast, the influence of the MO, NAO, and SCA patterns on wintertime temperature means reached the significance threshold only at highly elevated areas in the Pyrenees and west of the Iberian system. As depicted, the EAWR and WeMO influences on mean temperature were markedly weaker in complex terrain areas during winter months. Also, the dependency between mean temperature and the EAWR and WeMO modes showed a NW-SE gradient. This relationship was markedly weaker to the west, particularly along the Cantabrian coastland, and to the northeast (Catalonia). On the other hand, the NAO influence on mean temperature variability seemed to have a clear south-north gradient.

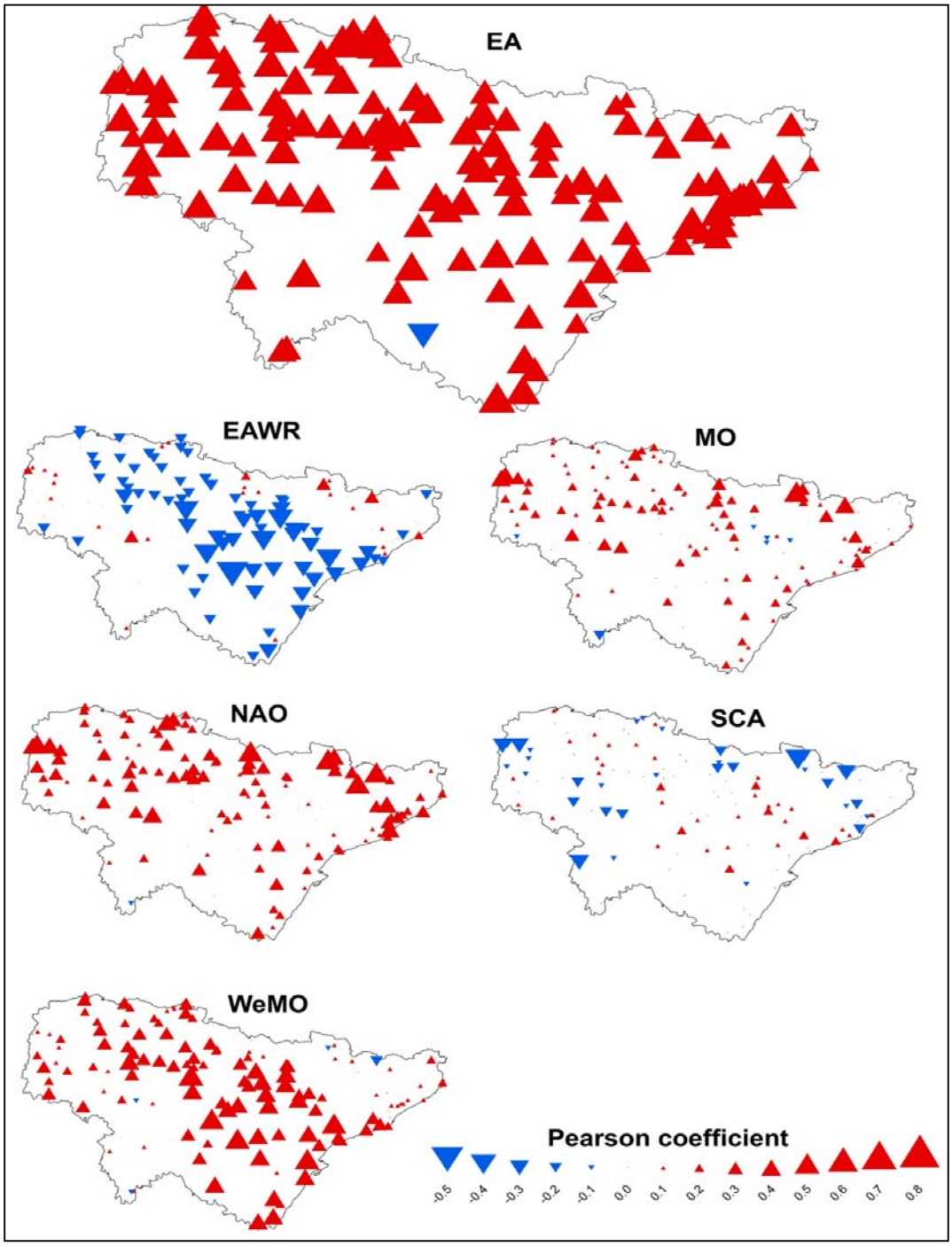

Figure 4.26: Spatial distribution of Pearson correlation coefficients between standardized anomalies of winter mean temperature and the general atmospheric circulation. In some cases, the scale of the maps was set to improve their readability. However, the scale of the Pearson coefficient remained constant for all maps. Correlation coefficients above 0.28 were statistically significant at the 95% level.

Figure 4.27 indicates the spatial distribution of Pearson correlation coefficient between spring mean temperature and atmospheric patterns. The EA, SCA and WeMO modes were also the main drivers of mean temperature variability. Although the EA pattern had a broad spatial pattern across the study domain, the WeMO and SCA modes experienced a south-north gradient. In particular, the influence of these modes on springtime mean temperature was more pronounced northward. Also, areas close to the Mediterranean Sea indicated higher correlation with the SCA and MO, while they showed less and statistically insignificant correlation with the WeMO.

As illustrated in Figure 4.28, the influence of the EA pattern on summer mean temperature was higher close to the Mediterranean Sea, particularly in Catalonia. Similarly, the Pearson correlation between summer mean temperature and the SCA mode was less evident close to the Cantabrian Sea, while it increased eastward and southward. The picture summarizing the role of the EAWR and MO modes only showed significant correlation in the Pyrenees and along western parts of the Iberian system. For the NAO, the spatial patterns were almost uniform with less spatial differences. Similar to spring, the WeMO experienced a south-north gradient, with more intense association in areas close to the Cantabrian Sea northwest.

In comparison to other seasons, the spatial contrasts in the relationships between autumn mean temperature and the general circulation patterns were less apparent (Figure 4.29). Overall, the EAWR, MO, and NAO patterns showed a uniform pattern, with no marked differences.

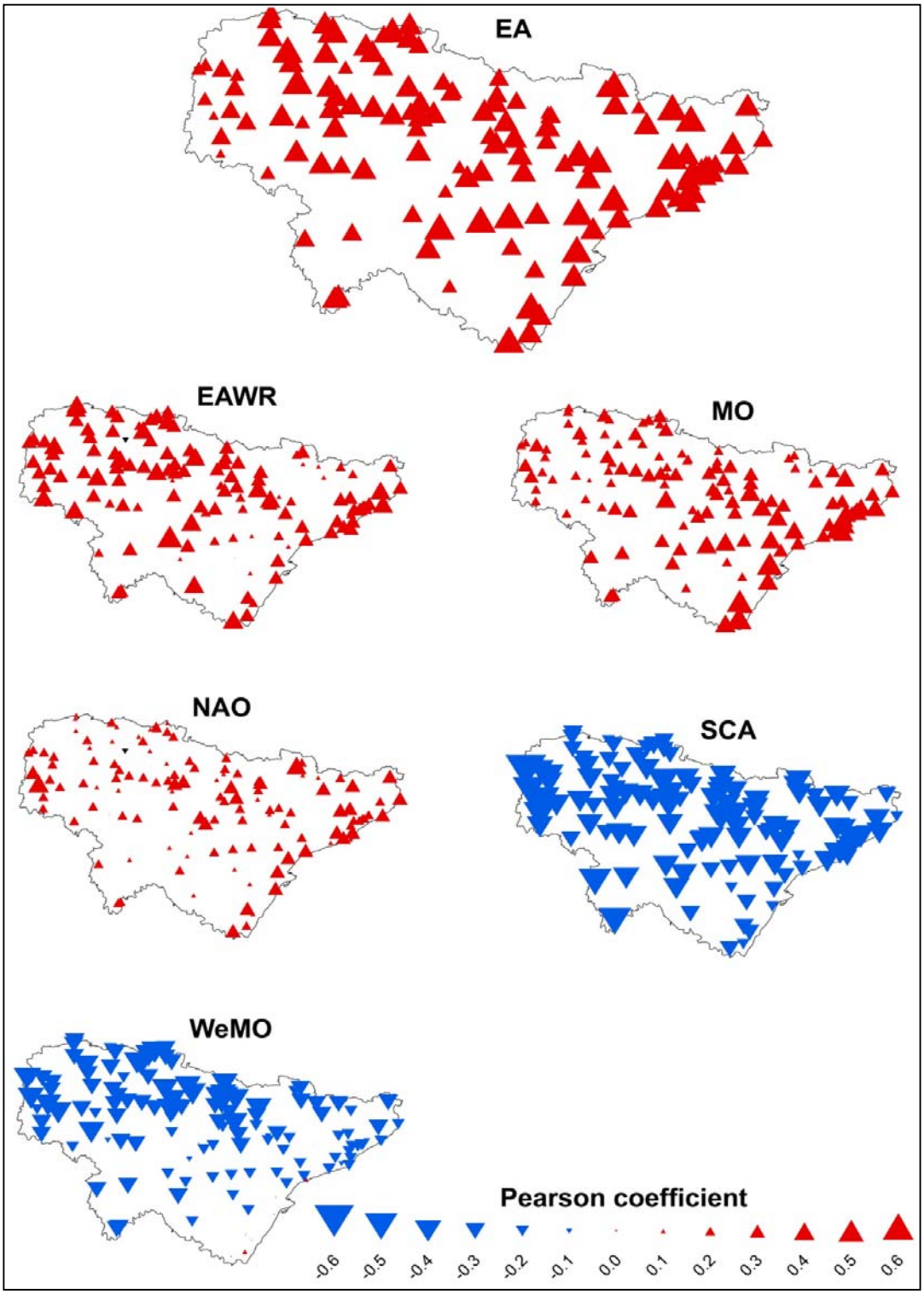

Figure 4.27: Same as Figure 4.26, but for spring.

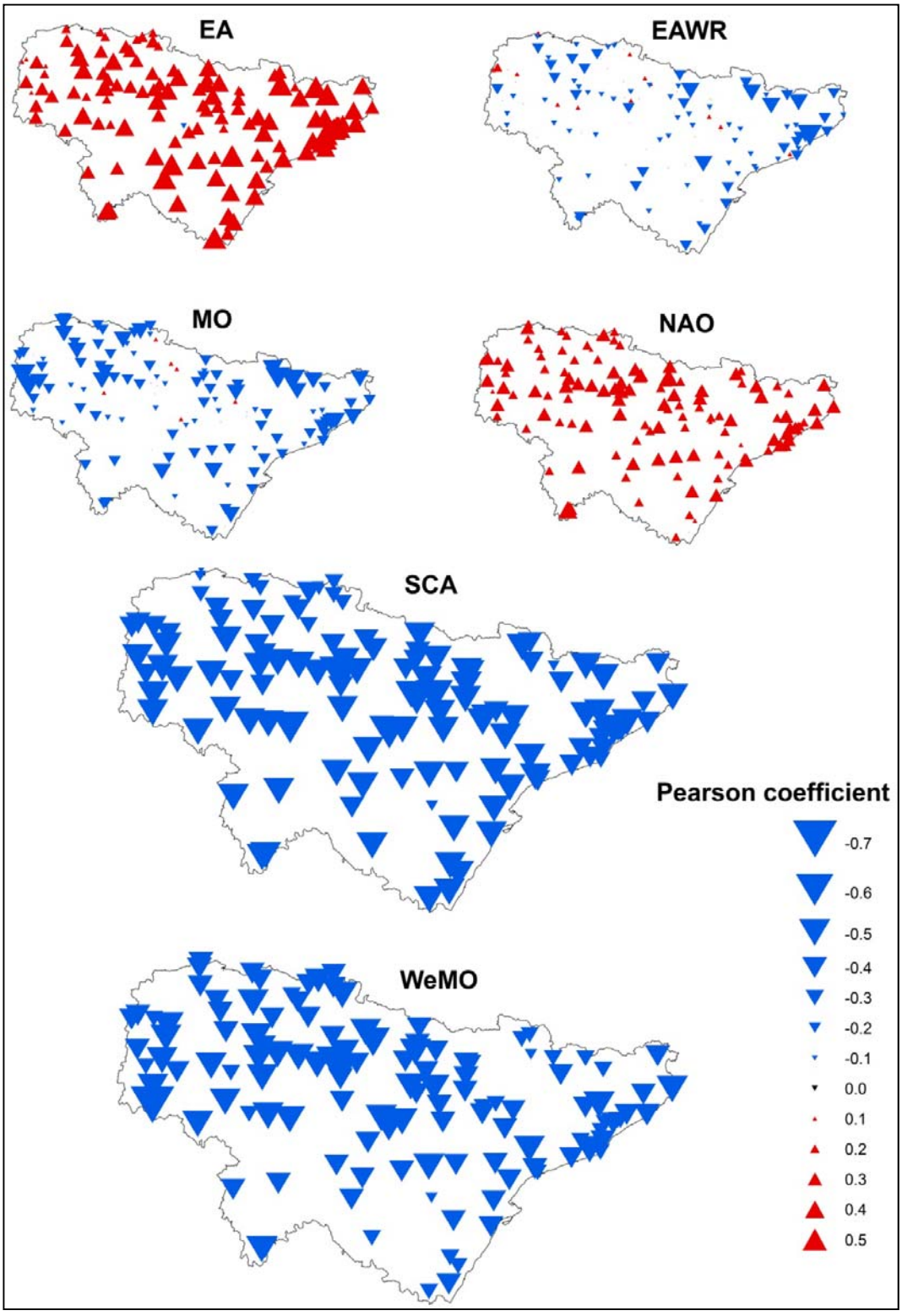

Figure 4.28: Same as Figure 4.26, but for summer.

Conversely, the relationship between the EA pattern and mean temperature was higher close to the Mediterranean Sea and the Cantabrian Sea, whereas it became weaker in mainland areas.

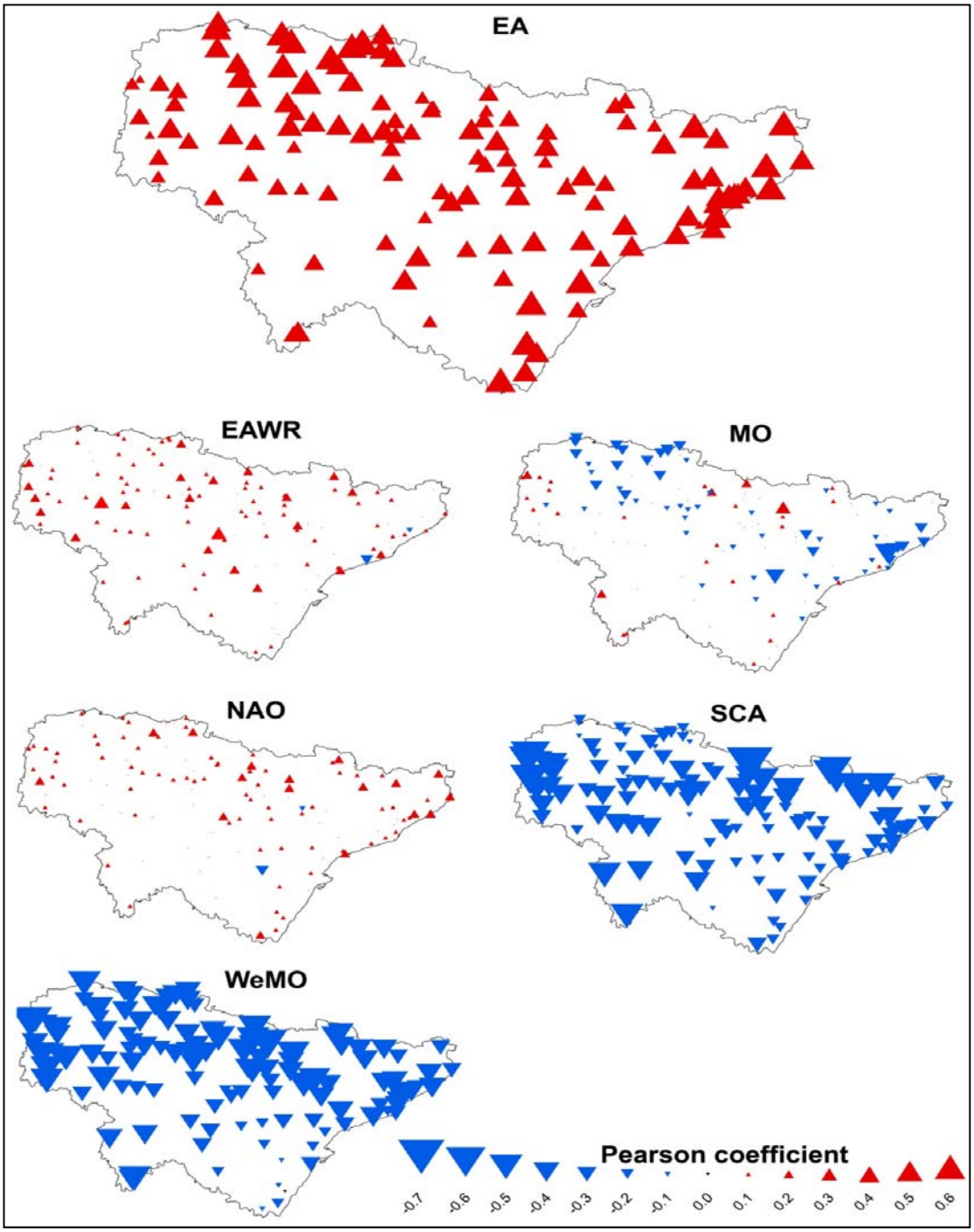

Figure 4.29: Same as Figure 4.26, but for autumn.

Interestingly, the connection of autumn mean temperature with the SCA showed a clear dependency with elevation. In particular, the correlation was stronger at highly elevated localities in the north (the Pyrenees) and to the south and the west (the Iberian system); meanwhile it was less apparent in coastal and inland areas of low elevation.

To explain in detail the SLP configurations beyond the observed spatial structure of the dependency between temperature and teleconnection indices, features of anomalous seal level pressure (SLP) corresponding to the key atmospheric circulation (herein, the EA+, WeMO- and SCA-) were presented by means of the climate composite maps. These physical processes can be seen as a good indicator of air advection through land-sea interactions. The results on the configuration of mean SLP anomalies associated with each dominant pattern are presented in Figure 4.30. The major centers of atmospheric action and their seasonal variations in terms of both strength and position are also described.

In winter, the interannual variability of temperature was mainly dependent on the positive EA. As illustrated in Figure 4.30, the positive EA is primarily linked to a north (low)-south (high) dipole of pressure anomalies, with a vast anticyclonic center over North Africa and the Mediterranean and a negative anomaly across northwestern Europe and west of the British Isles. This configuration would tend to bring anomalous S and SW warm air to the Iberian Peninsula, causing higher temperatures. As the study area is located downstream from the Atlantic Ocean, the Atlantic air advections bring relatively warmer air over the study domain.

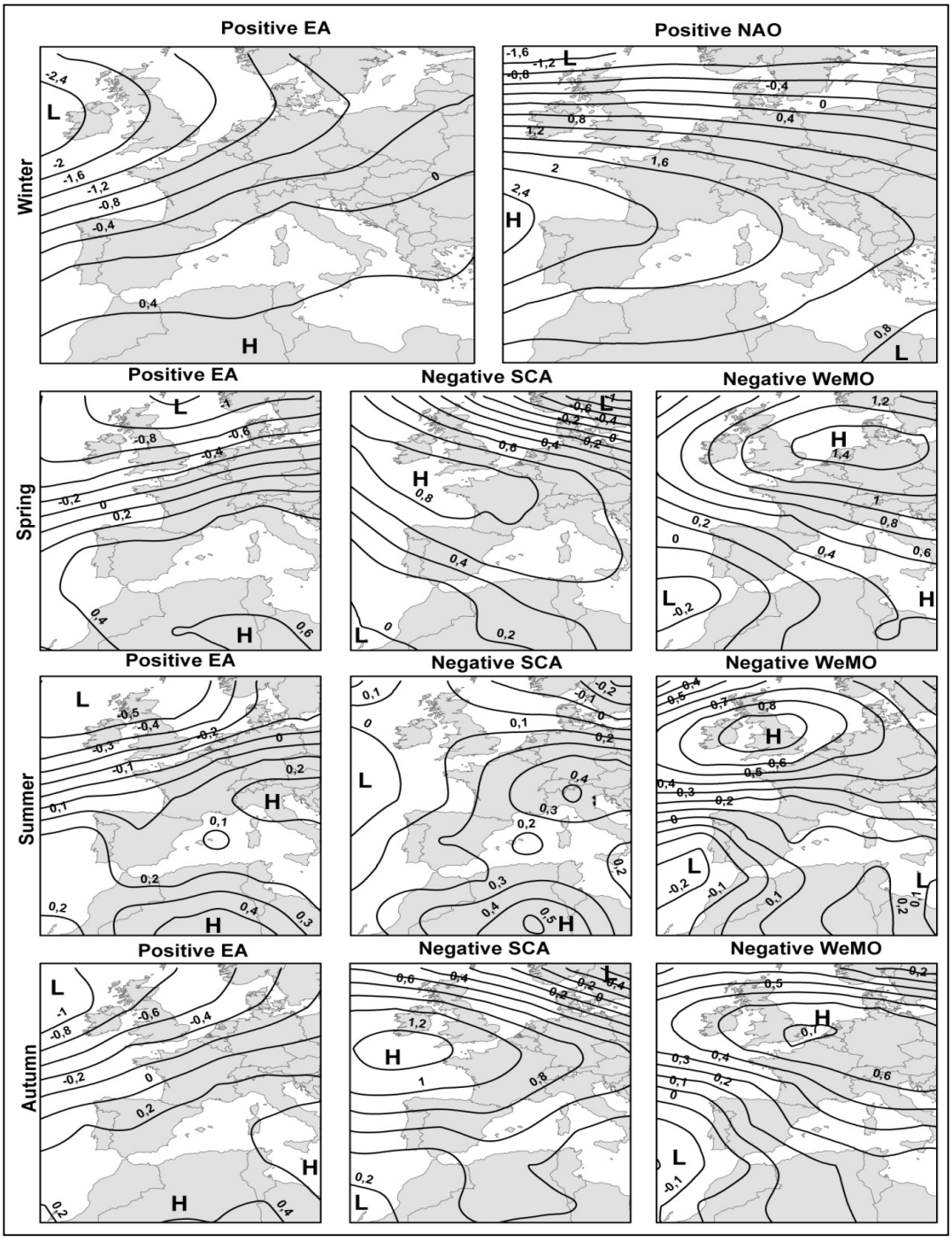

Figure 4.30: (a) Average sea level pressure (SLP) anomalies (hPa) over the period 1960-2006 corresponding to the most significant atmospheric patterns. The anomalies were derived from the daily NCEP/NCAR reanalysis data provided by the NOAA/OAR/ESRL PSD (http://www.nws.noaa.gov) for the base period 1960-2006.

While the positive phase of the NAO significantly correlated with maximum temperature during winter, it merely correlated with mean temperature in terrain complex areas in the north and the west (see Figure 4.26). Overall, as depicted in Figure 4.30, the positive phase of the NAO is largely associated with an increase in zonal circulation over Western Europe. This feature was clearly evident where the isobars had zonal direction.

Figure 4.30 also indicates that the positive EA during springtime has two main anomaly centers, located over the Sahara and NW Europe. Pressure anomalies during this mode reveal that the study area is particularly influenced by dry and warm air flows originating from the positive pressure anomaly over North Africa and moving toward the Iberian Peninsula. On the other hand, the anomalous pressure associated with the negative SCA during spring is mainly characterized by the zonal circulation, where the Atlantic blocks move eastward to cover broad areas of the Iberian Peninsula and Western Europe. This configuration often corresponds to very weak Icelandic lows, enhancing the advection of the westerlies from the Atlantic Ocean. The westerly and southwesterly flows affect much of the western areas of the study domain, explaining the stronger correlation found in these areas. In the years of negative WeMO, a distinct dipole in SLP anomaly is observable, with an anticyclonic anomaly placed over northern Europe and a negative anomaly located throughout North Africa and the Azores. Throughout this configuration, the Azores High moves northward covering broad areas of the British Isles and northwestern Europe. In short, spring is mainly characterized by the northerly displacement of the subtropical high corresponding to the positive EA. This positive anomaly is located over vast areas of the

western Mediterranean basin and North Africa, bringing southerly and southeasterly warm winds over the Iberian Peninsula. These easterly and southerly anomalous flows are associated with higher temperature, mostly highlighted along the Mediterranean coast and the Pyrenees. Owing to the orographic barriers, the influence of these atmospheric flows is less apparent over inland areas. On the other hand, the main feature associated with the negative modes of SCA and WeMO is the presence of the European/Atlantic blockings over large area of central and Western Europe, favoring for above-normal temperature.

In summer, the interannual variability of temperature was largely linked to the negative modes of the SCA and WeMO, and the positive mode of the EA. As depicted in Figure 4.30, summers of low SCA are characterized by a dominance of a high SLP anomaly over the Iberian Peninsula, central Europe, and North Africa. At the same time, two dipoles of negative anomaly appear on Scandinavia and western of the British Isles. This configuration reinforces the easterly advection of warm air flow from the Mediterranean Sea. This water body acts as a source of humidity for warm air masses originating over the Sahara, suggesting warmer conditions. In the study domain, these easterly and southerly flows cause above-normal temperature; the most affected regions being the eastern and southern portions. On the other hand, the WeMO negative mode is associated with a high pressure anomaly over the northeastern Atlantic. In accordance, an opposite dipole prevails in North Africa. This configuration increases the advection of the Westerlies, transferring warm oceanic air over the study domain. However, due to orographic effects, the influence of these warm flows is

constrained to the northwestern parts of the region, with less effect in central areas. Also, this study suggested that summer mean temperature correlated positively with the EA mode, although this dependency was markedly weaker and less significant, as compared to the negative phases of the SCA and WeMO. Figure 4.30 also illustrates SLP configurations corresponding to summers of positive EA values. As illustrated, the positive mode of the EA during summer is well linked to two main centers of action. The first is the high pressure anomaly over the Mediterranean basin and North Africa. The latter is the low pressure anomaly over Western Europe and the northern Atlantic. The subtropical high migrates northward to be located over North Africa and the Mediterranean Sea. Also, the low Icelandic is placed eastward to be located over the British Isles and parts of Scandinavia. This configuration supports strong southerly and southwesterly advections, which transport tropical moisture from the Mediterranean toward the study domain, particularly southern and eastern areas.

During autumn, the EA positive mode is characterized by a clear pole with low anomalous pressure located in the northwestern Europe and another dipole of opposite sign placed over the Mediterranean Sea and the Sahara. In particular, the high SLP migrates northward to be located over North Africa and the Mediterranean Sea, whereas the low Icelandic is placed eastward to be positioned over the British Isles and parts of Scandinavia (approximately between 55º and 65ºN). As a result, southerly and southwesterly flows affect the study domain. A similar mechanism is associated with the negative SCA configuration. However, throughout the negative WeMO mode, a branch of the Azores High extends northward to be placed over the Iberian Peninsula and vast areas of the

Western Europe, which acts as a block for the passage of the Icelandic cyclones eastward. The SLP anomalies corresponding to the negative WeMO imply northerly flows, enforcing the advection of cold air from northern Europe to the region of interest. This configuration can likely be responsible for the observed temperature downtrend, particularly in northern portions.

In summary, it seems that temperature variations over the study domain are mainly linked to the position of the centers of SLP positive (negative) anomaly over the mid Atlantic and the western Mediterranean. This position varies significantly from one season to another and among the leading atmospheric circulations, as a consequence of the displacement of the Azores High and the Icelandic lows.

4.4.1.2. Land-atmosphere coupling forces

Land-atmosphere coupling forces (e.g., soil moisture and cloudiness) can exert a strong control on temperature variations over the study domain. In some seasons (e.g., summer), temperature variations cannot only be driven by atmospheric circulation, particularly at the regional scale. Other forces such as changes in land surface, including soil moisture, can explain much of this variability.

4.4.1.2.1. Soil moisture

The relationship between changes in soil moisture and temperature variability in the study domain was explored through correlation analysis. The results are summarized in Table 4.9. As presented, there were clear seasonal differences in the response of temperature to soil moisture feedback. Notably, the influence of soil moisture on temperature variations appeared to be stronger during spring

and summer, the seasons which also exhibited the highest warming rates in the region from 1960 to 2006. Contrarily, the strength of this relationship degraded markedly during winter and autumn. During spring, the Pearson correlation coefficient varied from -0.38 (minimum temperature) to -0.7 (maximum temperature), while it lied between -0.53 (minimum temperature) and -0.57 (maximum temperature). Most of these coefficients were found statistically significant at $p<0.01$.

Table 4.9: Pearson correlation coefficients of seasonal maximum, minimum and mean temperatures with cloud cover and soil moisture over the study domain. Bold numbers indicate statistically significant correlation at $p<0.05$. The correlation was calculated between regional time series calculated for the whole area for each parameter.

Season	Variable	Soil moisture	Cloud cover
Winter	maximum	-0.13	0.09
	minimum	**0.27**	**0.60**
	mean	0.09	**0.40**
Spring	maximum	**-0.7**	**-0.60**
	minimum	**-0.38**	**-0.28**
	mean	**-0.62**	**-0.48**
Summer	maximum	**-0.57**	**-0.60**
	minimum	**-0.53**	**-0.40**
	mean	**-0.66**	**-0.50**
Autumn	maximum	-0.27	-0.21
	minimum	-0.02	0.10
	mean	-0.17	-0.08

As shown in Table 4.9, the strongest correlation between temperature variation and soil moisture was found during spring (r = -0.7 with maximum temperature). This association is illustrated in Figure 4.31, which notably indicates that years of anomalous warmer temperature during spring were generally characterized by a significant deficit in soil moisture. This can be clearly seen in two periods: from mid of the 1960s to 1980 and during the last two decades.

For summertime, the results also suggest that standardized anomalies in soil moisture were negatively correlated with anomalous temperature ($p < 0.01$). Nevertheless, this correlation was stronger for maximum and mean temperatures (-0.57) than for minimum temperature (-0.53). Table 4.9 also informs that the connection between temperature and soil moisture was stronger during daytime relative to nighttime. The only exception was found during winter as minimum temperature correlated better with soil moisture (0.27) than maximum temperature (-0.13). During wintertime, this feedback was found positive with minimum temperature, which came in contrast with other seasons.

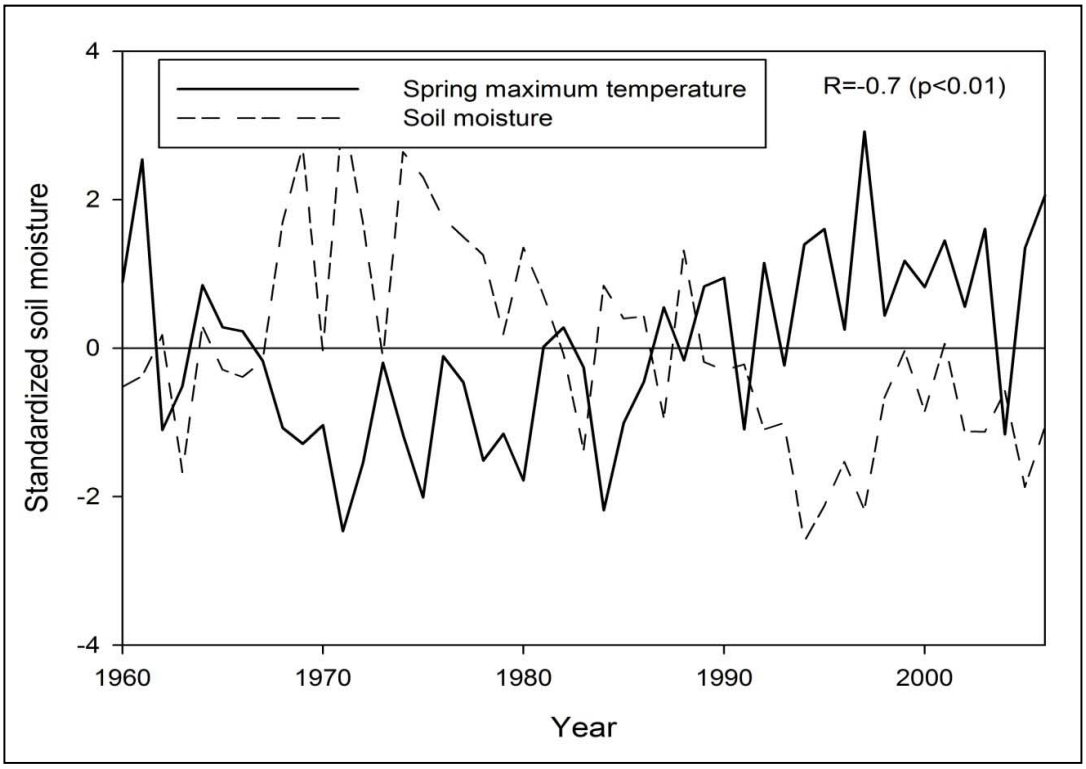

Figure 4.31: The negative feedback between soil moisture and maximum temperature during spring season from 1960 to 2006.

4.4.1.2.2. Cloudiness

Cloudiness is another key factor influencing the Earth's radiation budget. The strong role of the seasonal cycle of insolation suggests that climate system is likely sensitive to changes in cloudiness, particularly during summer. The dependency between cloud cover and temperature variations was investigated at a seasonal scale for maximum, minimum and mean temperatures in the region. A summary of the results is also given in Table 4.9. As presented, it seems that cloudiness had a significant influence on temperature variations during winter, spring and summer. Temperature only showed weaker dependency with cloudiness during autumn season, with correlation coefficients ranging from -0.08 to -0.21. The results suggest positive (negative) feedback during winter (spring and summer). As indicated, it seems that cloudiness is a key driver of temperature variability during summer. The feedback was found negative for maximum (-0.6), minimum (-0.43) and mean (-0.54) temperatures. This relationship was statistically significant at high level of probability (99%), which suggests strong causal links between the amount of cloudiness and summer temperature over the study domain. Similarly, a strong positive feedback between cloudiness and minimum temperature was found during winter, with r = 0.6. The well-fitted temporal evolution of both winter minimum temperature and cloudiness, as revealed from Figure 4.32, clearly implies that a considerable portion of temperature variations during wintertime can be explained by cloudiness feedback.

Taken together, two main findings can be inferred in this context. First, for both cloud cover and soil moisture, the results suggest stronger influence on

temperature variations during spring and summer than in winter and autumn. These feedbacks were generally negative assuming that an increase (decrease) in temperature anomalies often corresponds to a negative (positive) anomaly of soil moisture and cloud cover. Winter was the only season in which both cloudiness and soil moisture experienced positive feedback with temperature. Second, the influence of the examined land surface-atmosphere forces had a diurnal cycle, with more influence during daytime than nighttime. These diurnal differences were more apparent during spring with regard to other seasons.

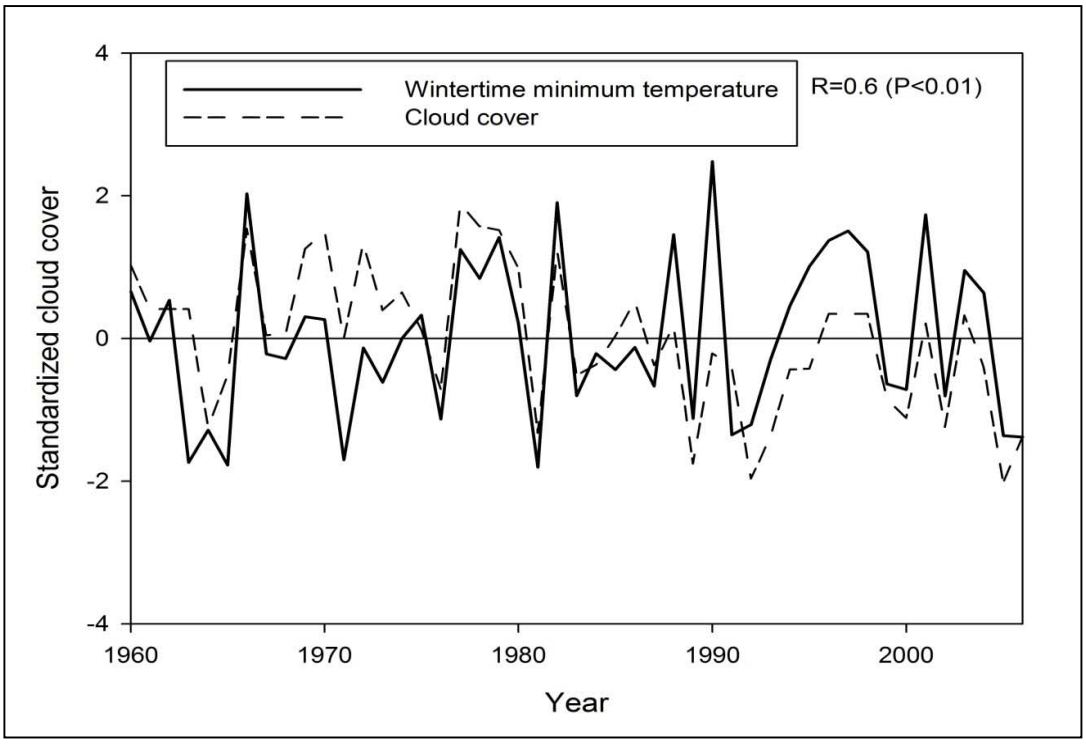

Figure 4.32: The positive feedback between cloud cover and wintertime minimum temperature in the study domain from 1960 to 2006. Standardized anomalies of both fields are provided from 1960 to 2006.

4.4.2. Influence of large-scale atmospheric circulation on temperature extremes

4.4.2.1. Influence on moderate extreme events

In this section, the influence of the atmospheric circulation patterns on temperature extremes was assessed based on the spatial regionalization of summertime extreme events defined in section 5.3.1 and plotted in Figure 4.20 (CL1 to CL4). Figure 4.33 depicts Pearson correlation values between the general atmospheric circulation and the regional time series of extreme temperature indices in the period 1960-2006. This association was calculated for the regionally weighted time series computed for the delineated four clusters.

Similar to mean temperature conditions, the connection between the circulation patterns and temperature extremes was found statistically significant ($p<0.05$) only for the EA+, SCA- and WeMO- patterns. Among them, the WeMO represents an east-west dipole; meanwhile the EA and SCA are north-south dipoles. On the other hand, the NAO was found a weak predictor of temperature extremes during summer season. Similarly, the role of the MO pattern was irrelevant in the region.

For the established homogenous sub-regions, it seems that the SCA pattern is a key controller of temperature extremes, with correlation coefficients ranging between -0.20 and -0.64. However, it can be noted that the influence of the SCA on day-time extremes (e.g., max_summer, WD and TX90p) was much stronger than its influence on night-time extremes (e.g., min_summer, TXn, TNn and TN90p). In particular, correlation coefficients with day-time extremes were in the

range of -0.41 and -0.54, whereas they varied from -0.29 to -0.49 for night-time extremes.

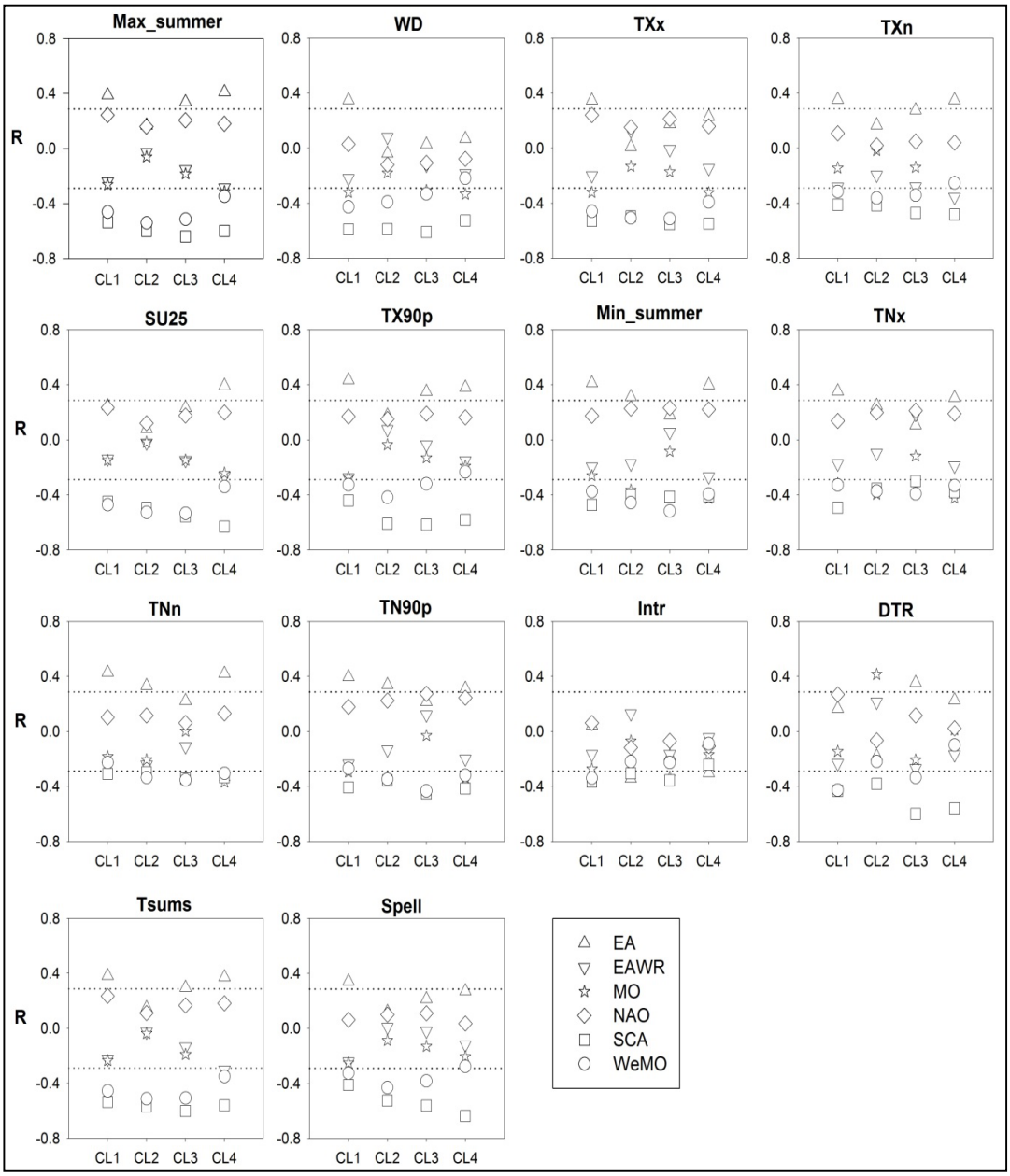

Figure 4.33: Pearson correlation coefficients (*r*) between detrended time series of summer extremes and the main modes of atmospheric circulation over the period 1960-2006. Dotted lines show the upper and lower limits of the 95% level of significance.

A quick view of the association between the SCA circulation pattern and temperature extremes at sub-regional scale reveals some significant spatial differences (Figure 4.33). The influence of the negative SCA on most of summer temperature extremes was generally less marked in the Mediterranean region (CL1) and, in contrast, much stronger in the highly elevated regions (CL3 and CL4). A clear example corresponding to DTR showed a significant correlation with the negative SCA in all the defined sub-regions, but with higher values in CL3 (r = -0.60) and CL4 (r = -0.56), compared with CL1 (r = -0.43) and CL2 (r = -0.38). This spatial pattern likely resembles that of the Spell index, which exhibited the strongest relationship with the SCA negative phase in CL4 (r = -0.64) and CL3 (r = -0.56), relative to CL1(r = -0.41) and CL2(r = -0.52). It can thus be inferred that the influence of SCA on extreme temperature in the region is clearly elevation dependent, with more (less) influence at high (low) elevation sites.

The correlation of summer temperature extremes with the positive EA was generally positive although it did not necessarily reach the statistical significance threshold, as being the case with the WD, INTR, SU25 and Spell indices. In contrast to the SCA pattern, the strongest association between the EA positive phase and temperature extremes was markedly apparent along the Mediterranean coast (CL1) for the majority of the indices. Contrarily, this influence declined in mainland and over complex terrain sub-regions. Similar to the SCA pattern, the WeMO correlated better with maximum temperature indices than with minimum temperature indices. Spatially, it can be noted that the impacts of the WeMO pattern on temperature extremes were more pronounced in continental and low elevated areas than in coastal and highly elevated regions.

In summary, among all circulation patterns, the most significant during summer season were the EA+, WeMO- and SCA-. Figure 4.34 indicates the temporal evolution of the atmospheric circulation patterns from 1960 to 2006. As depicted, a significant positive trend was exclusively exhibited for the EA index, meanwhile a statistically downward trend with remarkable decadal variability was found for the EAWR, MOI and SCA patterns. In particular, the EA experienced a negative phase until the end of the 1970s, followed by a noticeable rise since the mid of the 1990s. By contrast, a decline in the MOI, WeMO and SCA patterns was observed since 1980. This figure also indicates that the NAO showed a negative trend from the mid of the 1980s, which comes in direct contrast with the strong signal of temperature during this period.

4.4.2.1.1. SLP configurations

In order to better understand the mechanisms of atmospheric flows and land-sea interactions during summer season, the SLP configurations corresponding to the significant circulation patterns in the region (i.e., EA+, WeMO- and SCA-) were summarized by means of the composite climate analysis and the canonical correlation functions. For each dominant circulation mode, the composite maps were plotted based on SLP anomalies corresponding to summers of positive or negative values from 1960 to 2006, depending on the phase under investigation (i.e., positive or negative). This dependency is depicted in Figures from 5.35 to 5.37. SLP canonical variates are plotted in left panels, whereas their corresponding temperature variates are illustrated in right panels. The sign of canonical correlation coefficients for the SLP and temperature anomaly indicates the direction of the co-variability (i.e., correlated (+) or anticorrelated (-)).

Figure 4.35 (panel A) shows the averaged anomalies of SLP over western and southwestern Europe during summers with positive EA values. As illustrated, the positive mode of the EA pattern is mainly associated with a strong dipole over the North Atlantic (approximately 50ºN, 30ºW) and dominance of anticyclones over the Mediterranean and central and Eastern Europe. This situation also corresponds to an increase in the anticyclonic activity over the Iberian Peninsula, while the Azores High extends northward.

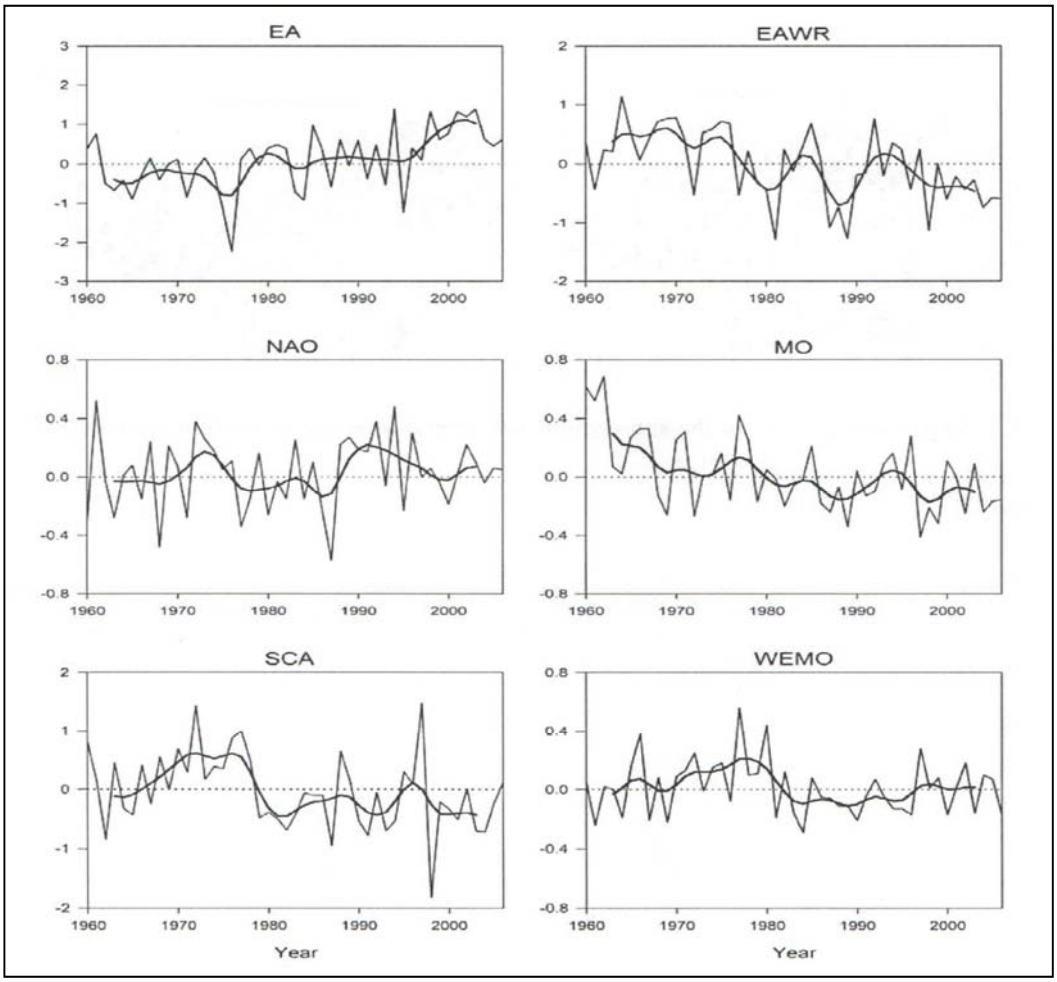

Figure 4.34: Temporal evolution of the large-scale atmospheric circulation patterns during summers of the period 1960-2006. Bold lines refer to a low-pass Gaussian filter of 9 years.

Under this SLP configuration, the advection of the westerly and southwesterly winds over the Iberian Peninsula is enhanced, while the easterly flows transport moisture from the Mediterranean along a SE-NW gradient. Correspondingly, there is a weak moisture transport from the north Atlantic during this configuration, which induces a decrease in precipitation over the study domain. The anomalous low precipitation demonstrates positive feedback with soil moisture anomalies, which in turn has a positive feedback with temperature anomaly. The impacts of the westerly, southwesterly and easterly flows on the study domain are largely constrained by local terrain. For example, the central portions (e.g., the Ebro valley) are weakly affected by these flows as a consequence of the surrounded orographic lifting (i.e. the Iberian and Cantabrian systems). Contrarily, the EA exerts more important influence along the Mediterranean coast, particularly with the increase in the warm and moist flows from the Mediterranean and the mid of the Atlantic. Owing to the weak contrast between SLP over the Mediterranean Sea and closing land areas during the positive EA as revealed by SLP isopleths, the influences of these inflows can not extend to mainland, particularly with prevalence of high pressure anomalies in most of the peninsula as a consequence of local heating effects (see Figure 4.35, panel A). In short, the EA positive phase exerted a remarkable influence on the increase in frequency and intensity of summer temperature extremes along the Mediterranean coast and high elevation sites.

Figure 4.35 (panels B and C) illustrates respectively the first and second canonical functions that explain the large proportion of variability in both SLP and temperature during the positive EA mode.

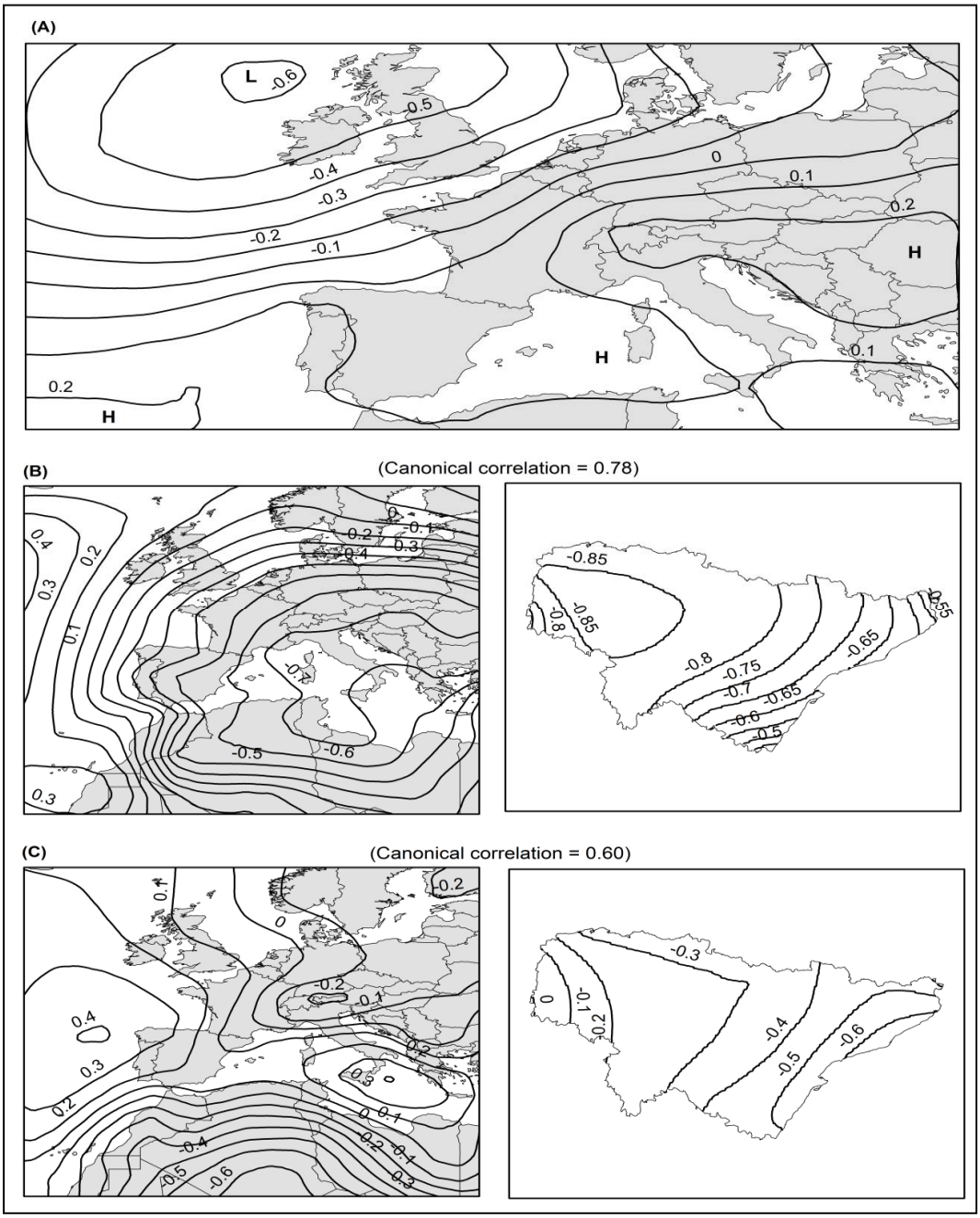

Figure 4.35: (A) Composite of sea level pressure (SLP) anomalies (hPa) corresponding to summers with positive EA values from 1960 to 2006. SLP anomalies at each grid were computed using the monthly mean and standard deviation for the long-term period (1960–2006). (B) The first leading canonical function of SLP and temperature anomalies co-variability during summers of the positive EA mode, (C) the same as (B) but for the second leading function. Isopleths show the Pearson correlation coefficient. Coefficients above 0.23 are statistically significant at the 95% level.

As shown, the canonical correlation coefficients of the first and second functions were 0.78 and 0.60, respectively. Spatially, it was found that temperature over central and western areas of the study domain are mainly controlled by SLP anomaly over the Mediterranean region, particularly the western basin (r = -0.7), whereas it is anticorrelated with SLP anomalies over the northern Atlantic. The second function suggests that temperature variations over the eastern portions of the study area were significantly influenced by SLP anomaly over central Europe and northern Africa, while they correlated negatively with SLP over the eastern Atlantic (panel C). Taken together, it can be noted that above-normal temperatures during summers of the positive EA values are mainly associated with a positive SLP anomaly over the Mediterranean, central Europe and North Africa on the one hand and a negative SLP anomaly placed over the east Atlantic on the other hand.

Figure 4.36 (panel A) illustrates the composite of SLP anomaly during summers of negative SCA values from 1960 to 2006. As depicted, the negative phase of the SCA pattern produced similar configuration to the positive EA, with clear high pressure anomaly over central Europe. This high pressure anomaly extends westward to cover the Iberian Peninsula and southward to include parts of the Mediterranean region and North Africa.

On the other hand, a low pressure system predominates over the north Atlantic and vast areas of northern Europe and Scandinavia. This atmospheric circulation indicates that the advection of northern flows over the peninsula is largely restricted during the negative mode of SCA, as a consequence of dominance of

anticyclonic conditions over the European mainland, giving rise to increased above-normal temperature. This situation comes clearly in contrast with SLP features during summers of positive SCA values, where the anticyclonic anomalies predominate over the Scandinavian region favoring for the advection of northern cold-air flows toward the Iberian Peninsula.

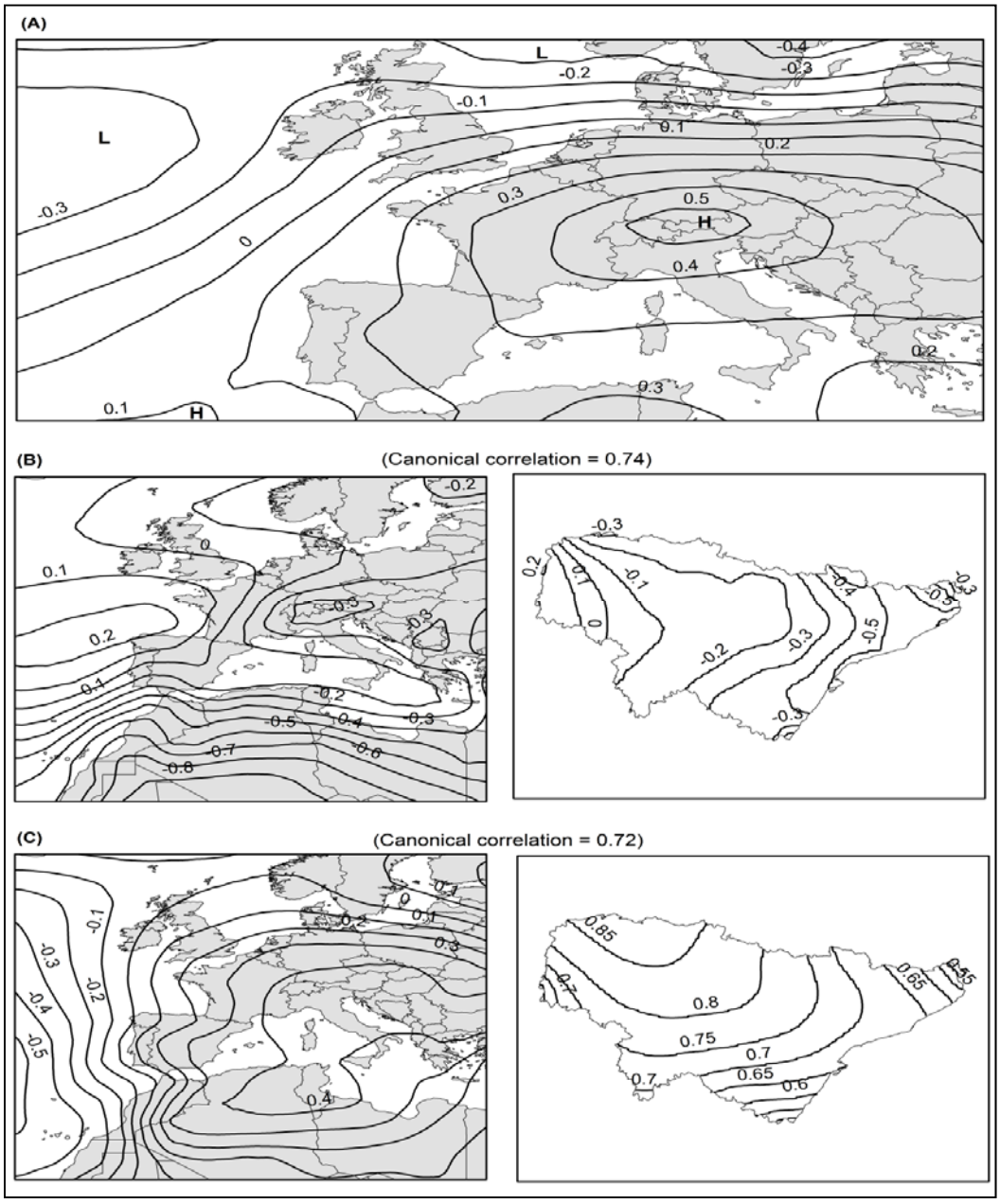

Figure 4.36: Same as Figure 4.35, but for summers with negative SCA values.

Figure 4.36 (panels B and C) suggests two main functions that explained the co-variability between SLP anomaly and temperature during summers of the negative SCA. The first canonical function had a canonical correlation coefficient of 0.74. On the other hand, the second function showed captured 17.3% of temperature variance, with a canonical correlation coefficient of the order of 0.72. A quick comparison between panels B and C suggests that higher temperature along the northeastern parts of the study domain were mainly controlled by the high pressure anomaly over northern Africa (*r* between -0.2 and -0.8) and central Europe (*r* = -0.3). Similarly, the anomalous high temperatures over western areas were significantly connected to the SLP positive anomaly located over the Mediterranean region and central and southern Europe. These spatial patterns clearly match those patterns observed during the positive phase of the EA mode.

Spatial variations of SLP anomalies corresponding to summers of negative WeMO values are illustrated in Figure 4.37 (panel A). As shown, the atmospheric circulation corresponding to the negative mode of the WeMO pattern is mainly associated with a remarkable increase in the zonal circulation activity. Obviously, summers with negative WeMO values are characterized by a strong positive SLP anomaly over the whole Europe with a maximum over the Northwestern Europe and in particular the British Isles (up to +1.0 hPa). In contrast, SLP shows a slight negative pressure anomaly over western parts of Iberia. This is mainly associated with the northward shift of the Azores high. In contrast to the meridional flows which are clearly constrained during the negative WeMO as a consequence of the European blockings, zonal flows from the Mediterranean Sea

are promoted causing above-normal temperature over eastern proportions of the study area.

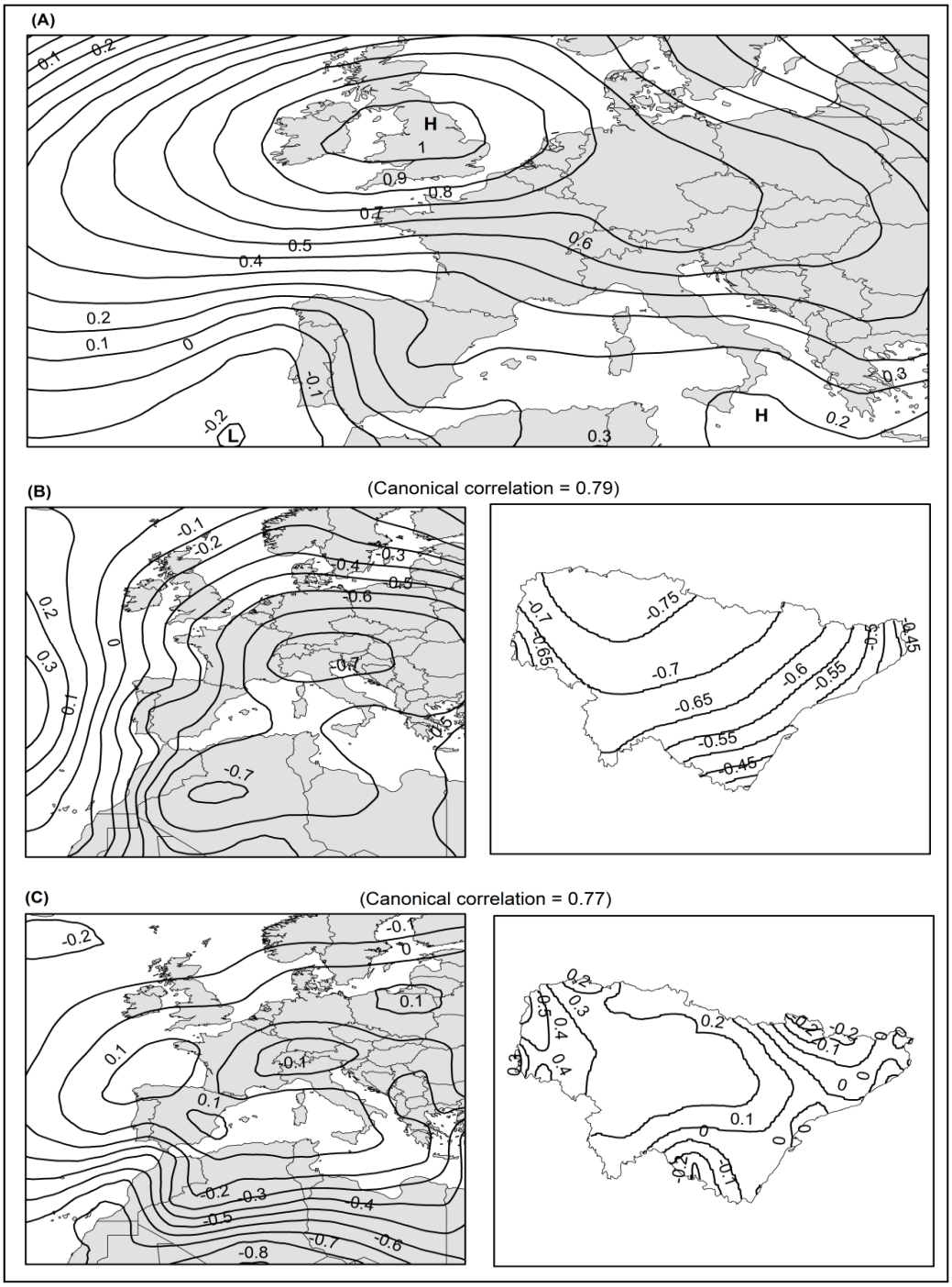

Figure 4.37: Same as Figure 4.35, but for summers with negative WeMO values.

Figure 4.37 (panels B and C) depicts the main spatial patterns of SLP-temperature co-variability during the negative WeMO mode. The results suggest two main functions, with canonical correlation of 0.79 and 0.77 for the first and second functions, respectively. The spatial association between temperature variations and centers of action of SLP anomaly resembles well those detected for both the positive EA and the negative SCA patterns.

4.4.2.2. Influence on the anomalously severe extreme events

In this section, a comparison between the circulation patterns corresponding to very warm days (VWD) and very cold nights (VCN) from 1960 and 2006 is provided. These events represent the most anomalously extreme records as they were defined as daily Tmax >99th for VWD, and daily Tmin <1st percentile of local temperature distribution for VCN. Prior to making this comparison, it was important to compare between circulation patterns during these severe heat events and those corresponding to the normal thermal conditions. This comparison highlights the differences between normal and less frequent events. It also indicates how circulation patterns may behave differently under these contrasted conditions. Simply, days of normal summer (winter) conditions were calculated as days of maximum (minimum) temperature higher than the 25 percentile and lower than the 75 percentile relative to each station's own summer (winter) climatological temperature ranges. Then, the daily anomalies of SLP, 200hPa and 500hPa corresponding to these extreme heat days were averaged and plotted.

Figure 4.38 (panel A) depicts anomaly of SLP and geopotential fields corresponding to the mean conditions of climate during summers of the period

1960-2006. As depicted, it can be noted that a positive surface and geopotential anomaly stretches over the Iberian Peninsula : >0.2hPa for the SLP, >0.8gpm for the 200hPa and >4gpm for the 500hPa level during normal conditions. Interestingly, a similar pattern was also visible at all levels from the surface to the mid troposphere although this pattern was less accentuated and smaller in magnitude at surface compared with the warm anomaly composites at upper levels (i.e., 200hPa and 500hPa). Apparently, a lack of significant pressure gradient was evident during these normal summer days, which implies a broad high prevailing over Iberia.

Figure 4.38 (panel B) reveals the SLP and 200hPa and 500hPa geopotential height anomaly associated with VWD from 1960 to 2006. Relative to summer normal conditions, there was a higher surface anomaly with a main center over the mainland Europe (between 3 and 4.2 hPa). Also, when considering other geopotential height (e.g., 200hPa or 500hPa) a similar but stronger low and mid-troposphere geopotential anomaly is observed, with different values (>12 gpm for 200hPa and >60 gpm for 500hPa). Spatially, the center of action was shifted northeast to be located over the Bay of Biscay and mainland France.

A quick comparison between panels A and B in Figure 4.38 suggests that weather patterns during the most extreme warm events showed differences from the norm conditions. The common conditions show a slight positive pressure anomaly over Iberia and the mid of the Atlantic ocean (west to the peninsula). Conversely, the days of extremely high temperature exhibited a very strong and persistent high blocking which moves northward further to be placed over central

Europe. This enhances the presence of a ridge or anticyclone over central Europe.

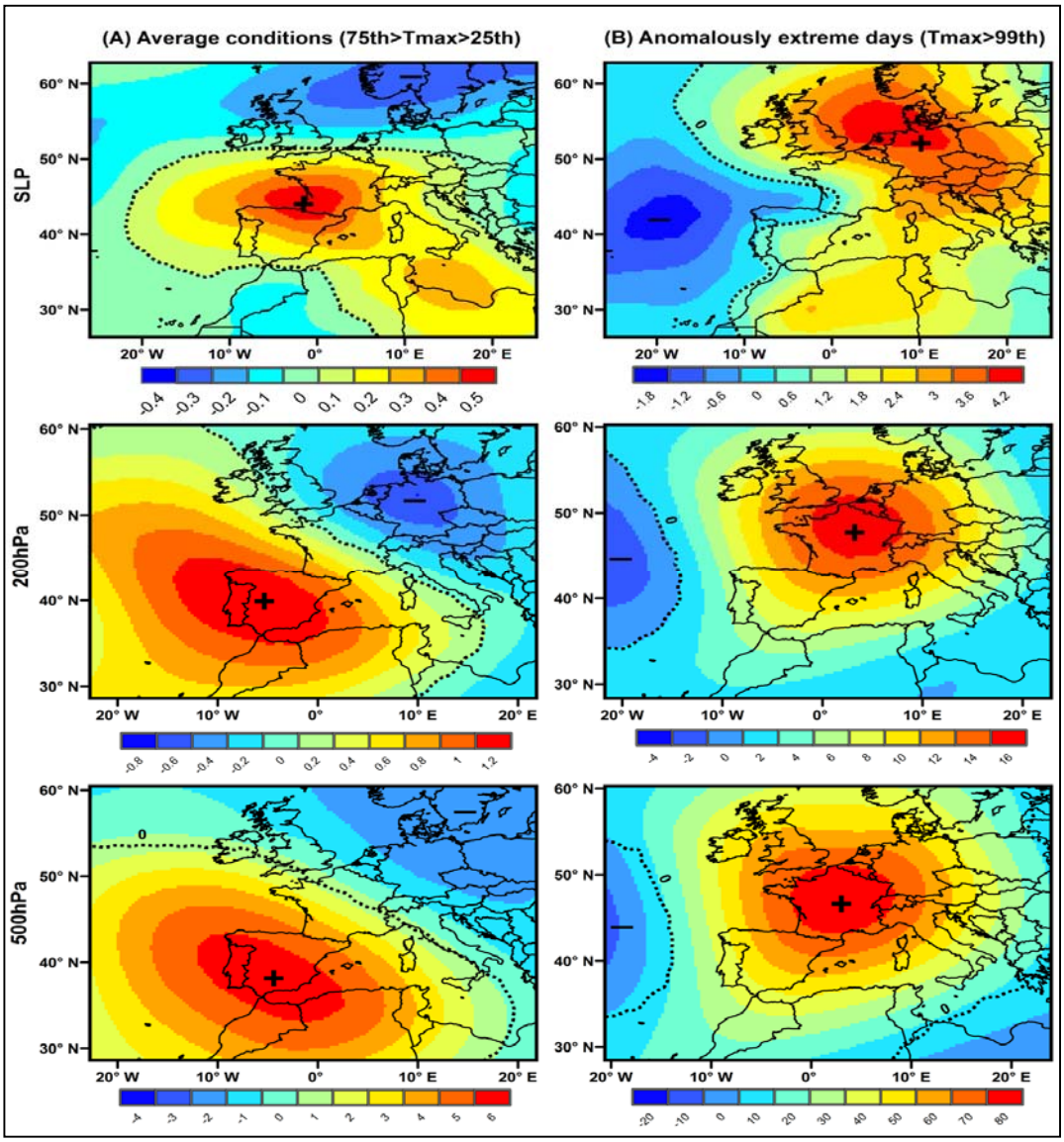

Figure 4.38: Composite anomalies of SLP (hPa), 200hPa and 500hPa geopotential height fields (gpm) during summertime (MJJA) (panel A) against the mean state of summertime temperature (panel B) during VWD. All calculations were based on the period from 1960 to 2006. Due to lack of significant gradient during normal conditions, panel A has its own scale to highlight the spatial modes corresponding to this circulation and also to facilitate comparison of spatial differences between normal and VWD conditions.

Accordingly, it can be noted that the European blockings and Atlantic ridges are the main drivers of the occurrence of VWD. In the study domain, this configuration corresponds to a negative anomaly of SLP and geopotential fields east of the Atlantic Ocean. This situation enforces a strong inflow from the continental central Europe to southern and southwestern regions.

Figure 4.39 represents anomaly of circulation conditions during VCN compared to wintertime ordinary variations. The average conditions during winter months (25th<daily Tmin<75th percentiles, relative to the long-term winter average) were characterized by a clear north-south dipole with the dominance of anticyclonic conditions over much area of Europe, including the Iberian Peninsula. This situation also corresponds to a northeastward displacement of the Atlantic subtropical high to be located west of the Iberian Peninsula. In contrast, a negative anomaly was mainly located over Northern Europe extending from the British Isles to Scandinavia. According to this configuration, there was a high frequency of westerly mild flows into Europe, favoring for less severely cold nights. On the other hand, the anomaly composite of days which witnessed severe low temperatures reveals a similar spatial distribution as in the normal conditions (right panel), though reversed. The negative surface and geopotential anomaly was represented as a long belt extending diagonally from the southwestern to the central part of Europe. However, it was maximized over the western basin of the Mediterranean (>4 hPa for SLP, >16 gpm for 200hPa and >75 gpm for 500hPa).

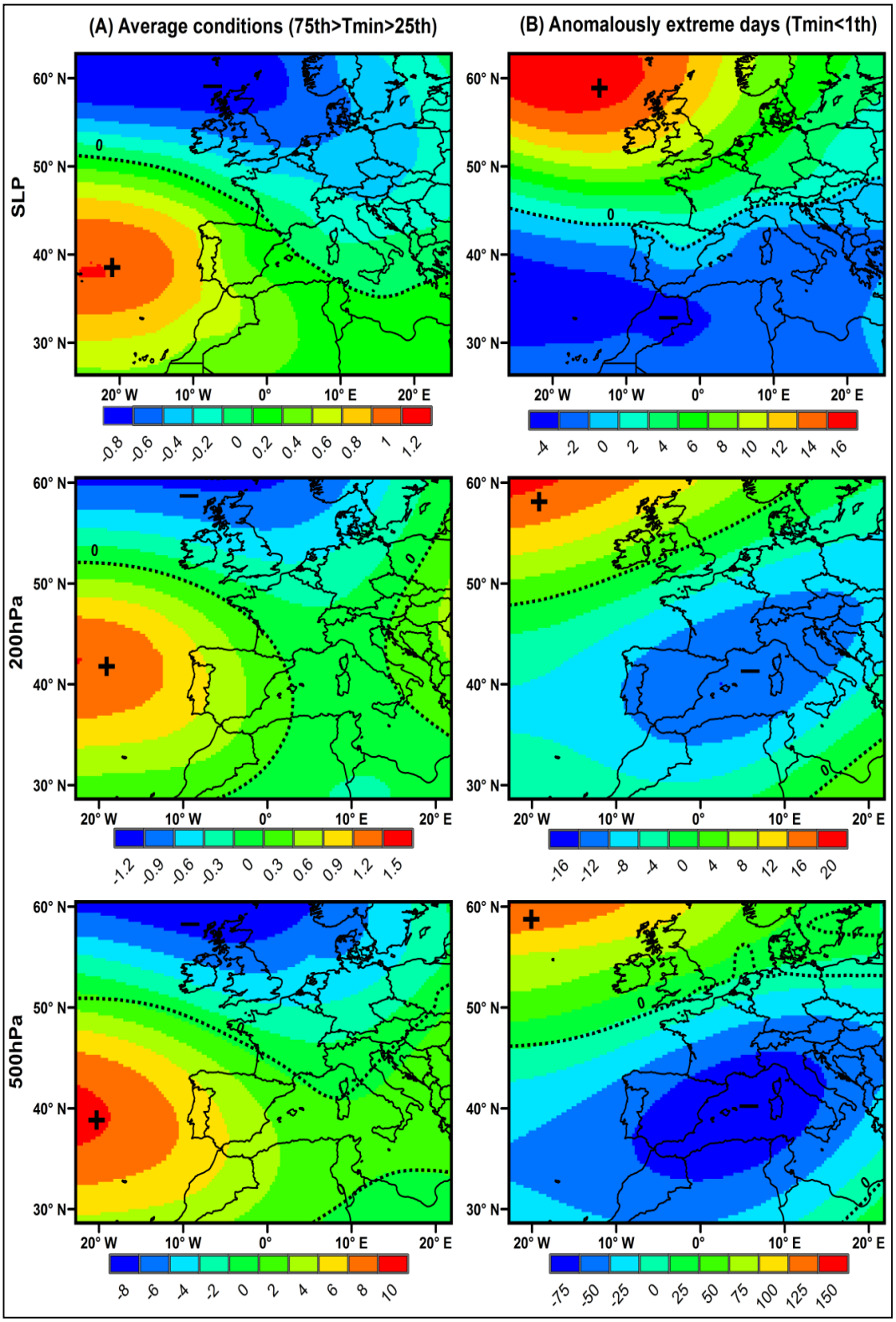

Figure 4.39: Same as Figure 4.38, but for VCN.

Correspondingly, the positive anomaly showed a strong gradient over the Northern Atlantic and Europe (Figure 4.39, panel B). This configuration was also visible at the surface level and low and mid troposphere, enforcing the meridional circulation over the study domain with strong advection of northerly and northeasterly cooler air flows.

To explore air advections controlling very heat temperature variations in the region, the connection between the spatial variability of VWD/VCN and the main centers of large-scale atmospheric circulation patterns was analyzed by means of the canonical correlation. For each canonical pair (variate), the results are presented in two maps: one for the dependent variable (i.e., anomaly of atmospheric fields) and the latter for independent variables (i.e., temperature anomaly during these VWD/VCN). This pair of maps provides an explanation of the physical reasoning of VWD/VCN canonical variate by identifying the main centers of action of circulation patterns that significantly correlate with the spatial modes of VCN/VWD over the study domain.

4.4.2.2.1. Mean Sea Level (MSL)

Figure 4.40 depicts three surface synoptic patterns that explained regional variability of VWD over northeast Spain. The first leading function (canonical r = 0.7) revealed strong and statistically significant positive correlation between anomalously higher temperature over the western areas of the study domain and SLP regime over the Iberian Peninsula near to the Cantabrian Sea. The second and third functions suggested that the behavior of VWD temperature along the coastal regions was mainly driven by SLP anomaly over the mid latitudes of the

Atlantic Ocean and the Western Mediterranean. As illustrated, it can be seen that positive temperature anomalies along the Cantabrian Sea were well correlated with pressure anomaly west of the Mediterranean basin (the second function), while the intensity and frequency of VWD in the Mediterranean observatories were strongly driven by the positive SLP anomalies over North Africa and Central and Northern Europe (the third function).

An interesting note is that the influence of increasing convection as a consequence of local heating effects, as revealed in the first function, was broadly consistent across the entire domain. This pattern was monopole with positive correlation with temperature anomalies in all sites although the highest significance occurred close to the Cantabrian system in the west and the lowest were found near to the Mediterranean Sea. On the other hand, the second and third functions suggested more spatial contrasts, indicating that more frequent VWD on the Cantabrian Sea always correspond to relatively fewer number of VWD on the Mediterranean Sea and vice versa.

Figure 4.41 represents three main synoptic conditions that explained sub-regional variability of VCN at sea level. All these patterns imply that the anomaly pattern over the North Atlantic region was the main controller of the occurrence of VCN over northeast Spain. The first function (canonical r = 0.65) indicated a generally negative correlation between SLP north of the British Isles and magnitude of temperature during VCN over the study area. In particular, high (low) pressure anomaly north of Ireland implies more (less) severe cold nights in the whole domain, with few spatial differences (Figure 4.41, panel A).

Importantly, the regional response of VCN to SLP anomaly over the Atlantic waters was largely dependent on the location of the Atlantic SLP center action. The first function revealed the strong influence of the Arctic flows when the highs are located over the British Isles.

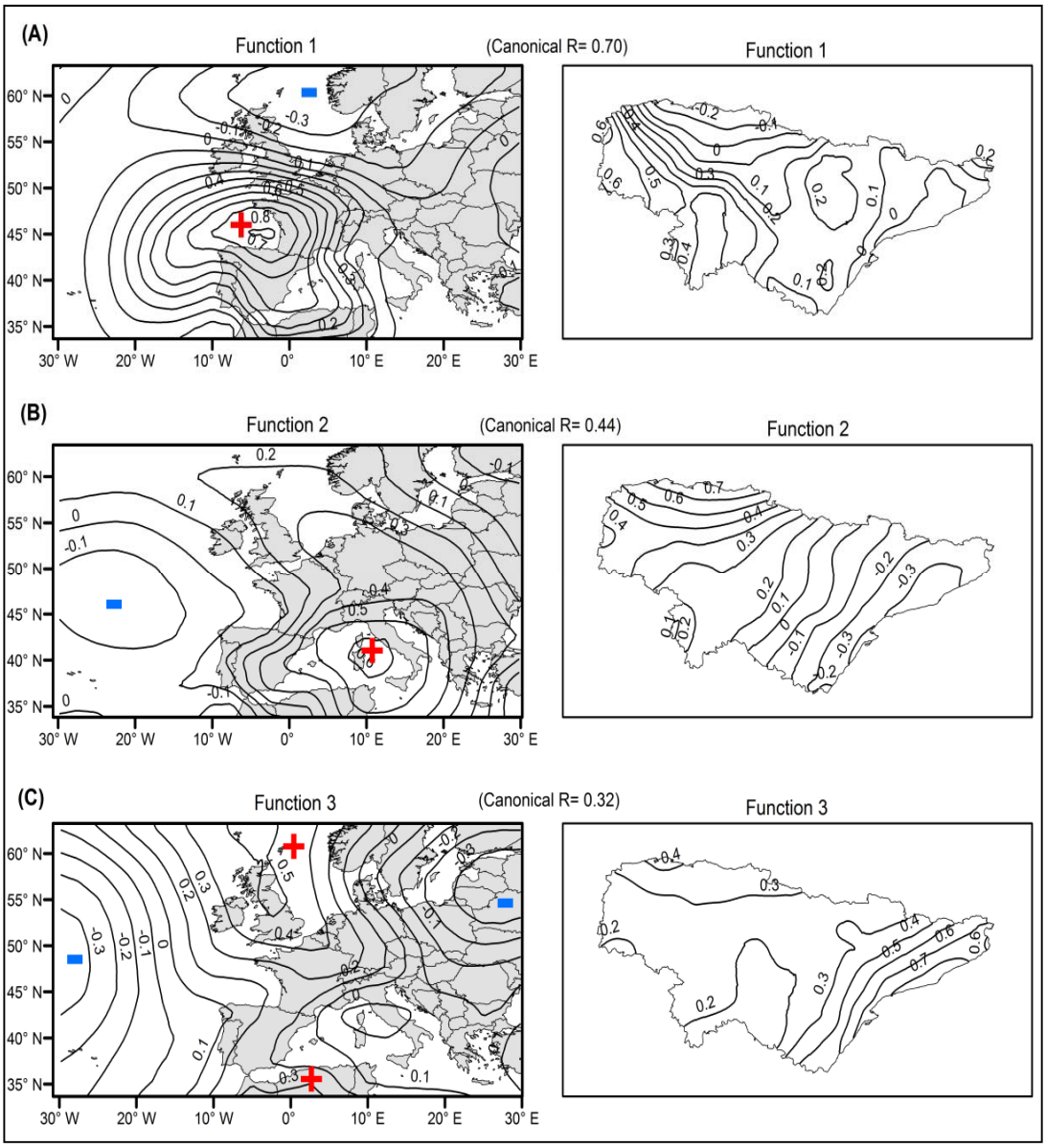

Figure 4.40: Pearson correlation coefficient between anomalies of SLP (left) and temperature anomalies (right) during the VWD across the study domain (coefficients above 0.15 are statistically significant at the 95% confidence level).

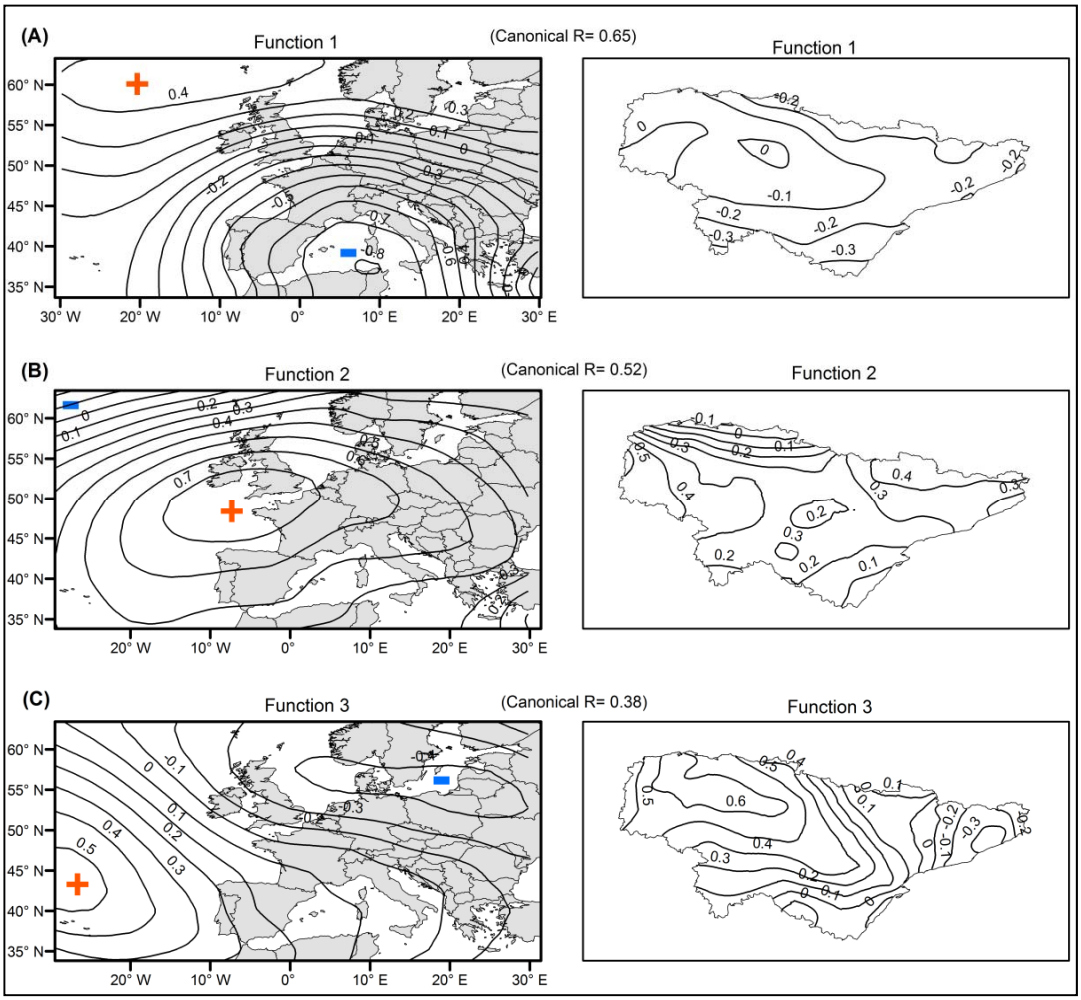

Figure 4.41: Same as Figure 4.40, but for VCN.

The second function suggested less (more) intense VCN over the elevated areas to the west and the Pyrenean mountains northward (r > 0.4) when high (low) anomaly was placed near to the Iberian Peninsula. The third function suggested the possible influence of the Azores high that can extend further to the Eastern Mediterranean during winter months. The displacement of the Azores assumes that temperature intensity in the whole domain, apart from Catalonia in northeast,

was negatively influenced demonstrating warmer conditions and less frequent VCN.

4.4.2.2.2. 200hPa Level

Figure 4.42 suggests three canonical functions, with correlation coefficients varying from 0.14 to 0.64. The first function demonstrated that the positive 200hPa anomaly over the Iberian Peninsula was highly correlated with VWD temperature in northeast Spain. High anomaly at this geopotential induces stability at this upper level causing above-normal temperature and in turn clear skies. This synoptic pattern fitted well with the first function detected at the surface level (Figure 4.40). The very high correlation (highest values above - 0.9) ensured that, during summer months, very high temperature over the western parts of the study area significantly relate to high geopotential anomaly over the Cantabrian Sea. For temperature variate, the highest values of correlation coefficient (larger than 0.8) occurred over the western portions. Contrarily, low pressure anomalies over the peninsula imply less frequent and intense warm days in the western part of the study domain. The second function indicated that the most extreme warm days along the Mediterranean were mainly connected to the pressure anomaly over the British Isles ($r > 0.6$, $p<0.05$) and the Western Mediterranean ($r > 0.4$, $p<0.05$) although the direction was reversed. In particular, high anomaly over the western Mediterranean basin was positively correlated with more intense over the Mediterranean observatories in the region. Also, a negative (positive) anomaly across northern Europe and the British isles assumed more (less) intensity of VWD close to the Mediterranean coast. These anomalies bring warm and moist air from the high anomaly over the eastern

Mediterranean and North Africa to the peninsula, causing above-normal temperature in coastal observatories. This dependency is reversed in mainland areas (i.e., the Ebro valley) as the correlation became negative, but statistically insignificant. The third function characterized the possible influences of the warm masses from the Sahara and North Africa. The intensive warm days over the study domain were associated, to large extent, with the strong advection of warm and very dry air originating over North Africa. The correlation coefficients on temperature variate suggested a markedly SE-NW gradient, with more (less) intense warm days in south and east (north and west).

Figure 4.43 illustrates the main leading 200hPa synoptic patterns that explain VCN spatial variations during the winter season. Overall, the first function (canonical r = 0.73) indicated that VCN minimum temperature anomaly in vast areas of the study domain was positively correlated with 200hPa anomaly over the peninsula. Low anomaly assumes more frequent and intense cold nights. This situation also highlights the strong influence of the Icelandic High as they cause anomalous advection of cold winds from the anticyclones near to the British Islands and Scandinavia to the deep cyclones over the Iberian Peninsula. As shown in Figure 4.43, while the first and second canonical functions highlight the possible influence of meridional circulation as the cooler air flows moved from the north (Islands High) to southern Europe and the Mediterranean, the third function mainly featured the influence of the zonal circulation. The anomalous high (low) over the north Atlantic around (55ºN, 25ºW) and the anomalous low (high) in the Central Europe suggested more influence of the zonal circulation with western and northwestern (eastern and northeastern) advections over

southern and southwestern Europe. The enhanced (weaker) westerlies cause less (more) frequent VCN in northeast Spain.

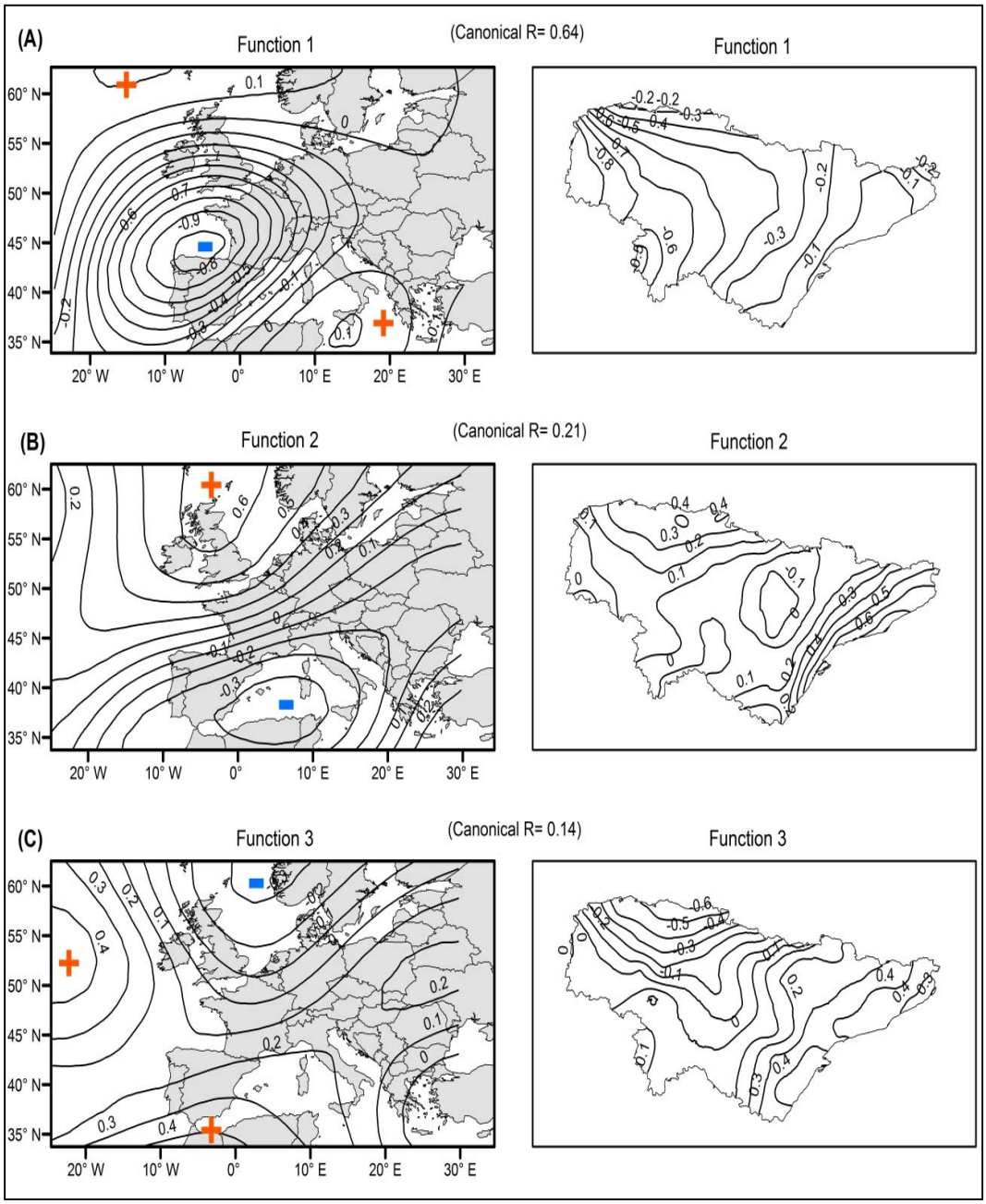

Figure 4.42: Pearson correlation coefficient between anomalies of 200hPa geopotential height field (left) and temperature anomalies (right) during the VWD across the study domain (coefficients above 0.15 are statistically significant at the 95% confidence level).

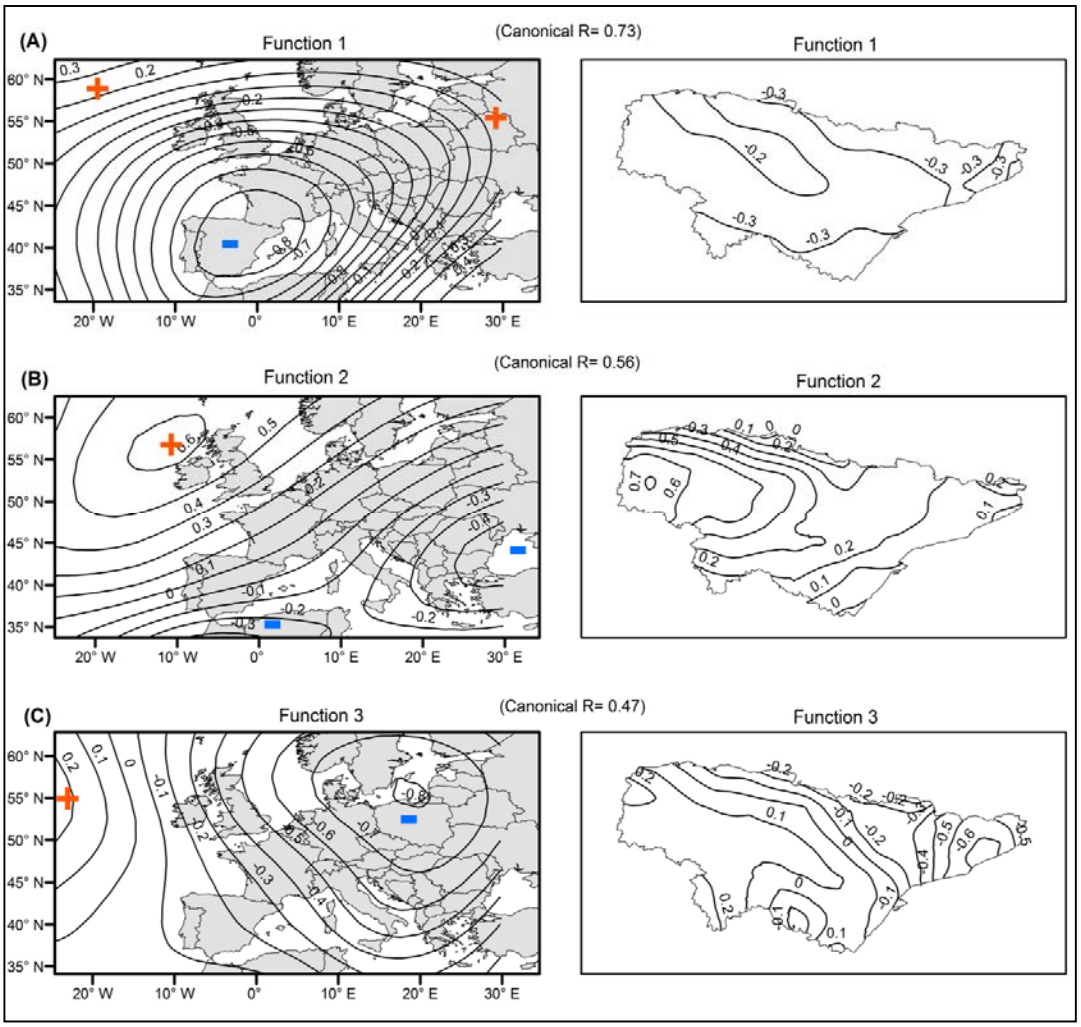

Figure 4.43: same as Figure 4.42, but for VCN.

4.4.2.2.3. 500hPa Level

Figure 4.44 reveals three statistically significant canonical functions (at 95% confidence level). The canonical correlation coefficients ranged from 0.31 to 0.72. Similar to SLP and 200hPa patterns, the first function (r = 0.77) indicates a statistically significant positive correlation between 500hPa geopotential anomaly north to the peninsula and high temperature anomalies across the whole domain. This suggested that VWD were almost entirely controlled by the activity of

anticyclones formed over the Peninsula in general and the Cantabrian Sea in particular. Also, the severity of warm temperature extremes increased westward over the study domain. The intensity of temperature on this function was suggested to be enhanced by the Azores anticyclones, which induce a strong heat and humid advection from the Atlantic. The second function (r = 0.45) highlighted the influence of high anomaly of 500hPa over the western Mediterranean and North Africa on intense temperature in the Mediterranean portions of the study domain. The correlation coefficient reached its highest values (r = - 0.6) in the central Ebro valley. Contrarily, the 500hPa positive anomaly in the western Mediterranean was anticorrelated with intensity of VWD close to the Cantabrian Sea.

In accordance of the first function explaining 200hPa-VCN co-variability, the first function, as illustrated in Figure 4.45, indicates that a deep depression placed over the Iberian Peninsula is favoring for more intense cold nights as it encourages strong advection of northerly cooler flows from the north (Figure 4.45). The results also suggested a statistically significant positive relationship between 500hPa anomaly over the Atlantic Ocean west to the Iberian Peninsula and cold extreme days in the western windward areas of the study domain. Figure 4.45 obviously reveals that cooler air masses over the study domain were strongly linked to low anomaly over the mid latitudes of the Atlantic Ocean, suggesting advections from cooler continental areas in Central Europe. Conversely, this function also implies that zonal advection from the Atlantic was dominated by high humidity advection enhanced by strong anomaly of the westerlies, which was favoring for less intense cold nights.

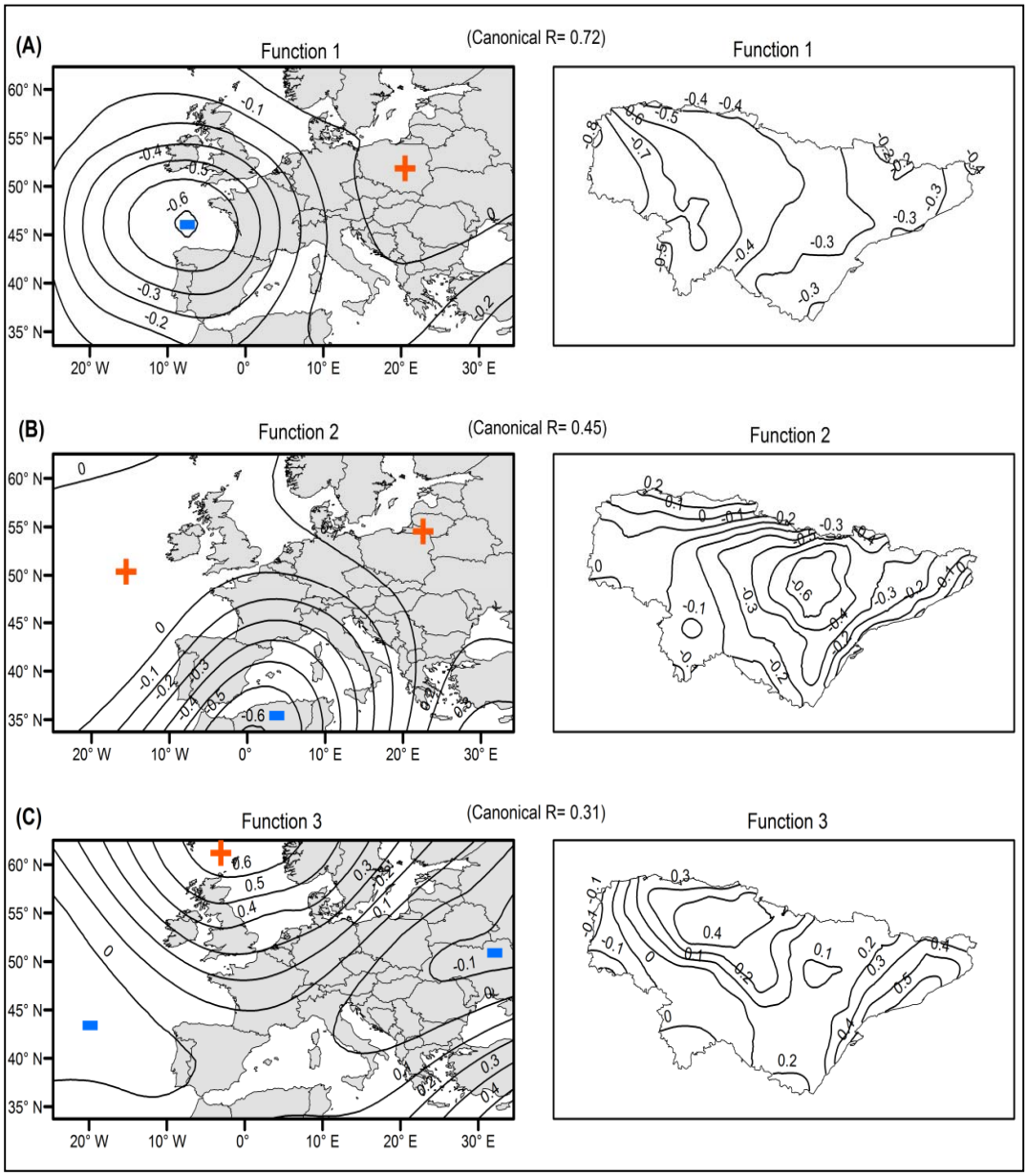

Figure 4.44: Pearson correlation coefficient between anomalies of 500hPa geopotential height field (left) and temperature anomalies (right) during the VWD across the study domain (coefficients above 0.15 are statistically significant at the 95% confidence level).

On the other hand, the third function indicated a negative correlation between anomalies of 500hPa over North Africa and intensity of VCN in the Mediterranean

areas. Under this configuration, the lower tropospheric flows over the western Mediterranean and North Africa, in addition to the warm sea water, enhance the cyclones formation. This situation strengthens the cooler air flows from the north and northeast.

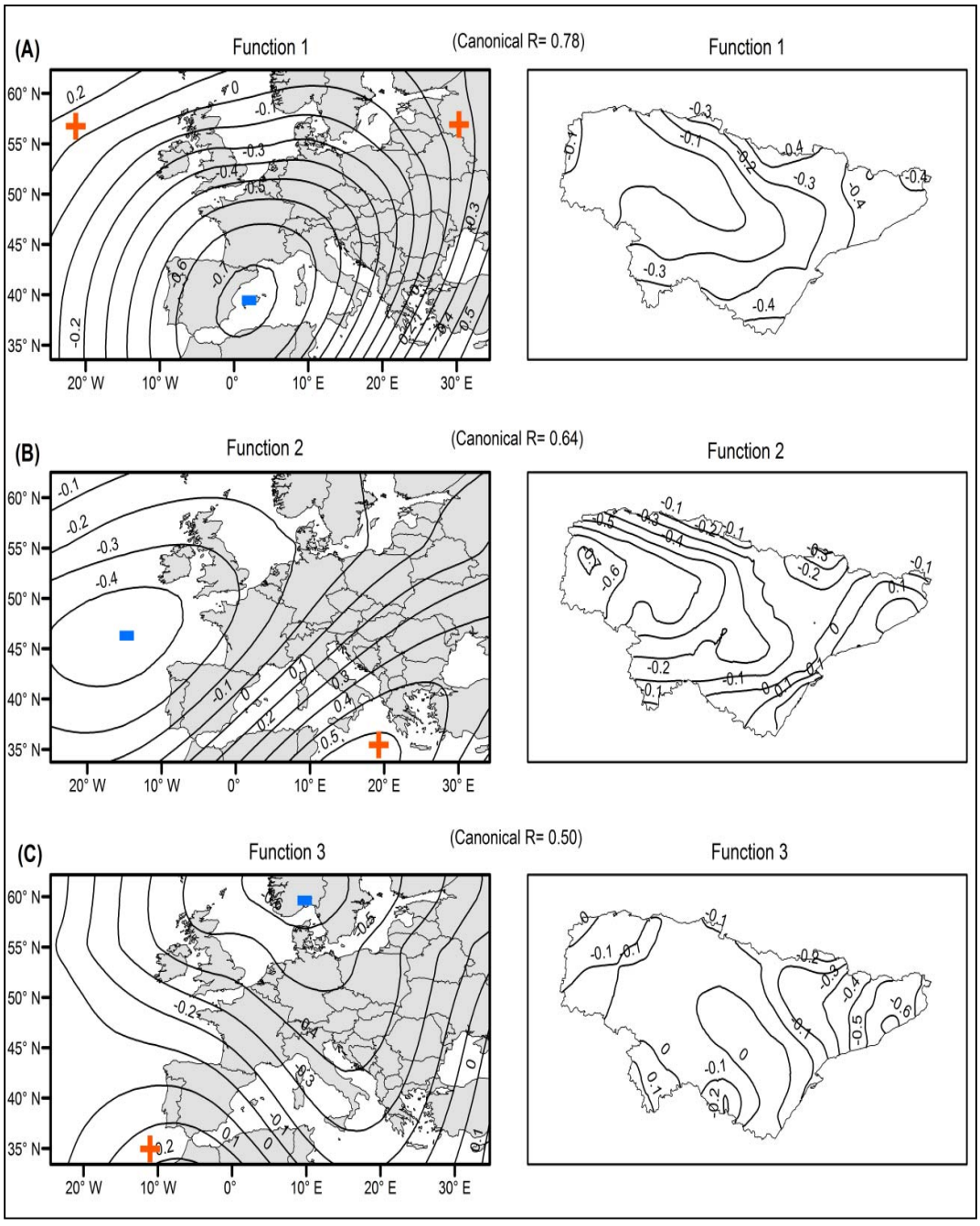

Figure 4.45: Same as Figure 4.44, but for VCN.

A quick inspection of the main functions explaining the connections between 500hPa field and VCN/VWD suggests that the degree of co-variability between 500hPa field and anomalous temperatures was more apparent during VCN when compared with VWD. The canonical correlation coefficients corresponding to 500hPa-VCN functions were generally higher than those of 500hPa-VWD functions. This suggests a higher co-variability between 500hPa over Western Europe and the Mediterranean and anomalous temperature in the study region during winter months than in summer months. This can be seen in the context that temperature variability during wintertime largely depends on air advections at the lower tropospheric layer (e.g., 500hPa level).

4.5. Future changes of temperature during the 21st century

4.5.1. Model Validation results

Various statistical measures were calculated on a seasonal basis to assess the model performance, through comparing the modeled and observed temperature in the period from 1971 to 2000. Boxplots summarizing the validation results using the MBE, YK, IVE and Willmott's D statistics are illustrated in Figures 5.46 and 5.47 for maximum and minimum temperatures, respectively.

As illustrated in Figure 4.46 (panel A), the averaged temperature biases in the CNRM, DMI-APR, METO and MPI simulations for maximum temperature were small, generally less than 1°C, for winter (CNRM=0.2ºC, DMI-APR=-0.4ºC, METO=0.3ºC and MPI=-0.3ºC), spring (CNRM=0.1ºC, DMI-APR=-0.3ºC, METO=-0.5ºC and MPI=-0.9ºC) and autumn (CNRM=-0.6ºC, DMI-APR=0ºC, METO=0.6ºC and MPI=-0.4ºC). As opposed to the winter, spring, and autumn

seasons, the difference between the observed and modeled data was much higher during summer. The CNRM, DMI-APR, METO, and MPI ensembles showed larger bias, with values of 0.9, 1.7, 3.6 and -1.1ºC, respectively.

Moving to the IVE coefficients (Figure 4.46, panel B), the same finding was also confirmed as the CNRM, DMI-APR, METO showed the best performance, with near-to-zero values. More specifically, the CNRM, DMI-APR, METO and MPI simulations gave the best validation results in winter (CNRM=0.1ºC, DMI-APR=-0.15ºC, METO=0.1ºC and MPI=-0.14ºC), spring (CNRM=0.13ºC, DMI-APR=-0.16ºC, METO=0.16ºC and MPI=-0.2ºC), summer (CNRM=0.03ºC, DMI-APR=0ºC, METO=-0.07ºC and MPI=0.11ºC) and autumn (CNRM=0.14ºC, DMI-APR=0.11ºC, METO=0.07ºC and MPI=-0.13ºC).

Figure 4.46 (panel C) also suggests smaller YK coefficients for the CNRM (METO) simulation in all seasons, with values of -0.04ºC (0ºC) in winter, -0.01ºC (0.09ºC) in spring and 0.09ºC (0.03ºC) in summer. Nonetheless, as illustrated in Figure 4.46 (panel C), the YK results indicated that the DMI-APR failed to capture the general symmetry of seasonal maximum temperature, given an opposite (i.e. negative) asymmetry sign to other simulations. This change in the YK from close-to-zero to negative values implies that this ensemble failed to reproduce the maximum temperature distribution, which is more likely to be asymmetric with a tendency to increase extreme cold events. This was mainly evident for all seasons, apart from summer, suggesting less skill of this ensemble in reproducing the asymmetry of maximum temperature.

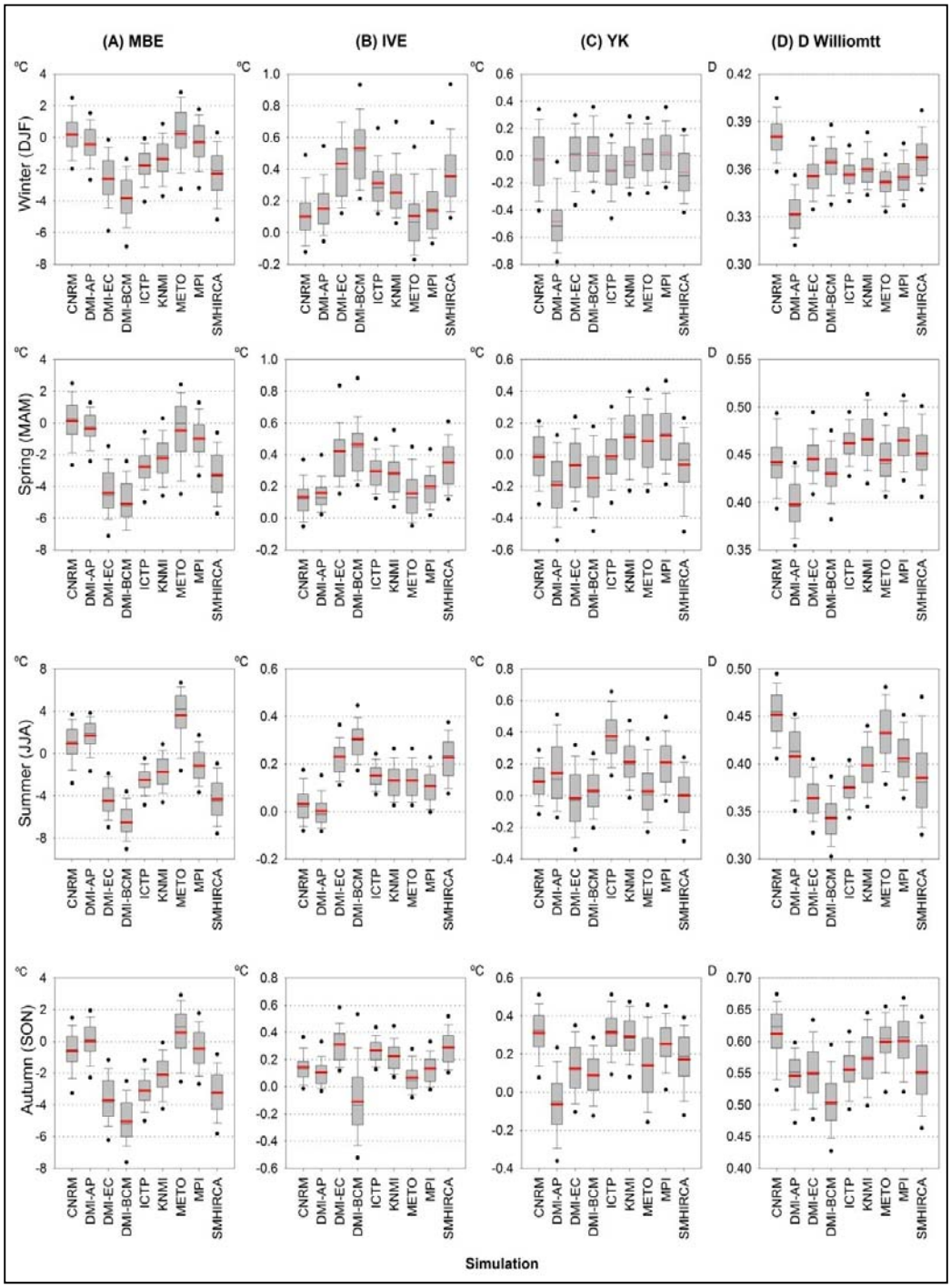

Figure 4.46: Cross-validation results for maximum temperature based on comparing the modelled and observed data for the control period (1971- 2000) for 9 different RCMs simulations. The red line represents the mean and the black line indicates the median.

The Willmott's D statistic also gave reasonable results for the CNRM and METO simulations. For the CNRM (MPI) simulations, the Willmott's D magnitude varied from 0.38 (0.36) during winter to 0.61 (0.60) during autumn.

Combining the results from the different statistics, it can be noted that the CNRM, MPI and METO models gave the most satisfactory results. Interestingly, while these RCMs are driven by different GCMs (i.e., APREGE for CNRM, ECHAM5 for MPI and HadCM3Q16 for METO), they still show similar spatial patterns of temperature changes during the run period (1971-2000), as revealed by the exploratory PCA factors. Accordingly, the CNRM, MPI and METO simulations can be used with a degree of confidence to provide reliable estimates of changes in seasonal maximum temperature over the study domain under the A1B climate change emission scenario during the 21st century.

A summary of the validation results for the seasonal minimum temperature is presented in Figure 4.47. The results suggested three ensembles that gave the best performance for all seasons: ICTP, KNMI and METO. Those models simulated well the daily records of minimum temperature with no significant biases. For the ICTP, KNMI and METO simulations, the findings identified an average MBE of 0.76, 1 and 0.7ºC in winter, -0.54, 0.48, and -0.05ºC in spring and -0.3, 0.7 and 1.2ºC in autumn, respectively. In summer, the CNRM and MPI models showed reasonable results in conjunction with the KNMI model. During this season, the averaged biases for the KNMI, MPI and CNRM ensembles were 0.05, 1 and 1.1ºC, respectively. The same finding was confirmed by the IVE coefficient, which showed magnitudes roughly close to the ideal zero value for the ICTP, KNMI and METO simulations (Figure 4.47, panels B and C). Those

ensembles were also reasonably good at reproducing the observed symmetry of seasonal minimum temperature series, as revealed by the YK statistic.

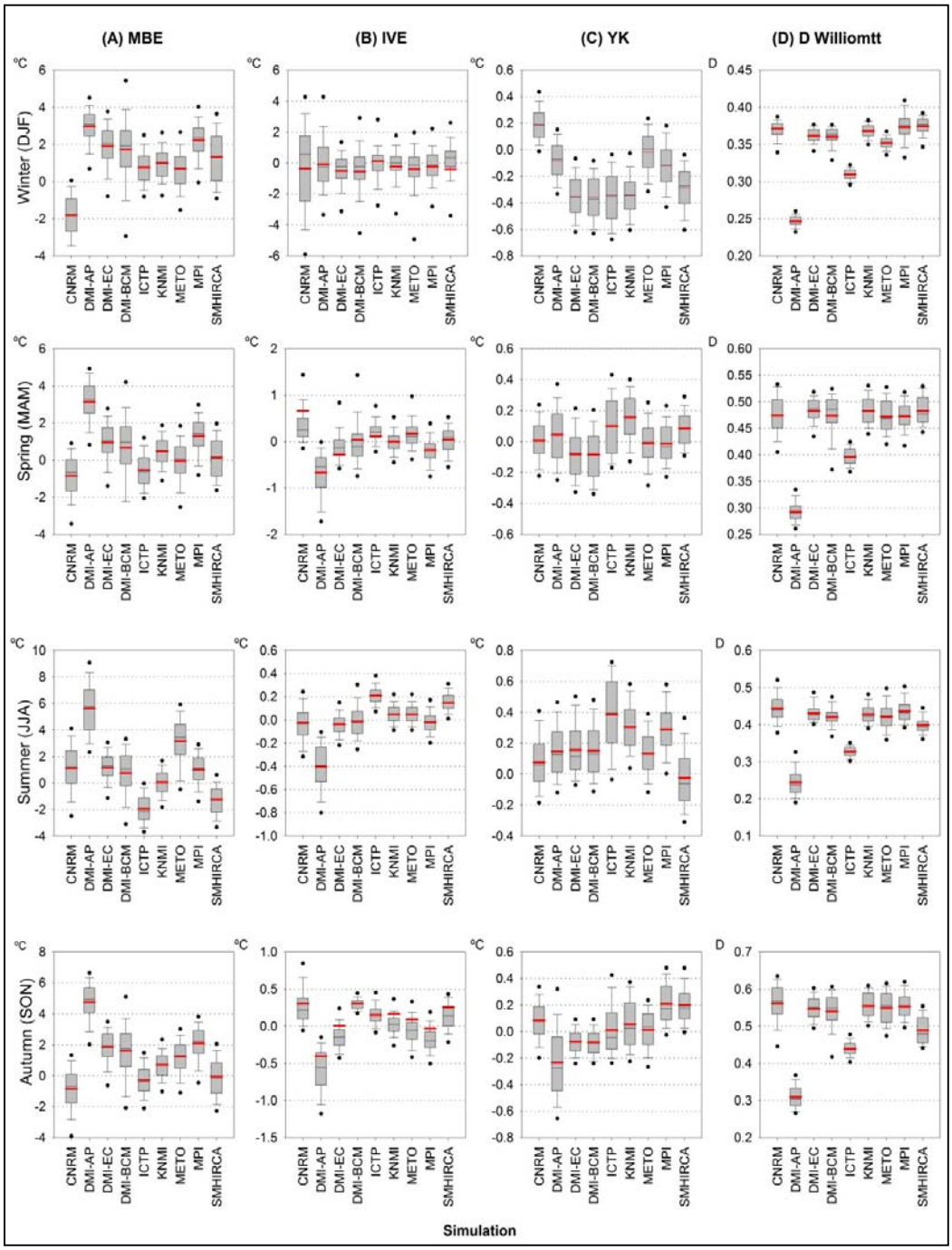

Figure 4.47: Same as Figure 4.46, but for minimum temperature.

Through the PCA, the ICTP, KNMI and METO ensembles also simulated well the spatial patterns of seasonal trends, implying that they can provide a reasonable skill in analyzing changes and variability of the simulated data in the future.

Overall, according to the validation results for simulated minimum temperature data, the ICTP, KNMI and METO ensembles correctly reproduced the main characteristics of the observed climate (e.g., the mean, variance, skewness and symmetry). Accordingly, the models with the best agreement with the observed station data were selected. Herein, the decision was made to select the ICTP, KNMI and METO, as being the models with the overall best performance, to simulate future changes in minimum temperature. As presented in Table 3.4, this group of models is driven by three different GCMs (Arpège, ECHAM5 and HadCM3Q16). Herein, inclusion of more than a single model is advantageous to estimate a wider range of possible responses of the climatic system to elevated GHG emissions.

In the attempt to assess changes in extreme events in the future, an additional pair of statistics was also used to assess the sensitivity of the models to capture the anomalous extremes events (i.e., VCN and VWD). In this context, the coefficient of variance (CV) and changes in the magnitude of the 1st (99th) percentiles for the modelled and observed data were computed for the 9 different models. This assessment was important to test the ability of the models to produce the values of the anomalous temperature as well as the variance of the series. It is noteworthy indicating that these measures were only calculated for summer (MJJA) and winter (NDJF) seasons. The results are presented in Figure 4.48.

For summer (left panel), the results reveal a good performance of the MPI and KNMI models. The 99th percentile was well modeled by these ensembles although they were a bit underestimated by -1.19ºC and -1.16ºC, respectively. Similarly, the ratio of coefficient of variance (CV), calculated for the modelled and observed data gave good results for the MPI and KNMI simulations with values generally close to 1.

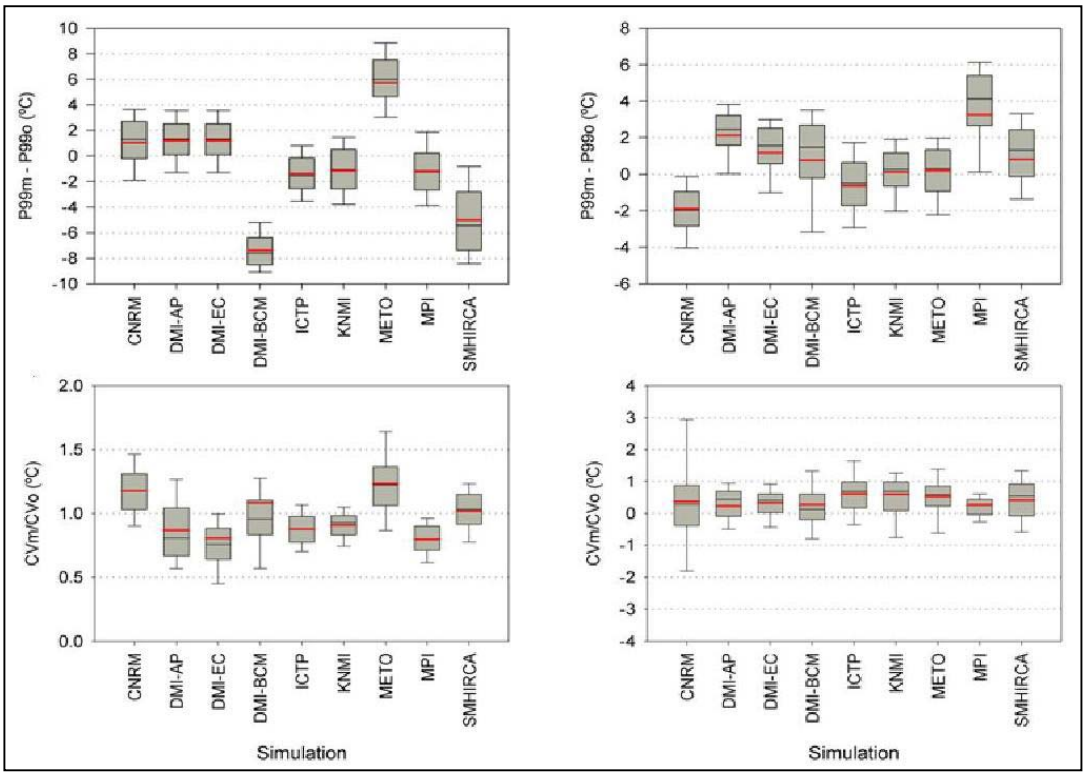

Figure 4.48: Comparison between (upper) differences in the magnitude of the 99th and 1st percentiles, and (lower) changes in the coefficient of variance. Red line shows the average, while the black line indicates the median. Left (right) panels belong to summer (winter).

For winter (right panel), the models with the best performance in terms of the ratio of the coefficient of variance were the METO, ICTP and KNMI. These models were also able to capture the 1st percentile magnitude of wintertime

minimum temperature, with differences of 0.2, -0.7 and 0.1ºC, respectively. Interestingly, these biases were markedly smaller compared with differences in the magnitude of the 99th percentile for daily maximum temperature during summer season. Interestingly, this was also the case for extreme maximum temperatures in highly elevated areas with cooler temperatures. Following the validation results, two different RCMs were used to simulate VWD (MPI and KNMI), while three models were used to project changes in VCN (METO, ICTP and KNMI).

4.5.2. Future changes in temperature means

After having confidence in model performance for the control period (1971-2000), the projected future changes in the seasonal maximum and minimum temperatures for the time slices 2021-2050 and 2071–2100 were assessed, relative to the control period. Figure 4.49 shows the seasonal maximum and minimum temperature anomalies for the 20th and 21st century over the whole region. For each individual simulation, the anomalies were first computed relative to the 30-year observed (1971-2000) long-term mean for the region grid points. In order to detect temperature change signal for each season under the A1B emission scenario, an inter-model anomaly was then calculated as the average of the anomalies of the selected simulations.

Figure 4.49 informs that both mean maximum and minimum temperatures exhibited positive anomaly with regard to the 1971-2000 period. This anomaly was much stronger during the last decades of the 21st century. However, this warming had some seasonal differences.

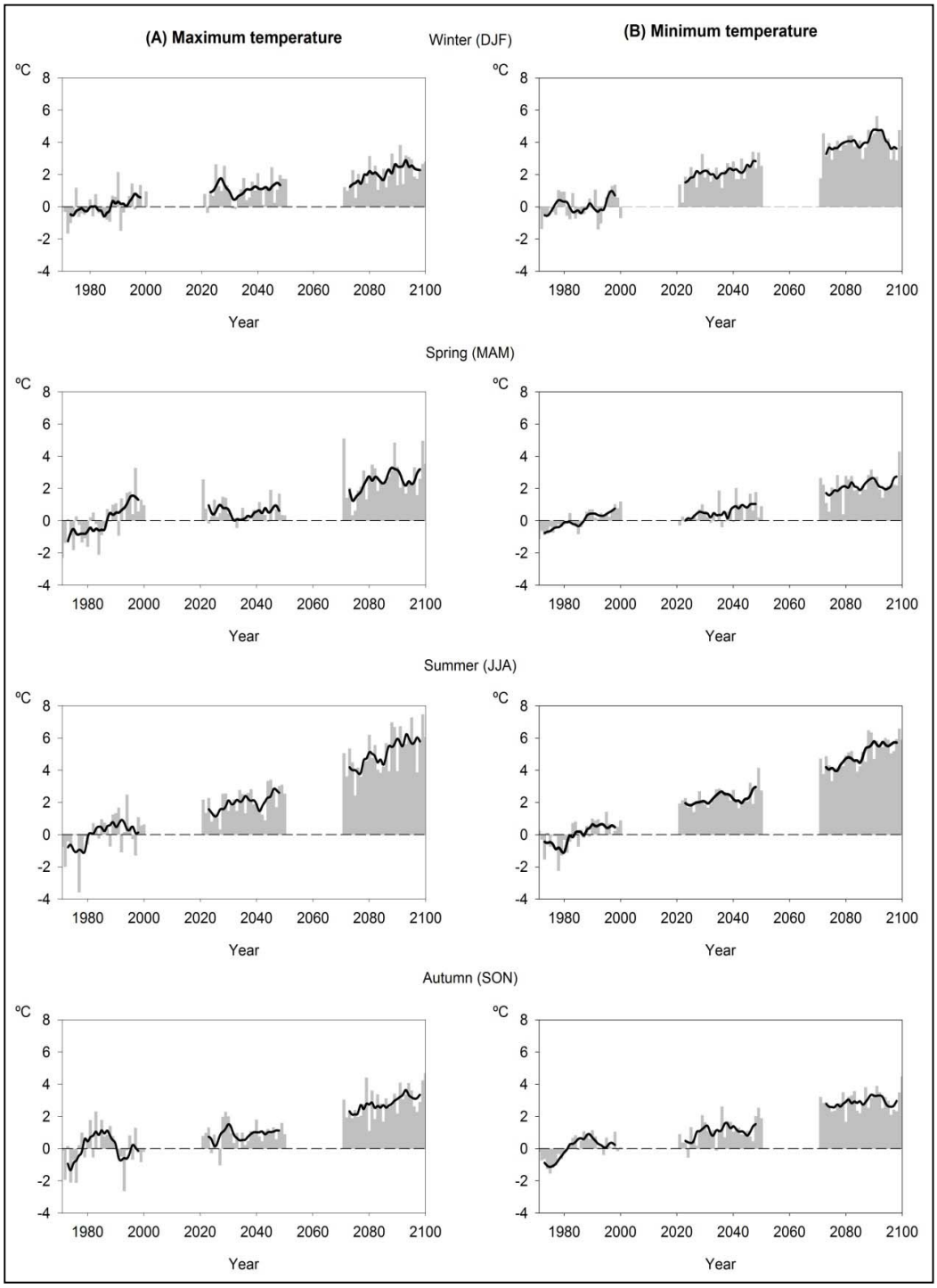

Figure 4.49: The observed and simulated time series of areally averaged seasonal temperature from 1971 to 2100, presented as bars. A 7-yrs low pass filter is calculated and mapped as solid lines. The anomalies are calculated relative to the control period (1971-2000) for each season.

From 2021 to 2050, the predicted warming during the summer and winter periods, under the A1B emission scenario, were larger than the transition seasons (i.e., spring and autumn). The projected increases were in the order of 2, 1.1, 0.9 and 0.6ºC for summer, winter, autumn and spring maximum temperatures, respectively. Similarly, minimum temperature became warmer, but at rates faster than those of maximum temperature. In particular, the average minimum temperatures were warmer than observations by approximately 0.5–2.3°C, depending on the season. The highest increase occurred during summer (2.3ºC) and winter (2.1ºC), relative to autumn (1.1ºC) and spring (0.5ºC).

Similarly, the projected changes of maximum and minimum temperatures over the period from 2071 to 2100 showed rapid shift toward more warming conditions relative to both the baseline (1971–2000) and near future (2021–2050) simulations. This trend was evident for all seasons, with rather similar rates of increase for maximum and minimum temperatures. As presented, there was a high likelihood of increase in maximum temperature by 5.1, 2.8, 2.6 and 2.1ºC during summer, autumn, spring and winter, compared with a simulated warming of about 5, 2.9, 2.2 and 3.9ºC for minimum temperature, respectively.

The spatial structure associated with changes in the maximum and minimum temperature anomalies are given in Figure 4.50. These patterns are presented for the 2021-2050 and 2071-2100 time slices, based on computing an inter-model average for the best-validated simulations for each season (as defined previously in section 5.5.1). As depicted in Figure 4.50 (panel A), the main spatial pattern corresponding to maximum temperature was the high positive anomaly over the central Ebro valley, with higher increases in winter and summer. In the

Ebro valley, the projection for the A1B emission scenario over the 21st century was that maximum air temperature may increase in the range of 3-4ºC and 1-2ºC during summer and winter respectively compared to the present climate. From 2021 to 2050, all solutions also produced a slight negative anomaly over parts of the Pyrenees, which had an opposite sign to the entire region in all seasons, with a maximum reduction in cold seasons (winter [2-3°C] and spring [1-2ºC]). These changes were less pronounced during warmer seasons (i.e., summer and autumn). However, a projected increase in the temperature maxima across the Pyrenees is expected by the end of the century, particularly during summer.

In particular, the RCMs predicted an increase in the summer maximum temperature by 3.5ºC to 5ºC over the region by the end of the century. Another notable feature was that the warming pattern exhibited a meridional gradient with somewhat higher values in the south than in the north. In areas close to the Cantabrian Sea, maximum temperature was generally lower relative to the continental and southern portions by roughly 2ºC in winter and 3ºC in summer.

Figure 4.50 (panel B) illustrates the spatial distribution of minimum temperature changes during the 21st century with regard to the present climate. As depicted, a positive anomaly prevailed during winter and summer from 2021 to 2050, particularly over continental grids. Correspondingly, a slight increase was experienced during spring and autumn. Similar to maximum temperature, the Pyrenees was expected to exhibit a slightly negative anomaly during spring and autumn. From 2071 to 2100, temperature anomalies showed a steady increase on an east-west gradient. While the Cantabrian system to the west and southwest exhibited the strongest positive anomaly (above 4.5 and 6ºC in winter

and summer, respectively), a relatively less warming occurred close to the Mediterranean and the Cantabrian Sea.

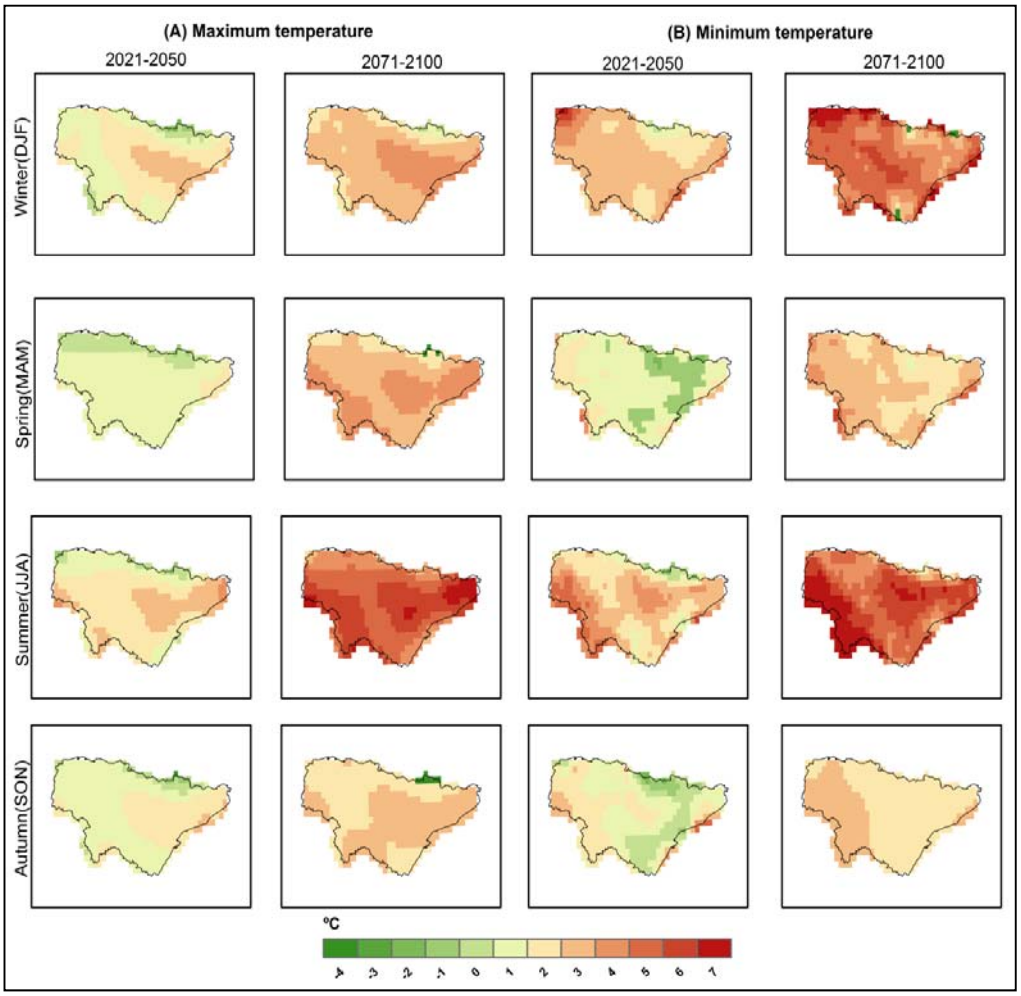

Figure 4.50: Spatial distribution of seasonal maximum and minimum temperature anomalies (ºC) over the study domain. The anomaly was defined as departures from the observed long-term mean (1971-2000).

Figure 4.51 reveals the Gaussian probability distributions of the winter and summer maximum temperatures calculated from the Pyrenean grid cells with altitude above 1000 m. The probability distribution had a near normal distribution during the period from 1971 to 2000, with a mean value of 6.8ºC for winter and

22.2ºC for summer. On the other hand, those of the future periods were quite diverse but generally very elongated, with significant shifts toward the positive tail. The only exception corresponds to the winter temperature from 2021 to 2050, which exhibited a slight decrease in the mean by 0.3ºC relative to the observed climate.

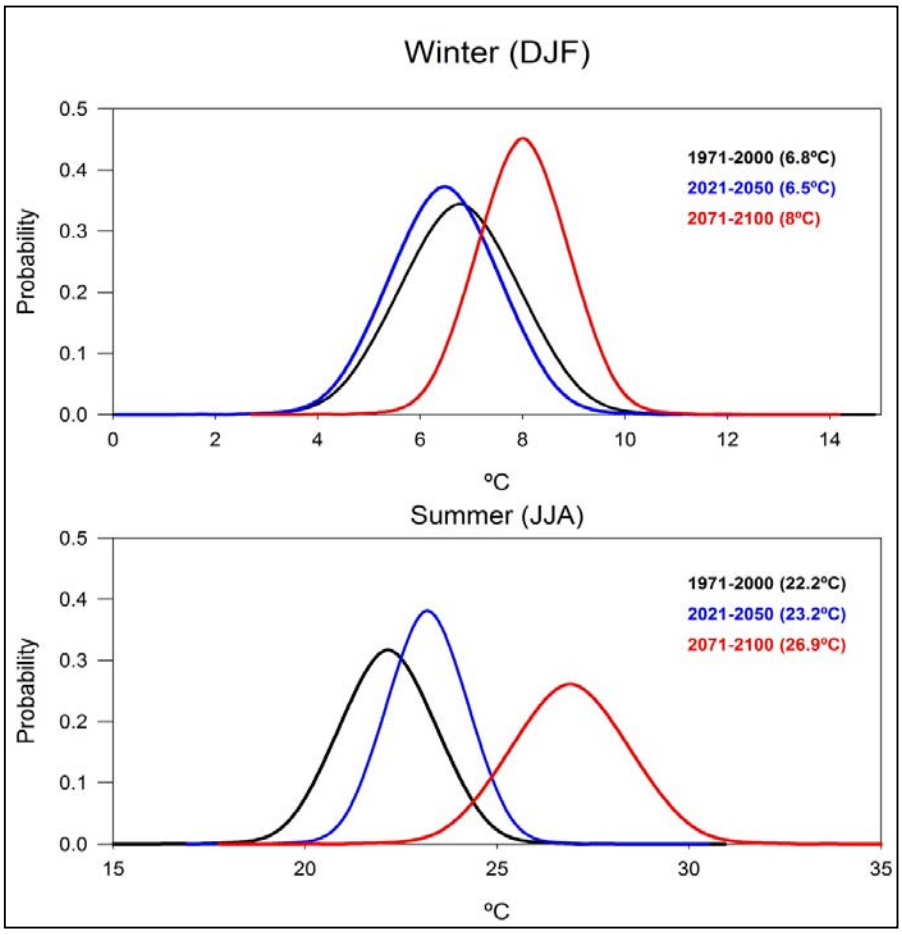

Figure 4.51: Gaussian distribution for (upper) wintertime and (lower) summertime maximum temperatures for the 1971-2000, 2021-2050 and 2071-2100 periods for the Pyrenees region. The inter-model average was calculated as an average of temperature from the grids with altitude above 1000 m in this region. Numbers between brackets indicate the mean value corresponding to each bell curve.

Conversely, there was a general consistency about high likelihood of increase in winter and summer maximum temperatures by the end of the century. This warming was more pronounced during summer with an increase rate of 4.7ºC, compared with the present climate. In summer, the temperature distribution was flatter, suggesting that temperature values are more disperse from the mean, a situation which favors for more warm events. This feature was enhanced by the increase in the standard deviation during summer, which came in contrast with maximum temperature during winter.

4.5.3. Future changes in temperature standard deviation

Figure 4.52 shows the spatial distribution of changes in the standard deviation of the seasonal mean maximum and minimum temperatures across the region over the 21st century. For each grid box, changes in the standard deviation were simply calculated as the difference between the standard deviation of the future simulations (2021-2050 and 2071-2100) and the reference period (1971–2000).

A quick inspection of Figure 4.52 clearly reveals that, in accordance with changes in the mean, standard deviation presented an overall increase during the 21st century, except for the winter season. Also, this warming was much higher at the end of the century. The projected changes were larger in summer and spring than in the winter and autumn. The only exception corresponded to the autumn maximum temperature as the standard deviation during the first half (2021-2050) of the century was larger than that of the latter half (2071-2100). Averaged over the whole region, the models simulated an increase in the standard deviation of summer maximum temperatures from 2071 to 2100 by 0.5ºC (proportional to

9.8% of the mean increase). In spring, the rise in the standard deviation of the mean maximum temperature was nearly 0.36ºC (proportional to 13.9% of the mean increase). In contrast to other seasons, the standard deviation of wintertime minimum temperature clearly decreased, particularly from 2021 to 2050, suggesting that temperature values were more likely to be located around the mean value. Accordingly, a prorogated distribution of wintertime minimum temperature is expected under the A1B emission scenario, suggesting more or less symmetrical (Gaussian) distribution of temperature, with a tendency to less extreme cold events.

In summer, the highest increases in both the mean and the standard deviation, compared with other seasons, indicate a substantial shift with positively skewed and more widening and flattening temperature distributions in the future. This finding suggests more intense and frequent warm summer extremes over the region, especially during the late 21st century, which also accompanies to a projected increase in the inter-annual variability of summer maximum and minimum temperatures.

Spatially, the projected increase in the standard deviation was fairly inhomogeneous over the entire domain, indicating some regional differences, which mostly come in agreement with those of the mean temperature changes. For maximum temperature, the largest standard deviation values tended to be located in mainland portions, particularly over the central Ebro valley during summer. On the other hand, the highest increase for minimum temperature variability was principally situated over mountains located to the west of the study

area, while the least were centered close to the Mediterranean and the Cantabrian coasts to the north and the east.

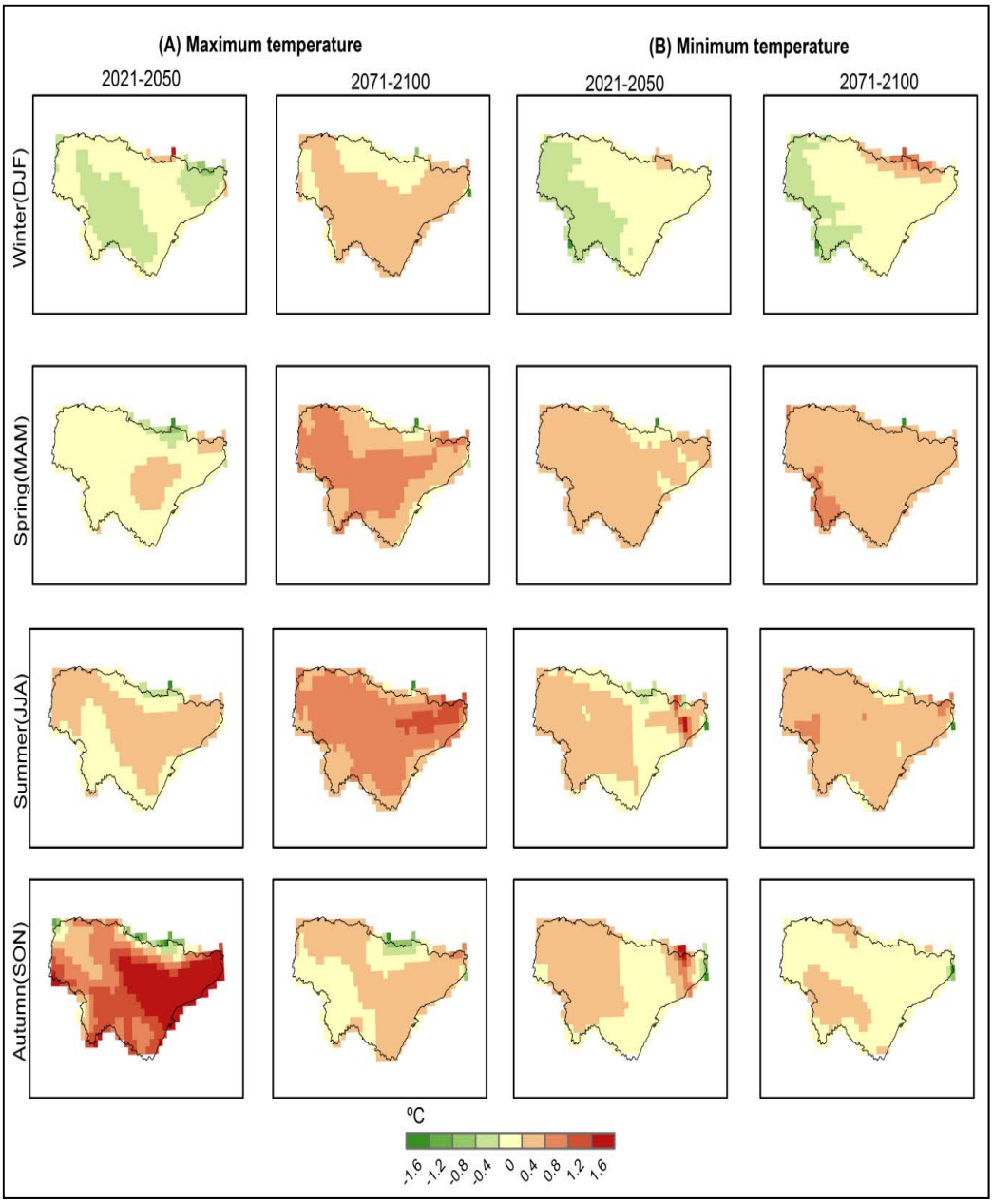

Figure 4.52: Changes (2021–2050 minus 1971–2000 and 2071–2100 minus 1971–2000) in standard deviation of seasonal surface air temperature (°C) based on the ensemble average calculated for each season.

4.5.4. Future changes in the time-varying percentiles

In order to compare between changes in the statistical distribution of the warm and cold tails of temperature time series, this work obtained seasonal time series of the main time-varying percentiles (i.e., the 10th, 25th, 75th and 90th) for the control and future time slices. For each ensemble, these percentiles were calculated for each grid on a seasonal basis. Seasonal differences between the characteristics (i.e., mean, standard deviation and trends) of the simulated and observed percentiles time series are presented in this section and plotted in Figures from 5.53 to 5.56.

4.5.4.1. Winter season (DJF)

Figure 4.53 (panel A) summarizes changes in the magnitude of the percentiles for the winter maximum and minimum temperatures during the 21st century, computed relative to the present climate. For maximum temperature, the magnitudes of all percentiles increased steadily with no significant differences among various percentiles. With respect to the observed percentiles, the warming rate was in the range of 1.1 to 1.3ºC for the period 2021-2050 and 2.4 to 2.6ºC for the period 2071-2100. Also, there were no significant differences among the percentiles of the warm and cold tails of temperature distribution. For minimum temperature, on the other hand, Figure 4.53 (panel B) indicates that the percentiles of the simulated temperature showed rapid warming relative to those of maximum temperature. This can be expected given that the projections suggested more increase in the wintertime minimum temperature than in the maximum temperature in the course of the 21st century. The highest increase occurred for the lower percentiles as the magnitude of the 10th and 25th

increased by 2.7 and 2.6ºC, respectively, for the near-future (2021-2050) simulation, which were roughly doubled over the 2071-2100 period, with a warming of 4.8 and 4.7ºC, respectively.

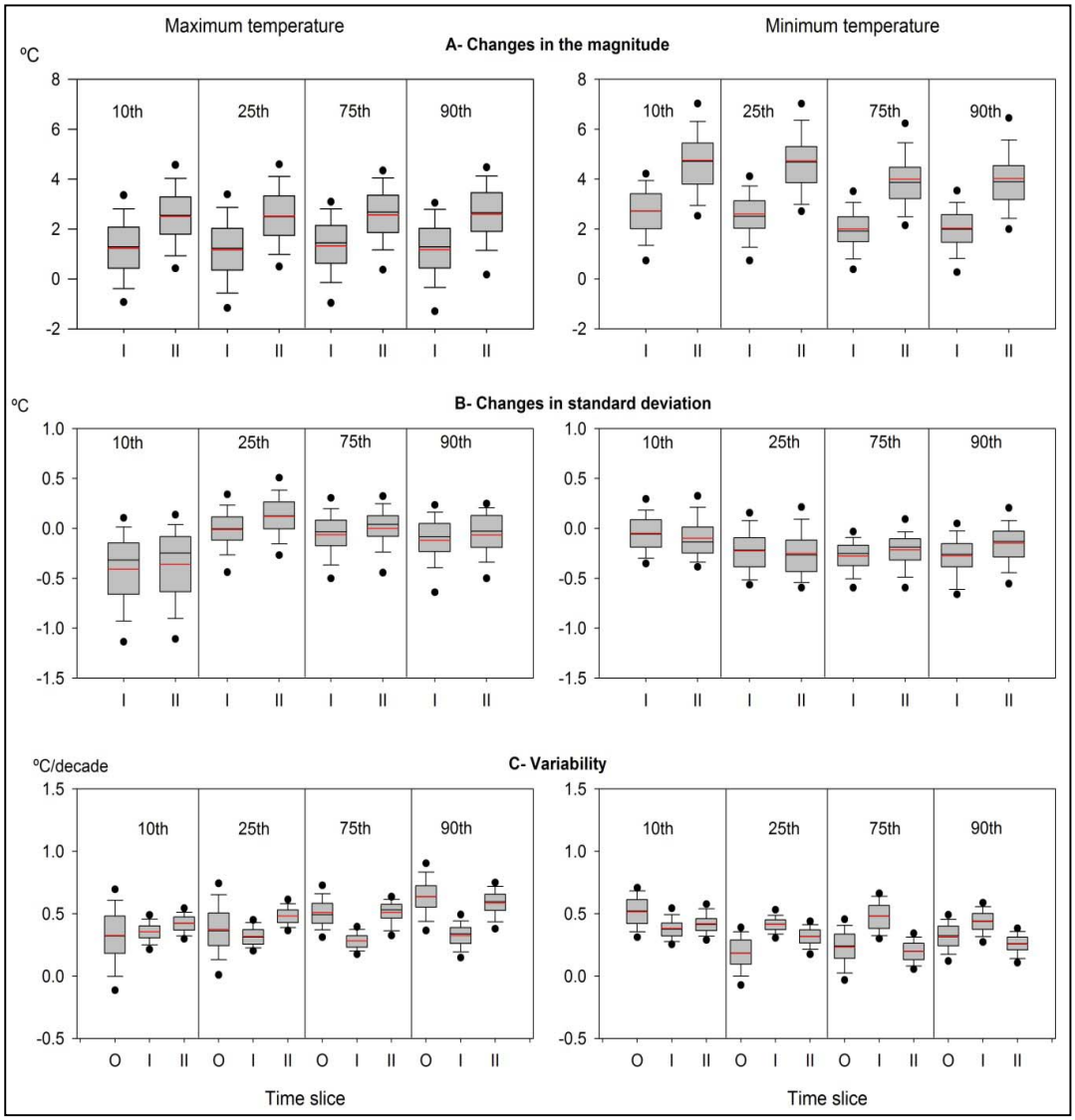

Figure 4.53: Boxplots representing changes in (a) the magnitude (ºC), (b) standard deviation (ºC) and (c) interannual variability (ºC decade^{-1}) of the time-varying percentiles time series during winter (DJF) season for the observed data from 1971 to 2000 (O), the 2021-2050 period (I) and the 2071-2100 period (II). In panels A and B, the results are given as (future-base), so that I indicates (2021-

2050 simulation menus base climate) and II denotes (2071-2100 minus base climate).

Figure 4.53 (panel B) also illustrates changes in the standard deviation of the time-varying percentiles time series over the 21st century. Similar to changes in the standard deviation of the mean temperature, the majority of the maximum (minimum) temperature percentiles showed an increase (decrease) in their standard deviations, compared with the present climate.

For minimum temperature, the decreasing rate was in the range of -0.2 and -0.3ºC for the period 2021-2050 and -0.1 and -0.2ºC from 2071 to 2100. The projected warming in the magnitude and standard deviation of maximum temperature time-varying percentiles could influence the frequency and intensity of daytime warm events, which are more likely to increase during the winter season.

Figure 4.53 (panel C) suggests that most maximum temperature percentiles substantially showed less interannual variability compared with the recent past climate (1971-2000). This was clearly evident from 2021 to 2050, with generally insignificant trends (magnitudes roughly less than 0.3ºC decade^{-1}, $p<0.05$). For the 2071-2100 period, although there was a remarkable increase in the magnitudes of the percentiles compared with the real-world climate, the trends were generally comparable with the observed trends, particularly for those of the warm tail percentiles (i.e., the 75th and 90th). In particular, the findings indicated that linear trends in the 75th and 90th percentiles were, on average, 0.51(0.51) and 0.64(0.58ºC decade^{-1}) for the periods 1971-2000 (2071-2100). This will

undertake more warming during the 2071-2100 time slice compared with the control period. This change is not necessarily related with an increase in the year-to-year variability. The same finding can also be seen for the percentiles of minimum temperature (Figure 4.53, panel C), particularly for the period from 2071 to 2100. This feature can also be better identified when comparing direction (sign) of the trends for the observed (1971-2000) and the simulated (2071-2100) climate. Results on the cross-tabulation analysis employed to explore pairwise relationships between the categorical trends in the minimum temperature 10th percentile during the winter season for the period 1971-2000 against the simulation (2071-2100) are reported in Table 4.10.

Table 4.10: Results of the cross-tabulation analysis applied to trends in the 10th percentile time series for wintertime minima from 2071 to 2100 against the observed trends. The statistical significance was assessed at the 95% level using the Mann-Kendall's Tau test. The numbers indicate the percentage of grids in the ensemble that projected the same sign of changes as the observed temperature.

	+	N+	N-	-
+	2.6	11.9	1.5	0.0
N+	2.2	73.7	8.1	0.0
N-	0.0	0.0	0.0	0.0
-	0.0	0.0	0.0	0.0

As presented, the grids were classified into four main categories, following the results of the trend analysis: statistically significant positive [+, $p<0.05$], statistically significant negative [-, $p<0.05$], statistically insignificant positive [N+, $p>0.05$] and statistically insignificant negative [N-, $p>0.05$]). As presented, regardless of the rapid increase in their percentile magnitudes, 76.3% of the grids in the ensemble projected the same sign as observed. In most cases, this can be explained by the fact that the rapid increase in the magnitude of the percentiles at

the end of the century corresponded to a decrease in the standard deviation of wintertime temperature.

4.5.4.2. Spring season (MAM)

Results on changes in the time-varying percentiles during spring season (MAM) from 1971 to 2100 are summarized in Figure 4.54. A visual inspection reveals two main findings. First, the percentiles steadily showed an increase in their magnitude, indicating that the current warming will continue during the 21st century. In contrast to the winter season, rates of warming were similar for the two comparable periods: 2021-2050 and 2071-2100 for both maximum and minimum temperatures, with negligible differences. In particular, changes in maximum temperature percentiles varied from 0.66 to 3.5ºC during the course of the 21st century, which corresponded to an upward of 1.1 to 3.4ºC for minimum temperature percentiles. One interesting note is that the warming rates of the time-varying percentiles during spring were markedly much higher than those of the mean. A representative example is the 75th and 90th percentiles from 2021 to 2050 which moved towards more extremes, with increases of 1.8 and 1.9ºC, respectively, while mean maximum temperature roughly warmed by 0.6ºC, relative to the observed climate. This finding, together with the strong increase of the standard deviation during spring, implies that high-intensity temperature will get warmer at rates exceeding that of the mean. Second, there were remarkable differences between the interannual variability of the percentiles during the observed and the simulated climate.

While the percentiles of spring season showed strong warming trend from 1971 to 2000, they exhibited less variability during the 21st century, especially for the cold percentiles. Interestingly, the upper percentiles (75th and 90th) of maximum temperature exhibited a downward tendency from 2021 to 2050, at linear rates of -0.23 and -0.32ºC decade^{-1}, respectively. Accordingly, it can again be noted that, in the future, the increase in the magnitude of temperature percentile does not necessarily correspond to more interannual variations.

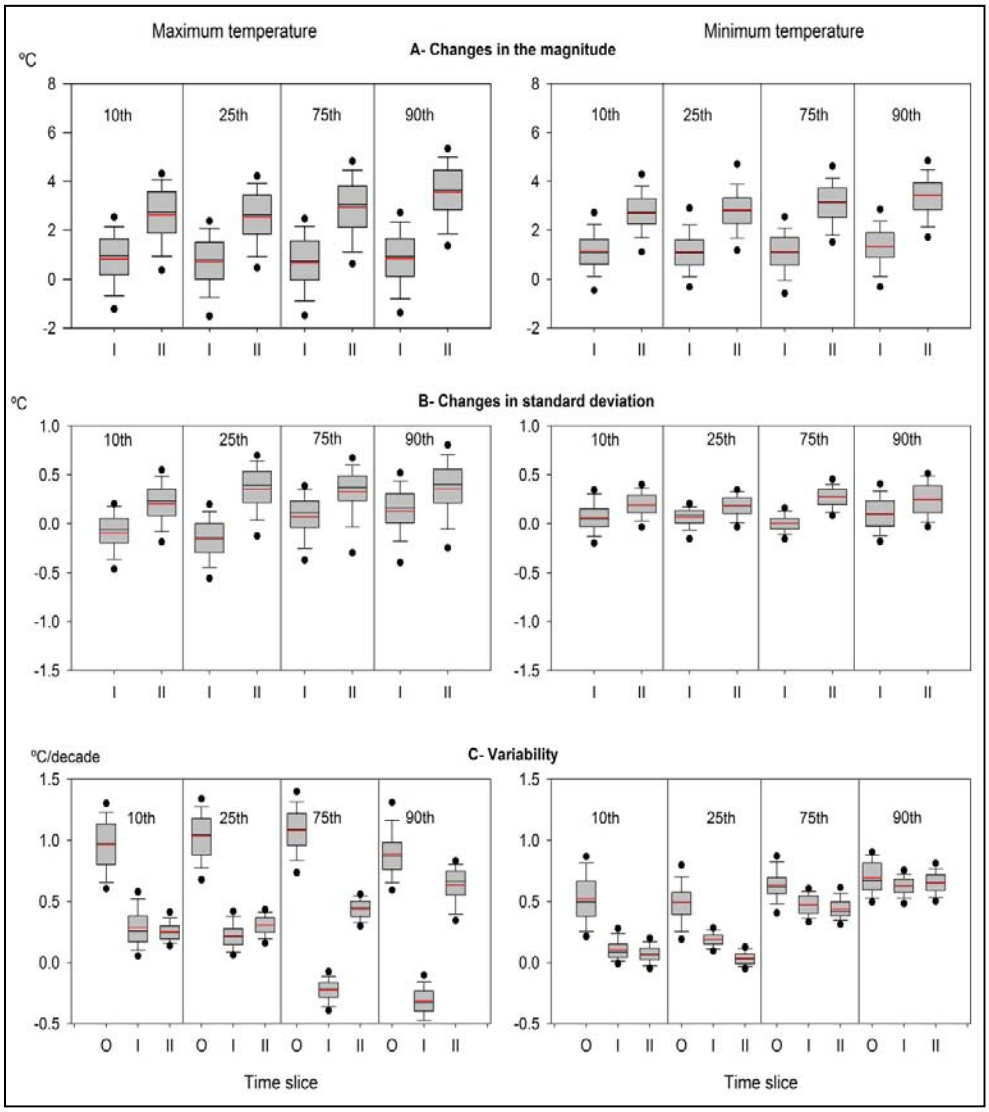

Figure 4.54: Same as Figure 4.53, but for spring.

4.5.4.3. Summer season (JJA)

Changes in the magnitude, standard deviation and interannual variability of the time-varying percentiles during summer season are given in Figure 4.55. Similar to the wintertime, the magnitude of the percentiles exhibited a “systematic” future increase for both maximum and minimum temperatures. Also, changes in the percentiles corresponding to minimum temperature were faster than those of maximum temperature. With regard to the current climate, the magnitudes of the 10th, 25th, 75th and 90th percentiles increased by 1.4, 1.3, 1.8 and 1.8ºC for maximum temperature from 2021 to 2050, while their changes had the order of 2.4, 2, 2.3 and 2.5ºC for minimum temperature, respectively. This picture was markedly reversed at the latter half of the 21st century, as the percentiles of maximum temperature increased faster than those of minimum temperature.

In contrast to wintertime temperature, Figure 4.55 (panel A) informs that changes in the upper percentiles exceeding those of the lower percentiles. One clear example is the change in the 90th percentile from 2071 to 2100, which corresponded to a rise of 5.9 and 5.3ºC for maximum and minimum temperatures, respectively, compared with 4.3 and 4.8ºC for the 10th percentile. Similarly, the time-varying percentiles of summer experienced a clear increase in their standard deviation, relative to the control period, which also came in contrast to the winter season. This has been the case for both maximum and minimum temperatures although the increasing rates were much stronger for the cold tail 10th and 25th percentiles.

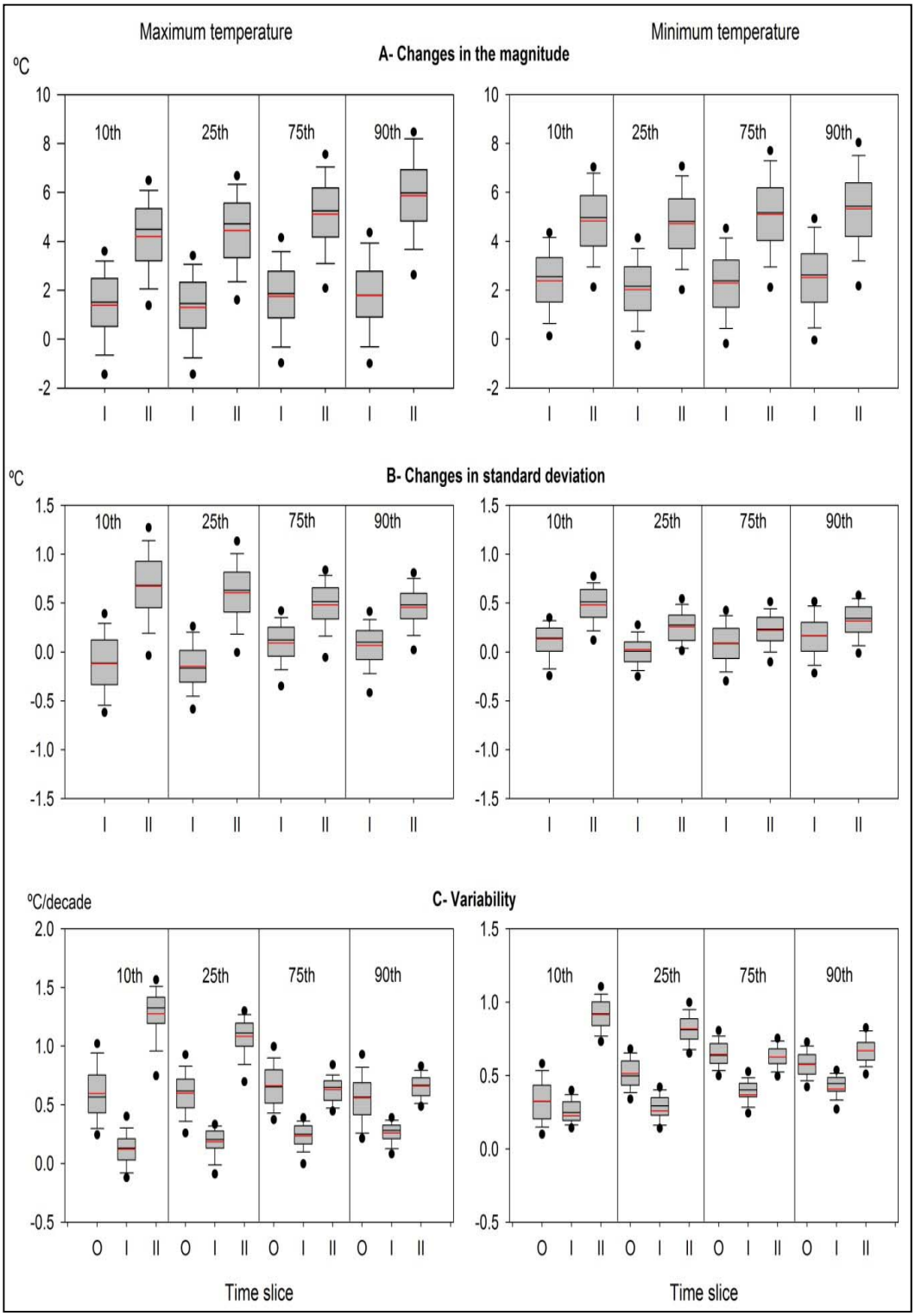

Figure 4.55: Same as Figure 4.53, but for summer.

For the period 2071-2100, the results suggested a rapid increase in the standard deviation of the 10th (0.7ºC) and 25th (0.6ºC) percentiles. In response to the projected increase in the magnitude and standard deviation of the time-varying percentiles, the summer season was expected to exhibit a remarkable increase in the temperature interannual variability over the 21st century. This feature was clearly observed at the late of the century, particularly for the cold tail percentiles (i.e., the 10th and 25th). All the trends were positive and statistically significant (at the 99% level), with magnitudes of change in the range of 0.5-1.7ºC decade^{-1} for the 10th percentile and 0.5-1.4ºC decade^{-1} for the 25th percentile.

4.5.4.4. Autumn season (SON)

Figure 4.56 depicts changes in the magnitude, standard deviation and trends of the time-varying percentiles calculated for autumn maximum and minimum temperatures during the 20th and 21st century. In accordance with other seasons, the results also suggest increase in the magnitude of all percentiles during the 21st century, being more highlighted at the end of the century. Similar to spring season and also in contrast to summer and winter, there were no significant differences between changes in the upper and lower percentiles either for maximum or minimum temperature. On the other hand, while standard deviation of maximum temperature time-varying percentiles showed a markedly rapid warming with respect to the 1971-2000 period, there were no changes in the standard deviation of minimum temperature percentiles. The main modes of variability characterizing autumn time-varying percentiles were the markedly increase (decrease) in the interannual variations of upper (lower) percentiles of maximum (minimum) temperature.

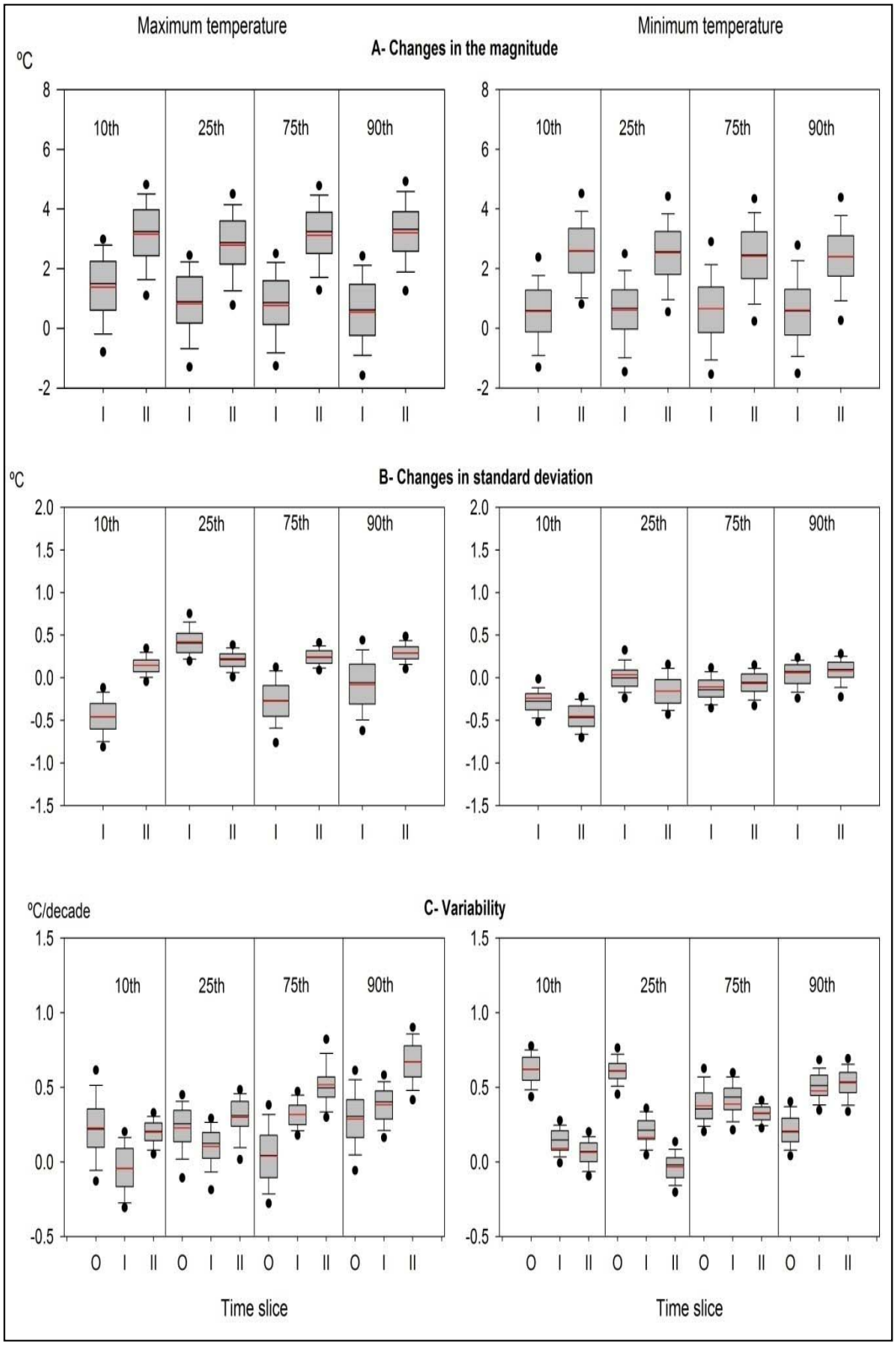

Figure 4.56: Same as Figure 4.53, but for autumn.

4.5.5. Future changes in extreme events

Figure 4.57 shows changes in the 99th percentile magnitude over the periods (2021-2050) and (2071-2100) as compared to the control period (1971-2000). Under the A1B emission scenario, all models agree that the 99th percentile magnitude will be reduced by an average of -1.6ºC and -1ºC following the KNMI and MPI simulations during the period 2021-2050 respectively. Nonetheless, Figure 4.57 also depicts clear spatial differences as grid points along the Mediterranean coast and across the Ebro valley exhibited positive differences in the 99th percentile values (nearly by 2-3ºC), suggesting warmer conditions than the observed climate. Interestingly, other regions demonstrated a decrease in the magnitude of the 99th percentile. Interestingly, this spatial structure was reflected by both the MPI and KNMI models. Although these extremely severe warm events are characterized by high natural variability, the similarity between the models in terms of the magnitude, sign and spatial variability of simulated changes confirms the skill of these models in responding a similar parameterization scheme.

During the period 2071-2100, this magnitude will markedly be more intensified, with an average increase of 3 and 4.2ºC for the KNMI and MPI ensembles, respectively. These substantial projected increases in the 99th percentile temperature magnitudes strongly indicate that more heat stress could dramatically be intensified across the region during the last decades of this century, which could have considerable impacts on different disciplines in the study domain, such as hydrology, agriculture, water resources management, forestry, and human health in .

From the spatial perspective, the regional differences among the models from 2071 to 2100 showed similar patterns. The distribution of the 99th percentile changes seemed to be elevation dependent, with rapid increase at lowest elevations (e.g., the Mediterranean coasts and the Ebro valley) and weak warming at high elevation sites to the west (i.e., the Cantabrian system) and southwest (i.e., the Iberian system).

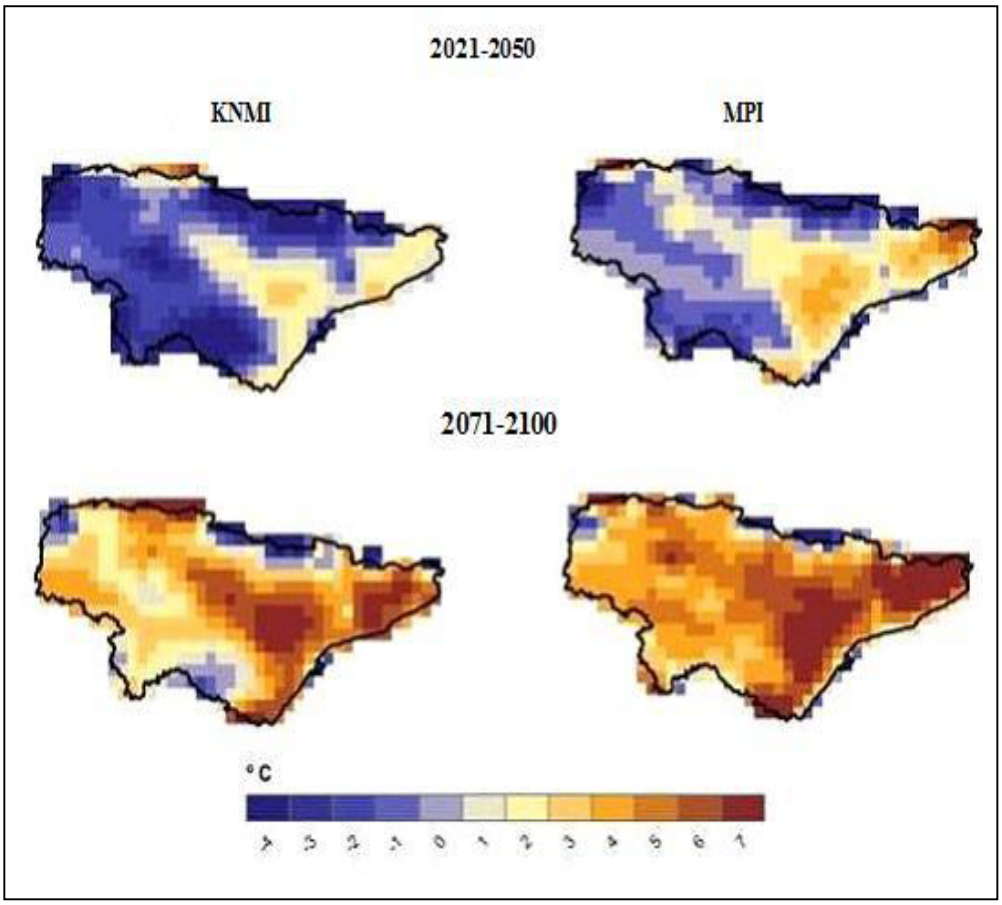

Figure 4.57: Change (prediction minus current climate) in the magnitude of the 99th percentile daily maximum air temperature during summer.

Figure 4.58 depicts changes in summer frequency of VWD during the periods 2021-2050 and 2071-2100, as compared with the control integration. As illustrated in the upper panel, a generalized decreasing in the number of VWD is

detected for the near future (2021-2050). This cooling of VWD was more pronounced along the Cantabrian, the Mediterranean and at elevated sites in the west, whereas it was less evident in lowlands and inland. A similar pattern was also observable during the period 2071-2100 (lower panel), but with rapid increase in the frequency of VWD near the coast, while there was a relatively weaker warming in continental areas.

Simulated changes in the magnitude of the 1st percentile of wintertime minimum temperature, calculated as difference between this magnitude for the 30 yr minimum temperatures in baseline (1971-2000) and future scenario periods (2021-2050) and (2071-2100) are presented in Figure 4.59. Analogous to the expected warmer climate in future, changes in the 1st percentile magnitude tended to increase gradually over the two time slices: 2021-2050 and 2071-2100 under the A1B emission scenario. This result suggests that the VCN will become substantially less severe in future as the cold tail of daily minimum temperature shifts toward warmer conditions. However, this increase slightly occurred over 2021-2050 with an average of 0.16, 0.29 and 0.43ºC for the ICTP, KNMI and METO ensembles, respectively. Contrarily, the projected warming of the 1st percentile will sharply be larger over the last three decades of the 21th century, with an average of 1.94, 2.4 and 3.3ºC for the ICTP, KNMI and METO ensembles, respectively. For the two time slices under investigation, spatial variations in the magnitude of the 1st percentile appeared robust and similar between models, with more warming in the west and close to the Cantabrian Sea and less increase and, even a decrease, in the eastern parts and over the northern Pyrenees.

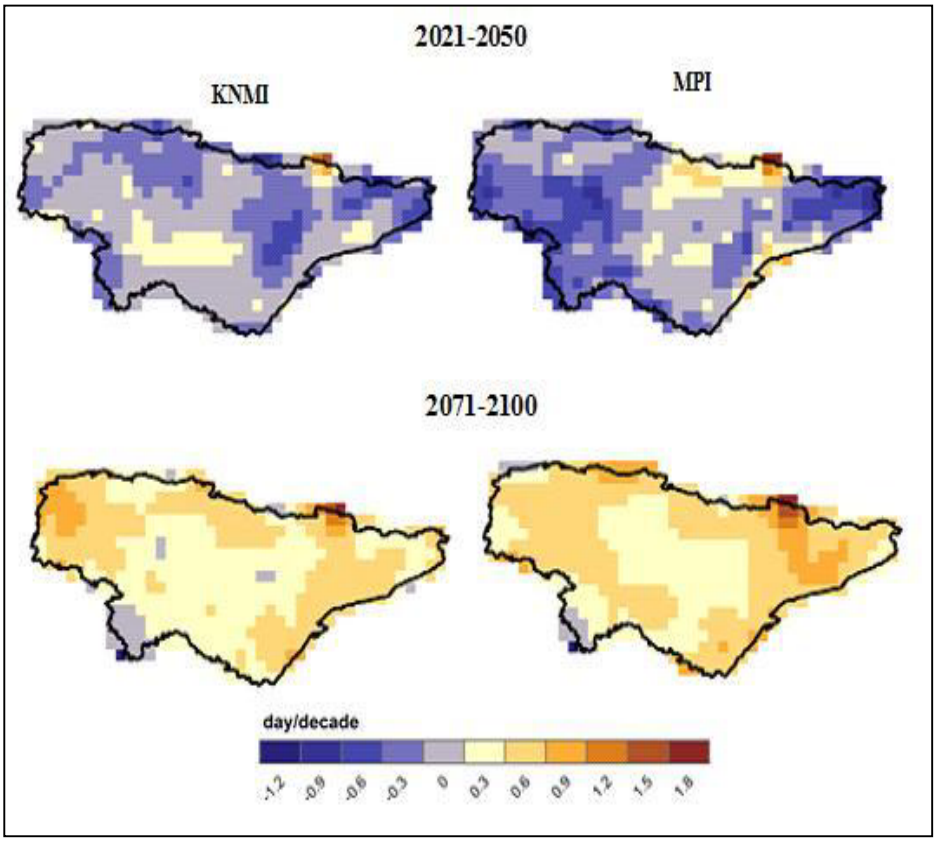

Figure 4.58: Same as Figure 4.57, but for changes in the number of days per each summer in which the maximum temperature exceeded the 99th percentile of summertime daily distributions.

Changes in the frequency of VCN are given in Figure 4.60. The observed changes fitted well with spatial changes in the magnitude of the 1st percentile. Given that the last period of this century will be warmer than the near future decades, a less frequent and intense VCN will be expected by the end of the century. The results suggest that the most elevated sites to the west will exhibit less severe cold conditions in the two simulated periods than eastern portions, particularly those close to the Mediterranean Sea.

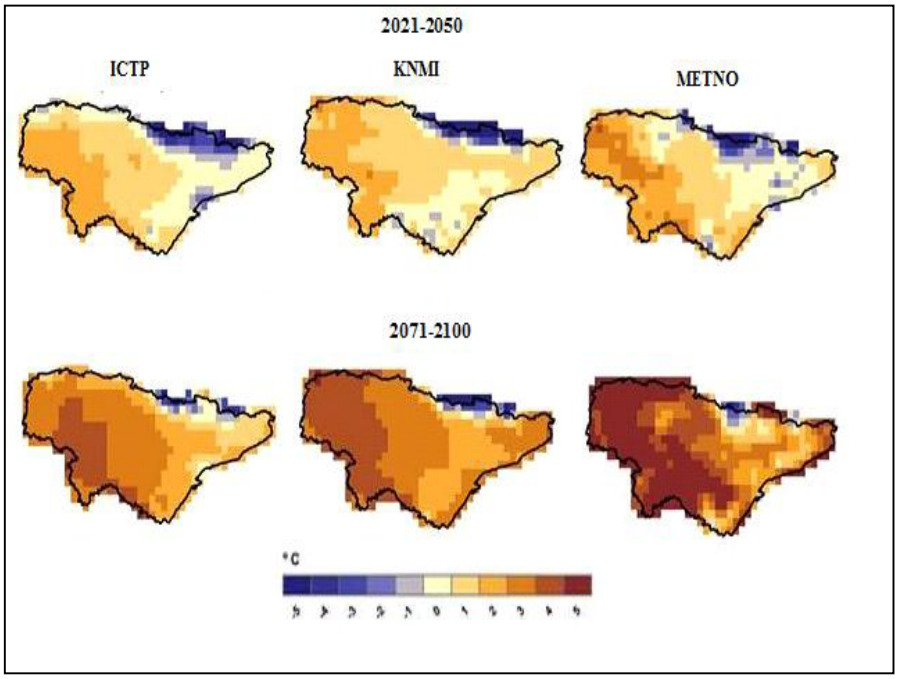

Figure 4.59: Changes in the magnitude of the 1st percentile daily minimum air temperature during winter.

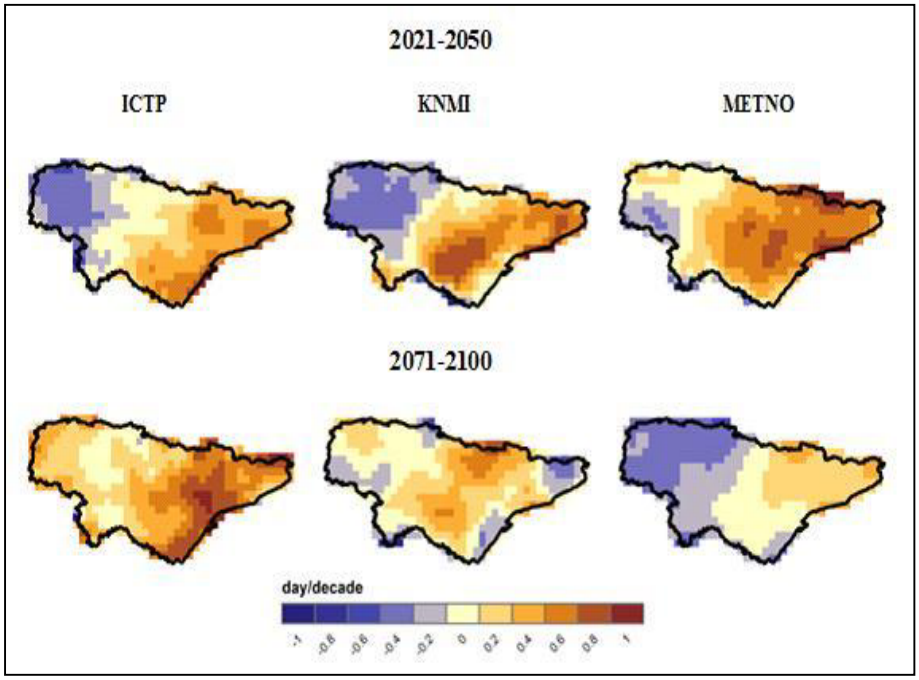

Figure 4.60: Same as Figure 4.59, but for changes in the frequency of VCN during winter.

4.5.6. The dependency between changes in the mean temperature and changes in the corresponding time-varying percentiles

Conventionally, changes in the warm and cold tails of temperature distribution are as interesting as changes in the mean, particularly for regional climate impact and assessment studies. It is therefore important to identify whether changes in the upper and lower percentiles of temperature distribution may already be detectable and consistent with changes in the mean conditions. In the following section, the results on this dependency for both the present and future climates are presented. As expected, higher correlation suggests a consistency among changes in the mean and the corresponding time-varying percentiles in the magnitude and/or the sign (direction) of changes. Conversely, lower correlation can be seen as an indicator of disagreement.

Figure 4.61 presents correlation coefficients between changes in the mean maximum temperature and changes in the time-varying percentiles on a seasonal basis. Both fields (i.e., maximum temperature and percentiles values) were calculated at each grid box. The association was then assessed for both the observed (1971-2000) and the future simulations (2021-2050 and 2071-2100). As illustrated in Figure 4.61, the simulated changes in the warm tail (i.e., the 75th and 90th percentiles) of winter maximum temperature during the last decades of the 21st century remarkably correlated well with changes in the mean maximum temperature. The Pearson correlation coefficients were approximately close to 0.8. Conversely, the relationship was generally weaker for the cold tail percentiles (i.e., 10th and 25th percentiles), with correlation magnitudes roughly below 0.3. a similar dependency was also evident during the period 2021-2050.

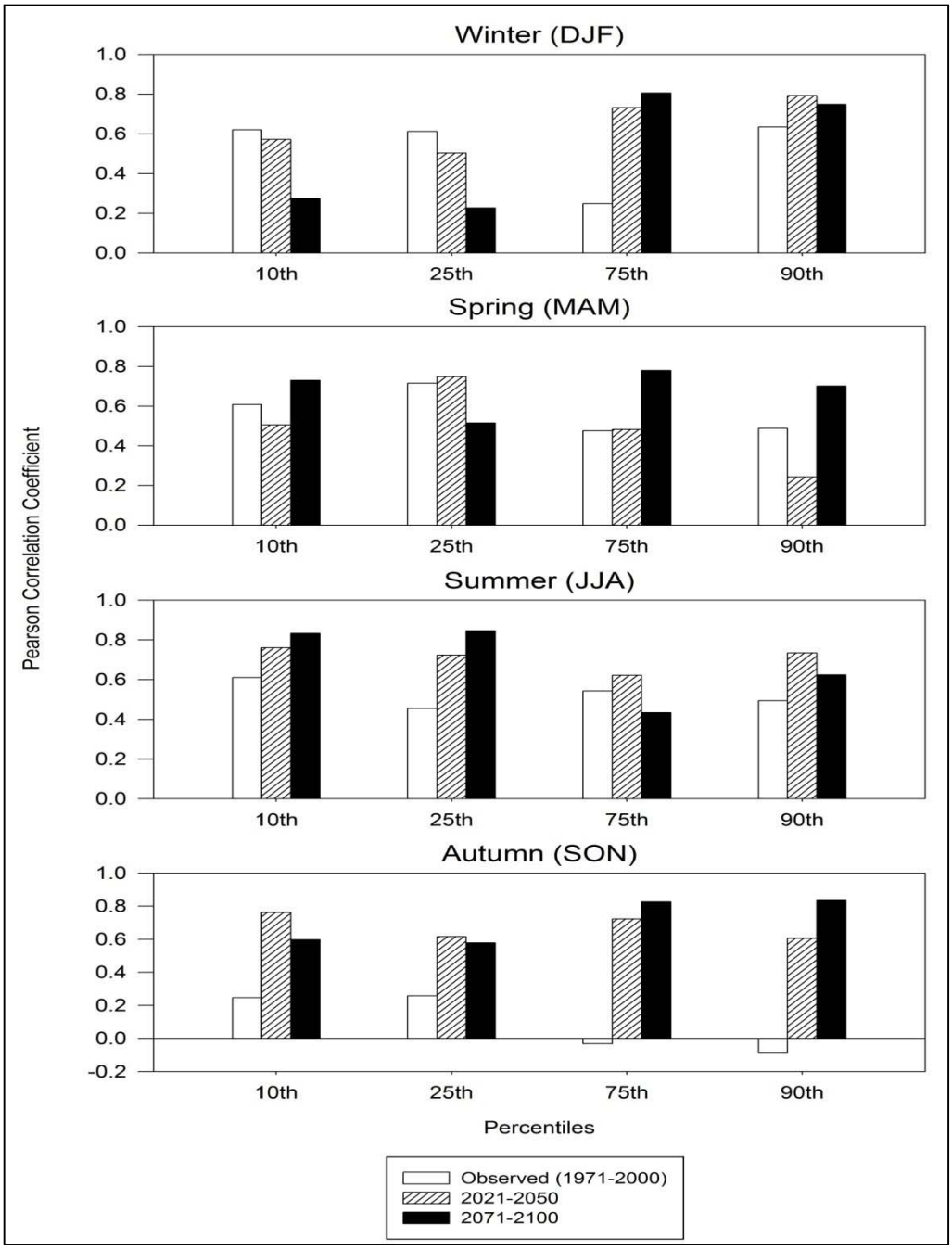

Figure 4.61: Pearson correlation coefficient (*r*) between changes in the seasonal mean maximum temperature time series and changes in the seasonal time-varying percentiles series calculated for maximum temperature during the control period and the 2021-2050 and 2071-2100 time slices. The calculation was computed for changes in each pixel in the study domain.

However, it differed for the observed data (1971-2000), as changes in the percentiles of the cold tail of maximum temperature distribution were generally higher than those of the upper tail percentiles. Recalling the strong positive anomaly of the projected wintertime maximum temperature during the 21st century, the10th and the 25th percentiles poorly followed changes in the mean temperature. This provides strong evidence that changes in winter maximum temperature in the future will not only be driven by changes in the mean temperature, but they will also be influenced by a shift in the entire temperature distribution. This finding must also be seen in the context that winter was the only season that experienced a decrease in the standard deviation during the 21st century.

Moving to the summer season, the projected changes in the mean maximum temperature were more consistent with changes in the percentiles of the lower than the upper tail temperature distribution. This feature comes in direct contrast to winter season. As presented, the correlation coefficient reached 0.83 and 0.85 for the 10th and 25th percentiles, which were reduced to 0.43 and 0.62 for the 75th and 90th percentiles, respectively. The positive anomaly of standard deviation during summer season can possibly explain these findings, giving more influence to changes of the mean (standard deviation) on the cold (warm) tail of temperature distribution. For the upper percentiles, the strong positive anomaly of both the mean and standard deviation implies an overall decrease in the left hand side of the temperature distribution (cooler and milder low temperatures), while the right-hand side (high temperatures) skews positively.

Figure 4.61 also shows that, for spring and autumn, there was similar dependency between changes in the mean maximum temperature and changes in their corresponding percentiles, with weaker (stronger) influence on changes in the cold (warm) tails of temperature distributions. This feature was clearly reversed for the observed and the 2021-2050 simulated climates, particularly for spring. Exceptionally, changes in the autumn mean maximum temperature were not consistent with change in their corresponding time-varying percentiles over the control period. This association was generally weak (*r* lower than 0.2) and even negative for the upper tail percentiles. This indicates that some changes in the warm tail of maximum temperature distribution might exceed the raise of the mean values during autumn.

Figure 4.62 summarizes the dependency between changes in the mean minimum temperature and their corresponding time-varying percentiles from 1971 to 2100. The results give a strong indication on the increase in the variability of warm tails of minimum temperature during winters and summers at the last decades of the 21st century. As presented, it seems that changes in the 90th percentile time series of winter and summer minimum temperatures correlated well with changes in the mean, with Pearson correlation coefficients of 0.82 and 0.76, respectively. The strength of this relationship became weaker for the cold tail percentiles, particularly during summer. The correlation between changes in the summer minimum temperature and the corresponding 10th (25th) percentiles was only 0.52 (0.46). This indicates that, for minimum temperature, there was a rapid increase in the high-intensity and warm temperature extremes relative to cooler temperature events.

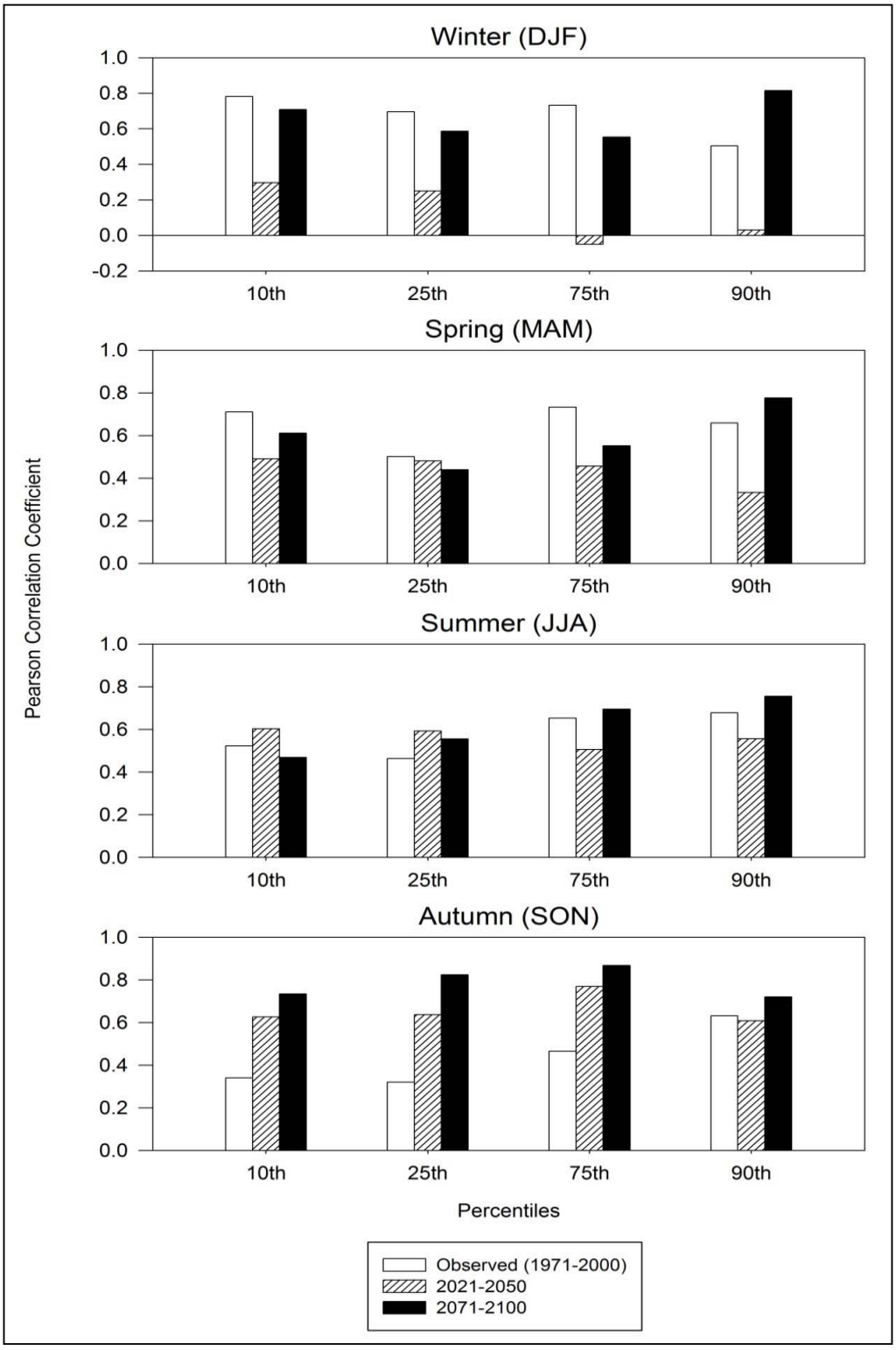

Figure 4.62: Same as Figure 4.61, but for mean minimum temperature.

For winter, Figure 4.62 suggests that the interannual variability of the 75th and 90th time series of minimum temperature from 2021 to 2050 can be expected to decrease as the mean winter gets warmer. This clearly implies that an increase in wintertime minimum temperature corresponds to a decrease in the variability of the 75th and 90th time over the period 2021-2050.

For summer season, a comparison of Figures 5.61 and 5.62 indicates that the 10th and 25th percentile correlated weaker for minimum temperature than for maximum temperature, while the correlation of the 75th and 90th increased more with minimum temperature than with maximum temperature. This gives indication that extreme events corresponding to warmer minimum temperature would increase more rapid than those of maximum temperatures. Contrarily, changes in the 10th percentile of winter minimum temperature were more consistent with changes in the mean, while it poorly responded to changes in the mean for the 10th percentile of maximum temperature. Moving to spring season, it can be seen that changes in upper tail of the minimum temperature distribution tended to be significantly driven by changes in the mean, with more shift toward warmer values by the end of the century. This feature remarkably agrees well with the pattern detected for the observed temperature.

In contrast to other seasons, the warm percentiles of minimum temperature in autumn show a slight negative correlation with the mean trends over the study domain from 2021 to 2050. This association was statistically insignificant ($p<0.05$), with r values of -0.03 and -0.05 for the 75th and 90th percentiles, respectively. Also, it seems that the relationship between changes in autumn

minimum temperature and changes in the warm tail of daily minimum temperature was markedly much stronger than changes in the cold tail. In general, this relationship was found consistent over the 20th and 21st century.

4.5.7. The dependency between changes in the mean temperature and the frequency of extreme events

This research also looked at changes in the relationship between the mean (hereafter: M) temperature and standard deviation (hereafter: S) in the one hand and the frequency (hereafter: F) of extreme events on the other hand. This was mainly to explore whether changes in the frequency of anomalously severe heat events (i.e., VCN and VWD) over the study domain are more linked to changes in the occurrence of these days (as revealed by changes in the standard deviation) and/or to changes in the intensity (as revealed by changes in the mean) of temperature during these days.

For each grid, the association between the frequency of these days (F+/F-) and changes in (i) the mean (M+/M-) (ii) standard deviation (S+/S-) and (iii) combined effects of changes in the mean and standard deviation (e.g., M+/S+, M+/S-, M-/S-, M+/S-) were examined for each ensemble. For instance, this assessment helps exploring whether an increase in the mean (M+) and/or the standard deviation (S+) could induce an increase in the frequency (F+) of these extreme events. The results are summarized in Figure 4.63. The findings suggested that intense severe warm events during the period 2071-2100 can be explained by the combined effect of positive changes in both the standard deviation and the mean of summer maximum temperature.

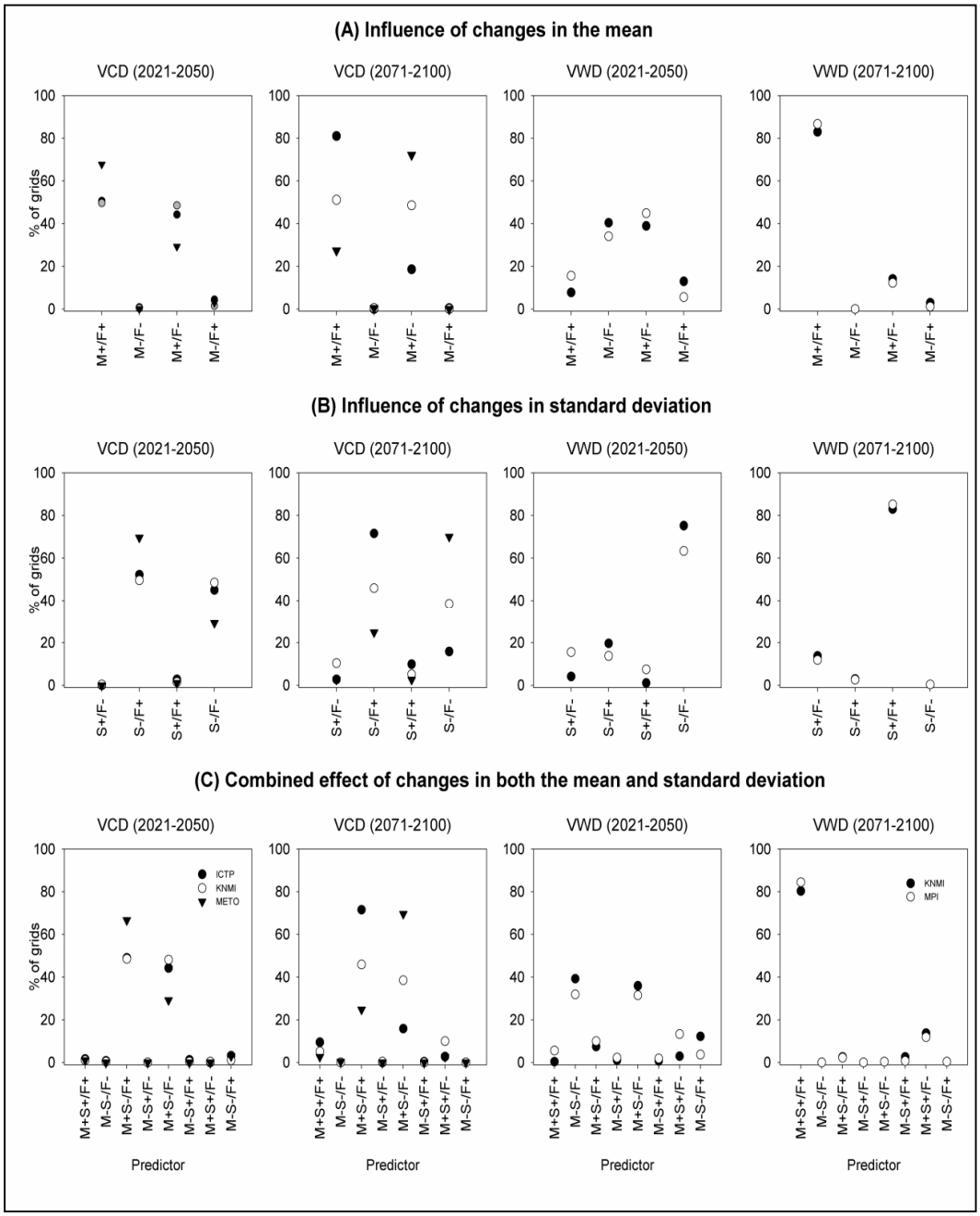

Figure 4.63: Relationships between simulated changes in the frequency of extreme events (labeled as F+ for increase in the occurrence and F- for the decrease) and changes (i.e., increase [+] vs. a decrease [-]) in the mean (M) and/or the standard deviation (S).

The positive change in the mean (M+) was spatially consistent with the increase in the occurrence (frequency) of warm events (F+) in more than 80% of the grids across the study area. The same finding was observed for S+ with F+ and also for M+S+ with F+. However, this effect was markedly minimized during the 2021-2050 period, with less frequent VWD, due to the weak change in the standard deviation of summer maximum temperature.

The results also suggest that the decrease in the standard deviation had more influence on VWD when compared with the impact of the decrease in the mean. For VCN, on the other hand, this dependency was more stable with a steady decrease in the standard deviation in both time slices (2021-2050) and (2071-2100) and an increase in the minimum mean temperature in spite of its slow rates in the first decades of the 21st century. Accordingly, it can be demonstrated that the shift toward higher minimum temperatures in the next decades cannot be the solely factor responsible for the observed decrease in the frequency of very cold nights across the study domain.

CHAPTER FIVE

DISCUSSION

5. DISCUSSION

5.1. Observed changes in seasonal temperature means

5.1.1. Temperature long-term trends (1920-2006)

The results concerning the observed trend in the mean temperature from 1920 to 2006 reveal that the study domain exhibited an increase during the 20th century. This warming was much more pronounced during the last few decades, with the largest increase occurred during summer and spring periods. The observed trend in temperature from 1920 to 2006 has notably been consistent with earlier findings in the Iberian Peninsula (e.g., Quereda et al., 2000), the Mediterranean (e.g., Brunetti et al., 2006) and Europe (e.g., Parry, 2000). For instance, according to the present work, the annual mean temperature increased at a rate of 0.96ºC from 1920 to 2006. In the Mediterranean region, Parry (2000), for example, reported that the annual mean temperature over Europe has risen at a rate of 0.80ºC over the 20th century. Similarly, Brunetti et al. (2006) recorded an increase of 1ºC in the Italian mean temperature during the last century. Over the Iberian Peninsula, Quereda et al. (2000) noted that the annual mean temperature in the Spanish Mediterranean region has increased at a rate of 0.71ºC in the last century. Similarly, over the period from 1920 to 2006, the study domain experienced an increasing trend of 0.7ºC in the mean maximum temperature, which has also been analogous to the finding of Karl et al. (1993) and Easterling et al. (1997) for the globe (0.82ºC/century). Nonetheless, although the annual minimum temperature showed stronger rise (1.22ºC) from 1920 to 2006, compared with both maximum and mean temperature, this trend is still lower than the global trend reported by Easterling et al. (1997) (1.79ºC/century).

This work also indicates that the temporal evolution of temperature over the study domain showed a remarkable interdecadal variability for all analyzed thermal variables (i.e., maximum, minimum and mean temperatures), with main departure toward cooling during the 1920s, 1930s and 1960s. Contrarily, temperature exhibited a general positive anomaly during the 1940s, 1970s, 1980s, 1990s and 2000s. This interdecadal variations of seasonal temperature generally fit well with other regional and global studies (e.g., Tett et al., 1999; Rodriguez-Puebla et al., 2001a). Notably, there has been a clear tendency toward warming at both the annual and seasonal timescales since the mid of the 1970s. This general behavior also agrees well with numerous previous regional (e.g., Labajo et al., 1998; Brunet et al., 2002; Esteban-Parra et al., 2003; Morales et al., 2005; Brunet et al., 2007a) and global studies (e.g., Parker et al., 1994; Tett et al., 1999; Jones and Moberg, 2003; Luterbacher et al., 2004). According to Brunet et al. (2002), a clear warming has been mainly registered over the peninsular Spain in two periods: during the 1940s and from the mid-1970s onwards. Other regional studies (e.g., Labajo et al., 1998; Morales et al., 2005) also reported a remarkable change in the behavior of the annual maximum, minimum, and mean temperatures after the year 1972. In accordance with the IPCC (2007), the unusual warmest years over the whole period (1920-2006) were restricted to the past two decades. Over this period, the study area also witnessed anomalous warming temperatures in 1990, 1997, 1998, 2003, and 2006.

Herein, it is also worthwhile to indicate that the network covering the period 1920-2006 was not dense enough, as being represented only by a sample of 19 observatories. Nonetheless, the final conclusion on the observed trends can still be seen with high level of confidence. The derived results seem to clearly delineate similar temporal

patterns to those observed for Iberia, Europe and the globe. In addition, given that the observatories employed in this study are not only located in rural sites and small towns, but also include urban cities, the "global" warming observed in much of the study domain implies that this trend is a consequence of natural variability reflecting global warming conditions. This sounds interesting since it confirms the assumption that the observed temperature variations in the region are only due to climatic processes rather than other non-climatic factors such as urbanization or industrialization. Also, given that the long-term changes of temperature are not well captured in many studies over Europe in general and in the Iberian Peninsula in particular due to lack of reliable data in the early decades of the past century, these results can considerably contribute to improving the current knowledge on long-term temperature variability and change within a larger spatial context, including the Iberian Peninsula, the Mediterranean and the Western Europe.

5.1.2. Observed seasonal and annual temperature trends (1960-2006)

5.1.2.1. Maximum temperature

The linear trend analysis of maximum temperature suggests a warming trend in all seasons. The strongest signal occurred during summer and spring. The only exception is seen in autumn since 43% of observatories exhibited a negative tendency at the 95% level. This finding is of special interest given that earlier studies (e.g., Houghton et al., 2001; Klein Tank et al. 2005; Martinez et al., 2010) also reported a downward trend in autumn temperature in Spain and wide regions across Europe, being the sole exception among all seasons. For example, Martinez et al. (2010) reported a generalized decreasing in autumn maximum temperature in Catalonia (NE Spain).

In general, there is a conclusive evidence on the increase in maximum temperature in NE Spain, which is comparable to previous works in the Iberian Peninsula (e.g., Quereda et al., 2000; Esteban-Parra et al., 2003; Morales et al., 2005; Miro et al., 2006; Rodriguez-Puebla et al., 2010; Martinez et al. 2010), the Mediterranean (e.g., Maheras and Kutiel, 1999; Brunetti et al., 2000, 2006) and Europe (e.g., Jones et al., 1999a). For instance, Martinez et al. (2010) indicated a general warming trend in the annual maximum temperature in Catalonia (NE Spain) with a value of 0.5ºC decade^{-1}, the greatest increase occurred during summer and spring.

Spatially, it is noted that the largest warming occurred in coastal areas along the Mediterranean and the Cantabrian Seas, whereas mainland observatories experienced less warming. However, this general picture still has some seasonal differences. An interesting aspect is the dominance of a statistically insignificant pattern of trends in the Ebro basin during autumn. A possible explanation of this pattern is probably linked to the location of this semi-closed basin between the Pyrenees northward, the Catalan system to the east and the Iberian system to the south and southwest. This feature is favorable for below-normal temperature as a consequence of the frequent occurrence of fog, particularly during wind-calm days corresponding to anticyclonic conditions.

Also, during summer and spring seasons, there is a noticeable south-north gradient of warming, with the strongest warming in southern part of the study domain. This feature can largely be attributed to the strong advection of warm and dry air masses from the Sahara during these periods of the year. Another important spatial feature is that the spatial distribution of the trends in annual temperature seems to be spatially more consistent with the distribution of trends in summer and spring than in winter and

autumn. This result has recently been confirmed in other global (e.g., Jones and Moberg, 2003) and regional studies (e.g., Morales et al., 2005; Brunet et al., 2006; Abarca Rio and Mestre, 2006). For instance, in their study on the region of Castilla-Leon (northern Spain), Morales et al. (2005) observed that maximum temperature showed more increase in summer and spring compared with winter and autumn, particularly since the 1970s.

5.1.2.2. Minimum temperature

Similar to maximum temperature, the strongest warming in minimum temperature occurred during summer and spring, whereas autumn exhibited little warming. This observable tendency toward warming is compatible with a number of works over the Iberian Peninsula such as Rodriguez-Puebla et al. (2010) who noted an upward trend of 0.20ºC decade^{-1} in the annual minimum temperature over the Iberian Peninsula. This amount of change closely matches the warming rate in the study area (0.21ºC decade^{-1}).

5.1.2.3. Mean temperature

The trend analysis results inform that majority (93%) of observatories exhibited statistically significant trends during summer and spring ($p<0.05$). Contrarily, 46.1 (15.6%) of observatories did show insignificant trend during autumn (winter). Similar temporal features have already been identified in previous works (e.g., Hulme and Sheard, 1999; Esteban-Parra et al., 2003; Pausas, 2004; Scherrer et al., 2006). For example, Hulme and Sheard (1999) found the highest (lowest) warming in the Iberian mean temperature during summer (winter). Similarly, Pausas (2004) reported a clear upward increase in the annual and summer mean temperature in the Mediterranean region of the Iberian Peninsula over the period 1950-2000. More recently, Capilla

(2008) observed an upward increase in the annual mean temperature in Valencia, largely occurred during spring and summer. Over a larger spatial extent, Scherrer et al. (2006) confirmed the same finding in Europe, indicating a remarkable warming trend in mean temperature anomaly between 1961 and 1990. The strongest signal occurred during summer, whereas there was no trend in autumn. Also, based on the gridded data of New et al. (2000), Jacobeit et al. (2003) found a distinct summer warming for the 1969-1998 period over the Mediterranean.

The mean temperature trends in the study domain seem to have a spatial component, with clear coastal-continental contrasts. Nonetheless, this observational spatial structure comes in direct contrast to the simulated data as revealed by different regional climate models (RCMs). One representative example is López-Moreno et al. (2008b) who projected strongest warming in the inland observatories rather than in coastal localities. Based on the simulations of a set of global climate models (GCMs), the IPCC (2007) also documented less warming near the coasts compared to continental areas. These contradicting features sound interesting from the scientific point of view indicating that further contribution of these variations is still possible to explain forces beyond these differences.

5.1.2.4. Diurnal temperature range (DTR)

Assessment of seasonal changes in DTR over the study area suggests three seasons with positive trend: summer, winter, and spring. This can simply be explained by the rapid increase in maximum temperature than in minimum temperature. Contrarily, autumn was the only season with a decreasing trend in much of the region. This simply corresponded to a rapid increase in autumn minimum temperature (0.19ºC

decade^{-1}) than in maximum temperature (0.07ºC decade^{-1}). Studies on some regions in the Iberian Peninsula: including the central Ebro valley (Abaurrea et al., 2001), northeastern Spain (Brunet el al., 2001), mainland Spain (Folland et al., 2001), southern Spain (Morales et al., 2005), and the whole Spain (Brunet et al., 2005, 2006) have revealed positive DTR due to larger increase in maximum temperature than in minimum temperature. The same finding has also been confirmed elsewhere in the world: e.g. Italy (Brunetti et al., 2006) South Korea (Jung et al., 2002), India (Rupa Kumar et al., 1994), South Africa (Kruger and Shongwe, 2004), eastern Canada (Easterling et al., 1997) and the British Isles (Horton, 1995). For instance, Brunetti et al. (2006) noted a higher increase in the Italian maximum temperature than in minimum temperature throughout the last five decades of the 20th century. At the global scale, Vose et al. (2005) confirmed the same finding during the period 1979-2004. Nonetheless, it is noteworthy indicating that the observed positive trend in DTR during winter and spring does not fit also well with other regional (e.g., Esteban-Parra et al., 1995, 2003; Staudt, 2004; Staudt et al., 2005) and global studies (e.g., Karl et al., 1993; Dai et al., 1997). According to the IPCC (2007), minimum temperatures increased at nearly twice the rate of maximum temperatures in the globe during the second half of the 20th century. One possible reason for these divergent trends is that the overall conclusions on DTR variability may differ considerably according to the period of study. For example, considering longer time interval (1920-2006) in this research did show consistent results with those given in Karl et al. (1993) and Dai et al. (1997). This is simply a consequence of the asystematic behavior of minimum and maximum temperatures. In the study domain, maximum temperature remained constant or has increased slightly in the pre-1970s, whereas it has abruptly exhibited warmer conditions than minimum temperature in the more recent decades, especially

since 1980. The evidence on a divergent behavior of DTR stresses the need of caution given that they may differ markedly according to the period of study under consideration. Also, this study indicates that the DTR results at the annual scale vary considerably from those obtained at the seasonal scale. It is therefore believed that further research is still demanded to explain in depth the interdependency between DTR and precipitation or cloudiness variability at different temporal scales. This investigation can give insights into the dependency between precipitation at a seasonal scale, as a main driver of DTR evolution, and DTR variability. This relationship has already been discussed in detail in previous works (e.g., Jones, 1991; Lough, 1997; Power et al., 1998).

The results of this thesis confirm that the observable warming during the 20st century is mainly attributed to the rapid increase during the last three decades. The warming for the 1920-1959 period was less extreme than that in 1960-2006. For example, the warming rate of the annual mean temperature from 1960 to 2006 was doubled relative to the period 1920-1959. Over the Iberian Peninsula, this finding has been compatible with Brunet et al. (2005) who noted that the Spanish mean temperature from 1973 onwards has increased five times larger than the period from 1850 to 1973. Interestingly, spring mean temperature revealed a strong upward trend from 1960 to 2006 (0.66ºC decade^{-1}). Abaurrea et al. (2001) also observed a very strong warming in springtime temperature in the central Ebro valley from 1975 to 1997 (1.43ºC decade^{-1}). Over Europe, Xoplaki et al. (2005) also recorded the strongest signal in spring temperature during the last half millennium in the period from 1975 to 2004. This very strong signal implies critical implications on hydrology and water resources management in the region, as a consequence of the early snow cover melting,

particularly at the headwaters of the main hydrological divisions in the study area (López-Moreno and Garcia-Ruiz, 2004). According to Batalla et al., (2004), the rivers originating in the Pyrenees contribute to nearly 72% of the Ebro discharge, which is the largest in the peninsula (Figure 5.1). The Pyrenean Rivers have their maximum flow during spring because their flow regime is related more to snow melting rather than to rainfall. Therefore, their streamflow is very sensitive to the timing of snow melting which can be largely influenced by spring warming, particularly at the onset of the season.

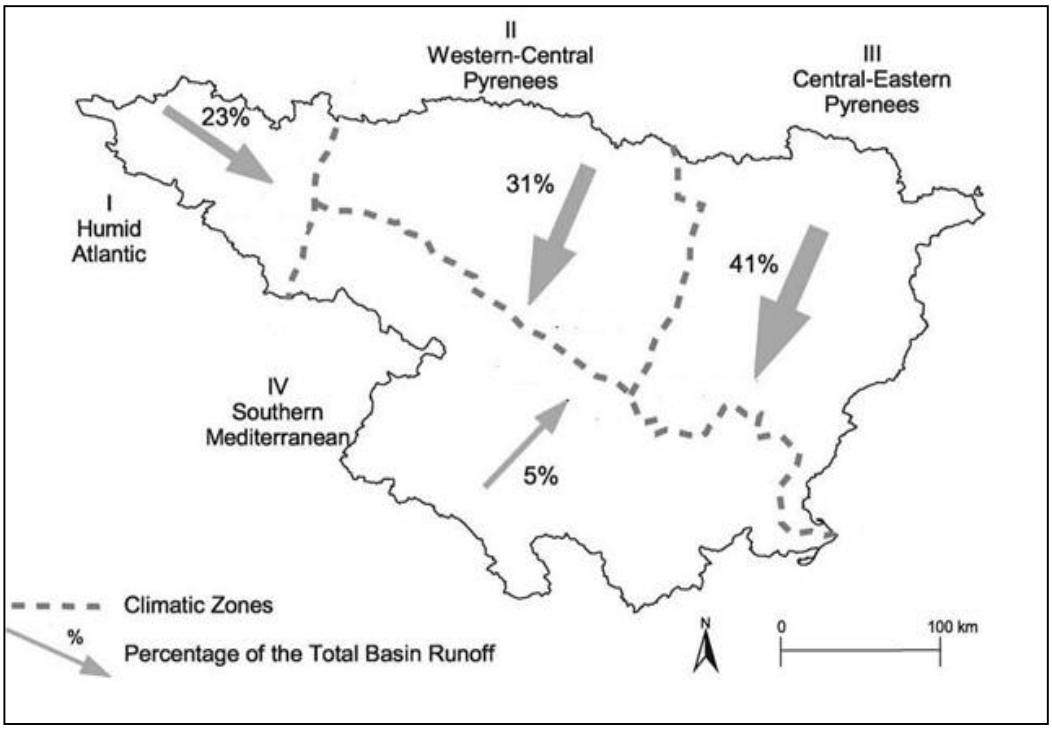

Figure 5.1: The main watersheds of the Ebro River. The percentages indicate the relative contribution of each watershed to the total basin runoff. (After Battalla et al., 2004)

Spatially, a quick comparison between Figures 5.3, 5.4 and 5.5 clearly shows that the warming in maximum, minimum, and mean temperatures is dominated across much of

northeastern Spain. This uptrend is more pronounced in coastal areas. The observed upward trend in most of observatories reveals that this increase has a climatological meaning. The detected changes can thus be attributed to either natural variability of climate or global warming or both of them.

5.2. Observed changes in temperature extremes

In this research, several methodological procedures have been considered in order to limit the possible effects of serial correlation and cross-correlation, which could add considerable uncertainty to trend assessment of extreme events. The results indicate that temperature series are likely free from serial correlation. This can be expected given that temperature often shows low persistence at the annual time scale with respect to monthly or seasonal time scales. In the same context, temperature extreme indices were proved as unbiased by the influence of cross correlation. Thus, the obtained results on trends in temperature extremes can be considered with a level of confidence. In this section, observed changes in warm, cold and variability extreme indices are discussed.

5.2.1. Changes in warm extremes

The results indicate an overall upward tendency in the frequency and intensity of warm extremes across much of the study area. This upward trend is generally compatible with previous findings (e.g., Frich et al., 2002; Klein Tank and Können; 2003; Alexander et al., 2006; IPCC, 2007). According to Alexander et al. (2006), there have been considerable changes in warm temperature extremes in the globe. For example, more than 70 % of the land-area observatories showed statistically significant uptrend in warm nights over the period 1951-2003. For the Mediterranean region numerous

studies also assessed the impact of climate change on temperature extremes (e.g., Klein Tank and Können, 2003; Kostopoulou and Jones; 2005; Diffenbaugh et al., 2005; Hertig et al., 2010). Among them, Klein Tank and Können (2003) found a significant positive trend in the warm tails of the European daily temperature over the second half of the 20th century. The same finding has recently been confirmed by Kostopoulou and Jones (2005) for the eastern Mediterranean and by Politano (2008) and Hertig et al. (2010) for the Western Mediterranean. For the Iberian Peninsula there has been few limited number of studies that examined the behavior of warm extremes (e.g., Burgueño et al., 2002; Miro et al., 2006; Brunet et al., 2007b; Della-Marta et al., 2007a,b). Among them, Brunet et al. (2007b) gave evidence on larger changes in high temperature extremes in Spain from 1955 to 2006. Similarly, Della-Marta et al. (2007b) pointed out that temperature of the Western Europe, including Iberia, has become more extreme, with the increase being more confined to summer. At the regional scale, Miro et al. (2006) reported a significant increase in the frequency of warm and extreme temperature days in Valencia from 1958 to 2003.

The increase in the frequency and severity of warm temperature extremes can mainly be linked to the rapid warming in maximum temperature compared with minimum temperature. In their study covering the whole Spain, Brunet et al. (2007b) found higher rates of change in maximum temperature rather than in minimum temperature over the period 1850-2005 (0.11º versus 0.08ºC decade^{-1}). In the study domain, this finding has been confirmed, suggesting that the most remarkable warming in mean temperature from 1960 to 2006 occurred during spring (0.66ºC decade^{-1}) and summer (0.41ºC decade^{-1}). Warm extremes are more likely to occur during these periods of the year.

Spatially, the trends in warm extremes were more pronounced in the coastal areas along the Mediterranean Sea and the Cantabrian Sea, whereas less warming was evident in mainland areas. The roughly contrasting coastal-continental pattern of warm extremes can be due to the prolonged strength of sea surface temperature (SST). Recently, many studies reported strong relationship between temperature extremes and SST. For example, Vincent et al. (2011) found strong influence of SST on variability of warm extremes in the countries of the Western Indian Ocean, with correlation coefficient ranging between 0.6 and 0.87. Black and Sutton (2006) also linked the 2003 European heat wave with variations in SST anomalies of both the Mediterranean Sea and the Indian Ocean. However, this warming can also be attributed to the strong influence of the general large-scale atmospheric circulation. Rodriguez-Puebla et al. (2010) attributed much of the warming in warm days (WD) across the Iberian Peninsula to changes in the Scandinavian pattern and the 500 hPa geopotential height field over the North Atlantic. Similarly, Politano (2008) linked the 1998 unprecedented warm winter in the Mediterranean region with the anomalous geopotential height at 500hPa and 200hPa levels. Fischer et al. (2007) also suggested the anticyclonic activity as a key driver of warm events in Europe. Cassou and Philips (2005) found strong association between the 1994 warm summer over France and the Atlantic blockings.

Altogether, these results strongly suggest the possible linkage between warm extremes during summertime over the domain and large-scale atmospheric circulation and geopotential heights. Given the notable increase in the frequency and severity of warm temperature events, which could have significant implications for hydrology,

ecology and agriculture, assessing this kind of research could provide a concrete base to better understanding of the spatial and temporal variability of warm extremes at this sub-regional scale. In the same context, the results of this work show more warming in warm extremes close to the coasts. Thus, it is also important to assess the impact of closing water bodies on warm extremes by means of simulations from different atmosphere-ocean climate models.

5.2.2. Changes in cold extremes

The Mann-Kendall results confirm that most of the cold temperature extremes related to the frequency and intensity showed a decreasing but statistically insignificant trend ($p<0.05$). The only exception corresponds to the annual high minimum temperature (TNx), which showed upward trend of 0.3ºC decade^{-1} in the whole domain. This uptrend can be linked to the increase in the mean minimum temperature during the summer season, which has been confirmed in other regional (e.g., Zhang et al., 2005) and global studies (e.g., Frich et al., 2002). In the study domain maximum temperature has increased faster than minimum temperature over the whole period 1960-2006, which suggests lower variance in the cold tail of temperature distribution. A number of studies worldwide confirmed this little change in cold extremes. For example, New et al. (2006) pointed out that indices related to the minimum temperature for southern Africa showed less warming compared with those of maximum temperature. In central and south Asia, Klein Tank et al. (2006) reported that most cold temperature indices exhibited significant warming in the period from 1961 to 2000. Also, Moberg et al. (2006) gave consistent conclusions in their study of trends in daily temperature extremes in Europe. In Iberia, Brunet et al. (2007b) reported a decrease in cold temperature extremes across much of Spain during the last few decades. In this

context, it is worthwhile to indicate that the occurrence of cold temperature extremes showed a clear decadal variation in the study area. Cold events were more frequent during the 1960s and 1970s. This situation has been reversed from the late 1970s onwards, due to the rapid warming in minimum temperature in the last two decades. This observation agrees well with the results of Bermejo and Ancell (2009), who reported a significant increase in minimum temperature across Spain after 1980. Accordingly, it is important to seek out the driving forces that can describe the interdecadal variability of cold extremes. Physical factors such as atmospheric circulation and sea surface temperature could be among other forces.

5.2.3. Changes in variability extremes

Similar to cold extremes, trends in variability extremes were less prevalent since insignificant trends were noted for majority of indices, with the exception of temperature sums (Tsums). For instance, the growing season length (GSL) significantly increased in only 14.8% of observatories. This finding is in line with Alexander et al. (2006) who indicated that around 16.8% of land observatories worldwide have experienced significant positive trends in the growing season length (GSL). In the study area, the less temporal variability of most of the indices can largely be explained by the inconsistence changes in maximum and minimum temperature during the past few decades. The evolution of the diurnal temperature range (DTR) is a clear example that summarizes the asymmetric evolution of both maximum and minimum temperature. As noted by many studies (e.g., Dai et al., 1997; Easterling et al., 2000), the globe has experienced a general negative trend in diurnal temperature range (DTR) that is largely a consequence of the rapid increase in minimum temperatures rather than maximum temperatures. In this work, the trends in DTR were

mixed between positive (49.2%) and negative (50.8%), being statistically insignificant in 71.9% of all observatories. This behavior is mostly due to the rapid warming of maximum temperature in recent decades, which is inconsistent with changes in minimum temperature over the same period. An inspection of DTR variability from 1960 to 2006 clearly revealed that DTR decreased during the 1960s, which was then reversed from the 1970s, suggesting less marked changes over the whole period (1960-2006).

The evolution of the intra-annual extreme temperature range (Intr) index can also be explained by the asymmetric evolution of very warm days (TX99p) and very cold days (TN1p) indices. Although these two indices summarize the evolution of the most extreme events in terms of their frequency, they can, to some extent, provide a good indication on the variability in Intra-annual extreme temperature range (Intr). The relationship between trends in both TX99p and TN1p is given in Figure 5.2, which are not linearly well-fitted (r = 0.01). This weak dependence between the two indices can be seen in the context that the frequency of very warm days (TX99P) showed a strong uptrend; more highlighted during the last few decades (refer to Figure 5.11). In contrast, the decrease in the frequency of very cold nights (TN1p) did not occur at the same rate (see Figure 5.13).

Overall, a comparison of the trends in warm and cold temperature extremes indicates that the impact of climate change on temperature is mainly accompanied by higher shift in the warm tail rather than in the cold tail. Trends in warm extremes are of greater magnitudes than cold extremes. These findings are compatible with previous works (e.g., Klein Tank and Können 2003; Kostopoulou and Jones 2005; Alexander et

al., 2006; Moberg et al., 2006). In the study domain the major changes in temperature extremes are focused on frequency and intensity of warm extremes. This finding fits well with the results of Klein Tank and Können (2003) for Europe, Politano (2008) for the Mediterranean, Beniston (2009) for Switzerland and Brunet et al. (2007b) for the peninsular Spain. The results demonstrate that changes in cold extremes were largely related to changes in the magnitude (e.g., CN, TNx, and TNn) rather than changes in the frequency of cold events (e.g., TX10p, TN10p, ID0, and FD0). By contrast, changes in warm extremes were due to the combined change of frequency and magnitude. Taken together, it can be inferred that the study area seems to be more sensitive to global warming during the warmer periods of the year, while it shows less sensitivity to this warming during the cold periods.

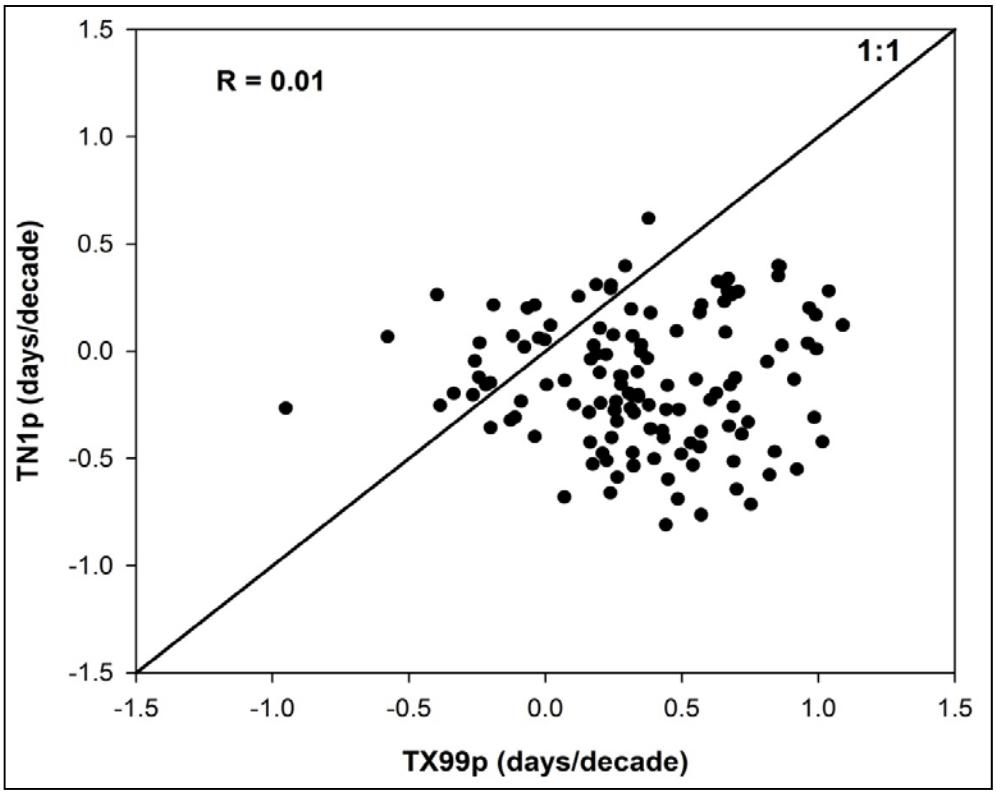

Figure 5.2: Scatter plot of the relationship between the observed trends in TX99p and TN1p.

5.3. Spatial regionalization of temperature extreme events

In this thesis, an attempt was made to divide the study domain into sub-regions as homogenous as possible based on characteristics of summer extreme events (e.g., frequency, intensity and persistence). The motivation for this classification was the high spatial variability of climate in the region due to its complex topography. The summer season was selected for this regionalization because the present study reported that the mean summer surface air temperature in northeastern Spain has increased by about 1.9ºC since 1960, with a warming rate of about 0.41°C decade^{-1}, which represents the strongest signal among all seasons. This can be clearly seen, at a broader scale, in the numerous summers with the anomalously record-breaking warm events in the recent decades over the Mediterranean and Europe (e.g., 1998, 2003, 2005 and 2010). These unusual events caused various drastic impacts on both the physical (e.g., agriculture, ecology, forest fire, and hydrology) and human environments (e.g., mortality and energy demand).

In this research, the multivariate statistics, including the principal component analysis (PCA) and cluster analysis (CA), were employed to divide the study domain into relatively homogenous climate regions. This kind or regionalization helps assessing the driving forces beyond the detectable spatial modes. Although the procedure followed to obtain homogenous regions can be seen as arbitrary and user defined given that the selection of clustering algorithm and the number of clusters was subjectively defined, the obtained results can be seen as satisfactory for many reasons. First, this study followed the standard procedure applied by many previous studies (e.g., Baeryswil and Rebetez, 1997; Romero et al., 1999; Papadimas et al., 2011) to obtain climatic homogenous regions. In particular, the climatic data were first

summarized by means of factor analysis to reduce data dimensions. Second, the scores of the retained factors were examined by cluster analysis to delineate the final homogenous regions. Also, given that the clustering procedure is unsupervised as the number of clusters is defined objectively, it was important to verify its goodness of fit. For this reason, the obtained classification was validated by means of the Silhouette width index to ensure its stability and goodness. Through this two-step statistical procedure, this work intended to use multiple statistics (i) to define the number of retained factors, (ii) to select the appropriate clustering algorithm, (iii) to detect the number of retained clusters, and (iv) to validate the clustering outputs. Combining the results from different statistics is advantageous to check for consistency between various statistics and in turn ensure the reliability of the findings.

According to this scheme, four sub-regions were indentified: the Mediterranean region, the Cantabrian region and the inland region, the moderately elevated areas, and the highly elevated areas. These sub-regions have clear climatic and geographical meanings, with relatively clear physiographic boundaries. According to previous knowledge, these defined sub-regions match well with the dominant climate regimes over the study domain. Given that the regionalization of extremes is challengeable due to very rarity of these events, relative to regionalization of the mean values, the obtained sub-regions are reasonably found homogenous and well separated. Interestingly, although the network density in high-elevation sites is generally irregular compared with other data-rich regions (only 14.4 % of the observatories are located above 1000 m), the clustering procedure, as being distinctly identified in CL4, skillfully captured the variability of temperature extremes at these highly elevated and scattered localities. This can probably be explained by the free-air advection at the mountains

summits and along the free-drainage slopes. Pepin and Lundquist (2008) confirmed this finding for elevated sites with annual 0º isotherm across the globe, suggesting that inter-site variance of temperature at those sites is expected to be lower than moderate and low elevation sites, as a consequence of the weak influence of local factors near surface such as land use changes.

A detailed assessment of the linear trends in extreme temperature indices in the established sub-regions indicates some important findings. Overall, there is a general tendency toward warming in temperature extremes for all sub-regions. However, this warming has a spatial component. For summer cold and warm temperature indices, the strongest signals were found in the most elevated areas (CL4) and along the Mediterranean (CL1). This probably suggests that orography and distance to the Mediterranean Sea play a key role in the temporal evolution of summer extremes in NE Spain. Accordingly, it can be assumed that changes in the summer extreme temperature are relatively complex and thus behave disproportionately over space as the climate warms. In this small area of complex orography, this finding implies that changes in these extremes are governed by different physical and dynamical considerations within the climate system.

The temporal evolution of summer temperature extremes close to the Mediterranean Sea (CL1) coincides with the observed changes found across many Mediterranean areas (e.g., Frich et al., 2002; Klein Tank and Können, 2003; Kostopoulou and Jones, 2005; Brunet et al., 2005; Hertig et al., 2010). For example, Klein Tank and Können (2003) found upward trend in warm temperature extremes over the Mediterranean region from 1976 to 1999. Also, Kostopoulou and Jones (2005) found that summer

was the season of the most significant increase in maximum temperature extremes in the eastern Mediterranean. For the western Mediterranean, Hertig et al. (2010) recently observed a strong warming trend in summer maximum temperature, more intense over the Iberian Peninsula. Brunet et al. (2006) also reported rapid increases in warm days over Spain since 1973, more apparent close to the coasts. The same finding has also been previously confirmed by Brunet et al. (2007b) who assessed variability of extreme temperatures in Spain, providing evidence on larger changes in warm temperature extremes during the 20th century, as compared with cool extremes. Given that the Mediterranean is a close basin, temperature variability at coastal sites seems to be closely linked to Sea Surface Temperature (SST) variations. Santoleri et al. (1994) found an increase of 1.5ºC in mean SST across the western Mediterranean, mostly faster during summer and winter compared with spring and autumn. Xoplaki et al. (2003a) also noted a significant warming trend of the Mediterranean Sea Surface Temperature (SST) west of 20°E over the period 1950-1999, while the eastern Mediterranean basin experienced cooling. More recently, Salat and Pascual (2007) showed a similar upwarding trend in SST along the Catalan coast (NW the Mediterranean).

The results also confirm that high mountain areas are more vulnerable to the global warming, compared with lowlands. These mountain environments are more likely to be affected by climate change and therefore they can be an early indicator of climate variability and change for the nearby low elevated areas. Accordingly, these results can be of particular importance in the context of the possible impacts of the global climatic change on behavior of temperature extremes in areas of complex topography. At the global scale, few studies also have been undertaken to assess elevation

dependency on climate change signals in areas of large temperature gradient. Among these few studies are Giorgi et al. (1997) and Beniston et al. (1997) for the Alps, Fyfe and Flato (1999) for the Rocky, Chen et al. (2003) for the Tibetan Plateau, Coronato and Bisigato (1998) for the Andes and López-Moreno et al. (2011) for the Mediterranean mountains. In previous works over the region, it has been unclear whether the mountainous areas are undergoing a global warming, particularly with low density of temperature observatories in much of these areas. In the study domain, the rapid warming at high elevations appears to be of great importance for ecological and hydrological systems and climate impact assessment. Rapid changes could lead to significant changes in their natural vegetation and thus impacts on ecosystems and biodiversity. Species at high altitudes are therefore expected to undergo rapid change due to greater magnitudes of warming.

5.4. Driving forces of observed changes and variability

5.4.1. Influences on seasonal mean temperature

5.4.1.1. Influence of teleconnections

The Pearson correlation coefficient was used to assess the strength and direction of association between the general atmospheric circulation patterns and temperature series over the period 1960-2006. This correlation provided valuable information on the strength of the phase of each particular teleconnection pattern. In general, the results suggest a predominant influence of the EA+, SCA-, and WeMO- patterns on interannual variability of temperature in the region. Other atmospheric circulation patterns (i.e., NAO, EAWR, and MO) are proven to be weaker predictors of seasonal temperature variations in the study domain. The correlation coefficient did not reach the statistical significance threshold for majority of observatories in most of the

seasons. The relationship between the NAO and temperature in the study area only applies for winter season. Recent work has indicated that the EA is a leading climate mode in Western Europe and the North Atlantic sector (e.g., Woollings et al., 2010; Moore et al., 2011), In the Iberian Peninsula, numerous studies also reported strong linkage between the positive EA and temperature variations. For instance, Sáenz et al. (2001a) noted that winter temperature variations in the northern Iberian Peninsula are mainly associated with the EA index. In the same way, Maheras and Kutiel (1999) attributed much of temperature variability in the Mediterranean region to the EA positive mode. Also, at a hemispheric scale, Hurrell (1996) reported that the NAO is responsible for a considerable amount of variability in land winter temperature north of 20ºN, with strong statistical significance ($p < 0.01$). In the Iberian Peninsula, numerous studies have also linked the increase in winter temperature to the positive mode of the NAO (e.g., Hurrell, 1995; Marshall et al., 2001). However, other works also suggest low and insignificant correlation between the NAO and temperature (e.g., Sáenz et al., 2001b; Slonosky et al., 2001).

Interestingly, the results also indicate that the leading circulation modes interacted differently with temperature in the region, with both negative and positive correlations. This strongly implies that the impacts of these circulation patterns on temperature are spatially dependent. For this reason, the composite climate maps of anomalous sea level pressure (SLP) corresponding to the key atmospheric circulation modes were built, providing information on the land-sea interactions in the study domain.

A detailed inspection of the configurations of SLP anomalies associated with each dominant circulation pattern reveals that the observed warming in mean temperature at the seasonal timescale can be linked to two main atmospheric configurations: the first is the increase in the zonal circulation compared with the meridional circulation. The second factor is the dominance of the Atlantic anticyclones over Western Europe.

The zonal circulation enhancement implies an increase in the easterly and westerly air flows relative to northern and southern flows. In the study domain, this situation is clearly evident during winter, particularly in the last decades. In winter, there is a strong pressure gradient with the Azores High and the Icelandic Low being well developed resulting in enhanced zonal winds. Figure 5.3 compares the average of SLP anomaly during winter for the 1960-1979 and 1980-2006 periods over much area of Europe and North Africa. This comparison can likely give an indication on recent changes in the zonal circulation over Europe during the last three decades. As illustrated, SLP over northern Europe tends to be anomalously low in the recent decades compared with earlier decades, implying that blocking may be weakened over these areas. This feature induces an increase in the westerlies reinforcement over Europe, which leads to warm winters in central and southern Europe. As shown in Figure 5.3, the increase in zonal circulation in recent decades often corresponds to an increase in anticyclones frequency. This feature leads to a reduction in cloud cover, and in turn an increase in warm air advection as a result of the increase in the incoming solar radiation during daytime hours (Esteban-Parra et al., 2003). These findings come in agreement with other earlier studies. For example, Slonosky et al. (2001) attributed much of the variability in the European wintertime temperature to changes in the zonal circulation. In the same context, Quadrelli et al. (2001) reported a

significant increase in the Atlantic blockings that affect the Western and southern Europe during winter months.

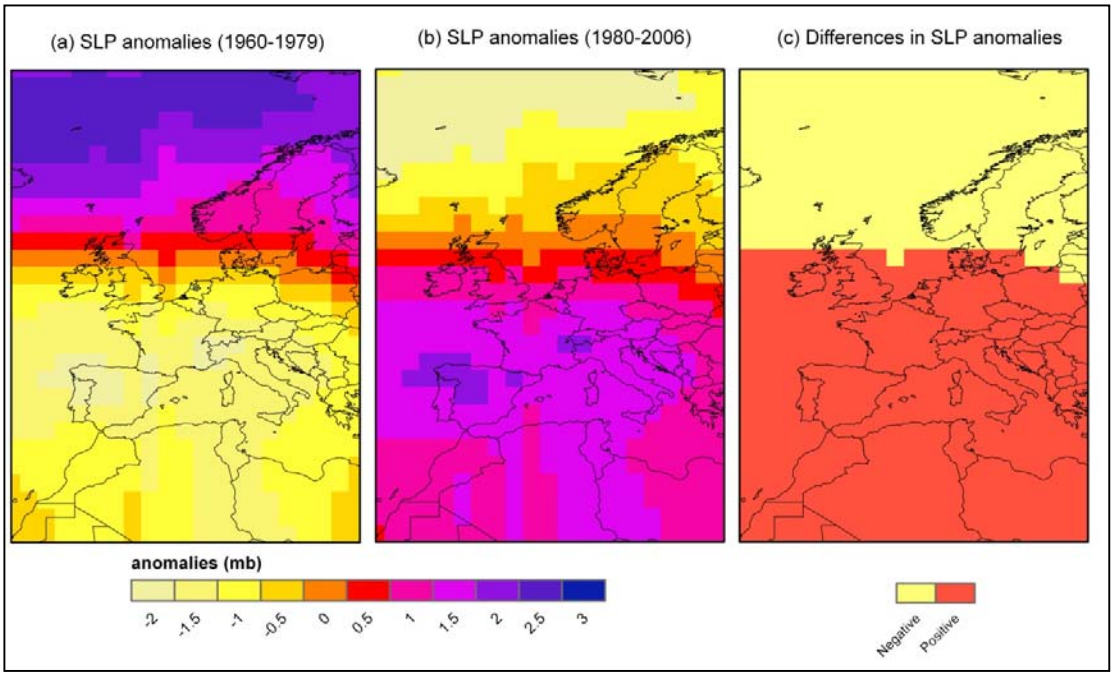

Figure 5.3 Differences in winter SLP anomalies between the two periods: 1960-1979 and 1980-2006, as indicator of changes in the zonal circulation. The anomaly was calculated from the NCEP/NCAR daily data for each grid using the reference period 1960-2006. Panel (c) has a binary value indicating the direction (i.e. positive/negative) of the difference in the anomaly between the two periods for each grid.

Given that the study domain is located in a transitional zone between the Atlantic and the Mediterranean configurations, the dominating atmospheric systems are the subtropical Azores High, the polar Icelandic Low and the continental surface highs (winter) and lows (summer). Accordingly, the Atlantic and Mediterranean air advections bring relatively warmer air over the study domain. More specifically, the composite SLP anomaly corresponding to the positive phase of the NAO is largely associated with an increase in zonal circulation over Western Europe. This

configuration corresponds to higher-than-normal western flows, which are accompanied with amplification of the warm Atlantic air advection to the study domain. This configuration can be responsible for the warming observed along the Cantabrian Sea and highly elevated sites in the Iberian system. This influence gets weaker in inland areas. Herein, it is however worthwhile to indicate that the dependency between the NAO and winter temperature variability is very sensitive to locations of the SLP anomalies centers. This is particularly because Southern Europe and the Mediterranean region are characterized by weaker SLP gradient in relations to northern and central Europe. As a consequence, a different behavior of southern Europe temperature from one year to another can be expected. In their study on the whole Mediterranean, Maheras and Kutiel (1999) pointed out that the high (low) temperature anomalies over the western Mediterranean is markedly related to the location of a low (high) pressure in the Atlantic ocean along the western Iberian Peninsula. This can be clearly seen during autumn season as there is a small pressure gradient over the Iberian Peninsula, which does not permit strong advection of atmospheric flows. This feature may explain the weak warming observed in this season, particularly in southern and central areas, compared with other seasons. During summer, the WeMO negative mode is also associated with the increase in zonal circulation, mainly originating from the positive pressure anomaly over the North Atlantic. This configuration increases the advection of the Westerlies, transferring warm oceanic air over the Cantabrian region, with less effect in central areas.

The second key factor responsible for the warming in mean temperature in the study area is the dominance of the Atlantic anticyclones over Western Europe, particularly during the negative modes of the SCA and WeMO and the positive mode of the EA.

The persistence of the anticyclonic configurations is markedly apparent during the last three decades. This can clearly be seen in Figure 5.4, which mapped averaged SLP data derived from the grids covering the study domain from 1960 to 2006. As indicated, there is a clear tendency toward increasing in the SLP means over the study domain. This is more pronounced during the last two decades. The only exception is the statistically insignificant trend ($p<0.05$) in the surface pressure during autumn. There is a tendency toward a decrease in the last three decades, with clear interannual behavior. These weak anticyclones can explain the weak warming and even the decrease found in some areas over the region during autumn. Blackburn and Hoskins (2001) found the same association during the positive SCA in summer, indicating that Western Europe is mainly associated with predominance (weakness) of the cyclonic (anticyclones) conditions. This behavior enhances the advection of the surface westerlies from the Atlantic toward southern Europe and the Mediterranean. The westerlies cause the transport of mild airflow that could weaken heat severity. Nonetheless, it is noteworthy indicating that the center action of the positive anomaly of anticyclones varies among seasons, between northwestern Europe and central Europe. This situation plays a key role in the above-normal temperature during spring and summer as these anticyclones act as blocks to the passage of the Icelandic cyclones and Atlantic fronts which are favoring for the northerly cooler flows. Previous works attributed the cooling of summer temperature in the first years of the 1980s to the weak of Atlantic anticyclonic, which favored strong and more frequent northerly cold flows over central and southern Europe (e.g., Metaxas et al. 1991; Reddaway and Bigg 1996; Kutiel and Maheras 1998). This situation has been reversed in the recent decades as summer corresponded to a well developed and stable Azores High predominating over large areas of the Mediterranean and continental Europe.

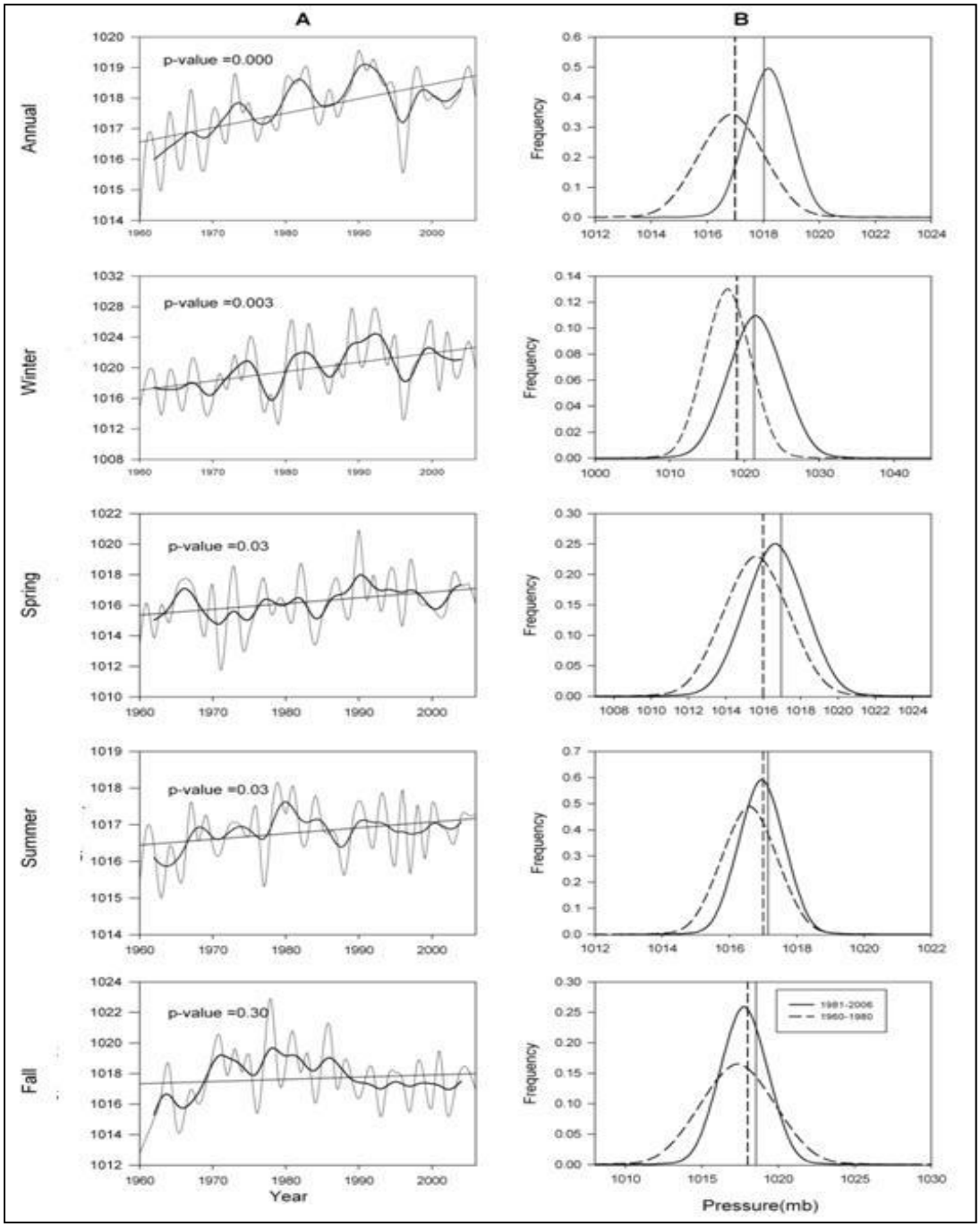

Figure 5.4: (A) Seasonal and annual temporal variations of mean SLP (hPa) over the study domain and, (B) differences in SLP in the two sub-periods 1960-1980 and 1981-2006, as indicator of blocking behavior. All calculations were made based on the averaged values of the 2.5º by 2.5º grid resolution covering he study domain. In right panels, changes in the mean values are represented by the vertical lines.

In addition, the persistence of anticyclones enhances the advection of air flows from one direction for consecutive days, which can be responsible for above normal temperature. For example, the EA+ configuration during winter and summer is mainly associated with predominance of anticyclonic conditions over the Mediterranean and North Africa, which would tend to bring anomalous S and SW warm air to the Iberian Peninsula, causing higher temperatures over the region. This configuration has been noted in earlier works (e.g., Sumner et al., 2001; Muñoz-Diaz and Rodrigo, 2004). Similarly, the SCA- during summer is characterized by prevalence of anticyclonic conditions at the surface level over Iberia, Central Europe, and North Africa. This configuration reinforces easterly and southerly flows from the Mediterranean, causing above-normal temperature over the study region.

5.4.1.2. Influence of land-atmosphere coupling

While numerous studies explained interannual variability of temperature as driven by large-scale atmospheric circulation (e.g., Sáenz et al., 2001a, b; Brunet et al., 2007b; Rodriguez-Puebla et al. 2010), the impact of these circulations is season dependent, with the stronger (weaker) effect during winter (summer). In particular, summer is generally characterized by a quasi-stationary circulation anomaly. Therefore, in response to the localized diabatic heating at the surface level, distinctive cyclonic (anticyclonic) circulation predominates in the lower (upper) layers of the troposphere during summertime (Chen, 2001). This thermally forced circulation is also coupled with other heat sources during this season, including heat radiation, maximum insolation, clear skies and light wind. Warmer temperature during summer can therefore be partially driven by this large stability and strong persistence in atmospheric circulation.

Over Iberia, this configuration can act as blockings to the passage of the Icelandic cyclones and Atlantic fronts, which bring cold air from Scandinavia and Eurasia. Trigo et al. (1999) defined a major cyclonic center over Iberia during summer season (36º-42ºN, 10ºW-0º). It is mainly originated from the thermal effect of warm land, besides the influence of land-sea interaction. Thomas et al. (2010) indicated that the dominance of cyclonic conditions during summer is more highlighted in the mainland peninsula and over mountainous regions, leading to more stability.

While the large-scale atmospheric modes can largely be responsible for temperature variations in some seasons (e.g., winter), land-atmosphere coupling processes (e.g., cloudiness and soil moisture) can explain large proportion of temperature variability in the summer periods. Based on simulated data from four different RCMs, Seneviratne et al. (2006), for example, noted that the projected changes in the interannual variability of climate in Europe would largely be driven by land-surface-atmosphere coupling. Among the land surface-atmosphere forces, cloudiness and soil moisture might be considered the two most important parts with significant feedbacks with temperature. Both are key drivers of mass and energy transfer in the globe.

Previous studies linked changes in land surface, including soil moisture, with climate variations (e.g., Huang et al. 1996; Douville 2003; Koster and Suarez 2003; Koster et al., 2004, Seneviratne et al. 2006; Fischer et al., 2007). Soil moisture plays a critical role in influencing surface energy and water balance components mainly through its effects on evapotranspiration or latent heat flux. Given that the study area is located in the mid-latitudes between dry and wet conditions; its climate is more likely to be influenced by changes in soil moisture. In this semi-arid region, soil moisture is a

limiting factor for evapotranspiration and thus exerts strong impact on the land energy balance. In this context, an attempt was made to quantify the relationship between the variability of surface temperature and soil moisture availability. It was revealed that changes in soil-atmosphere interactions can partially contribute to the observed trends in temperature evolution, particularly during spring and summer. This feedback was found negative and statistically significant at the 99% level as low soil moisture at the surface level during summer and spring seasons always causes a decrease in latent cooling and in turn above-normal temperature. A recent study by Zhang and Dong (2010) found that soil moisture feedbacks accounted for 5-20% of temperature variability in the transitional zones of eastern Asia. Similarly, Seneviratne et al. (2006) attributed much of variation (60%) in summer temperature variability in the transitional zones over Europe to soil moisture feedbacks. In summer and spring, soil moisture deficit can damp evapotranspiration and consequently more energy is partitioned into sensible heat, enhancing surface air temperature. Moreover, soil moisture can also modify surface air temperature through altering other components of surface energy balance (e.g., surface albedo, atmospheric water, clouds, and thermal properties of soil). Recalling that surface evapotranspiration is likely to inhibit the rising of daytime temperature through evaporative cooling, it can be expected that the dependency of soil moisture will be stronger during daytime (i.e., maximum temperature), while it decreases with nighttime temperature. This finding agrees well with previous works, which found strong feedback between soil depletion and maximum temperature than with minimum temperature (e.g., Dai et al., 1999; Durre et al., 2000; Diffenbaugh et al., 2005; Alfaro et al., 2006; Fischer et al., 2007; Zhang et al., 2009; Zhang and Dong, 2010; Lorenz et al., 2010).

Spatially, soil moisture feedback is likely to be greater on dry slopes, where soil moisture is determined by recent precipitation and time since snowmelt, and least near streams, where soil moisture persists at higher levels. In the study domain, a strong coupling of soil moisture with precipitation is expected during summertime. This is particularly because the study domain is located in a transition zone between dry and wet climates. Also, there is a high spatial and temporal variability of precipitation in the region. The influence of reduced soil moisture on summer temperature variations is also expected to be more highlighted along the coastal and mountainous regions compared with lowlands. This is basically because these regions often receive higher amounts of precipitation compared with areas of low altitude. Thus, the persistence of negative soil moisture anomalies is expected to be higher when there is a decrease in the amount of precipitation. This feature may partially explain the higher temperature warming observed in coastal areas and at highly elevated sites with respect to continental and lowlands. For example, Vautard et al (2007) indicated that a shortage in winter precipitation over the Mediterranean region often causes above-normal temperature in the following summer season. Fink et al. (2004) also demonstrated that the 2003 anomalous warm summer in Central and Western Europe was accompanied by a remarkable deficit in precipitation during the preceded winter. Recently, Seneviratne et al. (2006) showed observational evidence on strong impact of deficit in soil moisture on warm extremes in southeastern Europe.

Another important factor affecting temperature variations is cloudiness through radiation feedbacks. Cloudiness directly affects the global climate system by transferring energy in the atmosphere. The decrease in cloudiness often affects energy and heat transfer throughout insolation, suggesting above-normal temperature

during the daytime. Conversely, cloudy days are mostly linked to decrease in sunshine and in turn more evaporation and cooling. However, this study strongly suggests that the relationship between cloudiness and temperature is highly dependent on season, with positive (negative) feedbacks during winter (spring and summer). In contrast to summer, increasing cloudiness causes warmer temperature during winter. Dai et al. (1997) explained the association between surface air temperature and cloudiness in the context of radiation fluxes. In short, the cloudiness effect has a negative feedback during summertime as, under decreasing cloudiness, the incoming shortwave radiation is lower than the outgoing longwave radiation. This feature would be reversed in cloudy days. In winter, this association shows highly significant inverse relationship, indicating warmer minimum temperature during cloudy weather. In their study on the USA, Plantico et al. (1990) indicated that assessing interrelationships between trends or anomalies of temperature and cloud cover could significantly contribute to the understanding of climate change processes. They found a correlation coefficient in the order of -0.44 and -0.13 between cloud cover and maximum and minimum temperature, respectively, during summer (JJA) season. Herein, it is also worthwhile to indicate that this correlation is expected to be higher during years of positive anomalies of sea surface temperature (SST) as warmer surface water leads to less cloud amount.

5.4.2. Influence of large-scale circulation on extreme events

5.4.2.1. Influence on summer temperature extremes

Pearson correlation values between the general atmospheric circulation and the regional time series of extreme temperature during summers (JJA) of the period 1960-

2006 were computed for the established sub-regions following principal component ad cluster analyses. In general, this relationship was found statistically significant ($p<0.05$) for the EA+, SCA- and WeMO- patterns. Though the relationship between the NAO and winter temperature over large portions of the Mediterranean and Europe is confirmed (Hurrell, et al., 2003), the NAO seems to be a weak predictor for temperature extremes during summer season. This finding also agrees well with Trigo and Palutikof (2001) who found that the NAO poorly explained variability in atmospheric circulation during summer months, as compared with other seasons. In their study on the entire Europe, Beranova and Huth (2008) found the strongest connections between the EA mode and temperature in southern France and NE Spain.

The obtained results suggest that the behavior of temperature extremes during summer is mainly driven by atmospheric circulation during the positive EA, and the negative modes of the SCA and WeMO. This clearly implies that the dependency between temperature extremes and teleconnection indices resembles what was previously obtained for the mean temperature conditions. Similarly, the impacts of these configurations seem to have a spatial structure, with clear regional contrasts among the defined sub-regions. Accordingly, the co-variability between SLP as independent variable and summertime (JJA) temperature as dependent variable was explored for the period from 1960 to 2006. This co-variability was explored for the leading circulation modes by means of the composite climate analysis and the canonical correlation.

In summary, it can be concluded that the variability of summer temperature extremes in NE Spain is particularly related to the circulation modes that produce high pressure

anomalies over much of Europe and the Mediterranean Sea. A series of studies found a statistically positive trend in SLP over the whole Mediterranean and most of the continental Europe during warm summers of recent decades (e.g., Reddaway and Bigg, 1996; Xoplaki, 2002). For example, Xoplaki (2002) noted an upward trend in both surface pressure and different geopotential heights over the eastern Atlantic and most of continental Europe west of 30ºE. However, the canonical functions obtained in this work suggest that the spatial variability of temperature anomalies over northeastern Spain varies considerably according to SLP anomaly variations, which markedly differs its position, strength and influence domain from one prominent mode to another

5.4.2.2. Influence on the anomalously severe temperature extremes

With a focus on anomalous and very extreme temperature events, the PCA results denote that that changes in these events do not scale proportionately over the study domain. Changes are not found uniformly in all areas of the domain. The large-scale atmospheric circulation at SLP, 200hPa and 500hPa levels was proven to be able to explain spatial variability in very extreme temperature events (i.e., VCN and VWD). The results derived from both the composite maps and the canonical correlation analysis pointed out that the patterns of the 200hPa and 500hPa anomaly fields resemble that of the SLP modes. The spatial patterns of SLP and upper air (i.e., 200hPa and 500hPa) anomalies remain more or less consistent during both VCN and VWD. This more or less similarity implies that cyclones/anticyclones are developed simultaneously at these different levels. This indicates a stationary vertical structure of pressure, suggesting that extreme temperature variability at the seasonal scale (i.e., winter vs. summer) is forced by similar modes of pressure at mid and shallow

troposphere; a result that has been confirmed in earlier works over Western and southwestern Europe (Ulbrich et al., 1999).

The results also indicate that changes in VCN can be attributed to two main synoptic conditions. First, they are related to low surface and geopotential anomalies at the 200hPa and 500hPa geopotential heights over the Peninsula, which encourage strong advection of cold polar air masses originating from the anticyclones over Scandinavia. This finding has been reported in recent works (e.g., Klein Tank and Können, 2003; Prieto et al., 2004). For example, Klein Tank and Können (2003) attributed much of variation in cold extremes over the Western Europe and the Mediterranean winters to cold airflows from the snow-covered European continent and the northern Atlantic Ocean. Similarly, Prieto et al. (2004) identified the Arctic synoptic pattern as responsible for much of variability in cold days over the Iberian Peninsula. According to this explanation, the decrease in the frequency and intensity of these cold events can mainly be linked to a decrease (increase) in the meridional (zonal) circulation over the Western Europe in recent years. Werner et al. (2000) reported an increase in the mean residence time of zonal circulation during wintertime in the North Atlantic/European sector since the 1970s. This also agrees well with the previous finding which indicates that warmer winters in northeast Spain are mainly linked to the increase in zonal circulation, as revealed by more warm advections from west and southwest. This situation corresponds to weaker flows from cooler continental areas in north Europe as a consequence of the increase in the frequency of the Atlantic blockings. The second dominant pattern corresponding to the occurrence of VCN is linked to the presence of deep anticyclones over the study area for several days, which help local factors (e.g., fog) to generate VCN. Prieto et al. (2004) demonstrated

that this situation is responsible for the occurrence of cooler temperatures in the Iberian Peninsula when there is a general absence of any significant pressure gradient. The persistence of this circulation for uninterrupted days can likely enhance the occurrence of VCN conditions.

The findings on VWD assume that the warmest days during summer corresponded to strong anomalies at different levels (i.e., SLP, 200hPa and 500hPa) over Central Europe, while a negative anomaly is located over the Atlantic Ocean near to the Iberian Peninsula. Numerous studies reported a significant increase in pressure at MSL and different geopotential levels (e.g., 200hPa, 500hPa, 850hPa and 1000hPa) over the Mediterranean and Western Europe during summers of recent decades (e.g., Maheras et al., 1998, 1999; Wanner et al., 1997; Schonwiese et al., 1998; Xoplaki, 2002). For instance, Maheras et al. (1998) indicated a statistically significant increase for the 500 hPa level over the western Mediterranean. This finding has also been confirmed by Wanner et al. (1997), but for a broad geographical domain including the eastern Atlantic sector and much of the continental Europe. More recently, Xoplaki (2002) found statistically significant uptrend in both the 500hPa and 1000hPa geopotential heights from the tropics to the midlatitudes during summer months, the European regions west of 30ºE being the areas with the most significant trend. This configuration enhances advance of warm-dry air flows from the enhanced ridges from overheated European plains to the west and southwest. This situation comes in agreement with previous regional (e.g., Trigo and DaCamara, 2000; Lorenzo et al., 2008) and continental studies (e.g., Post et al., 2002). For example, Lorenzo et al. (2008) showed that the northeastern flows showed their high frequency over northern Spain during warmer summers, while southwestern advections had their least

frequency. In addition, a minimized influence of the westerly air flows during the most extreme warm events is evident, suggesting more influence of the Mediterranean Sea flows (i.e., easterly and northeasterly) compared with the Cantarbrian Sea flows (i.e. westerly and northwesterly). Over the peninsula, Trigo and DaCamara (2000) found the least frequency of the W and NW weather types during the May-August period of each year.

A comparison between canonical functions to assess co-variability between anomalous VCN/VWD temperature and geopotential fields indicates that no single function can solely explain this interrelationship. This suggests a high degree of variability among these fields and temperature over the region. Overall, the canonical correlation functions during VWD suggest that the severity and frequency of VWD can be understood as a function of the changing relationship between the centers of anomaly on the Mediterranean and the Atlantic. In general, VWD seems to be highly correlated with surface and geopotential anomaly in adjacent seas (i.e., the mid Atlantic and the Mediterranean). On the other hand, VCN showed low correlations with surface temperature in adjacent waters. This may imply that changes in sea surface temperature (SST) can possibly act as a key driver for the extremely severe warm days. Colman (1997) and Colman and Davey (1999) discussed the association between the European summer temperature and SST anomalies in the North Atlantic during the preceding winter. Black and Sutton (2006) also highlighted the role of the SST anomalies in the Mediterranean on the European heat wave of 2003.

However, the results also suggest that the spatial variability of VWD and VCN cannot be explained solely by changes in atmospheric circulation. Other mechanisms should

be considered to explain the occurrence of these events. According to Ogi et al. (2005), surface-atmosphere feedback mechanisms such as soil moisture, long periods of clear-sky conditions, subsidence, the Northern Hemisphere annular mode, northward extension of the Hadley cell, and an upper-troposphere double jet can significantly contribute to more frequent VWD (Black et al., 2004; Trigo et al., 2005). For example, soil moisture can strongly enhance convection, favoring for a higher increase in the frequency of these days in regions characterized by dry soils. Similarly, the anomalous warm days can be linked with lack of water availability (e.g., precipitation) and changes in cloud cover anomalies. Likewise, the synoptic conditions corresponding to VCN are still far from completely determining their mechanisms given that other local processes (e.g., snow pack, surface albedo) can have potential impact.

5.5. Future changes of temperature during the 21st century

Understanding the impacts of future climate change on northeast Spain, a region characterized by complex climatological and topographical features, is important for different environmental, hydrological, agricultural and socioeconomic applications. In order to obtain confidence in a future climate projection, it was necessary to evaluate the ability of different RCMs to adequately capture the characteristics of the observed regional climate. Using projections from different models rather than just relying on a single outcome is preferred because it allows deepening current knowledge of the uncertainties associated to the climatic change in the region. An ensemble of different simulations makes the projected changes representative of average or conservative conditions in the region. To meet this end, multiple simulations from 9 RCMs were assessed for their ability not only to reproduce the main statistical characteristics (i.e. the mean, skewness, symmetry and interannual variations) of time series, but also to

simulate spatial structure of the observed trends. The performance of the models was assessed against a gridded observational daily dataset obtained using a dense observational network during the reference period (1971–2000). This dataset is complete (i.e. no missing values); homogenous and dense, which is advantageous for validating simulated data. In this regard, numerous accuracy estimators were calculated on a seasonal basis to assess the performance of the models, including: the Mean Bias Error (MBE), the Yule–Kendall (YK) skewness and the ratio of coefficient of variance (CV). A quick comparison between the simulations which most accurately reproduce observed climate suggests that they tend to underestimate maximum temperature, while they overestimate minimum temperature over large parts of the region. This finding agrees well with other previous studies (e.g., Giorgi et al., 2004; Gonzalez-Aparicio and Hidalgo, 2011). This feature was more pronounced during winter and autumn relative to summer and spring. This can probably be explained by the inadequate representation of some components of the land-surface schemes, such as precipitation, soil moisture, surface fluxes and convective parameters. Moberg and Jones (2004) attributed much of the warm bias in mean temperature over southern Europe to poor simulation of soil moisture. Also, the absolute values of the bias were found higher for minimum temperature than for maximum temperature. Modelling minimum temperature can be constrained by very local conditions near land surface, such as local topography, vegetation cover and wind speed, which are quite complicated and difficult to resolve by the current RCMs spatial resolution (≈ 25 km). Numerous works informed that there is a general tendency of RCMs to overestimate precipitation during rainy seasons (particularly winter), which can in turn induce cold bias of maximum temperature. Many authors (e.g., Giorgi and Marinucci, 1996) attributed much of bias in climate models during summertime to lack of adequate

treatment of cumulus convection, a predictable process which plays a key role in temperature variations during this season. Another interesting note is that, apart from winter minimum temperature, majority of the models exhibited positive YK and IVE values for either daily maximum or minimum temperatures. A possible explanation for this feature is that the interannual variability of temperature decreases as the spatial scale of the study domain gets smaller (Giorgi and Bi, 2005). Recalling that the study area is quite small (≈160,000 km^2), temperature is not expected to vary greatly over space. Nonetheless, the complex topography of the study domain and its geographical location introduce changes over short distances. This is particularly clear with minimum temperature, which shows high gradient over short distances during cold seasons (i.e., winter and spring), particularly in areas of complex topography which are more prone to thermal invasions.

This study provides strong evidence that the current substantial warming over the study domain will continue during the 21st century. Model output indicates that mean temperature might increase for most of the study domain, with values ranging from 2.4ºC (spring) to 5.1ºC (summer). The strongest warming anomalies are expected to occur in winter and summer, with a more increase in the latter half of the 21st century. This seasonality of warming and their corresponding values are in the midrange of the predicted warming, as reported in previous works over the whole Mediterranean region (e.g., Giorgi and Bi, 2005; IPCC, 2007). According to the IPCC (2007), the warming rate of the mean temperature at the end of the current century lies in the range of 2.3ºC to 5.3ºC, under the A1B emission scenario. Similarly, over Europe, future changes in temperatures derived from five different GCMs under four global scenarios indicated that the annual temperature would rise in the range of 1ºC to 4ºC $decade^{-1}$

(IPCC, 2007). This features also fit well with the observed changes in maximum and minimum temperatures over the study domain from 1960 to 2006. The only exception is that spring will warm at weaker rates compared with the observed warming.

The projections also indicate that the projected minimum temperature will increase at larger rates than maximum temperature, suggesting a decrease in the diurnal temperature range in the future. This diurnal differential rate of warming is opposite to the observed changes in the region. However, this feature is generally in accordance with other global (Alexander et al. 2006) and regional (Esteban-Parra et al., 1995; Staudt et al., 2005) works.

The findings of future changes in temperature characteristics for the study domain find coincident change patterns. The overall changes are coincident over all seasons, suggesting more increase in mainland areas, and particularly over the central Ebro valley for maximum temperature and the Iberian and Cantabrian systems for minimum temperature. Overall, this spatial structure of the projected changes suggests less warming in coastal grids. Interestingly, the RCMs showed a remarkable agreement in spatial distribution for all seasons, although the magnitudes varied distinctly. This good agreement between the projected changes was interesting because the inter-model averages were computed from RCMs forced by different GCMs. While this spatial component is clearly opposite to the observed changes from 1960 to 2006 in which the largest changes in temperature are generally confined to coastal areas, these regional differences agree well with some recent projections (e.g., Hanssen-Bauer et al., 2005; López-Moreno et al., 2008b; Jerez et al., 2012). For example, Jerez et al. (2012) projected more increase in summer and winter temperatures over mainland and

western areas of the Iberian Peninsula. Similarly, López-Moreno et al. (2008b) reported more increase in mean temperature over land grid points along the Pyrenees (NE Spain), relative to the coastal grids. At the national scale, Alcamo et al. (1996) projected an increase of 2-3ºC in temperature over Spain using simulations from the IMAGE model, the largest warming occurred in the Ebro watershed. Over Europe, Hanssen-Bauer et al. (2005) found that a common feature for projected temperature change in Scandinavia was the large increase in continental areas than in coastal areas. The contrasted spatial modes between observed and simulated climate may imply considerable changes in the strength of the physical processes responsible for this warming. While the SST is regarded as a key driver of climate change in the region during the second half of the 20th century, there will probably be an enhanced negative feedback of soil moisture and the associated albedo in the future. Changes in the patterns of this dependency need further and detailed assessment in the future.

The results also demonstrated that the Pyrenees is more prone to negative anomaly (in the range of -0.5ºC to -3ºC) in maximum temperature during the mid 21st century (2021-2050). This result can be of particular importance from the hydrological point of view given that this mountainous region encompasses the headwaters of the main hydrological divisions in the study domain (López-Moreno and Garcia-Ruiz, 2004). One possible reason for this “unexpected” negative anomaly is that the simulated anomalies were computed based on an inter-model average of different simulations with diverse formulations. These models may vary in their response to climate change in very high-elevation regions. There are different formulations of the RCMs with varied representation of some components of the land-surface schemes such as

precipitation, soil moisture, snow-albedo feedbacks, surface fluxes and convective parameters. Another possible reason might be related to the uncertainty related to the use of the Inverse Distance Weighting (IDW) interpolation algorithm to obtain a gridded dataset based on the observational data (1971-2000). This Pyrenees has a relatively uneven network of observatories. Accordingly, the observed temperature might be overestimated as a consequence of the combined effect of topography gradient and the edge impact as access to data from the French Pyrenees was unavailable to limit this effect during interpolation. Overall, according to this finding, a late snow cover melting could be expected in the region in the next few decades, which could have potential implications in the area of water resources management. This picture has completely been reversed at the end of the 21st century, fitting the result of López-Moreno et al. (2008b) that projected a 1.7–3.1°C rise in the wintertime temperature across the Pyrenees by the end of the current century under the A2 emission scenario using a set of RCMs developed under the PRUDENCE project.

The results also indicate that changes in the mean temperature are accompanied by changes in the corresponding time-varying percentiles. This denotes that changes in temperature extremes are mainly due to the shift of the whole distribution rather than changes only in the mean. This also suggests that changes in extremes of daily temperatures in the study domain were due to changes in both the mean and the variance. The overall warming is more highlighted during summer, implying that there is consensus among models and the ensemble mean about high likelihood of increase in extreme warmer minimum and maximum temperature in the future. This range comes in agreement with Hertig et al. (2010) who projected an increase in the

magnitude of the upper percentiles of summer maximum temperature over the western Mediterranean during the 21st century.

A comparison between the role of changes in the mean temperature on trends of the maximum and minimum temperature time-varying percentiles during the 21st century reveals that the projected increase in both the mean and magnitudes of the time-varying percentiles generally corresponds to lower interannual variability in the future. The results gave little evidence on a statistically significant change in inter-annual temperature variations. The only exception was found during summer, which exhibited a future increase in the interannual variability of temperature. This implies a more likelihood to exhibit severe extreme warm events in the future. This finding was confirmed by Schär et al. (2004) for the whole Europe.

This study highlights the finding that the large absolute change in the mean during the first and the late halves of the 21st century does not necessary correspond to an increase in the temperature variability in the future. Therefore, future temperature changes over the study domain cannot only be inferred from changes in the mean, especially with respect to temperature changes at the lower and upper ends of the maximum and minimum temperature distributions. These results imply that we cannot only rely on changes in the mean to infer changes in the corresponding time-varying percentiles. Hertig et al. (2010) confirmed the same finding for the whole Mediterranean region, indicating that changes in the 90th and 5th percentiles of summer maximum and winter minimum temperatures, respectively, do not follows the same rates of changes of the mean values.

Based on the performance of 9 RCMs over the study domain, future changes in VWD and VCN were also assessed for the 2021-2050 and 2071-2100 periods. It can be seen that changes in the VCN over the study area are more linked to changes in the intensity of temperature during these days than to changes in the VCN frequency. This can be seen when comparing rates of change in the 1st percentile with changes in the frequency of VCN. This comparison may suggest that changes in the mean of minimum temperature during winter season are significant, while changes in the standard deviation are less evident. This situation leads to few changes in the frequency of these events while there is a significant change in the magnitude of temperature recorded during these days. This finding has been confirmed by Prieto et al. (2004) for cold days across the Iberian Peninsula, suggesting no significant changes in the standard deviations of daily minimum temperature distribution. Similarly, the magnitude of the 99th percentile of summer maximum temperature increased at rates greater than those of the 1st percentile of winter minimum temperature during the second half of the 21th century. This indicates a rapid increase in the warm tail of daily temperature distribution than in the cold tail. This picture has been reversed in the earlier decades (2021-2050) as the 1st percentile of daily minimum temperature has risen at rates higher than the 99th percentile of daily maximum temperature, suggesting rapid warming of minimum temperature than maximum temperature in earlier decades of the 21st century.

The results on changes in both the mean and the time-varying percentiles can be valuable to assess the potential impacts of climate change on hydrology, human activities, agriculture and economy and can also be useful to monitor these influences at the regional scale. Recalling that warm extreme events are mostly expected to

occur during summer season (JJA), the enhanced summer temperature increase for the study domain, particularly, at the end of the current century, could have various hydrological and environmental consequences. These impacts could include, for example, the increase in drought severity, forest fires and energy consumption and the degradation of agricultural production. Moreover, it can lead to higher evaporation rates that transport larger amounts of water vapor into atmosphere, inducing accelerated changes in the hydrological cycle over the region. In addition, shallow snowpacks as caused by the projected warming can lead to drier soils, longer growing season, and higher moisture stress for plants. In other words, it can be expected that the growing season will begin earlier due to melting of snowpacks, while soil moisture will become depleted sooner as a consequence of the rapid snow melting. Also, this warming can significantly influence the timing of streamflow in the study domain, which may increase water demands and stress in the region. Following Rodriguez et al. (2005), an increase of 1ºC in the Spanish mean annual temperature in the future can be responsible for a reduction of nearly 5-14% in water yields, while a more intense increase of 4ºC could reduce water yields by 22%.

The projected rapid warming at high elevation regions by the end of the century (e.g., the Pyrenees and the Iberian systems) could have a wide range of impacts with potentially severe consequences for the biodiversity in these vulnerable environments. For example, changes in the timing of snowmelt could affect plant phenology and induce early season temperature regimes (Inouye et al. 2002; Dunne et al. 2003). This warming may also alter conditions that determine the distribution of habitats and phenologies of the plants. Thuiller et al. (2005) indicated that a projected global warming of 3.6°C could induce a loss of more than 50% of plant species in the

Mediterranean mountain region. This loss is likely to be maximized over northern Spain, reaching 80% of species. In the same context, the model results projected a rapid increase in maximum temperature over the Ebro valley. This suggests that the Ebro valley may become warmer and drier in the future. This projected warming may intensify the hydrological cycle resulting in higher evaporation losses, higher irrigation water requirements, and an overall increase in water resource demand for domestic, agricultural, and industrial use. Such changes in hydrological system and water resources could have a direct effect on society, environment and economy.

Taken together, the results of this work on the projected temperature future changes should be taken with much consideration by local decision makers, highlighting the need to adopt their future policy and development plans to meet future demands.

CHAPTER SIX

CONCLUSION

6. CONCLUSION

The present thesis examined changes in the annual and seasonal distribution of daily maximum and minimum temperatures for northeastern Spain. A better understanding of the ongoing changes in the temperature means and extremes was the primary objective. Further aims involved the analysis of large-scale atmospheric circulation patterns at different geopotential levels as well as the Mean Sea Level (MSL) pressure based on climate composites analysis and canonical variates in order to quantify the driving forces beyond the observed variability. Finally, this work aimed to assess future climate projections of seasonal temperature and their spatial variations to improve the understanding and prediction of the long-term trends of temperature means and extremes simulations. To achieve all these goals, it was necessary to develop a homogenous dataset with high spatial and temporal resolution. The next few paragraphs answer the main research questions raised during this work.

(1) To what extent the daily temperature dataset can be trustworthy to examine temperature changes in the study domain?

In addition to data availability, the quality and homogeneity of temperature time series are prerequisites for detailed, reliable and trustworthy assessment and attribution of temperature changes. In this work a dense daily temperature database spanning the period between 1900 and 2006 has been developed for the study domain. The raw data provided by *the Spanish Meteorological Agency (AMET)* were subjected to a vigorous quality control procedure to eliminate any spurious values. Then, a reconstruction scheme was performed to fill in missing values by linear regression.

Potential discontinuities in the time series, as caused by any of the non-climatic factors (e.g., changes in locations, instruments, observers, observing practices, and surrounding environments) were also evaluated. When a statistically significant breakpoint was identified, a correction model was applied to adjust the detected breaks. A monthly correction factor based on the combined results of all homogeneity tests was then computed and interpolated to daily data. This dataset comprises the most long, complete, reliable and spatially dense time series over northeastern Spain, encompassing its major climate regimes (i.e., Mediterranean, oceanic, continental and mountainous).

(2) How are seasonal temperature variations distributed in space and time in the study domain?

The evolution of seasonal and annual temperatures has been investigated over the period 1920-2006 and the sub-period 1960-2006. By means of the non-parametric Spearman *Rho* statistic, it was possible to assess presence of trends in the temperature series. Overall, there is strong evidence on an increasing trend in temperature at both seasonal and annual timescales. This finding implies that the regional trends of temperature on either yearly or seasonal scales are closely related to changes in the global climate system. The largest warming occurred during the last few decades, especially from the mid of the 1970s. This warming was faster during spring and summer than in winter and autumn. Spatially, the coastal areas warmed at higher rates than in the mainland areas, demonstrating that there is a distinct coastal-continental gradient in temperature variations across the region.

(3) How did indices of extreme temperature change in space and time in the study domain?

Using a 47-year daily dataset of maximum and minimum temperature from 128 meteorological observatories, the spatial and temporal variability of temperature extremes were analyzed for the period 1960-2006. The trends were assessed by means of the Mann-Kendall statistic after the removal of the significant lag-1 serial correlation using a prewhitening procedure. The trend analysis of extreme events suggests that there has been an increase in both the frequency and intensity of warm extremes (e.g., TX90p, TN90p, TR20 and TXx) rather than in cold extremes (e.g., TN10P, FD0, ID0 and TNn). The indices with significant trends were less for cold events than for warm events, suggesting an obvious shift toward more warm extremes. This upward trend in warm extremes has been more pronounced in the last two decades, corresponding to the rapid warming in the mean maximum temperature. The variability of warm temperature extremes seems to have a spatial component. The presence of positive trends along the Mediterranean and the Cantabrian seas suggests possible effects of atmospheric circulation patterns and SST on extreme variations in the study domain.

In this study, the full procedure used to classify daily temperature extremes during summer season (JJA) is also described. The main objective was to delineate spatially coherent regions employing 14 temperature-based extreme indicators derived from a 47-year of daily information (1960-2006). Multivariate statistics (i.e., principal components analysis and cluster analysis) did an adequate job in providing a useful classification that gave insights into spatial variability of summer temperature extremes. Four sub-regions with climatic and geographic meanings were indentified:

the Mediterranean region, the Cantabrian region and the inland region, the moderately western and southern areas, and the highly elevated areas. The temporal evolution of summer temperature extremes for the established sub-regions was examined. While the spatial domain of this study is quite limited (≈160,000 km^2), a high degree of inter-regional variability in characteristics of temperature extremes (i.e., frequency, intensity and persistence) was evident. In general, a warming trend was exhibited for both maximum and minimum temperatures, being more pronounced at high elevation sites and along the Mediterranean coastland.

(4) To what extent changes in temperature means and extreme events in the region can be explained as driven by the large-scale atmospheric circulation patterns?

This study endeavors to make an advance in the understanding of the temperature variability and change by assessing the connection between the large-scale circulation and temperature anomalies at both seasonal and annual scales. The observed warming in maximum, minimum and mean temperatures can be linked to two main configurations: the first is the increase in the zonal circulation compared with the meridional circulation. This feature suggests an increase in the easterly and westerly air flows relative to the northern and southern flows. The second factor is the dominance of the Atlantic anticyclones over Western Europe, particularly during the negative modes of the SCA and WeMO. The correlation of the large-scale atmospheric circulation with temperature extremes also showed that temperature extremes in NE Spain are mainly explained by three configurations (SCA-, WeMO- and EA+). The negative mode of the SCA pattern proved to be capable of explaining most of

variability in summer temperature extremes at sub-regional scale, with more influence in the highly elevated areas. In contrast, the impact of the EA positive phase was more highlighted in the Mediterranean region compared with mainland portions. However, recalling that the influence of SLP on temperature extreme may be interrupted by certain local conditions (e.g., vegetation canopy, land use changes and topography), a detailed study on variability of VWD and VCN based on atmospheric circulation at various geopotential heights (i.e., surface sea, 500hPa and 200hPa) was provided. The VCN (VWD) was defined for each time series from the 1st (99th) percentiles of daily minimum (maximum) temperature distributions. This work identified the main synoptic patterns that contribute to the occurrence of these extremely severe events. Attribution of this dependency is still lacking and worth investigating over the Iberian Peninsula at both coarse and fine spatial scales. The links between centers of action of the large-scale circulation patterns over the Mediterranean and the Western Europe on one hand and regional variations of the anomalous events over the study domain on the other hand were explored by means of the composite maps and canonical correlation analysis. The composites of SLP, 200hPa and 500hPa fields during VWD suggested that these days are linked to the replacement of the strong ridges from the Iberian Peninsula toward central Europe. The most evident features associated with this situation are the quasi-stationary anticyclonic circulation anomaly over Central Europe. The strength of these anticyclones conditions over mainland Europe is much stronger, as compared to those placed over Iberia suggesting strong advection of the easterly and northeasterly warmer dry air to the study domain. On the other hand, the occurrence of VCN is mainly enhanced by the increase in the meridional circulation, which encourages strong advection of arctic flows to the depression centered over the western Mediterranean. In few instances, these cold events were connected to the

persistence of anticyclones over the peninsula for several days, particularly with the lack of any significant circulation gradient.

(5) Will temperature means and extremes exhibit in the future more or less similar changes in terms of both the amount (magnitude) and sign (direction) of change to those of the present-time?

It is widely known that changes in GHG concentrations will not only impact temperature means, but they will also influence the warm/cold tail of temperature distributions. Therefore, it was of particular importance to assess future changes in both temperature means and extremes over the region. In this work, nine RCM experiments available through the EU-ENSEMBLE project and forced by different GCMs simulation, were assessed for their ability not only to reproduce the main statistical characteristics (i.e., the mean, skewness, symmetry and interannual variations) of observed temperature, but also to simulate spatial structure of the observed trends.

To estimate the amount of future changes most accurately, it was necessary to compare climate simulated data with observational data. The performance of the models was assessed against a gridded observational daily dataset obtained using a dense observational network during the control period (1971–2000). The validation statistical measures (e.g., MBE, YK, IVE and Willmott's D of agreement statistics) were calculated on a seasonal basis to assess the models performance. These statistics gave insights on changes in the means, variance, symmetry and interannual variability of temperature series and accordingly they can be employed as guidance for selecting

models to be used in projecting temperature future changes. An inter-model comparison suggests that not all the models describe the present climate with similar accuracy. Based on the validation results, this work looked at the range of projections from different models rather than just relying on a single outcome, allowing deepening the knowledge of the uncertainties associated to the climatic change across the study domain. The models with the best agreement with the observed station data were selected with a level of confidence and used to provide guidance on the behavior of future seasonal temperature changes over the region.

To account for changes in the mean and extremes of temperature distribution, this study compared present-day climate with future climate projections in terms of changes in the high-order statistics (i.e., the mean and standard deviation) as well as a set of time-varying percentiles (i.e., the 10th, 25th, 75th and 90th). Analysis of the simulated seasonal temperature datasets, driven by the A1B emission scenario, suggests that the projected regional warming in both the mean and extreme events is expected to continue during the 21st century. The projected changes in future climate, as simulated by RCMs, include a continuation of increases in maximum and minimum surface air temperatures, with the greatest increases occurring over mainland and at high altitudes. The results also suggest strong warming anomalies in winter and summer during the 21st century, with a more increase in the latter decades of the century. The projections also indicate that the magnitude of climate change signal will be greater for minimum temperature than for maximum temperature, suggesting a decrease in the diurnal temperature range in the future.

Spatially, there is a general consensus among the models in the projected seasonal temperature changes of: (1) a positive anomaly of seasonal maximum and minimum temperatures over mainland areas, particularly in the central Ebro valley; (2) a slight positive temperature anomaly over the Pyrenees; and (3) a weaker positive temperature anomaly along the Cantabrian Sea relative to the Mediterranean and continental portions.

This work also tested the ability of high-resolution simulations of the RCMs to project changes in VCN and VWD frequencies under the A1B emission scenario during the 21th century. The results indicate a symmetric decrease in the frequency of VCD during the periods: 2021-2050 and 2071-2100. On the other hand, VWD will be more frequent during the late of the century (0.8 day decade^{-1}) compared with 2021-2050 (0.1 day decade^{-1}). The results also imply that changes in the frequency of these very extreme heat events will be more linked to changes in both the mean and standard deviations of daily temperature distributions.

(6) What is more important in the future: changes in the mean or the variability of temperature?

The results indicate that changes in the mean temperature are often accompanied by changes in the corresponding time-varying percentiles, suggesting shifts in the whole bell curves (i.e., the warm and cold tails). This overall warming was more highlighted during summer, implying that there is consensus among models about high likelihood of increase in extreme warmer minimum and maximum temperature during summer in the future. The results of this study also indicate that the large absolute change in the

mean during the first and the late halves of the 21st century does not necessary correspond to an increase in the temperature variability. Therefore, future temperature changes over the study domain cannot only be inferred from changes in the mean, especially with respect to temperature changes at the lower and upper ends of the maximum and minimum temperature distributions. Changes in the variance of the temperature distribution could have larger impacts on extreme events like change in the mean. These seasonal differences also imply that we cannot only rely on changes in the mean to infer changes in the corresponding time-varying percentiles.

(7) What are the potentials of the results obtained in this work?

The results derived from this study can contribute to understanding the climate change signal associated with the seasonal temperature variability in northeast Spain. This work represents one of the first attempts to explore spatial and temporal characteristics of temperature variations at sub-regional scale in the Iberian Peninsula. Given the high spatial and temporal scales of the dataset used in this work, the present study can contribute to the limited number of studies focusing on temperature variability at the regional scale in Iberia. Moreover, this work provides an insight into the possible mechanisms and physical processes that may relate spatial and temporal variability of regional temperature with the large-scale atmospheric circulation patterns.

Given that the study domain is characterized by complex topography and geography, which play a considerable role in determining the climate and weather at regional and local scales, the results on long-term variability of temperature in this Atlantic/ Mediterranean region can be placed in a larger climate context, providing insights into temperature variability in the Mediterranean and southwestern Europe. In addition,

information on the behavior of temperature on this fine scale can be essential for different impact assessment applications in the region. The results obtained in this work could therefore be meaningful for various applications related to hydrological modeling, agroclimatology, water resources management and drought monitoring.

Northeastern Spain has several characteristics that make it interesting for the study of temperature trends. These features include the altitude, latitudinal location, complex topography, and the high spatial and temporal variability of climate. Accordingly, there are great disparities in the variability of temperature at various spatial and temporal scales. Owing to its diversity, the study domain provides an interesting test ground to assess the ability of different RCMs to reproduce temperature future projections. Unfortunately, in contrast to the global scale, there is generally less confidence in estimates of how the climate will change to global warming at regional scale. Only few projections have been studied in the region due to lack of high quality data on a daily basis. The projected change in temperature, as simulated by RCMs forced by different GCM experiments, was within the range of changes simulated by other works in the Mediterranean and Western Europe. The results of this work can thus represent an important milestone step in the prediction of future temperature, as caused by the global warming, under different climate scenarios in the Iberian Peninsula. Therefore, the results intend to complement the series of studies on climate future changes in Iberia by evaluating projected changes in temperature means and extremes over the study domain during the 21st century. The results on future simulations can also contribute to enhancement of climate change adaptation and disaster management as the observed changes could have considerable implications in various areas, such as hydrology, ecology, mortality rates and energy demand and consumption. For

instance, the enhanced summer temperature increase for the study domain, particularly at the end of the current century, could have various hydrological and environmental consequences. These impacts could include, among others, the increase in drought severity, forest fires and energy consumption and the degradation of agricultural production. Moreover, it can lead to higher evaporation rates that transport larger amounts of water vapor into atmosphere, inducing accelerated changes in the hydrological cycle over the region. Accordingly, there is a need to understand the hydrological processes possibly altered by climate change, such as evaporation, surface runoff, drought conditions and water availability.

To conclude, this study can be advantageous compared with earlier studies examining temperature changes and variability in the study domain in several ways. First, it depends on a dataset of long, complete, reliable and spatially well-covered time series, which encompasses the main climate regimes in northeastern Spain (i.e. oceanic, Mediterranean, and continental). Previous studies were only restricted to very smaller number of observatories, where reliable data were available. Second, this study can provide a more comprehensive view of long-term variability on seasonal and annual timescales in a way that can significantly contribute to more accurate and robust climate projections. Third, the high spatial and temporal resolution of this dataset suggest that the projected future changes must be taken with much consideration by local decision makers, highlighting the need to adopt their future policy and development plans on a more local scale to meet future demands.

CHAPTER SEVEN

CONCLUSIONES

7. CONCLUSIONES

En esta tesis doctoral se han analizado los cambios en la distribución anual y estacional de las temperaturas máximas y mínimas diarias en el noreste de España. Uno de los principales objetivos fue obtener una mejor comprensión de los cambios en los valores medios y en los extremos térmicos. Otros objetivos incluyeron el análisis de la influencia de los patrones generales de circulación atmosférica a diferentes niveles de geopotencial, así como a nivel del mar (SLP); todo ello basado en clasificaciones y variables canónicas para cuantificar los factores atmosféricos que controlan la variabilidad de la temperatura. Finalmente, este trabajo también ha tenido como objetivo evaluar las proyecciones futuras de la temperatura estacional y sus variaciones espaciales, con el fin de mejorar la comprensión y la predicción de las tendencias a largo plazo, tanto en los valores medios como en los extremos.

(1) ¿En qué medida la base de datos generada a escala diaria resulta adecuada para identificar los cambios térmicos en el área de estudio?

Además de la disponibilidad de datos, la calidad y homogeneidad de las series de temperatura son un requisito esencial para llevar a cabo una evaluación detallada y fiable sobre los cambios de temperatura en la región. En este trabajo se ha desarrollado una base de datos diaria de temperatura con una elevada densidad espacial. Los datos brutos proporcionados por la Agencia Estatal de Meteorología (AEMET) fueron sometidos a un cuidadoso procedimiento de control de calidad para eliminar los valores falsos de las series. A continuación, se llevó a cabo un proceso de reconstrucción para unir diferentes observatorios y rellenar determinados valores. Se evaluaron potenciales discontinuidades en las series temporales no causadas por

factores climáticos (p. ej., cambios en la ubicación de la estación, instrumental, los observadores, prácticas de observación y entorno). Cuando se identificó un punto de ruptura estadísticamente significativo, se aplicó un modelo de corrección para ajustar los problemas detectados. Se obtuvo un factor de corrección mensual, basado en el resultado combinado de diferentes pruebas de homogeneidad, que se interpoló a los diferentes datos diarios. La base de datos desarrollada constituye la serie temporal a escala diaria más completa, fiable y densa espacialmente sobre el noreste de España.

(2) ¿Cómo son las variaciones estacionales de temperatura en el área de estudio?

La evolución de las temperaturas estacionales y anuales se ha caracterizado para los periodos 1920-2006 y 1960-2006. Las tendencias se evaluaron mediante un test estadístico no paramétrico. En general, se registra una clara tendencia hacia el aumento de la temperatura a ambas escalas: estacional y anual. Este resultado implica que las tendencias regionales identificadas en la región, tanto anual como estacionalmente, están muy relacionadas con los cambios observados en el sistema climático mundial. Las principales tasas de calentamiento se han registrado en las últimas décadas, especialmente desde mediados de la década de 1970. El calentamiento es más rápido en primavera y verano que en invierno y otoño. Espacialmente, las zonas costeras muestran mayores tasas de calentamiento que las zonas continentales.

(3) ¿Cómo varían los índices de temperatura extrema en el espacio y el tiempo en el área de estudio?

7. CONCLUSIONES

Se analizó la variabilidad espacial y temporal de las temperaturas extremas durante el período 1960-2006 mediante datos diarios de temperatura máxima y mínima de 47 en 128 observatorios meteorológicos. La tendencia se evaluó por medio del test de Mann-Kendall después de eliminar la correlación serial mediante un procedimiento de *prewhitening*. El análisis de tendencias de los eventos extremos indica un aumento en la frecuencia e intensidad de los extremos cálidos (TX90p, TN90p, TR20 y Txx) frente a la evolución de los extremos fríos (TN10P, FD0, ID0 y TNn). La frecuencia de tendencias significativas fue menor para los eventos fríos que para los cálidos, lo que sugiere un cambio hacia condiciones con extremos más cálidos. Esta tendencia al alza en los extremos cálidos ha sido más pronunciada en las dos últimas décadas, correspondiéndose con un rápido aumento en las temperaturas máximas. La variabilidad de la temperatura máxima extrema parece tener un componente espacial. Las mayores tendencias positivas registradas a lo largo de las costas mediterránea y cantábrica sugieren posibles efectos diferenciadores de los patrones de circulación atmosférica y de la temperatura del mar.

Se ha descrito un completo procedimiento para clasificar los valores diarios extremos de temperatura durante el verano. El principal objetivo consistió en delimitar espacialmente regiones coherentes a partir de 14 indicadores basados en las temperaturas máximas entre 1960 y 2006. Se utilizó estadística multivariante (análisis de componentes principales y análisis clúster) para llevar a cabo una clasificación espacial coherente con información sobre la variabilidad espacial de las temperaturas extremas de verano. El grado de bondad de la clasificación se evaluó por medio del índice de Silhouette. Se identificaron cuatro sub-regiones: i) la región del Mediterráneo, ii) la región cantábrica y zonas del interior, iii) las áreas más

occidentales y meridionales y iv) las zonas más elevadas. Se examinó la evolución temporal de las temperaturas extremas de verano para las diferentes regiones establecidas, destacando que, si bien el dominio espacial del estudio queda muy limitado espacialmente (≈ 160.000 km^2), existe un elevado grado de variabilidad espacial en las características de las temperaturas extremas (frecuencia, intensidad y persistencia). En general, la tendencia hacia un mayor calentamiento se observó en los observatorios ubicados a mayor altitud y a lo largo del litoral mediterráneo.

(4) ¿Hasta qué punto los cambios en los valores medios y en los eventos extremos pueden explicarse por patrones de circulación atmosférica a gran escala?

En este trabajo también se ha analizado la conexión de la temperatura en la región con la variabilidad en la circulación atmosférica para el período 1960-2006. El incremento térmico observado en las temperaturas máximas, mínimas y medias puede estar relacionado con cambios en algunos patrones de circulación: i) en primer lugar, con el aumento de la circulación zonal con relación a la circulación meridional, lo que implica un aumento de los flujos del oeste respecto a los flujos del norte o del sur y ii) en segundo lugar, un mayor dominio de los anticiclones atlánticos en Europa Occidental, especialmente coincidiendo con los modos negativos de la SCA y WeMO. La correlación de la circulación atmosférica a gran escala con las temperaturas extremas también mostró que las temperaturas extremas en el NE de España se explican principalmente por las configuraciones de tres patrones generales de circulación (SCA, WeMO y EA). El modo negativo del patrón SCA explica la mayor parte de la variabilidad de las temperaturas extremas de verano a escala subregional, con una mayor influencia en los observatorios de mayor altitud. En contraste, el

impacto de la fase EA positiva resulta más destacado en la región del Mediterráneo en comparación con las zonas continentales. Sin embargo, y considerando que la influencia de las configuraciones de presión en superficie sobre las temperaturas extremas puede estar perturbado por ciertas condiciones locales (p. ej., la vegetación, cambios de uso del suelo y la topografía), también se ha realizado un estudio detallado sobre la variabilidad en los días más cálidos (VWD) y días más fríos (VCN) basado en la circulación atmosférica a diferentes niveles de geopotencial (superficie, 500hPa y 200hPa). Los VCN (VWD) se definieron a partir de los percentiles 1(99) de la distribución de temperaturas mínimas (máximas) diarias. Se identificaron los principales patrones sinópticos que determinan la ocurrencia de este tipo de días. La relación entre los patrones de circulación a gran escala sobre el Mediterráneo y Europa occidental, por un lado, y las variaciones regionales de los extremos térmicos en el área de estudio, por otro, se analizó mediante mapas de compuestos y análisis de correlación canónica. Los compuestos correspondientes a los campos de presión a nivel del mar, 200hPa y 500hPa durante los VWD sugieren un desplazamiento de los sistemas de altas presiones desde la Península Ibérica hacia el centro de Europa. La característica más evidente asociada a esta situación es la existencia de una circulación anticiclónica cuasi-estacionaria sobre el centro de Europa. La intensidad de dichas condiciones anticiclónicas sobre Europa continental es mucho mayor, en comparación con las ubicadas sobre la Península Ibérica, lo que implica la presencia de advecciones fuertes de aire caliente y seco del este y nordeste al área de estudio. Por otro lado, la ocurrencia de VCN se ve reforzada por un aumento de la circulación meridional, que fomenta la advección fuerte de masas de aire ártico hacia condiciones de bajas presiones dominantes sobre el Mediterráneo occidental. En algunos casos, estos eventos fríos están conectados a la persistencia de anticiclones sobre la

península durante varios días, con una falta total de cualquier gradiente de circulación significativo.

(5) ¿la magnitud y el signo de los cambios en los valores medios y los extremos de temperatura son equiparables a los cambios observados?

Se asume que el incremento en las concentraciones de gases de efecto invernadero influirá no solamente en los valores medios, sino también afectará a los valores más extremos. Por lo tanto, resultaba de gran importancia evaluar los cambios esperados para el futuro en los valores medios y en los extremos de temperatura en la región. Para ello se utilizó un conjunto de simulaciones basadas en modelos regionales de cambio climático (RCMs), disponibles a partir del proyecto UE-ENSEMBLE. Se utilizaron nueve RCMs, enmarcados por diferentes modelos generales de circulación. Se evaluó la capacidad de los modelos para reproducir las características estadísticas de las series de temperatura observada (media, asimetría y variaciones interanuales), pero también para simular la estructura espacial de las tendencias. Para estimar con mayor precisión los cambios futuros, se llevó a cabo una comparación de los datos modelizados con los datos observados. La capacidad de cada modelo para reproducir los datos observados se llevó a cabo mediante una rejilla a escala diaria a partir de una densa red de observatorios para el período de referencia (1971-2000). Se calcularon diferentes test de validación estadística (MBE, YK, IVE y la D de Willmott) a escala estacional para evaluar la capacidad de los modelos. Estos estadísticos aportaron información sobre los cambios en los valores medios, varianza, simetría y variabilidad interanual de las series térmicas y se utilizaron como criterio para seleccionar los modelos utilizados para evaluar las proyecciones de temperatura para el futuro. La comparación entre modelos sugiere que no todos los modelos describen

el clima actual con una precisión similar. En base a los resultados de la validación, el análisis de las proyecciones futuras se centró en diferentes modelos en vez de depender de un solo modelo, lo que permite analizar las posibles incertidumbres asociadas al cambio climático en la región. Se seleccionaron aquellos modelos que muestran una mejor coincidencia con los datos observados, y dichos modelos se utilizaron para determinar el comportamiento futuro de la temperatura a escala estacional en la región.

Para tener en cuenta los cambios en las medias y los valores extremos de la distribución de temperatura, se realizó una comparación entre el periodo de control y las condiciones futuras mediante los cambios en las estadísticas de orden superior (media y desviación estándar), además de en un conjunto de variables que informan sobre la frecuencia de la distribución (percentiles 10, 25, 75 y 90). El análisis de los datos de temperatura estacionales a partir del escenario de emisiones A1B sugiere que el calentamiento detectado a partir de los datos observados continuará durante el siglo XXI, tanto en el caso de los valores medios, como de los extremos térmicos. Los cambios proyectados para el clima futuro por los RCMs muestran la continuación del aumento de las temperaturas medias, máximas y mínimas, con un mayor incremento en las áreas continentales y en las zonas más elevadas. Los resultados también muestran un mayor calentamiento en invierno y verano, mucho más acusado durante la segunda mitad de siglo. Las proyecciones también indican que la magnitud de la señal de cambio climático es mayor para las temperaturas mínimas que para las máximas, lo que sugiere una disminución en el rango de temperatura diurna para el futuro. Espacialmente, hay una coincidencia general entre los modelos: i) la anomalía positiva en las temperaturas máximas y mínimas, especialmente en las zonas

centrales del valle del Ebro, ii) un menor incremento en los Pirineos, y iii) el menor aumento en la zona cantábrica con relación a la región mediterránea y continental.

Este trabajo también muestra la capacidad de las simulaciones de alta resolución a partir de los modelos climáticos regionales para proyectar los cambios en las frecuencias de VCN y VWD en el escenario de emisiones A1B durante el siglo XXI. Los resultados indican una disminución simétrica en la frecuencia de VCN en los períodos: 2021-2050 y 2071-2100. Por otro lado, los VWD serán más frecuentes durante la segunda mitad del siglo (0.8ºC día/década) en comparación con el periodo 2021-2050 (0.1ºC día/década). Los resultados implican que los cambios en la frecuencia de estos eventos muy extremos estarán vinculados a cambios tanto en la media como en la desviación estándar de las distribuciones de temperatura diaria.

(6) ¿Qué son más importantes en el futuro: los cambios en la media o en la variabilidad de la temperatura?

Los resultados indican que los cambios en la temperatura media se ven acompañados de cambios en los percentiles, lo que sugiere cambios en el conjunto de la distribución (es decir en las colas de valores máximos y mínimos). Este calentamiento es más destacado durante el verano, lo que implica que existe un consenso entre los modelos sobre la alta probabilidad de aumento de los valores máximos y mínimos extremos durante los veranos en el futuro. Los resultados de este estudio indican también que el cambio absoluto en la temperatura media durante la primera y segunda mitades del siglo XXI no se corresponde necesariamente con un aumento en la variabilidad de la temperatura. Por lo tanto, los cambios futuros de temperatura en el área de estudio no sólo se deducen de los cambios en los valores medios, especialmente con relación a

los cambios térmicos correspondientes a los extremos inferior y superior de las distribuciones de temperatura máxima y mínima. Los cambios en la varianza de la distribución de temperatura podrían tener notables impactos en la frecuencia de los eventos extremos.

(7) ¿Cuál es el potencial de los resultados obtenidos en este trabajo?

Este estudio de doctorado puede contribuir a la comprensión de los procesos de cambio climático relacionados con la variabilidad estacional de la temperatura en el noreste de España. Este trabajo constituye uno de los primeros intentos de analizar las características espaciales y temporales de las variaciones de temperatura a escala subregional en la Península Ibérica. Teniendo en cuenta la escala espacial y temporal de los datos utilizados en este trabajo, este estudio contribuye al escaso número de estudios centrados en la variabilidad de la temperatura a escala regional en la Península Ibérica. Por otra parte, este trabajo aporta ideas sobre los posibles mecanismos y procesos físicos relacionados con la variabilidad espacial y temporal de la temperatura regional, incluyendo patrones de circulación atmosférica a gran escala.

Teniendo en cuenta que el área de estudio se caracteriza por una compleja topografía y geografía, que juegan un papel importante en las características climáticas a escala regional y local, los resultados a largo plazo sobre la variabilidad de la temperatura en esta región deben ser ubicados en un contexto climático más amplio, proporcionando información sobre la variabilidad de las temperaturas en el Mediterráneo y el suroeste de Europa.

7. CONCLUSIONES

La zona de estudio presenta varias características que la hacen interesante para el estudio de las tendencias térmicas. Estas características incluyen la altitud, la localización latitudinal, una topografía compleja, y la alta variabilidad espacial y temporal del clima. En consecuencia, existen grandes diferencias en la variabilidad de la temperatura a diferentes escalas espaciales y temporales. Debido a su diversidad, el área de estudio resulta idónea para evaluar la capacidad de los diferentes modelos climáticos regionales para reproducir las proyecciones de temperatura en el futuro. Frente a las constatadas evidencias globales, en general, existe una menor confianza en las estimaciones de cambio a escala regional. De hecho a escala regional se han llevado a cabo pocas estimaciones debido a la falta de datos de alta calidad a escala diaria. En el área de estudio, los cambios proyectados en la temperatura están dentro del rango de los cambios simulados por otros trabajos en el Mediterráneo y Europa occidental. Por lo tanto, los resultados de este trabajo representan un paso más en el conocimiento de las predicciones de temperatura en el futuro en la Península Ibérica. Los resultados complementan los estudios existentes sobre los cambios futuros en la Península Ibérica, incluyendo la evaluación de las proyecciones en los valores medios y extremos de temperatura durante el siglo XXI. Además, los resultados de las simulaciones para el futuro pueden contribuir a la mejora de la adaptación al cambio climático y a una mejor gestión de los eventos extremos, debido a que los cambios observados tendrán implicaciones importantes en la hidrología, ecología, la salud, y en la demanda y consumo de energía. Por ejemplo, el aumento de las temperaturas en verano proyectadas para finales de siglo, podría tener notables consecuencias hidrológicas y ambientales. Los impactos incluirían, entre otros, el aumento de los incendios forestales, una mayor severidad de las sequías, el incremento del consumo de energía, y menores producciones agrícolas. Por otra parte, el incremento puede

dar lugar a mayores índices de evaporación, con un incremento del transporte de agua a la atmósfera, induciendo cambios acelerados en el ciclo hidrológico sobre la región. En consecuencia, existe una amplia necesidad de comprender los procesos hidrológicos que pueden quedar alterados por el proceso de calentamiento, tales como la evaporación, la escorrentía superficial, la sequía y la disponibilidad de agua en su conjunto.

Para concluir, este estudio aporta novedades con relación a estudios anteriores que han examinado los cambios de temperatura y su variabilidad en la zona de estudio. En primer lugar, el estudio se ha basado en una base de datos larga, completa, de fiabilidad y con una elevada densidad espacial, que engloba los principales regímenes climáticos en el noreste de España (es decir, oceánico, mediterráneo y continental). Los estudios anteriores habían contemplado habitualmente un pequeño número de observatorios. En segundo lugar, este estudio puede proporcionar una visión más completa de la variabilidad a largo plazo a escalas temporales estacional y anual, contribuyendo a aportar proyecciones climáticas más precisas y robustas. En tercer lugar, la alta resolución espacial y temporal de los datos sugieren que los cambios proyectados en el futuro se deben tomar muy en consideración por parte de los gestores locales, poniendo de relieve la necesidad de adoptar política de adaptación en un futuro.

CHAPTER EIGHT

OUTLOOK

8. OUTLOOK

In this chapter, a further discussion of the limitations of this study and also areas of required future research is provided.

This PhD thesis contributes to an enhanced understanding of the regional climate variability for northeast Spain by addressing changes in seasonal and annual temperatures based a currently new compiled daily dataset. This dataset represents the more reliable, complete and homogenous instrumental dataset available for the region. A methodological improvement of the reconstruction and homogenization procedures is achieved through providing different measures to assess the role of homogenization on spatial and temporal consistency of daily temperature time series. These measures prove that available information from this dataset is particularly useful for different applications in the region. Over the last few years, further research has been conducted on testing different reconstruction and homogeneity techniques. Nonetheless, almost all of them have not provided any measure of dataset validation.

This work also makes advance in investigating the dynamical forcing behind temperature variations over the past centuries. As emphasized throughout this thesis there are many important aspects of recent present climate variability which need to be addressed further in future research. Due to the limitation of time, these important issues have not been addressed in this thesis. In the following paragraphs a few of them are listed and briefly discussed.

- The present work indicates that changes in the anomalous SLP can contribute to better understanding of interannual temperature variations in northeastern Spain. Features of anomalous seal level pressure (SLP) gave a reasonable physical explanation of the spatial differences in the role of the different atmospheric patterns on temperature in the study area. These physical processes can be a good indicator of air advection through land-sea interactions. Nonetheless, spatial patterns of temperature cannot be fully explained by changes in mean SLP, given that the study area is located in a region more vulnerable to climate change. In addition, differences in land surface characteristics such as vegetation canopy, surface albedo and orography can further influence the advection or/and vertical motions of atmospheric flows. This can lead to changes in surface heat exchanges with the atmosphere and in turn local disturbances in the dominant synoptic flows responsible for the interannual variability of temperature. Therefore, an assessment of the possible connection between temperature variations and the large-scale atmospheric circulation at different geopotential height levels as well as sea surface temperature (SST) fields is suggested to support the physical mechanisms noted at the ground level. The role of SST and its interaction with the land and atmosphere can significantly contribute to understanding temperature variations in the region. This is not surprising considering the fact that ocean and land masses are strongly coupled by fluxes of energy and mass. Surrounding water bodies could act as a regulator of thermal and flows interactions between land and closing waters. In addition, changes in the oceanic moisture fluxes can also drive changes in climate variability. This sounds important given that much of the strongest signals in temperature

across the region were found near the coast. Thus, further investigations are clearly needed to clarify reasons responsible for these spatial differences. A spatial and temporal classification of the main spatial modes of these circulation fields can give more insights into spatial and temporal signatures of temperature in the region. Variations in SST can be analyzed based on in situ measurements as well as, for the most recent years, satellite observations.

- This thesis suggests a feedback between temperature variations and soil moisture. This relationship showed large interseasonal changes, with more dependency during summer and spring seasons. However, a major challenge in exploring this dependency is the lack of dense records of these fields to explore differences in the regional response. In a complex region such as NE Spain, a resolution of approximately 2º latitude by 2º latitude of gridded data is still coarse to capture changes in soil moisture over space. The amount of soil deficit is expected to vary spatially over short distances, particularly with the high spatial variability of precipitation. Soil moisture near to the ground level is largely sensitive to vegetation canopy, topography and land use patterns. In addition, the regions experiences larger changes among wet and dry extremes. Taken together, in order to assess how soil moisture behaves in a seasonal timeframe for the study domain, a finer gridded dataset enhanced by intensive real world data resampled from a network with a reasonable spatial coverage of settings can markedly improve knowledge of this dependency and assess its spatial differences. In the same context, the connection between temperature and soil moisture across the region highlights the question whether there is a feedback between changes in precipitation and temperature variability. This

sounds critical in the study domain as precipitation is characterized by very high spatial and temporal variability in this topographically and climatologically complex region. With the new available daily temperature dataset, which spatially and temporarily overlaps with the already available dense precipitation network for the region (Vicente-Serrano et al., 2010), further work is still demanded to improve further the understanding of the way in which temperature variability is driven by precipitation variations. Although it is hard to directly attribute the observed trend in temperature to the evolution of precipitation in such area of complex topography as it is difficult to distinguish between the predictor and predictand variable in this association, it is still important to search for possible underlying relationship between temperature and precipitation variability. This dependency is still lacking and needs further investigation at a more regional and local scale. In the regard, the possible impact of droughts and wetnesses episodes can also be investigated. The Standardized Precipitation Index (SPI) and the recently developed Standardized Precipitation Evapotranspiration Index (SPEI) (Vicente Serrano et al., 2011c) can be employed to explore dependency between temperature variations and precipitation deficit at multiple time scales.

- As shown in this thesis, the East Atlantic (EA) atmospheric circulation is a very promising and valuable predictor of present climatic conditions in the study domain. However, little is known about the relationship between peaks of this mode and temperature variability in the region. The suggested role of the EA on temperature variability needs to be more explored as the underlying dynamics of this mode are not well covered in the region. In this regard, one promising

approach is to use the spectral analysis to quantify the extent to which daily temperature in the region is linked to daily variability of the EA values. Moreover, recalling the varied spatial response to this circulation pattern, this assessment could assess the impacts of changes in the action centers of this pattern at the daily scale on changes in the temperature stress across the region. A deeper insight of this configuration could be gained, for example, by investigating distinct extreme values and explaining their dynamical patterns. This analysis can also extend further to assess the influence of the combination of different dominant circulation modes (e.g., the NAO and EA) on temperature. In the dynamic climate system, there is often an interchangeable effect of circulation modes on temperature. Thus, such combination can provide a more reliable explanation of temperature variability in the region rather than relying on a single circulation mode.

- As shown in this thesis, the positive anomaly of maximum, minimum and mean temperatures in the region was considerably related to the rapid increase in the European anticyclones and the Atlantic blockings over the study domain in recent decades. Therefore, more research in this direction is needed. In particular, this feature motivates a future work to objectively classify weather types in the region. A daily catalogue of different weather types such as cyclone (C), anticyclone (A), and zonal and meridional weather types is needed for the region. This classification can help exploring possible influences of the main weather types on temperature variations in the region as it summarizes a wide variability of flows that can affect the region. Weather type variations are a major part explaining changes in the relationship between the large-scale

atmospheric circulation and climate in transitional regions in the mid latitudes. In a future research, the temporal variability of the large-scale atmospheric circulation patterns can be linked to temporal evolution of weather types frequencies.

- Assessment of temperature future changes in the region reveals that there are large differences in the ability of different RCMs to capture seasonal variations in the study domain. Determining sources of these variations is out of the scope of this thesis although it sounds important in climate studies. Therefore, future research should therefore try to distinguish the various sources of these biases. This can probably include sources of dynamic origin (e.g., changes in soil moisture and land cover) or those originating from climatic source (e.g., changes in climatic boundary). Also, developing new methods and approaches to account for the bias in the RCMs is mainly related to understand different sources of these errors.

- Apart from summer, all future simulations projected a decrease in the interannual variability of temperature means. In other words, the substantial projected increase in the mean temperature in the future does not correspond to an increase in temperature interannual variability across the region. This suggests assessing day to day future variability in the region relative to the present climate conditions. This kind of assessment would therefore not only be interesting, but it will allow defining changes in the central tendency of temperature series compared with standard deviation. Day to day variability can have further implications in various hydrological and biological applications as

there is, for example, daily biological temperature threshold beyond it the productivity of plants and forests may be influenced.

- This thesis gave much attention to assess future changes in temperature means and extremes across NE Spain. Nonetheless, the exact processes that explain these projected changes remain an open question. For this reason, it is still important to assess circulation and weather-type changes under enhanced GHG emission scenarios in the future. Also, future projections of SST should be taken into account in future research questions.

- The central Ebro valley is projected to exhibit a strong warming anomaly for the next few decades, which could significantly alter the hydrological cycle in this watershed. Therefore, it is of particular interest to look at the major environmental, ecological and hydrological threats that may correspond to such changes. This can possibly include frequency of floods and drought events, and acceleration of erosion and desertification.

- This thesis has exclusively focused on present and future climate variability across the northeastern portions of the Iberian Peninsula. However, this assessment should be performed in other regions of the peninsula, making the best use of the available dense network of temperature observatories for each region. This will give insights on the regional contrasts across the peninsula, which can exert different social, ecological and economical impacts from local to regional scale.

BIBLIOGRAPHY

REFERENCES

Abarca del Río, R., Mestre, O. (2006). Decadal to secular time scales variability in temperature measurements over France, Geophysical Research Letters, 33, L13705, DOI:10.1029/2006GL026019.

Abaurrea, J., Asin, J., Erdozain, O., Fernández, E. (2001). Climate variability analysis of temperature series in the Medium Ebro River Basin, In Detecting and Modeling Regional Climate Change edited by Brunet, M., Lopez, D., pp 109–118, Springer, New York.

Adamowski, K., Bougadis, J. (2003). Detection of trends in annual extreme rainfall, Hydrological Processes, 17, 3547-3560.

Adams, R.M., Brian, H. H., Stephanie, L., Neil, L. (1998). Effects of Global Climate Change on Agriculture: An Interpretative Review, Climate Research, 11 (1). 19-30.

Agresti, A. (1992). A survey of exact inference for contingency tables, Statistical Science, 7 (1). 131-153.

Aguilar, E., Auer, I., Brunet, M., Peterson, T.C., Weringa, J. (2003). Guidelines on climate metadata and homogenization. World Climate Programme Data and Monitoring WMO-TD No. 1186, World Meteorological Organization: Geneva, 51 pp.

Aguilar, E., Peterson, T.C., Obando, P.R., Frutos, R., Retana, J.A., Solera, M., Soley, J., Garcia, I.G., Araujo, R.M., Santos, A.R., Valle, V.E., Brunet, M., Aguilar, L., Alvarez, L., Bautista, M., Castanon, C., Herrera, L., Ruano, E., Sinay, J.J., Sanchez, E., Oviedo, G.I.H., Obed, F., Salgado, J.E., Vazquez, J.L., Baca, M., Gutierrez, M., Centella, C., Espinosa, J., Martinez, D., Olmedo, B., Espinoza, C.E.O., Nunez, R., Haylock, M., Benavides, H., Mayorga, R.(2005). Changes in precipitation and temperature extremes in Central America and northern South America, 1961-2003, Journal of Geophysical Research- Atmospheres, 110, D23107, DOI 10.1029/200.

Aguilar, E., Aziz Barry, A., Brunet, M., Ekang, L., Fernandes, A., Massoukina, M., Mbah, J., Mhanda, A., do Nascimento, D. J., Peterson, T. C., Thamba Umba, O., Tomou, M., Zhang, X. (2009). Changes in temperature and precipitation extremes in western central Africa, Guinea Conakry, and Zimbabwe, 1955-2006, Journal of Geophysical Research- Atmospheres, 114, D02115, DOI:10.1029/2008JD011010.

Ahrens, B. (2006). Distance in spatial interpolation of daily rain gauge data, Hydrology and Earth System Sciences, 10, 197–208.

Albregtsen, F., Maltby, P. (1981). Solar cycle variation of sunspot intensity, Solar Physics, 71, 269–283.

Alcamo, J., Kreileman, G.J.J., Leemans, R. (eds). (1996). Integrated scenarios of global change: results from the IMAGE 2.1 model. Spec Iss Global Environmental Change, 6(4),255–394.

Alexander, L.V., Zhang, X., Peterson, T.C., Caesar, J., Gleason, B., Tank, A.M.G.K., Haylock, M., Collins, D., Trewin, B., Rahimzadeh, F., Tagipour, A., Kumar, K.R., Revadekar, J., Griffiths, G., Vincent, L., Stephenson, D.B., Burn, J., Aguilar, E., Brunet, M., Taylor, M., New, M., Zhai, P., Rusticucci, M., Vazquez-Aguirre, J.L. (2006). Global observed changes in daily climate extremes of temperature and precipitation, Journal of Geophysical Research- Atmospheres, 111, D05109,

DOI: 10.1029/2005JD006290.

Alexandersson, H. (1986). A homogeneity test to precipitation data, Journal of Climatology, 6, 661-675.

Alfaro, E. J., Gershunov, A., Cayan, D. (2006). Prediction of summer maximum and minimum temperature over the central and western United States: The roles of soil moisture and sea surface temperature, Journal of Climate, 19, 1407–1421, DOI:10.1175/JCLI3665.1.

Allen, R.J., DeGaetano, A.T. (2001). Estimating missing daily temperature extremes using an optimized regression approach, International Journal of Climatology 21, 1305 –1319.

Asquith, W.H. (2003). Modeling of runoff-producing rainfall hyetographs in Texas using L-moment statistics: Austin, Texas, University of Texas at Austin, Ph.D. dissertation, 386 pp.

Auer, R., Böhm, A., Jurkovi, A., Orlik, R., Potzmann, W., Schöner, M., Ungersböck, M., Brunetti, T., Nanni, M., Maugeri, K., Briffa, P., Jones, D., Efthymiadis, O., Mestre, J.M., Moisselin, M., Begert, R., Brazdil, O., Bochnicek, T., Cegnar, M., Gaji-Čapka, K., Zaninovíc, E., Majstorovi, S., Szentimrey, S., Mercalli, L. (2005). A new instrumental precipitation dataset for the greater Alpine region for the period 1800–2002, International Journal of Climatology, 25, 139–166.

Baeryswil, P.A., Rebetez, M. (1997). Regionalization of precipitation in Switzerland by means of principal component analysis, Theoretical and Applied Climatology, 58, 31-41.

Balairon, L. (1997). El clima mediterraneo y sus caracter´ısticas en el contexto de la circulacion general atmosferica. In El Paisaje Mediterraneo a Traves del Espacio y del Tiempo. Implicaciones en la Desertificacion, Ibanez JJ, Valero B, Machado C (eds.). Geoforma Ediciones, Logrono, 131–160.

Barnett, V., Lewis, T. (1994). Outliers in statistical data. 3rd edition. John Wiley & Sons. Chichester. 584 pp.

Barnston, A.G., Livezey, R.E. (1987). Classification, seasonality and persistence of low-frequency atmospheric circulation patterns, Monthly Weather Review, 115, 1083–1126.

Barriopedro, D., Fischer, E.M., Luterbacher, J., Trigo, R.M., and Garcia-Herrera, R. (2011). The Hot Summer of 2010: Redrawing the Temperature Record Map of Europe, Science, 332, 220-224, DOI: 10.1126/science.1201224.

Barry, R.C., Chorley, R.J. (1987). Atmosphere, Weather and Climate, 5th ed. Routledge, New York, USA, 459pp.

Bartzokas, A, Metaxas, D.A., Ganas, I.S. (1994). Spatial and temporal sea-surface temperature covariances in the Mediterranean, International Journal of Climatology, 14, 201–213.

Batalla, R.J., Gómez, C.M., Kondolf, G.M. (2004). Reservoir-induced hydrological changes in the Ebro River basin (NE Spain), Journal of Hydrology, 290, 117–136.

Beer, J., Muschler, R., Kass, D., Somarriba, E. (1998). Shade management in coffee and cacao plantations, Agroforestry Systems, 38, 134–164.

Begert, M., Schlegel, T., Kirchhofer, W. (2005). Homogeneous temperature and precipitation series of Switzerland for 1864 to 2000, International Journal of Climatology, 25, 65-80.

9. REFERENCES

Begueria-Portugues, S., Vicente Serrano, S.M. (2006). Mapping the hazard of extreme rainfall by peaks-over-threshold extreme value analysis and spatial regression techniques, Journal of Applied Meteorology, 45, 108–124.

Bejaran, R.A., Camilloni, I.A. (2003). Objective method for classifying air masses: an application to the analysis of Buenos Aires (Argentina) urban heat island intensity, Theoretical and Applied Climatology, 74, 93–103.

Bejarano, M.D., Marchamalo, M., García de Jalón, D., González del Tánago, M. (2010). Flow regime patterns and their controlling factors in the Ebro basin (Spain), Journal of Hydrology, 385, 323–335.

Beniston, M., Rebetez, M., Giorgi, F., Marinucci, M. R. (1994). An analysis of regional climate change in Switzerland, Theoretical and Applied Climatology, 49, 135–159.

Beniston, M., Diaz, H. F., Bradley, R. S. (1997). Climatic change at high elevation sites: an Overview, Climatic Change, 36, 233–251.

Beniston, M., Stephenson, D.B. (2004). Extreme climatic events and their evolution under changing climatic conditions, Global and Planetary Change, 1 – 9.

Beniston, M. (2004). The 2003 heat wave in Europe. A shape of things to come? Geophysical Research Letters, 31, L02022.

Beniston, M., Stephenson, D.B., Christensen, O.B., Ferro, C.A.T., Frei, C., Goyette, S., Halsnaes, K., Holt, T., Jylha, K., Koffi, B., Palutikof, J., Scholl, R., Semmler, T., Woth, K. (2007). Future extreme events in European climate: an exploration of regional climate model projections, Climatic Change, 81, 71–95.

Beniston, M., Goyette, S. (2007). Changes in variability and persistence of climate in Switzerland, exploring 20th century observations and 21st century simulations, Global and Planetary Change, 57, 1-20.

Beniston, M. (2009). Decadal-scale changes in the tails of probability distribution functions of climate variables in Switzerland, International Journal of Climatology, 29, 1362-1368.

Beranova, R., Huth, R. (2008). Time variations of the effects of circulation variability modes on European temperature and precipitation in winter, International Journal of Climatology, 28, 139-158.

Bermejo, M., Ancell, R. (2009). Observed changes in extreme temperatures over Spain during 1957-2002 using Weather Types, Revista de Climatologia, 9, 45-61.

Black, E., Sutton, R. (2006). The influence of oceanic conditions on the hot European summer of 2003, Climate Dynamics, 28, 53–66.

Blackburn, M., Hoskins, B.J. (2001). The UK-record breaking wet autumn 2000., pp:38-40, in UK Universities Global Atmospheric Modeling Programme, UGAMP Newsletter 24, Meteorological Department, University of Reading, UK.

Boé, J., Terray, L. (2008). Uncertainties in summer evapotranspiration changes over Europe and implications for regional climate change, Geophysical Research Letters, 35, L05702, DOI: 10.1029/2007GL032417.

Bohm, R., Auer, I., Brunetti, M., Maugeri, M., Nanni, T., Schoner, W. (2001). Regional temperature variability in the European Alps: 1760-1998 from homogenized instrumental time series, International Journal of Climatology, 21, 1779-1801.

Bolle, H.I. (2003). Mediterranean Climate: Variability and Trends, Springer Verlag, Berlin, 372pp.

Bonell, M., Summer, G. (1992). Autumn and winter daily precipitation areas in Wales, 1982–1983 to 1986–1987, International Journal of Climatology, 12, 77–102.

9. REFERENCES

Bordi, I., Fraedrich, K., Petitta, M., Sutera, A. (2006). Large-scale assessment of drought variability based on NCEP/NCAR and ERA-40 re-analyses, Water Resources Management, 20, 899–915.

Bordi, I., Sutera, A. (2007). Drought monitoring and forecasting at large scale, **In:** Methods and Tools for Drought Analysis and Management, Series Water Science and Technology Library, edited by: Rossi, G., Vega, T., and Bonaccorso, B., Springer Verlag, vol. 62, 490 pp.

Bouza-Deaño, R., Ternero-Rodríguez, M., Fernández-Espinosa, A.J. (2008). Trend study and assessment of surface water quality in the Ebro River (Spain), Journal of Hydrology, 361, 227– 239.

Box, G., Jenkins, G. (1970). Time series analysis: Forecasting and control, San Francisco, CA, Holden-Day, 575pp.

Brands, S., Herrera, S., San-Martín, S., Gutiérrez, J.M. (2011a). Validation of the ENSEMBLES global climate models over southwestern Europe using probability density functions, from a downscaling perspective, Climate Research, 48, 145-161.

Brands, S., Taboada, J.J., Cofiño, A.S., Sauter, T., Schneider, C. (2011b). Statistical downscaling of daily temperatures in the NW Iberian Peninsula from global climate models: validation and future scenarios, Climate Research, 48,163–176.

Breiling, M., Charamza, P. (1999). The impact of global warming on winter tourism and skiing: a regionalized model for Austrian snow conditions, Regional Environmental Change, Vol. 1, No. 1, 4-14.

Brown, S.J., Caesar J., Ferro, C.A.T. (2008). Global changes in extreme daily temperature since 1950, Journal of Geophysical Research- Atmospheres, 113, D05115, DOI: 10.1029/2006JD008091.

Brunet, M., Aguilar, E., Saldie, O., Lopez, D. and Sigro, J. (2001). The variation and trends of the surface air temperature in the Northeastern of Spain from middle nineteenth century onwards, In Brunet, M. and Lopez, D. (Eds.). Detecting and Modelling Regional Climate Change and Associated Impacts, Springer, Berlín-Heidelberg-New York, 81-93

Brunet, M., Sigro, J., Saldie, O., Aguilar, E., Jones, P.D., Moberg, A., Walther, A., Lopez, D. (2005). Spatial Patterns of Long-term Spanish Temperature Change, Geophysical Research Abstracts, Vol. 7, 04007.

Brunet M., Saldie, O., Jones, P., Sigro, J., Aguilar, E., Moberg, A., Lister, D., Walther, A., Lopez, D., Almarza, C. (2006). The development of a new dataset of Spanish daily adjusted temperature series SDATS 1850-2003, International Journal of Climatology, 25, 1777-1802.

Brunet, M., Jones, P.D., Sigro, J., Saladie, O., Aguilar, E., Moberg, A., Della-Marta, P.M., Lister, D., Walther, A., López, D., (2007a). Temporal and spatial temperature variability and change over Spain during 1850-2005, Journal of Geophysical Research- Atmospheres, 112, D12117, DOI:10.1029/2006JD008249.

Brunet, M., Sigro, J., Jones, P.D., Saladie, O., Aguilar, E., Moberg, A., Walter, A. (2007b). Long- term changes in extreme temperatures and precipitation in Spain, Contribution to Science, 3, 331-342.

Brunetti, M, Buffoni, L, Maugeri, M, Nanni, T. (2000). Trends of minimum and maximum daily temperatures in Italy from 1865 to 1996, Theoretical and Applied Climatology, 66, 49–60.

Brunetti, M, Buffoni, L, Mangianti, F, Maugeri, M, Nanni, T. (2004). Temperature, precipitation and extreme events during the last century in Italy, Global and Planetary Change, 40, 141–149.

Brunetti, M., Maugeri, M., Monti, F., Nanni, T. (2006). Temperature and precipitation variability in Italy in the last two centuries from homogenized instrumental time series, International Journal of Climatology, 26, 345–381.

Bueh, C., Nakamura, H. (2007). Scandinavian pattern and its climatic impact, Quarterly Journal of the Royal Meteorological Society, 133, 2117–2131, DOI: 10.1002/qj.173.

Burgueño, A., Lana, X., Serra, C. (2002). Significant hot and cold events at the Fabra Observatory, Barcelona (NE Spain), Theoretical and Applied Climatology, 71, 141–156.

Burn, D.H., Cunderlik, J.M. (2004). Hydrological trends and variability in the Liard River basin, Hydrological Sciences, 49 (1). 53–67.

Caesar, J., Alexander, L., Vose, R. (2006). Large-scale changes in observed daily maximum and minimum temperatures: Creation and analysis of a new gridded data set, Journal of Geophysical Research- Atmospheres, 111, D05101, DOI: 10.1029/2005JD006280.

Camiz, S., Pillar, V.D. (2007). Comparison of single and complete linkage clustering with the hierarchical factor classification of variables, Community Ecology, 8(1). 25-30.

Campisano, A, Cancelliere A, Rossi, G. (2002). Una procedura semi-automatica per il controllo di qualità dei dati pluviometrici e termometrici **In:** Atti del XXVIII Convegno di Idraulica e Costruzioni idrauliche. Potenza 16–19 settembre 2, 415 –424.

Capel-Molina, J.J. (1981). Los climas de España. Oikos Tau, Barcelona.

Capilla, C. (2008). Time Series Analysis And Identification Of Trends In A Mediterranean Urban Area. Global and Planetary Change, 63, 275-261. D.O.I.:10.1016/j.gloplacha.2007.10.001

Cassou, C., Terray, L. (2005). Tropical Atlantic Influence on European Heat waves, Journal of Climate, 18, 2805-2811.

Caussinus, H., Mestre, O. (2004). Detection and correction of artificial shifts in climate series, Applied Statistics, 53, 405–425.

Chen, P. (2001). Thermally forced stationary waves in a quasigeostrophic system, Journal of Atmospheric Sciences, 58, 1585–1594.

Chen, B.D., Chao, W.C. Liu, X.D. (2003). Enhanced climatic warming in the Tibetan Plateau due to doubling CO2, a model study, Climate Dynamics, 20,401–413.

Choi, G., Collins, D., Ren , Trewin, B., Baldi, M., Fukuda, Y., Afzaal, M., Pianmana, T., Gomboluudev, P., Huong, P., Thi ,T., Lias, N., Kwon, W., Boo, K., Cha, Y., Zhou, Y. (2009). Changes in means and extreme events of temperature and precipitation in the Asia-Pacific Network region, 1955-2007, International Journal of Climatology, 29(13). 1906-1925.

Christensen, J.H., Carter, T.R., Rummukainen, M. (2007). Evaluating the performance and utility of regional climate models: the PRUDENCE project, Climatic Change, 81, Supplement 1, 1-6, DOI: 10.1007/s10584-006-9211-6.

Christopher, S., Gerd, J. (2003). Hot news from summer 2003, Nature, 432, 559-560.

Chust, G., Borja, A., Caballero A., Irigoien, X., Saénz, J., Fontán, A., Moncho, R., Marcos, M., Liria, P., Hidalgo, J., Valle M., Valencia, V. (2011) Climate Change

impacts on the coastal and pelagic environments in the southeastern Bay of Biscay: a review, Climate Research, 48, 307-332

Ciais, P. H., Reichstein, M., Viovy, N., Granier, A., Ogeé, J., Allard, V., Aubinet, M., Buchmann, N., Bernhofer, C., Carrara, A., Chevallier, F., De Noblet, N., Friend, A., Friedlingstein, P., Grünwald, T., Heinesch, B., Keronen, P., Knohl, A., Krinner, G., Loustau, D., Manca, G., Matteucci, G., Miglietta, F., Ourcival, J.M., Papale, D., Pilegaard, K., Rambal, S., Seufert, G., Soussana, J.F., Sanz, M.J., Schulze, E.D., Vesala, T., Valentini, R. (2005). Europe-wide reduction in primary productivity caused by the heat and drought in 2003, Nature, DOI: 10.1038/nature03972.

Clark WAV, Hosking PL. 1986. Statistical Methods for Geographers. New York. John Wiley & Sons.528pp.

Colman, A. (1997). Prediction of summer central England temperature from preceding North Atlantic winter sea surface temperature, International Journal of Climatology, 17, 1285-1300.

Colman, A., Davey, M. (1999). Prediction of summer temperature, rain-fall and pressure in Europe from preceding winter North Atlantic ocean temperature, International Journal of Climatology, 19 , 513 – 536.

Coppola, E., Giorgi, F. (2010). An assessment of temperature and precipitation change projections over Italy from recent global and regional climate model simulations, International Journal of Climatology, 30, 11-32.

Coronato, F., Bisigato, A. (1998). A temperature pattern classification in Patagonia, International Journal of Climatology, 18 (7). 765-773.

Corte-Real, J, Zhang, Z, Wang, X. (1995). Large-scale circulation regimes and surface climatic anomalies over the Mediterranean. Int J Climatol 15, 1135–1150.

Costa, A. C., Soares, A. (2006). Identification of inhomogeneities in precipitation time series using SUR models and the Ellipse test. **In:** Caetano, M. Painho, M. (eds.). Proceedings of Accuracy 2006 - 7th International Symposium on Spatial Accuracy Assessment in Natural Resources and Environmental Sciences, Instituto Geográfico Português, 419-428

Costa, A. C. Soares, A. (2009a). Trends in extreme precipitation indices derived from a daily rainfall database for the South of Portugal, International Journal of Climatology, 29, 1956-1975.

Costa, A.C., Soares, A. (2009b). Homogenization of climate data: review and new perspectives using Geostatistics, Mathematical Geosciences, 413, 291–305.

Cox, D.R., Stuart, A. (1955). Some quick sign tests for trend in location and dispersion, Biometrika, 42, 80–95.

Cressie, N.A.C.(1993). Statistics for spatial data. Revised edition. John Wiley and Sons. New York. 900pp.

Dai, A., Del Genio., A.D., Fung, I.Y. (1997). Maximum and minimum temperature trends for the globe, Nature, 386, 665-667.

Dai, A., Trenberth, K.E., Karl, T.R. (1999). Effects of clouds, soil moisture, precipitation and water vapor on diurnal temperature range, Journal of Climate, 12, 2451–2473.

De Castro, M. J. Martin-Vide, M. Brunet, M., (2005). The climate of Spain: Past, present and scenarios for the 21st century Publicaciones Ministerio de Medio Ambiente 207 - 218 pp.

De Luis, M., Raventos, J. Gonzales-Hidalgo, J.C., Sanchez, J. R & Cortina, J. (2000)

Spatial analysis of rainfall trends in the region of Valencia (East Spain), International Journal of Climatology, 20: 1451-1469.

De Luis, M., Vicente Serrano, S.M., González Hidalgo, J.C., Raventós, J. (2003). Aplicación de las Tablas de Contingencia (Crosstab análisis) al análisis espacial de tendencias climáticas. Cuadernos de Investigación Geográfica 29, 23-34.

De Luis, M.., González-Hidalgo, J.C., Longares, L.A., Stepanek, P. (2009). Seasonal precipitation trends in the Mediterranean Iberian Peninsula in second half of 20th century International, International Journal of Climatology, 29, 1312-1323.

DeGaetano, A.T. (1989). A climatic classification of plant hardiness in the United States and Canada and the effects of temperature fluctuations on the hardiness of woody ornamentals, Ph.D. Dissertation, Rutgers University, New Brunswick, NJ, pp. 295.

DeGaetano, A. T. (2001). Spatial grouping of United States climates stations using a hybrid clustering approach, International Journal of Climatology, 21, 791–807.

Della-Marta PM, Wanner H. (2006). A method of homogenizing the extremes and mean of daily temperature measurements, Journal of Climate 19, 4179–4197.

Della-Marta, P. M., Haylock, M.R., Luterbacher, J. Wanner, H. (2007a). Doubled length of western European summer heat waves since 1880, Journal of Geophysical Research- Atmospheres, 112, D15103, DOI: 10.1029/2007JD008510.

Della-Marta, P.M., Luterbacher, J., von Weissenfluh, H., Xoplaki, E., Brunet, M., Wanner, H. (2007b). Summer heat waves over western Europe 1880–2003, their relationship to large-scale forcings and predictability, Climate Dynamics, 29, 251–275.

Déqué, M., Marquet, P., Jones, R.G. (1998). Simulation of climate change over Europe using a global variable resolution general climate model, Climate Dynamics, 14, 173–189.

Deque, M., Jones, R.G., Wild, M., Giorgi, F., Christensen, J.C., Hassell, D.C., Vidale, P.L., Rockel, B., Jacob, D., Kjellstrom, E., de Castro, M., Kucharski, F., van den Hurk, B. (2005). Global high resolution versus Limited Area Model climate change projections over Europe: quantifying confidence level from PRUDENCE results, Climate Dynamics, 25, 6, 653-670.

Diaz, H.F., Murnane, R.J. (Eds.) (2008). Climate Extremes and Society. Cambridge University Press, Cambridge (UK), 340 pp.

Díaz, J., Garcia, R., Velázquez de Castro, F., Hernandez, E., López, C., Otero, A. (2002). Effects of extremely hot days on people older than 65 years in Seville (Spain) from 1986 to 1997, International Journal of Biometeorology, 46,145–149.

Díaz, J., García-Herrera, R., Trigo, R.M., Linares, C., Valente, M.A., De Miguel, J.M., Hernández, E. (2006). The impact of summer 2003 heat wave in Iberia: how should we measure it? International Journal of Biometeorology, 50,159–166.

Diffenbaugh, N. S., Pal, J.S., Trapp, R.S., Giorgi, F. (2005). Fine-scale processes regulate the response of extreme events to global climate change, Proceedings of National Academic Science, U.S.A., 102, 15,774–15,778, DOI:10.1073/pnas.0506042102.

Dillon, W. R., Goldstein, M. (1984). Multivariate Analysis: Methods and Applications, New York, Wiley, 587pp.

Domonkos, P. (2001). Temporal accumulations of extreme daily mean temperature

anomalies, Theoretical and Applied Climatology, 68, 17–32.

Douglas, E.M., Vogel, R.M., Kroll, C.N. (2000). Trends in floods and low flows in the United States: impact of spatial correlation, Journal of Hydrology, 240, 90-105.

Douville, H. (2003). Assessing the Influence of Soil Moisture on Seasonal Climate Variability with AGCMs, Journal of Hydrometeorology, 4, 1044-1066.

Ducré-Robitaille, J.F., Vincent, L.A., Boulet, G. (2003). Comparison of techniques for detection of discontinuities in temperature series, International Journal of Climatology 23, 1087-1101.

Dunne, J. A., Harte, J., Taylor, K. J. (2003). Subalpine meadow flowering phenology responses to climate change: integrating experimental and gradient methods, Ecological Monogrphs, 73, 69–86.

Durre, I., Wallace, J., Lettenmaier, D. (2000). Dependence of extreme daily maximum temperatures on antecedent soil moisture in the contiguous United States during summer, Journal of Climate, 13, 2641–2651, DOI: 10.1175/ 1520-0442.

Easterling, D.R., Peterson, T.C. (1995). A new method of detecting undocumented discontinuities in climatological time series, International Journal of Climatology 15, 369-377.

Easterling, D.R., Horton, B., Jones, P.D., Peterson, T.C., Karl, R.R., Parker, D.E., Salinger, M.J., Razuvayev, V., Plummer, N., Jamason, P., Folland, C.K. (1997) Maximum and minimum temperature trends for the globe, Science, 277, 364-367.

Easterling, D.R., Meehl, G.A., Parmesan, C., Changnon, S.A., Karl, T.R., Mearns, L.O. (2000). Climate extremes: observations, modeling, and impacts, Science, 289, 2068-2074.

Eischeid, J.K., Baker, C.B., Karl, T., Diaz, H.F. (1995). The quality control of long-term climatological data using objective data analysis, Journal of Applied Meteorology, 34, 2787-2795.

Eischeid, J.K., Pasteris, P.A., Diaz, H.F., Plantico, M.S., Lott, N.J. (2000). Creating a serially complete national daily time series of temperature and precipitation for the western United States, Journal of Applied Meteorology, 39, 1580–1591.

Ek, M.B., Holtslag, A.A.M. (2003). Influence of soil moisture on boundary-layer cloud development, Journal of Hydrometeorology, 5, 86–99.

El Kenawy, A., López-Moreno, J. I., Vicente-Serrano, S.M. (2012). Trend and variability of surface air temperature in northeastern Spain (1920–2006): linkage to atmospheric circulation, Atmospheric Research, 106, 159-180.

Emori, S., Brown, S.J. (2005). Dynamic and thermodynamic changes in mean and extreme precipitation under changed climate, Geophysical Research Letters, 32, L17706, doi:10.1029/2005GL023272.

Errasti, I., Ezcurra, A., Sáenz, J., Ibarra-Berastegi, G. (2011). Validation of IPCC AR4 models over the Iberian Peninsula, Theoretical and Applied Climatology, 103, 1-2, 61-79, DOI: 10.1007/s00704-010-0282-y.

Esteban, P., Martin-Vide, J., Mases, M. (2006). Daily atmospheric circulation catalogue for Western Europe using multivariate techniques, International Journal of Climatology, 26, 1501–1515.

Esteban-Parra, M. J., Rodrigo, F.S., Castro-Díez, Y. (1995). Temperature trends and change points in the Northern Spanish Plateau during the last 100 years, International Journal of Climatology, 15, 1031-1042.

Esteban-Parra, M. J., Pozo-Vázquez, D., Rodrigo, F. S., Castro-Díez, Y. (2003). Temperature and Precipitation Variability and Trends in Northern Spain in the Context of the Iberian Peninsula Climate, **In** Bolle, H. J. (ed.). Mediterranean Climate Variability and Trends, Springer, Berlin, pp. 259–276.

Everitt, B.S., Dunn, G. (1991). Applied Multivariate Data Analysis, Edward Arnold, London, 342pp.

Feng, S., Hu, Q., Qian, Q. (2004). Quality control of daily meteorological data in China 1951-2000: a new dataset, International Journal of Climatology, 24, 853-870.

Fang, X.Q., Wang, A.Y., Fong, S.K., Lin, W.S., Liu, J. (2008). Changes of reanalysis-derived Northern Hemisphere summer warm extreme indices during 1948–2006 and links with climate variability, Global and Planetary Change, 63, 67–78.

Fernandez-Mills, G., Lana, X., Serra, C. (1994). Catalonian precipitation patterns: principal component analysis and automated regionalization, Theoretical and Applied Climatology, 49, 201–212.

Ferro, C. A. T., Hannachi, A., Stephenson, D.B. (2005). Simple nonparametric techniques for exploring changing probability distributions of weather, Journal of Climate, 18, 4344–4354.

Fischer, E. M., Seneviratne, S.I., Luthi, D., Schar, C. (2007). Contribution of land-atmosphere coupling to recent European summer heat waves, Geophysical Research Letters, 34, L06707, DOI: 10.1029/2006GL029068.

Folland, C.K., Parker, D.E. (1995). Correction of instrumental biases in historical sea surface temperature data. Quarterly Journal of the Royal Meteorological Society 121, 319-367.

Folland, C. K., Karl, T. P., Christy, J. R., Clarke, R. A., Gruza, G. V., Jouzel, J., Mann, M. E., Oerlemans, J., Salinger, M. J., and Wang, S. W. (2001). Observed climate variability and change, **In**: Chapter 2 of climate change 2001; the scientific basis, Contribution of Working Group I to the Third Assessment Report of the Intergovernmental Panel on Climate Change (IPCC), edited by: Houghton, J. T., Ding, Y., Griggs, D. J., Noguer, M., van der Linden, P. J., and Xiaoxu, D., Cambridge University Press, Cambridge, 99–181.

Frei, C., Schar, C. (2001). Detection probability of trends in rare events: Theory and application to heavy precipitations in the Alpine region, Journal of Climate*,* 14, 1568-1584.

Font-Tullot, I., 1983. Climatología de España y Portugal. Sección de Publicaciones del Instituto Nacional de Meteorología, Madrid. 422pp.

Frich, P., Alexander, L.V., Della-Marta, P., Gleason, B., Haylock, M., Klein Tank, A.M.G., Peterson, T. (2002). Observed coherent changes in climatic extremes during the second half of the twentieth century, Climate Research, 19, 193-212.

Fyfe, J.C, Flato, G.M. (1999). Enhanced climate change and its detection over the rocky mountains, Journal of Climate, 12, 230–243.

Gaffen, D.J., Ross, R.J. (1999). Climatology and trends of U.S. surface humidity and temperature, Journal of Climate 12 (3). 811–828.

Gao, X., Pal, J.S., Giorgi, F. (2006). Projected changes in mean and extreme precipitation over the Mediterranean region from high resolution double nested RCM simulations, Geophysical Research Letters, 33,L03706.

García-Herrera, R., Díaz, J., Trigo, R. M., Hernández, E. (2005). Extreme summer temperatures in Iberia: health impacts and associated synoptic conditions, Annales Geophysics, 23, 239-251.

Ghil, M., Allen, M. R., Dettinger, M. D., Ide, K., Kondrashov, D., Mann, M. E., Robertson, A. W., Saunders, A., Tian, Y., Varadi, F., Yiou, P. (2002). Advanced spectral methods for climatic time series, Review of Geophysics, 40(1), 1003 41pp, DOI: 10.1029/2000GR000092.

Gimeno, L., Trigo, R.M., Gómez-Gesteira, M. (2011). Regional climate change in the NW Iberian Peninsula, Climate Research, 48, 105-108.

Giorgi, F., Marinucci, M.R. (1996). An investigation of the sensitivity of simulated precipitation to model resolution and its implications for climate studies, Monthly Weather Review, 124, 148-166.

Giorgi, F., Hurrel, J.W., Marinucci, M.R., Beniston, M. (1997). Elevation dependency of the surface climate change signal: a model study, Journal of Climate, 10, 288–296.

Giorgi, F., Mearns, L.O. (1999). Regional climate modelling revisited. An introduction to the special issue, Journal of Geophysical Research- Atmospheres, 104, 6335-6352.

Giorgi, F., Bi, X., Pal, J. (2004). Mean, interannual variability and trends in a regional climate change experiment over Europe. II. Climate change scenarios (2071–2100). Climate Dynamics, 23, 839-858.

Giorgi, F., Bi, X. (2005). Regional changes in surface climate interannual variability for the 21st century from ensembles of global model simulations, Geophysical Research Letters, 32, L13701, DOI:10.1029/2005GL023002.

Giorgi, F. (2006). Climate change hot-spots, Geophysical Research Letters, 33, DOI: 10.1029/2006GL025734.

Glahn, H.R., Lowry, D.A. (1972). The use of model output statistics MOS in objective weather forecasting, Journal of Applied Meteorology 11, 1203–1211.

Gleason B. (2002). Global daily climatology network, VI.0. National Climatic Data Center: Asheville.

Gokturk, O.M., Bozkurt, D., Sen, O.L., Karaca, M. (2008). Quality control and homogeneity of Turkish precipitation data, Hydrological Processes, 22, 3210–3218.

Gong, X., Richman, M.B. (1995). On the application of cluster analysis to growing season precipitation data in North America east of the Rockies, Journal of Climate, 8, 897–931.

González-Aparicio, I., Hidalgo, J. (2011). Dynamically based future daily and seasonal temperature scenarios analysis for the northern Iberian Peninsula, International Journal of Climatology, DOI: 10.1002/joc.2397.

González-Hidalgo, J.C., De Luis, M., Raventós, J., Sánchez, J.R. (2003). Daily rainfall trend in the Valencia Region of Spain, Theoretical and Applied Climatology 75, 117–130.

González-Hidalgo, J.C., De Luis, M., Vicente Serrano, S.M., Saz, M.A., Štěpánek, P., Raventós, J., Cuadrat, J.M., Creus, J.M., Ferraz, J.A. (2004). Monthly rainfall data base for Mediterranean Coast of Spain: reconstruction and quality control World Meteorological Organization: TD No 1236, Geneve. 105 –116.

González-Hidalgo, J.C., Lopez-Bustins, J.A., Stepanek, P., Martin-Vide, J., de Luis, M. (2009). Monthly precipitation trends on the Mediterranean façade of the Iberian Peninsula during the second half of the 20th century (1951-2000), International Journal of Climatology, 29(10). 1415-1429.

Gonzalez-Hidalgo, J.C., Brunetti, M., de Luis, M. (2010). Precipitation trends in

Spanish hydrological divisions, 1946–2005, Climate Research, 43, 215–228.

Gonzalez-Rouca, J.F., Jiménez, J.L., Quesada, V., Valero, F. (2001). Quality control and homogeneity of precipitation data in the Southwest of Europe, Journal of Climate, 14(5). 964-978.

Greenwood, J.A., Landweher, J.M., Natales, N.C. (1979). Probability weighted moments: definition and relation to parameters of several distributions expressable in inverse form, Water Resources Research, 15, 1049–1054.

Guttman, N.B. (1993). The use of L-Moments in the determination of regional precipitation climates, Journal of Climatology, 6, 2309–2325.

Guttman, N.B., Hosking, J.R.M., Wallis, J.R. (1993). Regional precipitation quantile values for the continental United States computed from L-Moments, Journal of Climatology, 6, 2326–2340.

Hamed, K.H. (2008). Trend detection in hydrologic data: The Mann-Kendall trend test under the scaling hypothesis, Journal of Hydrology, 349, 350-363.

Hanemann, M., Labandeira, X., Loureiro, M.L. (2011). Climate change, energy and social preferences on policies: exploratory evidence for Spain, Climate Research, 48, 343–348.

Hansen, J.E., Lacis, A.A. (1990). Sun and dust versus greenhouse gases: An assessment of their relative roles in global climate change, Nature, 346, 713-719, DOI:10.1038/346713a0.

Hanssen-Bauer, I., Achberger, C., Benestad, R.E., Chen, D., Førland, E.J. (2005). Statistical downscaling of climate scenarios over Scandinavia: A review, Climate Research, 29 (3), 255-268.

Harvey, D.I., Mills, T.C., (2003). Modeling trends in central England temperatures. Journal of Forecasting, 22, 35–47.

Hawkins, D. M. (1977). Comments on A new statistic for testing suspected outliers. Communications in Statististics, A 6, 435-8.

Haylock, M., Nicholls, N. (2000). Trends in extreme rainfall indices for an updated high quality data set for Australia, 1910–1998, International Journal of Climatology, 20, 1533–1541.

Haylock, M.R., Cawley, G.C., Harpham, C., Wilby, R.L., Goodess, C.M. (2006) Downscaling heavy precipitation over the United Kingdom: a comparison of dynamical and statistical methods and their future scenarios, International Journal of Climatology, 26, 1397–1415.

Haylock, M.R., Hofstra, N., Klein Tank, A.M., Klok, E.J., Jones, P.D., New, M. (2008). A European daily high-resolution gridded data set of surface temperature and precipitation for 1950–2006, Journal of Geophysical Research- Atmospheres, 113, D20119, DOI: 10.1029/2008JD010201.

Hegerl, G.C., Zwiers, F. W., Braconnot, P., Gillett, N.P., Luo, Y., Marengo Orsini, J.A., Nicholls, N., Penner, J.E., Stott,P. A. (2007). Understanding and Attributing Climate Change. **In:** Climate Change 2007, The Physical Science Basis. Contribution of Working Group I to the Fourth Assessment Report of the Intergovernmental Panel on Climate Change [Solomon, S., D. Qin, M. Manning, Z. Chen, M. Marquis, K.B. Averyt, M. Tignor, Miller, H.L. (eds.).

Hellman, J. (2002) The effect of an environmental change on mobile butterfly larvae and the nutritional quality of their hosts, Journal of Animal Ecology 71, 925-936.

Herrera, S., Gutiérrez, J.M., Ancell, R., Pons, M.R., Frías, M.D., Fernández, J. (2012).

Development and analysis of a 50–year high–resolution daily gridded precipitation dataset over Spain (Spain02), International journal of Climatology, International Journal of Climatology, 32 (1), 74–85.

Hertig, E., Seubert, S., Jacobiet, J. (2010). Temperature extremes in the Mediterranean area: trends in the past and assessments for the future, Natural Hazards and Earth System Sciences, 10, 2039–2050.

Hewitt, C.D., Griggs, D.J. (2004). Ensemble-based predictions of climate changes and their impacts, EOS, Transactions American Geophysical Union, 85, DOI: 10.1029/2004EO520005.

Hofstra, N., Haylock, M., New, M., Jones, P., Frei, C. (2008). The comparison of six methods for the interpolation of daily European climate data, Journal of Geophysical Research- Atmospheres, 113, D21110, DOI: 10.1029/2008JD010100.

Hofstra, N., Haylock, M., New, M., Jones, P. (2009). Testing E-OBS European high-resolution gridded dataset of daily precipitation and surface temperature, Journal of Geophysical Research- Atmospheres, 114, D21101, DOI: 10.1029/2009JD011799.

Hofstra, N., New, M., McSweeney, C. (2010). The influence of interpolation and station network density on the distributions and trends of climate variables in gridded daily dataset, Climate Dynamics, 35:5, 841-858.

Holt, T. (1999). A classification of ambient climatic conditions during extreme surge events off Western Europe, International Journal of Climatology, 19, 725–744.

Horton, B. (1995). The geographical distribution of changes in maximum and minimum temperatures, Atmospheric Research, 37, 101–117.

Hosking, J.R.M., Wallis, J.R. (1997). Regional frequency analysis: an approach based on L-moments. Cambridge University Press, Cambridge, U.K, 224pp.

Houghton, J.T., Ding, Y., Griggs, D.J., Noguer, M., Van der Liden, P.J., Dai, X., Maskell, K & Lohnson, C.A. (2001). Climate change 2001, The Scientific Basis. Cambridge University Press. Cambridge, 881 pp.

Huang, J., Van den Dool, H., Georgakakos, K. (1996). Analysis of model calculated soil moisture over the United States (1931–1993) and applications to long-range temperature forecasts, Journal of Climate, 9, 1350–1362.

Hubbard, K.G., Goddard S, Sorensen WD, Wells N, Osugi TT. (2005). Performance of quality assurance procedures for an applied climate information system, Journal of Atmospheric and Oceanic Technology, 22(1), 105-112.

Hubbard, K.G., You, J. (2005). Sensitivity Analysis of Quality Assurance Using the Spatial Regression Approach: A Case Study of the Maximum/Minimum Air Temperature, Journal of Atmospheric and Oceanic Technology, 22(10), 1520-1530.

Hubbard, K.G. (2001). Multiple station quality control procedures in automated weather stations for applications in agriculture and water resources management, AGM-3 WMO/TD No. 1074. 248pp.

Hubbard, K.G., You, J. (2005). Sensitivity Analysis of Quality Assurance Using the Spatial Regression Approach: A Case Study of the Maximum/Minimum Air Temperature, Journal of Atmospheric and Oceanic Technology, 22(10). 1520-1530.

Hulme, M., Sheard, N. (1999). Escenarios de Cambio Climático para la Península Iberica. Climatic Research Unit- University of East Anglia, Norwich, UK. 6 pp.

Hurrell, J.W. (1995). Decadal trends in the North Atlantic Oscillation: regional temperatures and precipitation, Science, 269, 676-679.

Hurrell, J.W. (1996). Influence of Variations in Extratropical Wintertime Teleconnections on Northern Hemisphere Temperatures, Geophysical Research Letters, 23 (6), 665-668.

Hurrell, J.W., Kushnir, Y., Ottersen, G., Visbeck, M. (2003). An overview of the North Atlantic Oscillation. **In:** Hurrell, J.W., Kushnir, Y., Ottersen, G., Visbeck, M. (eds.) The North Atlantic Oscillation, American Geophysical Union, Washington, DC, pp 1–35.

Inouye, D. W., Morales, M., Dodge, G. (2002). Variation in timing and abundance of flowering by Delphinium barbeyi Huth (Ranunculaceae): the roles of snowpack, frost, and La Niña, in the context of climate change, Oecologia, 139:543–550.

IPCC (2007). Climate Change 2007, The Physical Science Basis. Contribution of Working Group I to the Fourth Assessment Report of the Intergovernmental Panel on Climate Change.

Jacobeit, J., Wanner, H., Luterbacher, J., Beck, C., Philipp, A., Sturm, K. (2003). Atmospheric circulation variability in the North-Atlantic-European area since the midseventeenth century, Climate Dynamics, 20, 341-352.

Jansen, E., J. Overpeck, J., Briffa, K., R., Duplessy, J.C., Joos, F., Masson-Delmotte, V., Olago, D., Otto-Bliesner, B., Peltier, W.R., Rahmstorf, S., Ramesh, R., Raynaud, D., Rind, D., Solomina, O., Villalba, R., Zhang, D. (2007). Palaeoclimate. In Climate Change 2007, The Physical Science Basis. Contribution of Working Group I to the Fourth Assessment Report of the Intergovernmental Panel on Climate Change. S. Solomon, D. Qin, M. Manning, Z. Chen, M. Marquis, K.B. Averyt, M. Tignor, Miller, H.L. (eds.), Cambridge University Press, pp. 433-497.

Jarvis, C.H., Stuart, N. (2001a). A comparison between strategies for interpolating maximum and minimum daily air temperatures: The selection of 'guiding' topographic and land cover variables, Journal of Applied Meteorology, 40, 1060-1074.

Jarvis, C.H., Stuart, N. (2001b). A comparison between strategies for interpolating maximum and minimum daily air temperatures: The interaction between number of guiding variables and the type of interpolation method, Journal of Applied Meteorology, 40, 1075-1084.

Jerez, S., Montavez, J.P., Gómez-Navarro, J.J., Jiménez, P.A., Jiménez-Guerrero, P., Lorente, R., González-Rouco, J.F. (2012). The role of the land-surface model for climate change projections over the Iberian Peninsula, Journal of Geophysical Research- Atmospheres, 117, D01109, DOI: 10.1029/2011JD016576.

Jones, D.A., Trewin, B.C. (2002). On the adequacy of historical Australian daily temperature data for climate monitoring, Australian Meteorological Magazine, 51, 237-50.

Jones, P.D., Raper, S.C.B., Bradley, R.S., Diaz, H.F., Kelly, P.M., Wigley, T.M.L. (1986). Northern Hemispheric surface air temperature variations 1851–1984, Journal of Climatology and Applied Meteorology, 25, 161–179.

Jones, P.D. (1991). Historical records of cloud cover and climate for Australia, Australian Meteorological Magazine, 39 (1991), pp. 181−189.

Jones, P.D., Briffa, K.R. (1992). Global surface air temperature variations during the twentieth century: Part 1 spatial temporal and seasonal details, the Holocene, 2,165-179.

Jones, P.D. (1994). Hemispheric surface air temperature variations: A reanalysis and an update to 1993, Journal of Climate, 7, 1794-1802.

Jones, P.D., Hulme, M. (1996). Calculating regional climatic time series for temperature and precipitation: methods and illustrations, International Journal of climatology, 16, 361-377.

Jones, P.D., New, M., Parker, D.E., Martin, S., Rigor, I.G. (1999a). Surface air temperature and its changes over the past 150 years, Review of Geophysics, 37,173-199.

Jones, P.D., Horton, E.B., Folland, C.K., Hulme, M., Parker, D.E., Basnett, T.A. (1999b). The use of indices to identify changes in climatic extremes, Climatic Change, 42,131–149.

Jones, P.D., Jones, R.N., Nicholls, N., Sexton, D.H.M. (2001). Global temperature change and its uncertainties since 1861, Geophysical Research Letters, 28, 2621-2624.

Jones, P.D., Moberg, A. (2003). Hemispheric and large scale surface air temperature variations: An extensive revision and an update to 2001, Journal of Climate, 16, 206-223.

Kalkstein, L. S., Tan, G., Skindlov, J.A. (1987). An evaluation of three clustering procedures for use in synoptic climatological classification, Journal of Applied Meteorology, 26, 717–730.

Kalnay, E., Kanamitsu, M., Kistler, R., Collins, W., Deaven, D., Gandin, L., Iredell, M., Saha, S., White, G., Woollen,J., Zhu, Y., Chelliah, M., Ebisuzaki, W., Higgins, W., Janowiak, J., Mo, K.C., Ropelewski, C., Wang, J., Leetmaa, A., Reynolds, R., Jenne, R., Joseph, D. (1996). The NCEP/NCAR 40-year reanalysis project. Bulletin of American Meteorological Society, 77, 437-470.

Karl, T.R., and Coauthors. (1993). A new perspective on recent global warming: Asymmetric trends of daily maximum and minimum temperature, Bulletin American Meteorological Society, 74, 1007-1023.

Karl, T.R., Knight, R.W. (1997). The 1995 Chicago heat wave: How likely is a recurrence?, Bulletin of the American Meteorological Society, 78, 1107-1119.

Katz, R.W., Brown, B.G. (1992). Extreme events in a changing climate: variability is more important than averages, Climatic Change, 21, 289–302.

Kemp, W.P., Burnell, D.G., Everson, D.O., Thomson, A.J. (1983). Estimating missing daily maximum and minimum temperatures, Journal of Climatology and Applied Meteorology 22, 1587–1593.

Kendall, M. (1975). Multivariate Analysis. Charles Griffin & Company, London.

Keyantash, J., Dracup, J. A. (2002). The quantification of drought: an evaluation of drought indices, American Meteorological Society, 83, 1167–1180.

Kirono, D.G.C., Kent, D.M. (2011). Assessment of rainfall and potential evaporation from global climate models and its implications for Australian regional drought projection, International Journal of Climatology, 31, 1295-1308.

Kjellström, E. (2004). Recent and future signatures of climate change in Europe, Ambio, 33, 193-298.

Kjellstrom, E., Barring, L., Jacob, D., Jones, R., Lenderink, G., Schar, C. (2007). Modelling daily temperature extremes: recent climate and future changes over

Europe, Climatic Change, 81, 249–265.

Klein Tank, A., Wijngaard, J., Können, G., Böhm, R., Demarée, G., Gocheva, A., Mileta, M., Pashiardis, S., Hejkrlik, L., Kern-Hansen, C., Heino, R., Bessemoulin, P., Müller-estermeier, G., Tzanakou, M., Szalai, S., Pálsdóttir, T., Fitzgerald, D., Rubin, S., Capaldo, M., Maugeri, M., Leitass, A., Bukantis, A., Aberfeld, R., Van Engelen, A., Forland, E., Mietus, M., Coelho, F., Mares, C., Razuvaev, V., Nieplova, E., Cegnar, T., Antonio López, J., Dahlström, B., Moberg, A., Kirchhofer, W., Ceylan, A., Pachaliuk, O., Alexander, L., Petrovic, P. (2002). Daily dataset of 20th-century surface air temperature and precipitation series for the European climate assessment, International Journal of Climatology, 22, 1441–1453.

Klein Tank, A.M.G., Können, G.P. (2003). Trends in indices of daily temperature and precipitation extremes in Europe, 1946–99, Journal of Climate, 16, 3665-3680.

Klein Tank, A., Konnen, G., Selten, F. (2005). Signals of anthropogenic influence on European warming as seen in the trend patterns of daily temperature variance, International Journal of Climatology, 25, 1 – 16.

Klein Tank, A. M. G., Peterson, T. C., Quadir, D. A., Dorji, S., Zou, X., Tang, H., Santhosh, K., Joshi, U. R., Jaswal, A. K., Kolli, R. K., Sikder, A. B., Deshpande, N. R., Revadekar, J. V., Yeleuova, K., Vandasheva, S., Faleyeva, M., Gomboluudev, P., Budhathoki, K. P., Hussain, A., Afzaal, M., Chandrapala, L., Anvar, H., Amanmurad, D., Asanova, V. S., Jones, P. D., New, M. G., Spektorman, T. (2006). Changes in daily temperature and precipitation extremes in central and south Asia, Journal of Geophysical Research-Atmospheres, 111, D16105, DOI: 10.1029/2005JD006316.

Klok, E.J., Tank, A. (2009). Updated and extended European dataset of daily climate observations, International Journal of Climatology, 29, 1182–1191.

Koster, R.D., Suarez, M.J. (2003). Impact of land surface initialization on seasonal precipitation and temperature prediction, Journal of Hydrometeorology, 4, 408–423.

Koster, R. D., Dirmeyer, P., A. Guo, Z., Bonan, G., Chan, E., Cox, P., Gordon, C. T., Kanae, S., Kowalczyk, E., Lawrence, D., Liu, P., Lu, C., Malyshev, S., McAvaney, B., Mitchell, K., Mocko, D., Oki, T., Oleson, K., Pitman, A., Sud, Y. C., Taylor, C. M., Verseghy, D., Vasic, R., Xue, Y., Yamada, T., (2004). Regions of strong coupling between soil moisture and precipitation, Science, 305, 1138–1140.

Kostopoulou, E., Jones, P. (2005). Assessment of climate extremes in Eastern Mediterranean, Meteorological and Atmospheric Physics, 89, 69–85.

Kostopoulou, E., Tolika, K., Tegoulias, I., Giannakopoulos, C., Somot, S., Anagnostopoulou, C., Maheras, P. (2009). Evaluation of a Regional Climate Model using in-situ temperature observations over the Balkan Peninsula, Tellus A, 61, 357-370.

Kruger, A. C., Shongwe, S. (2004). Temperature trends in South Africa: 1960–2003, International Journal of Climatology, 24, 1929– 1945.

Kürbis, K., Mudelsee, M., Tetzlaff, G., Brázdil, R. (2008). Trends in extremes of temperature, dew point and precipitation from long instrumental records from central Europe. **In:** Raabe A (Ed.) Scientific Reports, No. 42, Institute of Meteorology, University of Leipzig, Leipzig, Germany, pp1–16.

Kuglitsch, F.G., Toreti, A., Xoplaki, E., Della-Marta, P.M., Zerefos, C.S., Türkes, M., and Luterbacher, J. (2010). Heat Wave Changes in the Eastern Mediterranean since 1960, Geophysical Research Letters, 37, L04802, DOI: 10.1029/2009GL041841.

Kundzewick, Z.W., Robson, A.J. (2000). Detecting Trend and Other Changes in Hydrological Data, World Climate Programme – Data and Monitoring, World Meteorological Organization, Geneva.

Kutiel, H., Maheras, P. (1998). Variations in the temperature regime across the Mediterranean during the last century and their relationship with circulation indices, Theoretical and Applied Climatology, 61, 39–53.

Kyselý, J., Huth, R. (2006). Changes in atmospheric circulation over Europe detected by objective and subjective methods, Theoretical and Applied Climatology, 85, 19-36.

Labajo, J.L., Piorno, A., Izquierdo, M.J. (1998). Temporal behaviour of the annual mean pressure on the Northern Spanish Plateau between 1945 and 1994, International Journal of Climatology, 18, 637– 647.

Lana, X,, Burgueño, A. (1996). Extreme winter minimum temperatures in Catalonia (northeast Spain): expected values and their spatial distribution, International Journal of Climatology, 16, 1365–1378.

Landman, W. A., Mason, S. J., Tyson, P. D. Tennant, W. J. (2001). Retro-active skill of multi-tiered forecasts of summer rainfall over southern Africa, International Journal of Climatology, 21, 1-19.

Lettenmaier, D.P., Wood, E.F., Wallis, J.R. (1994). Hydro-climatological trends in the continental United States, Journal of Climate, 7, 586-607.

Li, Q, Dong, W. (2009). Detection and adjustment of undocumented discontinuities in Chinese temperature series using a composite approach, Advances in Atmospheric Sciences, 26(1). 143-153.

Linacre, E. (1992). Climate Data and Resources: A Reference and Guide. Routledge. London. 366 pp.

Lionello, J., Bhend, A., Buzzi, P.M., Della-Marta, S., Krichak, A., Jansà, P., Maheras, A., Sanna, I.F., Trigo, R. (2006). Cyclones in the Mediterranean region: climatology and effects on the environment. **In:** Lionello, P., Malanotte-Rizzoli, P., Boscolo, R., Mediterranean Climate Variability, Elsevier, Amsterdam, pp. 324–372.

Lolis, C.J., Bartzokas, A., Katsoulis, B.D. (2004). Relation between sensible and latent heat fluxes in the Mediterranean and precipitation in the Greek area during winter, International Journal of Climatology, 24, 1803-1816.

Lopez-Bustins, J.A., Martin-Vide, J., Sanchez-Lorenzo, A. (2008). Iberian winter rainfall trends based upon changes in teleconnection and circulation patterns, Global and Planetary Change, 63 (2-3), 171-176.

López-Moreno, J.I., García-Ruiz, J.M. (2004). Influence of snow accumulation and snowmelt on streamflow in the Central Spanish Pyrenees, International Journal of Hydrological Sciences, 49, 1–16.

López-Moreno, J.I., Beguería, S., García-Ruiz, J.M. (2006). Trends in high flows in the Central Spanish Pyrenees: response to climatic factors or to land-use change? Hydrological Sciences, 51 (6), 1039–1050.

López-Moreno, J.I., Goyette, S., Beniston, M. (2008). Climate change prediction over complex areas: spatial variability of uncertainties and predictions over the

Pyrenees from a set of regional climate models, International Journal of Climatology, 28, 1535-1550.

López-Moreno, J.I., Vicente-Serrano, S.M., Angulo-Martínez, M., Beguería, S., Kenawy, A. (2010). Trends in daily precipitation on the northeastern Iberian Peninsula, 1955-2006, International Journal of Climatology, 30, 1026-1041.

López-Moreno, J.I., Vicente-Serrano, S.V., Angulo-Martínez, M, Beguería, S, Kenawy, A. (2010). Trends in daily precipitation on the northeastern Iberian Peninsula, 1955-2006, International Journal of Climatology. 30: 1026–1041.

López-Moreno, J.I., Vicente-Serrano S.M., Morán-Tejeda E., Lorenzo J., Kenawy, A. and Beniston, M. (2011). NAO effects on combined temperature and precipitation winter modes in the Mediterranean mountains: Observed relationships and projections for the 21st century, Global and Planetary Change, 77, 62-76.

Lorenzo, M.N., Taboada, J.J., Gimeno, L. (2008). Links between circulation weather types and teleconnection patterns and their influence on precipitation patterns in Galicia (NW Spain), International Journal of Climatology, 28(11).1493–1505.

Lorenz, R., Jaeger, E.B., Seneviratne, S.I. (2010). Persistence of heat waves and its link to soil moisture memory, Geophysical Research Letters, 37, L09703, DOI: 10.1029/2010GL042764.

Lough, J.M. (1997). Regional indices of climate variation: temperature and rainfall in Queensland, Australia, International Journal of Climatology, 17, 55−66.

Love, D., Hallbauer, D., Amos, A., Hranova, R. (2004). Factor analysis as a tool in groundwater quality management: two southern African case studies, Physics and Chemistry of the Earth, 29(15-18), 1135-1143.

Lucio, P.S., Conde, F.C., Cavalcanti, I.F.A., Serrano, A.I., Ramos, A.M., Cardoso A.O. (2007). Spatiotemporal monthly rainfall reconstruction via artificial neural network – case study: south of Brazil, Advances in Geosciences, 10, 67-76.

Luterbacher, J., Dietrich, D., Xoplaki, E., Grosjean, M., Wanner, H. (2004). European seasonal and annual temperature variability, trends, and extremes since 1500, Nature, 303, 1499-1503.

Maheras, P., Kutiel, H., Vafiadis, M. (1998). Tendances spatiales et temporelles de la pression atmospherique de surface et des geopotentieles de 500 hPa en Europe et en Mediterranee durant la derniere periode 1950–1994, Publ AIC, 11, 345–351.

Maheras P, Kutiel H. (1999). Spatial and temporal variations in the temperature regime in the Mediterranean and their relationship with circulation during the last century, International Journal of Climatology, 19, 745–764.

Maheras, P., Xoplaki, E., Davies, T., Martin-Vide, J., Bariendos, M., Alcoforado, M. (1999). Warm and cold monthly anomalies across the Mediterranean basin and their relationship with circulation, 1860–1990, International Journal of Climatology, 19, 1697–1715.

Marshall, J., Kushnir, Y., Battisti, D., Chang, P., Czaja, A., Hurrell, J.W., Mc Cartney, M., Saravanan, M., Visbeck, M. (2001). Review: North Atlantic climate variability, International Journal of Climatology, 21, 1863–1898.

Martinez, M.D., Serra, C., Burgueño, A., Lana, X. (2010). Time trends of daily maximum and minimum temperatures in Catalonia (NE Spain) for the period 1975-2006, International Journal of Climatology, 30, 267-290.

Martin-Vide, J., Gomez, L. (1999). Regionalization of peninsular Spain based on the length of dry spells, International Journal of Climatology, 19, 537–555.

Martn-Vide, J., Olcina, J. (2001). Climas y tiempos de España, Madrid, Alianza Editorial, 258 pp.

Martin-Vide, J. (2004). Spatial distribution of a daily precipitation concentration index in peninsular Spain, International Journal of Climatology, 24, 959–971.

Martin-Vide, J., Lopez-Bustins, J.A. (2006). The Western Mediterranean Oscillation and rainfall in the Iberian Peninsula, Int. J. Climatol., 26 (11). 1455-1475.

McKee, T. B., Doesken, N. J., Kleist, J. (1993). The relationship of drought frequency and duration to time scales, **In:** Proc. of the 8th Conference on Applied Climatology, 17–22 January, Anaheim, CA, American Meteorological Society, Boston, MA, 179–184.

Medina-Ramon, M., Zanobetti, A., Cavanagh, D.P., Schwartz, J. (2006). Extreme temperatures and mortality: assessing effect modification by personal characteristics and specific cause of death in a multi-city case only analysis, Environ, Health Perspect, 114, 1331–1336.

Meehl, G. A., Thomas Karl, A., David, B., Easterling, R., Stanley, B., Changnon, C Roger Pielke JR., A David Changnon,D Jenni Evans, E Pavel YA. Groisman, B Thomas R. Knutson, F Kenneth E. Kunkel, C Linda O. Mearns, A Camille Parmesan, G Roger Pulwarty, H Terry Root, I Richard T. Sylves, J Peter Whetton, K, Zwiers, F. (2000). An introduction to trends in extreme weather and climate events: Observations, socioeconomic impacts, terrestrial ecological impacts, and model projections, Bulletin American Meteorological Society, 81, 413– 416.

Meehl, G.A., Tebaldi, C. (2004). More intense, more frequent and longer lasting heat waves in the 21st century, Nature, 305, 994-997.

Meisel, J.E., Turner, M.G. (1998). Scale detection in real and artificial landscapes using semivariance analysis, Landscape Ecology, 13, 347-362.

Menne, M.J., Williams, J.R. (2005). Detection of undocumented change points using multiple test statistics and composite reference series, Journal of Climate 18, 4271-4286.

Menne, M.J., Williams, C.N., Vose, R. S. (2009). The U.S. historical climatology network monthly temperature data, version 2, Bull. Amer.Meteor.Society 90 (7). 993-1007.

Metaxas, D.A., Bartzokas, A., Vitsas, A. (1991). Temperature fluctuations in the Mediterranean area during the last 120 years, International Journal of Climatology, 11, 897–908

Miller, C., Urban, D. L. (1999). A model of surface fire, climate and forest pattern in the Sierra Nevada, California, Ecological Modelling, 114, 113–135.

Milligan, G. W., Cooper, M. C. (1985). An Examination of procedures for determining the number of Clusters in a data Set, Psychometrika, 50, 159–179.

Miro, J.J., Estrela, M.J., Milan, M. (2006) Summer temperature trends in a Mediterranean area (Valencia region), International Journal of Climatology, 26, 1051-1073.

Moberg, A., Jones, P. (2004). Regional climate model simulations of daily maximum and minimum near-surface temperatures across Europe compared with observed station data 1961-1990, Climate Dynamics, 23, 695-715.

Moberg, A., Jones, P.D. (2005). Trends in indices for extremes in daily temperature and precipitation in central and Western Europe 1901-1999, International Journal of Climatology, 25, 1173-1188.

Moberg, A., Jones, P. D., Lister, D., Walther, A., Brunet, M., Jacobeit, J., Alexander, L. V., Della-Marta, P. M., Luterbacher, J., Yiou, P., Chen, D. L., AK. Tank, M. G., Saladie, O., Sigro, J., Aguilar, E., Alexandersson, H., Almarza, C., Auer, I., Barriendos, M., Begert, M., Bergstrom, H., Bohm, R., Butler, C. J., J. Caesar, A. Drebs, D. Founda, F. W. Gerstengarbe, Micela, Maugeri, G., M., Osterle, H., Pandzic, K., Petrakis, M., Srnec, L., Tolasz, R., Tuomenvirta, H., Werner, P. C., Linderholm, H., Philipp, A., Wanner, H. , Xoplaki, E. (2006). Indices for daily temperature and precipitation extremes in Europe analyzed for the period 1901-2000, Journal Of Geophysical Research-Atmospheres, 111(D22):D22106.

Mohan, S., Arumugam, N. (1996). Relative importance of meteorological variables in evapotranspiration: Factor analysis approach, Water Resources Management, 10(1),1-20.

Moore, G.W.K., Pickart, R.S., Renfrew, I.A. (2011). Complexities in the climate of the subpolar North Atlantic: a case study from 2007, Quarterly Journal of the Royal Meteorological Society, 137, 757–767.

Morales, C. G., Ortega, M.T., Labajo, J.L., Piorno, A. (2005). Recent trends and temporal behavior of thermal variables in the region of Castilla-Leon (Spain). Atmosfera, 18, 71– 90.

Muñoz-Díaz, D., Rodrigo, F. S. (2004). Spatio-temporal patterns of seasonal rainfall in Spain (1912-2000) using cluster and principal component analysis: comparison, Annales Geophysics, 22, 1435-1448.

Murphy, S.J., Washington, R. (2001). United Kingdom and Ireland precipitation variability and the North Atlantic sea-level pressure field, International Journal of Climatology, 21, 939–959.

Nakicenovic, N., Alcamo, J., Davis, G., de Vries, B., Fenhann, J., Gaffin, S., Gregory, K., Gr¨ubler, A., Jung, T.Y., Kram, T., La Rovere, E.L., Michaelis, L., Mori, S., Morita, T., Pepper, W., Pitcher, H., Price, L., Riahi, K., Roehrl, A., Rogner, H.H., Sankovski, A., Schlesinger, M., Shukla, P., Smith, S., Swart, R., van Rooijen, S., Victor, N., Dadi, Z. (2000). IPCC Special Report on Emissions Scenarios, Cambridge University Press: Cambridge, United Kingdom.

New, M., B. Hewitson, D.B., Stephenson, A., Tsiga, A., Kruger, A., Manhique, B., Gomez, C.A.S., Coelho, D.N., Masisi, E., Kululanga, E., Mbambalala, F., Adesina, H., Saleh, J., Kanyanga, J., Adosi, L., Bulane, L., Fortunata, M.L., Mdoka, R. L. (2006). Evidence of trends in daily climate extremes over southern and west Africa, Journal of Geophysical Research, 111: D14102, DOI: 10.1029/2005JD006289.

Nogues-Bravo, D., Aaujo, M.B., Errea, M.P., Martinez-Rica, J.P. (2007). Exposure of global mountain systems to climate warming during the 21st century, Global environmental change, 17, 420-428.

Norusis, M.J. (1988). The SPSS guide to data analysis, SPSS/PC+ Advanced statistics, V20, SPSS Inc., Chicago, 420pp.

NRC (National Research Council). (2002). Abrupt Climate Change. Inevitable Surprises. Committee on Abrupt Climate Change. Ocean Studies Board, Polar Research Board, 20 Board on Atmospheric Sciences and Climate. National

Academy Press. Washington, DC

Oberhauser K. Peterson A. T. (2003). Modeling current and future potential wintering distributions of eastern North American monarch butterflies. Proceedings of the National Academy of Sciences, USA 100: 14063-14068.

Ogi, M., Yamazaki, K., Tachibana, Z. (2005). The summer northern annular mode and abnormal summer weather in 2003, Geophysical Research Letters, 32,L04706, DOI: 10.1029/ 2004 GL 021528.

Oke, T.R. (1987). Boundary layer climates. 2nd ed. Routledge, 435pp.

Oliver, J.E. (1973). Climate and Man's Environment: an introduction to applied climatology, John Wiley & Sons, New York, 200 pp.

Ollero, A. (2010). Channel changes and floodplain management in the meandering middle Ebro River, Spain, Geomorphology, 117, 247–260.

Oñate,J.J., Pou,A. (1996). Temperature variations in Spain since 1901, A preliminary analysis, International Journal of Climatology, 16, 805-815.

Palutikof, J.P. (2003). Analysis of Mediterranean climate data: measured and modeled. **In**: Bolle, H.J. (Ed.), Mediterranean Climate Variability and Trends. Springer-Verlag, Berlin, pp. 133–153.

Pandzic K, Likso T. (2010). Homogeneity of average annual air temperature time series for Croatia, International Journal of Climatology, 30, 1215–1225.

Papadimas, C. D., Bartzokas, A., Lolis, C. J., Hatzianastassiou, N. (2011). Sea-level pressure-air temperature teleconnections during northern hemisphere winter, Theoretical and Applied Climatology, DOI: 10.1007/s00704-011-0523-8.

Parker, D. E., Jones, P. D., Bevan, A., Folland, C.K. (1994). Interdecadal changes of surface temperature since the 19th century, Journal of Geophysical Research 99, 14373-14399.

Parmesan, C., Yohe, G. (2003). A globally coherent fingerprint of climate change impacts across natural systems, Nature, 421, 37–42. (DOI:10.1038/nature01286)

Parmesan, C. (2006). Ecological and evolutionary responses to recent climate change, Annual Review of Ecological Evolution Sciences, 37, 637–669.

Parry, M.L. (2000). Assessment of potential effects and adaptations for climate change in Europe: The Europe Acacia Report. UK: Jackson Environment Institute, University of East Anglia

Pasho, E., Camarero, J.J., De Luis, M., Vicente-Serrano, S.M. (2011a). Spatial variability in large-scale and regional atmospheric drivers of Pinus halepensis growth in eastern Spain, Agricultural and Forest Meteorology, 151,1106-1119.

Pasho, E., Camarero, J.J., de Luis, M., Vicente-Serrano, S.M. (2011b). Impacts of drought at different time scales on forest growth across a wide climatic gradient in north-eastern Spain, Agricultural and Forest Meteorology, 151,1800-1811.

Patz, J., Campbell-Lendrum, D., Holloway, T., Foley, J. (2005). Impact of Regional Climate Change on Human Health, Nature, 438 (7066). 310–317, DOI: 10.1038/nature04188.

Pausas, J.G. (2004). Changes in fire and climate in the eastern Iberian Peninsula (Mediterranean basin), Climatic Change, 63, 337-350.

Peel, M.C., Finlayson. B.L., McMahon, T.A. (2007). Updated world map of the Kppen-Geiger climate classification, Hydrology and Earth System Sciences, 11, 1633-1644.

Pepin, N.C., Lundquist, J.D. (2008). Temperature trends at high elevations: patterns across the globe, Geophysical Research Letters, 35, L14701, DOI: 10.1029/2008GL034026.

Peterson, T.C., Easterling, D.R. (1994). Creation of homogeneous composite climatological reference series, International Journal of Climatology, 14, 671-680.

Peterson, T.C., Vose, R.S. (1997). An overview of the global historical climatology network temperature database, Bulletin American Meteorological Society, 78, 2837-2850.

Peterson, T.C., Easterling, D.R., Karl, T.R., Groisman, P., Nicholls, N., Plummer, N., Torok, S., Auer, I., Boehm, R., Gullett, D., Vincent, L., Heino, R., Tuomenvirta, H., Mestre, O., Szentimrey, T., Salinger, J., Forland, E.J., Hanssen-Bauer, I., Alexandersson, H., Jones, P., Parker, D. (1998). Homogeneity adjustments of in situ atmospheric climate data: a review, International Journal of Climatology, 18, 1493–1517.

Petrovic, P. (2004). Detecting of inhomogeneities in time series using Real Precision Method **In:** Fourth seminar for homogenization and quality control in climatological databases, Budapest: Hungary, 6–10 October 2003, WCDMP-No 56 WMO, Geneva, 79–88.

Philipp, A., Della-Marta, P.M., Wanner, H., Fereday, D.R., Jones, P.D., Moberg, A., (2007). Long-term variability of daily North Atlantic-European pressure patterns since 1850 classified by simulated annealing clustering, Journal of Climate, 20, 4065-4095.

Plantico, M.S., Karl, T.R., Kukla, G., Gavin, J. (1990). Is recent climate change across the United States related to rising level of anthropogenic greenhouse gases? Journal of Geophysical Research- Atmospheres, 95,16, 617-16,637.

Plaut, G., Simonnet, E. (2001). Large-scale circulation classification, weather regimes, and local climate over France, the Alps and Western Europe, Climate Research, 17, 303-324.

Politano, L. (2008). Extreme temperature events in the Mediterranean, MA thesis, Institute of Geography, University of Bern, 80pp.

Post, P., Truija, V., Tuulik, J. (2002). Circulation weather types and their influence on temperature and precipitation in Estonia, Boreal Environmental Research, 7, 281−289.

Power, S., Tseitkin, F., Torok, S., Lavery, B., Dahni, R., Mc-Avaney, B. (1998). Australian temperature, Australian rainfall and the Southern Oscillation, 1910–1992: Coherent variability and recent changes, Australian Meteoroligical Magazine, 47, 85–101.

Pozo-Vázquez, D., Esteban-Parra, M.J., Rodríguez, F.S., Castro-Diez, Y. (2001). A study of NAO variability and its possible non-linear influences on European surface temperature, Climate Dynamics, 17, 701-715.

Prieto, L., García-Herrera, R., Díaz, J., Hernández, E., Del Teso, T. (2004). Minimum extreme temperatures over Peninsular Spain, Global and Planetary Change, 44, 59-71.

Przybylak, R. (2000). Diurnal temperature range in the Arctic and its relation to Hemispheric and arctic circulation patterns, International Journal of Climatology, 20, 231-253.

Quadrelli, R., Pavan, V., Molteni, F. (2001). Wintertime variability of Mediterranean precipitation and its links with large-scale circulation anomalies, Climate Dynamics, 17, 457–466.

Quereda, J., Gil, A., Perez, A., Olcina, J., Rico, A., Monton, E. (2000). Climatic warming in the Spanish Mediterranean: Natural trend or urban effect, Climatic Change, 46, 473–483.

Ramos-Calzado P, Gómez-Camacho J, Pérez-Bernal F, Pita-López MF. (2008). A novel approach to precipitation series completion in climatological datasets: application to Andalusia, International Journal of Climatology 28, 1525–1534.

Reddaway, J., Bigg, G. (1996). Climatic change over the Mediterranean and links to the more general atmospheric circulation, International Journal of Climatology, 16, 651-661.

Reek, T., Doty, S.R., Owen, T.W.A. (1992). Deterministic approach to the validation of historical daily temperature and precipitation data from the cooperative network, Bulletin American Meteorological Society, 73, 753–762.

Reimann, C., Filzmoser, P., Garrett, R.G. (2002). Factor analysis applied to regional geochemical data: problems and possibilities, Applied Geochemistry, 17, 185-206.

Richardson, K., Steffen, W., Schellnhuber, H.J. (2009). Synthesis report: Climate change: Global risks, challenges and decisions; Copenhagen 2009, 10-12 March. Climate Congress, Copenhagen, University of Copenhagen, 39pp.

Rigol, J. P., Jarvis, C. H., Stuart, N. (2001). Artificial neural networks as a tool for spatial interpolation, International Journal of Geographical Information Science, 15(4), 323-344.

Robeson, S. M. (2004). Trends in time-varying percentiles of daily minimum and maximum temperature over North America, Geophysical Research Letters, 31, L04203, DOI: 10.1029/2003GL019019.

Robeson, S.M., Doty, J.A. (2005). Identifying rogue air-temperature stations using cluster analysis of percentile trends, Journal of Climate, 18, 1275-1287.

Rodríguez-Puebla, C., Encinas, A.H., Nieto, S., Garmenia, J. (1998). Spatial and temporal patterns of annual precipitation variability over the Iberian Peninsula, International Journal of Climatology, 18, 299–316.

Rodríguez-Puebla, C., Encinas, A.H., Sáenz, J. (2001a). Winter precipitation over the Iberian peninsula and its relationship to circulation indices, Hydrology and Earth System Sciences, 5, 233–244.

Rodríguez-Puebla, C., García-Casado, L.A., Frías, M.D. (2001b). Trend and interannual variations in air temperature over Iberian Peninsula, In 13th symposium on global change and climate variations, 13-17 January 2002, Orlando, Florida, American Meteorological Society, Boston, USA, 106-108.

Rodríguez-Puebla, C., Encinas, A.H., García-Casado, L.A., Nieto, S. (2010). Trends in warm days and cold nights over the Iberian Peninsula: relationships to large-scale variables, Climatic Change, 100, 667-684.

Rodríguez-Puebla, C., Nieto, S. (2010). Trends of precipitation over the Iberian Peninsula and the North Atlantic Oscillation under climate change conditions, International Journal of Climatology, 30 (12), 1807–1815.

Romero, R., Guijarro, J.A., Ramis, C., Alonso, S. (1998). A 30-year 1964–1993 daily rainfall data base for the Spanish Mediterranean regions: first exploratory study, International Journal of Climatology, 18(10), 541–560.

Romero, R., Sumner, G., Ramis, C., Genoves, A. (1999). A classification of the atmospheric circulation patterns producing significant daily rainfall in the Spanish Mediterranean area, International Journal of Climatology, 19, 765–785.

Root, T. L., Price, J. T., Hall, K. R., Schneider, S. H., Rosenzweig, C. J. A. (2003) Fingerprints of global warming on wild animals and plants, Nature, 421, 57–60.

Rousseeuw, P.J. (1987). Silhouettes: a graphical aid to the interpretation and validation of cluster analysis, Journal of Computational and Applied Mathematics, 20, 53-65.

Ruddiman, W. (2003). The Anthropogenic Greenhouse Era Began Thousands of Years Ago, Climatic Change, 61, 259–260.

Ruiz-Ramos, M., Minguez, M. I. (2010). Evaluating uncertainty in climate change impacts on crop productivity in the Iberian Peninsula, Climate Research, 44, 69–82.

Ryan, M., S. Archer, R. Birdsey, C. Dahm, L. Heath, J. Hicke, D. Hollinger, T. Huxman, G. Okin, R. Oren, J. Randerson, Schlesinger, W. (2008). Land Resources. **In:** The effects of climate change on agriculture, land resources, water resources and biodiversity. A Report by the U.S. Climate Change Science Program and the Subcommittee on Global Change Research, Washington, DC., USA, 362 pp.

Sabater, S., Munoz, I., Feio, M.J., Roman, A.M., Graca, M.A. (2009). The Iberian Rivers. **In:** Tockner K, Robinson Ch, Uhlinger U (eds.). Rivers of Europe. Elsevier, pp 113-149.

Sáenz J., Zubillaga J., Rodríguez-Puebla, C. (2001a). Interannual winter temperature variability in the north of the Iberian Peninsula, Climate Research, 16, 169-179.

Sáenz J., Rodríguez-Puebla C., Fernández J., Zubillaga J. (2001b). Interpretation of interannual winter temperature variations over southwestern Europe. Journal of Geophysical Research-Atmospheres, 106, 20641-20651.

Salat, J., Pascual, J. (2007). Climatological trend from 32 years of observations at L'Estartit station, near the Catalan coast (NW Mediterranean). Rapp. Comm. Int. Mer Medit., 38,196pp.

Salinger, M. J., Griffiths, G.M. (2001). Trends in New Zealand daily temperature and Rainfall extremes, International Journal of Climatology, 21, 1437-1452.

Sánchez, E., Domínguez, M., Romera, R., López de la, F., Noelia, G., Miguel, A., Gallardo, C., Castro, M. (2011). Regional modeling of dry spells over the Iberian Peninsula for present climate and climate change conditions, Climatic Change, 107 (3), 625- 634, DOI - 10.1007/s10584-011-0114-9.

Santoleri, R, Böhm, E., Schiano, M.E. (1994). The sea surface temperature of the Western Mediterranean Sea: historical satellite thermal data. **In**: La Violette PE (ed) Seasonal and interannual variability of the Western Mediterranean Sea. Coastal and Estuarine Studies 46, American Geophysical Union, Washington, DC, pp 155–176.

Savic, S., Petrovic, P., Milovanovic, B. (2010). Homogenization of Mean Air Temperature Data Series from Serbia, Geophysical Research Abstracts, Vol. 12, EGU2010-5521-1.

Schär C, Vidale, P.L., Luthi, D., Frei, C., Haberli, C., Liniger, M.A., Appenzeller, C. (2004). The role of increasing temperature variability in European summer heat waves, Nature, 427, 332–336.

Scherrer, S.C., Appenzeller, C., Laternser, M. (2004). Trends in Swiss Alpine snow

days: The role of local- and large-scale climate variability. Geophysical Research Letters 31: L13215.

Schindler, D. W. (1997). Widespread Effects of Climatic Warming on Freshwater Ecosystems in North America, Hydrological Processes, 11, 1043-1067.

Schönwiese, C.D., Walter, A., Rapp, J., Meyhöfer, S., Denhard, M. (1998). Statistical analysis of climate variability and anthropogenic climate signals in global and regional analysis. Institute of Meteorology and Geophysics, University of Frankfurt, NO. 102.

Schulte, A., Mrosek, T. (2006). Analysis and assessment of the forestry and wood-processing industry cluster in the State of North Rhine-Westphalia, Germany, Forstarchiv, 4, 136–141.

Semenov, M.A., Donatelli, M., Stratonovitch, D., Chatzidaki, E., Baruth, B. (2010). ELPIS: A dataset of local-scale daily climate scenarios for Europe, Climate Research, 44, 3-15.

Seneviratne, S.I., Lüthi, D., Litschi, M., Schär, C. (2006). Land-atmosphere coupling and climate change in Europe, Nature, 443, 205–209.

Serra, C., Burgueno, A., Lana, X. (2001). Analysis of maximum and minimum daily temperatures recorded at Fabra Observatory (Barcelona NE Spain) in the period 1917–1998, International Journal of Climatology, 21, 617– 636.

Serra, C., Martínez, M.D., Lana, X., Burgueño A. (2010). Extreme normalized residuals of daily temperatures in Catalonia (NE Spain). sampling strategies return periods and clustering process, Theoretical and applied Climatology, 101, 1-17.

Serreze, M.C., Clark, M.P., McGinnis, D.L., Robinson, D.A. (1998). Characteristics of snowfall over the eastern half of the United States and relationships with principal modes of low-frequency atmospheric variability, Journal of Climate 11(2). 234-250.

Shen, S.S.P., Dzikowski, P., Li, G., Griffith, D. (2001). Interpolation of 1961–1997 daily climate data onto Alberta polygons of ecodistrict and soil landscape of Canada, Journal of Applied Meteorology, 40, 2162–2177.

Sheng, J., Zwiers, F. (1998). An improved scheme for time-dependent boundary conditions in atmospheric general circulation models, Climate Dynamics, 14, 609 –613.

Simmonds, I., Murray, R. J. (1999). Southern extratropical cyclone behavior in ECMWF analyses during the FROST special observing periods, Weather and Forecasting, 14, 878-891.

Slonosky, V.C., Jones, P.D., Davies, T.D. (1999). Homogenization techniques for European monthly mean surface pressure series, Journal of Climate, 12, 2658-2672.

Slonosky, V.C., Jones, P.D., Davies, T.D. (2001). Instrumental pressure observations and atmosphere circulation from the 17th and 18th centuries: London and Paris. International Journal of Climatology, 21, 285-298.

Slonosky, V., Yiou, P. (2002). Does the NAO index represent zonal flow? The influence of the NAO on North Atlantic surface temperature, Climate Dynamics, 19(1), 17–30, DOI:10.1007/s00382-001-0211-y.

Smoyer-Tomic, K. E., Kuhn, R., Hudson, A. (2003). Heat wave hazards: An overview of heat wave impacts in Canada, Natural Hazards, 28, 463– 485.

Snell, S.E., Gopal, S., Kaufmann, R.K. (2000). Spatial interpolation of GCM forecasts using artificial neural networks, Journal of Climate, 13, 886-895.

Sneyers, R. (1990). On the Statistical Analysis of Series of Observations, WMO Tech. Note No. 143, 192pp.

Sneyers, R. (1992). On the use of statistical analysis for the objective determination of climatic change, Meteorologische Zeitschrift, 1, 247–256.

Solomon, S., Qin, D., Manning, M., Chen, Z., Marquis, M., Avery, K.B., Tignor, M., Miller, H.L. (eds) (2007). Climate Change: The Physical Science Basis. Contribution of Working Group I to the Fourth Assessment Report of the Intergovernmental Panel on Climate Change, Cambridge University Press, Cambridge.

Staudt, M. (2004). Detection de cambios termicos en la Peninsula Iberica con datos homogeneos regionales. PhD thesis, University of Granada, Spain.

Staudt, M., Esteban-Parra, M. J., Castro-Diez, Y. (2005). Evolution and changes in Spanish monthly maximum and minimum temperatures with homogenized data, European Geosciences Union, General Assembly 2005, Geophysical Research Abstract, 7, 06754.

Staudt, M., Esteban-Parra, M.J., Castro-Diez, Y. (2007). Homogenization of long-term monthly Spanish temperature data, International Journal of Climatology, 27, 1809-1823.

Stepanek, P. (2004). AnClim- software for time series analysis (for windows). Department of Geography, Faculty of Natural Sciences, Masaryk University: Brno; 1.47 MB.

Stepanek, P. (2008). ProClimDB – software for processing climatological datasets CHMI regional office Brno: http://wwwclimahomeu/ ProcData/html.

Stepanek, P., Mikulová, K. (2008). Homogenization of air temperature and relative humidity monthly means of individual observation hours in the area of the Czech and Slovak Republic. **In:** 5th Seminar for Homogenization and Quality Control in Climatological Databases. Hungarian Met. Service, Budapest, Hungary, 147−163.

Stepanek, P.R., Reznickova, L., Brazdil, R. (2008). Homogenization of daily air pressure and temperature series for Brno (Czech Republic) in the period 1848–2005, **In:** Proceedings of the Fifth seminar for homogenization and quality control in climatological databases (Budapest, 29 May–2 June 2006). WCDMP, WMO, Geneva, CD-ROM.

Stepanek, P., Zahradníček, P., Skalák P. (2009). Data quality control and homogenization of the air temperature and precipitation series in the Czech Republic in the period 1961-2007. Advances in Science Research, 3, 23-26.

Stooksbury, D.E., Idso, C.D., Hubbard, K.G. (1999). The effects of data gaps on the calculated monthly mean maximum and minimum temperatures in the continental United States: a spatial and temporal study, Journal of Climate, 12, 1524–1533.

Sumner, G. N., Homar, V., Ramis, C. (2001). Precipitation seasonality in eastern and southern coastal Spain, International Journal of Climatology, 21,219–247.

Sumner, G. N., Romero, R., Homar, V., Ramis, C., Alonso, S., Zorita, E. (2003). An estimate of the effects of climate change on the rainfall of Mediterranean Spain by the late 21st century, Climate Dynamics, 20, 789-805.

Syrakova, M., Steanova, M. (2008). Homogenization of Bulgarian temperature series, International Journal of Climatology, 29, 1835-1849.

Taplador, F., Sánchez, E., Romera, R. (2009). Exploiting an ensemble of regional

climate models to provide robust estimates of projected changes in monthly temperature and precipitation probability distribution functions, Tellus, 61A, 75-71.

Tett, S. F. B., Stott, P. A., Allen, M. R., Ingram, W. J., Mitchell, J. F. B. (1999). Causes of twentieth-century temperature change near the Earth's surface, Nature, 399, 569-572.

Thomas, CD, Alison, C., Green, R.E., Bakkenes, M., Beaumont, L.J., Collingham, Y.C., Barend F. N. Erasmus, de Siqueira, M.F., Grainger, A., Hannah, L., Hughes, L., Huntley, B., van Jaarsveld, A.S., Midgley, G.F., Miles, L., Ortega-Huerta, M.A., Peterson, T., Phillips, O.L., Williams, S.E., (2004). Extinction risk from climate change, Nature, 427, 145–148.

Thomas, C.D. (2010). Climate, climate change and range boundaries, Diversity and Distributions, 16(3), 488-495.

Thornton, P.E., Running, S.W., White, M.A. (1997). Generating surfaces of daily meteorology variables over large regions of complex terrain, Journal of Hydrology, 190, 214–251.

Thuiller, W., Lavorel, S., Araujo, M.B., Sykes, M.T., Prentice, I.C. (2005). Climate change threats to plant diversity in Europe. Proc. Natl Acad. Sci. USA, 102, 8245–8250.

Trenberth K.E., Jones, P.D., Ambenje, P., Bojariu, R., Easterling, D., Klein Tank, A., Parker, D., Rahimzadeh, F., Renwick, J.A., Rusticucci, M. (2007). Observations: surface and atmospheric climate change. In Climate Change 2007. The Physical Science Basis, Contribution of WG 1 to the Fourth Assessment Report of the Intergovernmental Panel on Climate Change, Solomon, S., Qin, D., Manning, M., Chen, Z., Marquis, M.C., Averyt, K.B., Tignor M. and H.L., Miller (Eds.), Cambridge University Press, Cambridge, New York, pp. 235–336.

Trigo, I.F., Davies, T.D., Bigg, G.R. (1999). Objective climatology of cyclones in the Mediterranean region, Journal of Climate, 12, 1685–1696.

Trigo, R.M., DaCamara, C. (2000). Circulation Weather Types and their impact on the precipitation regime in Portugal, Int J of Climatology, 20, 1559-1581

Trigo, R.M., Palutikof, J.P. (2001). Precipitation scenarios over Iberia: a comparison between direct GCM output and different downscaling techniques, Journal of Climate, 14, 4422-4446.

Tuomenvirta, H. (2001). Homogeneity adjustments of temperature and precipitation series - Finnish and Nordic data, International Journal of Climatology, 21, 495-506.

Ulbrich, U., Christoph, M., Pinto, Corte-Real, J.G. (1999). Dependence of winter precipitation over Portugal on NAO and baroclinic wave activity, International Journal of Climatology, 19, 379-390.

Urban, D.L., Miller, C., Stephenson, N.L., Halpin, P.N. (2000). Forest pattern in Sierran landscapes: the physical template, Landscape Ecology, 15, 603–620.

Van de Beek, C.Z., Leijnse, H.,. Torfs, P.J.J.F, Uijlenhoet, R. (2010). Semivariance of rainfall in The Netherlands as a function of accumulation interval. **In:** Proceedings of the 10th International Precipitation Conference, 23–25 Jun. 2010, Coimbra, Portugal.

Vargas, M., García, M. C., Moya, F., Tel, E., Parrilla, G., Plaza, F., Lavín, A. (2008). Cambio climático en el Mediterráneo español. Instituto Español de Oceanografía, 170 pp.

Vautard, R., Yiou, P., D'Andrea, F., de Noblet, N., Viovy, N., Cassou, C., Polcher, J., Ciais, P., Kageyama, M., Fan, Y. (2007). Summertime European heat and drought waves induced by wintertime Mediterranean rainfall déficit, Geophysical Research Letters, 34, L07711 DOI:10.1029/2006GL028001.

Vautard, R., Yiou, P., Oldenborgh, G. J. V. (2009). Decline of fog, mist and haze in Europe over the past 30 years, Nature Geoscience, 2 (2), 115-119.

Vicente-Serrano, S.M. (2006). Spatial and temporal analysis of droughts in the Iberian Peninsula (1910-2000), Hydrological Sciences, 51, 83-97.

Vicente-Serrano, S. M., López-Moreno, J.I. (2006). The influence of atmospheric circulation at different spatial scales on winter drought variability through a semiarid climatic gradient in north east Spain, International Journal of Climatology, 26, 1427–1456.

Vicente-Serrano, S. M., Cuadrat-Prats, J. M. (2007). Trends in drought intensity and variability in the middle Ebro valley (NE of the Iberian peninsula) during the second half of the twentieth century, Theoretical and Applied Climatology, 88, 247–258.

Vicente-Serrano, S. M., Beguería, S., López Moreno, J.I., El Kenawy, A., Angulo, M.M. (2009). Daily atmospheric circulation events and extreme precipitation risk in northeast Spain: Role of the North Atlantic Oscillation, the Western Mediterranean Oscillation, and the Mediterranean Oscillation, Journal of Geophysical Research- Atmospheres, 114, D08106, DOI: 10.1029/2008JD011492.

Vicente-Serrano, S.M., Beguería, S., López-Moreno, J., Garcia-Vera, M., Stepanek, P. (2010). A complete daily precipitation database for North-East Spain: reconstruction, quality control and homogeneity, International Journal of Climatology, 30, 1146-1163.

Vicente-Serrano, S.M., López-Moreno, J.I., Drumond, A., Gimeno, L., Nieto, R., Morán-Tejeda, E., Lorenzo-Lacruz, J., Beguería, S., Zabalza, J. (2011a). Effects of warming processes on droughts and water resources of the NW Iberian Peninsula (1930–2006), Climate Research, 48, 203–212.

Vicente-Serrano, S.M., Trigo, R.M., López-Moreno, J.I., Liberato, M.L.R., Lorenzo-Lacruz, J., Beguería, S., Morán-Tejeda, E., El Kenawy, A. (2011b). The 2010 extreme winter North Atlantic Oscillation in Iberian Precipitation: anomalies, driving mechanisms and future projections. Climate Research 46, 51–65, DOI: 10.3354/cr00977.

Vicente-Serrano, S.M., Beguería, S., López-Moreno, J.I., Angulo, M., El Kenawy, A. (2011c). A global 0.5° gridded dataset (1901-2006) of a multiscalar drought index considering the joint effects of precipitation and temperature, Journal of Hydrometeorology, 11(4), 1033-1043.

Vincent, L. (1998). A technique for the identification of inhomogeneities in Canadian temperature series, Journal of Climate, 11, 1094–1104.

Vincent, L.A., Gullett, D.W. (1999). Canadian historical and homogeneous temperature datasets for climate change analyses, International Journal of Climatology, 19, 1375 –1388.

Vincent, L.A., Zhang, B., Bonsal, R., Hogg, W.D. (2002). Homogenization of daily temperatures over Canada, Journal of Climate, 15, 1322–1334.

Vincent, L. A., Peterson T. C., Barros V. R., Marino M. B., Rusticucci M., Carrasco G., Ramirez E., Alves L. M., Ambrizzi T., Bwrlato M. A., Grimm A. M., Marengo J.

A., Molion L., Moncunill D. F., Rebello E., Anunciacao Y. M., Quintana J., Santos J. L., Baez J., Coronel G., Garcia J., Trebejo I., Bidegain M., Haylock M. R., Karoly D., (2005). Observed trends in indices of daily temperature extremes in South America 1960–2000, Journal of Climate, 18, 5011–5023.

Vincent, L.A. Aguilar E., Saindou M., Hassane A. F., Jumaux G., Roy D., Booneeady P., Virasami R., Randriamarolaza L. Y. A., Faniriantsoa F. R., Amelie V., Seeward H., Montfraix B. (2011). Observed trends in indices of daily and extreme temperature and precipitation for the Countries of the Western Indian Ocean, 1961-2008, Journal of Geophysical Research- Atmospheres, 116, D10108, DOI:10.1029/2010JD015303.

Visser M. E., Both C. (2005). Shifts in phenology due to global climate change: the need for a yardstick. Proc. R. Soc. B 272, 2561–2569. (DOI:10.1098/rspb.2005.3356)

Von Storch, H., Navvara, A. (1995). Analysis of climate variability-applications of statistical techniques. Springer-verlag, New York, 352pp.

Von Storch, H., Zwiers, F.W. (1999). Statistical Analysis in Climate Research. Cambridge University Press, 484 pp.

Vose, R.S., Schmoyer, R.L., Steurer, P.M., Peterson, T.C., Heim, R., Karl, T.R., Eischeid, J. (1992). The global historical climatology network: long-term monthly temperature precipitation sea level pressure and station pressure data. ORNL/CDIAC-53 NDP-041 Carbon Dioxide Information Analysis Center. Oak Ridge National Laboratory. Oak.

Wallington, T.J., Srinivasan, J., Nielsen, O.J., Highwood, E.J. (2004). Greenhouse gases and global warming. **In**: Sabljic A, (editor). Environmental and Ecological Chemistry. Oxford: Eolss Publishers, 424p.

Wang, Y., Cheng H., Edwards R.L., He Y., Kong X., An Z., Wu J., Kelly M.J., Dykoski C.A., Li X. (2005). The Holocene Asian Monsoon: Links to solar changes and North Atlantic climate, Science, 308, 854-7.

Wanner, H., Rickli, R., Salvisberg, E., Schmutz, C., Schüepp., M. (1997). Global climate change and variability and its influence on Alpine climate: concepts and observations, Theoretical and Applied Climatology, 58, 221–243.

Webster, R., Oliver, M.A. (2001). Geostatistics for Environmental scientists. Wiley, Chichester, UK, 271 pp.

Werner, P.C., Gerstengarbe, F.W., Fraedrich, K., Oesterle. H. (2000). Recent climate change in the North Atlantic/European sector, International Journal of Climatology, 20, 463 – 471.

Wetterhall, F., Halldin, S., Xu, C.Y. (2007). Seasonal properities of four statistical-downscaling methods in central Sweden, Theoretical and Applied Climatology. 87, 123-137.

Whiteman, C. D. (2000). Mountain Meteorology, Oxford University Press, New York. ISBN 01951327108, 355pp.

WHO (2003). The health impacts of 2003 summer heat-waves. Briefing note for the Delegations of the fifty-third session of the WHO (World Health Organization) Regional Committee for Europe. 12 pp.

Wijngaard, J.B., Klein Tank, A.M.G., Können, G.P. (2003). Homogeneity of 20th century European daily temperature and precipitation series, International Journal of Climatology, 23, 679–692.

Wild, M., Gilgen, H., Roesch, A., Ohmura, A., Long, C.N., Dutton, E.G., Forgan, B., Kallis, A., Russak, V., Tsvetkov, A. (2005). From dimming to brightening: Decadal changes in surface solar radiation, Science, 308, 847–850, DOI:10.1126/science.1103215.

Willmott, C.J. (1982). Some comments on the evaluation of model performance, Bulletin American Meteorological Society, 63, 1309 -1313.

Willmott, C.J., Matsuura, K. (1995). Smart interpolation of annually averaged air temperature in the United States, Journal of Applied Meteorology, 34, 2577-2586.

WMO (1966). Climatic change, Technical note, World Meteorological Organization, Geneva, 79pp.

WMO (2009) Climate Data and Monitoring: Guidelines on Analysis of extremes in a changing climate in support of informed decisions for adaptation, WCDMP No.72. WMO/TD-No, 1500.

Wolting, G., Bouvier, C.H., Danloux, J., Fritsch, J.M. (2000). Regionalization of extreme precipitation distribution using the principal components of the topographical environment, Journal of Hydrology, 233, 86–101.

Wood, J.M., Tataryn, D.J., Gorsuch, R.L. (1996). Effects of under- and overextraction on principal axis factor analysis with varimax rotation, Psychological Methods, 1, 354-365.

Woollings, T. (2010). Dynamical influences on European climate: an uncertain future. Philosophical Transactions of the Royal Society A – Mathematical Physical and Engineering Sciences, 368, 3733–3756.

Xoplaki, E. (2002). Climate variability over the Mediterranean. PhD thesis, University of Bern.

Xoplaki, E, Gonzalez-Rouco, J.F., Luterbacher, J., Wanner, H. (2003a) Mediterranean summer air temperature variability and its connection to the large-scale atmospheric circulation and SSTs, Climate Dynamics, 20, 723–739 DOI 10.1007/s00382-003-0304-x.

Xoplaki, E, Gonzalez-Rouco, F.J., Gyalistras, D., Luterbacher, J., Rickli, R., Wanner, H. (2003b) Interannual summer air temperature variability over Greece and its connection to the large-scale atmospheric circulation and Mediterranean SSTs 1950–1999, Climate Dynamics, 20, 523–536 DOI 10.1007/s00382-002-0291-3.

Xoplaki, E., Luterbacher, J., Paeth, H., Dietrich, D., Steiner, N., Grosjean, M., Wanner, H., 2005. European spring and autumn variability and change of extremes over the last half millennium, Geophysical Research Letters, 32.L15713 DOI:10.1029/2005GL023424.

Yin, Z.Y. (1993). Spatial pattern of temporal trends in moisture conditions in the Southeastern United States, Geografiska Annaler. Series A, Physical Geography 75 (1-2). 1-11.

You, J., Hubbard, K.G. (2006). Quality control of weather data during extreme events, Journal of Atmospheric and Oceanic Technology, 23(2), 184–197.

You, J., Hubbard KG, Goddard S. (2008). Comparisons of methods for spatially estimating station temperatures in a quality control system, International Journal of Climatology, 28, 777-787.

Young, K.C. (1992). A three-way model for interpolating monthly precipitation values, Monthly Weather Review, 120, 2561-2569.

Young, F.J., Hammer, R.D. (2000). Defining geographic soil bodies by landscape

position, soil taxonomy, and cluster analysis, Journal of American Society of Soil Sciences, 64, 989–998.

Yue, S., Pilon, P, Phinney, B., Cavadias, G. (2002). The influence of correlation on the ability to detect trend in hydrological series, Hydrological Processes, 16, 1808–1829.

Yue, S., Wang, C.Y. (2002). Applicability of prewhitening to eliminate the influence of serial correlation on the Mann-Kendall test, Water Resources Research, 38(6), 1068, 2002.

Yue, S., Wang, C.Y. (2004). The Mann-Kendall test modified by effective sample size to detect trend in serially correlated hydrological series, Water Resources Management, 18(3), 201–218, 2004.

Zhang, J., Wang, W. C, Wu, L. (2009). Land–atmosphere coupling and diurnal temperature range over the contiguous United States, Geophysical Research Letters, 36, L06706, DOI: 10.1029/2009GL037505.

Zhang, J., Dong, W. (2010). Soil moisture influence on summertime surface air temperature over East Asia, Theoretical and Applied Climatology, 100, 221–226.

Zhang, X., Vincent, L. A., Hogg, W. D., Niitsoo, A. (2000). Temperature and precipitation trends in Canada during the 20th century, Atmosphere-Ocean, 38(3), 395–429.

Zhang, X. Aguilar E., Sensoy, S., Melkonyan, H., Tagiyeva, U., Ahmed, N., Kutaladze, N., Rahimzadeh, F., Taghipour, A., Hantosh, T., Albert, P., Semawi, M., Karam, Ali, M., Said Al-Shabibi, M.H., Al-Oulan, Z., Zatari, T., Al Dean Khelet, I., Hamoud, S., Sagir, R., Demircan, M., Eken, M., Adiguzel, M., Alexander, L., Peterson, T.C., Wallis, T. (2005). Trends in Middle East climate extreme indices from 1950 to 2003, Journal of Geophysical Research- Atmospheres, 110, D22104, DOI: 10.1029/2005JD006181.

Zwick, W.R., Velicer, W.F. (1986). Comparison of five rules for determining the number of components to retain, Psychological Bulletin, 99, 432-442.

APPENDICES

APPENDIX A

List of the observatories of the final dataset with their main characteristics.

WMO-Station code	Observatory	Province	Latitude (North)	Longitude	Altitude (meter a.s.l)	Starting date (MM/DD/YYYY)	End date (MM/DD/YYYY)
1060	AMURRIO 'INSTITUTO'	ALAVA	43.05	3.01W	219	1/1/1955	12/31/2006
9091O	VITORIA 'AEROPUERTO DE FORON -DA'	ALAVA	42.88	2.72W	508	1/1/1913	12/31/2006
0069	PANTA DE FOIX	BARCELONA	41.26	1.65E	104	1/1/1912	12/31/2006
0181	SANT SADURNI D'ANOIA	BARCELONA	41.44	1.8E	125	1/1/1941	12/31/2006
0158O	MONTSERRAT	BARCELONA	41.59	1.84E	730	1/1/1968	12/31/2006
0111	CABRIANES	BARCELONA	41.8	1.9E	246	1/1/1929	12/31/2006
0072A	BEGUES SAN EUDALD	BARCELONA	41.34	1.93E	360	1/1/1950	12/31/2006
0076	AEROPORT DE BARCELONA EL PRAT	BARCELONA	41.3	2.08E	6	1/1/1938	12/31/2006
0229I	SABADELL AERODROMO	BARCELONA	41.53	2.1E	130	1/1/1900	12/31/2006
0120	MOIA	BARCELONA	41.82	2.1E	800	1/1/1916	12/31/2006
0200E	BARCELONA FABRA	BARCELONA	41.42	2.12E	420	1/1/1926	12/31/2006
0200R	BARCELONA CAN BRUIXA	BARCELONA	41.38	2.13E	58	1/1/1969	12/31/2006
0222	CALDES DE MONTBUI	BARCELONA	41.61	2.17E	180	1/1/1933	12/31/2006
0203	ELS HOSTALETS DE BALENYA	BARCELONA	41.85	2.26E	570	1/1/1930	12/31/2006
0208	GRANOLLERS	BARCELONA	41.61	2.29E	154	1/1/1950	12/31/2006
0213	CARDEDEU	BARCELONA	41.64	2.36E	195	1/1/1920	12/31/2006
0211	LLINARS DEL VALLES	BARCELONA	41.63	2.4E	193	1/1/1943	12/31/2006
0356	VILANOVA SAU EL TORTADES	BARCELONA	41.9	2.44E	850	1/1/1965	12/31/2006
0263	SANT CELONI	BARCELONA	41.69	2.5E	155	1/1/1940	12/31/2006
2290	CASTROGERIZ	BURGOS	42.29	4.14W	808	1/1/1959	12/31/2006
2121	GUMIEL DEL MERCADO 'LA VENTO- SILLA'	BURGOS	41.72	3.82W	800	1/1/1949	12/31/2006
2331	BURGOS 'VILLAFRIA'	BURGOS	42.36	3.63W	890	1/1/1943	12/31/2006
9046	ESPINOSA DE LOS MONTEROS'IB'	BURGOS	43.08	3.56W	762	1/1/1929	12/31/2006
9044	MIÐON	BURGOS	42.95	3.5W	595	1/1/1959	12/31/2006

2114	HONTORIA DE VALDEARADOS 'QUIN-TANILLA DE RECUERDA'	BURGOS	41.76	3.5W	870	1/1/1967	12/31/2006
2304	SANTO DOMINGO DE SILOS	BURGOS	41.96	3.42W	1003	1/1/1956	12/31/2006
9037	OÐA-IBERDUERO	BURGOS	42.73	3.41W	598	1/1/1942	12/31/2006
2113	ARAUZO DE MIEL	BURGOS	41.86	3.39W	1010	1/1/1964	12/31/2006
2319	PANTANO DE ARLANZON	BURGOS	42.28	3.34W	1140	1/1/1932	12/31/2006
9105	PRADOLUENGO	BURGOS	42.33	3.2W	960	1/1/1961	12/31/2006
2079	HONTORIA DEL PINAR	BURGOS	41.85	3.16W	1041	1/1/1967	12/31/2006
9069	MIRANDA DE EBRO	BURGOS	42.68	2.96W	520	1/1/1929	12/31/2006
9008	ARROYO DE VALDEARROYO	CANTABRIA	42.97	4.06W	845	1/1/1966	12/31/2006
1144	MOLLEDO DE PORTOLIN	CANTABRIA	43.15	4.04W	242	1/1/1961	12/31/2006
1131I	TORRELAVEGA 'SNIACE'	CANTABRIA	43.36	4.04W	70	1/1/1967	12/31/2006
1109	PARAYAS 'AEROPUERTO'	CANTABRIA	43.43	3.82W	6	1/1/1924	12/31/2006
1124	VILLACARRIEDO	CANTABRIA	43.23	3.8W	212	1/1/1948	12/31/2006
1111	SANTANDER CMT	CANTABRIA	43.49	3.8W	52	1/1/1957	12/31/2006
8438	SEGORBE	CASTELLON	39.85	0.49W	364	1/1/1942	12/31/2006
8448A	VALL D'UIXË	CASTELLON	39.82	0.21W	79	1/1/1961	12/31/2006
8455	BETX═	CASTELLON	39.93	0.2W	102	1/1/1957	12/31/2006
9563	CASTELLFORT	CASTELLON	40.5	0.18W	1181	1/1/1943	12/31/2006
8492	ATZENETA DEL MAESTRAT	CASTELLON	40.22	0.17W	400	1/1/1943	12/31/2006
9562	MORELLA	CASTELLON	40.62	0.1W	990	1/1/1920	12/31/2006
8494O	VILLAFAMES H S	CASTELLON	40.12	0.06W	295	1/1/1937	12/31/2006
8518	VINARÊS 'VIVEROS ALCANAR'	CASTELLON	40.54	0.44E	100	1/1/1957	12/31/2006
9585	LA MOLINA OBSERVATORI	GIRONA	42.33	1.94E	1704	1/1/1929	12/31/2006
0317	NURIA	GIRONA	42.39	2.16E	1967	1/1/1906	12/31/2006
0323	RIPOLL PROGRES	GIRONA	42.2	2.19E	680	1/1/1900	12/31/2006
0354B	VILADRAU AGUES	GIRONA	41.84	2.42E	865	1/1/1964	12/31/2006
0367	AEROPORT DE GIRONA COSTA BRAVA	GIRONA	41.9	2.76E	127	1/1/1935	12/31/2006
0281	BLANES	GIRONA	41.67	2.79E	18	1/1/1911	12/31/2006
0281A	BLANES MARIMURTRA	GIRONA	41.68	2.8E	60	1/1/1947	12/31/2006
0423	PERELADA	GIRONA	42.31	3.01E	20	1/1/1927	12/31/2006
0292A	BEGUR LOS ALGARROBOS	GIRONA	41.93	3.19E	185	1/1/1900	12/31/2006

3103	PANTANO EL VADO	GUADALAJARA	41	3.3W	980	1/1/1942	12/31/2006
3086	SALTO DE ZORITA	GUADALAJARA	40.34	2.88W	642	1/1/1950	12/31/2006
3082	SALTO DE BOLARQUE	GUADALAJARA	40.36	2.83W	620	1/1/1931	12/31/2006
3131	VALDELCUBO	GUADALAJARA	41.23	2.68W	1011	1/1/1964	12/31/2006
3130	SIGUENZA 'EL BOSQUE'	GUADALAJARA	41.07	2.64W	950	1/1/1933	12/31/2006
3013	MOLINA DE ARAGON	GUADALAJARA	40.85	1.89W	1063	1/1/1961	12/31/2006
1049O	ELGUETA-AIXOLA	GUIPUZCOA	43.16	2.51W	262	1/1/1967	12/31/2006
1049	BERGARA 'ALBITXU'	GUIPUZCOA	43.13	2.43W	205	1/1/1945	12/31/2006
1037	LEGAZPIA	GUIPUZCOA	43.06	2.33W	402	1/1/1958	12/31/2006
1035U	AYA-LAURGAIN	GUIPUZCOA	43.25	2.17W	320	1/1/1917	12/31/2006
1024E	SAN SEBASTIAN 'IGUELDO'	GUIPUZCOA	43.31	2.04W	252	1/1/1916	12/31/2006
1035	LASARTE-MICHELIN	GUIPUZCOA	43.27	2.02W	85	1/1/1956	12/31/2006
1024	SAN SEBASTIAN 'ATEGORRIETA'	GUIPUZCOA	43.32	1.95W	8	1/1/1963	12/31/2006
1014	FUENTERRABIA 'AEROPUERTO'	GUIPUZCOA	43.36	1.79W	8	1/1/1955	12/31/2006
9210E	BAILO PUENTE LA REINA	HUESCA	42.56	0.8W	595	1/1/1967	12/31/2006
9207	HECHO	HUESCA	42.74	0.75W	860	1/1/1931	12/31/2006
9474	LA PEÐA 'EMBALSE'	HUESCA	42.39	0.74W	589	1/1/1914	12/31/2006
9206E	BINACUA	HUESCA	42.55	0.7W	762	1/1/1969	12/31/2006
9206	SANTA CRUZ DE LA SEROS	HUESCA	42.52	0.68W	820	1/1/1969	12/31/2006
9489	LA SOTONERA 'EMBALSE'	HUESCA	42.11	0.67W	413	1/1/1923	12/31/2006
9208	ARAGUES DEL PUERTO	HUESCA	42.71	0.67W	980	1/1/1968	12/31/2006
9470I	BOTAYA	HUESCA	42.49	0.65W	940	1/1/1969	12/31/2006
9205	AISA DE JACA	HUESCA	42.68	0.62W	1040	1/1/1968	12/31/2006
9491	ALMUDEVAR-GRANJA CHE	HUESCA	42.03	0.59W	390	1/1/1929	12/31/2006
9470E	BERNUES	HUESCA	42.48	0.58W	920	1/1/1950	12/31/2006
9202	JACA	HUESCA	42.57	0.55W	800	1/1/1929	12/31/2006
9198	CANFRANC LOS ARA/ONES	HUESCA	42.75	0.52W	1160	1/1/1910	12/31/2006
9900	NUENO	HUESCA	42.27	0.44W	726	1/1/1900	12/31/2006
9898	HUESCA MONFLORITE	HUESCA	42.08	0.33W	541	1/1/1943	12/31/2006
9461	YEBRA DE BASA	HUESCA	42.49	0.28W	910	1/1/1900	12/31/2006
9907I	GRAÐEN MONTE SODETO	HUESCA	41.89	0.25W	365	1/1/1960	12/31/2006

9910	PALLARUELO DE MONEGROS	HUESCA	41.71	0.21W	356	1/1/1900	12/31/2006
9885	PANZANO	HUESCA	42.21	0.17W	650	1/1/1969	12/31/2006
9814	TORLA	HUESCA	42.63	0.11W	1053	1/1/1963	12/31/2006
9893E	LASTANOSA-LASESA	HUESCA	41.86	0.07W	410	1/1/1968	12/31/2006
9866	BARBASTRO 'COMARCAL'	HUESCA	42.04	0.13E	338	1/1/1953	12/31/2006
9832A	NAVAL 'D.G.A.'	HUESCA	42.19	0.15E	590	1/1/1950	12/31/2006
9828U	CAMPORROTUNO	HUESCA	42.34	0.16E	560	1/1/1930	12/31/2006
9829	MEDIANO 'EMBALSE'	HUESCA	42.32	0.2E	504	1/1/1931	12/31/2006
9918	TAMARITE DE LITERA 'LA MELUSA'	HUESCA	41.78	0.37E	218	1/1/1935	12/31/2006
9914E	TAMARITE DE LITERA	HUESCA	41.86	0.39E	318	1/1/1958	12/31/2006
9853	SERRADUY 'DGA'	HUESCA	42.32	0.57E	775	1/1/1965	12/31/2006
9761	SANTA ANA 'EMBALSE'	HUESCA	41.88	0.58E	390	1/1/1955	12/31/2006
9118	SANTO DOMINGO DE LA CALZADA	LA RIOJA	42.44	2.92W	638	1/1/1950	12/31/2006
9131I	MANSILLA EMBALSE	LA RIOJA	42.17	2.89W	900	1/1/1967	12/31/2006
9136	ANGUIANO VALVANERA	LA RIOJA	42.23	2.87W	1020	1/1/1949	12/31/2006
9121	HARO	LA RIOJA	42.58	2.85W	479	1/1/1936	12/31/2006
9145	CENICERO BODEGA	LA RIOJA	42.48	2.65W	437	1/1/1966	12/31/2006
9145A	CENICERO INDUSTRIAL	LA RIOJA	42.48	2.64W	430	1/1/1949	12/31/2006
9170	LOGROÐO-AGONCILLO	LA RIOJA	42.45	2.33W	352	1/1/1948	12/31/2006
9769I	LLEIDA TORRERIBERA	LLEIDA	41.61	0.7E	217	1/1/1930	12/31/2006
9714I	LA SENTIU DE SIO SIFO DE SIO	LLEIDA	41.8	0.83E	240	1/1/1950	12/31/2006
9729	MOLLERUSSA IES AGRARIA L'URGELL	LLEIDA	41.62	0.86E	268	1/1/1961	12/31/2006
9729A	MOLLERUSSA C U	LLEIDA	41.63	0.89E	250	1/1/1967	12/31/2006
9772E	LA POBLA DE CERVOLES	LLEIDA	41.37	0.91E	663	1/1/1969	12/31/2006
9652E	ALOS DE BALAGUER FORESTAL	LLEIDA	41.95	0.95E	860	1/1/1936	12/31/2006
9772	VILOSELL	LLEIDA	41.38	0.95E	665	1/1/1968	12/31/2006
9660	SANT MAURICI LLAC	LLEIDA	42.58	1E	1920	1/1/1953	12/31/2006
9650	ARTESA DE SEGRE	LLEIDA	41.9	1.05E	320	1/1/1968	12/31/2006
9686	GERRI DE LA SAL	LLEIDA	42.33	1.07E	595	1/1/1900	12/31/2006

9713	AGRAMUNT	LLEIDA	41.79	1.1E	349	1/1/1966	12/31/2006
9657	ESTERRI D'ANEU	LLEIDA	42.62	1.13E	940	1/1/1900	12/31/2006
9680	SORT PIRAGUISME	LLEIDA	42.41	1.13E	680	1/1/1929	12/31/2006
9649	PONTS	LLEIDA	41.93	1.2E	360	1/1/1963	12/31/2006
9619	LA SEU D'URGELL	LLEIDA	42.36	1.46E	692	1/1/1930	12/31/2006
0127O	PORT DEL COMTE	LLEIDA	42.17	1.56E	1800	1/1/1909	12/31/2006
9269	ALSASUA	NAVARRA	42.89	2.18W	525	1/1/1921	12/31/2006
9174	SARTAGUDA	NAVARRA	42.37	2.05W	310	1/1/1920	12/31/2006
9182U	LERIN	NAVARRA	42.48	1.97W	435	1/1/1950	12/31/2006
9279	ALLOZ 'EMBALSE'	NAVARRA	42.7	1.95W	475	1/1/1965	12/31/2006
9276	PUENTE LA REINA	NAVARRA	42.67	1.82W	346	1/1/1928	12/31/2006
1021	ARTICUTZA	NAVARRA	43.21	1.8W	305	1/1/1938	12/31/2006
9281	FALCES	NAVARRA	42.39	1.79W	292	1/1/1920	12/31/2006
9283	CADREITA	NAVARRA	42.21	1.71W	268	1/1/1920	12/31/2006
9301	MONTEAGUDO	NAVARRA	41.96	1.69W	410	1/1/1929	12/31/2006
1006	SANTESTEBAN	NAVARRA	43.13	1.66W	131	1/1/1920	12/31/2006
9252	OLITE	NAVARRA	42.49	1.65W	395	1/1/1938	12/31/2006
9255	CAPARROSO	NAVARRA	42.34	1.65W	304	1/1/1953	12/31/2006
9262	PAMPLONA OBSERVATORIO	NAVARRA	42.82	1.64W	442	1/1/1900	12/31/2006
9257E	EUGUI ESTERIBAR	NAVARRA	42.96	1.52W	615	1/1/1968	12/31/2006
9258	ZUBIRI	NAVARRA	42.93	1.5W	536	1/1/1966	12/31/2006
9246	CARCASTILLO LA OLIVA	NAVARRA	42.37	1.47W	340	1/1/1920	12/31/2006
9305	BUÐUEL	NAVARRA	41.98	1.45W	242	1/1/1964	12/31/2006
9232	ARTIEDA	NAVARRA	42.72	1.32W	450	1/1/1954	12/31/2006
9224	JAVIER CASTILLO	NAVARRA	42.6	1.22W	455	1/1/1929	12/31/2006
9223	YESA 'EMBALSE'	NAVARRA	42.62	1.19W	515	1/1/1940	12/31/2006
2363	PANTANO DE COMPUERTO	PALENCIA	42.86	4.83W	1140	1/1/1958	12/31/2006
2362	PANTANO DE CAMPORREDONDO	PALENCIA	42.9	4.74W	1253	1/1/1932	12/31/2006
2370	SALDAÐA	PALENCIA	42.52	4.74W	912	1/1/1944	12/31/2006
2370A	SALDAÐA 'I.L.'	PALENCIA	42.52	4.74W	912	1/1/1958	12/31/2006
2374A	CARRION DE LOS CONDES 'C.D.'	PALENCIA	42.34	4.6W	839	1/1/1931	12/31/2006
2401B	PALENCIA ESCL CAP AGRARIA	PALENCIA	42.01	4.56W	760	1/1/1961	12/31/2006
2232	PANTANO DE REQUEJADA	PALENCIA	42.91	4.53W	1024	1/1/1961	12/31/2006
2236	PANTANO DE CERVERA	PALENCIA	42.87	4.53W	1000	1/1/1967	12/31/2006
2234	CERVERA DE PISUERGA	PALENCIA	42.86	4.5W	1013	1/1/1932	12/31/2006

2403	VENTA DE BAÐOS 'AZUCARERA'	PALENCIA	41.92	4.5W	720	1/1/1934	12/31/2006
2386	MONZON DE CAMPOS	PALENCIA	42.12	4.49W	754	1/1/1948	12/31/2006
2278	OSORNO	PALENCIA	42.41	4.36W	809	1/1/1900	12/31/2006
2257	ALAR DEL REY	PALENCIA	42.66	4.31W	851	1/1/1932	12/31/2006
2243	PANTANO DE AGUILAR	PALENCIA	42.79	4.28W	903	1/1/1959	12/31/2006
2095	SAN ESTEBAN DE GORMAZ	SORIA	41.57	3.2W	860	1/1/1932	12/31/2006
2085	EL BURGO DE OSMA	SORIA	41.59	3.07W	895	1/1/1932	12/31/2006
2081	SAN LEONARDO DE YAGUE	SORIA	41.83	3.07W	1033	1/1/1935	12/31/2006
2010	ABEJAR	SORIA	41.81	2.79W	1130	1/1/1900	12/31/2006
2017I	BARRIOMARTIN 'MOLINO PIQUERAS'	SORIA	42	2.49W	1260	1/1/1968	12/31/2006
2030	SORIA 'OBSERVATORIO'	SORIA	41.77	2.47W	1082	1/1/1943	12/31/2006
9981A	TORTOSA OBSER. DEL EBRO	TARRAGONA	40.82	0.49E	48	1/1/1910	12/31/2006
9951	FLIX SEO	TARRAGONA	41.23	0.53E	56	1/1/1941	12/31/2006
0001	EL PERELLO	TARRAGONA	40.87	0.72E	142	1/1/1969	12/31/2006
9971	TIVISSA	TARRAGONA	41.04	0.73E	310	1/1/1912	12/31/2006
9961	CABACES	TARRAGONA	41.25	0.73E	357	1/1/1967	12/31/2006
0002I	VANDELLOS CENTRAL NUCLEAR	TARRAGONA	40.96	0.87E	34	1/1/1968	12/31/2006
0019	VIMBODI RIUDEBELLA	TARRAGONA	41.37	1.04E	590	1/1/1931	12/31/2006
0016B	REUS CENTRE LECTURA	TARRAGONA	41.15	1.11E	138	1/1/1934	12/31/2006
0017	VILASECA DE SOLCINA	TARRAGONA	41.11	1.15E	53	1/1/1931	12/31/2006
0016A	REUS AEROPORT	TARRAGONA	41.15	1.16E	73	1/1/1961	12/31/2006
0022	MONTBLANC	TARRAGONA	41.38	1.17E	340	1/1/1968	12/31/2006
9999	ODON	TERUEL	40.88	1.57W	1110	1/1/1944	12/31/2006
9998	TORNOS	TERUEL	40.96	1.44W	1018	1/1/1969	12/31/2006
9372	CELLA	TERUEL	40.46	1.29W	1023	1/1/1959	12/31/2006
9547	LA PUEBLA DE HIJAR	TERUEL	41.22	0.44W	245	1/1/1900	12/31/2006
9567	GALLIPUEN 'EMBALSE'	TERUEL	40.88	0.41W	680	1/1/1920	12/31/2006
1083	ARCENTALES	VIZCAYA	43.24	3.22W	220	1/1/1967	12/31/2006
1059	PUNTA GALEA GOLF	VIZCAYA	43.38	3.02W	90	1/1/1946	12/31/2006
1082	BILBAO 'AEROPUERTO'	VIZCAYA	43.3	2.91W	39	1/1/1947	12/31/2006

1075E	ARANZAZU	VIZCAYA	43.15	2.79W	98	1/1/1967	12/31/2006
9366	LA TRANQUERA 'EMBALSE'	ZARAGOZA	41.26	1.79W	660	1/1/1926	12/31/2006
9311C	BORJA 'AYUNTAMIENTO'	ZARAGOZA	41.83	1.53W	440	1/1/1968	12/31/2006
9390	DAROCA OBSERVATORIO	ZARAGOZA	41.12	1.41W	779	1/1/1919	12/31/2006
9428E	CALATORAO COOPERATIVA	ZARAGOZA	41.51	1.32W	360	1/1/1940	12/31/2006
9331F	EL BAYO	ZARAGOZA	42.19	1.26W	360	1/1/1965	12/31/2006
9433U	ALAGON AZUCARERA	ZARAGOZA	41.77	1.12W	235	1/1/1928	12/31/2006
9220	SIGUES	ZARAGOZA	42.63	1.02W	495	1/1/1900	12/31/2006
9219I	SALVATIERRA DE ESCA	ZARAGOZA	42.67	1.02W	580	1/1/1969	12/31/2006
9434	ZARAGOZA AEROPUERTO	ZARAGOZA	41.66	1.01W	247	1/1/1900	12/31/2006
9322	BIEL	ZARAGOZA	42.39	0.94W	760	1/1/1966	12/31/2006
9515	MONEVA-EMBALSE	ZARAGOZA	41.18	0.83W	650	1/1/1938	12/31/2006
9499	ZARAGOZA AULA DEI	ZARAGOZA	41.73	0.81W	225	1/1/1950	12/31/2006
9481	MARRACOS	ZARAGOZA	42.09	0.77W	400	1/1/1961	12/31/2006
9495	ZUERA EL VEDADO	ZARAGOZA	41.88	0.65W	298	1/1/1965	12/31/2006
9509	OSERA DE EBRO	ZARAGOZA	41.54	0.58W	172	1/1/1969	12/31/2006
9574	CASPE-AYUNTAMIENTO	ZARAGOZA	41.24	0.04W	145	1/1/1954	12/31/2006

APPENDIX B

LIST OF ORIGINAL PUBLICATIONS

During his PhD study, Ahmed El Kenawy contributed to and became a co-author on six research articles extracted from this thesis. These articles are referred to as follows:

I. **El Kenawy, A.**, López-Moreno, J. I., and Vicente-Serrano, S. M. (2011). Recent trends in daily temperature extremes over northeastern Spain (1960–2006), Natural Hazards & Earth System Sciences, 11, 2583-2603.

II. **El Kenawy, A**., López-Moreno, J.I., Vicente-Serrano, S.M., Stepanek, P. (2012). An assessment of the role of homogenization protocols in the performance of daily temperature series and trends: application to northeastern Spain. International Journal of Climatology, DOI: 10.1002/joc.3410.

III. **El Kenawy, A**., López-Moreno, J. I., Vicente-Serrano, S.M. (2012). Trend and variability of surface air temperature in northeastern Spain (1920–2006): linkage to atmospheric circulation, Atmospheric Research, Vol.106, 159-180.

IV. **El Kenawy, A.**, López-Moreno, J. I., and Vicente-Serrano, S. M. Summer temperature extremes in northeastern Spain: spatial regionalization and links to atmospheric circulation (1960-2006). Theoretical and Applied Climatology (under review).

V. **El Kenawy, A.**, López-Moreno, J. I., Brunsell, N.A., Vicente-Serrano, S.M. Anomalously severe cold nights and warm days in northeastern Spain: their spatial variability, driving forces and future projections. Global and Planetary Change (under review).

VI. **El Kenawy, A.**, López-Moreno, J. I., Brunsell, N.A., Vicente-Serrano, S.M. Assessing simulations of daily temperature variability and change in

northeastern Spain during the 21st century. International Journal of Climatology (under review).